# Seismic Bond Model for Concrete Reinforcement and the Application to Column-to-Foundation Connections

Von der Fakultät Bau- und Umweltingenieurwissenschaften
der Universität Stuttgart zur Erlangung der Würde eines
Doktor-Ingenieurs (Dr.-Ing.) genehmigte Abhandlung

Vorgelegt von

**Christoph Mahrenholtz**

aus Braunschweig

| | |
|---|---|
| Hauptberichter: | Prof. Rolf Eligehausen |
| Mitberichter: | Prof. Stefano Pampanin |
| | Prof. Jan Hofmann |

Tag der mündlichen Prüfung: 1. August 2012

Institut für Werkstoffe im Bauwesen der Universität Stuttgart

2012

**Abstract**

The efficient application of reinforced concrete relies on the combined strengths of steel reinforcement, which is strong in tension, and concrete, which is strong in compression. In general, the interaction concentrates on the end anchorage of reinforcing bars where the load is transferred to the concrete via the steel-concrete-bond. During an earthquake, the bond of anchorages is at risk for two reasons: The seismic excitation of the reinforced concrete structure loads the reinforcement cyclically and, at the same time, generates cracks which open and close cyclically. In joints, the cracks may run parallel along reinforcing bars anchoring adjoining members. The combination of cyclic loads and cyclic cracks leads to a more pronounced bond damage.

The damage is secondary for large anchorage lengths with hooks detailed according to conventional design provisions. Large anchorage lengths with hooks are obstructive during construction and preclude post-installation of reinforcing bars. In order to develop an advanced design concept which allows the reduction of the anchorage length for column-to-foundation connections, two core topics were investigated in the course of the doctoral research which are discussed following the introduction (Chapter 1), the presentation of the state of the art (Chapter 2), as well as the explanation of the research approach and background (Chapter 3).

First, the bond behaviour under simultaneous load and crack cycling was studied at micro level as existing bond models do not consider the effect of crack cycling. This study allowed extending the applicability of a hysteretic energy model for reinforcing bars subjected to simultaneous load and crack cycling (Chapter 4). In addition, the possibility to simulate the bond damage by means of the finite element method was shown (Chapter 5).

Second, column-to-foundation connections were studied at macro level. An anchorage detailing without hooks is advantageous for construction and allows the post-installation of column starter bars in the foundation. Post-installed columns are in particular suitable for the seismic retrofit of soft ground floor stories which failure is one of the most common reasons for total structural collapses during earthquakes. Large scale experimental tests were conducted (Chapter 6) and supplemented by a large number of numerical tests (Chapter 7).

The gained knowledge enabled the enhancements of the bonded anchor design provisions (Chapter 8). Based on the enhanced design provisions, a design concept for column-to-foundation connections is proposed which allows the post-installation of columns (Chapter 9). The design concept was developed in particular for seismic load cases. The thesis concludes in summarising the most significant results and pointing out which open questions in the field of post-installed reinforcing bars should be answered in future (Chapter 10).

**Kurzfassung**

Der effiziente Einsatz von Stahlbetonbau beruht auf die kombinierten Stärken des Bewehrungsstahls, der hohe Zugfestigkeiten aufweist, und des Betons, der hohe Druckfestigkeiten aufweist. Im Allgemeinen konzentriert sich das Zusammenwirken auf die Endverankerung der Bewehrungsstäbe, wo die Last über den Stahl-Beton-Verbund in den Beton eingeleitet wird. Die Verankerungen werden bei einem Erdbeben aus zwei Gründen stark beansprucht: Die seismische Anregung eines Stahlbetontragwerks bewirkt ein zyklisches Belasten der Bewehrung und zugleich das Auftreten von Rissen, die sich zyklisch öffnen und schießen. In Stahlbetonrahmenknoten können die Risse entlang der Bewehrung verlaufen, die ein angeschlossenes Bauteil verankern. Die Kombination aus zyklischer Last und zyklischen Rissen beschleunigt die Verbundschädigung.

Bei nach herkömmlichen Bemessungsvorschriften ausgebildeten großen Verankerungslängen mit Haken ist die Schädigung sekundär. Große Verankerungslängen mit Haken sind jedoch hinderlich während der Bauausführung und schließen die nachträgliche Installation von Bewehrungsanschlüssen aus. Um ein neuartiges Bemessungskonzept zu entwickeln, das die Reduzierung der Verankerungslänge für Stützen-Fundament-Anschlüssen ermöglicht, wurden im Rahmen der Promotionsarbeit zwei große Themenbereiche untersucht, die nach der Einleitung (Kapitel 1), dem Erörtern des gegenwärtigen Kenntnisstandes (Kapitel 2) sowie der Erläuterung des Forschungsansatzes und des Hintergrundes (Kapitel 3) besprochen werden.

Zunächst wurde auf der Mikroebene das Verhalten des Verbundes unter gleichzeitiger Beanspruchung von zyklischer Last und zyklischem Riss untersucht, da bisherige Verbund-Modelle nicht die Einwirkung zyklischer Risse berücksichtigen. Durch die Untersuchungen wurde der Anwendungsbereich eines energetischen Verbund-Models auf Bewehrungen erweitert, die einer gleichzeitigen Belastung aus zyklischer Last und zyklischem Riss unterliegen (Kapitel 4). Zudem konnte gezeigt werden, dass die Verbundschädigung mit der Finiten-Element-Methode simuliert werden kann (Kapitel 5).

Anschließend wurde auf der Makroebene Stützen-Fundament-Anschlüsse untersucht. Eine Verankerung der Stützenanschlussbewehrung ohne Haken hat nicht nur baupraktische Vorteile, sondern ermöglicht auch einen nachträglichen Stützenbewehrungsanschluss im Fundament. Nachträglich eingebaute Stützen sind eine besonders geeignete Erdbebenertüchtigungsmaßnahme für strukturell zu schwach ausgeführte Erdgeschosstragwerke, deren Versagen eine der häufigsten Ursachen für den Totaleinsturz von Gebäuden während eines Erdbebens ist. Hierzu wurden experimentelle Großversuche durchgeführt (Kapitel 6) und ergänzt durch eine große Anzahl von numerische Versuchen (Kapitel 7).

Die gewonnenen Erkenntnisse ermöglichten die Weiterentwicklung der Bemessungsvorschriften für Verbundanker (Kapitel 8). Basierend auf die weiterentwickelten Bemessungsvorschriften wird ein Bemessungskonzept für Stützen-Fundament-Anschlüsse vorgeschlagen, das den nachträglichen Einbau von Stützen erlaubt (Kapitel 9). Das Bemessungskonzept wurde insbesondere für Erdbebenlastfälle entwickelt. Abschließend werden die wesentlichen Untersuchungsergebnisse zusammengefasst und dargelegt, welche offene Fragen im Bereich von nachträglichen Bewehrungsanschlüssen noch in Zukunft beantwortet werden sollten (Kapitel 10).

**Acknowledgement**

First things first – I would like to thank my PhD advisor Professor Rolf Eligehausen for supporting my research career. It was a pleasure to conduct seismic research with him in the transition zone of anchor technology and reinforced concrete engineering. His strong commitment to my dissertation at the Institut für Werkstoffe im Bauwesen (IWB), Universität Stuttgart, encouraged me to travel to the other side of the world for a research period down under at the University of Canterbury (UC) in Christchurch, New Zealand.

Special thanks go to Professor Stefano Pampanin for hosting me at the cradle of modern seismic engineering, namely the Department for Civil and Natural Resources Engineering of the UC. The shaking and educative experience in Christchurch will stay in my mind forever. His participation in my research was a benefit and I am grateful having him as a co-reviewer of my thesis.

I thank my co-reviewer Professor Jan Hofmann for supporting my stay at UC and for giving me new research impulses and the opportunity to expand my technical knowledge at the IWB. The discussions were helpful to see things from a different perspective. Sincere thanks are given to Professor Ulrike Kuhlmann as chair of the examination board.

Conversations with Professor Hans-Wolf Reinhardt, former director of the IWB, always impressed me because of his abundant knowledge also beyond the field of civil engineering. Professor Josko Ožbolt was so kind to create my personal MASA release, and laboratory manager Bernd Schlottke who supported my shopping tours at hydraulic equipment suppliers.

As a follower of the educational ideal of the unity of research and teaching I really enjoyed my involvement in the Bologna process at our institute and in the course of Material Science managed by Lecturer Dr. Joachim Schwarte. It was great to work with my colleagues Alexander Assmann, Sören Sippel, Judit Tevesc, and Tim Weirich.

The German back office team, also in alphabetic order, Heidi Bauer, Gisela Baur, Silvia Choynacki, Regina Jäger, and Simone Stumpp deserve my thanks for keeping the engine running, and Monika Werner for organising every literature from the first paper on bond (written almost illegible by typewriter) to the latest paper on the behaviour of reinforced concrete structures under seismic excitation (as a DOI reference). Further, my thanks go to technicians Paul Geiger, Eugen Lindenmeier, and Peter Scherf who helped me with shock-loading anchors, controlling the actuators, and welding gadgets.

Also the support of the New Zealand team is greatly appreciated as it made my Kiwi Episode most enjoyable and memorable! I would like to mention in particular

Dr. Umut Akguzel (formerly at UC), a really good fellow who joined my large scale experiments while wrapping up his thesis, and furthermore, Dr. Weng-Yuen Kam (formerly at UC), as well as the technical staff members Peter Coursey, Mosese Fifita, Gavin Keats, David MacPherson, John Maley, Tim Perigo, and Stuart Toase. A super big thank-you goes to Elizabeth Ackermann, heart and soul of the department, for the linguistic proofreading. Another extra large thank-you goes to Nigel Snoep, fellow engineer, for the technical and linguistic proofreading of my thesis.

Valuable input and support was gratefully provided by Dr. Jörg Asmus (IEA Engineering Office), Dr. Thilo Pregartner (formerly at IWB), Dr. Werner Fuchs and Dr. Goran Periskic (both IWB), Dr. Stefan Fichtner (Regional Council Stuttgart), Dr. Matthew Hoehler and John Silva (both Hilti company), and Philipp Strater (Chemofast company).

To become friends with Akanshu Sharma (Bhabha Atomic Research Centre (BARC) and IWB) was in many aspects enriching. High speed testing in Mumbai, India was challenging but successful, not least because of the creative commitment of the technicians Shekhar Bodele and Rumachand Nandanwar.

The exchange of ideas with my colleagues Walter Berger and Ronald Blochwitz as well as the 'numerical advice' of Josipa Bošnjak was very supportive. Working with my co-workers Cenk Köse, Dénes Sándor, and Marina Stipetic was a pleasure. Student assistants Yangyang Gao, Wentao Zhu and Kai Liu were helpful to cope with my IT challenges. The feed back of Dr. Philipp Mahrenholtz (formerly at IWB) was very inspiring for my research as was his technical proofreading of the thesis.

Funding of the research presented in this thesis was largely provided by the German Research Foundation (DFG) under Grant No. EL 72/18-1. The proposal for the overseas research was awarded by a scholarship of the German Academic Exchange Service (DAAD). Both financial supports are greatly acknowledged.

Finally, I ask my daughter's pardon for me being bleary-eyed and not having as much time for playgrounds as I wished to have, and my wife’s for any inconvenience the PhD story may have caused.

**Table of Contents**

## Notation

### Acronyms and Abbreviations

| | |
|---|---|
| ACI | American Concrete Institute, standard developing organization, also taken as shortform for respective US-American normative standard |
| BOND | Procedural program to determine the strain distribution along an anchorage under monotonic and cyclic loading |
| C | Concrete \| Concrete failure |
| CC | Concrete Capacity |
| CEB | Concrete Euro-International du Béton |
| CEN | European Committee for Standardization |
| CPU | Central Processing Unit |
| CSM | Constant Stiffness Method |
| CV | Coefficient of Variation |
| DIN | Deutsches Institut für Normung (German Institute for Standardisation) |
| DCH, DCL | Ductility Class High, Ductility Class Low |
| DOF | Degree of freedoms |
| EC | Eurocode, European normative standard for structural design and construction work developed by the CEN |
| EN | European Standard |
| EOTA | European Organisation for Technical Approvals |
| ESR | ES-Report (US technical approval warranting by the ICC-ES) |
| ETA | European Technical Approval |
| FE | Finite Element |
| FEA | Finite Element Analysis |
| FEM | Finite Element Method |
| FEMAP | Finite Element Modelling And Post-processing, pre- and post-processing program |
| FEA | Finite element analysis |
| FIB | Federation International du Béton (International Federation for Structural Concrete) |
| FRP | Fibre Reinforced Polymers |
| ICC-ES | International Code Council – Evaluation Service, ICC-ES Report also taken as technical approval |
| IWB | Institut für Werkstoffe im Bauwesen (Institute of Construction Material of the University of Stuttgart) |
| LRFD | Load and Resistance Factor Design |
| MASA | MAcroscopic Space Analysis, finite element program |
| MCE | Maximum Credible Earthquake |
| MPII | Manufacturer's Printed Installation Instructions |
| MRF | Moment Resisting Frame |
| NZ | New Zealand |
| OS | Operation system |
| P | Pullout failure |
| PGA | Peak Ground Acceleration |
| PSF | Partial Safety Factor |
| RAM | Random Access Memory |
| RC | Reinforced Concrete |
| S | Steel \| Steel failure |
| SI | Système International d'Unités (International System of Units) |
| SDC | Seismic Design Category |

| | |
|---|---|
| SSM | Secant Stiffness Method |
| STM | Strut-and-Tie Model \| Strut-and-Tie Modelling |
| TS | Technical Specification |
| TSM | Tangent Stiffness Method |
| UB | Uniform Bond |
| UC | University of Canterbury, Christchurch |
| US | United States of America |

**Common subscripts**

| | |
|---|---|
| 0 | Short term \| Initial |
| ave | Average |
| c | Concrete |
| ccr | Cracked, cyclically crack width |
| col | Column |
| com | Compressed crack |
| con | Constant |
| cyc | Cyclic or cycle |
| cyl | Cylinder |
| cr | Cracked, constant crack width \| critical |
| d | Design |
| ef | Effective |
| f | Friction |
| fdn | Foundation |
| k | Characteristic |
| m | Mean |
| max | Maximum |
| min | Minimum |
| nom | Nominal |
| p | Pullout |
| ucr | Uncracked |
| s | Steel |
| y | Yield |

**Prefix**

| | |
|---|---|
| cal | Calculative analysis |
| exp | Experimental test |
| num | Numerical test |

**Latin Uppercase Letters**

| | |
|---|---|
| A | Area |
| $A_c$ | Cross section of concrete member |
| $A_s$ | Cross section of reinforcing bar \| Cross section starter bars of one face |
| $A_{s,bot}$ | Cross section of foundation bottom reinforcement |
| $A_{s,prov}$ | Provided cross section |
| $A_{s,req}$ | Required cross section |
| $A_{s,spl}$ | Cross section of foundation splitting reinforcement |
| $A_{s,top}$ | Cross section of foundation upper reinforcement |
| C | Compression (strut-and-tie model) \| Concrete failure mode |
| $C_d$ | Deflection amplification factors (IBC and ASCE 7) |
| E | Modulus of elasticity \| Load \| Energy \| Hysteretic energy (bond model) |

| | |
|---|---|
| $E_d$ | Dissipated energy of sub-assemblage (inter alia inter alia in the context of ACI 374.1) |
| $E_f$ | Hysteretic frictional energy (bond model) |
| $E_h$ | Modulus of hardening |
| $E_0$ | Initially dissipated energy (bond model) \| Initial modulus of elasticity |
| $E_{0f}$ | Initially dissipated frictional energy (bond model) |
| F | Column shear load |
| $F_{Ek}$ | Design load |
| $F_{Em}$ | Mean load |
| $F_{Ek}$ | Characteristic load |
| $F_{max}$ | Maximum connection shear load capacity |
| $F_R$ | Area of one transverse rib \| Resistance \| Connection shear load capacity (failure load as the minimum of $P_{R,y}$, $P_{R,p}$, and $P_{R,c}$) |
| $F_{Rm}$ | Mean resistance |
| $F_{Rk}$ | Characteristic resistance |
| $F_{R,c}$ | Connection shear load capacity corresponding to concrete breakout failure |
| $F_{R,p}$ | Connection shear load capacity corresponding to pullout failure |
| $F_{R,p/c}$ | Connection shear load capacity corresponding to minimum of pullout and concrete failure |
| $F_{R,y}$ | Connection shear load capacity corresponding to yield failure |
| G | Fracture energy |
| $K_p$ | Stiffness sub-assemblage (inter alia in the context of ACI 374.1) |
| L | Length |
| M | Moment \| Column bending moment |
| $M_{max}$ | Maximum connection bending moment capacity |
| $M_n$ | Nominal connection bending moment capacity (based on characteristic yield strength) |
| $M_R$ | Connection bending moment capacity according to bonded anchor design (minimum of $M_{R,}$, $M_{R,p}$, and $M_{R,c}$) |
| $M_{R,c}$ | Connection bending moment capacity corresponding to concrete breakout failure of anchorage ($N_{R,c} \cdot z$) |
| $M_{R,p}$ | Connection bending moment capacity corresponding to pullout failure of anchorage ($N_{R,p} \cdot z$) |
| $M_{R,p/c}$ | Connection bending moment capacity corresponding to minimum of pullout and concrete breakout failure of anchorage ($N_{R,p/c} \cdot z$) |
| $M_{R,y}$ | Connection bending moment capacity corresponding to yield failure of anchorage ($N_{R,y} \cdot z$) |
| $M_y$ | Connection bending moment capacity based on mean yield strength |
| $N_R$ | Anchorage capacity according to bonded anchor design (minimum of $N_{R,y}$, $N_{R,p}$, and $N_{R,c}$) |
| $N_{R,c}$ | Anchorage capacity corresponding to concrete breakout failure (concrete breakout capacity) |
| $N_{R,p}$ | Anchorage capacity corresponding to pullout failure (pullout capacity) |
| $N_{R,p/c}$ | Anchorage capacity corresponding to minimum of pullout and concrete breakout failure |
| $N_{R,y}$ | Anchorage capacity corresponding to yield failure (yield capacity) |
| $N_w$ | Sustained axial load |
| P | Pullout failure mode |
| R | Resistance \| Capacity \| Parameter (bond model) |
| S | Steel failure mode |

| | |
|---|---|
| T | Tension (strut-and-tie model) |
| V | Shear load or force |
| W | Width |
| Y | Yield failure mode |

**Latin Lowercase Letters**

| | |
|---|---|
| a | Rib height (reinforcing bar) |
| $a_1$, $a_2$, $a_{1f}$, $a_{2f}$ | Tuning parameters for hysteretic energy model |
| $b_{col}$ | Width of column |
| $b_{fdn}$ | Width of foundation |
| c | Rib distance (reinforcing bar) \| Centre-to-edge distance of anchorages |
| $c_{col}$ | Centre-to-edge distance of column reinforcement |
| $c_{cr,N}$, $c_{cr,Np}$ | Centre-to-centre distance of anchorages, in the context of designing |
| $c_d$ | Minimum of concrete cover and half of the clear distance between adjoining reinforcing bars |
| $c_{fdn}$ | Centre-to-edge distance of foundation reinforcement |
| d | Damage parameter \| Diameter |
| $d_0$ | Diameter of drilled hole |
| $d_s$ | Diameter of stressed steel cross section |
| $e_N$ | Eccentricity of the resulting tensile load on the tensioned anchorage |
| f | Frequency |
| $f_b$ | Bond strength between concrete and reinforcing bar |
| $f_c$ | Compressive cylinder strength of concrete |
| $f_{c,cube}$ | Compressive cube strength of concrete (C20/25: $f_c = f_{c,cube} / 1.25$; C50/60: $f_c = f_{c,cube} / 1.20$) |
| $f_{ct}$ | Tensile strength of concrete |
| $f_R$ | Related rib area |
| $f_s$ | Ultimate strength of steel (steel model) |
| $f_u$ | Ultimate strength of steel |
| $f_y$ | Yield strength of steel |
| h | Overall depth of a cross-section \| Average finite element size |
| $h_{col}$ | Depth of column |
| $h_{ef}$ | Effective embedment depth of anchor |
| $h_{fdn}$ | Height of foundation |
| $h_{min}$ | Minimum thickness of concrete member |
| k | Coefficient (concrete breakout capacity) \| Stiffness \| Number of ribs around perimeter \| k-factor (statistic) |
| $k_{sec}$ | Secant stiffness with reference to ultimate bond strength (bond model) |
| $k_8$ | Coefficient (concrete breakout capacity), in the context of designing |
| $\ell_b$ | Anchorage length of reinforcing bar |
| $\ell_{b,eq}$ | Equivalent anchorage length |
| $\ell_{b,min}$ | Minimum anchorage length |
| $\ell_{b,rqd}$ | Required anchorage length |
| $\ell_p$ | Depth of penetration of yielding and debonding |
| $\ell_{element}$ | Length of finite element \| Grid width of finite element mesh |
| n | Number of anchors or reinforcing bars within one group \| cycle counter |
| p | Pressure |
| $p_f$ | Probability of failure |
| s | Displacement (slip) \| Spacing \| Centre-to-centre spacing of anchorages |
| $s_{cr,N}$, $s_{cr,Np}$ | Edge length of prism activated by tensioned anchorage, in the context of designing |

| | |
|---|---|
| $s_u$ | Slip corresponding to bond strength determined in bond test |
| $s_1$ | Slip corresponding to bond strength defined for bond model (beginning of plateau) |
| $s_2$ | Slip corresponding to bond strength defined for bond model (end of plateau) |
| $s_3$ | Slip corresponding to solely frictional bond strength defined for bond model (mechanical bond strength deteriorated) |
| t | Time |
| v | Displacement |
| w | Crack width |
| $w_{max}$ | Maximum crack width |
| $w_{min}$ | Minimum crack width |
| $w_1$ | Upper crack width (crack cycling qualification tests) |
| $w_2$ | Lower crack width (crack cycling qualification tests) |
| x | Distance from surface measured from the loaded end of anchorage |
| y | Distance between point of load application on column and top of foundation |
| z | Internal lever arm column |
| z' | Internal lever arm foundation |

**Greek Uppercase Letters**

| | |
|---|---|
| $\Delta$ | Displacement |
| $\Delta_a$ | Allowable story displacement (IBC and ASCE 7) |
| $\Omega_i$ | Factor to account for various effects reducing or increasing the bond strength |
| $\Omega_c$ | Factor taking into account the effect of transverse concrete compression on bond strength |
| $\Omega_{cyc}$ | Factor taking into account the damage effect of cycling on bond strength |
| $\Omega_{cycf}$ | Factor taking into account the damage effect of cycling on frictional bond strength |
| $\Omega_{cyc(n=10)}$ | Factor taking into account the damage effect of cycling after 10 cycles |
| $\Omega_s$ | Factor taking into account the effect of inelastic steel strain on bond strength |
| $\Omega_w$ | Factor taking into account the effect of parallel concrete cracks on bond strength |

**Greek Lowercase Letters**

| | |
|---|---|
| $\alpha_1$, $\alpha_2$, $\alpha_5$ | Coefficients (anchorage length) |
| $\beta$ | Safety index \| Angle between rib and longitudinal axis of bar |
| $\gamma_{inst}$ | Installation partial safety factor |
| $\gamma_F$ | Partial safety factor of force |
| $\gamma_M$ | Partial safety factor of material |
| $\gamma_{Mc}$ | Partial safety factor of concrete failure |
| $\gamma_{Mc,seis}$ | Partial safety factor of concrete failure, seismic load case |
| $\gamma_{Mp}$ | Partial safety factor of pullout failure |
| $\gamma_{Mp,seis}$ | Partial safety factor of pullout failure, seismic load case |
| $\gamma_{Ms}$ | Partial safety factor of steel failure |
| $\gamma_{Ms,seis}$ | Partial safety factor of steel failure, seismic load case |

| | |
|---|---|
| $\varepsilon$ | Strain |
| $\varepsilon_c$ | Concrete strain in concrete member |
| $\varepsilon_s$ | Steel strain in reinforcing bar |
| $\varepsilon_u$ | Minimum uniform elongation |
| $\eta_1$, $\eta_2$ | Coefficients (bond strength) |
| $\theta$ | Angle (strut-and-tie model) \| Drift of sub-assemblage |
| $\theta_a$ | Drift at which acceptance is sought (in the context of ACI 374.1) |
| $\theta_i$ | Initial drift (in the context of ACI 374.1) |
| $\lambda$ | Overstrength factor |
| $\mu$ | Ductility \| Mean value |
| $\rho$ | Reinforcement ratio of longitudinal tension reinforcement |
| $\rho_{min}$ | Minimum reinforcement ratio |
| $\sigma$ | Normal stress \| Tensile stress \| Standard deviation |
| $\sigma_c$ | Concrete compressive stress in concrete member |
| $\sigma_{ct}$ | Concrete tensile stress in concrete member |
| $\sigma_s$ | Steel tensile stress in reinforcing bar |
| $\tau$ | Shear stress \| Bond stress |
| $\tau_f$ | Frictional bond strength (bond test) |
| $\tau_{f(n)}$ | Ultimate frictional bond strength at $n^{th}$ slip reversal (bond test and bond model) |
| $\tau_m$ | Mechanical bond strength (bond test) |
| $\tau_u$ | Ultimate bond strength (bond test) |
| $\tau_{uf}$ | Ultimate frictional bond strength (bond test) |
| $\tau_{u,res}$ | Ultimate bond strength for residual load test (bond test) |
| $\tau_1$ | Ultimate bond strength (bond model) |
| $\tau_{1(n)}$ | Ultimate bond strength at $n^{th}$ slip reversal (bond test and bond model) |
| $\tau_3$ | Ultimate frictional bond strength (bond model) |
| $\tau_R$ | Bond strength, in the context of designing (pullout capacity) |
| $\tau_{R,max}$ | Maximum transferable bond strength, in the context of designing |
| $\phi$ | Reinforcement bar diameter \| Strength reduction factor (IBC and ASCE 7) |
| $\phi_{m,min}$ | Minimum inner bending diameter |
| $\psi_c$ | Factor taking into account the effect of concrete strength on the capacity of reinforcing bar anchorages |
| $\psi_{cyc}$ | Factor taking into account the adverse effect of cyclic loading on the column-to-foundation connection capacity |
| $\psi_{cyc,N}$ | Ditto, in the context of designing |
| $\psi_{g,Np}$ | Factor taking into account the effect of failure surface of starter bar group on the capacity of reinforcing bar anchorages, in the context of designing |
| $\psi_M$ | Factor taking into account the beneficial effect of moment loading on the column-to-foundation connection capacity |
| $\psi_{M,N}$ | Ditto, in the context of designing |
| $\psi_{s,N}$, $\psi_{s,Np}$ | Factor taking into account the effect of disturbance of stress distribution due to foundation edges on the capacity of reinforcing bar anchorages, in the context of designing |
| $\psi_w$ | Factor taking into account the effect of cracked concrete on the capacity of reinforcing bar anchorages |

# 1 Introduction

## 1.1 Motivation for Research on Anchorages for Seismic Applications

In rural areas, earthquakes claim only few victims, mostly by rockfall and landslides. The traces of earthquakes are visible for a short time only (Figure 1.1a) before being recaptured by nature. Only in uninhabited locations with little erosion and vegetation, will earthquake traces be visible for a long time (Figure 1.1b).

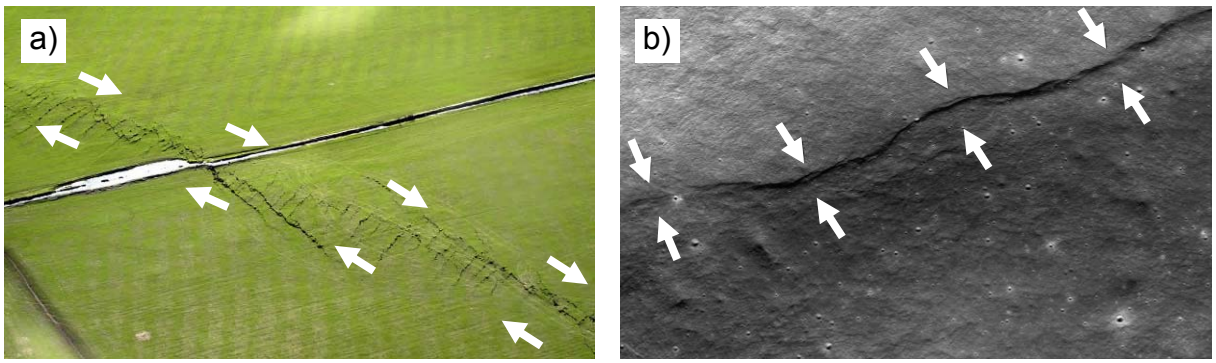


Figure 1.1 a) Greendale Fault, New Zealand, seismicity caused by strike-slip faulting (Source: GeoNet); b) Fault next to Gregory Crater, Moon, seismicity caused by contraction (Source: NASA/GSFC/Arizona State University/Smithsonian)

In urban areas, in contrast, earthquakes easily become a disaster as the civil structures respond to the destructive seismic waves and experience severe damage or a total collapse, killing tens of thousands of people every year. Unfortunately, areas with high density in population (Figure 1.2a) and seismic activity (Figure 1.2b) appear to coincide. A good agreement can be observed at the Great Rift Valley in Africa, the Adriatic and Aegean Plate in Europe, the collision rim of the Asian and Australian plate, and in particular the ring of fire (inter alia Chile, Mexico, California, Japan, Taiwan, and New Zealand).

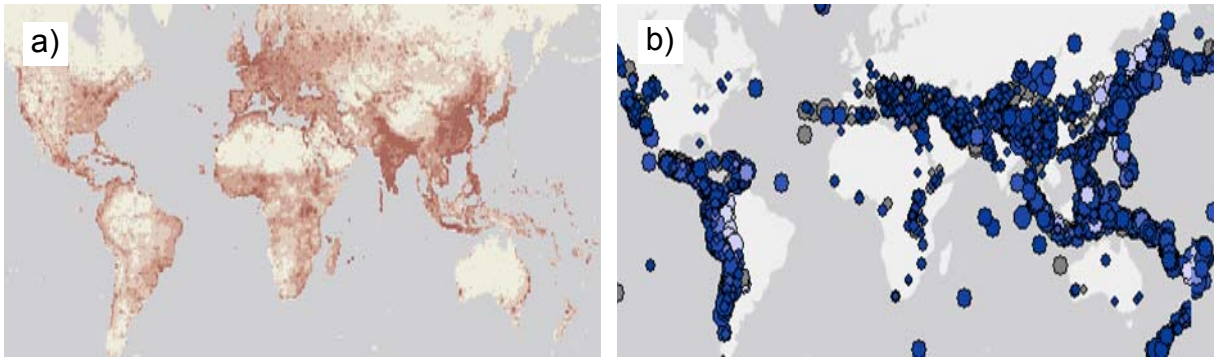


Figure 1.2 Density maps of a) population and b) earthquakes (Source: National Geographic)

In urban regions with high population density, the majority of buildings are reinforced concrete structures which are generally deemed to be a suitable building type for earthquake prone areas. However, recent earthquakes as the 1995 Kobe Earthquake in Japan, the 1999 Chi Chi Earthquake in Taiwan, the 2010 Maule Earthquake in Chile, and the 2011 Christchurch Earthquake in New Zealand showed not only the collapse of pre1970s buildings which are deemed in particular vulnerable to earthquakes (*EERI SER Kobe (1996)*, *EERI SER Chi-Chi (1999)*, *EERI SER Maule (2010)*, *EERI SER Christchurch (2011)*). But also a substantial number of reinforced concrete structures designed according to modern seismic design provisions proved to be vulnerable for seismic loads. As discussed in the following section, the reason for the failure of even modern buildings was either inadequate structural design or ground accelerations higher than anticipated.

Building owners and tenants prefer open space. Therefore, shear walls and columns are typically reduced to a minimum, in particular on the ground floor. This concept and the structural detailing of the connections often turn out to be inappropriate. For example, the total collapse of the six story CTV Building (Figure 1.3a) during the 2011 Christchurch Earthquake was probably caused by insufficient reinforcement detailing of the gravity columns (*Zahn, F. (2012)*). The collapse claimed 115 victims, which is more than half of the total number of victims (*Matthews, P. (2011)*, *EERI SER Christchurch (2011)*). Also in East and Southeast Asia buildings often show insufficient horizontal strengths. Here, arcade style buildings with commercially used ground floors are very common. These shop houses typically have open fronts at the street and are designed as moment resisting frame (MRF) reinforced concrete structures with masonry infill. Recent earthquakes such as the 1999 Chi Chi Earthquake (Figure 1.3b) revealed that insufficient earthquake resistance of low and mid-rise buildings caused fatal building collapses, accounting for the majority of the total death toll (*RMS (2000)*, *Liao, Y.-H. et al. (2005)*). To maximise the sales area, the ground floor often does not provide any shear wall parallel to the street and

consequently, the buildings are prone to fail in soft story mechanism (*Lee, G.-C.; Loh, C.-H. (1999)*, *EERI SER Chi-Chi (1999)*). Pancaking collapses due to soft story mechanism (Figure 1.3c) were also reported after the 2011 Tohoku Earthquake in Japan (*ISE (2012)*).


Figure 1.3 Failure of columns: a) CTV building before and after 2011 Christchurch Earthquake (Source: NZ Herald); b) and c) Shop houses after pancaking during 1999 Chi Chi and 2011 Tohoko Earthquakes (Source: EERI, ISE); d) Column-to-foundation connection failure during 2011 Tohoko Earthquake (Source: ISE)

Seismic maps published in building codes reflect the potential seismic hazard of the considered area. They are based on available geological data, stochastic evaluations, historic records, and collective memory. However, earthquake prognoses and associated demands are characterised by a large degree of uncertainty. Often, previous estimates later turn out to be insufficient. Regrettably, it requires disastrous earthquakes to prove wrong assumptions. For example, the peak ground acceleration (PGA) of the 2011 Christchurch Earthquake was about twice the acceleration assumed for the maximum credible earthquake (MCE) according to the building code (*Zahn, F. (2012)*). Furthermore, the earthquake gave evidence that the rule of thumb to define the vertical acceleration as one third of the horizontal acceleration is questionable as the PGAs recorded ranged from 0.2g to 1.41g in the horizontal and 0.06g to 2.21g in the vertical direction (*Bradley, A.; Cubrinovski, M. (2011)*). In the aftermath of devastating earthquakes, the seismic maps are frequently

redrawn to adapt the design ground accelerations, e.g. in New Zealand after the 2011 Christchurch Earthquake (Interim Advice *SESOC (2011)* for *NZS 1170.5 (2004)*). Other countries tighten the requirements of buildings in seismic zones as a precautionary measure, e.g. in Germany by the revised earthquake design code *DIN 4149 (2005)*.

The building stock of reinforced concrete structures which are deemed not to be earthquake-proof according to up-to-date knowledge is considerable. Because reinforced concrete structures have a long life span of 60 years or more, the problem does not take care of itself. Some countries are reluctant to deal with the socio-economic question of what to do with unsafe structures while others request the building owners to upgrade the buildings, at least to a certain fraction of the safety level in force for new buildings. Therefore, seismic retrofitting concepts are in the focus of earthquake engineering researchers. The reassessment of the building design in respect to earthquake strength may identify the need for additional structural elements. Post-installed anchorages play a key role for seismic retrofitting of reinforced concrete structures as pointed out in the following section.

## 1.2 Post-Installed Anchorages for Seismic Retrofitting

Seismic retrofitting includes precautionary retrofitting and repairing of structures which have already been moderately damaged by an earthquake. Several techniques are available to retrofit moment resisting frame concrete structures. Most retrofit solutions have in common that either post-installed concrete anchors or post-installed reinforcing bars are used to connect existing and retrofitting structural elements:

- Steel members and fibre reinforced polymer (FRP) elements are typically fixed with post-installed anchors (Figure 1.4a) to create a composite structure. This method is used for steel bracing, steel framed bracing and FRP or steel jacketing retrofitting solutions.
- Additional reinforced concrete elements, e.g. exterior buttresses, thickening of members, shear walls, column wing walls and additional columns, are generally connected to the existing structure using post-installed reinforcing bars (Figure 1.4b).

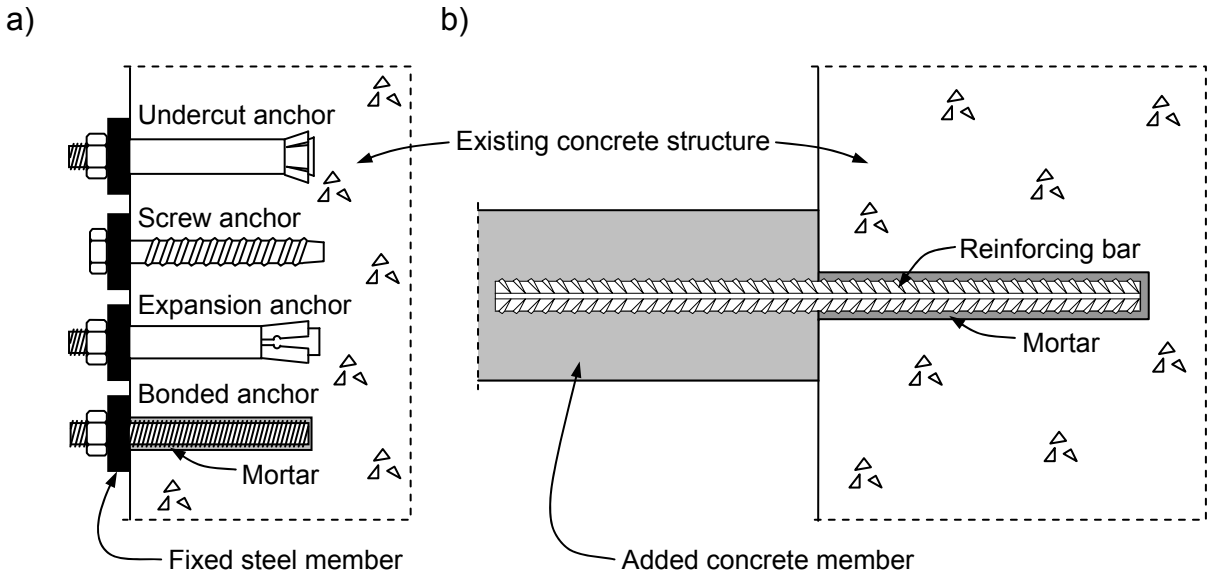


Figure 1.4 Schematic of a) various post-installed anchors and b) post-installed reinforcing bar to connect existing and retrofitting structural elements

An overview on the most common retrofitting schemes for reinforced concrete structures is given in Figure 1.5 and Table 1.1.

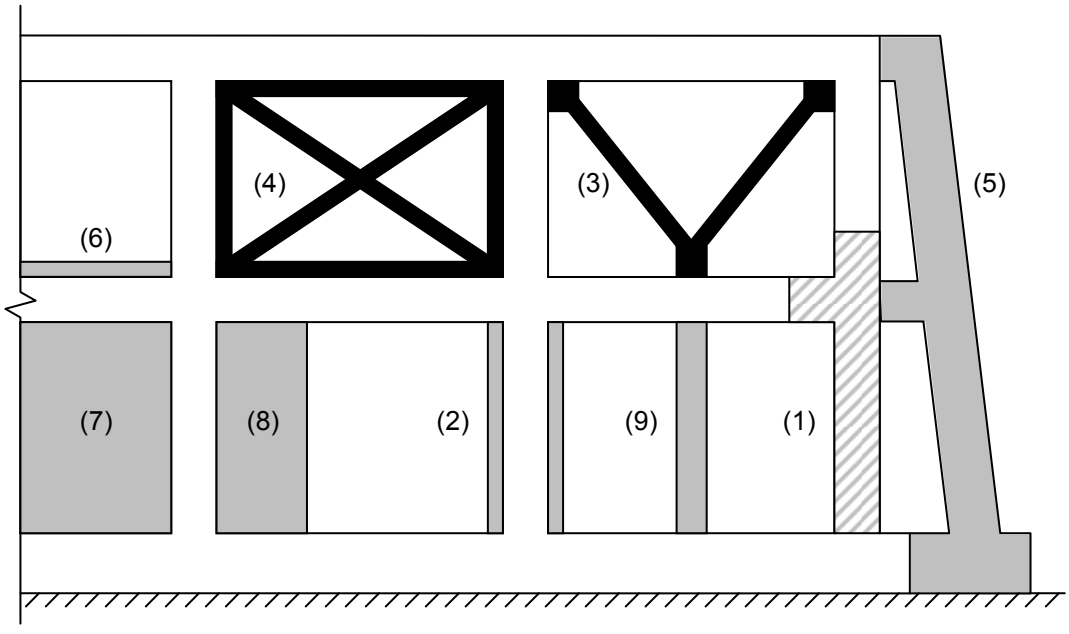


Figure 1.5 Overview of most common seismic retrofitting schemes for reinforced concrete structures

Table 1.1 Overview on seismic retrofitting solutions, schedular

| Solution | Remark |
|---|---|
| Post-installed anchors | |
| (1) FRP/steel jacketing/wrapping | Improving ductility, shear, lateral, and/or flexural strength; post-installed shear anchors transfer shear forces between existing column and jacketing element (e.g. *Aboutaha, R. et al. (1994)*), also used to retrofit beam-column-joints (e.g. *Tsonos, A. (2003)*) |
| (2) Concrete jacketing | Improving ductility, shear, lateral, and/or flexural strength; post-installed reinforcing bars connect longitudinal reinforcement of concrete jacket to existing structure (e.g. *Hwang, S.-J.; Kuo, W.-W. (2007)*) |
| (3) Steel bracing and<br>(4) Steel framed bracing | Improving strength, stiffness and ductility which can be specifically tuned; energy dissipation devices (dampers) can be conveniently integrated; lower mass compared to a concrete retrofitting elements, therefore, additional foundation works and increase of inertia forces avoided; elements can be prefabricated, allowing manual transport, clean and fast installation (e.g. *Mazzolani, F.; Della Corte, G. et al. (2009)*, *Jones, E.; Jirsa, J. (1986)*) |
| Post-installed reinforcing bars | |
| (5) Exterior buttresses | Providing additional horizontal strength, however, problematic because of architectonical handicap, requirement of vacant site, and necessity for additional foundation works |
| (6) Thickening of members | increasing strength and stiffness of slabs and walls; dowels to connect reinforced concrete topping; alternatively, steel or FRP mesh embedded in an additionally applied plaster layer (e.g. *Stempniewski, L.; Urban, M. et al. (2010)*). |
| (7) Shear walls | Increasing load capacity but decreasing deformation capacity significantly; reducing horizontal accessibility; post-installed reinforcing bars connect new shear wall to existing frame (e.g. *Shiohara, H. et al. (1986)*) |
| (8) Wing walls | Increasing load capacity but decrease deformation capacity moderately; limited horizontal accessibility; post-installed reinforcing bars connect wing wall to existing frame (e.g. *Yamamoto, Y.; Hattori, Y. et al. (2001)*) |
| (9) Additional columns | Increasing load capacity moderately and increase deformation capacity significantly; post-installed reinforcing bars connect new column to existing frame or slab and foundation |

Traditionally, solely cast-in-place anchorages were used to connect structural concrete elements. The development of lighter electrical powered rotary hammers in the 1970s allowed the drilling of holes more conveniently and faster. In addition, high performance mortars were developed. Therefore, post-installed anchoring became increasingly popular for fast track constructions, building re-uses, and seismic retrofit solutions. The combination of mortar, anchor or reinforcing bar, and installation technique is termed as a post-installation system.

Different installation techniques are available to post-install bonded anchors and reinforcing bars:

- Capsule technique: A capsule is placed in the drilled hole and the anchor or reinforcing bar is driven in by a machine with a simultaneous hammering and turning (Figure 1.6a).
- Injection technique: The mortar is injected into the hole and the anchor or reinforcing bar is inserted manually or mechanically (Figure 1.6b).
- Bulk technique: The mortar is externally mixed, poured into the hole and the anchor or reinforcing bar inserted.

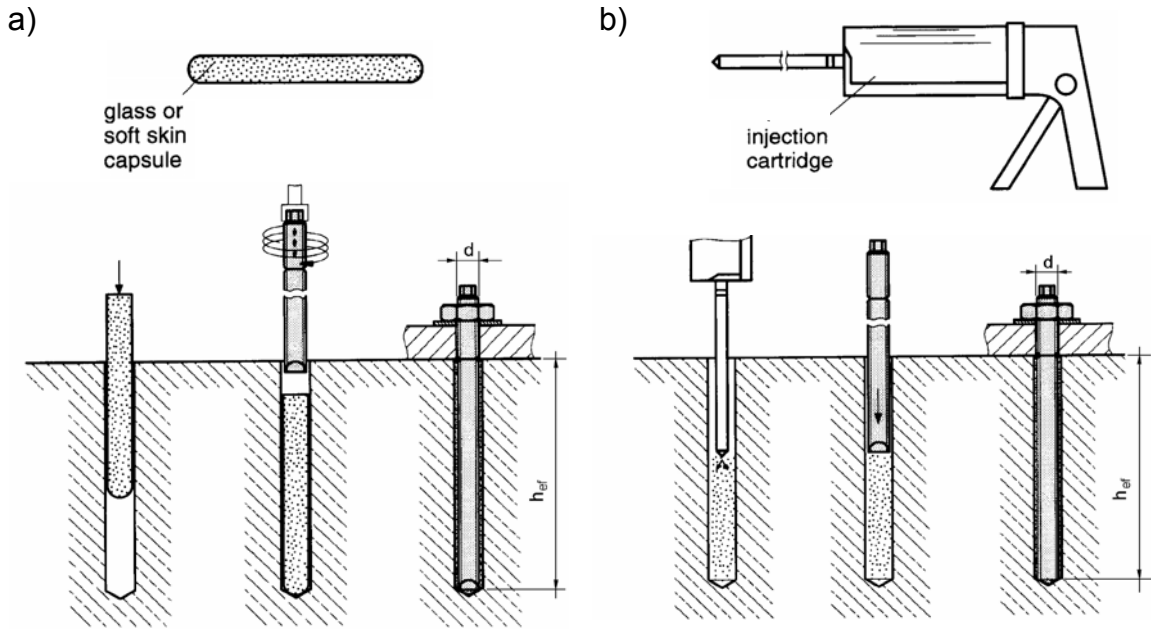


Figure 1.6 Installation techniques of bonded anchors: a) Capsule type; b) Injection type (*ETAG 001 (2006)*, Part 5)

For reinforcing bar post-installation, the injection technique is commonly used to mix and place the mortar because it is less labour intensive than the bulk technique and does not require the electrical powered spinning as with the capsule technique. Electrical driven injection guns are particularly suitable for the post-installation of reinforcing bars where a large quantity of mortar is needed.

In general, the post-installation of reinforcing bars is carried out according to the following installation sequence:

- Drilling the installation hole into concrete (Figure 1.7a)
- Cleaning the drilled hole by brushing and compressed air (Figure 1.7b)
- Injecting the mortar (Figure 1.7c)
- Installing the reinforcing bar (Figure 1.7d)

It is noted the the photos shown in Figure 1.7 are illustrative only. Contrary to the installation of bonded anchors, special drill rigs have to be used for the required large anchorage lengths of post-installed reinforcing bars. Further requirements for the post-installation of reinforcing bars are discussed in Section 2.3.1.1. The properties of post-installation systems relevant in the context of this thesis are addressed in Section 2.2.1ff. A general introduction to the characteristics of post-installation systems can be found in *Eligehausen, R.; Mallée, R. et al. (2006)*.

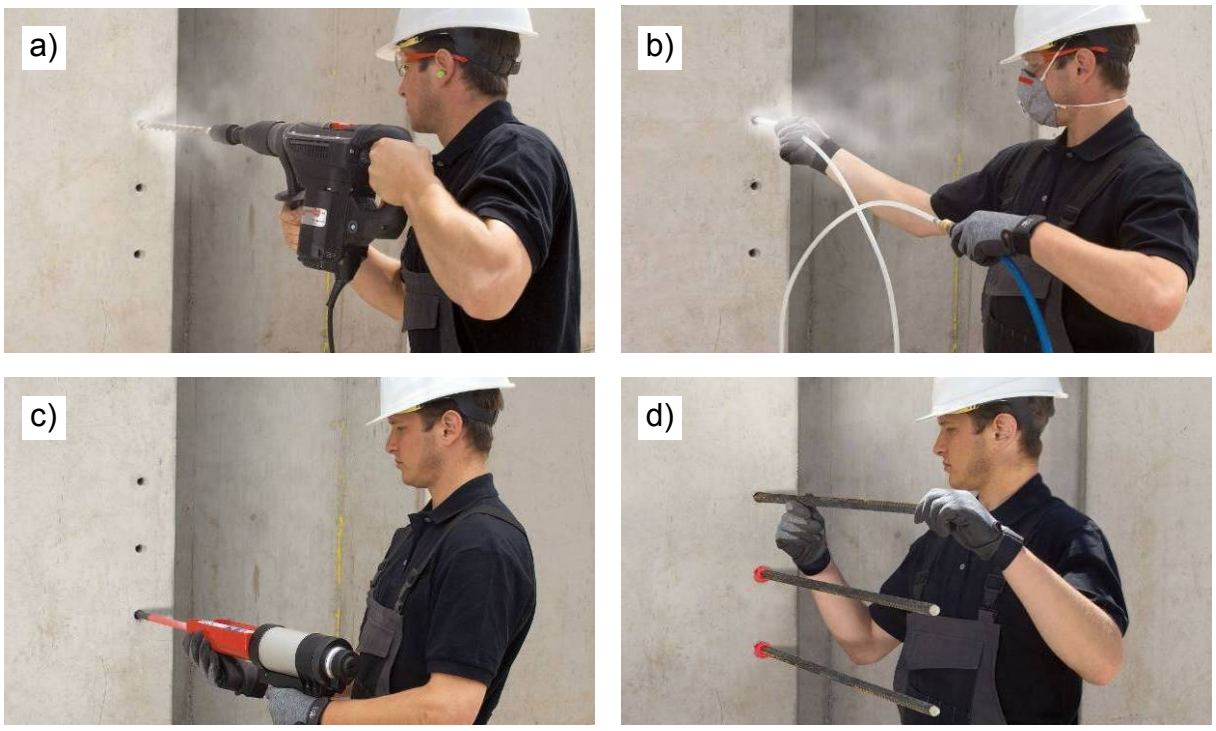


Figure 1.7 Installation sequence of post-installed reinforcing bars: a) Drilling; b) Cleaning; c) Injecting; d) Installing (Source: Würth)

The anchorage of some seismic retrofitting schemes using post-installed reinforcing bars, e.g. shear and wing walls (Figure 1.8a), is characterised by a high redundancy. Furthermore, the post-installed reinforcing bars are mostly loaded in shear and are located outside of the maximum stressed regions of the retrofitting element. On the contrary, the anchorage of post-installed column starter bars (Figure 1.8b) are highly stressed and predominantly loaded in tension.

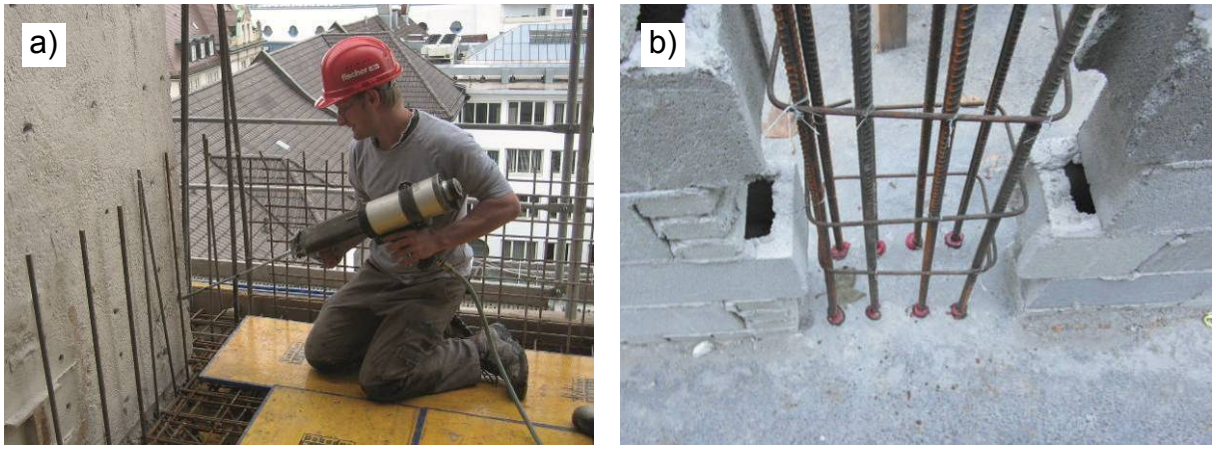


Figure 1.8 Application of post-installed reinforcing bars for: a) Shear walls (Source: Fischer); b) Columns (Courtesy: P. Mahrenholtz, University of Stuttgart)

Typically, columns are part of MRF structures which is the most popular reinforced concrete building type. The preferred strong column-weak beam failure mechanism of MRF structures relies on the development of plastic hinges at the column-to-foundation connections (Figure 1.9a). Typical seismic design deficiencies of MRF structures are poorly detailed gravity columns (Figure 1.9b) or an insufficient number of columns (Figure 1.9c), putting the structure at risk to fail in the soft story mechanism. Additional ground floor columns are deemed to be a first ranked seismic retrofit solution because of following advantages:

- Columns are more space saving and less obstructive than walls.
- The construction of columns is less expensive and time consuming if compared to other retrofitting schemes.
- Columns increase the strength without jeopardising the ductility (*Sugano, S. (1992)*).
- Seismic resistance of the ground floor is most critical provided that the building is regular from story to story (*Tsai, K.-C.; Hwang, S.-J. (2008)*).
- Columns allow the development of plastic hinges irrespective to the direction of seismic loading.

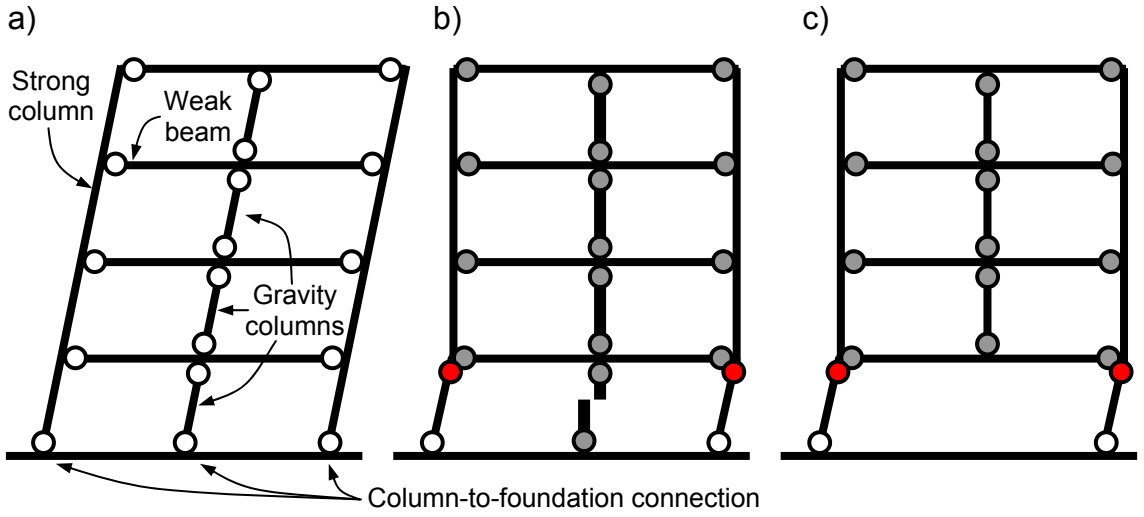


Figure 1.9 Example MRF structure with gravity columns in the centre line: a) Preferred plastic mechanism with location of plastic hinges. Structures with b) poorly detailed gravity columns or c) insufficient number of columns potentially collapse due to soft story mechanism

To date, the performance of post-installed reinforcing bars was studied by comparing their behaviour with the behaviour of cast-in-place reinforcing bars if subjected to monotonic loads (*Spieth, H.; Eligehausen, R. (2002)*) and cyclic loads (*Simons, I.; Eligehausen, R. (2008)*). It was shown that the performance is equivalent if qualified mortars are used. In conclusion, reliable post-installed reinforcing bar connections are possible, provided the starter bars are detailed in such a way that the full development length according to the reinforced concrete design codes is available.

However, foundations typically do not provide sufficient depth to accommodate the development length needed if the starter bars are designed without hooks. Because of their advantages, additional ground floor columns are installed despite the limited member depth available for anchoring. In practice, the starter bar detailing with reduced development lengths and without hooks is justified by engineering judgment on a questionable case by case basis (Figure 1.8b). This approach is risky in particular with respect to the seismic performance of post-installed starter bar anchorages when the demand is pushing the connection to its limit and robust behaviour is needed most. In particular failure of columns has catastrophic consequences unless the structure is capable to develop catenary actions for load redistribution (*Sasani, M.; Bazan, M. et al. (2007)*, *Yi, W.-J.; He, Q.-F. et al. (2008)*, *Su, Y.-P.; Tian, Y. et al. (2009)*).

Insufficient, unsuitable or defective anchorage to the existing concrete structure results in premature failure of the retrofitting element before the targeted deformation

or load capacity is reached. Erroneously chosen anchorage systems not fit for purpose remain unnoticed until a major earthquake occurs and the anchorage may turn out to be the weak link (e.g. *Henry, R.; Ingham, J. (2011)*, *Zareian, F.; Sampere, C. et al. (2012)*). Recognising this, the development of a sound design concept for retrofitting columns with post-installed anchorages is urgent. Figure 1.10 shows two examples of failed anchorages during the 2011 Christchurch Earthquake.

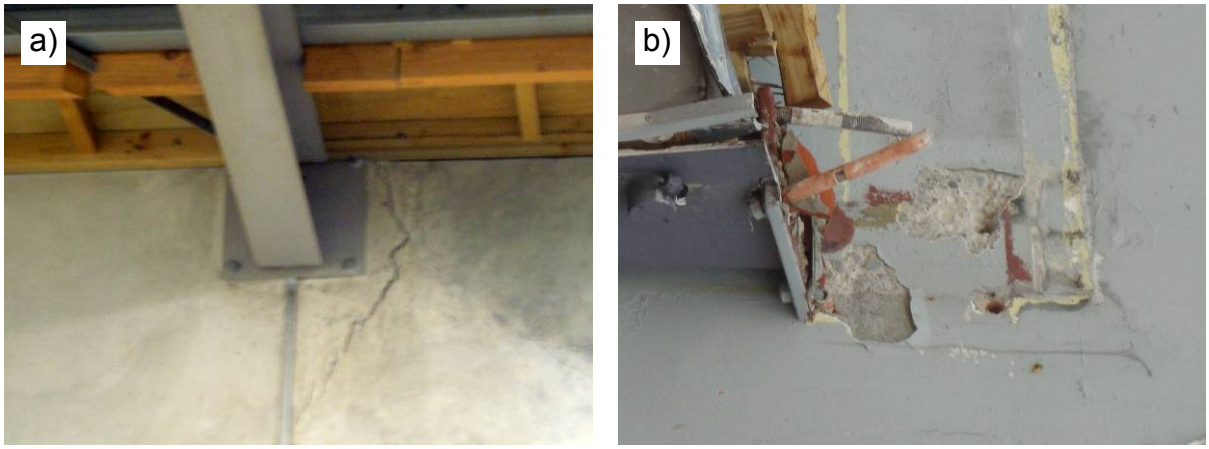


Figure 1.10 Failure of post-installed anchorages during 2011 Christchurch Earthquake: a) Concrete breakout failure (Courtesy: H. Derakhshan, P. Abercromby, R. Henry, University of Auckland); b) Pullout failure (Courtesy: J. Silva, Hilti North America)

## 1.3 Objective of the Research

The preceding sections highlighted the need for innovative design solutions which facilitate retrofitting of seismically vulnerable buildings. Applications with post-installed reinforcing bars are very promising; however, their suitability has not yet been proven for substandard anchorage lengths which are reduced with reference to the development length according to the reinforced concrete design standards.

The main objective of this thesis is to overcome the knowledge deficits in seismic behaviour of cast-in-place and post-installed reinforcing bars, and to provide the basics necessary to design column-to-foundation connections by means of post-installed reinforcing bars. To achieve this goal, a comprehensive research program was conducted. The development of the seismic bond model for concrete reinforcement and its application to column-to-foundation connections is presented in the following chapters:

- After the introduction, the state of the art is reported in Chapter 2. The review focuses on literature which is most relevant in the context of this thesis and

covers the field of bond between concrete and reinforcement, as well as reinforcing bar anchorages of structural connections.

- To provide the background of the pursued research approach, Chapter 3 presents the results of exploratory studies and identifies the research needed for the investigations discussed in the following four chapters.
- Improved testing methods and equipment allowed detailed experimental studies on bond of concrete reinforcement presented in Chapter 4. The test results were used to validate a bond model for cast-in-place and post-installed reinforcing bars under simultaneous load and crack cycling.
- Numerical studies on the bond behaviour between reinforcement and concrete, shown in Chapter 5, were conducted using a finite element program in which the bond model was implemented. After verifying the model by comparing the numerical with the experimental test data, the range of test parameters was extended.
- Large scale tests were carried out to investigate the performance of column-to-foundation connections subjected to seismic excitation. In Chapter 6, the results of the experimental studies on column-to-foundation connections which anchorage were cast-in-place or post-installed, are discussed and evaluated.
- The numerical studies on column-to-foundation connections are presented in Chapter 7. After benchmarking the numerical tests by means of the experimental tests, the finite element analyses allowed the investigation of column-to-foundation connections without scatter of the results and for an extended parametric range.
- The enhanced bonded anchor model for column-to-foundation connections presented in Chapter 8 is required for the statistical evaluation of the factors proposed to take into account the adverse effect of seismic loading and beneficial effect of moment loading on the connection capacity.
- The mechanical model is also needed for the design concept for post-installed column-to-foundation connections developed in Chapter 9. The concept is introduced and statistically evaluated on the basis of the performed investigations.
- In Chapter 10, the key findings and conclusions are summarised and open questions outlined.

# 2 State of the Art

The aim of this section is to provide an overview of the state of the art and to identify deficits in knowledge. After some general remarks given in Section 2.1, the literature in the field of steel-concrete-bond (Section 2.2) and structural reinforcement anchorages is reviewed (Section 2.3). Finally, further reading is recommended in Section 2.4 and the key points are summarised in Section 2.5.

## 2.1 General

Some technical terms used in the field of reinforced concrete have synonyms. In addition, the terms used in the context of the conventional anchorage design (Section 2.3.1.1) may differ from the terms used for bonded anchor design (Section 2.3.1.2) though essentially meaning the same. Table 2.1 clarifies which terms are preferred in this thesis.

Table 2.1 Preferred terms and synonymous terms

| Preferred term | Synonymous terms |
|---|---|
| anchor | fastener, fastening, and anchoring |
| mortar | adhesive material |
| anchorage | end anchorage of a reinforcing bar, bonded anchor |
| anchorage length $\ell_b$ | development length, embedment depth |
| anchorage diameter $\phi$ | reinforcing bar diameter, bonded anchor diameter |
| bond stress $\tau$ | bond between concrete and reinforcing bar or bonded anchor |
| slip s | (relative) displacement between reinforcing bar and concrete |
| rib | deformation, lug |

Further, it is noted that constant or varying crack widths of bond tests are measured additive to the initial hairline crack after completion of the test setup but before loading the reinforcing bar. In general, the units used in this thesis follow the SI convention. For the sake of clarity, the base unit 'MPa' is used for material strengths and the equivalent unit 'N/mm²' for stresses. The term 'experimental tests' desribes experimental studies carried out in the laboratory and the term 'numerical tests' computer-assisted numerical studies.

Because the US American reinforced concrete design code *ACI 318 (2011)* is the predominant standard applied in regions along the ring of fire, it is referred to in this thesis beside the European reinforced concrete design code *Eurocode 2 (2005)* and

*Eurocode 8 (2006)*. Reference is also made to the reinforced concrete design code *NZS 3101 (2006)* since this code is known to be at the forefront of seismic engineering codes and the large scale tests were conducted in New Zealand.

## 2.2 Bond between Reinforcing Bars and Concrete

In the following, aspects of the bond between reinforcement and concrete are discussed which are relevant in the context of this thesis. The review includes cast-in-place and post-installed reinforcing bars. Only ribbed bars are considered because virtually all reinforcing bars used nowadays are ribbed (Figure 2.1).

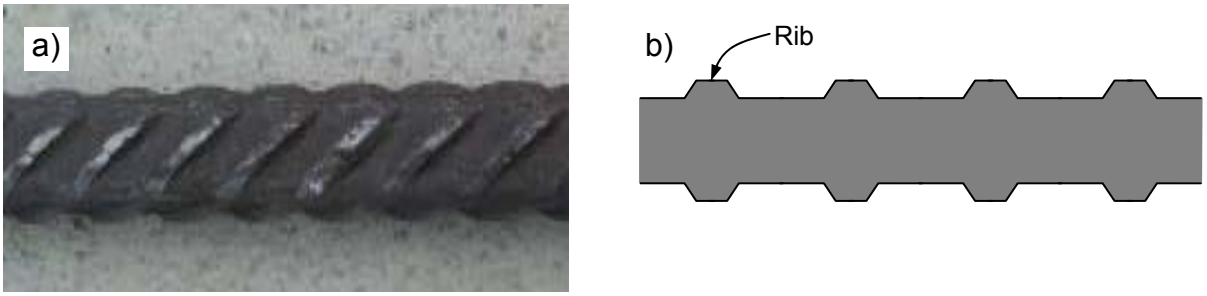


Figure 2.1 Ribbed reinforcing bar: a) Photo; b) Schematic

### 2.2.1 Definition of tensile stress and bond stress

A basic assumption for the reinforced concrete design is that the reinforcing bar is loaded in longitudinal direction only (Section 2.3.1.3). The resulting tensile stress $\sigma$ and bond stress $\tau$ for a reinforcing bar increment are shown in Figure 2.2.

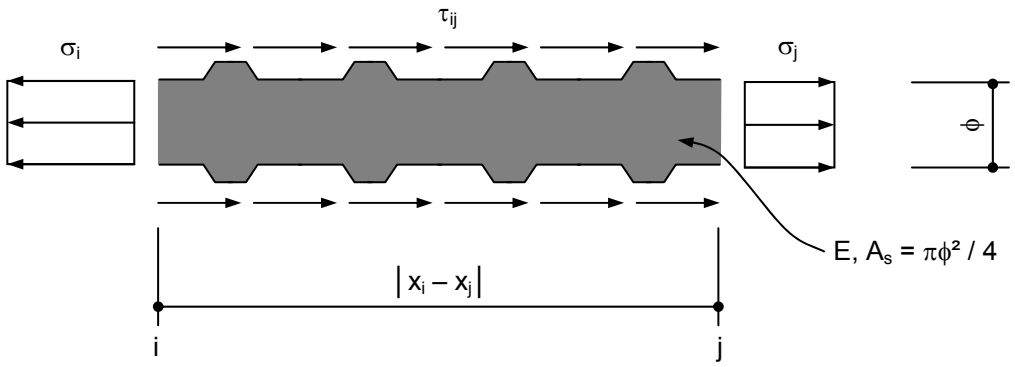


Figure 2.2 Tensile stress and bond stress at two locations i and j of a reinforcing bar increment with two loaded ends

The length of the reinforcing bar increment is defined by the two locations i and j. The elastic modulus E and the strain $\varepsilon$ are used to calculate the tensile stresses at the locations i and j:

$$\sigma_i = E \cdot \varepsilon_i \text{ and } \sigma_j = E \cdot \varepsilon_j \qquad \text{Equation 2.1}$$

The averaged bond stress between the locations i and j is calculated according to:

$$\tau_{ij} = \frac{EA(\varepsilon_i - \varepsilon_j)}{\pi\phi|x_i - x_j|} = \frac{E\phi(\varepsilon_i - \varepsilon_j)}{4|x_i - x_j|} = \frac{\phi(\sigma_i - \sigma_j)}{4|x_i - x_j|} \qquad \text{Equation 2.2}$$

Pullout tests on reinforcing bar increments cast-in-place or post-installed in concrete are termed bond tests (Section 2.2.2). The boundary conditions are defined by the stressed loaded end and the unstressed unloaded end (Figure 2.3a).

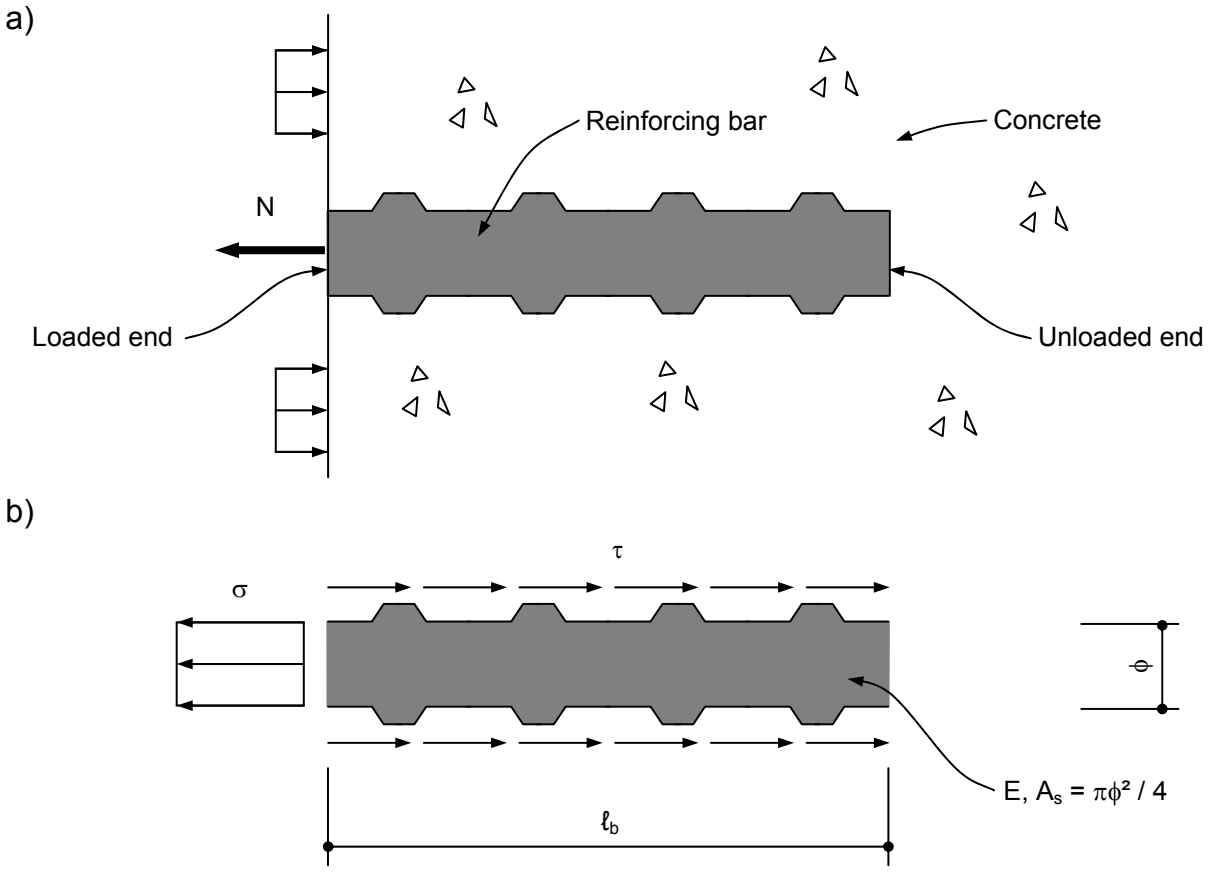


Figure 2.3 a) Schematic of pullout test; b) Tensile stress and bond stress of a reinforcing bar element with one loaded and one unloaded end

The boundary conditions allow calculating the tensile stress and average bond stress as follows (Figure 2.3b):

$$\sigma = \frac{4N}{\pi\phi^2} \qquad \text{Equation 2.3}$$

$$\tau = \frac{N}{\pi \phi \ell_b}$$ Equation 2.4

Averaging is only meaningful if an approximately constant bond stress distribution can be assumed (solid lines in Figure 2.4). Because of the elasticity of the reinforcing bar and the non-linearity of the bond, the shapes of the actual tensile stress and bond stress distribution increasingly deviate from the linear idealisation for larger anchorage lengths (dashed lines in Figure 2.4).

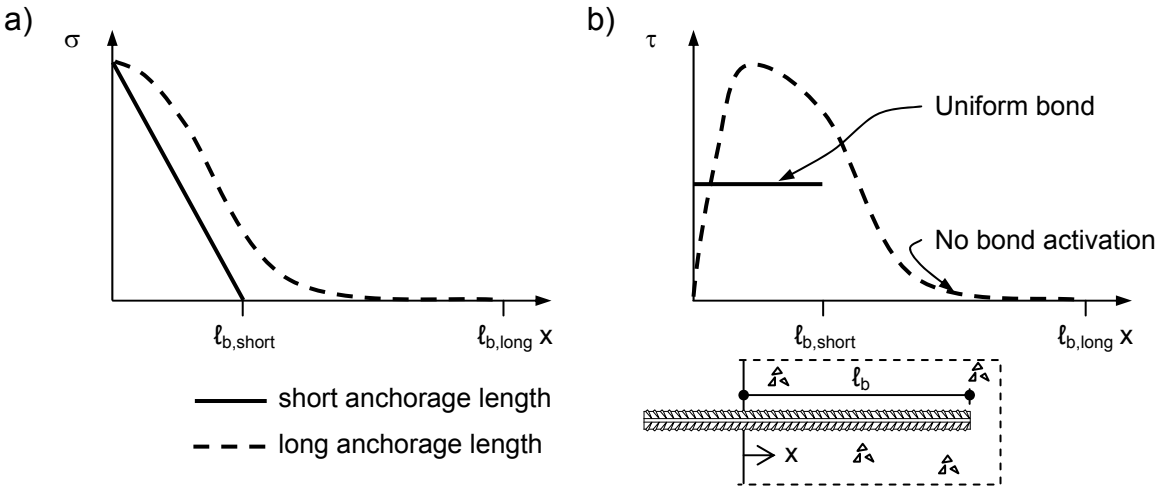


Figure 2.4 Schematic of a) tensile stress and b) bond stress distribution

For practical applications, e.g. to determine the pullout capacity of bonded anchors, a uniform approximation, also known as the uniform bond model (*Kunz, J.; Cook, R. et al. (1998)*), provides reasonable results for bonded lengths up to 25$\phi$ (*Cook, R.; Kunz, J. et al. (1998)*).

For bond tests on reinforcing bars, shorter bonded lengths than 25$\phi$ are used to allow an accurate determination of the bond strength. Typically, bond tests are conducted on reinforcing bars cast-in-place or post-installed with a bonded length of 5$\phi$. Smaller bonded lengths potentially lead to larger scatter and less significant results.

For the sake of completeness it is noted that analytical models describing the distribution of the bond stress along the anchorage length can be found in e.g. *Alsiwat, J.; Saatcioglu, M. (1992)*, *Russo, G.; Pauletta, M. (2006)*, *Rodriguez, M.; Muttoni, A. et al. (2007), Haskett, M.; Oehlers, D. et al. (2008),* and *Mazzarolo, E.; Scotta, R. et al. (2012)*.

### 2.2.2 Influence of setup and bond test types

The bond is significantly influenced by the surrounding state of stress which depends on the test method comprising test specimen, test setup, and test procedure.

*Noakowski, P.; Janovic, K. (1978)* carried out a literature research on bond. It was concluded that no bond test method can be considered to be universally valid for all practical applications. This is in line with the general conclusion of material sciences that every determined material property depends on the specific test method. For this reason it is important that the setup is defined precisely to allow comparability and reproducibility. The normalisation of the tested bond strength with reference to the actual concrete strength is discussed in *Harajli, M.; Mabsout, M. (2002)*.

Two standardised test setups specified in *RILEM/CEB/FIP (1982)* are used to determine the bond behaviour of concrete reinforcement: The beam test RC5 and the pullout test RC6. The slip at the unloaded end, not affected by the load driven elastic elongation of the bar, is measured as an estimate for the slip between reinforcing bar and concrete. Each beam test comprises two bond tests with a bonded length of 10$\phi$ (Figure 2.5a). A bonded length of 5$\phi$ is defined for the pullout test and a free pre-length, also termed debonded length, of 5$\phi$ is required to reduce the influence of the confining stresses (Figure 2.5b). For the sake of completeness it is noted that another standardised bond test for reinforcing bars is the beam-end test according to *ASTM A944 (2010)*.

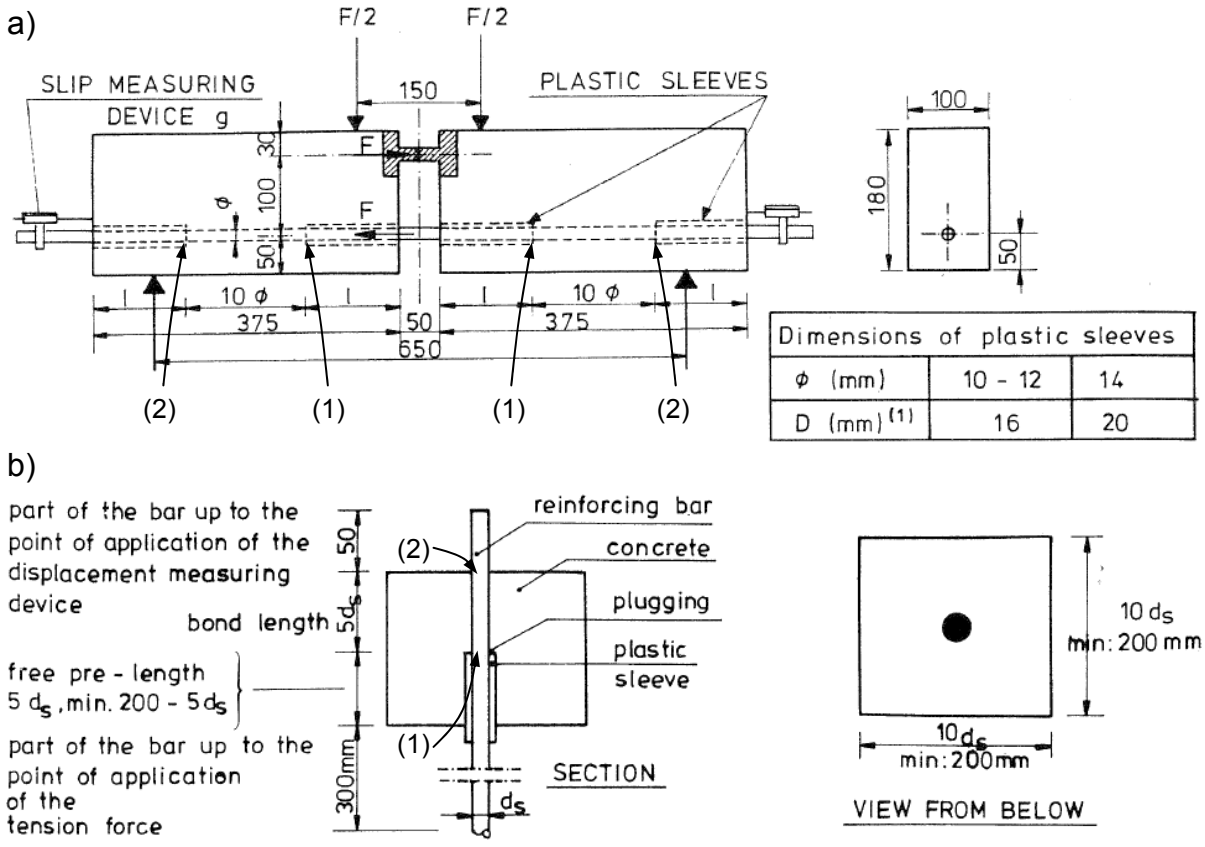


Figure 2.5 Defined test setup according to *RILEM/CEB/FIP (1982)*: a) Beam test RC5; b) Pullout test RC6; (1) loaded end and (2) unloaded end

For the qualification of bonded anchors, two standardised test setups, namely unconfined setup and confined setup, are used to assess the capacity by means of pullout tests (*ETAG 001 (2006)*, Part 5 or *ACI 355.4 (2010)*). The unconfined test setup requires a distance between anchor and testing rig of at least 2 times the embedment depth, allowing a conical concrete breakout to develop (Figure 2.6a). Two facts call for a different solution when carrying out tests to determine the bond strength. First, long anchorage lengths require very large concrete test specimens and, second, in particular anchors and reinforcing bars installed with high strength mortars experience either concrete breakout failure or steel failure. To determine the bond strength, the confined setup was developed which defines a reaction load bearing plate with a hole of 1.5 to 2 times the anchor diameter, allowing only steel or pullout failure by suppressing the concrete breakout failure (Figure 2.6b). Typically, short embedment depths of five times the diameter are used. Post-installed reinforcing bars are generally tested by a confined test setup (*EOTA TR 029 (2010)*). The influence of the confined test setup becomes negligible if a debonded length of $5\phi$ is provided (*Appl, J. (2009)*).

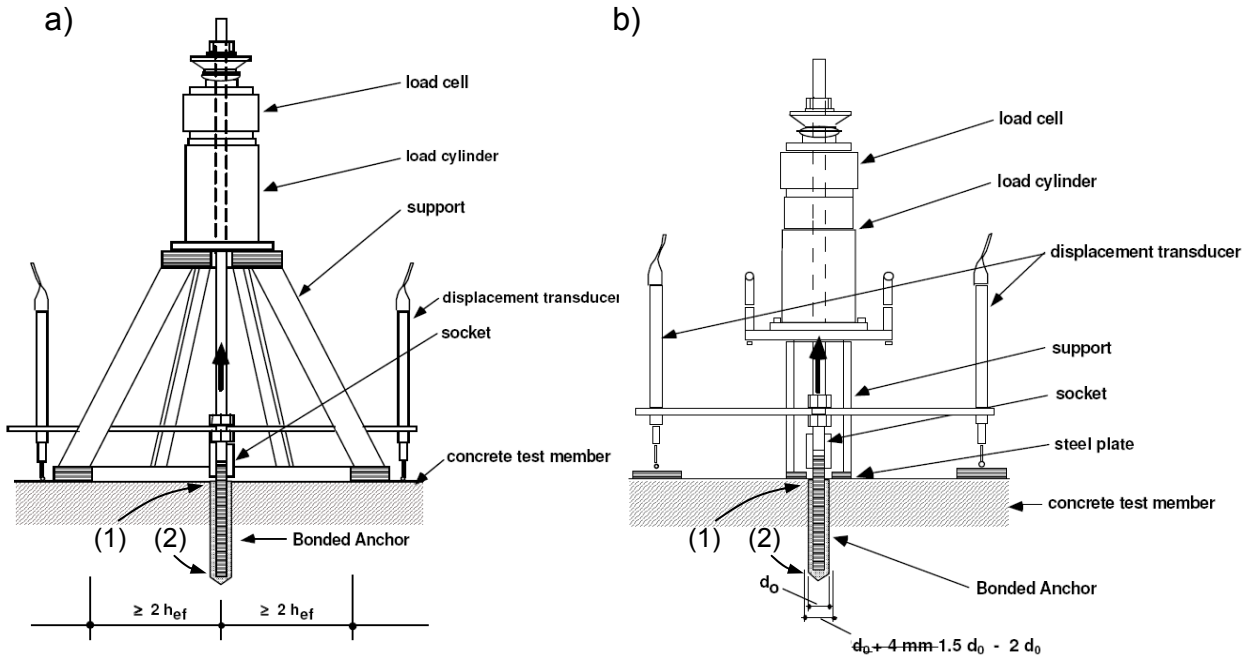


Figure 2.6 Defined test setups according to *ETAG 001 (2006)*, Part 5: a) Unconfined; b) Confined; (1) loaded end and (2) unloaded end

### 2.2.3 Influence of human factor

Good design and workmanship are the cornerstones for sustainable buildings and civil engineering structures. This is in particular true for reinforced concrete structures which require substantial structural detailing. In addition, construction is carried out in situ under sometimes adverse conditions and often tight schedules.

The post-installation of reinforcing bars require special attention, because carelessness and ignorance of the correct installation procedure may reduce the capacity of the anchorage. For example, omitting the cleaning easily reduces the bond strength by 50 % (e.g. *Wollmershauser, R.; Lee, M. (2008)*).

To reduce the human factor to a minimum, a strict adherence to the manufacturer's printed installation instructions (MPII) is required. The MPII stipulates installation details such as cleaning method, maximum setting and minimum curing times, as well as maximum setting and minimum curing temperatures. Trained installers further improve the installation quality (e.g. *Fuchs, W. (2007)*).

### 2.2.4 Constitutive law of bond

Figure 2.7 shows typical bond stress-slip curves of monotonic bond tests on reinforcing bars cast-in-place with a short bonded length. The bond stress-slip relationship is also termed as the constitutional law of bond.

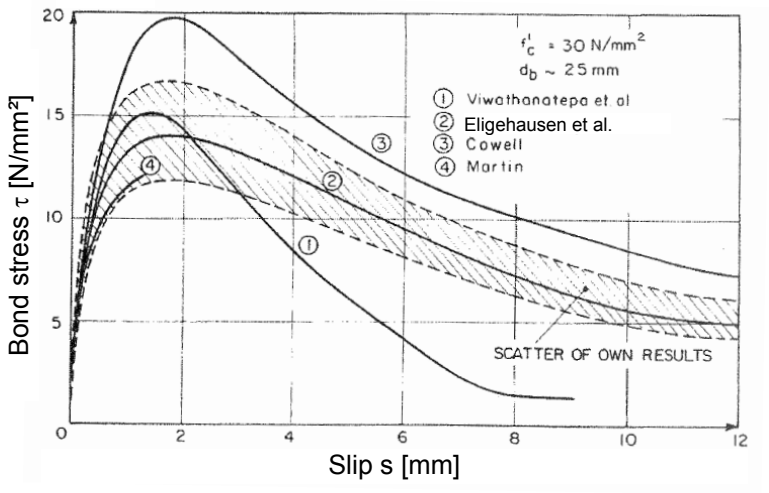


Figure 2.7 Examples of bond stress-slip curves (*Eligehausen, R.; Popov, E. et al. (1983)*)

The bond stress-slip behaviour of ribbed bars is characterised by a high initial stiffness which becomes softer with increasing load. The maximum bond stress is the bond strength. In the context of anchorage technology, the bond strength is commonly termed ‘ultimate bond stress’ and for this reason the variable $\tau_u$ is used. Consequently, the corresponding slip $s(\tau_u)$ is denominated as $s_u$. The slope of the initial part of the bond stress-slip curve and the peak bond stress mainly depends on the related rib area $f_R$ (Section 2.2.5) and the concrete strength (Section 2.2.6).

Figure 2.8a shows the tension and compression trajectories at the concrete shear key where the bond stress of the pulled reinforcing bar is transferred by means of

compressive stresses. The compressive stresses generate circumferential tensile stresses (Figure 2.8b). The circumferential tensile stresses may crack small concrete covers completely which appears as splitting crack parallel to the embedded reinforcing bar. The tensile stresses also generate local bond cracks which may break through to the concrete surface where these appear as primary transverse cracks (Figure 2.8c). Finally, shear cracks develop when the concrete key between the reinforcing bar ribs is sheared off (Figure 2.8a).

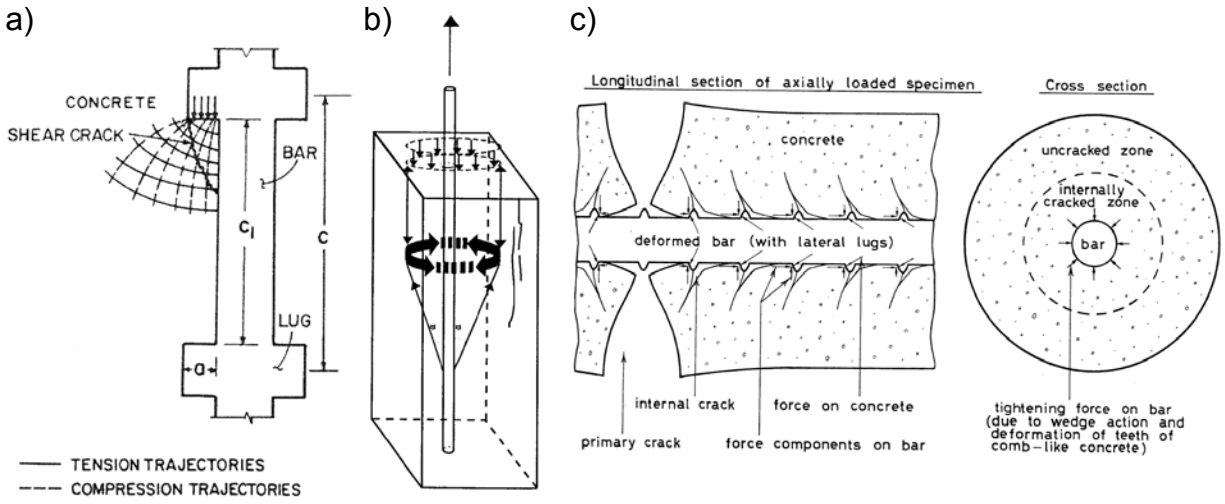


Figure 2.8 Stress trajectories and cracks developing during tension loaded concrete reinforcement (a) *Eligehausen, R.; Popov, E. et al. (1983)* after *Rehm, G. (1958)*; b) *Tepfers, R. (1973)*; c) *Goto, Y. (1971)*)

The successive phases of the bond mechanism during monotonic loading are shown in Figure 2.9 and described in the following:

- Adhesion is generally negligible when ribbed bars are used. Initially, the bond is mainly transferred by mechanical interlock. At low loading stages, the angle of the compressive stresses in relation to the longitudinal bar axis is relatively small, approximately 30 ° (Point A). Bond cracks develop due to the resulting circumferential tensile stresses. The length and width of the cracks depends on the confinement which is either generated by secondary reinforcement or sufficient concrete cover preventing splitting failure. Increasing the tensile stress in the bar further increases the slip because more local crushing takes place.
- Following, shear cracks in the concrete keys between the ribs are initiated (Point B). When the ultimate bond stress is reached, the concrete key between the ribs shear off partly or completely (Point C). The length of the shear crack is given in *Rehm, G. (1958)* as 6 times the rib height and in *Tepfers, R. (1973)* as 2 to 3 times the rib height. At this loading stage, the bond forces will spread into

the concrete under an increased angle of about 45 ° because of the wedging action of sheared off concrete.

- After passing the peak bond resistance $\tau_u$, an increasing part of the concrete is sheared off and less force is needed to shear off the remaining bits of the concrete keys and to smooth out the surface of the shear plane (Point D). The mechanical bond has almost vanished when the slip equals approximately the distance of the ribs (Figure 2.9c, Point E). Only the frictional bond resistance $\tau_{uf}$ at the cylindrical surface remains.

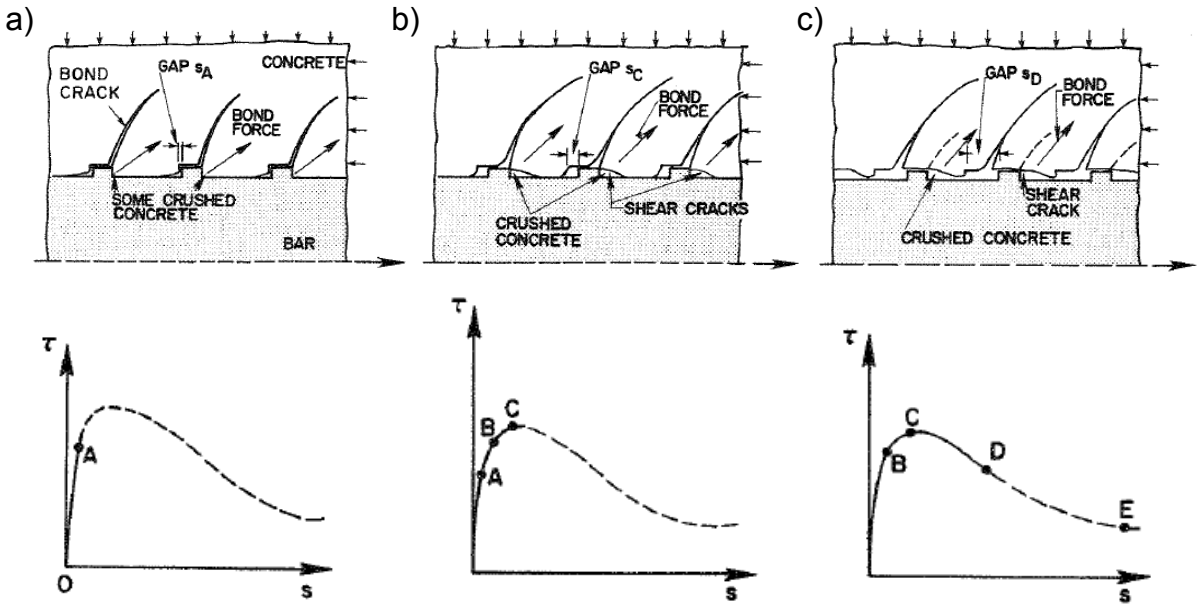


Figure 2.9 Mechanism of bond during monotonic loading (*Eligehausen, R.; Popov, E. et al. (1983)*): a) pre-peak; b) at peak; c) post-peak

Different models describing the monotonic bond stress-slip behaviour analytically were developed in the past. Most models (e.g. *Eligehausen, R.; Popov, E. et al. (1983)*, *Lowes, L.; Moehle, J. et al. (2004)*) simplify the bond stress-slip curve as follows (Figure 2.10a):

- The total bond strength is given by the superposition of mechanical bond $\tau_m$ and frictional bond $\tau_f$ which both increase until the ultimate bond stress $\tau_1 = \tau_u$ is reached at the slip $s_1$.
- The flattening bond stress-slip curve around the ultimate load is described by a horizontal plateau between the slip value $s_1$ and $s_2$.
- While the ultimate frictional bond stress $\tau_3 = \tau_{uf}$ sustains during further slip, the mechanical bond starts to decrease and is zero at a slip equivalent to the centre-to-centre distance of lateral ribs $s_3 = c$.

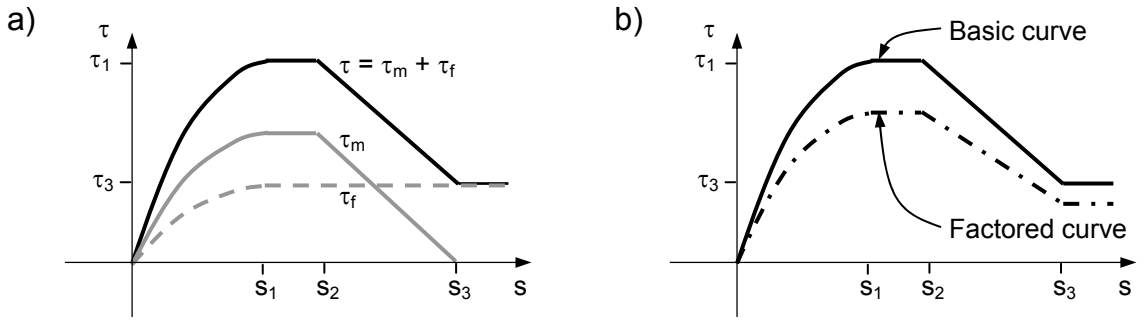


Figure 2.10 a) Schematic bond stress-slip model for monotonic loading; b) Schematic of basic and factored curve

The bond model is used to describe the constitutive law of any concrete reinforcement. The bond model is defined by the values $\tau_1$, $\tau_3$, $s_1$, $s_2$, and $s_3$ which are characteristic for the specific reinforcing bar and concrete properties. Therefore, the reinforcing bar and concrete properties have a constant effect on the bond behaviour which can be understood as a basic bond stress-slip curve. Moreover, the shape of the bond stress-slip curve is also influenced by several variable effects. The variable effects are often taken into account by factorising the basic bond stress-slip curve (Figure 2.10b). The systematic presentation of the constant and variable effects can be found in *Lettow, S. (2007)*. The constant and variable effects which are relevant in the context of this thesis are summarised in Table 2.2 and introduced in the following sections.

Table 2.2 Compilation of important constant and variable effects on the bond behaviour (after *Lettow, S. (2007)*)

| Constant effects | Variable effects |
|---|---|
| | Loading rate |
| | Sustained load |
| | Temperature |
| Reinforcing bar properties | Transverse concrete compression |
| Concrete properties | Parallel concrete cracks |
| | Inelastic steel strain |
| | Damage due to load cycling |
| | Damage due to crack cycling |

### 2.2.5 Effect of reinforcing bar properties

The most important property of the reinforcing bar in respect to the bond is the related rib area. The related rib area $f_R$ is the ratio of the axial cross section area of the rib and the shear surface of the bar. Details of the related rib area definition and

the minimum related rib area stipulated in the reinforced concrete codes are given in Appendix A: Conventional Anchorage Design.

Figure 2.11 shows the influence of the related rib area on bond strength and slip of cast-in-place reinforcing bars as tested by *Martin, H.; Noakowski, P. (1981)*. To the knowledge of the author, the influence of the related rib area on bond strength and slip of post-installed reinforcing bars has not been studied to date. It is reasonable to assume that the influence is significant only if failure occurs in the shear plane between reinforcing bar and mortar and will be secondary in comparison to other influencing factors.

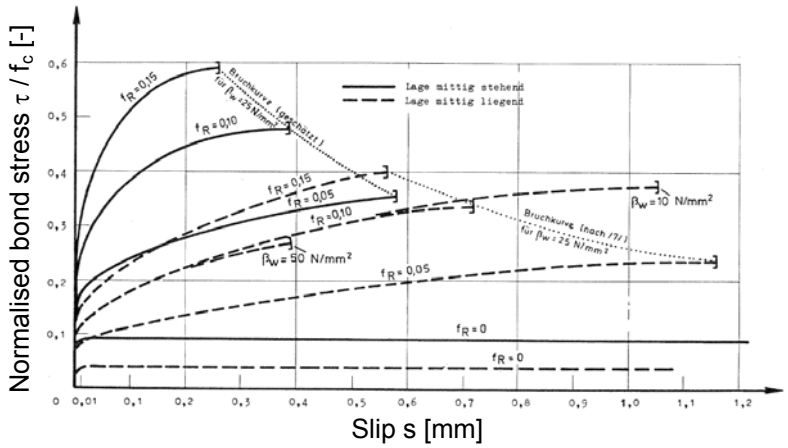


Figure 2.11 Influence of related rib area on bond strength and slip (*Martin, H.; Noakowski, P. (1981)*)

Because small related rib areas need less material and are therefore more economic, reinforcing bars commonly have a related rib area $f_R$ close to the minimum value stipulated in the standards. Consequently, the employment of any common reinforcing bar can be assumed to be representative and the related rib area is deemed not to be a relevant parameter to be tested in the context of this thesis.

The influence of the reinforcing bar diameter on the bond strength of cast-in-place and post-installed was controversially discussed in the past decades (e.g. *Eligehausen, R.; Popov, E. et al. (1983)*, *Hawkins, N.; Lin, I. et al. (1986)*). Partly, different conclusions were drawn. In summary, the influence of the reinforcing bar diameter on the bond strength is probably secondary which is in line with the European reinforced concrete design code *Eurocode 2 (2005)* where the bond strength is not a function of the reinforcing bar diameter smaller than or equal to 32 mm. The influence of the bar diameter on the mean bond strength of post-installed bars is small (*Spieth, H. (2003)*) or even insignificant as tests on reinforcing bars post-installed with epoxy mortar showed (*Mahrenholtz, C. (2009a)*). However, the bond strength given in some European technical approvals for post-installed reinforcing bars according to *EOTA TR 023 (2006)* provide bond

strengths depending on the reinforcing bar diameter, though the difference of the bond strength is only in the range of 10 percent for different concrete strengths. The approval scheme of post-installed reinforcing bars is briefly introduced in Section 2.3.1.1.

Aspects of steel stresses in terms of inelastic reinforcing bar strains are discussed in Section 2.2.12. Reference is also made to *Rehm, G. (1958)*, *Martin, H. (1973)*, *Viwathanatepa, S.; Popov, E. et al. (1979)*, *Royles, R.; Morley, P. et al. (1982)*, *Hawkins, N.; Lin, I. et al. (1986)*, *Rostasy, F.; Scheuermann, J. (1987)*, *Souroushian, P.; Choi, K.-B. (1989)* where the influence of further reinforcing bar properties on the bond is discussed.

### 2.2.6 Effect of concrete properties

The most important property of the concrete in respect to bond is the concrete strength. The influence of the concrete strength on the bond strength of cast-in-place bars was extensively studied in the past considering uncracked and cracked conditions with partly inconsistent results. An overview can be found in *Mainz, J. (1993)*. The international Model Code (*CEB-FIP Model Code 1990 (1993)*) considers the influence of the concrete strength on the bond strength proportionally to the power of ½. On the contrary, the present European reinforced concrete design code *Eurocode 2 (2005)* specified the power of ⅔. The same approach is used when determining the bond strength for post-installed reinforcing bars according to the *EOTA TR 023 (2006)* (Section 2.3.1.1).

*Menzel, C. (1939)* showed that the position of the reinforcing bar during concrete casting has a strong influence on the bond strength as illustrated in Figure 2.12. The main reason for the influence of the reinforcing bar position is that pores agglomerate below the reinforcing bars or the soffits of the ribs. Reinforcing bars cast in horizontally may show good or poor bond conditions depending on the location at the top or bottom of the concrete member. Generally good bond conditions are ascribed to vertical reinforcing bars, e.g. column starter bars anchored in the foundation. The concrete strength has only insignificant influence on the bond strength of post-installed anchors (*Cook, R.; Konz, R. (2001)*) and it is reasonable to assume the same for post-installed reinforcing bars.

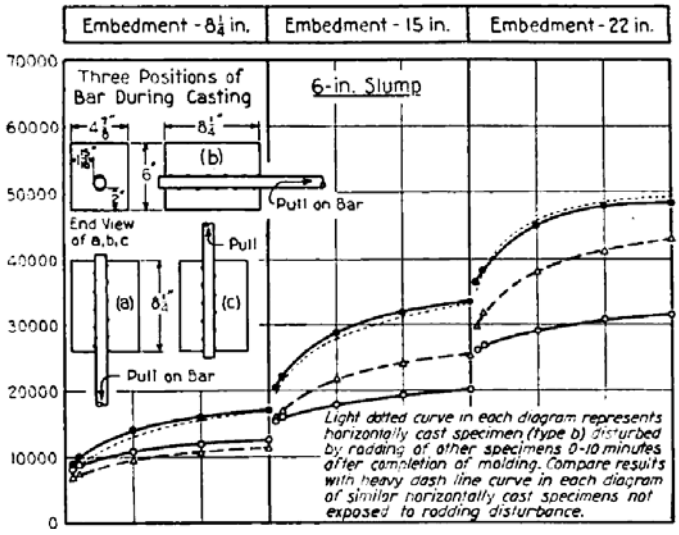


Figure 2.12 Influence of position of the reinforcing bar during casting concrete (*Menzel, C. (1939)*)

Aspects of concrete compression and cracks are discussed in Section 2.2.10 and Section 2.2.11. Reference is also made to *Rehm, G. (1958)*, *Martin, H. (1973)*, *Martin, H.; Noakowski, P. (1981)*, *Jirsa, J.; Breen, J. et al. (1982)*, *Russwurm, D.; Martin, H. (1993)*, and *Souroushian, P.; Choi, K.-B. et al. (1991)* where the influence of further concrete properties on the bond is discussed in more detail.

### 2.2.7 Effect of loading rate

For quasi-brittle materials like concrete, short term loading influences the material properties in a positive way (e.g. *Zielinski, A. (1982)*, *Curbach, M. (1987)*, *Eibl, J.; Curbach, M. (1989)*, *Bischoff, P.; Perry, S. (1991)*, *Malvar, L.; Ross, C. (1998)*, and *Sharma, A.; Ožbolt, J. et al. (2010)*). In *Eligehausen, R.; Popov, E. et al. (1983)* the influence of loading rate on the bond strength of cast-in-place reinforcing bars was investigated. A maximum loading rate of 170 mm/min (= 10,000 mm/sec) was chosen to simulate seismic conditions. For an assumed maximum displacement of about 2 mm, the peak load is reached after approximately 0.7 sec. The ultimate load was increased by about 15 % in comparison to tests at quasi-static loading rates. *Weathersby, J. (2003)* reported pullout capacities for impact-loaded specimens, failing after 0.005 sec, which were 1.75 times the capacities determined by quasi-static tests. *Hjorth, C. (1979)*, described a smaller influence of 30 % at the same loading rate. *Vos, E.; Reinhardt, H.-W. (1982)* employed Hopkinson bar tests on pullout specimens to achieve loading rates of 160 N/mm²/msec, resulting in a failure within about 0.0002 sec (Figure 2.13). In comparison to quasi-static loading rates, the bond strength increased by about 70 % for grade 20 concrete. However, the increase

became less significant for grade 50 concrete. Shock loading tests conducted on bonded anchors attaining the peak load within 0.25 sec and 0.1 sec (*Cook, R.; Collins, D. et al. (1992)* and *Hoehler, M. (2006)*, respectively) showed that the stiffness is not reduced and the bond strength increases by roughly 25 % compared to quasi-static loading conditions. It is reasonable to assume that also shock loaded post-installed reinforcing bars experience a similar beneficial effect.

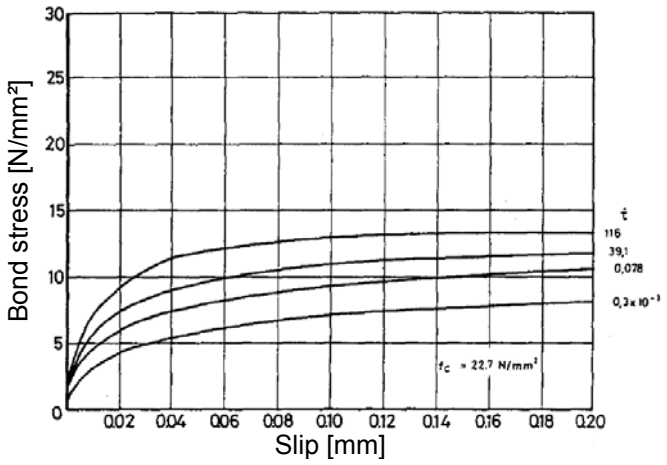


Figure 2.13 Influence of the loading rate on bond stress-slip curves (*Vos, E.; Reinhardt, H.-W. (1982)*)

It would stand to reason that high frequencies also beneficially influence the bond behaviour of reinforcing bars during crack cycling (Section 2.2.14). However, crack cycling tests on undercut anchors under various frequencies showed that the influence of high crack cycling frequencies on the load-slip behaviour is insignificant and overcasted by other scattering factors (*Mahrenholtz, C.; Eligehausen, R. et al. (2010)*, *Mahrenholtz, P.; Mahrenholtz, C. et al. (2012)*). It is assumed that this finding is also valid for crack cycling tests on reinforcing bars since mechanical interlock is also the main load transfer mechanism of ribbed reinforcing bars (Section 2.2.4). In summary, conducting crack cycling tests on reinforcing bars at quasi-static frequencies is deemed to be a conservative simplification of testing.

Technically relevant earthquake induced oscillations range between a frequency of 1 Hz and 10 Hz (e.g. *Eibl, J.; Keintzel, E. (1989)*, *Hoehler, M. (2006)*). *Chung, L.; Shah, S. P. (1989)*) showed that the anchorage capacity of beam-column joints increase for high frequency load cycling (1 Hz) by 20 to 25 % in comparison to low frequency load cycling (0.0025 Hz). *Dhakal, R.; Pan, T.-C. (2003)* carried out cyclic beam-column joint tests at various cycling rates and made suggestions for test setup and test procedure. However, general conclusions of the influence of the load cycling frequency are not reported. Based on a comprehensive literature review of the effects of the loading rate on reinforced concrete, *Fu, H.; Erki, M. et al. (1991)*

concluded that the significant increase of strength due to dynamic loading may shift the failure mode from a preferred ductile manner to a less desirable brittle mode. On the contrary, *Kulkarni, S.; Shah, S. (1998)* report the opposite on the basis of experiments and computations. *Gutierrez, E.; Magonette, G. et al. (1993)* tested column-to-foundation connections and concluded that material property scatter are of the same order of magnitude as the loading rate effects. In summary, also testing of column-to-foundation connections at quasi-static loading rates is an acceptable simplification.

### 2.2.8 Effect of sustained load

Concrete creeps under sustained loads which also influences the bond between reinforcement and concrete. Figure 2.18 shows the effect of sustained loads on the bond stress-slip curve. According to *Sippel, T. (1996)*, creeping reduces the consoles between the reinforcing bar ribs and therefore reduces the bond strength of cast-in-place reinforcing bars. Most mortars used to post-install reinforcing bars are made of resins which develop a pronounced creep behaviour. Based on the investigations of *Rehm, G.; Franke, L. (1978)*, *Jagfeld, P. (1980)*, *Rehm, G.; Franke, L. et al. (1980)*, and *Rehm, G.; Franke, L. (1982)*, it can be concluded that the long-term bond strength of epoxy mortars are roughly 60 % of the short-term bond strength (*Eligehausen, R.; Mallée, R. et al. (2006)*).

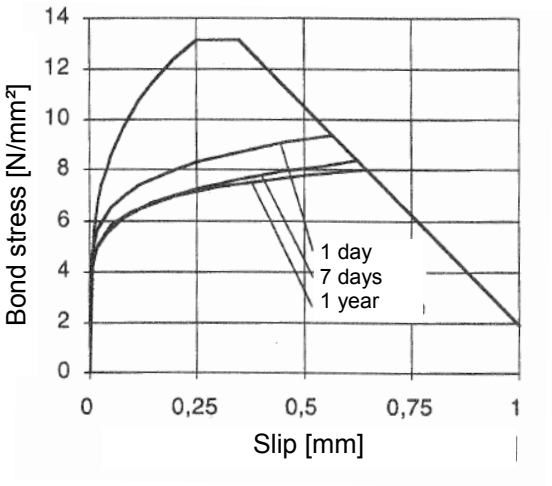


Figure 2.14 Effect of sustained loads on bond stress-slip curve (*Sippel, T. (1996)*)

However, columns are mainly vertically loaded which predominantly affects the concrete. The reinforcement is loaded in tension only if the column is horizontally loaded. Since horizontal loads are caused by wind and seismic actions, the tensioning of the starter bars is only temporary. In conclusion, the effect of sustained

loads on the bond strength of cast-in-place and post-installed column-to-foundation connections is deemed to be irrelevant.

### 2.2.9 Effect of temperature

Cast-in-place bars are not sensitive to temperature provided that the concrete is cast within the temperature range of about +5 °C to +50 °C. For the sake of completeness, reference is made to *Rostasy, F.; Scheuermann, J. (1987)* and *Royles, R.; Morley, P. et al. (1982)* who studied the bond behaviour of cast-in-place bars at extreme low temperatures and high temperatures, respectively. On the contrary, the bond behaviour of post-installed reinforcing bars is very sensitive to the installation and curing temperature (*Cook, R.; Konz, R. (2001)*). Typical mortars are based on resins which are irreversibly formed by the chemical reaction with the hardener. The two components are mixed to a ratio where the thermoset can perfectly cure in theory. In this case, the conversion reaches 100 % which means that all potential cross-links are formed. The degree of cross-linking is a function of time and temperature (*Dallner, C. (2008)*, *Hülder, G. (2008)*). At lower temperatures and curing times which have to be anticipated for resin based mortars used at construction sites, the conversion remains comparatively low. As a consequence, resin based mortars may develop increased creep rates and reduce in ultimate strength (Figure 2.15). Research presented in *Mahrenholtz, C.; Eligehausen, R.; Hofmann, J. et al. (2012)* showed that the bond strength of post-installed bonded anchors is reduced most if the post-installation was carried out at low temperatures and the loading at high temperatures. It is reasonable to assume that the temperature effect is identical for post-installed reinforcing bars.

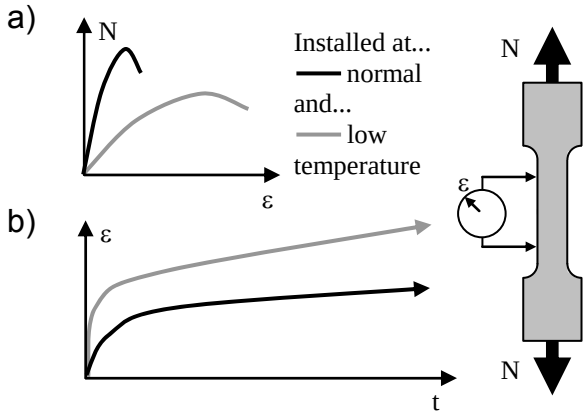


Figure 2.15 Influence of the conversion on the mechanical properties of resin based mortars: a) Short-term; b) Long-term (*Mahrenholtz, C.; Eligehausen, R.; Hofmann, J. et al. (2012)*)

For this reason, starter bars of column-to-foundation connections should not be post-installed at low temperatures and sufficient curing time is essential.

### 2.2.10 Effect of transverse concrete compression

Concrete compressive stresses generate a confinement of the reinforcing bar. Therefor it is irrelevant whether the concrete was previously cracked. The transverse concrete compression increases the bond strength of concrete reinforcement. This effect was investigated extensively, e.g. by *Dörr, K. (1980)*, *Gambarova, P.; Rosati, G. et al. (1989)*, *Malvar, L. (1992)*, and *Engström, B.; Magnusson, J. et al. (1998)*. The experimental test results were used by *Lowes, L.; Moehle, J. et al. (2004)* to propose an equation describing the confining effect as a function of the concrete transverse stress $\sigma_c$ and the concrete strength $f_c$ (Figure 2.16a):

$$\Omega_c = 1.75 - 0.35\exp\left(-40\left|\frac{\sigma_c}{f_c}\right|\right) - 0.4\exp\left(-\left|\frac{\sigma_c}{f_c}\right|\right) = \frac{\tau_{com}}{\tau_{ucr}} \qquad \text{Equation 2.5}$$

To estimate an increased bond stress-slip curve accounting for the effect of transverse concrete compression, the monotonic bond stress-slip curve is multiplied by the factor $\Omega_c$ (Figure 2.16b). For example, a compression of 15 percent of the concrete compressive stress yields a bond strength which is increased by about 150 percent if compared to the bond strength relaxed concrete.

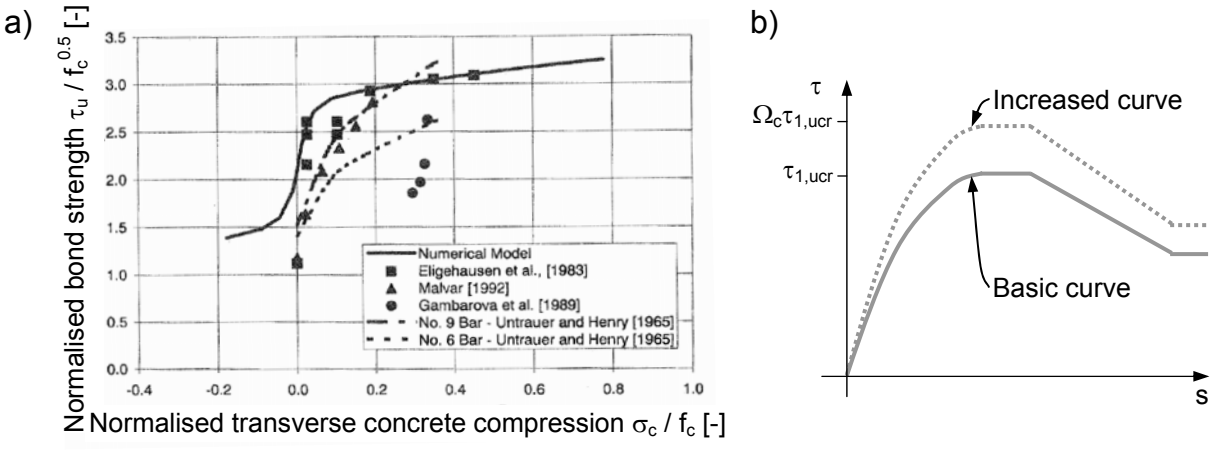


Figure 2.16 a) Literature research of *Lowes, L.; Moehle, J. et al. (2004)* on the bond strength increasing effect of transverse concrete compression; b) Model for the bond stress-slip relation to account for the same

To the knowledge of the author, no studies were conducted to date to determine the effect of transverse concrete compression on post-installed reinforcing bars. Because of their identical working principle, however, the assumption that the effect of transverse concrete compression is equal for post-installed and cast-in-place reinforcing bars is justified.

### 2.2.11 Effect of parallel concrete cracks

Concrete tensile stresses irreversibly crack the concrete when surpassing the concrete tensile strength. Parallel concrete cracks reduce the bond strength of concrete reinforcement. Also this effect was investigated extensively, e.g. by *Gambarova, P.; Rosati, G. (1996)*, *Idda, K. (1999)* and *Kreuser, R.; Purainer, R. (2003)*. Equations were developed to consider the influence of the crack width related to the rib height. However, the proposed equations are complex and the allowable parametric range is limited. Therefore, the experimental test results presented in *Gambarova, P.; Rosati, G. (1996)*, *Eibl, J.; Idda, K. et al. (1997)*, *Idda, K. (1999)*, *Simons, I. (2007)*, and *Lindorf, A.; Lemnitzer, L. et al. (2009)* were evaluated in *Mahrenholtz, C. (2011a)* to develop a simple equation as a function of the crack width and the reinforcing bar diameter for crack widths w smaller than the rib height a and with the assumption that a ≈ $\phi$ / 10 (Figure 2.17a):

$$\Omega_w = 1 - (10w / \phi) = \frac{\tau_{cr}}{\tau_{ucr}} \qquad \text{Equation 2.6}$$

The factor $\Omega_w$ may be used to multiply the monotonic bond stress-slip curve to specify reduced bond stress-slip curves to account for the effect of concrete cracks parallel to the embedded reinforcing bar (Figure 2.17a). For example, a reinforcing bar $\phi$ = 16 mm loaded in a crack w = 0.3 mm develops a bond strength of about 80 percent of the bond strength in uncracked concrete.

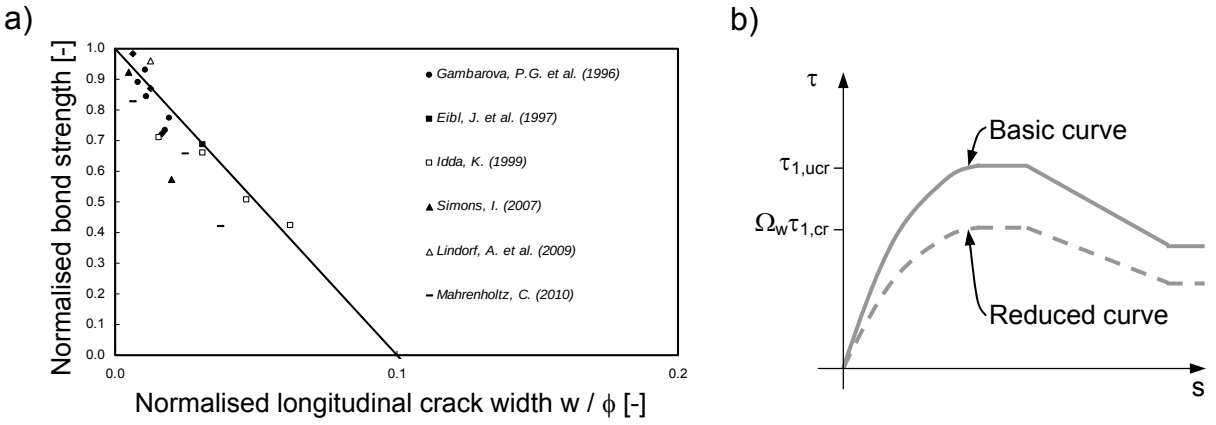


Figure 2.17 a) Literature research of *Mahrenholtz, C. (2011a)* on the bond strength reducing effect of parallel concrete cracks; b) Model for the bond stress-slip relation to account for the same

The effect of parallel concrete cracks on post-installed reinforcing bars was studied by *Simons, I. (2007)*. The effect of parallel concrete cracks on bonded anchors was investigated by *Mészároš, J. (2002)*. The findings made therein for bonded anchors are also valid for post-installed reinforcing bars because of the identical working

principle. Generally, a large scatter in the bond strength reduction due to cracks was observed which was attributed to the fact that the bond strength is sensitive to the unique geometry of the installation hole. In addition, the applied sequence to drill the installation hole after cracking the concrete inevitable led to very different trajectories of the crack. However, a simplified and conservative assumption after *Eligehausen, R.; Mallée, R. et al. (2006)* is that post-installed reinforcing bars loose half of the bonded surface due to cracks which theoretically surround the mortar semi-circularly. Consequently, post-installed reinforcing bars experience theoretically bond strength reductions of 50 percent.

### 2.2.12 Effect of inelastic steel strain

Pulled reinforcing bars are axially extended and transversely contracted resulting in a reduction of the bond strength. Vice versa, pushed reinforcing bars are axially contracted and transversely extended resulting in an increase of the bond strength. The influence of contracted or extended reinforcing bar diameters on the bond strength is deemed to be negligible as long the reinforcing bar remains in the elastic range. On the contrary, positive inelastic steel strains reduce the bond strength significantly because the steel necking virtually disconnects the reinforcing bar from the concrete. Also the excessive slip associated with the inelastic steel strains damages the bond irreversibly. Figure 2.18a depicts the effect of inelastic steel strain on strain and bond stress as tested by *Shima, H.; Chou, L.-L. et al. (1987)*.

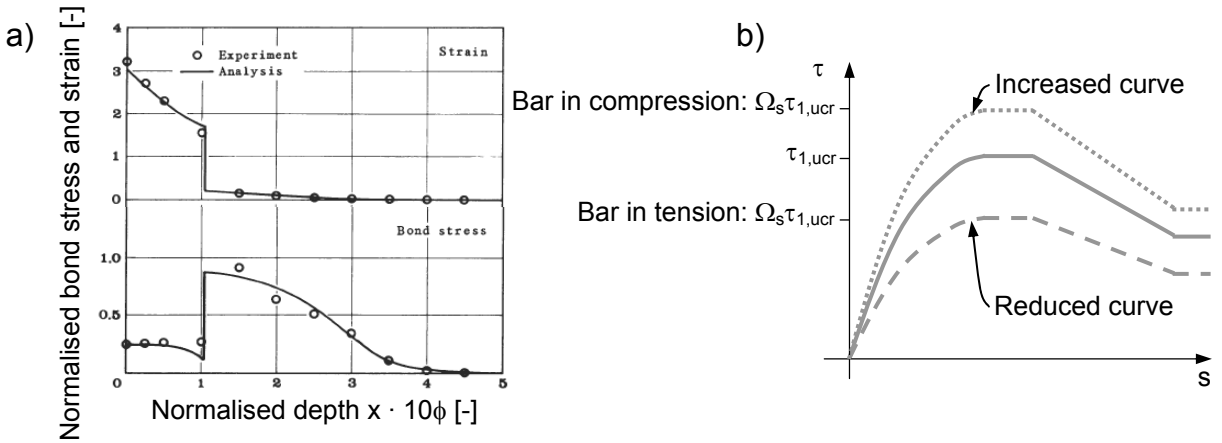


Figure 2.18 Bond strength reducing effect of inelastic steel strains (*Shima, H.; Chou, L.-L. et al. (1987)*); b) Model for the bond stress-slip relation to account for the same

*Lowes, L.; Moehle, J. et al. (2004)* used the test data of *Shima, H.; Chou, L.-L. et al. (1987)* and *Viwathanatepa, S.; Popov, E. et al. (1979)* and developed the following equation to consider the effect of inelastic steel strains:

$$\Omega_s = \left\{ \begin{array}{l} 1.0 + 1.4\left(1 - \exp\left(0.4\left(1 + \dfrac{\varepsilon}{\varepsilon_y}\right)\right)\right) \\ 0.1 + 0.9\left(\exp\left(0.4\left(1 - \dfrac{\varepsilon}{\varepsilon_y}\right)\right)\right) \end{array} \right\} \text{ for } \left\{ \begin{array}{l} \varepsilon < -\varepsilon_y \\ \varepsilon > \varepsilon_y \end{array} \right\} \qquad \text{Equation 2.7}$$

Multiplying the monotonic bond stress-slip curve by the factor $\Omega_s$ results in an increased bond stress-slip curve if the reinforcing bar is compressed and in a reduced bond stress-slip curve if the reinforcing bar is tensioned beyond the yield strength (Figure 2.18b). The effect of inelastic steel strains is further discussed in *Kobarg, J. (1986)*, *Engström, B. (1992)*, and *Rodriguez, M.; Muttoni, A. et al. (2007)*).

The effect of inelastic steel strains on post-installed reinforcing bars was not studied to date. It is reasonable to assume that post-installed reinforcing bars behave similar to cast-in-place reinforcing bar with respect to the effect of inelastic steel strains.

### 2.2.13 Damage effect of load cycling

Cast-in-place and post-installed reinforcing bars under load cycling experience accumulating bond damage. The testing scheme typically used to evaluate the damage effect of load cycling is briefly explained in the following. The damage effect is evaluated by means of test specimens for which the reinforcing bar is installed in the concrete member with a bonded length $\ell_b$. The slip s is measured at the unloaded end of the reinforcing bar (Figure 2.19a). Typically, the reinforcing bar is subjected to slip reversals between $s_{max}$ and $s_{min}$. The resulting bond damage is expressed by a decreasing bond stress response (Figure 2.19b). Figure 2.19c shows typical bond stress-slip curves of cyclic bond tests on cast-in-place reinforcing bars.

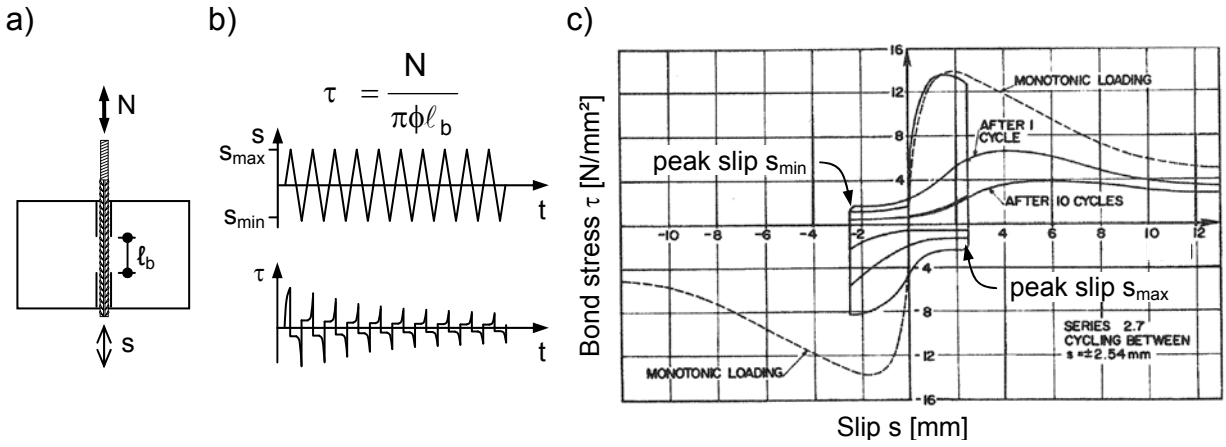


Figure 2.19 a) Load cycling test in uncracked concrete; b) Cyclic slip between peak slip $s_{max}$ / $s_{min}$ and resulting bond stress $\tau$, versus time t; c) Example for bond stress-slip curves affected by load cycling (*Eligehausen, R.; Popov, E. et al. (1983)*)

In the following, the successive phases of the bond mechanism during cyclic loading are shown in Figure 2.20 and described according to *Eligehausen, R.; Popov, E. et al. (1983)*:

- The initial positive bond stress-slip curve up to the first reversal at the peak slip $s_{max}$ is identical to the monotonic bond stress-slip curve (Point A) which bond mechanism is discussed in Section 2.2.4.
- The slip after unloading (Point F) equals to the gap between the reinforcing bar rib and concrete which remains after the recovery of the elastic concrete deformation. During slipping in the reversed direction, little frictional bond stress is built up. When the reinforcing bar rib is in contact with the concrete (Point H), the initial negative bond stress-slip curve shows a sharp rise in stiffness. The bond stress is increasing as the slipping continues to the peak slip $s_{min}$ (Point I).
- The following slip reversal is similar to the previously described slip reversal. However, the bond stress is increasing again when crushed concrete pieces are pressed against the previous bearing face (Point L) and reaches its maximum at peak slip (Point M).

The bond damage experienced due to the cycling depends on the peak slip values. For slip reversals before the development of shear cracks, $s_{max} < 0.5s_u$, the initial bond stress-slip curves in the positive domain as well as in the negative domain follows the monotonic bond stress-slip curve (Figure 2.20a). For larger peak slip values, e.g. $s_{max} = s_u$, the bond damage becomes effective for the initial negative slip because the resistance of the concrete key is reduced due to the radiating cracks of the adjacent concrete key which developed during the initial positive slip (Figure 2.20b). This effect becomes more prominent for peak slips beyond the slip $s_u$ corresponding to the ultimate bond strength $\tau_u$ during the monotonic loading, for example $s_{max} = 2.0s_u$ (Figure 2.20c).

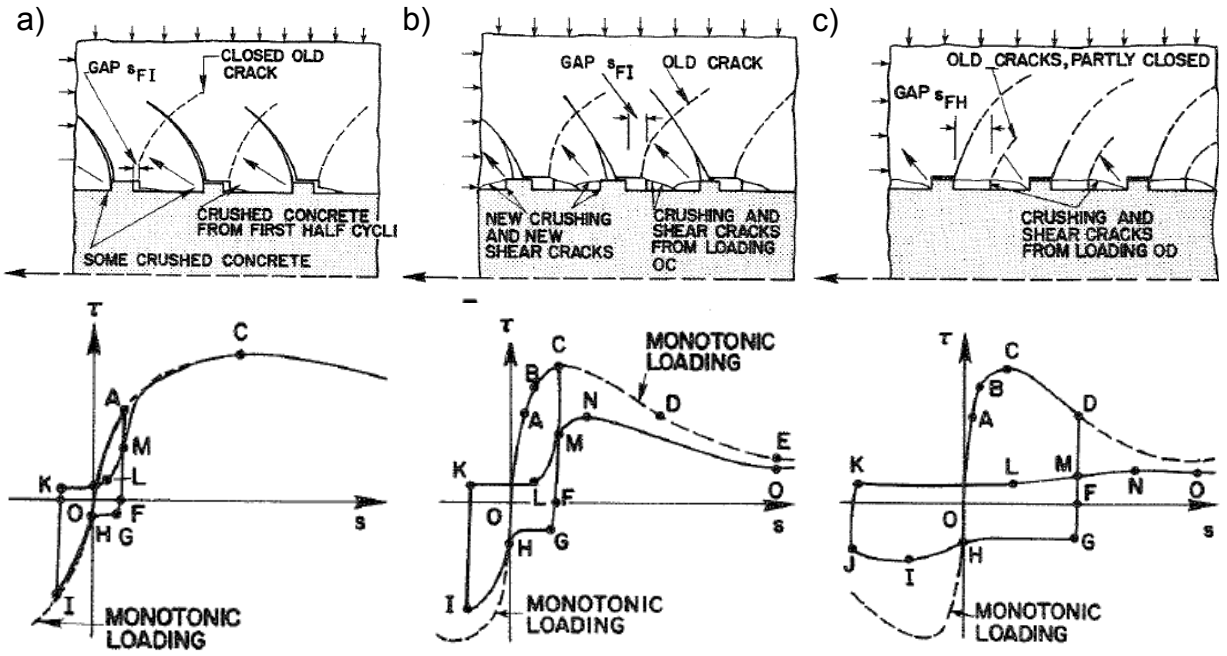


Figure 2.20 Mechanism of bond during cyclic loading (*Eligehausen, R.; Popov, E. et al. (1983)*): a) pre-peak; b) at peak; c) post-peak

Models to describe the influence of cyclic loading on the bond of reinforcing bars situated in uncracked concrete were developed by e.g. *Morita, S.; Kaku, T. (1973)*, *Viwathanatepa, S.; Popov, E. et al. (1979)*, *Hawkins, N.; Lin, I.-J. et al. (1982)*, *Eligehausen, R.; Popov, E. et al. (1983)*, and *Hawkins, N.; Lin, I. et al. (1986)*. A comparison of some of the models is presented in *Verderame, G.; De Carlo, G. et al. (2009)*. The hysteretic energy model proposed in *Eligehausen, R.; Popov, E. et al. (1983)* was extensively applied by researchers in the past (e.g. *Monti, G.; Spacone, E. et al. (1993)*, *Lowes, L.; Moehle, J. et al. (2004)*, *Lettow, S. (2007)*) and proved to be suitable to study reinforced concrete elements under cyclic loading. The hysteretic energy model is also used in the context of this thesis and is introduced briefly in the following.

The hysteretic energy model is based on the assumption that half of the dissipated energy E is converted into bond damage while the other half is transformed into heat. The bond damage is expressed by the reduction of the monotonic bond stress-slip curve. Figure 2.21a illustrates schematically the conceptual approach. The ultimate bond strength at the $n^{th}$ slip reversal is denominated $\tau_{1(n)}$. The damage parameter d is introduced to describe the accumulated bond damage as a function of the dissipated energy E. The definition of the damage parameter d is rewritten in the following to determine the damage factor:

$$\Omega_{cyc} = \exp\left(-a_1 (E/E_0)^{a_2}\right) = \frac{\tau_{1(n)}}{\tau_1} = 1 - d \qquad \text{Equation 2.8}$$

The energy consumed under monotonic loading $E_0$ is used to normalise the exponent. For the tuning parameters $a_1$ and $a_2$ *Eligehausen, R.; Popov, E. et al. (1983)* suggested $a_1 = 1.2$ and $a_2 = 1.1$. Figure 2.21b depicts schematically the progression of damage parameter d and factor $\Omega_{cyc}$ as a function of the relative consumed energy $E / E_0$. The multiplication of the monotonic bond stress-slip curve by $\Omega_{cyc}$ results in the reduced bond stress-slip curve which bond strength increasingly attains smaller values as the bond damage accumulates.

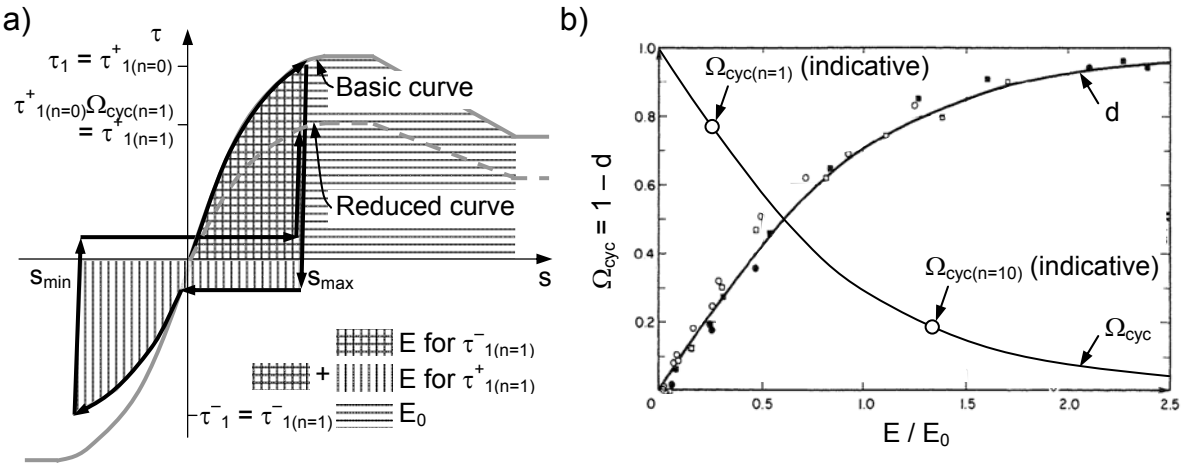


Figure 2.21 Hysteretic energy model to describe the reduction of the total bond strength due to cyclic loading (after *Eligehausen, R.; Popov, E. et al. (1983)*: a) Schematic; b) Factor $\Omega_{cyc}$ and damage parameter d

The frictional component of the dissipated energy $E_f$ is used to define the bond stress-slip relation between the peak slip reversals. Figure 2.22a illustrates schematically the conceptual approach. The ultimate frictional bond strength at the $n^{th}$ slip reversal is denominated $\tau_{f(n)}$. The deterioration of frictional bond is estimated by an additional damage parameter which is a function of the dissipated energy $E_f$:

$$\Omega_{cycf} = \exp\left(-a_{1f}\left(E_f / E_{0f}\right)^{a_{2f}}\right) = \frac{\tau_{f(n)}}{\tau_f} = 1 - d_f \qquad \text{Equation 2.9}$$

The energy $E_{0f}$ used to normalise the exponent is equal to $\tau_3 \cdot s_3$. The bond stress $\tau_3$ and slip $s_3$ are defined according to Figure 2.10. For the tuning parameters $a_{1f}$ and $a_{2f}$ *Eligehausen, R.; Popov, E. et al. (1983)* proposed $a_{1f} = 1.2$ and $a_{2f} = 0.67$. Figure 2.22b depicts schematically the progression of damage parameter $d_f$ and factor $\Omega_{cycf}$ as a function of the relative consumed energy $E_f / E_{0f}$. The multiplication of the frictional component of the monotonic bond stress-slip curve by $\Omega_{cycf}$ allows describing the bond stress-slip curve between the slip reversals. Also the frictional component of the bond strength attains increasingly smaller values as the bond damage accumulates.

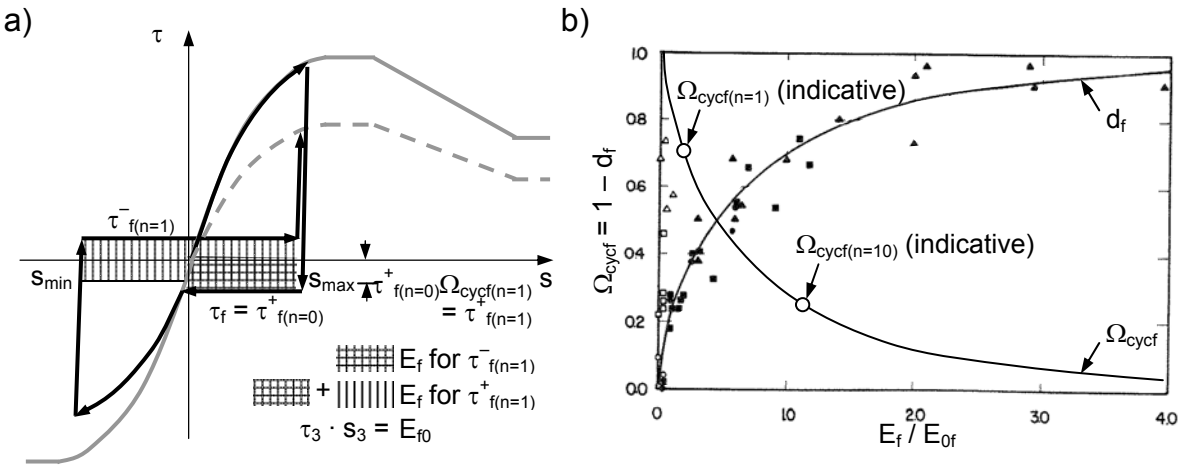


Figure 2.22 Hysteretic energy model to describe the reduction of the frictional bond strength between the slip reversals due to cyclic loading (after *Eligehausen, R.; Popov, E. et al. (1983)*: a) Schematic; b) Factor $\Omega_{cycf}$ and damage parameter $d_f$

The damage functions describe the deterioration of the bond strength with reference to a given monotonic bond stress-slip curve irrespective of the number of cycles and peak slip values. Therefore, the hysteretic energy model predicts the damage of bond under any cyclic loading. The model is valid for standard bar diameters and concrete strengths as well as for various slip histories of up to 30 load cycles. For this reason the model is suitable to describe the response to seismic events which is characterised by a limited number of pronounced cycles (*Rodriguez, M.; Zhang, Y.-G. et al. (1995)*, *Dutta, A.; Mander, J. (2001)*, *Malhotra, P. (2002)*, *Hoehler, M. (2006)*). The model is not valid for high cycle fatigue which has been subject of other investigations (e.g. *Rehm, G.; Eligehausen, R. (1979)*, *Pochanart, S.; Harmon, T. (1989)*, *Lindorf, A.; Lemnitzer, L. et al. (2009)*). The hysteretic energy model is explained in detail in *Eligehausen, R.; Popov, E. et al. (1983)* and *Mahrenholtz, C. (2011b)*.

*Simons, I. (2007)* validated the hysteretic energy model for post-installed reinforcing bars under load cycling for uncracked and cracked concrete. It is noted that *Simons, I. (2007)* proposed other tuning parameters $a_1$ and $a_2$ which possibly can be explained by the different geometry and material properties of the test specimens used. For example, the related rib area of the reinforcing bars tested in *Eligehausen, R.; Popov, E. et al. (1983)* was about $f_R = 0.10$ whereas the related rib area of the reinforcing bars used in *Simons, I. (2007)* was $f_R = 0.08$. The related rib area is considered as the governing parameter with respect to bond strength (Section 2.2.5). Notably, *Simons, I. (2007)* suggested identical tuning parameters for reinforcing bars cast-in-place and post-installed using epoxy mortar. Another fundamental observation described in *Simons, I. (2007)* for load cycling tests was that post-installed reinforcing bars experience less bond damage than cast-in-place

reinforcing bars if the monotonic bond tests on the post-installed reinforcing bars showed higher bond strengths than the monotonic bond tests on the cast-in-place reinforcing bars.

### 2.2.14 Damage effect of crack cycling

In the past decades, the effect of crack cycling on cast-in-place and post-installed reinforcing bars was rarely studied. To the knowledge of the author, the only tests available in the literature are tests on reinforcing bars to evaluate the sensitivity to crack width cycling as part of post-installed mechanical and bonded anchor qualification testing according to *ETAG 001 (2006)* or *ACI 355.4 (2010)*. The intention of the crack width cycling qualification tests is to assess the suitability of post-installed anchors located in cracks where width is subject to changes due to movable live loads. Post-installed anchors are allowed to be used for safety relevant connections if the acceptance criteria of all qualifications tests were met. Connections using post-installation systems approved on the basis of post-installed anchor qualification guidelines can be designed as an anchor according to the provisions introduced in Section 2.3.1.2. The post-installation system comprises of the anchor or reinforcing bar, installation technique, and mortar.

Following, the testing scheme stipulated in *ACI 355.4 (2010)* is explained in brief. The anchor is installed in a concrete test member which is pushed and pulled to generate crack cycling (Figure 2.23a). After applying the constant load $N_w = 0.3N_{Rk}$ on the anchor, 1000 crack cycles between a lower crack width of 0.1 mm and an upper crack width of 0.3 mm are conducted (Figure 2.23b). The lower crack width is allowed to increase to 0.2 mm, however, a minimum crack width difference of $w_1 – w_2 = 0.1$ mm has to be kept during testing. If necessary, the amplitude applied on the concrete test member is adjusted to maintain the minimum differential. The acceptance criteria of the crack cycling test is the displacement limit of 2 mm after 20 cycles and 3 mm after 1000 cycles. The characteristic resistance $N_{Rk}$ of the anchor is iteratively determined in the course of the qualification testing. It is noted that the anchor qualification guideline *ETAG 001 (2006)* stipulates an almost identical crack movement test, however, the constant load is differently defined.

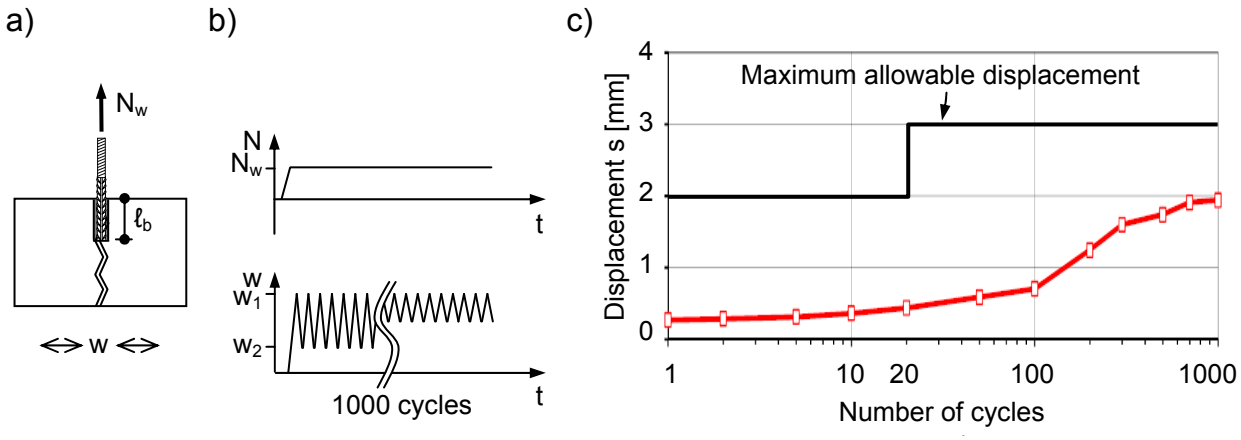


Figure 2.23 a) Crack cycling test at constant load; b) Load $N_w$ and cyclic crack width between peak crack widths $w_1$ and $w_2$ versus time t; c) Displacements measured for #4 (1/2 in.) reinforcing bar post-installed with epoxy mortar (after *Hahn, C. (2008)*)

Figure 2.23c provides the displacement curve of a reinforcing bar post-installed with an epoxy mortar as an example. The bonded length was $\ell_b = 8\phi$. It is evident that the tested post-installation system faced no difficulties to cope with the crack cycling. Also the subsequent pullout test to determine the residual capacity did not show any reduction compared to the monotonic reference tests conducted on reinforcing bars post-installed in cracked concrete.

However, the boundary condition of the crack cycling test according to current post-installed anchor qualification testing guidelines do not reflect the conditions present in joints of reinforced concrete structures during earthquakes. The seismic loading conditions on reinforcing bar anchorages of structural connections are subjected to larger crack openings and to full crack closings. In fact, the cracks will be compressed as the reinforced concrete structure responds to the seismic excitation (Section 3.3). For the sake of completeness it is noted that the German Guideline for fastenings in nuclear power plants and other nuclear technical facilities *DIBt KKW Leitfaden (2010)* defines a similar crack cycling test comprising 10 cycles between the lower crack width of 1.0 mm and upper crack width of 1.5 mm. The upper crack width is larger than anticipated for seismic events in an attempt to compensate for the compressed cracks (*Mahrenholtz, C. (2009b)*). However, this test regime was never applied on bonded anchors since these cannot cope with such large crack widths.

Realistic seismic conditions of large crack width opening and compressed crack closing were simulated for crack cycling tests on post-installed mechanical and bonded anchors which were part of a comprehensive seismic test program (*Mahrenholtz, C. (2009c)*). The crack protocol was arranged by stepwise increasing crack widths. After 32 cycles the maximum crack width was reached. The maximum

crack width was defined as $w_{max}$ = 0.8 mm. The minimum crack width $w_{min}$ equalled to a compression stress on the concrete member of $0.15f_c$.

Figure 2.24a shows the load-displacement curves of crack cycling tests on post-installed threaded rods M12 (diameter 12 mm). Epoxy mortar was used and the bonded length was 96 mm. The test series comprised three tests of which two failed prematurely. One test just endured the crack cycling, however, the residual load capacity was below the constant load.

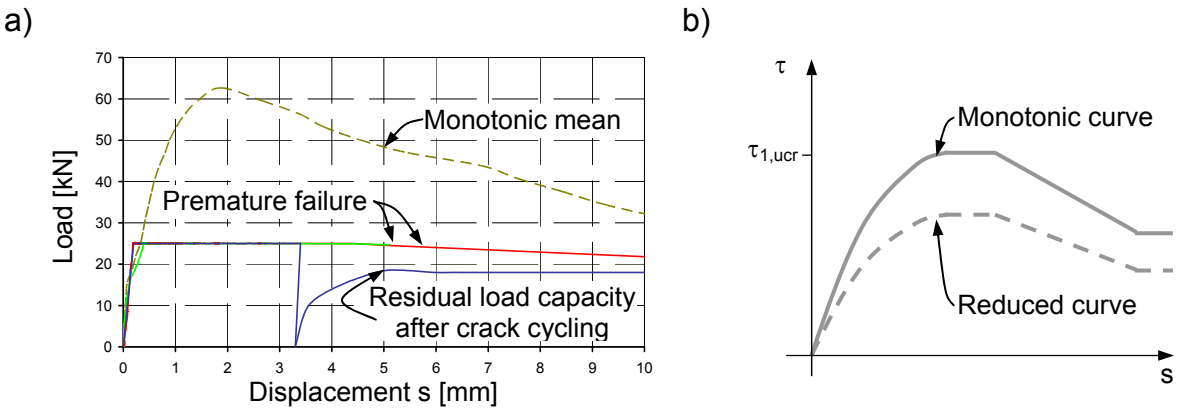


Figure 2.24 a) Load-displacement curves of crack cycling tests on threaded rod M12 post-installed with epoxy mortar (after *Mahrenholtz, C. (2009c)*); b) Model for the bond stress-slip relation to account for the bond damage due to crack cycling

Since the load transfer mechanism of bonded anchors and reinforcing bars is in principle identical (Section 2.3.1.2), the findings are instructive also for post-installed and cast-in-place reinforcing bar anchorages. This is in particular true because the shear plane of failure was between mortar and concrete. In conclusion, substantial reduction of bond strength due to crack cycling under seismic conditions has to be expected for reinforcing bars (Figure 2.24b).

To date, no model exists taking into account the effect of crack cycling on cast-in-place and post-installed reinforcing bars. For the sake of clarity it is pointed out that the term cyclic loading embraces also the effects derived from crack cycling.

### 2.2.15 Superpositioning of effects

The combination of the individual models developed for the analytical determination of the bond strength influencing factors ($\Omega_c$, $\Omega_w$, $\Omega_{cyc}$, $\Omega_s$) allows the consideration of all effects acting at the same time. For this purpose, the algorithms of the models, Equation 2.5 to 2.8, are superposed by multiplication:

$$\Omega = \begin{Bmatrix} \Omega_c \cdot \Omega_{cyc} \cdot \Omega_s \\ \Omega_w \cdot \Omega_{cyc} \cdot \Omega_s \end{Bmatrix} \begin{Bmatrix} \sigma_c \geq 0.0\ \mathrm{N/mm^2}\ \text{(transversal compression)} \\ w \geq 0.0\ \text{mm (longitudinal cracks)} \end{Bmatrix} \qquad \text{Equation 2.10}$$

Multiplying the basic bond stress-slip curve (Section 2.2.4) with the factor $\Omega$ defines a factored bond stress-slip curve which considers the so far accumulated damage and momentary acting effects (Figure 2.25).

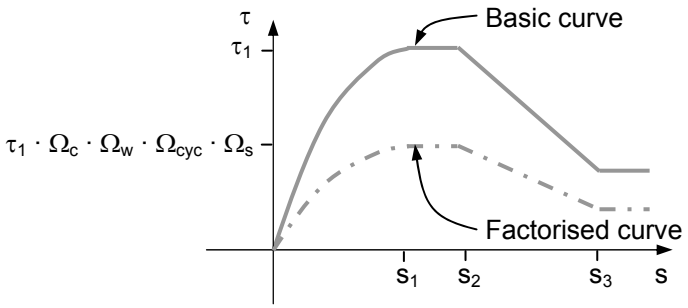


Figure 2.25 Effect of transverse concrete compression, effect of parallel concrete crack, damage effect of load cycling, and effect of inelastic steel strains superposed by multiplication of the factors $\Omega_c$, $\Omega_w$, $\Omega_{cyc}$, and $\Omega_s$

### 2.2.16 From reinforcing bar increments to reinforcing bar sections

The bond model defines the local bond behaviour of one reinforcing bar increment. The bond model can be understood as a non-linear spring which is defined by differential equations. In order to study the global bond behaviour of longer reinforcing bar sections, a sequence of increments is used which nodes are held by non-linear springs representing the bond model (Figure 2.26).

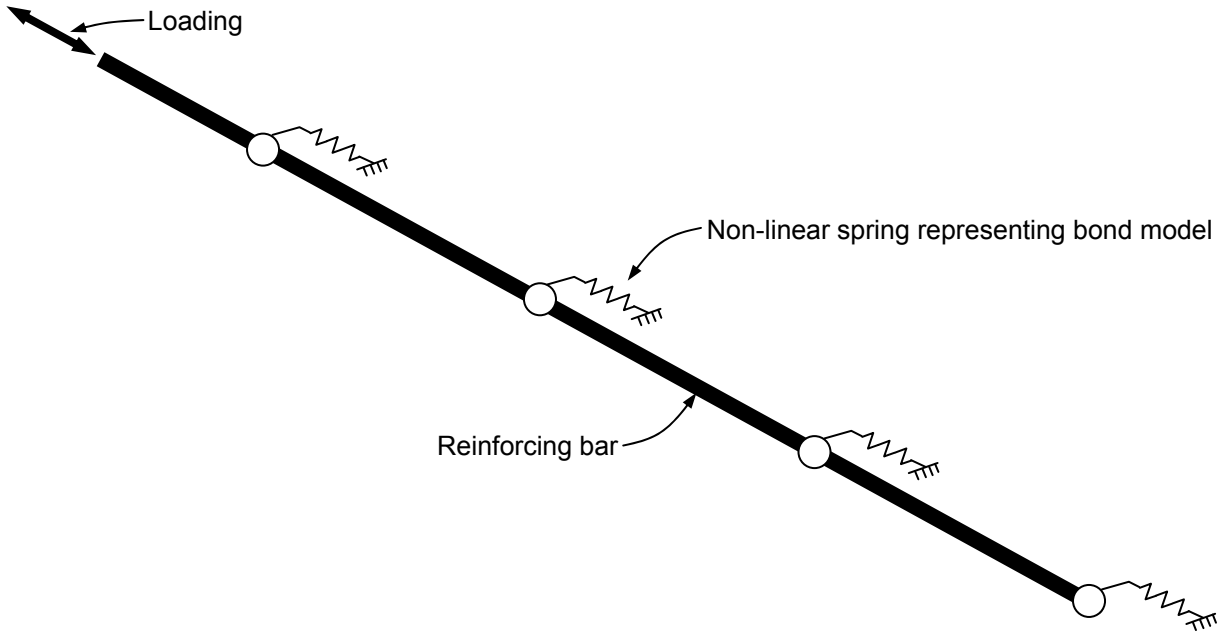


Figure 2.26 Reinforcing bar section as a sequence of increments held by non-linear springs representing the bond model

The differential equations have to be iteratively solved to determine the strain distribution. The iteration requires a procedural program, e.g. BOND (*Ciampi, V.; Eligehausen, R. et al. (1982)*). In order to realistically study structural members, e.g. column-to-foundation connections, the effects of transverse concrete compression, parallel concrete cracks, and inelastic steel strains have to be considered in a generic way. Therefore, the hysteretic energy model (*Eligehausen, R.; Popov, E. et al. (1983)*) was implemented in finite element programs, e.g. MASA (*Ožbolt, J. (1999a)*) and successfully tested (*Eligehausen, R.; Lettow, S. et al. (2003)*). The finite element method (FEM) provide further benefits such as the absence of material property scatter and the possibility to extract results which are difficult to measure in reality, e.g. reinforcement and concrete strains. A general description of the FEM and its application in engineering science can be found elsewhere (e.g. *Strang, G.; Fix, G. (2008)*). The three-dimensional finite element program MASA is introduced in Section 5.1.1, as this program was used for the numerical studies presented in this thesis.

## 2.3 Reinforcing Bar Anchorages for Structural Connections

In the following, some relevant aspects of reinforcing bar anchorages are discussed. Reinforcing bar anchorages are used to connect structural members, e.g. column

and foundation (Figure 2.27). Cast-in-place and post-installed anchorages were considered for the literature review.

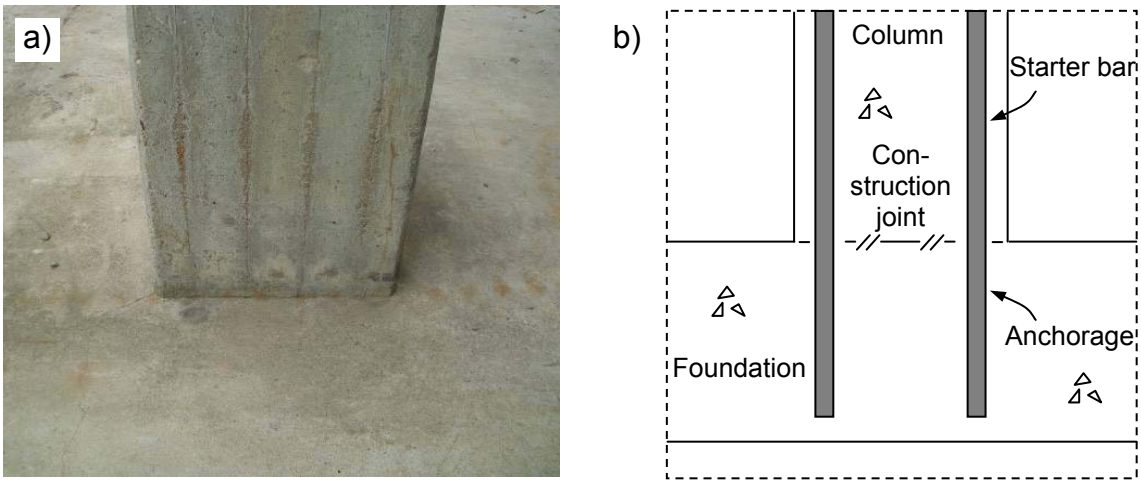


Figure 2.27 Column-to-foundation connection as an example for structural connections: a) Photo; b) Schematic

### 2.3.1 Coexisting design approaches for anchorages in concrete

Modern reinforced concrete design codes provide two coexisting approaches for the design of anchorages: The conventional approach for designing reinforcing bar anchorages, in the following abbreviated as 'conventional anchorage design', and the application of design provisions for bonded anchors, in the following termed as 'bonded anchor design'. The concepts were developed for different problems and have advantages and disadvantages. Some aspects of both concepts relevant in the context of this thesis are briefly discussed in the following. Figure 2.28 shows the range of application of both concepts with respect to the concrete cover and anchorage length.

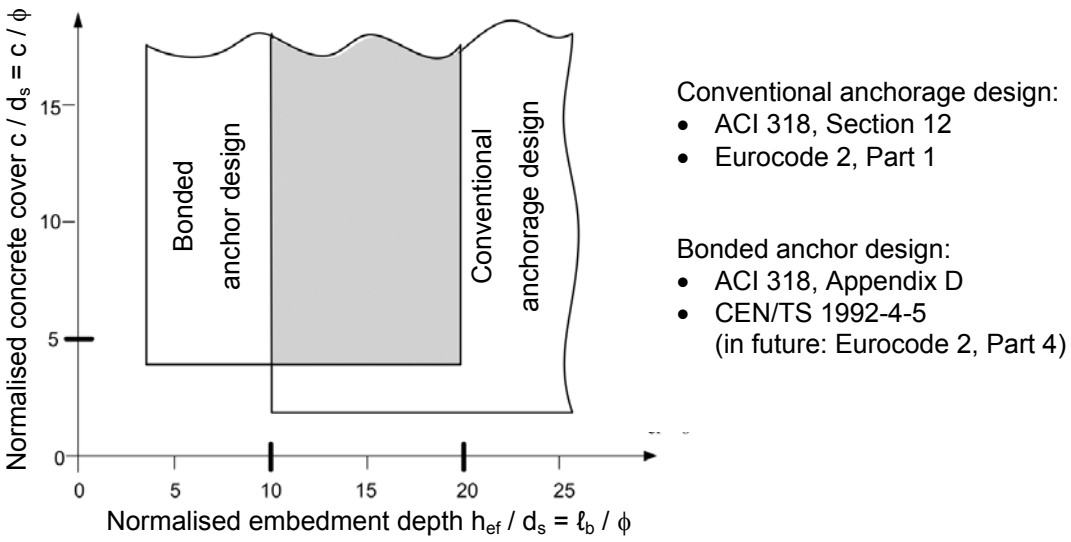


Figure 2.28 Range of application of conventional anchorage design and bonded anchor design (after *Fellinger, M. (2009)*)

Anchorages detailed according to conventional anchorage design require large anchorage lengths but allow small concrete covers. On the contrary, anchorages detailed according to the bonded anchor design are feasible also for small anchorage lengths if sufficient concrete cover is provided. Since the concrete cover of column starter bars anchored in the foundation slab is large, the bonded anchor design is a promising alternative to the conventional anchorage design. Both design approaches are discussed in the following two sections.

#### 2.3.1.1 Conventional anchorage design

For this approach, the reinforcing bars are considered to be loaded in pure tension. The forces are transferred to the concrete by bond, balanced either by local struts originating from splicing reinforcement (Figure 2.29a) or by a global strut which can be considered as a part of a truss system (Figure 2.29b). The principle of strut-and-tie modelling is discussed in Section 2.3.2.

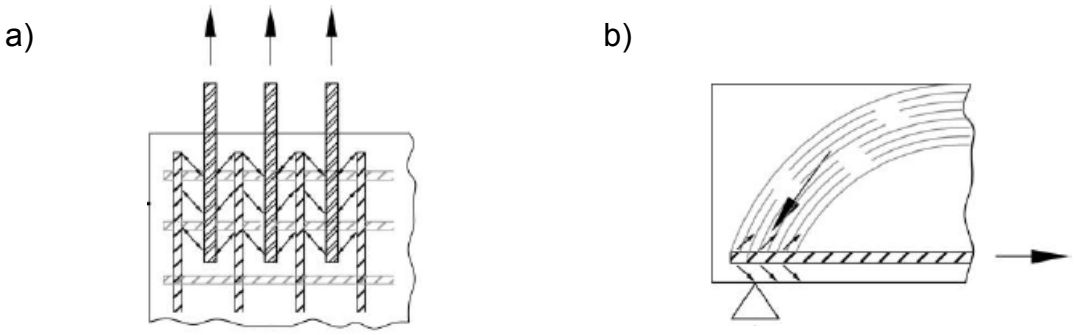


Figure 2.29 Balancing of bond stresses transferred by a) local struts and b) global strut (*Fib Bulletin No. 58 (2011)*)

The basic concept of the conventional anchorage design is to specify sufficient development lengths to ensure the reduction of bond stresses to uncritical low levels. For this reason, a failure of the anchorage by pullout is prevented as is the failure by concrete splitting despite small concrete covers. Therefore, anchorages designed according to the conventional anchorage design fail by yielding of the bar. The advantage of this design approach is an anchorage length which is universally valid regardless of the actual concrete member geometry. The disadvantage of this across-the-board approach is the long required anchorage length which is potentially over-conservative, e.g. for column starter bar anchorages where the confinement generated by the foundation prevents a splitting failure.

The conventional anchorage design is part of the reinforced concrete design codes. In the following, rules for the determination of the anchorage length according to the *Eurocode 2 (2005)* are quoted as an example. Only the most essential equations are given. Further details with respect to the determination of the anchorage length accordin to *Eurocode 2 (2005)* (Part 1, Section 8.4), *ACI 318 (2011)* (Section 12), and *NZS 3101 (2006)* (Section 8.6) are given in Appendix A: Conventional Anchorage Design.

The anchorage length is closely associated to the design bond strength $f_{bd}$ which is according to *Eurocode 2 (2005)*, Clause 8.4.2, defined by

$$f_{bd} = 2.25 \cdot \eta_1 \cdot \eta_2 \cdot f_{ctd} \qquad \text{Equation 2.11}$$

where $f_{ctd}$ is the design concrete tensile strength (*Eurocode 2 (2005)*, Table 3.1) and

- $\eta_1$ is taking into account the reinforcing bar position during casting ($\eta_1$ = 1.0, i.e. good bond conditions are assumed for the vertical column starter bars) and
- $\eta_2$ is taking into account the reinforcing bar diameter ($\eta_2$ = 1.0 for $\phi \leq 32$ mm, else (132 – $\phi$ [mm]) / 100).

The basic anchorage length $\ell_{b,rqd}$ required to transfer the tensile stress of a reinforcing bar is determined according to *Eurocode 2 (2005)*, Clause 6.9.4, by

$$\ell_{b,rqd} = \frac{\phi \sigma_{sd}}{4 f_{bd}} \qquad \text{Equation 2.12}$$

where $\phi$ is the reinforcing bar diameter and $\sigma_{sd}$ the design stress at the beginning of anchorage. The design anchorage length $\ell_{bd}$ is determined according to *Eurocode 2 (2005)*, Clause 6.9.5, by

$$\ell_{bd} = \alpha_1 \cdot \alpha_2 \cdot \ell_{b,rqd} \geq \ell_{b,min} \qquad \text{Equation 2.13}$$

where only those coefficients are given in the following which are potentially relevant in the context of this thesis, i.e.

- $\alpha_1$ taking into account the form of the bar ($\alpha_1$ = 1.0 for bars without hook, $\alpha_1$ = 0.7 for bars with hooks),
- $\alpha_2$ taking into account the confinement ($0.7 \leq \alpha_2 \leq 1.0$ for bars in tension, $\alpha_2 = 1 - 0.15\ (c_d - k\phi) / \phi$, where k = 1 for bars without hook, k = 3 for bars with hooks, $c_d > 3\ \phi$ is the minimum of concrete cover and half the clearance between adjacent bars).

The minimum anchorage length $\ell_{b,min}$ is the maximum of $0.3\ell_b$, $10\phi$, and 100 mm for bars in tension. The resulting code compliant anchorages typically require an anchorage length of about $40\phi$. Most joints, for example column-to-foundation connections, do not provide sufficient depth to accommodate the full anchorage length if detailed without hook. Also typical anchorage lengths detailed with hook still amounts to around $25\phi$.

Therefore, excess reinforcement is frequently designed to allow further reduction of the anchorage length. The excess reinforcement is reducing the steel stress $\sigma_s$ and therefore, Equation 2.12 yields smaller anchorage lengths. The reduction factor equals to the ratio $A_{s,req} / A_{s,prov}$ and $\ell_{b,prov} / \ell_{b,rqd}$ which is also termed utilisation ratio since it expresses to what extent the steel yield strength is utilised. Excess reinforcement, in turn, increases reinforcement congestions, material and labour costs. Moreover, *Eurocode 8 (2006)*, Clause 5.6.2 prohibits to take reduced utilisataion ratios into account for the determination of columns starter bar anchorage lengths under seismic loading. Other reinforced concrete design codes stipulate similar limitations on excess reinforcement for seismic load cases (Appendix A: Conventional Anchorage Design).

Also post-installed reinforcing bars may be designed according to the conventional anchorage design approach, provided that the post-installed reinforcing bars develop bond characteristics similar to cast-in-place reinforcing bars. The performance is

assessed according to the qualification guideline for post-installed reinforcing bars *EOTA TR 023 (2006)*. The tested properties are certified by means of European Technical Approval (ETA) documents. Qualifications of post-installed reinforcing bars are currently not carried out in the US.

Since the integrity of the concrete is potentially at risk due to the hammer drilling of the anchorage holes, the required concrete cover and clear spacing of post-installed reinforcing bars is increased. Currently, the nominal steel yield strength is limited to grade 500 ($f_y$ = 500 MPa) and the nominal concrete compressive strength to grade 60 ($f_{c,cube}$ = 60 MPa).

The performance assessment according to *EOTA TR 023 (2006)* is also evaluating the functioning of installation technique as well as the influence of water saturated concrete, sustained loads, freeze/thaw conditions, and the durability of the post-installation system. The assessment includes bond tests which have to give evidence that the post-installed reinforcing bar is capable to attain the same design values of bond strength with the same safety margin as cast-in-place reinforcing bars according to *Eurocode 2 (2005)*. *EOTA TR 023 (2006)* provides a diagram to compare mean and design bond values since the *Eurocode 2 (2005)* exclusively determines a *design* anchorage length $\ell_{bd}$ based on the *design* bond stress $f_{bd}$. The technical specifications of an approved post-installation system include all design data and the requirements for the Manufacturer's Printed Installation Instructions (MPII). The interrelationship of design, characteristic and mean bond strengths is discussed in Appendix A: Conventional Anchorage Design.

Post-installed reinforcing bars allow a monolithic connection between existing and new members of reinforced concrete structures, provided suitable mortars are used and the installation is carried according to the MPII. As a general rule in reinforced concrete, the existing concrete surface has to be roughened before the new concrete is placed against it (*Eurocode 2 (2005)*, Clause 6.2.5(2) and *ACI 318 (2011)*, Clause 11.6.9) to ensure a reliable transfer of shear forces. Figure 2.30 shows examples for the two possible connection types of post-installed reinforcing bars.

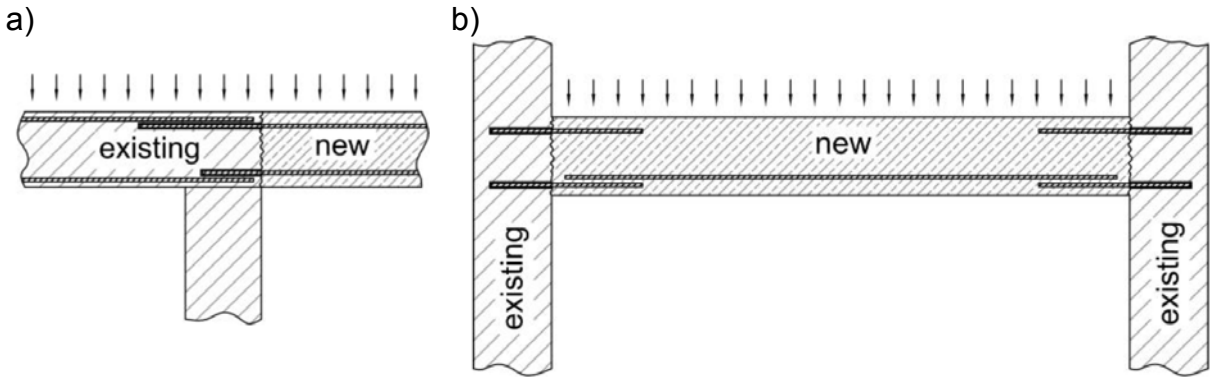


Figure 2.30 Connections with post-installed reinforcing bars for a) overlap joints ('splicing') and b) end anchoring ('anchorage') (*Fib Bulletin No. 58 (2011)*)

### 2.3.1.2 Bonded anchor design

The bonded anchor design provisions are given in *CEN/TS 1992-4 (2009)* which conversion to the *Eurocode 2 (2005)*, Part 4 is envisaged before long (*Feistel, G. (2012)*). Similar provisions are stipulated in *ACI 318 (2011)*, Appendix D which is referred to by design codes of many countries, e.g. *NZS 3101 (2006)*. The bonded anchor design provisions of *CEN/TS 1992-4 (2009)* are given in Appendix B: Bonded Anchor Design.

The general load transfer mechanism of bonded anchors is identical to that of reinforcing bar anchorages. Therefore, the bonded anchor design provisions are also applicable to post-installed and cast-in-place reinforcing bar anchorages. For better understanding of the mechanical background, the bonded anchor model is discussed which serves as the basis for the bonded anchor design provisions. Therefore, the quoted parameters are related to the mean material strengths. The failure load and corresponding failure mode of the anchorage is governed by one of the following capacities:

- Steel capacity (mode S): The steel of the bar fractures (Figure 2.31a1). The steel capacity of the bar with a stressed cross section of $A_s$ is based on the ultimate steel strength $f_u$:

  $N_{R,s} = A_s \cdot f_u$ Equation 2.14

  To comply with the common understanding of the conventional anchorage design in the context of column-to-foundation connections, the definition of the yielding capacity (mode Y) is required: Yielding is initiated at the loaded end of the anchorage when the yield strength $f_y$ is exceeded (Figure 2.31a2). The yielding capacity is defined as:

  $N_{R,y} = A_s \cdot f_y$ Equation 2.15

- Concrete breakout capacity (mode C): A conical concrete breakout develops from the unloaded end of anchorage (Figure 2.31b). The concrete breakout capacity is determined on the basis of the concrete capacity (CC) design model (*Fuchs, W.; Eligehausen, R. et al. (1995)*):

  $N_{R,c} = k \cdot f_c^{0.5} \cdot \ell_b^{1.5}$ Equation 2.16

  According to current experience (e.g. *Eligehausen, R.; Mallée, R. et al. (2006)*), k equals to $k_{ucr} = 14.6$ and $k_{cr} = 10.2$ for applications in uncracked and cracked concrete, respectively ($k_{ucr} = 0.7k_{ucr}$). Different k factors have to be used if the imperial unit instead of the metric system is used, or if the concrete compressive strength is determined by means of test cubes instead of test cylinders.

- Pullout capacity (mode P): The bond fails and the bar is pulled out. The pullout failure is also denoted as bond failure, or combined pullout and concrete failure because of the accompanying secondary concrete cone which develops near the surface (Figure 2.31c). The bond capacity is determined on the basis of the uniform bond (UB) design model (*Cook, R.; Kunz, J. et al. (1998)*):

  $N_{R,p} = \pi \cdot \phi \cdot \ell_b \cdot \tau_u$ Equation 2.17

  The bond strength $\tau_u$ generated in uncracked concrete equals $\tau_{u,ucr}$ which is reduced to the value $\tau_{u,cr}$ in case of cracked concrete.

It is noteworthy that the latter design model calculates the capacity on the basis of averaged bond strengths without considering the actual strain distribution.

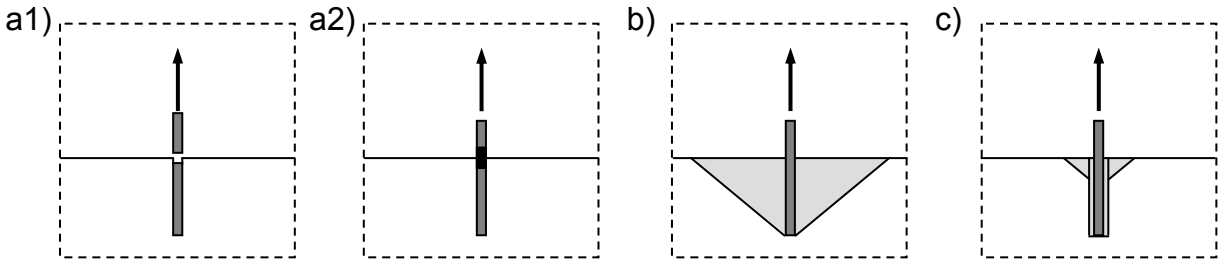


Figure 2.31 Individual bonded anchorage: a1) Steel failure mode; a2) Yielding failure mode; b) Concrete breakout failure mode; c) Pullout failure mode

The ultimate capacity available to anchor the tension load N of a reinforcing bar is governed by the minimum of the strengths according to Equation 2.15 to 2.17:

$N_R = \min\{N_{R,y}; N_{R,c}; N_{R,p}\}$ Equation 2.18

The ratio of the capacity $N_R$ corresponding to the governing failure mode and the yielding capacity $N_{R,y}$ indicates to what extent the reinforcing bar is utilised. Design values have to be used, i.e. $N_{Rd} / N_{Rd,y}$, to allow a meaningful comparison with the utilisation ratios according to the conventional anchorage design, i.e. $\ell_{b,prov} / \ell_{b,req}$.

It is evident that the ultimate capacity and corresponding failure mode depend on the material strengths and anchorage length as illustrated by the conceptual representation shown in Figure 2.32 for an individual bonded anchor. The yield, concrete and pullout capacities are plotted using representative geometry and material parameters. For smaller anchorage lengths mode C is governing, for medium lengths mode P and for larger lengths mode Y.

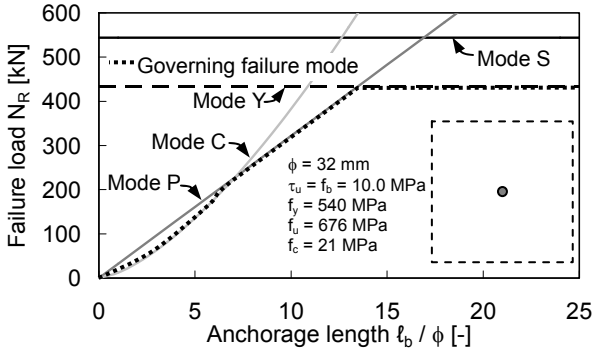


Figure 2.32 Conceptual representation of governing failure mode for individual bonded anchorage

Figure 2.33 illustrates the application of the bonded anchor model in the context of column-to-foundation connections. The column starter bars anchored in the foundation slab can be taken as an aligned group of bonded anchorages.

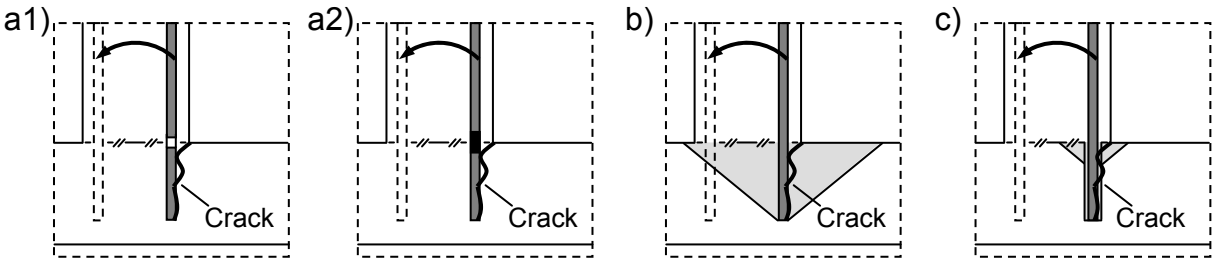


Figure 2.33 Column-to-foundation connection taken as a group of bonded anchorages: a1) Steel failure mode; a2) Yielding failure mode; b) Concrete breakout failure mode; b) Pullout failure mode

The conceptual representation in Figure 2.34 depicts the yield, concrete and pullout capacities per anchorage of an example column-to-foundation connection, which were determined for the assumption that the concrete is cracked.

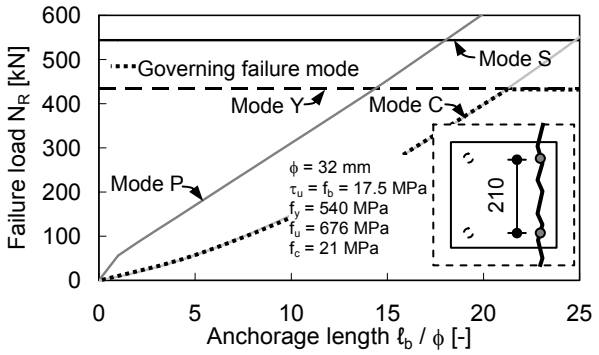


Figure 2.34 Conceptual representation of governing failure mode for a column-to-foundation connection taken as a group of bonded anchorages

Which mode governs depends not only on the specific material parameters of the reinforcing bar, concrete and mortar, but also on the geometry of the bonded anchor group and the concrete member the group is anchored in. Therefore, additional factors have to be considered when determining the concrete and pullout capacity to account for several effects such as the influence of anchorage groups, edge distances, and cracks. The additional factors relevant for the determination of the concrete and pullout capacity in the context of this thesis are given in Table 2.3.

Table 2.3 Additional factors to determine the mean capacity of an aligned group of bonded anchorages comprising of individual anchorages; denomination as defined above

| Effect | Pullout capacity | Concrete capacity |
|---|---|---|
| Overlapping influencing area | $\frac{A_{p,N}}{A_{p,N}^0} = \frac{A_{p,N}}{s_{cr,Np}^2}$<br>$s_{cr,Np} = 20 \cdot \phi \cdot \left(\frac{\tau_R[\text{MPa}]}{10}\right)^{0.5} = 2c_{cr,Np} \le 3 \cdot \ell_b$ [1)]<br>$A_{p,N}$ depends on installation geometry | $\frac{A_{c,N}}{A_{c,N}^0} = \frac{A_{c,N}}{s_{cr,N}^2}$<br>$s_{cr,N} = 2c_{cr,N} = 3 \cdot \ell_b$<br>$A_{c,N}$ depends on installation geometry |
| Edge | $\psi_{s,Np} = 0.7 + 0.3 \cdot \frac{c}{c_{cr,Np}} \le 1.0$ | $\psi_{s,N} = 0.7 + 0.3 \cdot \frac{c}{c_{cr,N}} \le 1.0$ |
| Group | $\psi_{g,Np} = \psi_{g,Np}^0 - \left(\frac{s}{s_{cr,Np}}\right)^{0.5} \cdot \left(\psi_{g,Np}^0 - 1\right) \ge 1.0$<br>$\psi_{g,Np}^0 = 0.5n + 0.5 - (0.5n - 0.5) \cdot \left(\frac{\tau_R}{\tau_{R,c}}\right)^{1.5} \begin{cases} \ge 1.0 & \text{2)} \\ \le n \end{cases}$ | - |
| Cracks | $\psi_{w,Np} = 0.5$ [3)] | $\psi_{w,N} = 0.7$ |

[1)] According to *Eligehausen, R.; Cook, R. et al. (2006)*

[2)] According to *Herzog, M. (2010)*, further explanations in Section 8.2.1

[3)] Rule of thumb according to *Eligehausen, R.; Mallée, R. et al. (2006)*, *Mészároš, J. (2002)*

The additional factors $\psi_i$ are multiplicatively superposed. It is noted that the anchor design codes, e.g. *CEN/TS 1992-4 (2009)*, do not define a specific factor $\psi_w$ to account for cracks because the values for $k_{ucr}$, $k_{cr}$, $\tau_{u,ucr}$, $\tau_{u,cr}$ are product specific and given in the approval document. The details of the group factors as well as information on the calculation of $A_{p,N}$ and $A_{c,N}$ are given in Appendix B: Bonded Anchor Design.

The parametric study provided in *Mahrenholtz, C. (2012a)* shows that the factors taking into account the effect of overlapping influencing areas and group effects capture three fundamental phenomena which are pointed out as follows:

- For a given constant total steel cross section and anchorage length, the total pullout capacity (but not the concrete capacity) is increased if the load is transferred by increasing the number of bars, since the bond area ($\phi \cdot \ell_b$) required for the load transfer is increased accordingly.

- Because of the overlapping stress fields, the capacity of an individual anchorage within a group is reduced. The reduction is more pronounced for the pullout capacity than for the concrete capacity.
- Parallel cracks reduce the pullout capacity of an anchorage more than the concrete capacity, which is reflected by the ratio of the k factors ($k_{ucr} = 0.7k_{ucr}$, Equation 2.16) and the ratio of the bond strengths ($\tau_{u,cr} = 0.5\tau_{u,ucr}$, Equation 2.17).

In Europe, post-installed anchors used for safety relevant connection have to be qualified. The qualification is conducted according to *ETAG 001 (2006)* and the tested properties are certified by means of European Technical Approval (ETA) documents. ICC-ES reports (ESR) are the US-American equivalents reporting qualification testing according to *ACI 355.2 (2007)* and *ACI 355.4 (2010)*. The approval documents provide characteristic values for k factors (Equation 2.16) and bond strengths (Equation 2.17), as well as other design provisions and installation instructions. The procedure of qualification is discussed e.g. in *Mahrenholtz, C. (2008)*.

#### 2.3.1.3 Comparison of the coexisting design approaches

The following Table 2.4 provides a comparison of the conventional anchorage design according to *Eurocode 2 (2005)* and bonded anchor design according to *CEN/TS 1992-4 (2009)*. It is noted that $\tau_R$ is the denomination of bond strength according to *CEN/TS 1992-4 (2009)*. A comparison of the two design approaches is made in Section 9.2.3.

Table 2.4 Comparison of conventional anchorage design and bonded anchor design

| | Conventional anchorage design | Bonded anchor design |
|---|---|---|
| Load cases | Tension | Tension, shear, combined tension and shear |
| Reaction | Balanced by concrete struts | Utilisation of concrete tensile strength |
| Failure modes[1)] | Bar yielding<br>Concrete splitting | Bar fracture (mode S)<br>Bar pullout (mode P)<br>Concrete breakout (mode C) |
| Total failure | Potential global collapse | Any failure is local only |
| Strength[1)] | $N_R = A_s f_y$ | $N_R = \min\{N_{R,s}, N_{R,p}, N_{R,c}\}$[2)] |
| Bond strength | Calculated<br>$f_{bd} = 2.25 \cdot \eta_1 \cdot \eta_2 \cdot f_{ctk} / \gamma_c$<br>Used to determine anchorage length | Tested and approved<br>$\tau_{Rd} = \tau_{Rk} / \gamma_c$<br>Used to determine pullout strength |
| Anchorage length | $\ell_{bd} = (\phi / 4) (\sigma_{sd} / f_{bd})$<br>$(\sigma_{sd} \leq f_{yd})$ | Resulting from uniform bond (UB) and concrete capacity (CC) design models |
| Condition of use | Load transfer does not rely primarily on concrete tensile stresses | Concrete remains essentially in the serviceability limit state |
| Ultimate limit state | Ultimate limit state of anchorage and structure reached at the same time | Failure of anchorage does not cause failure of structure |
| Concrete crack width | Service limit state: w = 0.3 mm[3)]<br>Ultimate limit state: w >> 0.3 mm | Uncracked: w = 0.0 mm ($\rightarrow \tau_{R,ucr}$)<br>Cracked: w = 0.3 mm[4)] ($\rightarrow \tau_{R,cr}$) |
| Typical concrete cover | $3\phi > c > 2\phi$ | $c >> 3\phi$ |
| Typical anchorage length | $\ell_b > 40\phi$ | $25\phi > \ell_b > 5\phi$ |
| Qualification guideline (post-installation) | EOTA TR 023 (2010) | ETAG 001 (2006) |
| Design code | EN 1992-1<br>(Eurocode 2, Part 1) | CEN/TS 1992-4<br>(in future: Eurocode 2, Part 4) |
| Modification | Universally valid anchorage length; $\alpha_i$ factors to take into account inter alia the effects of hooks, side cover, and transverse pressure | Geometry of concrete element and layout of grouped anchorages considered; $\psi_i$ factors to take into account various effects |

[1)] Tension only

[2)] Equation 2.15, 2.16, and 2.17

[3)] Mean value, recommended for low exposure classes

[4)] Mean value

### 2.3.2 Strut-and-tie modelling

Continuous zones of reinforced concrete members with linear strain distributions can be analysed by the theory of elasticity. In contrast, discontinuous zones with non-linear strain distributions, e.g. close to concentrated loads or cross sectional jumps, have to be analysed either by the finite element method (FEM) or by strut-and-tie modelling (STM) which is a versatile and practicable alternative. Modern reinforced concrete design codes such as *Eurocode 2 (2005)* and *ACI 318 (2011)* include provisions for STM. While *Eurocode 2 (2005)*, Clause 6.5.1(1) limits the use of STM expressively to discontinuity regions, *ACI 318 (2011)*, Clause A.2.1 permits to design structural concrete members by modelling the member or regions of the member as an idealised truss.

The STM is a well established method to determine the trajectories of the principal stresses in a concrete structure. The bundling of the trajectories leads to a truss model with struts loaded in compression and ties loaded in tension. Sufficient rotation capacity provided, the design of the imaginative truss is flexible. At a node, however, the angle between strut and tie should be larger than 30°. Smaller angles would lead to compatibility conflicts and large deformations. The analysis of the truss gives a good estimation of stresses in reinforcement and concrete. An instructive description of STM can be found in *Schlaich, J.; Schäfer, K. (2001)* and an example practical application to column-slab connections in *Alexander, S.; Simmonds, S. (1987)*.

*Bruckner, M. (2006)* studied column-to-foundation connections under monotonic loading. The column starter bars were detailed with hooks or as headed bars. It was shown that the design of the connection by means of the proposed three-dimensional strut-and-tie model is outmost complex and less practicable (Figure 2.35).

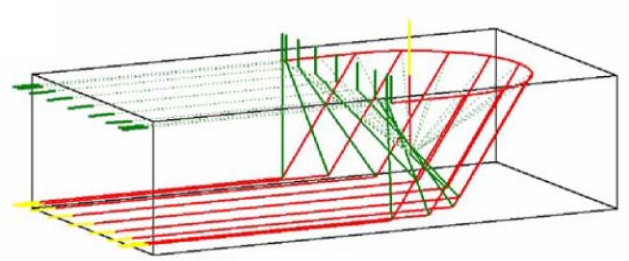

Figure 2.35 Three-dimensional strut-and-tie model of column-to-foundation connection, foundation shown only (*Bruckner, M. (2006)*)

The monotonic tests on post-installed wall-to-foundation connections presented in *Kupfer, H.; Münger, F. et al. (2003)* are instructive because of the similarity of column-to-foundation and wall-to-foundation connections. It was possible to design the connection using a two-dimensional STM (Figure 2.36a). *Hamad, B.; Hammoud, A. et al. (2006)* tested wall-to-foundation connections with different reinforcement

layouts and mortars used for post-installation. It was shown that the two-dimensional STM is not conservative for strut angles shallower than 35 ° (Figure 2.36b).

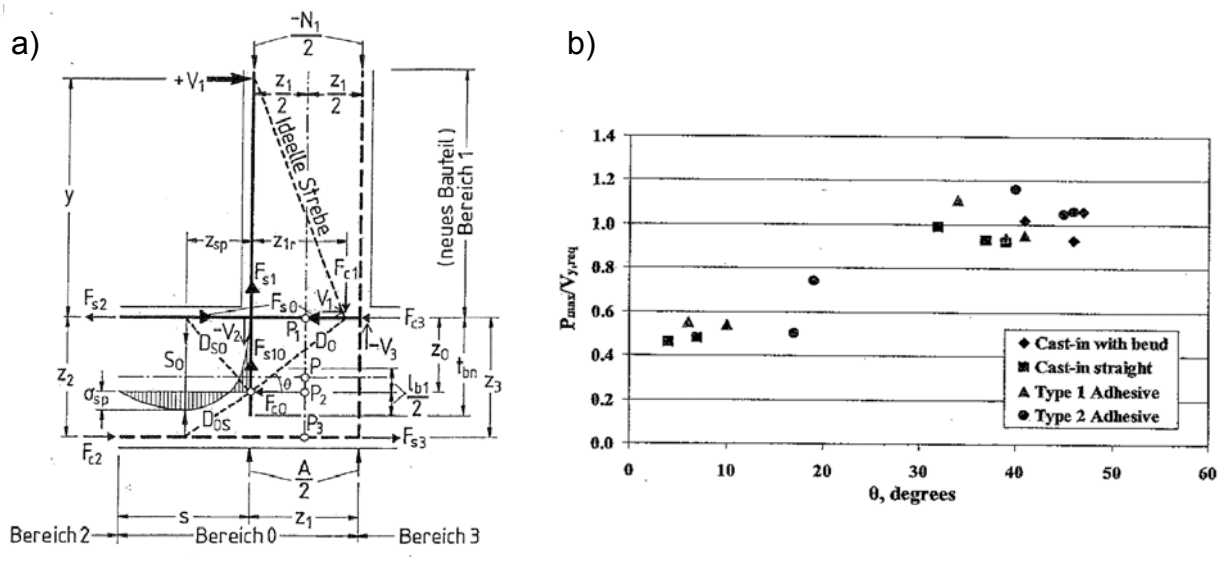


Figure 2.36 a) Two-dimensional strut-and-tie model for wall-to-foundation connections without hooks (*Kupfer, H.; Münger, F. et al. (2003)*); b) Ratio of tested and calculated capacities for various strut angles (*Hamad, B.; Hammoud, A. et al. (2006)*)

Also *Eligehausen, R.; Herzog, M. (2008)* pointed out that the STM suggested in *Kupfer, H.; Münger, F. et al. (2003)* may lead to unsafe results. Furthermore, the proposed STM is not straight forward and may lead to different results depending on the designer (*Eligehausen, R.; Herzog, M. et al. (2012)*).

The critical STM detail is the anchoring of the tensioned starter bars without hooks. Therefore, the objective of this thesis is to develop a design concept using a simple STM which starter bar anchoring is designed according to the bonded anchor design provisions (Section 2.3.1.2).

### 2.3.3 Beneficial effect of moment loading on connection capacity

*Zhao, G.-C. (1993)* studied the load behaviour of moment loaded anchor plates fitted with headed studs (Figure 2.37a) and observed that the external moment increases the concrete breakout capacity determined according to the bonded anchor model (Section 2.3.1.2). The factor $\psi_M$ was introduced to take this beneficial effect of moment loading into account which was defined as the ratio of the tested connection capacity and calculated concrete breakout capacity (Section 2.3.1.2). An advantage of this approach is that the factor $\psi_M$ also captures secondary effects which potentially reduce the connection capacity, making additional design checks as required at the STM approach (Section 2.3.2) unnecessary.

*Fichtner, S. (2011)* confirmed the observations of *Zhao, G.-C. (1993)* and used the data of *Varga, J. (1995)*, *Varga, J. (1996)*, *Bruckner, M.; Eligehausen, R. et al. (2001)* and other studies to develop two further equations describing the beneficial effect. The two proposed equations as a function of z-$h_{ef}$-ratio are shown in Figure 2.37b, where z equals the internal lever arm and $h_{ef}$ the anchorage length. In addition, the mean value of the ratio between tested and calculated factor $\psi_M$ and the coefficient of variation (CV) are given. Figure 2.37b also demonstrates that the differences between the suggested equations are small for the most relevant z-$\ell_b$ ratios between 0.5 and 1.5 and that the experimental and numerical tests show a large scatter in respect of factor $\psi_M$.

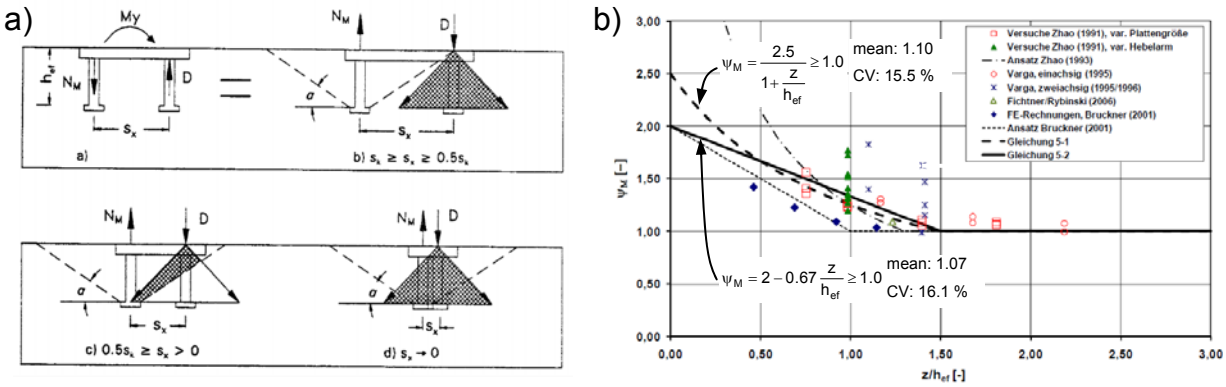


Figure 2.37 Examples for studies on connections subjected to external moment: a) Schematic for anchor plate fitted with headed studs (*Zhao, G.-C. (1993)*); b) Test results of various studies show increased capacity (*Fichtner, S. (2011)*)

The moment loading has also a beneficial effect on connections of two reinforced concrete members. This effect is generally described e.g. in *Paulay, T.; Priestley, N. (1992)* and *Priestley, N.; Seible, F. et al. (2007)*. Since column-to-foundation connections using cast-in-place anchor plates and reinforcing bars with short anchorage lengths are similar, *Herzog, M. (2008)* proposed to quantify the beneficial effect of moment loading also in the context of the bonded anchor model which then also consideres the pullout capacity (Section 2.3.1.2). Based on experimental and numerical studies on column-to-foundation connections under monotonic loading, *Herzog, M. (2010)* proposed the factor $\psi_M = 2.5 - (z / \ell_b)$ in where $\ell_b$ is the anchorage length of the column starter bars in the foundation. The equation was developed for column-to-foundation connections which columns were squarish and is deemed to be valid also for rectangular columns.

### 2.3.4 Adverse effect of cyclic loading on connection capacity

To date, only a limited number of literatures presenting research on column-to-foundation connections under cyclic loading can be found. Available literature dealing with column-to-foundation connection tests primarily focus on the general behaviour, e.g. plastic hinging at the column base, however, do not investigate the anchorage. The foundations of the test specimens are typically overdesigned in terms of reinforcement ratio and member thickness. Consequently, a realistic cracking along the column starter bar anchorage does not develop in the foundation stubs. Cast-in-place column-to-foundation connections where starter bars were detailed with hooks were studied by *Bousias, S.; Verzeletti, G. et al. (1995)* (Figure 2.38a). *Lee, J.-H. (2008)* compared the results of these experiments with the results derived from a two-dimensional finite element model to study the slip and stress distribution along column starter bar anchorages without hooks (Figure 2.38b).

*Riva, P. (2006)* carried out tests on precast columns which starter bars were grouted in cast-in-situ corrugated sleeve pipes (Figure 2.38c). The damage was mainly localised in the 20 mm grout layer between precast columns and foundation. *Tanaka, R.; Oba, K. (2001)* studied the behaviour of beam-column joints where the beam starter bars were cast-in-place and post-installed in the column stub. The configuration can also be interpreted as a column-to-foundation connection. However, realistic cracking of the compact stub in which the starter bars were anchored was impossible.

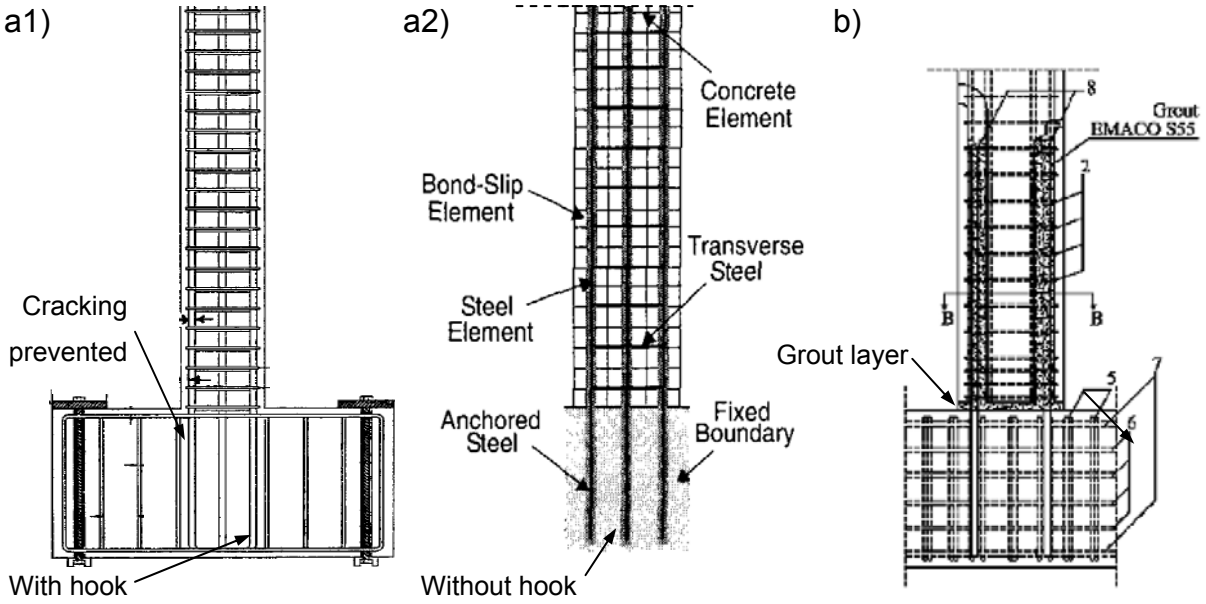


Figure 2.38 Examples for studies on column-to-foundation connections subjected to cyclic loading: a) Cast-in-place (*Bousias, S.; Verzeletti, G. et al. (1995)* and *Lee, J.-H. (2008)*); b) Post-installed (*Riva, P. (2006)*)

The above cited studies have in common that the cyclic tests are qualitatively described but no comparisons were made to monotonic tests. Furthermore, the adverse effect of cyclic loading was only taken into account regarding the damage effect of load cycling (Section 2.2.13). The damage effect of crack cycling (Section 2.2.14) was missed because the design of the foundation stubs did not allow pronounced cracking. Cracks with varying crack widths, however, have to be anticipated for column-to-foundation connections under seismic loading (Section 3.3).

## 2.4 Further Reading

The purpose of this chapter is not to discuss all literature available on bond of cast-in-place and post-installed reinforcing bars. Readers interested in further in-depth information on reinforced concrete – in particular in respect to bond and structural connections under seismic loading – are referred to the following bulletins which summarise relevant findings of the international research community:

- *CEB Bulletin d'information No. 131 (1979)* (RC under seismic action)
- *CEB Bulletin d'information No. 132 (1981)* (Bond in RC for seismic loading)
- *CEB Bulletin d'information No. 151 (1981)* (Bond behaviour of reinforcement)
- *CEB Bulletin d'information No. 158 (1984)* (Cracking and deformation)
- *CEB Bulletin d'information No. 187 (1988)* (RC under high loading rate)
- *CEB Bulletin d'information No. 120 (1991)* (RC under alternate actions)
- *CEB Bulletin d'information Nr. 213/214 (1993)* (CEB-FIP Model Code 1990)
- *CEB Bulletin d'information No. 216 (1994)* (Concrete and masonry anchors)
- *CEB Bulletin d'information No. 226 (1995)* (Design of concrete anchors)
- *CEB Bulletin d'information No. 230 (1996)* (RC under cyclic loading)
- *CEB State of the Art Report (1996)* (Anchors for seismic retrofitting)
- *Fib Bulletin No. 10 (2003)* (Bond behaviour of reinforcement)
- *Fib Bulletin No. 24 (2003)* (Seismic assessment and retrofit of RC buildings)
- *Fib Bulletin No. 58 (2011)* (Design of concrete anchors)

## 2.5 Summary and Conclusions

Substantial research was conducted in the past to study the bond stress-slip behaviour of concrete reinforcement by means of bond tests. The bond tests are generally carried out on concrete reinforcement with an incremental bonded length

for which a uniform bond stress distribution over the entire length can be assumed. While bond tests are typically conducted on concrete reinforcement with bonded lengths smaller than $10\phi$, the bond behaviour of bonded anchorings, e.g. cast-in-place or post-installed reinforcing bar anchorages, can be described by the uniform bond model for bonded lengths up to $25\phi$.

Five important influencing factors have been identified to be relevant for column-to-foundation connections under seismic loading:

- Effect of transverse concrete compression
- Effect of parallel concrete cracks
- Effect of inelastic steel strain
- Damage effect of load cycling
- Damage effect of crack cycling

The influence of crack cycling on the performance of reinforcing bars was not tested yet under seismic relevant boundary conditions. However, from crack movement tests conducted on post-installed reinforcing bars and anchors it is well known that crack cycling is very demanding. In conclusion, the adverse effect of seismically induced crack cycling on the bond behaviour of reinforcing bars needs to be carefully investigated.

The decomposed modelling of the bond-zone material and stress state influencing factors is suitable for numeric approaches which analyse the influencing factors using separate algorithms and superpose the results. To date, however, the influence of crack cycling on the bond strength was not studied by means of the finite element method (FEM). *Mullapudi, T. (2004)* simulated the load bearing behaviour of headed bolts in uncracked and cracked concrete. Acceptable results were generated only for monotonic loading. Though headed bolts are insensitive to cracks because of the load transfer by means of mechanical interlock, intensive calibration of an elastic buffer layer was required to achieve reasonable results for the simulation of the load-displacement behaviour for cracked concrete where crack width remained constant. *Simons, I. (2007)* dedicated a chapter to the numerical study of concrete reinforcement located in parallel cracks. However, the used finite element model did not simulate concrete cracking. Instead, the basic bond stress-slip curve was factored to mimic the reduced bond strength.

Post-installed reinforcing bar anchorages may be designed as cast-in-place anchorages according to *Eurocode 2 (2005)* if the post-installation system is qualified according to *EOTA TR 023 (2006)*. However, limitations in respect to concrete cover and clear spacing of the bars have to be met. Alternatively, post-installed reinforcing bar anchorages may be designed as bonded anchors according to *CEN/TS 1992-4-5*

*(2009)* if the post-installation system is qualified according to *ETAG 001 (2006)*. In summary, the reinforced concrete design codes provide two alternative approaches to design anchorages. The bonded anchor design potentially allows anchorage lengths which are reduced if compared to the conventional anchorage design.

Strut-and-tie models (STM) are suitable for the design of column-to-foundation connections. However, the critical detail is the anchoring of starter bars without hook. Several STM approaches proposed in the literature turned out to be impracticable or unconservative. Therefore, the bonded anchor design provisions are a promising alternative. In this case, the beneficial effect of the moment loading and the adverse effect of cyclic loading on the column-to-foundation connection capacity have to be considered. In particular the adverse effect of cyclic loading was not yet properly studied because the damage effect of crack cycling was not taken into account.

The chapter concluded with the recommendation of further literature collecting the findings of the international research community regarding the bond behaviour of cast-in-place and post-installed reinforcing bars as well as reinforced concrete members and structures under seismic loading.

# 3 Research Approach and Background

After some introductory notes in Section 3.1, exploratory crack cycling tests on cast-in-place and post-installed reinforcing bars are presented in Section 3.2. The effect of cyclic loading on column-to-foundation connections and the distribution of bond stress along the anchorage is examined in detail in Section 3.3. The concluded investigative steps required to develop a sound design concept for post-installed column-to-foundation connections is presented in Section 3.4. The key points are summarised in Section 3.5.

## 3.1 Introduction

As pointed out in Section 1.2, additional ground floor columns are a premier retrofit solution for moment resisting reinforced concrete frame structures (Figure 3.1a). The critical detail of post-installed column is the connection to the foundation. While cast-in-place column starter bars are commonly detailed with hooks in order to meet the requirements with respect to anchorage length (Figure 3.1b1), post-installed column starter bars have to be installed without hooks (Figure 3.1b2).

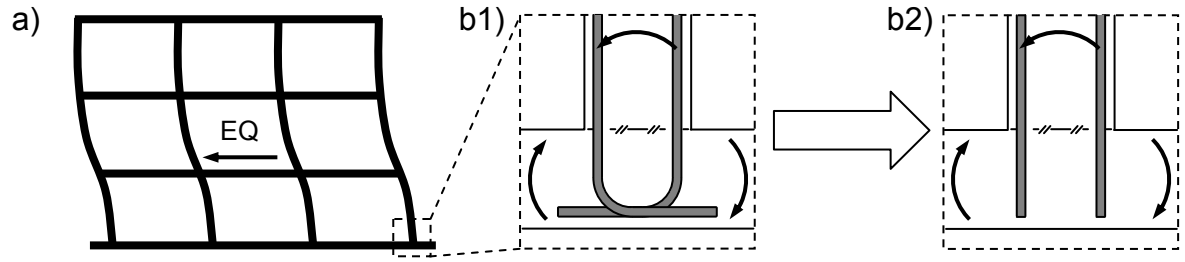


Figure 3.1 Column-to-foundation connection: a) Moment resisting reinforced concrete frame structure; b1) Anchorage with hook; b2) Anchorage without hook (after *Mahrenholtz, C.; Eligehausen, R.; Hofmann, J. (2011)*)

The limited member depth of the foundation inhibits long anchorage lengths required if designed as a conventional anchorage without hooks according to reinforced concrete design codes (Section 2.3.1.1). Excess reinforcement to reduce the required anchorage length cannot be used because most reinforced concrete design codes do not allow excess reinforcement for columns under seismic loading. Furthermore, excess reinforcement is uneconomic and difficult to be accommodated in small column cross sections.

Therefore, the objective of this thesis is to facilitate the design of column-to-foundation connections as a bonded anchor group (Section 2.3.1.2), paying particular attention to two effects:

- The beneficial effect of moment loading on the connection capacity (Section 2.3.3) which potentially allows the reduction of the anchorage length to the extent that hooks can be omitted for column-to-foundation connections.
- The adverse effect of cyclic loading on the connection capacity (Section 2.3.4) which requires sufficient long anchorages better coping with the seismic conditions present in the core of the connection.

As will be pointed out in Section 3.3, the seismic conditions are characterised by load cycling and crack cycling. Since the effect of crack cycling on the steel-concrete-bond was not studied to date considering seismic conditions, exploratory tests were conducted to evaluate the significance of the crack cycling effect.

## 3.2 Exploratory Tests on Bond Behaviour during Seismic Crack Cycling

One key conclusion of the literature review was that crack cycling strongly impairs the performance of anchorages (Section 2.2.14). However, this phenomenon was not investigated yet for reinforcing bars under seismic conditions. In fact and as pointed out in *Paulay, T.; Priestley, N. (1992)*, the conditions of the concrete surrounding embedded bars, in particular where extensive cracking may occur as a result of ineleastic response, are often inferior to those which prevailed in test specimens from which empirical code-specific rules for bar anchorages have been derived. To evaluate the damage effect of seismic crack cycling on cast-in-place reinforcing bars and reinforcing bars post-installed with epoxy mortar, two exploratory test programs were conducted which test parameters considered seismic conditions.

The test setup and procedure of the first exploratory test program (*Mahrenholtz, C. (2009d)*) were based on the provisions for the crack movement tests on anchors given in the qualification guideline for post-installed anchors, *ETAG 001 (2006)*, which was modified to serve for the purpose of seismic testing. The original intention of crack movement tests is to assess the functioning of post-installed anchors located in cracks which width is subject to changes due to moving live loads. *ETAG 001 (2006)* defines 1000 crack cycles between the maximum crack width of 0.3 mm and the minimum crack width of 0.1 mm.

Cast-in-place and post-installed reinforcing bars diameter $\phi$ = 12 mm and $\phi$ = 20 mm were tested. Epoxy mortar was used and the bonded length equalled $\ell_b = 8\phi$. Reference tests were conducted on reinforcing bars installed in wedge-split concrete members (Figure 3.2a). These concrete members were designed to allow for the generation and control of static cracks by means of wedges driven into sleeves

placed in preformed holes in the slab. The pullout tests yielded the monotonic capacity as the mean ultimate failure load $N_{u,m}$.

Strain concrete members were used for the crack cycling tests (Figure 3.2b). These concrete members allow the variation of crack width by pulling and releasing the longitudinal reinforcement by means of an actuator. This crack generation method is introduced in Section 4.2.1 in more detail. All four test locations of the strain concrete members were used at a time, making one test series. *Hoehler, M. (2006)* reported technical difficulties to generate a constant load by means of pressure controlled hydraulic cylinders. Therefore, disc springs sets were employed to generate the constant load $N_w$ (Figure 3.2c).

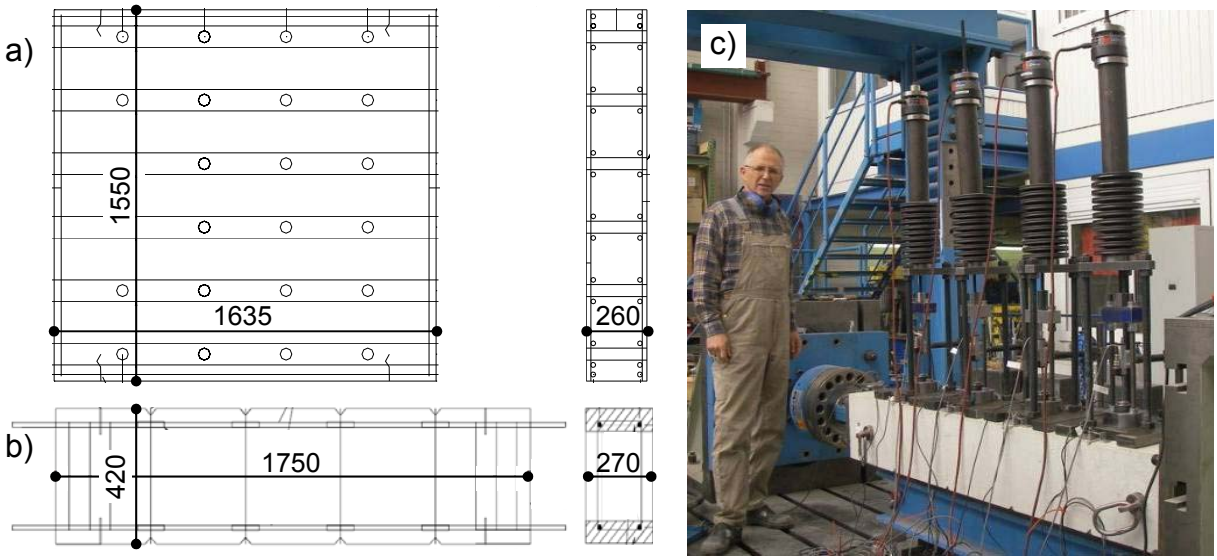


Figure 3.2 a) Wedge split concrete members; b) Strain concrete member; c) Setup 1st exploratory test program on crack cycling

The constant load $N_w$ (Figure 3.3a) was defined on the basis of the monotonic capacity as $0.4N_{u,m}$ yielding the targeted constant bond stress $\tau_w = 0.4\tau_{u,m}$. Contrary to the crack movement tests according to *ETAG 001 (2006)*, the tested maximum crack width $w_{max}$ was 0.8 mm, and the minimum crack width $w_{min}$ was taken as full crack closure assumed for a compression stress $0.15f_c$ over the cross section area. The definition of the maximum and minimum crack width represented seismic conditions and was based on considerations presented in Section 4.3.2.

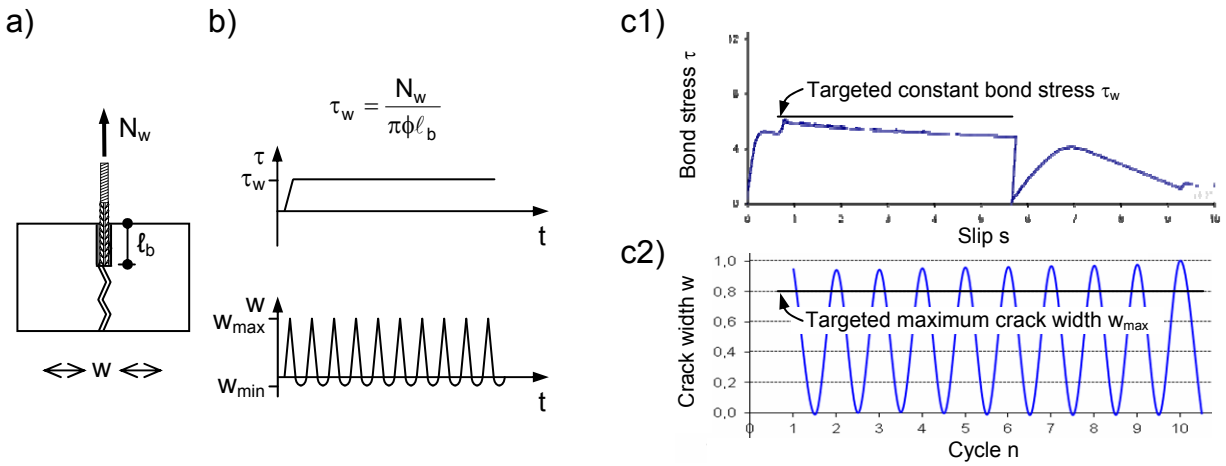


Figure 3.3 a) Crack cycling test at constant load; b) Constant bond stress $\tau_w$ and cyclic crack width between peak crack widths $w_{max}$ and $w_{min}$ versus time t; c) Measured bond stress and crack width (example after *Mahrenholtz, C. (2009d)*)

Establishing an experimentally determined relationship of actuator force and crack width allowed to run the test force controlled. The tested reinforcing bar was initially loaded by $N_w$ and then the crack cycled 10 times (Figure 3.3b). After completion of 10 cycles, the reinforcing bar was pulled out to determine the residual load capacity. The load, slip and crack width were measured (Figure 3.3c). Further details on the tests including the detailed discussion of the magnitude of the constant load $N_w$ can be found in *Mahrenholtz, C. (2009a)*.

The key findings of the conducted tests were:

- At least one test per series conducted on cast-in-place reinforcing bars experienced a premature failure (Figure 3.4a).
- On the contrary, post-installed reinforcing bars coped with the demanding test if the maximum crack width was not larger than 0.5 mm, however, the residual pullout capacity was reduced to about 30 % if compared to the reference pullout capacity (Figure 3.4b).

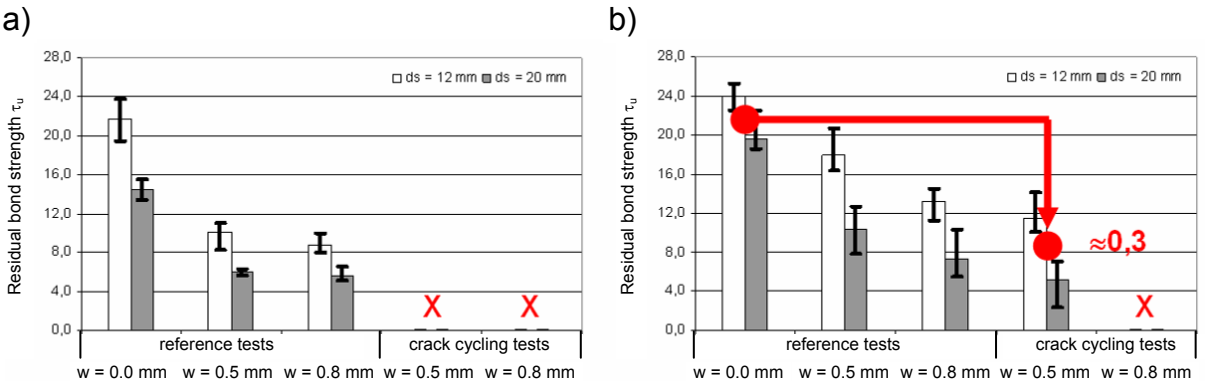


Figure 3.4 Test results of crack cycling tests at constant bond stress $\tau_w$ (*Mahrenholtz, C. (2009d)*): a) Cast-in-place reinforcing bars; b) Post-installed reinforcing bars

The poor performance in particular if compared to the results of load cycling tests on equivalent reinforcing bars demonstrates the high demands crack cycling is putting on reinforcing bars. High compression forces combined with large crack width results in a pronounced damage of the bond and slipping of the bar.

In conclusion, crack compression and large crack widths to be anticipated for seismic loading are critical, demonstrating that cast-in-place and post-installed reinforcing bars are more sensitive to crack cycling than to load cycling. Furthermore, the reinforcing bars post-installed with the used epoxy mortar performed better than the cast-in-place reinforcing bars.

The tests further revealed that the employed test setup (Figure 3.2c) is unsuitable to carry out crack cycling tests with the required precision:

- The targeted constant bond stress $\tau_w$ was not achieved within reasonable limits (Figure 3.3c1).
- The targeted maximum crack width $w_{max}$ was not met accurately (Figure 3.3c2).
- In addition, the use of one concrete member for the complete test series resulted in increased scatter because the cracks of the four testing positions developed differently (CV = 20 %).

To achieve reliable and reproducible results, the necessary improvements were identified as follows:

- One servo controlled actuator is needed to apply a constant load on the reinforcing bar during crack cycling.
- Another servo controlled actuator is required to control the crack width cycling based on real time crack width measurement.

- The approach to control reinforcing bar load and crack width by means of servo controlled actuators necessitates testing of one reinforcing bar at a time.
- Further, the control system and associated IT infrastructure has to be upgraded to cope with the increased demands in respect to input and output data.

After improving the test setup and laboratory equipment, the second exploratory test program was carried out (*Mahrenholtz, C. (2011b)*). To reduce the influence of systematic scatter, a specially developed concrete member accommodating a single testing position was used for the monotonic reference tests and cyclic tests. The diameter of the cast-in-place reinforcing bars was 16 mm and the bonded length 5$\phi$. The test specimen and the test setup were similar to the test setup introduced in Section 4.2.2 and is therefore not explained in detail here. Figure 3.5a shows a photo of setup and specimen.

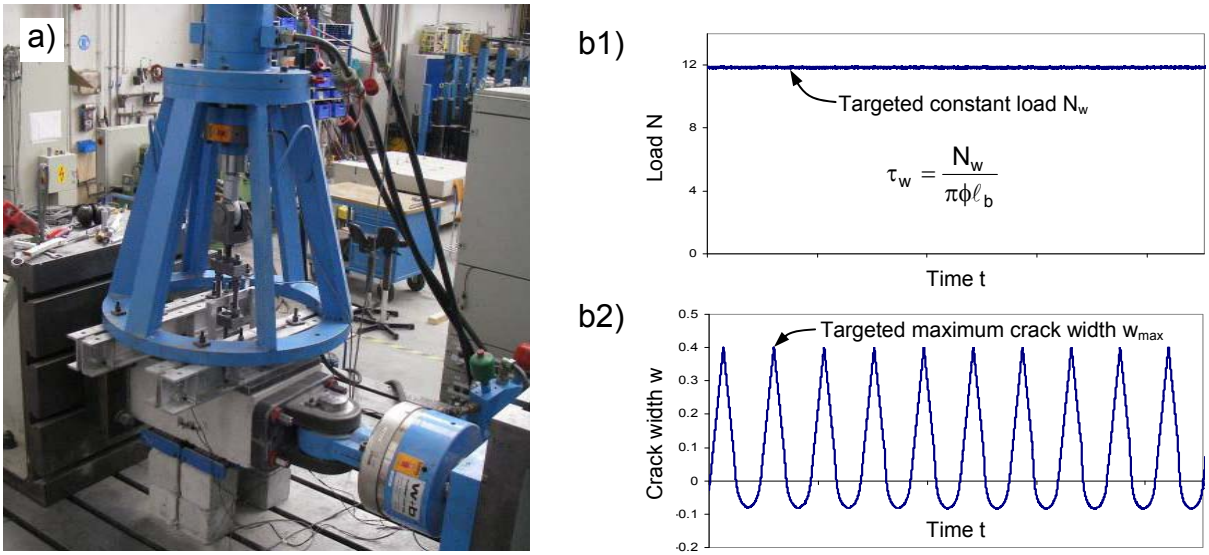


Figure 3.5 a) Setup 2nd exploratory test program on crack cycling; b) Measured load and crack width (example after *Mahrenholtz, C. (2011b)*)

In principle, the procedure of the testing remained unchanged (Figure 3.3a and Figure 3.3b). The diagrams shown in Figure 3.5b demonstrate the high accuracy the enhanced test setup is able to facilitate. The improved test setup made the generation of an absolute constant load possible (Figure 3.5b1) and prevented that the crack width overshoots the critical target $w_{max}$ (Figure 3.5b2).

Three different constant bond stress levels $\tau_w$ were defined for the cyclic tests which equalled 0.25, 0.50 and 0.75 multiples of the mean bond strength $\tau_{u,m}$ determined in monotonic reference tests. The crack cycling was continued till failure occurred. The bond stress-slip curves are shown in Figure 3.6a and the slip-time histories in Figure 3.6b.

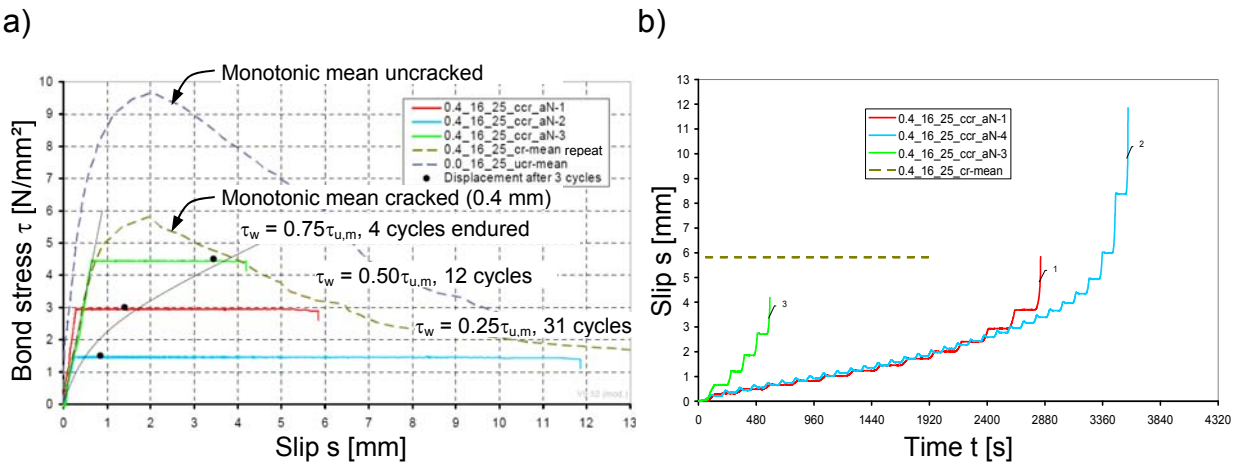


Figure 3.6 a) Bond stress-slip curves of crack cycling tests under constant bond stresses $\tau_w$ and b) slip versus time curves (*Mahrenholtz, C. (2011b)*)

Pullout failure occurred when the bond stress-slip curve of the crack cycling test came close to the bond stress-slip curve of the monotonic mean of the reference tests. Lower constant bond stresses $\tau_w$ resulted in smaller slips per cycle and in larger endurable slip before transecting the monotonic bond stress-slip curve. If the mean ultimate bond strength was utilised by 50 %, which is about the design load level (Section 9.1), only 12 cycles were completed.

In conclusion, the bond degradation effect of crack cycling was confirmed and requires further attention. The improved test setup enables the precise investigation of the damage effect.

## 3.3 Column-to-Foundation Connection Behaviour under Seismic Loading

In regions prone to strong earthquakes, the seismic load case governs the reinforcement design of columns and therefore requires careful consideration. The seismic excitation of a structure causes alternating bending moments, resulting in cyclic loading of the reinforcing bars and cyclic variation of the crack widths in reinforced concrete structures. In joints, e.g. column-to-foundation connections, the cracks may run along the starter bar anchorages. Therefore, phases succeed in which the starter bars are pulled and pushed while the cracks open and close (Figure 3.7a and Figure 3.7b). It is evident that load cycling and crack cycling are in the same phase and at the same frequency.

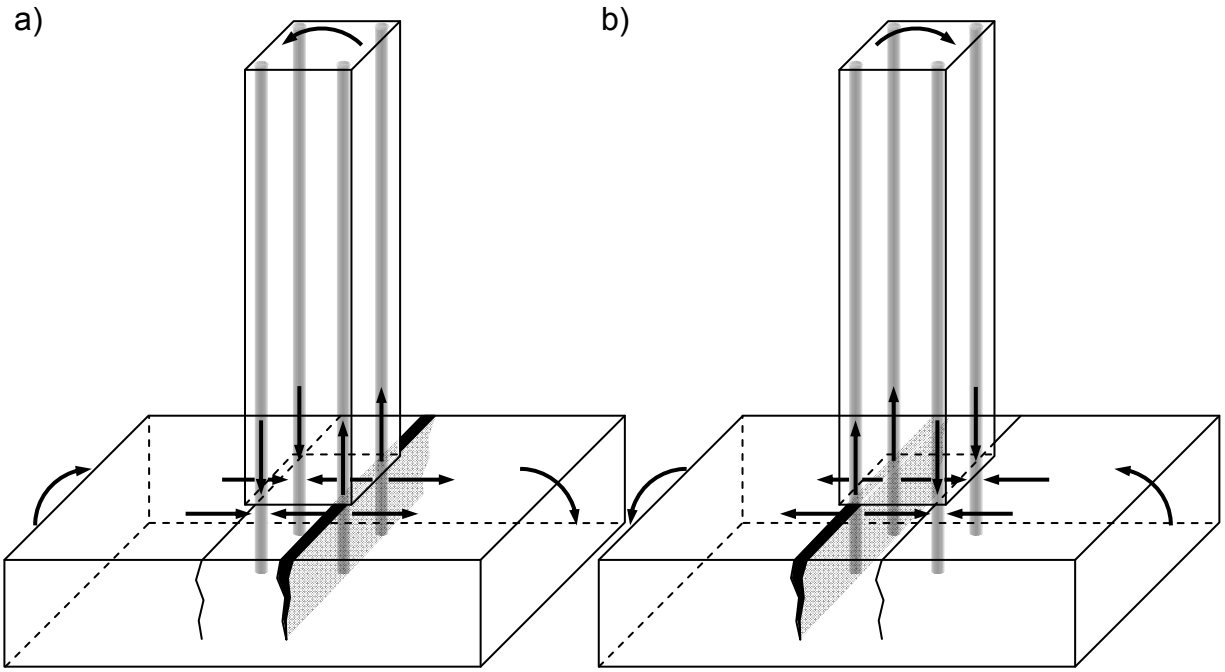


Figure 3.7 Two phases: a) Loading; b) Reversed loading

The review of the state of the art in Chapter 2 identified several effects which have a vital impact on the bond and therefore influence the capacity of anchorages. For column-to-foundation connections the anchorage capacity of starter bars is influenced by the following effects (Figure 3.8):

- Effect of transverse concrete compression: The crack is closed when the starter bar is pushed (Figure 3.8a) which increases the bond strength (Section 2.2.10).
- Effect of parallel concrete cracks: The crack is opened when the starter bar is pulled (Figure 3.8b) which reduces the bond strength (Section 2.2.11).
- Damage effect of simultaneous load and crack cycling: The repetition of loading (Figure 3.7a) and reversed loading (Figure 3.7b) of the connection causes load cycling and crack cycling (Figure 3.8c) which results in accumulating bond damage (Section 2.2.13 and Section 2.2.14).
- Effect of inelastic steel strains: Irrespective of the cracks, the exceedance of the yield strength in the starter bar (Figure 3.8d) reduces the bond strength (Section 2.2.12).

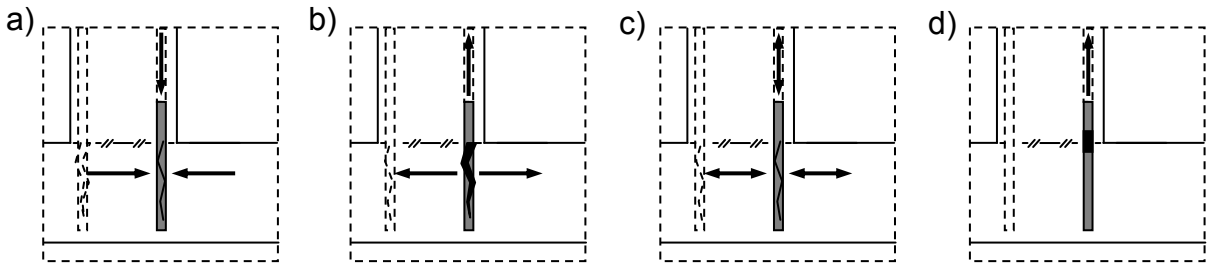


Figure 3.8 a) Effect of parallel concrete compression; b) Effect of transverse concrete cracks; c) Damage effect due to simultaneous load and crack cycling; d) Effect of inelastic steel strains

The effects also occur at code compliant anchorages with hooks, however, may then be considered as secondary since the tensile load of the starter bar can be transferred completely by the mechanical interlock of the hook. On the contrary, anchorages without hooks completely rely on the bond and are for this reason sensitive to bond damage effects.

Compression stress, crack width, and therefore the bond damage as well as the steel stress are not uniformly distributed over the anchorage length. The starter bar anchorage of the column-to-foundation connection (Figure 3.9a) is shown schematically in Figure 3.9b at the beginning of loading. For the sake of clarity it is pointed out that the starter bar location at the interface of column and foundation is termed loaded end of the anchorage though the reinforcing bar is not ending at that point. The actual end of the starter bar is termed unloaded end though the adjacent section of the bar is increasingly stressed because of increasing bond redistribution.

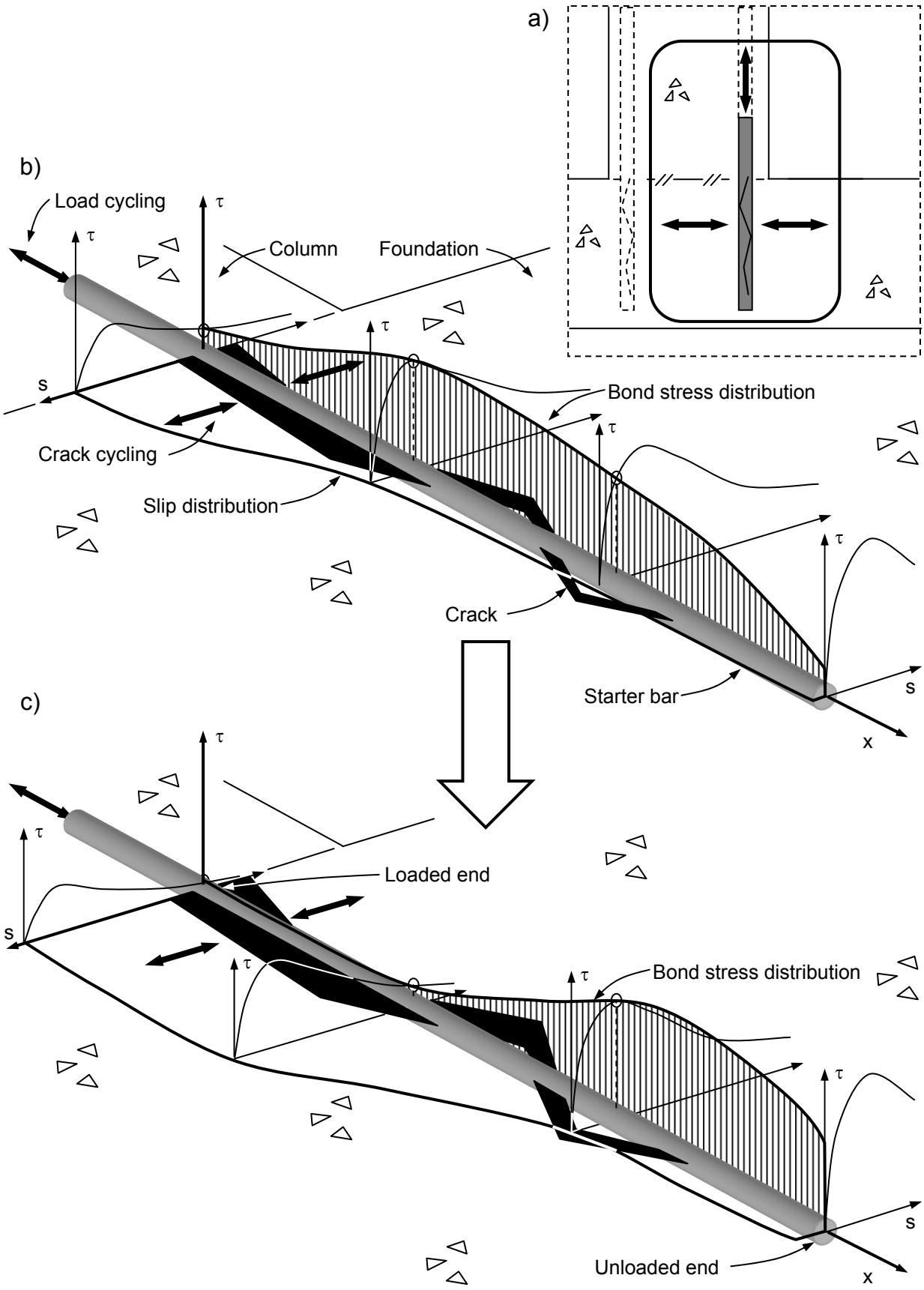


Figure 3.9 a) Column-to-foundation connection; Isometric view on starter bar anchorage of b) at the beginning of loading and c) after propagated damage, illustrating the redistribution of bond stresses from loaded to unloaded end

The momentary bond stress-slip curves are sketched for four locations of the anchorage which differ because of the

- momentary transverse concrete stress, which effect is expressed by the factor $\Omega_c$ (Section 2.2.10),
- momentary parallel concrete cracks, which effect is expressed by the factor $\Omega_w$ (Section 2.2.11),
- accumulated bond damage due to previous load cycling, which effect is expressed by the factor $\Omega_{cyc}$ (Section 2.2.13), and
- momentary inelastic steel strain, which effect is expressed by the factor $\Omega_s$ (Section 2.2.12).

The bond stress-slip curve describing the bond behaviour at the unloaded end of the anchorage is the virgin bond stress-slip curve, whereas the bond stress-slip curve at the loaded end of the anchorage is significantly reduced since it is the maximum loaded location with the most pronounced accumulated damage caused by load cycling and crack cycling. This leads to the question whether the existing bond model which includes the hysteretic energy model is capable to describe this more pronounced damage.

Continuous loading of the connection damages primarily the bond at the loaded end but the bond damage propagates to the unloaded end of the anchorage. Consequently, the load transfer by bond is increasingly redistributed to the unloaded end as illustrated in Figure 3.9c. Since simultaneous load and crack cycling damages the bond, the hypothesis is formulated that those column-to-foundation connections under cyclic loading experience a more pronounced redistribution of the bond stresses towards the unloaded end if compared to column-to-foundation connections under monotonic loading.

## 3.4 Investigative Steps

Enhancing the existing bonded anchor design provisions in order to develop a design concept for column-to-foundation connections where starter bars are detailed with reduced anchorage length, requires a solid research approach. As indicated in Section 1.3, the problem is solved by splitting up the task into several steps of experimental and numerical investigations, including bond tests on the reinforcing bar increments and large scale tests on column-to-foundation connections (Figure 3.10).

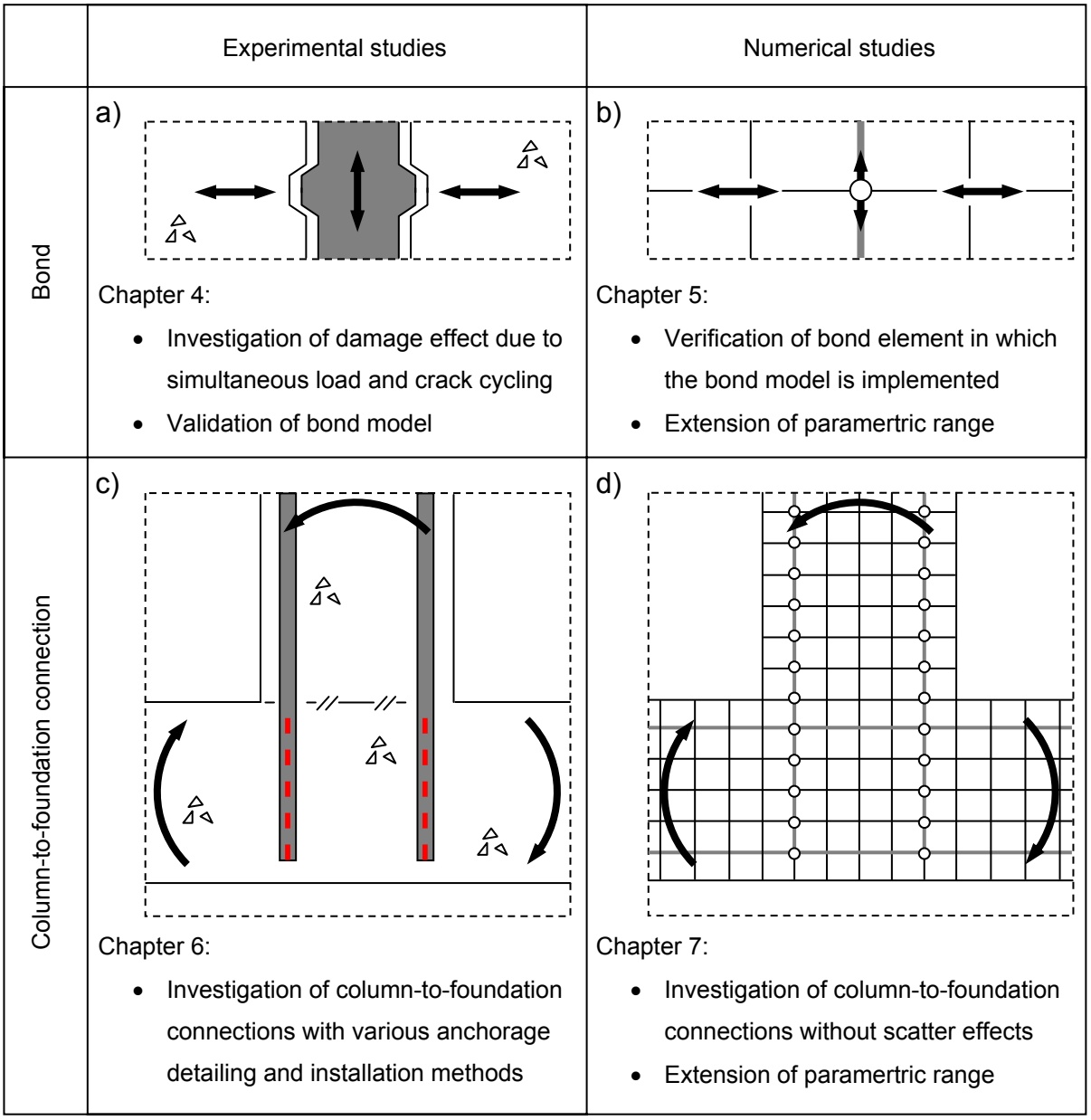


Figure 3.10 Investigative steps of experimental and numerical studies

First, the bond of concrete reinforcement is experimentally investigated under seismically relevant conditions (Figure 3.10a). Therefore, bond tests are carried out where the boundary conditions of the test setup reflect seismic conditions in terms of transverse compression, parallel cracks, as well as simultaneous load and crack cycling. The aim is to validate a bond model as a seismic bond model which takes into account all bond influencing factors relevant for seismic applications. This investigative step is discussed in Chapter 4.

Second, the seismic bond model implemented in a finite element program allows numerical studies on bond of concrete reinforcement increments (Figure 3.10b). By comparing the numerical with the experimental test results, the correct functioning of

the bond model is verified. Further simulations extend the parametric range of its application. This investigative step is discussed in Chapter 5.

Third, large scale experimental tests on column-to-foundation connections are carried out (Figure 3.10c). The studies deliver valuable data for evaluating the seismic performance of column-to-foundation connection anchorages and for benchmarking numerical simulations of column-to-foundation connections. Comparing the performance of cast-in-place and post-installed anchorages allow the development a general understanding of substandard column-to-foundation connection anchorages. This investigative step is discussed in Chapter 6.

Fourth, numerical studies on column-to-foundation connections are conducted by means of the finite element program (Figure 3.10d) using the seismic bond model already employed for the simulations on reinforcing bar increments. The cost effective numerical simulations make extensive investigations within a large parametric range and free of stochastic influences possible. This investigative step is discussed in Chapter 7.

The findings eventually allow coming up with a design concept for column-to-foundation connections based on enhanced bonded anchor design provisions. The design concept is primarily developed for post-installed column-to-foundation connections, but is also beneficial in the construction of cast-in-place column-to-foundation connections because it helps to reduce reinforcement congestions in the joint. Especially reinforcement conflicts in joints make the installation of reinforcing bars difficult and hamper the concrete flow during casting (e.g. *Lee, H.-J.; Yu, S.-Y. (2009)*, *Shakya, K.; Matsumoto, K. et al. (2012)*). The avoidance of honeycombing and therefore corrosion is particularly important for foundations which inaccessible underneath lies below the groundwater table. For this reason, headed bars have been proposed in the past (e.g. *Wallace, J.; McConnell, S. et al. (1998)*, *Chun, S.-C.; Oh, B.; Lee, S.-H.; Kang, H.-K. et al. (2009)*, *Chun, S.-C.; Oh, B.; Lee, S.-H.; Naito, C.-J. (2009)*, *Kang, H.-K.; Shin, M. et al. (2009)*). However, straight anchorages without heads are even less obstructive and can be post-installed.

## 3.5 Summary

Column starter bars of post-installed column-to-foundation connections have to be detailed without hooks. The resulting standard anchorage lengths according to the conventional anchorage design provisions (Section 2.3.1.1) cannot be accommodated in the foundation. The aim is therefore to enhance the bonded anchor design provisions (Section 2.3.1.2) by taking the beneficial effect of the moment loading on the connection capacity into account which may allow a sufficient reduction of the required anchorage length. The enhanced bonded anchor design

provisions could also be used for cast-in-place column-to-foundation connections. However, connections solely relying on bond are potentially at risk to fail in an unfavourable brittle fashion. Therefore, the adverse effect of cyclic loading on column-to-foundation connections capacities has to be considered.

The first ever conducted crack cycling tests on cast-in-place and post-installed reinforcing bars under seismic relevant boundary conditions yielded a number of unprecedented results. The tests showed that the damage effect of crack cycling is potentially more relevant than the damage effect of load cycling and therefore cannot be neglected. Consequently, bond tests on cast-in-place and post-installed reinforcing bars are required to verify the capability of the hysteretic energy model (*Eligehausen, R.; Popov, E. et al. (1983)*) to simulate the bond damage also for cyclic loading including crack cycling. A successful verification of the hysteretic energy model would validate the comprehensive bond model (Section 2.2.15) which includes the hysteretic energy model, as a seismic bond model.

The detailed examination of the column-to-foundation connection under cyclic loading shows that the starter bar anchorage capacity is influenced by transverse concrete compression, parallel concrete cracks, load cycling, and inelastic steel strains. In addition, the starter bar anchorage is subjected to crack cycling, an effect not yet studied. Load cycling and crack cycling are in the same phase and at the same frequency. The progressional bond damage during loading of column-to-foundation connection anchorages cause bond stress redistributions to regions where the damage is less, i.e. towards the unloaded ends. The distribution and redistribution of bond stress along anchorages depends on the bond influencing effects and is assumed to be more pronounced for cyclic loading if compared to monotonic loading. Since the bond stresses are not distributed uniformly, the bond behaviour has to be studied incrementally with respect to the distance from surface, momentary state of stress, and damage history.

Finally, the investigative steps of the research approach were outlined, illustrating the roadmap to achieve the aim of a sound design concept for column-to-foundation connections where starter bars are detailed without hooks and with potentially reduced, i.e. substandard anchorage lengths.

# 4 Experimental Studies on Bond

In this chapter, the experimental studies carried out at the IWB Laboratory of the University of Stuttgart to investigate the bond behaviour of seismically loaded reinforcing bars are presented. The aim of the studies was to verify a seismic bond model and to collect test data allowing the benchmarking of numerical studies presented in the following chapter. Some instructive notes on the employed instrumentation are given in Section 4.1. The experimental setup is introduced in Section 4.2. Following this, the experimental procedure including test parameters and test program as well as the load protocol are described in Section 4.3. The test results are discussed in Section 4.4. Finally, Section 4.5 summarises the key findings and conclusions of the experimental studies. The complete experimental test program of the studies on bond is reported in *Mahrenholtz, C. (2011b)*.

## 4.1 Basics

The setup introduced in Section 4.2 is based on the experience gained in the course of exploratory crack cycling tests on cast-in-place and post-installed reinforcing bars (*Mahrenholtz, C. (2009d)*) as well as crack cycling tests on post-installed anchors (*Mahrenholtz, C. (2009e)*, *Mahrenholtz, C.; Sharma, A. (2010)*). The finally employed instrumentation introduced in the following is generally recommended for tests on reinforcing bars and anchors. A comprehensive description of crack cycling tests can be found in *Mahrenholtz, C.; Silva, J. et al. (2012)*.

The simultaneous load and crack cycling tests presented in this chapter are displacement controlled by reinforcing bar slip and crack width. Both parameters are in the range of a millimetre. In order to gain micrometer accurate input signals for the servo control system, attention was paid on the measurement accuracy of crack width and reinforcing bar slip.

### 4.1.1 Crack width measurement

The qualification guidelines for post-installed anchors *ETAG 001 (2006)* as well as *ACI 355.2 (2007)* and *ACI 355.4 (2010)* suggest to measure the crack width using two transducers mounted on either side of the anchor. Placing the electronic transducers on top of the concrete member may lead to wrong estimates of the crack width at the level of bonded length due to the geometric inaccuracies of the concrete member and test setup (Figure 4.1a). For this reason, the two transducers mounted

on the sides of the concrete member, at the level of the bonded length are preferable (Figure 4.1b). To achieve the highest accuracy possible however, in total four transducers were employed for the simultaneous load and crack cycling tests introduced in this chapter. The centroid of the four transducers coincided with the centre of the bonded length (Figure 4.1c). The transducers were installed in aluminium mounting blocks glued by hot glue to the concrete member. The sensor heads extended to aluminium target angles attached to the concrete test member on the other side of the crack.

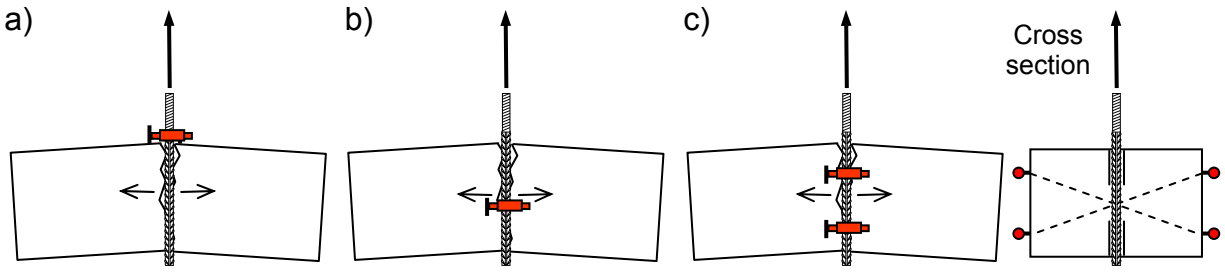


Figure 4.1 Measuring crack widths: a) Two transducers mounted on top; b) Two transducers attached on the sides; c) Four transducers to achieve best accuracy

### 4.1.2 Reinforcing bar slip measurement

Different technical solutions for measuring the reinforcing bar slip may be used. For example, *Spieth, H. (2003)* and *Simons, I. (2007)* used two transducers connected by a cantilever construction to the fixation of the reinforcing bar (Figure 4.1a). The slip was estimated by averaging the measurements of both transducers. However, the relative flexibility of the cantilever construction makes this solution less accurate. An alternative is to install the transducer on a heavy support construction (Figure 4.1b). A cable is connected to the transducer at one end, passes over a small sheave, and is connected to a magnet resting on the top of the reinforcing bar. This solution is more accurate, but only if the slip, stiffness, and eccentricities in the cable, sheave, and the connections are reduced to a minimum. As accuracy is paramount for this study, the simultaneous load and crack cycling tests presented in this chapter were carried out with the transducer mounted to a frame that bridges the crack. The sensor head of the transducer directly touched the reinforcing bar. To avoid the computational elimination of the elastic elongation of the reinforcing bar between the loaded end and the bonded length, the slip was measured at the unloaded end (Figure 4.1c). The frame was made of aluminium profiles which were fixed by hot glue to the concrete member. The hot glue was also used to connect the horizontal bar to the vertical poles. This solution allowed an easy adjustment of the system and once the hot glue was hardened, provided rigidity and stiffness.

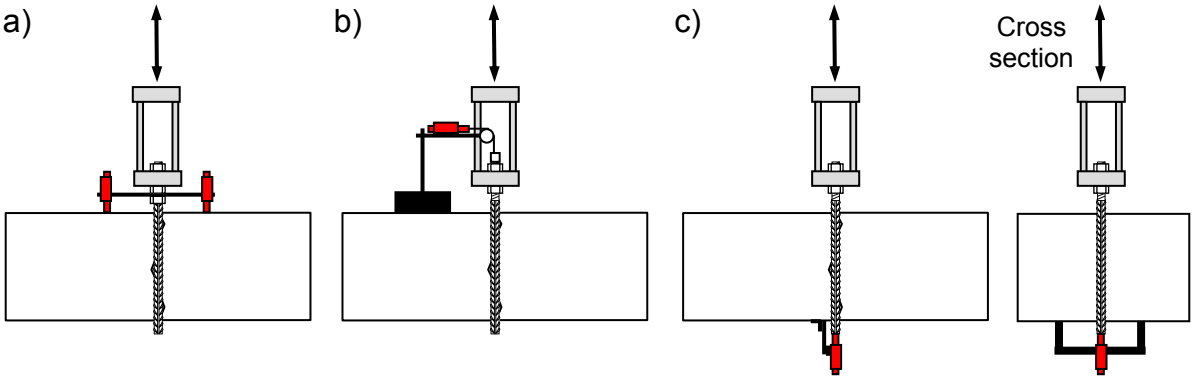


Figure 4.2 Measuring reinforcing bar slip: a) Cantilever construction; b) Heavy support construction; c) Frame with attached transducer and sensor head directly touching the reinforcing bar

## 4.2 Experimental Setup

### 4.2.1 Test specimens

For the experimental tests, reinforcing bars were either cast-in-place or post-installed in reinforced concrete members. The unit of concrete member and reinforcing bar used for testing is in the following termed ‘test specimen’. The reinforcing bars were physically debonded at top and bottom (Figure 4.3a). The debonding enabled a slip of the reinforcing bar along the bond free length. The bonded length was for all tests $5\phi$ for which the assumption of a constant bond stress generally applies (Section 2.2.2). The debonded length was for 16 mm reinforcing bars $5\phi$ to eliminate the influence of the confined setup on the bond strength (Section 2.2.2). The debonded length was increased or decreased for tests on 12 mm or 25 mm reinforcing bars respectively, according to the height of the test specimens.

The dimension of all concrete members was L / W / H = 600 mm / 400 mm / 240 mm (Figure 4.3b). The concrete members were reinforced by stirrups, and longitudinally placed high strength tie rods protruded at both ends. Two pilot holes and two thin metal sheets were provided in the centre at both sides to aid crack formation. The tie rods were debonded on both sides of these crack inducers to promote large cracks. Further information on the design of concrete members for cyclic testing can found in *Mahrenholtz, C. (2010)*. The specimens were manufactured by the precast company Rau, Ebhausen.

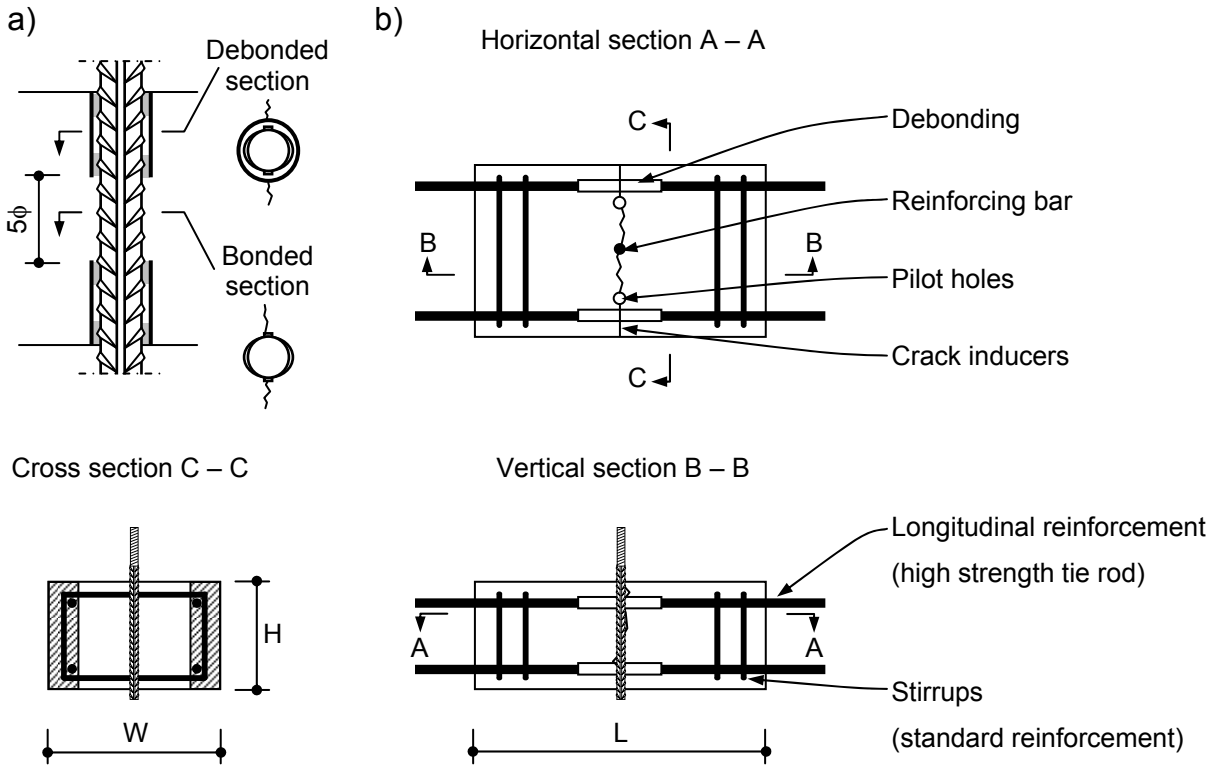


Figure 4.3 Layout of test specimen: a) Detail of reinforcing bar; b) Geometry and reinforcement (after *Mahrenholtz, C.; Eligehausen, R.; Hofmann, J. et al. (2011)*)

#### 4.2.1.1 Reinforcing bars

The tested B500B reinforcing bars complied with *DIN 488-1 (1986)* specifying a yield strength of $R_p = f_{yk} = 500$ MPa and an ultimate strength of $R_m = f_{uk} = 550$ MPa. Class B500B was used because it is the most common type in Europe. The loaded end of the reinforcing bars was threaded to allow a connection to the loading device. The reinforcing bars were cast-in-place in a horizontal position or post-installed. The measured mean related rib areas are given in Table 4.1. The stress-strain diagram was not determined for the used reinforcing bars because the loading stressed the reinforcing bars within the elastic range only ($\sigma < 0.4 f_y$). However, Figure 4.4 shows an example stress-strain diagram of a typical B500B reinforcing bar provided by the steel mill company BSW.

Table 4.1 Related rib area

| Diameter [mm] | Related rib area $f_R$ [-] |
|---|---|
| 12 | 0.06 |
| 16 | 0.07 |
| 25 | 0.08 |

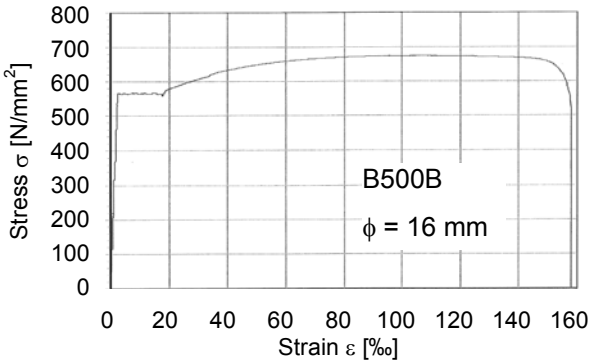


Figure 4.4 Typical stress-strain diagram

#### 4.2.1.2 Concrete

The concrete members were made of normal weight concrete C20/25 according to *Eurocode 2 (2005)* with a target concrete compressive strength of $f_{ck}$ = 20 MPa. The concrete members were produced according to *DIN 1045 (2001)* and *DIN 1048 (1991)* and reached a mean tested concrete compressive strength between $f_c$ = 19.2 and 24.3 MPa. Concrete class C20/25 was chosen because it is the most common type in Europe. The tested concrete strengths $f_c$ are given in Table C.1 and C.2 of Appendix C: Bond Test Data.

#### 4.2.1.3 Bond (mortar)

For tests on post-installed reinforcing bars, a two component mortar based on epoxy resin suitable for the post-installation of anchors and reinforcing bars was used. In Europe, the injection type system is approved for the post-installation of reinforcing bars. In addition, the mortar is approved for the post-installation of bonded anchors under fundamental load cases, whereas in the US, the mortar is additionally rated for the post-installation of bonded anchors at seismic applications. The installation was carried out according to the MPII (bore hole diameters $d_0$ = 16 mm, 20 mm, 32 mm for reinforcing bar diameters $\phi$ = 12 mm, 16 mm, 25 mm), and at normal ambient temperature to exclude temperature effects (Section 2.2.9). The bore hole diameter was A sophisticated installation procedure involving counter sink drilling and centring pins ensured the proper debonding and slip measuring at the unloaded end. Details of the installation procedure are given in *Mahrenholtz, C. (2011b)*.

Figure 4.5 shows close ups of the confined test setup and the pulled out reinforcing bar. The concrete consoles between the ribs of cast-in-place reinforcing bars have been crushed. The residual concrete was of powdery texture and could be easily removed by a brush with steel wires. The post-installed reinforcing bars sheared off along the perimeter of the reinforcing bar. The mortar consoles remained between the ribs and could be easily removed as limited adhesion to the smooth surface of

the reinforcing bar existed. The mean tested bond strength for diameter 16 mm bars cast-in-place and post-installed in uncracked concrete was $\tau_u$ = 7.74 MPa and $\tau_u$ = 28.15 MPa, respectively. The bond strengths are discussed in detail in Section 4.4.1 and are summarised in Table C.1 and C.2 of Appendix C: Bond Test Data.

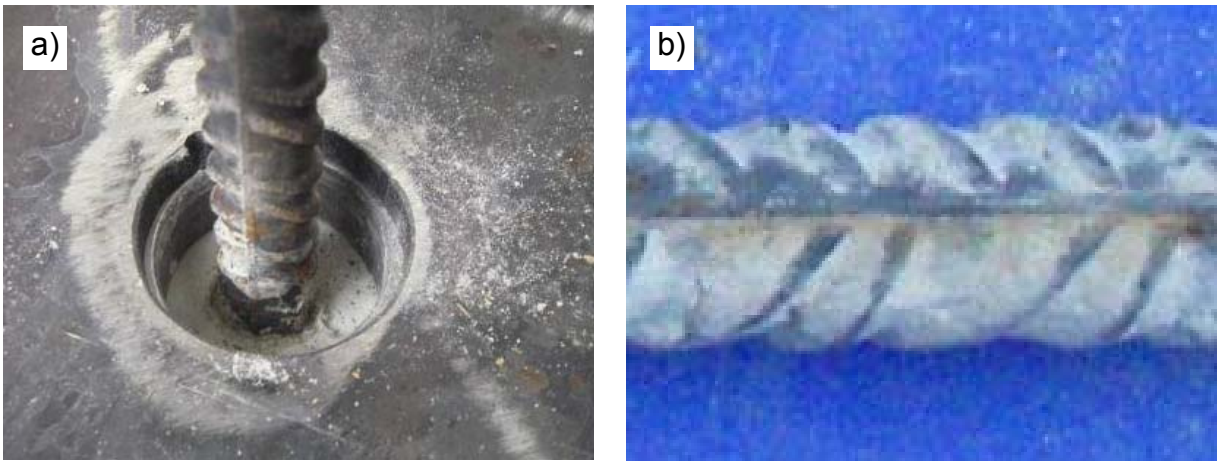


Figure 4.5 Close up of a) bearing plate for confined test setup and b) pulled out reinforcing bar (cast-in-place, as an example)

### 4.2.2 Test setup and erection sequence

Simultaneous load and crack cycling tests require that load cycling and crack cycling are controlled simultaneously. Therefore, a two axes servo control system was inevitable to process the input signal of crack width and slip measurements and to synchronise the output signal controlling the servo valves. The high demands regarding the precision of measuring reinforcing bar slip and crack width required an elaborate test setup (Figure 4.6). For the assembling of the test setup, the test specimen was sandwiched between two steel plates. The steel plates were fitted with inlets serving as bearing plates to provide a confined setup. Following, a 250 kN actuator for loading the reinforcing bar was placed with its support on the top steel plate. The support was anchored through to the bottom steel plate to get a self-equilibrated system, allowing loading the reinforcing bar cyclically. After placing the unit of test specimen, steel plate, support, and 250 kN actuator on a sliding bearing, the high strength tie rods of the concrete member were connected to the fixed bearing on one side and to a 630 kN actuator for loading the concrete member on the other side. Next, a loading device was attached to connect the reinforcing bar with the 250 kN actuator.

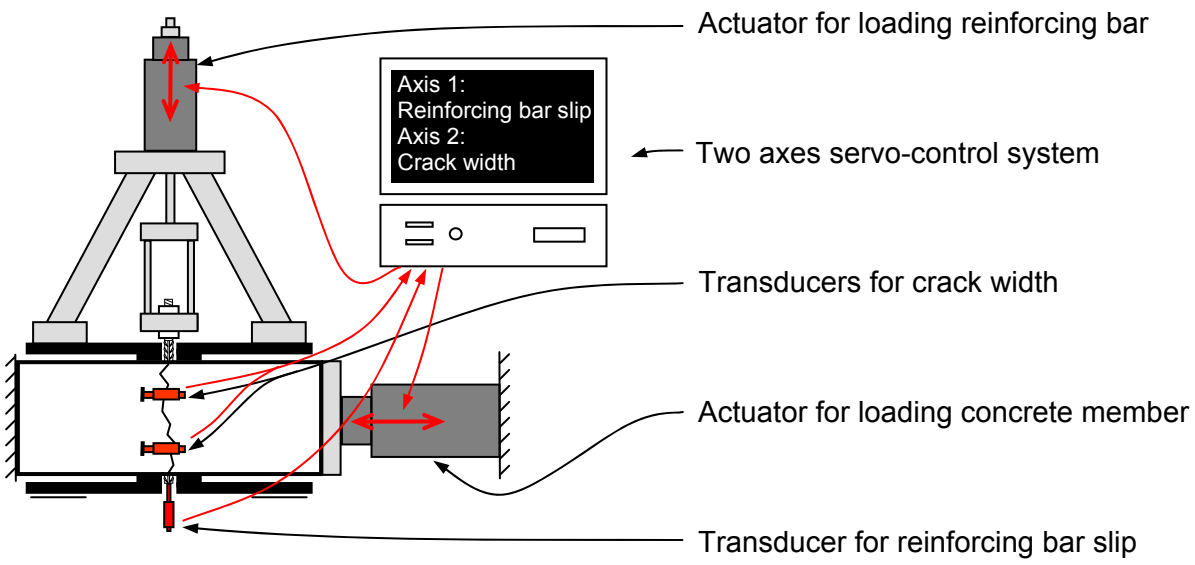


Figure 4.6 Schematic test setup

Four transducers measuring the actual crack width were installed on the sides of the concrete member. The centroid of the four points coincided with the centre of bonded length of the reinforcing bar. The averaged signal fed the servo control system to control the 630 kN actuator. A transducer measured the actual reinforcing bar slip at the unloaded end (Figure 4.7a). The signal was used by the servo control system to control the 250 kN actuator. The test setup enabled absolute symmetric boundary conditions for the pushing and pulling direction. The employed setup and servo-control system allowed displacement controlled loading. Therefore, postcritical testing (i.e. reinfocing bar slip exceeds peak bond stress) of the bond properties was feasible. Figure 4.7b shows the completed test setup.

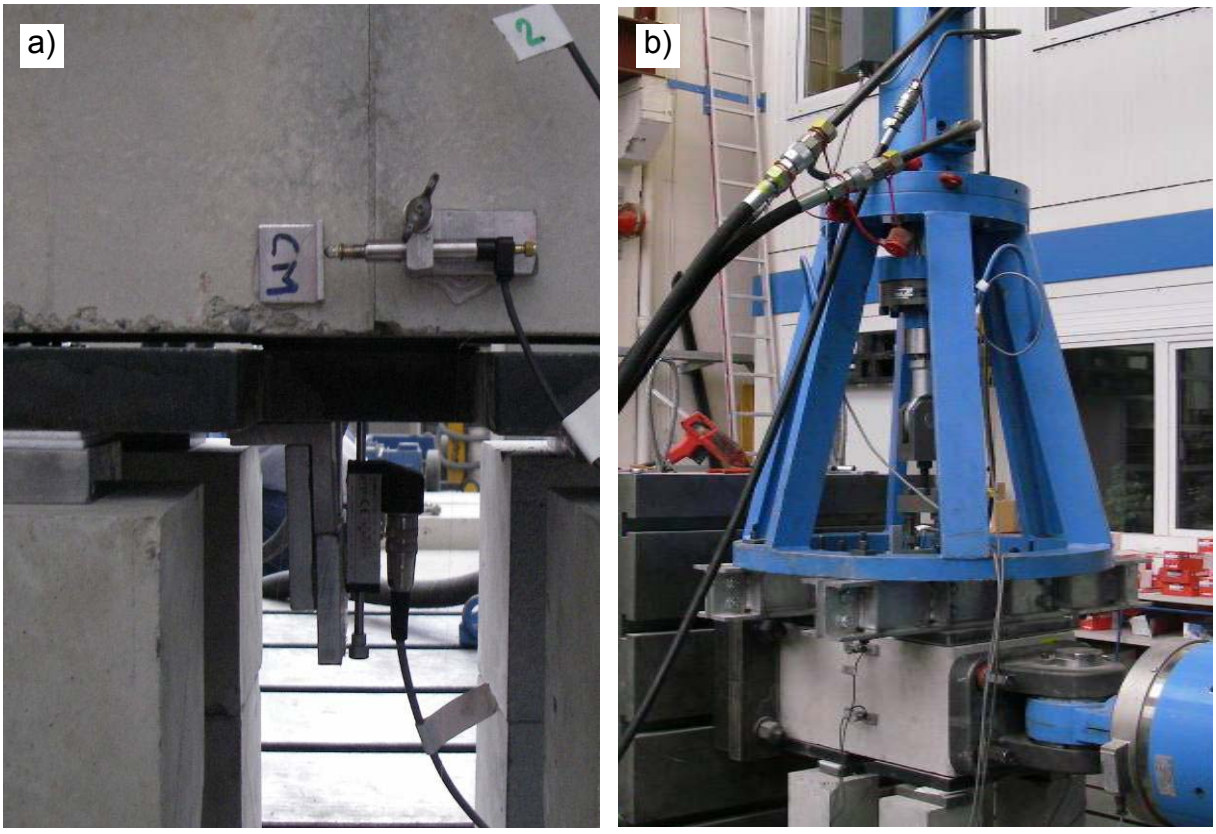


Figure 4.7 a) Close up of transducers; b) 250 kN actuator resting on test specimen which is mounted between abutment and 630 kN actuator

## 4.3 Experimental Procedure

### 4.3.1 Load protocol

In past decades, numerous studies directly or indirectly addressed the question what maximum crack width may occur during a seismic event. Some studies justify the assumption of a maximum crack width of 0.8 mm in flexural members outside of plastic hinges (e.g. *Nuti, C.; Santini, S. (2008)*, *Franchi, A.; Rosati, G. et al. (2009)*). Larger crack widths in joints of structural members are unlikely as long the joint core has not structurally disintegrated (e.g. *Kupfer, H.; Münger, F. et al. (2003)*, *Hamad, B.; Hammoud, A. et al. (2006)*). Therefore, $w_{max}$ = 0.8 mm was defined as the upper limit crack width tested. In addition, a hairline crack width of $w_{max}$ = 0.1 mm and a medium crack width of $w_{max}$ = 0.4 mm were tested to allow a sound evaluation of the influence of a range of lesser crack width.

The cyclic excitation of the reinforced concrete structure is not only closing the cracks but also compressing the mating surfaces on each side of the crack positions (Section 3.3). *Lowes, L.; Moehle, J. et al. (2004 d)* describes an increasing influence of transverse compression on the bond strength for stresses up to 15 % of the

concrete compressive strength, whereas a continued increase of compressive stress beyond 15 % of the concrete compressive strength does not significantly increase the bond strength further (Section 2.2.10). Therefore, the minimum crack width $w_{min}$ was defined as the crack width corresponding to a compression of the concrete member equal 15 % of the concrete compressive strength, i.e. $\sigma_c = 0.15 f_c$.

As explained in Section 4.2.2, all tests were conducted displacement controlled which facilitated postcritical testing. Monotonic loading tests were carried out for which the reinforcing bars were loaded while the concrete was either uncracked, cracked with a constant crack width $w_{max}$ or compressed with $\sigma_c = 0.15 f_c$. The peak slips $s_{max} = -s_{min}$ for the cyclic loading tests were defined on the basis of the slip $s_u$ of the monotonic loading tests in cracked concrete corresponding to the bond strength $\tau_u$ (Figure 4.8). Three different multiples of the slip $s_u$ corresponding to the ultimate load of the monotonic reference test, i.e. $0.5 s_u$, $1.0 s_u$, and $2.0 s_u$ were applied for the tests on cast-in-place reinforcing bars. The post-installed reinforcing bars were prone to buckling between the concrete surface and loading device due to the high strength and initial stiffness of the used epoxy mortar. Therefore, the peak slip was limited to $0.25 s_u$ for tests on post-installed reinforcing bars.

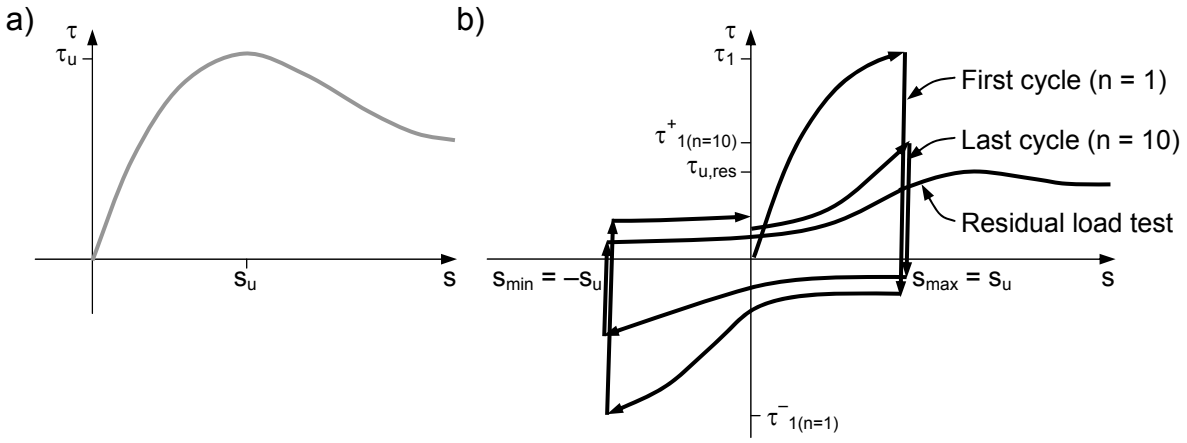


Figure 4.8 Ultimate slip value $s_u$ of a) monotonic test used to determine the peak slip value $s_{max}$ for b) cyclic test (example shown for $s_{max} = s_u$)

For reasons discussed in Section 3.3, the bond stress-slip behaviour of the cast-in-place and post-installed reinforcing bars was investigated under in-phase simultaneous load and crack cycling. The diagrams in Figure 4.9a depict the bond stress $\tau$ as a function of slip s and crack width w. To establish a base line for reference, tests on cyclically loaded reinforcing bars in constant width cracks were also conducted yielding the diagrams shown in Figure 4.9b.

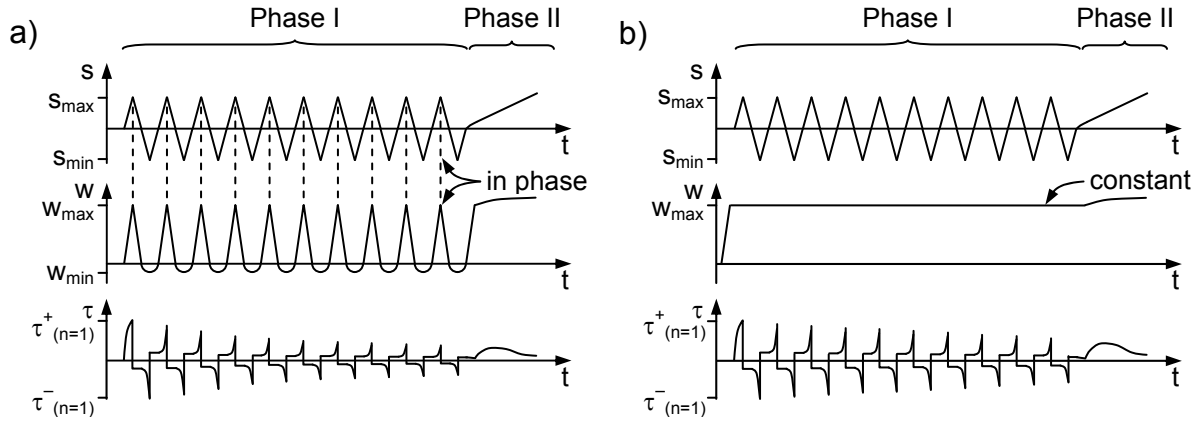


Figure 4.9 Cyclic slip s, cyclic crack width w, and resulting bond stress time histories for a) simultaneous load and crack cycling tests and b) load cycling tests in constant cracks (schematic, after *Mahrenholtz, C.; Eligehausen, R.; Hofmann, J. (2012)*)

The tests consisted of two phases. Phase I, cycling: The reinforcing bar was cyclically loaded between the peak slip values $s_{max}$ and $s_{min} = -s_{max}$. In parallel, the crack was opened and closed cyclically between $w_{max}$ and $w_{min}$. Phase II, pullout: To determine the residual load capacity, the crack was opened to $w_{max}$ and the reinforcing bar was pulled out monotonically.

Based on investigations studying the number of deformation cycles in reinforced concrete structures under seismic excitation (*Dutta, A.; Mander, J. (2001)*, *Malhotra, P. (2002)*, *Kunnath, S.; Chai, Y.-H. (2004)*), 10 uniform cycles were suggested in *Hoehler, M. (2006)* to be representative. Further, the results presented in *Eligehausen, R.; Popov, E. et al. (1983)* show that bond damage rapidly decelerate and becomes almost constant during the first 10 cycles (Figure 2.21b). Therefore, the number of cycles has been defined as 10.

Noteworthy, tests on headed bolts showed that out-of-phase load and crack cycling reduces significantly the slip of the anchorage (*Mahrenholtz, P.; Mahrenholtz, C. et al. (2013)*) if compared to in-phase load and crack cycling. This effect is even more pronounced for load and crack cycling at different frequencies. It is assumed that this finding is in principle also valid for reinforcing bars where the mechanical load transfer mechanism of the ribs is similar to that of headed bolts. Since slip comes along with a reduction of the concrete shear keys between the ribs, the pullout strength of the reinforcing bar is larger the lesser the bar slip is (Section 2.2.4). In conclusion, in-phase load and crack cycling is more demanding than out-of-phase cycling and is the critical load condition for structural connections. This is also in line with the considerations presented in Section 3.3.

### 4.3.2 Test program

Table 4.2 and Table 4.3 comprise the complete program for the tests on cast-in-place and post-installed reinforcing bars, indicating the various loading types, crack widths, and reinforcing bar diameters tested. In general, two repeats per test series were conducted. The details of the tests can be found in Table C.1 and C.2 of Appendix C: Bond Test Data.

Table 4.2 Experimental test program of tests on cast-in-place reinforcing bars

| Cast-in-place | Crack width $w_{max}$ [mm] | Bar diameter $\phi$ [mm] | Peak slip $s_{max} / s_u$ $-s_{min} / s_u$ [-] | Number of cycles $n_{cyc}$ [-] |
|---|---|---|---|---|
| Monotonic loading, compressed concrete | | | | |
| expCI20-w0.0-d16-com | – | 16 | – | – |
| Monotonic loading, uncracked concrete | | | | |
| expCI20-w0.0-d16-ucr | – | 16 | – | – |
| Monotonic loading, cracked concrete | | | | |
| expCI20-w0.1-d16-cr | 0.1 | 16 | – | – |
| expCI20-w0.4-d16-cr | 0.4 | 16 | – | – |
| expCI20-w0.8-d16-cr | 0.8 | 16 | – | – |
| expCI20-w0.4-d12-cr | 0.4 | 12 | – | – |
| expCI20-w0.4-d25-cr | 0.4 | 25 | – | – |
| Load cycling in constant cracks | | | | |
| expCI20-w0.1-d16-s1.0-con | 0.1 | 16 | 1.0 | 10 |
| expCI20-w0.4-d16-s0.5-con | 0.4 | 16 | 0.5 | 10 |
| expCI20-w0.4-d16-s1.0-con | 0.4 | 16 | 1.0 | 10 |
| expCI20-w0.4-d16-s2.0-con | 0.4 | 16 | 2.0 | 10 |
| expCI20-w0.8-d16-s0.5-con | 0.8 | 16 | 0.5 | 10 |
| expCI20-w0.8-d16-s1.0-con | 0.8 | 16 | 1.0 | 10 |
| expCI20-w0.4-d12-s0.5-con | 0.4 | 12 | 0.5 | 10 |
| Simultaneous load and crack cycling | | | | |
| expCI20-w0.1-d16-s0.5-cyc | 0.1 | 16 | 0.5 | 10 |
| expCI20-w0.1-d16-s1.0-cyc | 0.1 | 16 | 1.0 | 10 |
| expCI20-w0.4-d16-s0.5-cyc | 0.4 | 16 | 0.5 | 10 |
| expCI20-w0.4-d16-s1.0-cyc | 0.4 | 16 | 1.0 | 10 |
| expCI20-w0.4-d16-s2.0-cyc | 0.4 | 16 | 2.0 | 10 |
| expCI20-w0.8-d16-s0.5-cyc | 0.8 | 16 | 0.5 | 10 |
| expCI20-w0.8-d16-s1.0-cyc | 0.8 | 16 | 1.0 | 10 |
| expCI20-w0.4-d12-s0.5-cyc | 0.4 | 12 | 0.5 | 10 |
| expCI20-w0.4-d25-s0.5-cyc | 0.4 | 25 | 0.5 | 10 |

Table 4.3 Experimental program of tests on post-installed reinforcing bars

| Post-installed | Crack width $w_{max}$ [mm] | Bar diameter $\phi$ [mm] | Peak slip $s_{max} / s_u$ $-s_{min} / s_u$ [-] | Number of cycles $n_{cyc}$ [-] |
|---|---|---|---|---|
| Monotonic loading, uncracked concrete | | | | |
| expPI20-w0.0-d16-ucr | – | 16 | – | – |
| Monotonic loading, cracked concrete | | | | |
| expPI20-w0.4-d16-cr | 0.4 | 16 | – | – |
| Load cycling in constant cracks | | | | |
| expPI20-w0.4-d16-s0.25-con | 0.4 | 16 | 0.25 | 10 |
| Simultaneous load and crack cycling | | | | |
| expPI20-w0.4-d16-s0.25-cyc | 0.4 | 16 | 16 | 10 |

### 4.3.3 Servo control

Previous experience gained by tests on post-installed anchors showed that the actual shape of the load or crack time histories is irrelevant (*Mahrenholtz, C. (2009f)*, *Mahrenholtz, P. (2010)*). Both actuators were controlled by ramps to allow the synchronisation of the simultaneous load and crack cycling by means of the two axes servo control system. The crack opening was run crack width controlled with a targeted crack width $w_{max}$ and the crack closing force controlled with a targeted compression force $D_{max} = 0.15 f_c A_c$ where $A_c$ is the cross section of the concrete member. The reinforcing bar loading was run slip controlled between the targeted peak slips $s_{max}$ and $s_{min}$. All tests were run at quasi-static conditions as a simplifying but conservative approach (Section 2.2.7).

The servo control system provided a graphical user interface for programming the load protocol (Figure 4.10). The remarkably high accuracy achieved for crack width and slip control is demonstrated by the recorded slip and crack width time histories shown in Figure 4.11 for an example simultaneous load and crack cycling test as well as for an example load cycling test in constant cracks.

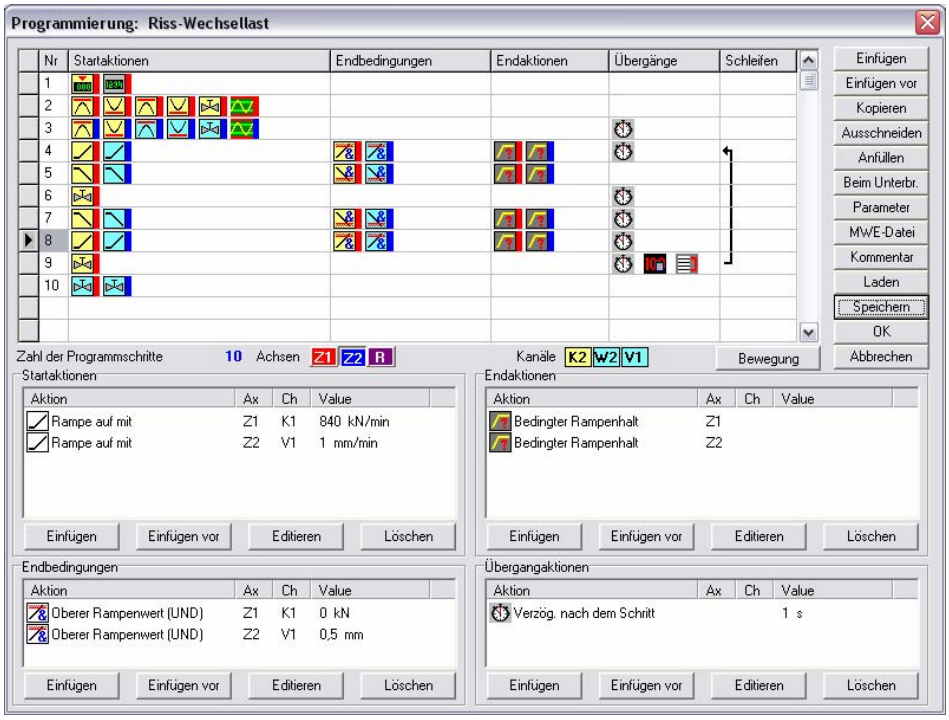


Figure 4.10 Servo control program

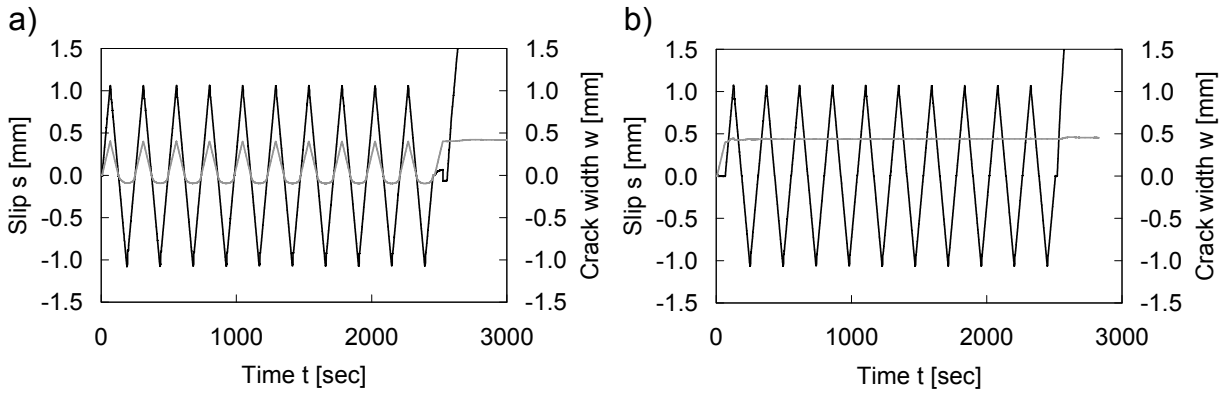


Figure 4.11 Example time histories of slip (black curves) and crack width (grey curves), recorded for a) an example simultaneous load and crack cycling test and b) an example load cycling test in constant cracks

## 4.4 Results and Discussion

### 4.4.1 General behaviour

All tested reinforcing bars failed by pullout prior to yielding of the reinforcing bar (Figure 4.12). The upper debonding sleeve was sometimes partly or completely dragged along with the reinforcing bars. The lower debonding sleeve of cast-in-place reinforcing bars always remained in the concrete test specimen. Post-installed

reinforcing bars were not furnished with lower debonding sleeves as the reinforcing bar ended at the unloaded end of the bonded length.

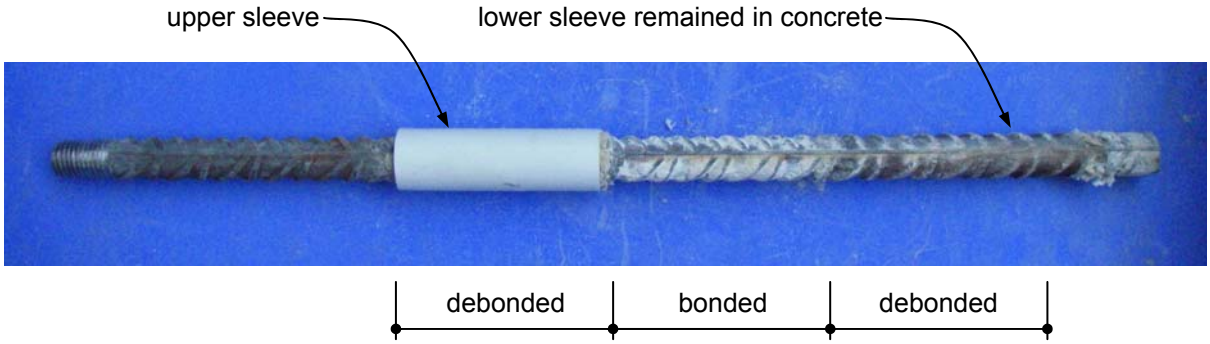


Figure 4.12 Typical pulled out reinforcing bar

In the next three sections (Section 4.4.1.1 to Section 4.4.1.3), the behaviour is described qualitatively. A quantitative evaluation is presented in the subsequent three sections (Section 4.4.1.4 to Section 4.4.1.6).

### 4.4.1.1 Monotonic loading

The general behaviour of bond tests on cast-in-place reinforcing bars under monotonic loading is described from a physical point of view in Section 2.2.4. In the following, some aspects of bond tests on cast-in-place and post-installed reinforcing bars in uncracked and cracked concrete under monotonic loading are discussed. Figure 4.13 shows the mean bond stress-slip curves of monotonic loading tests on 16 mm reinforcing bars cast-in-place and post-installed in grade 20 concrete.

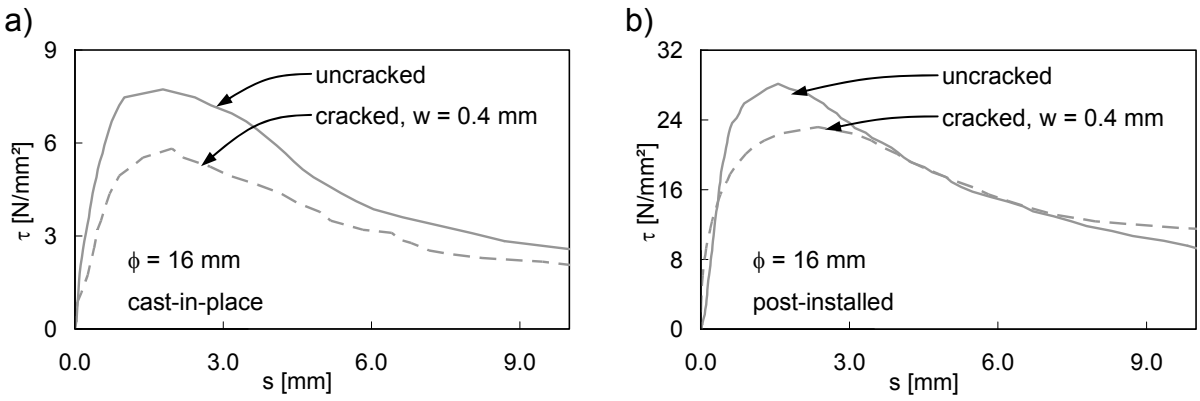


Figure 4.13 Bond stress-slip curves of experimental tests on a) cast-in-place and b) post-installed reinforcing bars subjected to monotonic loading

The tested bond strength of cast-in-place reinforcing bars in uncracked concrete is comparatively low which can be explained by the low concrete compressive strength of the used concrete member ($f_c$ = 19.1 MPa). The ratio of the bond strength corresponding to the tests on cast-in-place reinforcing bars in uncracked concrete and cracked concrete with a crack width of 0.4 mm is about 0.75 (Figure 4.13a). This ratio matches well to the influence of cracks on the bond strength reported in the literature (Section 2.2.11).

The tests on post-installed reinforcing bars in uncracked concrete demonstrate the high bond strength of current epoxy mortars used for reinforcing bar post-installation ($\tau_u$ = 28.1 N/mm²). The ratio of the bond strength corresponding to the tests on post-installed reinforcing bars in uncracked concrete and cracked concrete with a crack width of 0.4 mm is about 0.80 (Figure 4.13b). The reduction is relatively low if compared to the average reported in the literature (Section 2.2.11), however it is still within the band of scatter of the reported literature.

For the same reinforcing bar diameter, the bond stress-slip curves of cast-in-place and post-installed reinforcing bars reached the ultimate bond stress $\tau_u$ at approximately the same slip value of $s_u$. This observation allows modelling the bond stress-slip curve for post-installed reinforcing bars by multiplying the bond stress values of the bond stress-slip curve for cast-in-place reinforcing bars using the ratio of the corresponding bond strength as explained in Section 2.2.4.

Figure 4.14 shows the mean bond stress-slip curves of the monotonic loading tests on cast-in-place reinforcing bars illustrating the influence of reinforcing bar diameter and confinement in respect of parallel cracks and transverse compression.

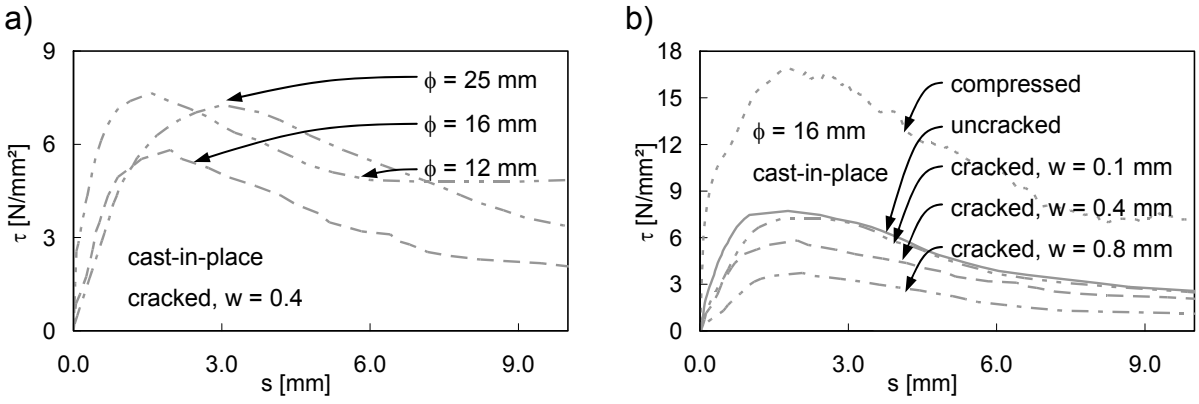


Figure 4.14 Bond stress-slip curves of experimental tests on cast-in-place reinforcing bars subjected to monotonic loading: a) Influence of reinforcing bar diameter; b) Influence of crack width

The curves given in Figure 4.14a are taken from tests in cracked concrete (w = 0.4 mm) and demonstrate that the influence of the reinforcing bar diameter on

the bond strength is not consistent. Diameter 16 mm reinforcing bars showed the lowest bond strength while larger and smaller diameters developed higher bond strengths. The inconsistency could be ascribed to scatter. In additio the concrete members used for the tests on diameter 16 mm reinforcing bars showed a low concrete compressive strength ($f_c$ = 19.1 MPa) if compared to the compressive strengths of the other concrete members.

The slip corresponding to the ultimate bond stress was reached between about 1.5 mm for diameter 12 mm reinforcing bars and approximately 3.0 mm for diameter 25 mm reinforcing bars.

Figure 4.14b illustrate that the bond strength is increasingly reduced with increasing width of the parallel cracks. Less than half of the bond strength which develops in uncracked concrete is attained in 0.8 mm cracks. In contrast, the bond strength is more than doubled if the applied transverse compression equals to 15 % of the concrete compressive strength. It is noteworthy that the confinement in terms of cracks parallel to the embedded reinforcing bar and transverse compression does not significantly influence the slip $s_u$ corresponding to the ultimate bond stress $\tau_u$. This phenomenon justifies the modelling of the bond stress-slip curve by means of factored basic curves to describe the influence of cracks parallel to the embedded reinforcing bar and transverse compression as described in Section 2.2.4. Since the bond strength is a function of the confinement but not the corresponding slip, the bond behaviour becomes increasingly stiffer with increasing compression stresses and increasingly softer with increasing crack widths.

All plots of the experimental tests under monotonic loading are presented in *Mahrenholtz, C. (2011b)* and the key results are given in Table C.1 and C.2 of Appendix C: Bond Test Data.

#### 4.4.1.2 Simultaneous load and crack cycling

The general bond stress-slip behaviour under simultaneous load and crack cycling is discussed in the following from a physical point of view. Figure 4.15a shows schematically of the bond stress-slip curve of simultaneous load and crack cycling tests on reinforcing bars which has been developed based on the conducted simultaneous load and crack cycling tests. In addition, the curves of monotonic tests on reinforcing bars located in compressed concrete, uncracked concrete and cracked concrete are plotted. The curves of all tests can be found in *Mahrenholtz, C. (2011b)*. Figure 4.15b shows the crack width-slip and compression stress-slip relation.

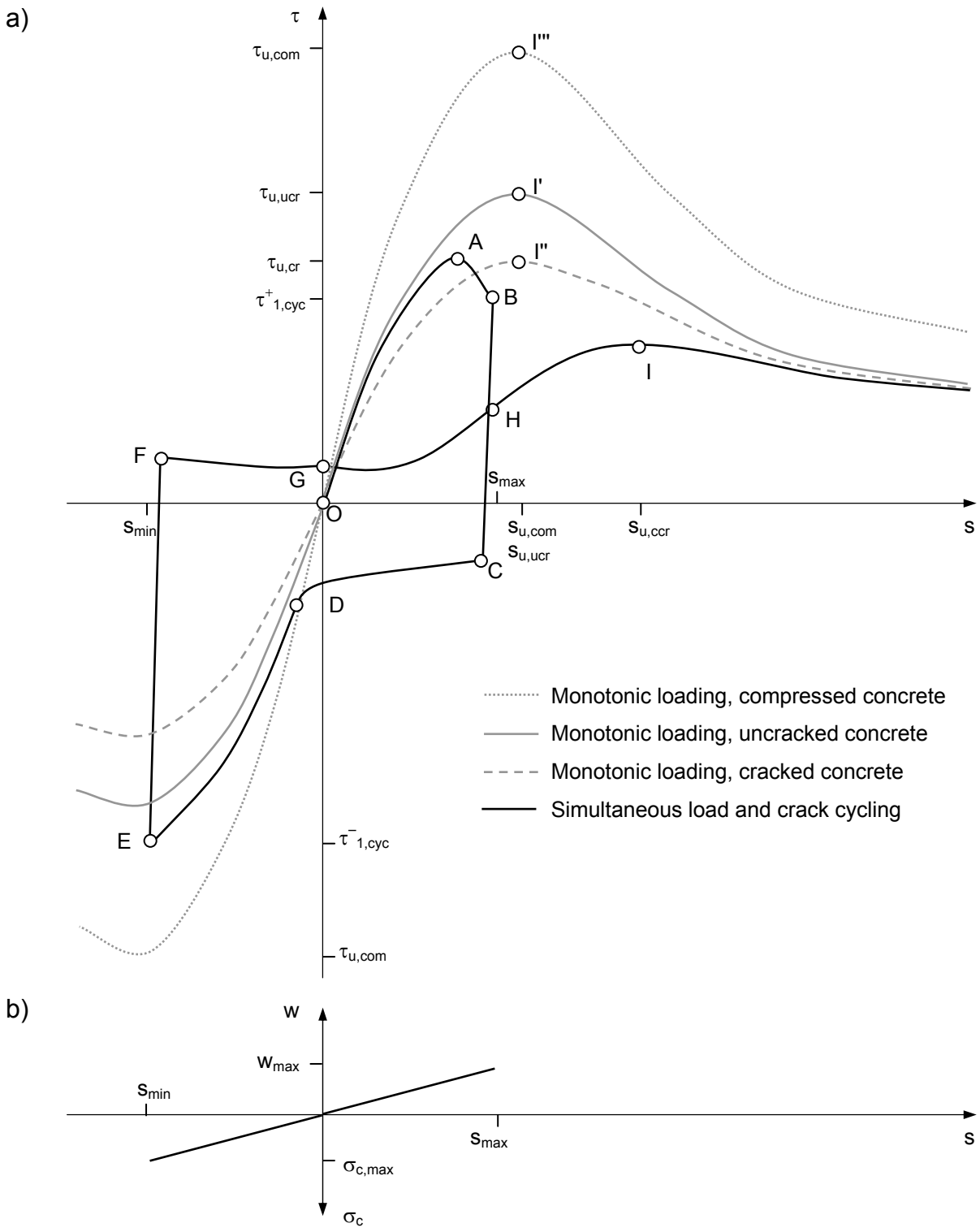


Figure 4.15 a) Schematic bond stress-slip curves of simultaneous load and crack cycling tests (first cycle and residual load test) and monotonic tests on reinforcing bars located in compressed concrete, uncracked concrete, and cracked concrete; b) Crack width-slip and compression stress-slip relation for simultaneous load and crack cycling tests

Monotonic loading of a reinforcing bar tested in uncracked concrete results in a bond stress-slip curve with the bond strength $\tau_{u,ucr}$ and its corresponding slip $s_{u,ucr}$ at Point I'. This curve is referred to as monotonic bond stress-slip curve of the reference test in uncracked concrete.

Monotonic loading of a reinforcing bar tested in cracked concrete is described by a similar but reduced curve with the bond strength $\tau_{u,cr}$ and corresponding slip $s_{u,cr}$ at Point I''. This curve is termed as the bond stress-slip curve of the monotonic reference test in cracked concrete.

Monotonic loading of a reinforcing bar tested in compressed concrete is described by a similar but increased curve with the bond strength $\tau_{u,com}$ and corresponding slip $s_{u,com}$ at Point I'''. This curve is named curve of the monotonic reference test in compressed concrete.

The slip values $s_{u,ucr}$, $s_{u,cr}$, and $s_{u,com}$ are approximately identical. The post peak behaviour is characterised by the gradual decrease of the bond resistance and a levelling off at slip values larger than the rib distance.

In the following, the bond stress-slip curves for reinforcing bars under simultaneous load and crack cycling are discussed in depth and compared to the monotonic bond stress-slip curves referred to above. The bond stress-slip curve first follows the curve of the monotonic loading in uncracked concrete and then deflects increasingly towards the curve of the monotonic loading in cracked concrete. The peak at Point A is generally located between the two curves. When the reinforcing bar slip reaches the assigned peak slip $s_{max}$, the bond stress at Point B is typically below the bond stress of the monotonic loading in cracked concrete. This is plausible because the energy consumption is larger when the crack is opened in phase with the load increase.

The stiff unloading branch leads from Point B to Point C at the beginning of the slip reversal. The load changes its direction and acts against the frictional bond. Further negative slip is slightly increasing the resistance which can be explained by the reduced crack width and crushed concrete trapped between the steel rib and the intact concrete console, adding mechanical bond resistance. The positive loop is completed when the reinforcing bar crosses its starting position (s = 0 mm).

The resistance is gradually picking up and swings into the parabolic shaped negative loading branch to Point D as the slip and transverse compression increases. The negative loading branch curve does not reach the curve of the reference test in compressed concrete because of the previously accumulated damage. The curve climaxes in Point E, defining the peak bond stress of the negative half cycle at the peak slip $s_{min}$. For tests with a peak slip of $s_{min} = 0.5s_u$, the absolute bond stress at Point E was slightly higher, for a peak slip of $s_{max} = 1.0s_u$ slightly lower than the bond

stress of the reference test in uncracked concrete. This observation was made for all tested maximum crack widths $w_{max}$.

As the slip is reversed the load drops from Point E to Point F, where only frictional bond remains. The releasing of the transverse compression load reduces the frictional bond resistance. Again, the reduction is partly counteracted by the mechanical bond resistance which is built up by the collection of the pulverised concrete between the steel rib and concrete console.

When the slip increases from zero slip (s = 0 mm), Point G, to the peak slip $s_{max}$, Point H, the frictional bond resistance is reduced due to the crack opening. This effect is later compensated by the gradual increase of mechanical bond resistance. The slip can be further increased to determine the residual resistance. The peak is reached after about 3 mm additional slip in Point I.

In the following, some aspects of bond tests on cast-in-place and post-installed reinforcing bars under simultaneous load and crack cycling are discussed in detail. For this reason, the bond stress-slip curves of the simultaneous load and crack cycling tests on 16 mm reinforcing bars cast-in-place and post-installed in grade 20 concrete are superposed with the corresponding mean bond stress-slip curves of monotonic loading tests as shown in Figure 4.16. For better visualisation only the first and the last cycle of the cyclic tests are shown.

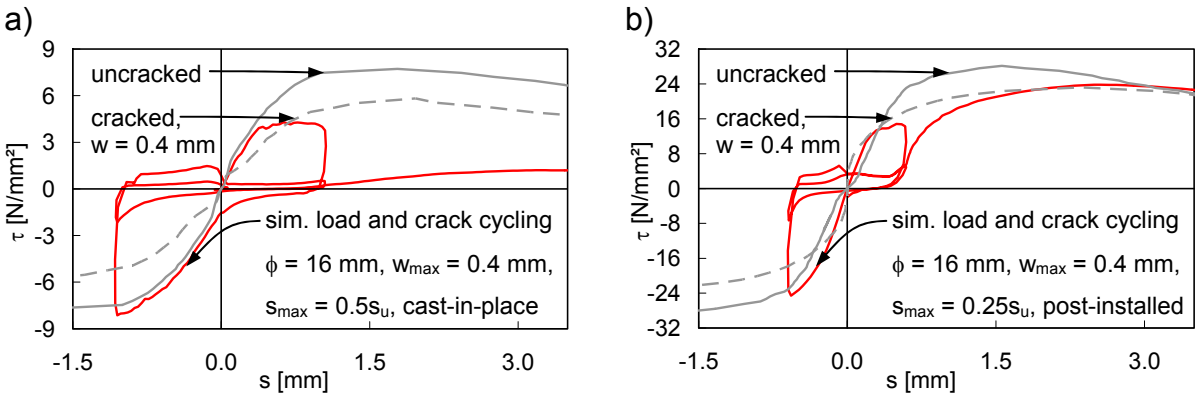


Figure 4.16 Bond stress-slip curves of experimental tests on a) cast-in-place and b) post-installed reinforcing bars subjected to simultaneous load and crack cycling

In the positive domain, the curves representing the simultaneous load and crack cycling on both cast-in-place reinforcing bars (Figure 4.16a) and post-installed reinforcing bars (Figure 4.16b) follow the curve of the monotonic loading test in uncracked concrete. Following, as the crack is gradually opened, the curves fall below the curve of the monotonic loading test in cracked concrete. As the imposed slip is reversed the crack is closed. The crack is increasingly compressed which increases the bond strength in the negative domain. The compression is

progressively released when the slip is reduced. The following cycles mainly consists of pinched hysteretic loops with little energy dissipation. The residual bond strength recorded during the final pullout of the reinforcing bar depends on the peak slip of the previous cycling. The simultaneous load and crack cycling on cast-in-place reinforcing bars between the peak slip of $\pm 0.5 s_u$ shown in Figure 4.16a is completed with a very low residual bond strength, while the simultaneous load and crack cycling on post-installed reinforcing bars between the peak slip of $\pm 0.25 s_u$ shown in Figure 4.16b develop residual bond strengths in the range of the ultimate bond strength of the corresponding monotonic loading test in cracked concrete.

In the following Figure 4.17 and Figure 4.18 the bond stress-slip curves of simultaneous load and crack cycling tests on cast-in-place reinforcing bars are shown to demonstrate the influence of various parameters.

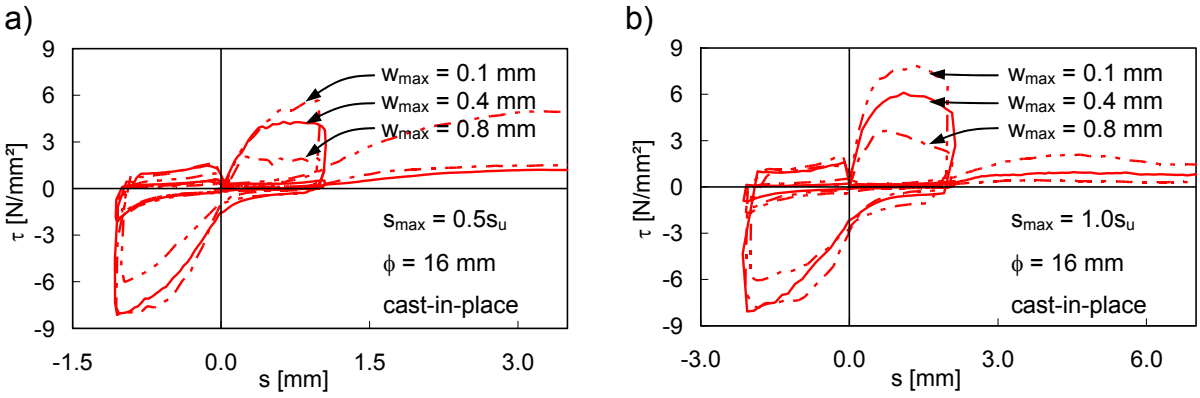


Figure 4.17 Bond stress-slip curves of experimental tests on cast-in-place reinforcing bars subjected to simultaneous load and crack cycling: Influence of maximum crack width $w_{max}$ for peak slip a) $s_{max} = 0.5 s_u$ and b) $s_{max} = 1.0 s_u$

The influence of the maximum crack width $w_{max}$ on the bond stress-slip curves of simultaneous load and crack cycling is illustrated in Figure 4.17a for peak slips $s_{max} = 0.5 s_u$ and in Figure 4.17b for peak slips $s_{max} = 1.0 s_u$. Clearly, larger maximum crack widths lead to smaller energy dissipation during the initial positive loop. Therefore, the corresponding initial negative loop shows larger bond strengths. However, final pullout tests carried out in cracks opened to the width identical to the maximum crack width of the previous crack cycling may attain higher residual bond strengths for simultaneous load and crack cycling characterised by higher energy dissipation for peak slips $s_{max} = 0.5 s_u$. For peak slips $s_{max} = 1.0 s_u$, the bond damage is less localised at the stretch between the slip reversals but the concrete is already significantly damaged at locations beyond the peak slip. This phenomenon was also observed by *Eligehausen, R.; Popov, E. et al. (1983)* for load cycling tests in uncracked concrete (Section 2.2.13).

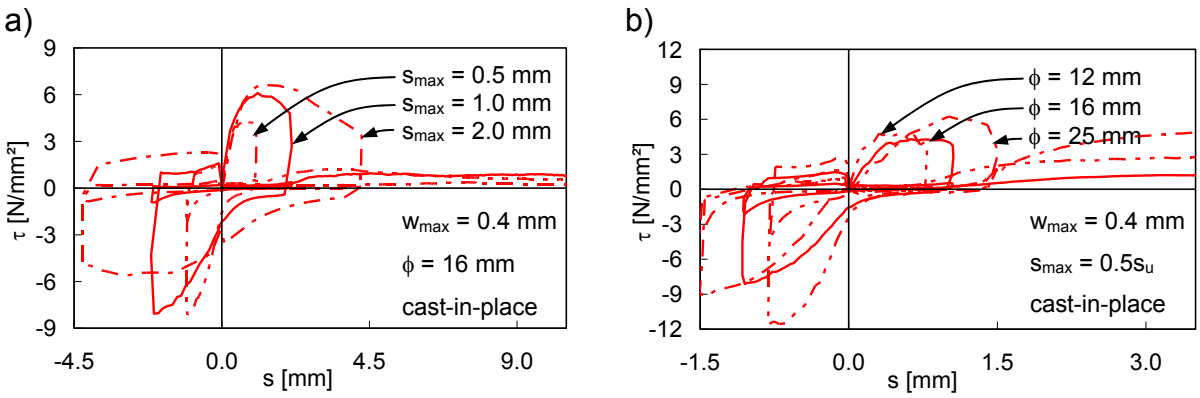


Figure 4.18 Bond stress-slip curves of experimental tests on cast-in-place reinforcing bars subjected to simultaneous load and crack cycling: Influence of a) peak slip $s_{max}$ and b) reinforcing bar diameter $\phi$ for maximum crack width $w_{max}$ = 0.4 mm

The influence of the peak slip $s_{max}$ on the bond stress-slip curves of simultaneous load and crack cycling is further demonstrated in Figure 4.18a. The influence of the initial positive hysteretic loop on the initial negative hysteretic loop is increasing with increasing peak slips. It is not possible to interpret the influence of the reinforcing bar diameter $\phi$ on the bond damage by means of the bond stress-slip curves of simultaneous load and crack cycling shown in Figure 4.18b because different reinforcing bar diameters are characterised by different basic bond stress-slip curves and therefore cannot be compared directly. It is more meaningful to compare the bond damage of the different reinforcing bar diameters which is presented in Section 4.4.2.

All plots of the experimental tests under simultaneous load and crack cycling are presented in *Mahrenholtz, C. (2011b)* and the key results are given in Table C.1 and C.2 of Appendix C: Bond Test Data.

#### 4.4.1.3 Load cycling in constant cracks

The general behaviour of bond tests on cast-in-place reinforcing bars under cyclic loading is described from a physical point of view in Section 2.2.13. In the following, some aspects of bond tests on cast-in-place and post-installed reinforcing bars in uncracked and cracked concrete under load cycling are discussed. In Figure 4.19 the bond stress-slip curves of the load cycling tests in cracked concrete on 16 mm reinforcing bars cast-in-place and post-installed in grade 20 concrete are superposed with the corresponding mean bond stress-slip curves of monotonic loading tests. For the sake of better readability, only the first and last hystereses are plotted.

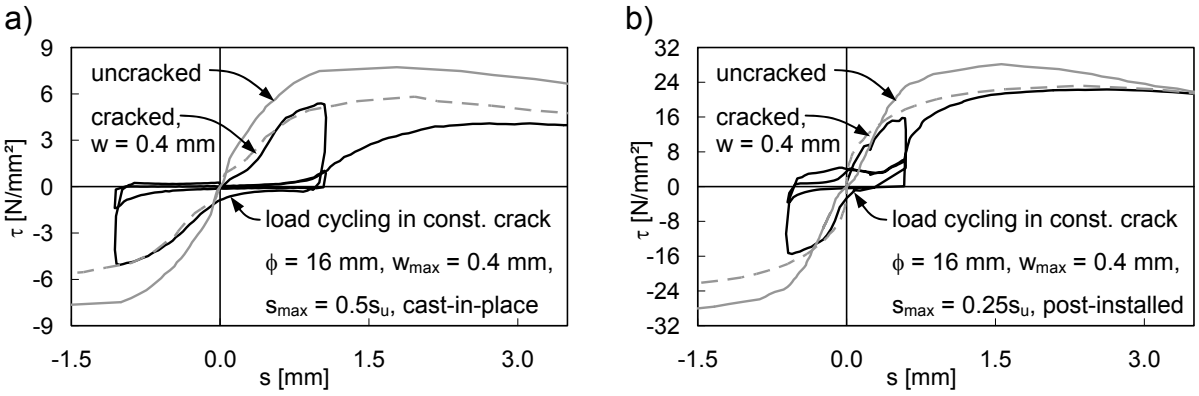


Figure 4.19 Bond stress-slip curves of experimental tests on a) cast-in-place and b) post-installed reinforcing bars subjected to load cycling in constant crack

Also the curves representing the load cycling in constant cracks for cast-in-place reinforcing bars (Figure 4.19a) and on post-installed reinforcing bars (Figure 4.19b) have a very similar behaviour which is principle identical to the bond behaviour in uncracked concrete described in Section 2.2.13.

In the following Figure 4.20 and Figure 4.21 the bond stress-slip curves of load cycling in constant cracks tests are presented to show the influence of various parameters.

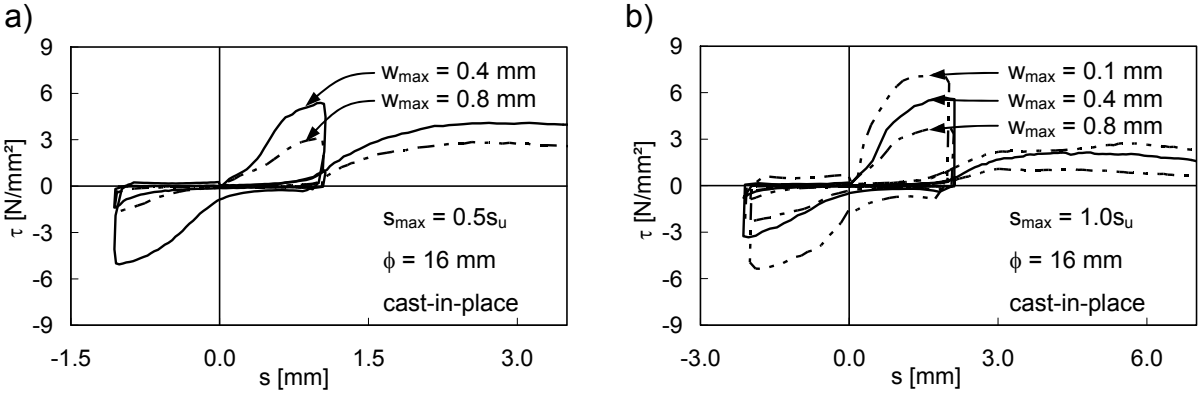


Figure 4.20 Bond stress-slip curves of experimental tests on cast-in-place reinforcing bars subjected to load cycling in constant crack: Influence of maximum crack width $w_{max}$ for peak slip a) $s_{max} = 0.5s_u$ and b) $s_{max} = 1.0s_u$

The influence of the maximum crack width $w_{max}$ on the bond stress-slip curves of load cycling in constant cracks is illustrated in Figure 4.20a for peak slips $s_{max} = 0.5s_u$ and in Figure 4.20b for peak slips $s_{max} = 1.0s_u$. As observed for simultaneous load and crack cycling, larger crack widths lead to smaller energy dissipation during the initial positive loop. However, in contrast to simultaneous load and crack cycling the

corresponding initial negative loop is similar to the initial positive loop and show higher bond strengths for smaller crack widths.

The final pullout bond test which was carried out in a crack opened to a width identical to the crack width of the previous crack cycling, shows generally higher residual bond strengths for load cycling if compared to simultaneous load and crack cycling tests, regardless of the peak slip ($s_{max} = 0.5s_u$ or $s_{max} = 1.0s_u$): If compared to residual bond strengths tests in larger crack widths, smaller crack widths always lead to higher residual bond strengths, although the previously dissipated energy was higher.

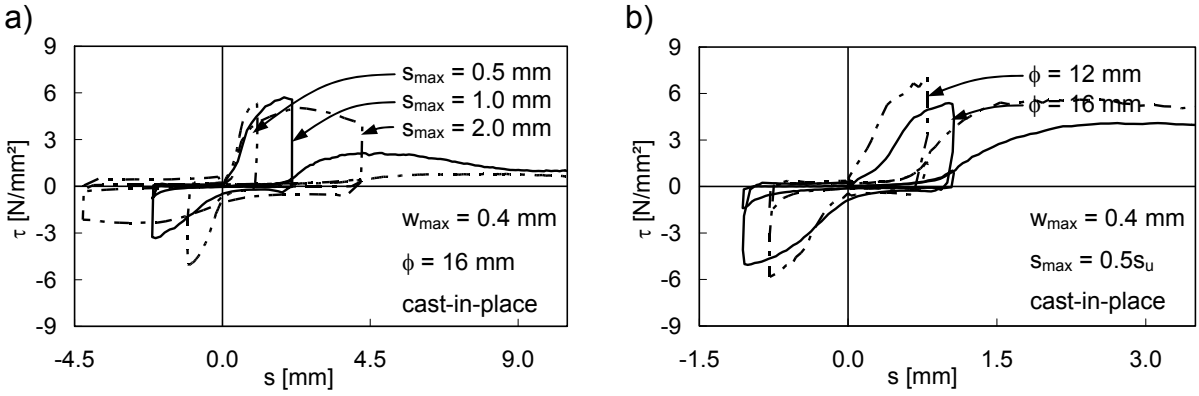


Figure 4.21 Bond stress-slip curves of experimental tests on cast-in-place reinforcing bars subjected to load cycling in constant crack: Influence of a) peak slip $s_{max}$ and b) reinforcing bar diameter $\phi$ for maximum crack width $w_{max} = 0.4$ mm

The influence of the peak slip $s_{max}$ on the bond stress-slip curves of load cycling in constant cracks is also demonstrated in Figure 4.21a. The influence of the initial positive hysteretic loop on the initial negative hysteretic loop is increasing with increasing peak slips. As pointed out in Section 4.4.1.3, it is impossible to interpret the influence of the reinforcing bar diameter $\phi$ on the bond damage by means of the bond stress-slip curves of load cycling shown in Figure 4.21b because different reinforcing bar diameters are characterised by different basic bond tress-slip curves and therefore cannot be compared directly. It is more reasonable to compare the bond damage of the different reinforcing bar diameters which is shown in Section 4.4.2.

All plots of the experimental tests under load cycling in constant cracks are presented in *Mahrenholtz, C. (2011b)* and the key results are given in Table C.1 and C.2 of Appendix C: Bond Test Data.

#### 4.4.1.4 Initial bond strength

For monotonic loading, the initial bond strength is equivalent to the ultimate bond strength $\exp\tau_u$. The mean ultimate bond strength recorded for cast-in-place 16 mm reinforcing bars under monotonic loading are given in Table 4.4. Characteristic values are not calculated since only two repeats per series were conducted. The coefficient of variation ranged from 0.7 % for uncracked concrete to 16.0 % for cracked concrete.

Table 4.4 Ultimate bond strength of experimental tests under monotonic loading for cast-in-place 16 mm reinforcing bars

| | | Compressed | Uncracked | Cracked | | |
|---|---|---|---|---|---|---|
| | | $\sigma_c = 0.15f_c$ | – | w = 0.1 mm | w = 0.4 mm | w = 0.8 mm |
| $\exp\tau_u$ | [N/mm²] | 13.17 | 7.73 | 7.41 | 5.82 | 3.80 |
| $\frac{\exp\tau_u}{\exp\tau_{u,ucr}}$ | [-] | 1.70 | 1.00 | 0.96 | 0.75 | 0.49 |

The tests on cast-in-place reinforcing bars situated in uncracked concrete carried out as a part of the test program given in Section 4.3.2 show bond strengths which are relatively low if compared to the other references. Therefore, the normalised values of the tests on reinforcing bars situated in compressed and cracked concrete reported in Table 4.4 are relatively high.

Table 4.5 allows the comparison of the ultimate bond strength of the conducted experimental tests with values reported in *Simons, I. (2007)* as well as with values calculated according to analytical models proposed in *Lowes, L.; Moehle, J. et al. (2004)*, *Gambarova, P.; Rosati, G. (1996)*, and *Idda, K. (1999)* which were developed on the basis of experimental tests. The bond strengths reported in the various references differ significantly, underlining the scatter immanent to bond properties. In summary, however, the bond strengths for cast-in-place 16 mm reinforcing bars under monotonic loading according to Table 4.3 are within the range of scatter and therefore plausible.

Table 4.5 Comparison of ultimate bond strength of experimental tests under monotonic loading for cast-in-place reinforcing bars according to various references

| | | Compressed | Uncracked | Cracked | | |
|---|---|---|---|---|---|---|
| | | $\sigma_c = 0.15 f_c$ | – | w = 0.1 mm | w = 0.4 mm | w = 0.8 mm |
| $exp\tau_u$ [1] | [N/mm²] | 12.78 | 7.73 | 7.41 | 5.24 | 3.80 |
| $\frac{exp\tau_u}{exp\tau_{u,ucr}}$ | [-] | 1.65 | 1.00 | 0.96 | 0.68 | 0.49 |
| $\frac{cal\tau_u}{cal\tau_{u,ucr}}$ [2] | [-] | 1.36 | 1.00 | – | – | – |
| $exp\tau_u$ [3] | [N/mm²] | – | 10.03 | 6.81 | 6.01 | |
| $\frac{exp\tau_u}{exp\tau_{u,ucr}}$ | [-] | – | 1.00 | 0.67 | 0.59 | – |
| $cal\tau_u$ [4] | [N/mm²] | – | 8.87 | 7.55 | 4.92 | 2.95 |
| $\frac{cal\tau_u}{cal\tau_{u,ucr}}$ | [-] | – | 1.00 | 0.85 | 0.55 | 0.33 |
| $cal\tau_u$ [5] | [N/mm²] | – | 10.26 | 6.26 | 3.81 | 2.53 |
| $\frac{cal\tau_u}{cal\tau_{u,ucr}}$ | [-] | – | 1.00 | 0.61 | 0.37 | 0.25 |

[1] According to *Mahrenholtz, C. (2011b)* (experimental, $\phi$ = 16 mm, expCI20-w0.0-d16-com ($f_c$ = 20.4 N/mm²), expCI20-w0.0-d16-ucr ($f_c$ = 19.2 N/mm²), expCI20-w0.1-d16-cr ($f_c$ = 19.2 N/mm²), expCI20-w0.4-d16-cr ($f_c$ = 23.7 N/mm²), expCI20-w0.8-d16-cr ($f_c$ = 19.2 N/mm²), normalised by $(19.2 \text{ N/mm}^2 / f_c)^{0.5}$, refer to Table 4.4)
[2] According to *Lowes, L.; Moehle, J. et al. (2004)* (analytical, refer to Equation 2.5)
[3] According to *Simons, I. (2007)* (experimental, $\phi$ = 20 mm, ME20(8d)w0 ($f_c$ = 22.9 N/mm²), ME20(10d)w1 ($f_c$ = 26.2 N/mm²), ME20(8d)w4 ($f_c$ = 21.9 N/mm²), normalised by $(19.2 \text{ N/mm}^2 / f_c)^{0.5}$)
[4] According to *Gambarova, P.; Rosati, G. (1996)* (analytical, for $f_c$ = 19.2 N/mm² and values for rib height and distance typical for $\phi$ = 16 mm)
[5] According to *Idda, K. (1999)* (analytical, for $f_c$ = 19.2 N/mm² and $\phi$ = 16 mm)

The initial bond strength $exp\tau_1$ of the simultaneous load and crack cycling and load cycling in constant cracks is defined as the ultimate bond strength during the first positive slip. The mean initial bond strength recorded for cast-in-place 16 mm reinforcing bars under cyclic loading are given in Table 4.6. Characteristic values are not given since only two repeats per series were conducted.

Table 4.6 Initial bond strength of experimental tests under simultaneous load and crack cycling and load cycling in constant cracks for cast-in-place 16 mm reinforcing bars

| $s_{max}$ / $s_u$ | [-] | 0.5 | | | 1.0 | | |
|---|---|---|---|---|---|---|---|
| $w_{max}$ | [mm] | 0.1 | 0.4 | 0.8 | 0.1 | 0.4 | 0.8 |
| $exp\tau_{1,cyc}$ [1)] | [N/mm²] | 5.74 | 4.90 | 2.01 | 8.05 | 5.76 | 3.71 |
| $exp\tau_{1,con}$ [2)] | [N/mm²] | – [3)] | 7.06 | 3.03 | 5.65 | 5.48 | 3.59 |
| $\frac{exp\tau_{1,cyc}}{exp\tau_{1,con}}$ | [-] | – | 0.69 | 0.66 | 1.42 | 1.05 | 1.03 |

[1)] Mean value of simultaneous load and crack cycling tests
[2)] Mean value of load cycling in cracked concrete tests
[3)] Not tested

For $s_{max} = 0.5s_u$, simultaneous load and crack cycling tests show smaller initial bond strengths if compared to the cyclic load tests in constant cracks where the initial bond strength ratio of the two test types is approximately 0.7. The ratio is larger than 1.0 for $s_{max} = 1.0s_u$. An apparent explanation for this phenomenon cannot be found but is certainly linked to the non-linearity of both, the bond stress-slip curve and the slip-damage correlation. The initial bond strengths recorded for all tests can be found in Table C.1 and C.2 of Appendix C: Bond Test Data.

#### 4.4.1.5 Bond strength after the 10th cycle

The bond strength after the 10th cycle $exp\tau^{+}_{1(n=10)}$ is defined as the ultimate bond strength during the last positive slip of the simultaneous load and crack cycling and load cycling in constant cracks. The mean initial bond strength recorded for cast-in-place 16 mm reinforcing bars are given in Table 4.7. Characteristic values are not given since only two repeats per series were conducted.

Table 4.7 Bond strength after the 10th cycle of experimental tests under simultaneous load and crack cycling as well as load cycling in constant cracks for cast-in-place 16 mm reinforcing bars

| $s_{max} / s_u$ | [-] | 0.5 | | | 1.0 | | |
|---|---|---|---|---|---|---|---|
| $w_{max}$ | [mm] | 0.1 | 0.4 | 0.8 | 0.1 | 0.4 | 0.8 |
| $exp\tau^{+}_{1(n=10),cyc}$ [1] | [N/mm²] | 0.93 | 0.79 | 0.28 | 0.46 | 0.19 | 0.21 |
| $exp\tau^{+}_{1(n=10),con}$ [2] | [N/mm²] | –[3] | 1.28 | 0.59 | 0.77 | 0.32 | 0.33 |
| $\frac{exp\tau^{+}_{1(n=10),cyc}}{exp\tau^{+}_{1(n=10),con}}$ | [-] | – | 0.62 | 0.47 | 0.60 | 0.59 | 0.64 |

[1] Mean value of simultaneous load and crack cycling tests

[2] Mean value of load cycling in cracked concrete tests

[3] Not tested

For both, $s_{max} = 0.5s_u$ and $s_{max} = 1.0s_u$, simultaneous load and crack cycling tests show smaller bond strengths after the 10th cycle if compared to the cyclic load tests in constant cracks. The ratio of the bond strengths after the 10th cycle corresponding to the two test types is approximately 0.6. This observation clearly demonstrates the increased bond damage due to crack cycling. The bond strength after the 10th cycle recorded for all tests can be found in Table C.1 and C.2 of Appendix C: Bond Test Data.

#### 4.4.1.6 Residual bond strength

The residual bond strength $exp\tau_{u,res}$ determined after the cycling gives evidence of the previously accumulated bond damage. The mean residual bond strengths tested after the simultaneous load and crack cycling and load cycling in constant cracks for cast-in-place 16 mm reinforcing bars are shown in Table 4.8. Characteristic values are not given since only two repeats per series were conducted. The coefficient of variation ranged from 1.8 % to 49.7 % for load cycling in constant cracks and from 11.5 % to 36.5 % for simultaneous load and crack cycling.

Table 4.8 Residual bond strength experimental tests under simultaneous load and crack cycling as well as load cycling in constant cracks for cast-in-place 16 mm reinforcing bars

| $s_{max}$ / $s_u$ | [-] | 0.5 | | | 1.0 | | |
|---|---|---|---|---|---|---|---|
| $w_{max}$ | [mm] | 0.1 | 0.4 | 0.8 | 0.1 | 0.4 | 0.8 |
| $exp\tau_{u,res,cyc}$ [1)] | [N/mm²] | 4.65 | 1.65 | 1.68 | 1.78 | 0.90 | 0.55 |
| $exp\tau_{u,res,con}$ [2)] | [N/mm²] | –[3)] | 4.59 | 2.82 | 2.43 | 1.74 | 1.27 |
| $\frac{exp\tau_{u,res,cyc}}{exp\tau_{u,res,con}}$ | [-] | – | 0.36 | 0.60 | 0.73 | 0.52 | 0.43 |

[1)] Mean value of simultaneous load and crack cycling tests

[2)] Mean value of load cycling in cracked concrete tests

[3)] Not tested

The residual bond strength is significantly lower for pullout tests after simultaneous load and crack cycling if compared to the residual bond strength of the pullout tests conducted after cyclic loads in constant cracks. The residual bond strength ratio of the two test types is between 0.36 and 0.73. The residual bond strengths measured for all tests can be found in Table C.1 and C.2 of Appendix C: Bond Test Data.

### 4.4.2 Bond damage

The example bond stress-slip hysteresis and pullout curves of cast-in-place reinforcing bars shown in Figure 4.17 and Figure 4.20 illustrate that the energy hysteresis and consequently the bond damage is more pronounced for cycled cracks if compared to constant cracks. However, a visual evaluation of bond damage by means of Figure 4.17 and Figure 4.20 allows only a qualitative interpretation of the accumulated bond damage. Also, the residual bond strength as a function of the various parameters as shown in Section 4.4.1.6 is only a rough indicator of the accumulated bond damage.

Therefore the damage effect on bond is determined in the following analytically according to the hysteretic energy model of *Eligehausen, R.; Popov, E. et al. (1983)* (Section 2.2.13). Figure 4.22 illustrates how the hysteretic energy model was applied on simultaneous load and crack cycling tests to analyse the bond damage and frictional bond damage between the slip reversals.

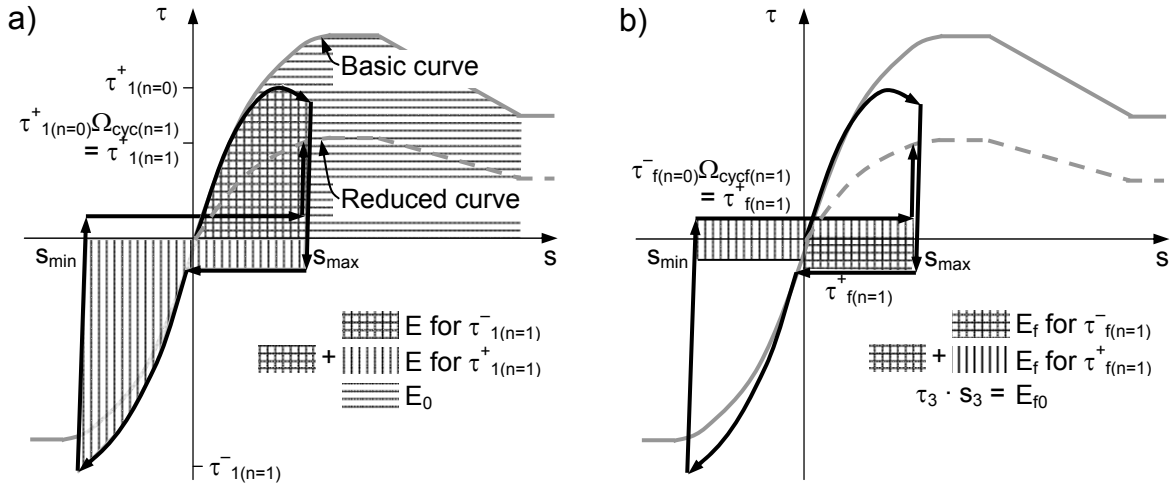


Figure 4.22 Hysteretic energy model to describe the a) bond damage, expressed by factor $\Omega_{cyc}$ and b) the frictional bond damage between the slip reversals, expressed by factor $\Omega_{cycf}$ due to simultaneous load and crack cycling

It is pointed out that in the following diagrams the factors $\Omega_{cyc}$ and $\Omega_{cycf}$ are used to express the accumulating bond damage and frictional bond damage between the slip reversals to be in line with the modelling of various effects presented in Section 2.2.10 to Section 2.2.13. In contrast, the diagrams presented in *Eligehausen, R.; Popov, E. et al. (1983)*, i.e. Figure 2.21b and Figure 2.22b, show the development of the damage parameters $d = 1 - \Omega_{cyc}$ and $d_f = 1 - \Omega_{cycf}$ as a function of the relatively dissipated energy $E / E_0$.

In order to calculate the relative dissipated energy in the context of bond damage, the dissipated energy E was normalised with reference to the energy $E_0$ dissipated during the monotonic test. Figure 4.23 depicts the factor $\Omega_{cyc}$ versus normalised dissipated energy $E / E_0$ for all tests of the test program (Table 4.2 and Table 4.3). For better readability, only the values after the first, the fifth and the tenth cycle are plotted. The bond damage follows roughly the same path for all tests carried out, independent of the testing parameters $s_{max}$, $\phi$, and $w_{max}$ and irrespective of whether the bars were cast-in-place or post-installed.

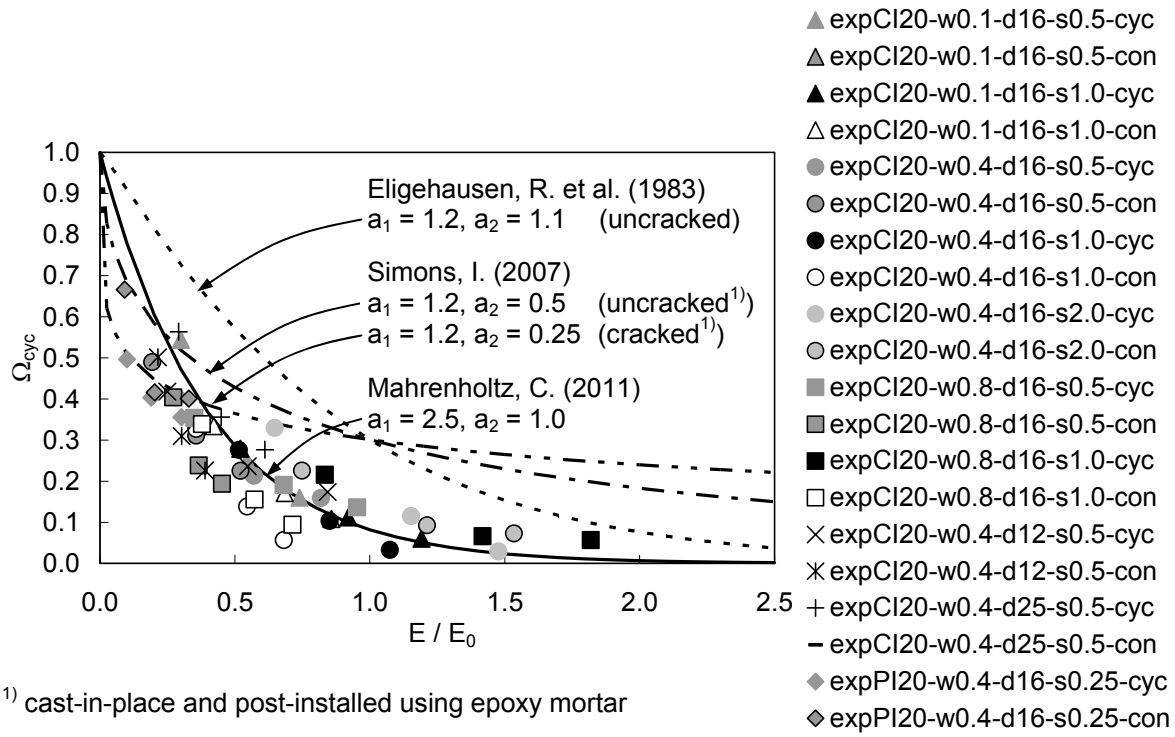


[1)] cast-in-place and post-installed using epoxy mortar

Figure 4.23 Factor $\Omega_{cyc}$ versus normalised energy dissipation E / $E_0$ to describe the bond damage of all tests (data points for cycle 1, 5, and 10 only)

The analytical description of the factor $\Omega_{cyc}$ according to *Eligehausen, R.; Popov, E. et al. (1983)* (dashed line), originally developed for uncracked concrete, is underestimating the bond damage for all conducted tests. According to *Eligehausen, R.; Popov, E. et al. (1983)*, the concrete strength does not influence the bond damage. This is plausible because of the normalisation of the dissipated energy with reference to the energy dissipated during the monotonic test. For the same reason the softening effect of the crack itself is not influencing the bond damage if described as shown in Figure 4.23. Therefore, a possible explanation for the difference between the tested bond damage (data points) and the bond damage predicted according to *Eligehausen, R.; Popov, E. et al. (1983)* (dashed line) are the different material properties of the test specimens used. For example, the related rib area $f_R \approx 0.07$ of the reinforcing bars used in the presented tests (Section 4.2.1.1) compared to $f_R = 0.10$ of the reinforcing bars tested in *Eligehausen, R.; Popov, E. et al. (1983)*. This assumption is supported by the fact that also the prediction of the bond damage for tests in uncracked concrete according to *Eligehausen, R.; Popov, E. et al. (1983)* (dashed line) and *Simons, I. (2007)* (dash-dotted line) show a significant difference.

The differences between the damage reported in *Simons, I. (2007)* for bond tests under load cycling in constant cracks (dash-double dotted line) and the damage determined for the bond tests under load cycling in constant cracks carried out

according to the test program given in Table 4.2 and Table 4.3 may also be ascribed to different material properties of the specimens used. Furthermore, the elastic elongation of the reinforcing bar between the bonded length and point of slip measurement may not have been deducted for the analyses presented in *Simons, I. (2007)* which leads to an underestimation of the bond damage. Besides, *Simons, I. (2007)* used a confined test setup while the tests presented in *Eligehausen, R.; Popov, E. et al. (1983)* and the tests according to the test program given in Table 4.2 and Table 4.3 where conducted on reinforcing bars which were furnished with a debonded pre-length to eliminate the effect of confinement (Section 2.2.2). Therefore, detailed comparisons with the results shown in *Simons, I. (2007)* appear to be of limited value due to the different parameters and bondary conditions used.

As in *Eligehausen, R.; Popov, E. et al. (1983)*, a visual best fit approach is deemed to be acceptable to tune the hysteretic energy model (Section 2.2.13). The bond damage of all tests carried out according to the test program (Table 4.2 and Table 4.3) can be described best using the tuning parameters $a_1 = 2.5$ and $a_2 = 1.0$. The resulting function is indicated by a solid line in Figure 4.23. Since the tested reinforcing bars showed a typical related rib area (Section 2.2.5), it is reasonable to assume that the proposed tuning parameters generally provide a good estimation of the bond damage for reinforcing bars with typical geometries.

In the following, the influence of the various test parameters on the bond damage is discussed in detail. To assist the reading of the following diagrams showing the development of the factors $\Omega_{cyc}$ as a function of $E / E_0$, it is mentioned that the damage is increasing with decreasing $\Omega_{cyc}$ values. Since the $\Omega_{cyc}$-$E / E_0$ correlation flattens with increasing bond damage it is easier to tell the damage on the basis of the relative dissipated energy $E / E_0$, in particular when considering the accumulated damage for the last cycle which data points are encircled. Data points corresponding to larger dissipated energy values indicate a more pronounced bond damage.

Figure 4.24 depicts the influence of peak slip and maximum crack width. The comparison of Figure 4.24a and Figure 4.24b with Figure 4.24c and Figure 4.24d shows that the energy dissipation and therefore the bond damage increases with increasing peak slip. The influence of the maximum crack width appears to be secondary, inconsistent, and overcast by scatter. In conclusion, tuning of the hysteretic bond model for various maximum crack widths is not meaningful and is a prerequisite for development a generic bond model.

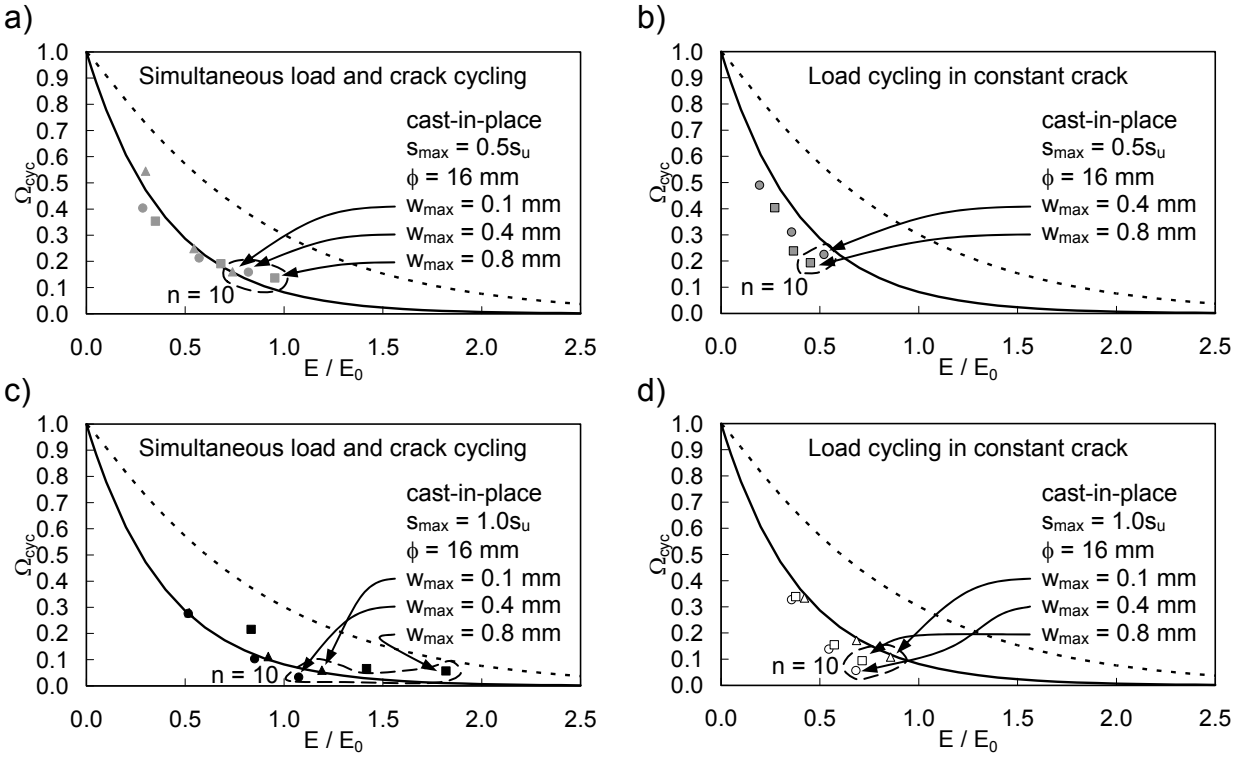


Figure 4.24 Influence of peak slip $s_{max}$ and maximum crack width $w_{max}$ on factor $\Omega_{cyc}$ for a) simultaneous load and crack cycling tests and b) load cycling tests in constant cracks (data points for cycle 1, 5 and 10)

Figure 4.25 shows that the influence of the reinforcing bar diameter on the bond damage is insignificant for the tested diameter range between 12 mm and 25 mm. This is true for both, the bond damage due to simultaneous load and crack cycling (Figure 4.25a) and the bond damage due to load cycling in constant cracks (Figure 4.25b). It is reasonable to assume that also the influence of bar diameters larger and smaller than those tested here is negligible.

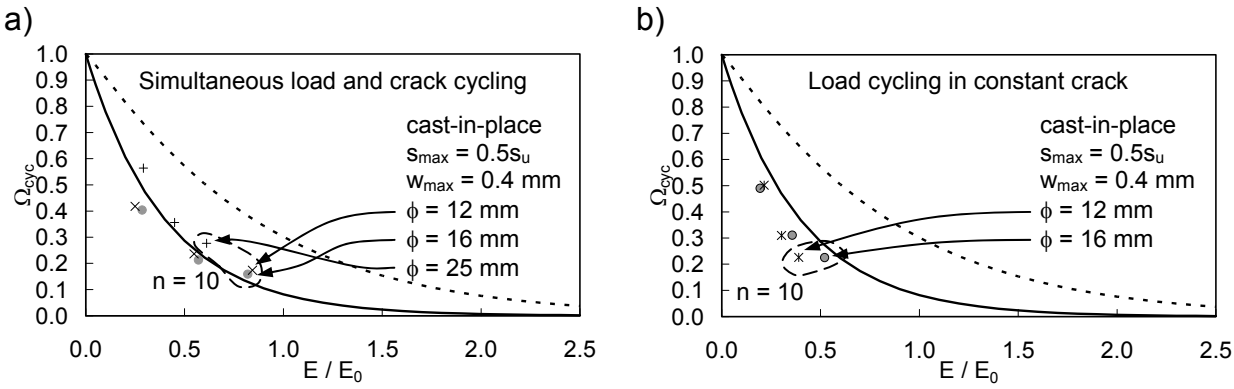


Figure 4.25 Influence of reinforcing bar diameter $\phi$, on factor $\Omega_{cyc}$ for a) simultaneous load and crack cycling tests and b) load cycling tests in constant cracks (data points for cycle 1, 5 and 10)

In general, the bond damage due to simultaneous load and crack cycling (Figure 4.24a, Figure 4.24c) is more pronounced if compared to the energy consumption due to load cycling in constant cracks (Figure 4.24b, Figure 4.24d). After n = 10 cycles, the energy dissipated in cyclic cracks is about two times larger than the energy dissipated in constant cracks. This can be attributed to the compression cycle of closed cracks which accelerates the bond damage.

Figure 4.26a and Figure 4.26b show that also the bond damage for peak slips $s_{max}$ larger $s_u$ is properly captured by the hysteretic energy model (*Eligehausen, R.; Popov, E. et al. (1983)*). Furthermore, Figure 4.26a and Figure 4.26b validate the application of the hysteretic energy model to describe the bond damage encountered by post-installed reinforcing bars because the agreement of the analytical and experimental results of the bond damage seems acceptable.

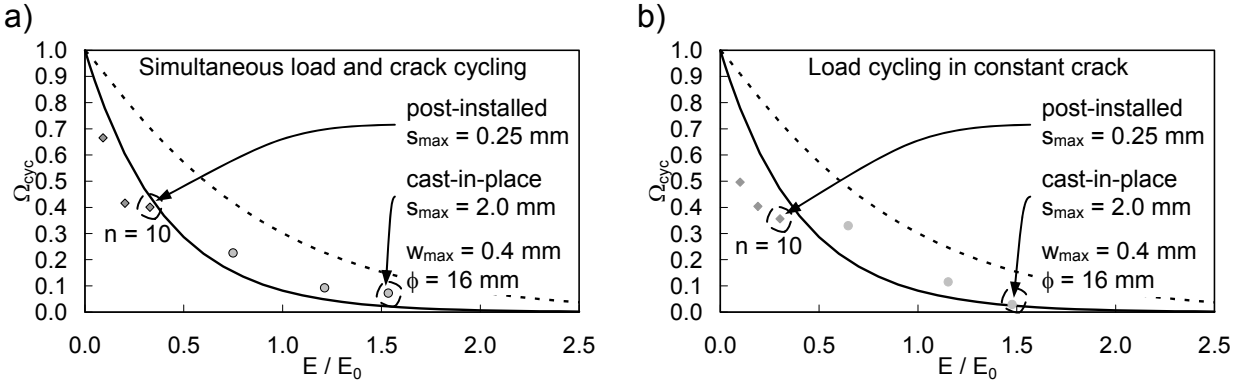


Figure 4.26 Influence of peak slip $s_{max}$ larger $s_u$ and installation method (cast-in-place and post-installed) on factor $\Omega_{cyc}$ for a) simultaneous load and crack cycling tests and b) load cycling tests in constant cracks (data points for cycle 1, 5 and 10)

Next the bond stress-slip relation between the slip reversals is evaluated according to the hysteretic energy model of *Eligehausen, R.; Popov, E. et al. (1983)* (Section 2.2.13). Figure 4.27 depicts the factor $\Omega_{cycf}$ versus normalised dissipated energy $E / E_{0f}$ for all tests of the test program (Table 4.2 and Table 4.3), plotting only the data points for the first, the fifth and the tenth cycle. The development of the frictional bond damage between the slip reversals is subject to large scatter which is in line with the studies presented in *Eligehausen, R.; Popov, E. et al. (1983)* (Figure 2.22b). The large scatter is attributed to the fact that the frictional bond stresses also show large scatter. Furthermore, the accuracy of the measured bond stresses well below 1 N/mm² is generally questionable because these results in very low forces (e.g. for $\phi$ = 16 mm: 1 N/mm² · $\pi$ · 16 mm · 5 · 16 mm = 4 kN) for which the load cell of the actuator is not calibrated that finely. Large scatters for tests in cracked concrete are also reported in *Simons, I. (2007)*.

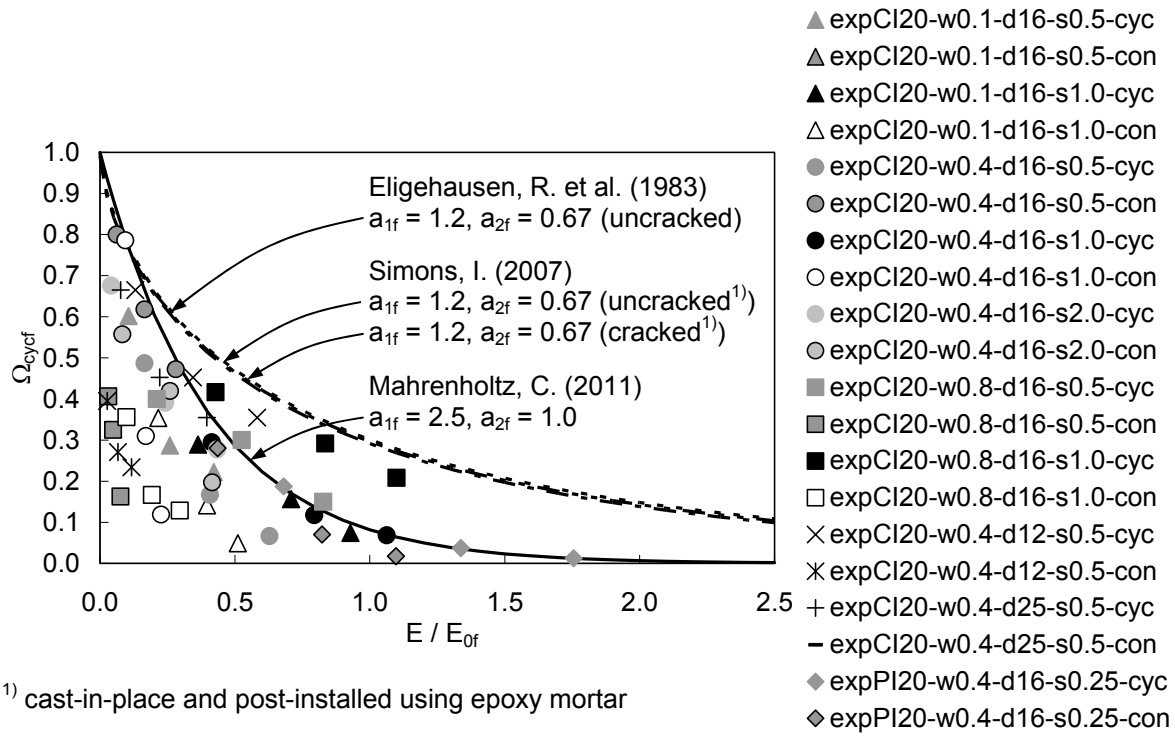


1) cast-in-place and post-installed using epoxy mortar

Figure 4.27 Factor $\Omega_{cycf}$ versus normalised energy dissipation E / $E_0$ to describe the frictional bond damage of all tests (data points for cycle 1, 5, and 10 only)

Due to the large scatter only less significant conclusions can be drawn. However, it is evident that by trend the analytical description of the factor $\Omega_{cycf}$ according to *Eligehausen, R.; Popov, E. et al. (1983)* (dashed line), which is identical to the proposal of *Simons, I. (2007)* (dash-dotted line), is underestimating the frictional bond damage between the slip reversals. The reason may be the same as for the bond damage, i.e. differences in either the setup or properties of the material used.

Like in *Eligehausen, R.; Popov, E. et al. (1983)*, a visual best fit approach is conducted to determine the tuning parameters $a_{1f}$ = 2.5 and $a_{2f}$ = 1.0 which are proposed for hysteretic energy model (Section 2.2.13) to describe the frictional bond damage between the slip reversals. The resulting function is indicated by a solid line in Figure 4.27.

In the following, the influence of the various test parameters on the frictional bond damage is discussed in detail. To assist the reading of the following diagrams showing the development of the factors $\Omega_{cycf}$ as a function of E / $E_{0f}$, it is pointed out that the damage is increasing with decreasing $\Omega_{cycf}$ values. Since the $\Omega_{cycf}$-E / $E_{0f}$ correlation flattens with increasing frictional bond damage it is more practicable to tell the damage on the basis of the relative dissipated energy E / $E_{0f}$, in particular when considering the accumulated damage for the last cycle for which the data points are

encircled. Data points corresponding to larger dissipated frictional energy values indicate more pronounced frictional bond damage.

Figure 4.28 illustrates the influence of peak slip and maximum crack width. A comparison of Figure 4.28a and Figure 4.28b with Figure 4.28c and Figure 4.28d shows that the energy consumption and consequently the frictional bond damage between the slip reversals is more pronounced for increasing peak slips. A statistically significant influence of the maximum crack width cannot be inferred.

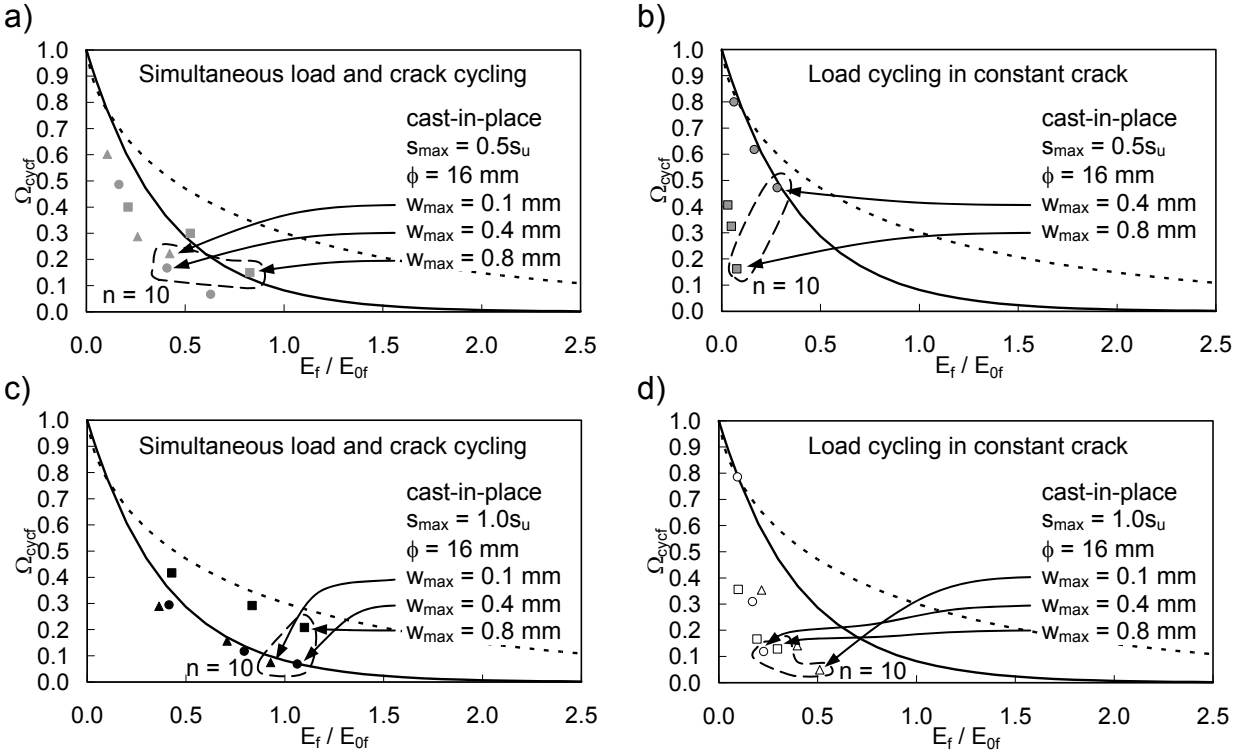


Figure 4.28 Influence of peak slip $s_{max}$ and maximum crack width $w_{max}$ on factor $\Omega_{cycf}$ for a) simultaneous load and crack cycling tests and b) load cycling tests in constant cracks (data points for cycle 1, 5 and 10)

From Figure 4.29, a statistically significant influence of the reinforcing bar diameter on the frictional bond damage factor cannot be readily concluded, neither for simultaneous load and crack cycling tests (Figure 4.29a) nor for load cycling tests in constant cracks (Figure 4.29b).

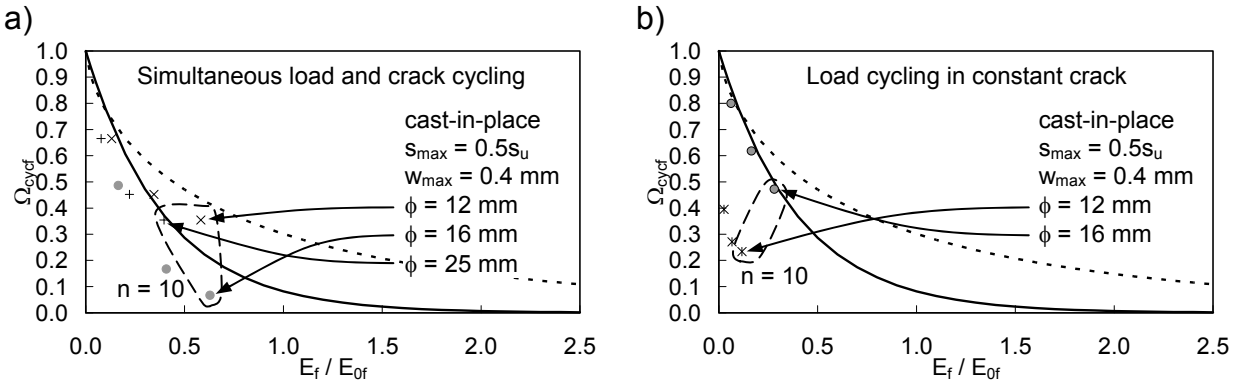


Figure 4.29 Influence of reinforcing bar diameter ϕ on factor $\Omega_{cycf}$ for a) simultaneous load and crack cycling tests and b) load cycling tests in constant cracks (data points for cycle 1, 5 and 10)

By trend, the frictional bond damage is more pronounced for simultaneous load and crack cycling (Figure 4.28a, Figure 4.28c) than for load cycling in constant cracks (Figure 4.28b, Figure 4.28d). After n = 10 cycles, the frictional energy dissipated in cyclic cracks is about two times larger than the frictional energy dissipated in constant cracks. In conclusion, the ratio of the damage experienced during cyclic cracks and constant cracks is similar for the bond damage and frictional bond damage.

Figure 4.30a and Figure 4.30b show that the hysteretic energy model (*Eligehausen, R.; Popov, E. et al. (1983)*) predicts the frictional bond damage between the slip reversals adequately also for peak slips $s_{max}$ larger than $s_u$. In addition, the hysteretic energy model is suitable to estimate the frictional bond damage on post-installed reinforcing bars because the agreement of the analytical and experimental results of the frictional bond damage seems acceptable.

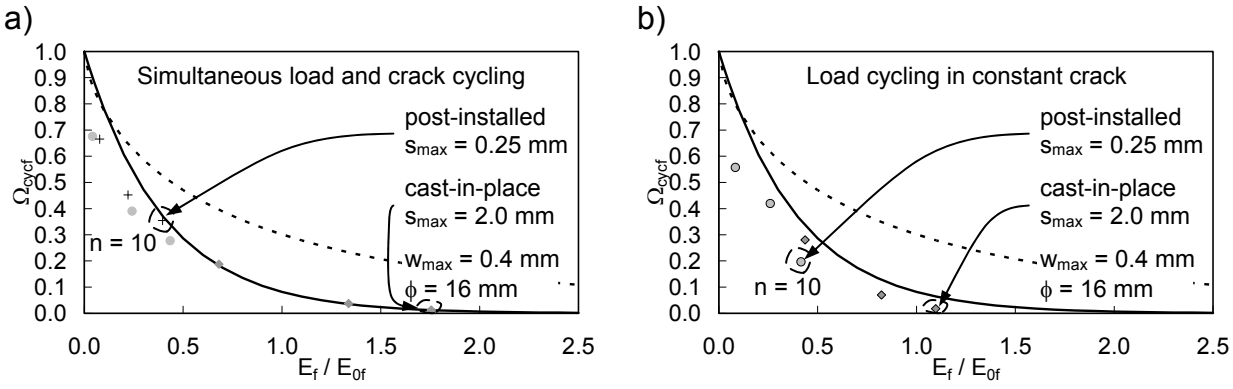


Figure 4.30 Influence of peak slip $s_{max}$ larger $s_u$ and installation method (cast-in-place and post-installed) on factor $\Omega_{cycf}$ for a) simultaneous load and crack cycling tests and b) load cycling tests in constant cracks (data points for cycle 1, 5 and 10)

## 4.5 Summary and Conclusions

The developed test setup proved to be capable to carry out tests of high complexity. The precise control of slip and crack histories allowed a sound and accurate analysis of the dissipated energy subject to critical test parameters. The simultaneous load and crack cycling tests on reinforcing bars were the first ever conducted and provided bond stress-slip curves which enabled a detailed discussion of the bond behaviour for the adverse condition during earthquake loading.

In general, the results of the monotonic reference tests and load cycling tests on reinforcing bars in cracked concrete were in line with observations made earlier. However, simultaneous load and crack cycling is characterised by an increased energy hysteresis and a more pronounced bond damage. This phenomenon is demonstrated by the dissipated energy which is approximately doubled if compared to load cycling in constant cracks. Because of the flattening bond damage-dissipated energy curve, however, the damage is not doubled due to crack cycling. According to *Mahrenholtz, C. (2011a)* cycled cracks increases the factor $\Omega_{cyc}$ approximately by the power of 1.25 if compared to constant cracks of the same crack width.

The experimental tests gave evidence that the hysteretic energy model (*Eligehausen, R.; Popov, E. et al. (1983)*) is capable to reflect the adverse condition of simultaneous load and crack cycling since Equation 2.8 and 2.9 allow adequate estimation of the bond damage effect. Most importantly the progressively decreasing values for the factor $\Omega_{cyc}$, reflect the bond strength reduction, cluster around one narrow band of scatter when plotted as a function of the normalised dissipated energy $E / E_0$, regardless of whether the crack is constant or cycled (Figure 4.23). Therefore, one set of tuning parameters are proposed which are independent from the actual concrete condition, i.e. uncracked, constantly cracked, cyclically cracked. This simplifying yet conservative approach allows the generic tuning of the hysteretic energy model which is then assumed to be valid for the complete reinforced concrete element. The frictional bond strength reduction expressed by the factor $\Omega_{cycf}$ is characterised by pronounced scatter as observed in *Eligehausen, R.; Popov, E. et al. (1983)*. $\Omega_{cycf}$ plotted as a function of the normalised dissipated frictional energy $E / E_{0f}$ (Figure 4.27) however, shows a similar correlation as the bond damage $\Omega_{cyc}$. Tuning parameters $a_1 = a_{1f} = 2.5$ and $a_2 = a_{2f} = 1.0$ are suggested for the cast-in-place reinforcing bars as well as for post-installed reinforcing bars and the epoxy mortar used.

The well known effects of transverse compressions and cracks parallel to the embedded reinforcing bar which come along with crack cycling are directly taken into account by the hysteretic energy model because transverse compression results in increased bond stress-slip curves and energy dissipations and parallel cracks result in reduced bond stress-slip curves and energy dissipations.

In conclusion, the bond behaviour of cast-in-place and post-installed reinforcing bars including seismic loading conditions can be comprehensively described by a bond model combining component-by-component known models replicating the influencing factors of transverse concrete compression (Section 2.2.10), parallel concrete cracks (Section 2.2.11), inelastic steel strain (Section 2.2.12), and damage effect (Section 2.2.13), provided the bond damage effect is captured according the hysteretic energy model. The components of such a comprehensive model indicate that the hysteretic energy model takes satisfactorily directly into account the increased bond damage due to simultaneous load and crack cycling.

# 5 Numerical Studies on Bond

In this chapter, the numerical studies conducted using a finite element model comprising solid, bar and bond elements are presented. The main objective was to show the capability of the bond element to take into account the realistic effect of simultaneous load and crack cycling and therefore to prove its suitability to be integrated in a model of a structural connection. A general introduction to the finite element program used as well as the pre- and post-processing program is given in Section 5.1. Relevant details of the numerical setup are explained in Section 5.2. Following this, the numerical procedure including the load protocol, test parameters and test program are introduced in Section 5.3. The test results are discussed in Section 5.4. Summary and conclusion are given in Section 5.6. The complete numerical test program of the studies on bond is reported in *Mahrenholtz, C. (2011c)*.

## 5.1 Basics

The realistic simulation of seismically loaded cast-in-place and post-installed reinforcing bars requires a capable finite element program which element library includes a bond element for discrete bond modelling. In addition, the finite element program including the bond element has to capture the effects of transverse compression and parallel cracks as well as the bond damage by means of the hysteretic energy model. A finite element program which meets these requirements is MASA, a program developed at the Institut für Werkstoffe im Bauwesen (IWB), University of Stuttgart, to conduct non-linear, three-dimensional, smeared fracture finite element analyses (FEA) of structures made of quasi-brittle materials. The engineering analysis program FEMAP is used for pre- and post-processing. The following explanation of the finite element method (FEM) implemented in MASA is partly an excerpt from *Sharma, A. (2008)* and *Ožbolt, J. (1999b)*.

### 5.1.1 MASA

Although different kinds of materials can be employed, MASA is mainly written to be used for the non-linear analysis of concrete and reinforced concrete structures. As the global solution strategy, three possibilities can be used: Constant stiffness method (CSM), tangent stiffness method (TSM), and secant stiffness method (SSM). While the stiffness matrix remains constant in the course of a computation applying

the CSM, the stiffness matrix is updated after a predefined number of iteration steps when the TSM or SSM is used.

In the following sections, the modelling of the reinforcing bars, concrete and bond is discussed.

#### 5.1.1.1 Modelling of reinforcing bar

The constitutive law for steel is described by the uniaxial stress-strain relation. The tri-linear curve is defined by the initial modulus of elasticity $E_0$, the hardening modulus $E_h$, the yield strength $f_y$ and the ultimate strength $f_s$. The relation for monotonic loading in Figure 5.1a and the relation for cyclic loading-unloading-reversed loading is shown in Figure 5.1b.

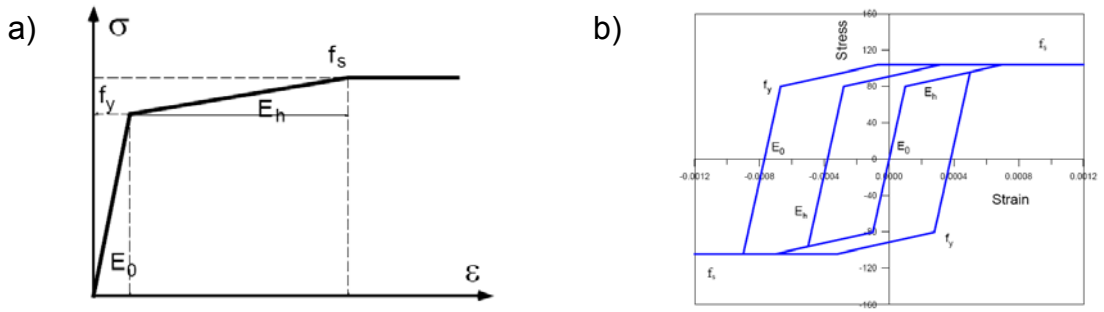


Figure 5.1 a) Monotonic steel stress-strain model (*Ožbolt, J. (1999b)*); b) Cyclic steel stress-strain model (*Ožbolt, J. (1999b)*)

The reinforcement is modelled by truss elements or bar elements with fixed end rotations. Both elements have three degree of freedoms (DOF) per node. The benefit of both element types is a substantially reduced number of DOF and thus work load for the computation compared to fully-fledged bar elements with six DOF at the nodes. If deformations of reinforced concrete members are governed by pure bending, the employment of truss elements provides good results. On the contrary, the dowel action of a shear dominated situation is better simulated by bar elements with fixed end rotations. For typical, shear and bending loaded structural connections, however, deformations are underestimated when the reinforcement is modelled by truss elements (Figure 5.2a) and overestimated when using bar elements with fixed end rotations (Figure 5.2b).

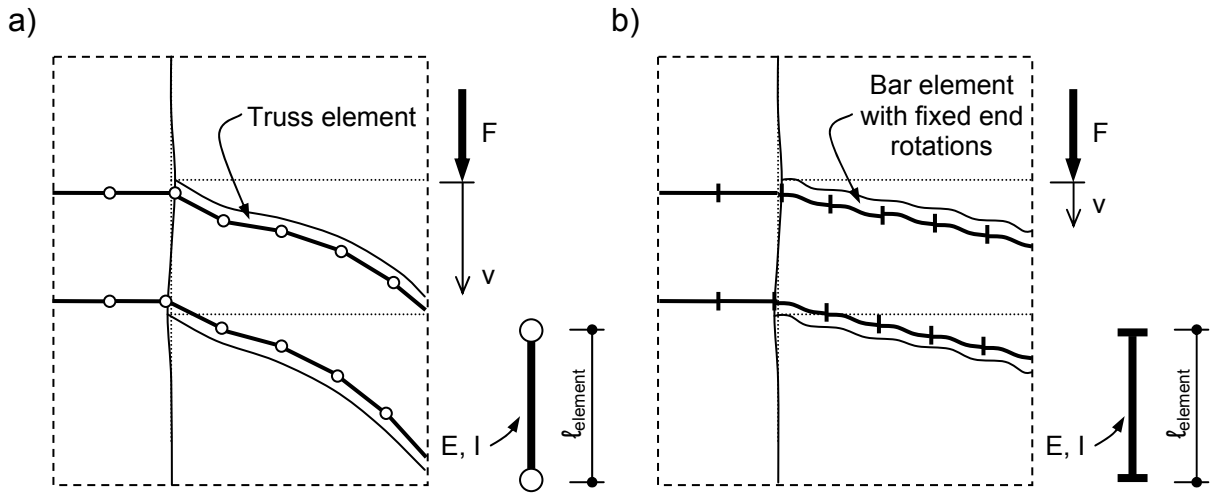


Figure 5.2 Influence on the deformation behaviour of a loaded structural connection: a) Truss elements leading to overestimated deformations; b) Bar elements with fixed end rotations resulting in underestimated deformations

The rotational stiffness $k = 4EI / \ell_{element}$ of the bar elements can be tuned by specifying imaginary lengths $\ell$ which differ from the real element length. This tuning may improve the accuracy of the simulation. For the sake of clarity, the elements modelling the reinforcing bars are termed in the following as bar elements if a differentiation between truss elements and bar elements with fixed end rotations is not required.

#### 5.1.1.2 Modelling of concrete

The microplane model is used to simulate the behaviour of the concrete (*Bažant, Z.; Ožbolt, J. (1990)*). For the microplane model the material is characterised by a relation between the stress and strain components on planes of various orientations (*Ožbolt, J.; Li, Y.-J. et al. (2001)*). These planes may be imagined to represent the damage planes or weak planes in the microstructure, such as contact layers between aggregate pieces in concrete (Figure 5.3).

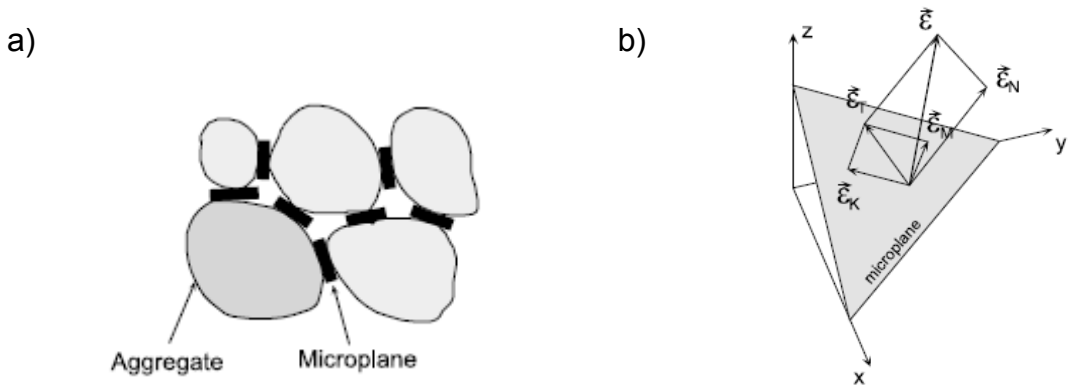


Figure 5.3 Microplane model: a) Load transfer over a number of idealised contact planes; b) Decomposition of the total macroscopic strain tensor on the microplane (*Ožbolt, J.; Li, Y.-J. et al. (2001)*)

The macroscopic response is obtained by integrating contributions of all microplanes. To model concrete for dominant compressive load realistically and to control the initial elastic value of the Poisson's ratio, the normal microplane component is decomposed into volumetric and deviatoric part. The loading-unloading-reloading rules for microplane components are schematically plotted for the volumetric component in Figure 5.4a and for the deviatoric component in Figure 5.4b.

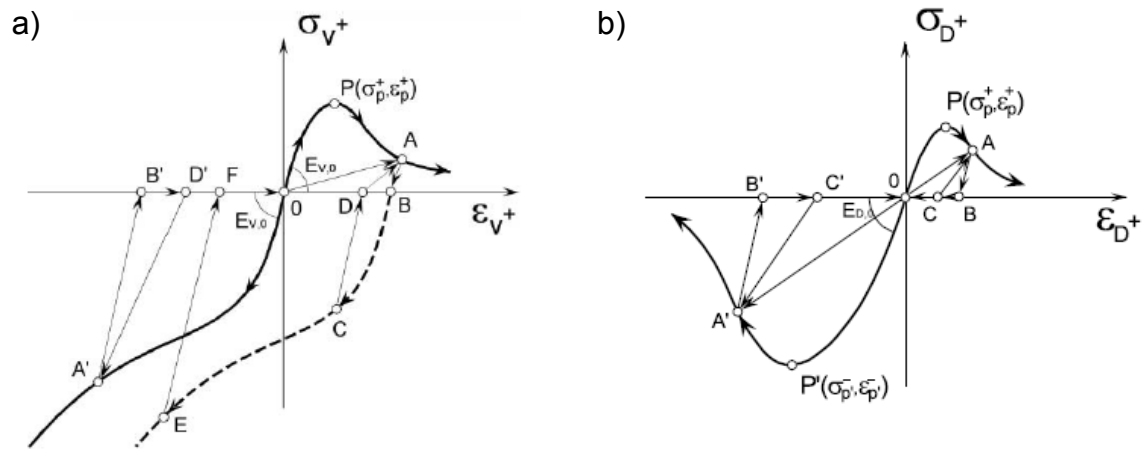


Figure 5.4 Loading-unloading-reloading rules for microplane components (*Ožbolt, J.; Li, Y.-J. et al. (2001)*): a) Volumetric component; b) Deviatoric component

Figure 5.5a and Figure 5.5b show the response of specimens subjected to uniaxial cyclic loading.

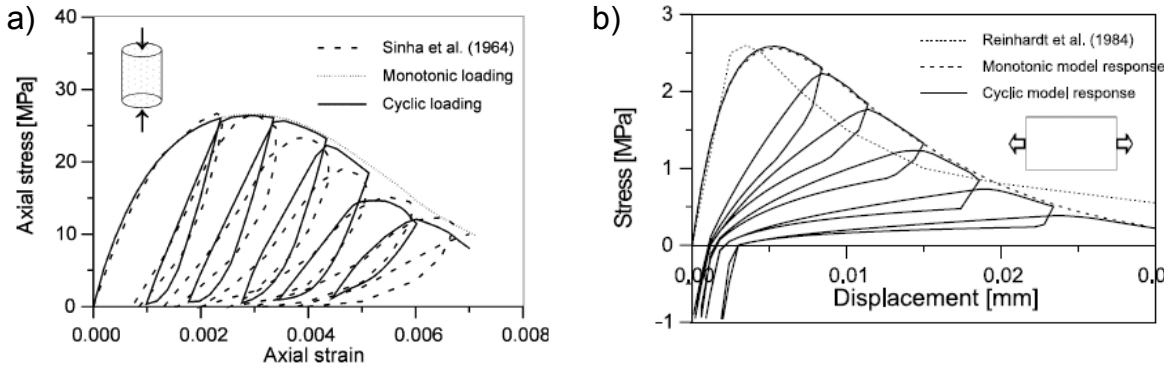


Figure 5.5 Monotonic and cyclic concrete stress-strain relation (*Ožbolt, J.; Li, Y.-J. et al. (2001)* and *Ožbolt, J. (1999b)*): a) Uniaxial compression; b) Uniaxial tension and compression

Cracking and material damage phenomena are modelled by the smeared crack method. The conventional local continuum smeared fracture analysis of materials which exhibits pronounced softening leads to results which are in general mesh dependent. The reason for this is localisation of damage and related energy consumption capacity which depends on the element size, i.e. for coarser finite element meshes the energy consumption capacity will be larger and vice versa (Figure 5.6).

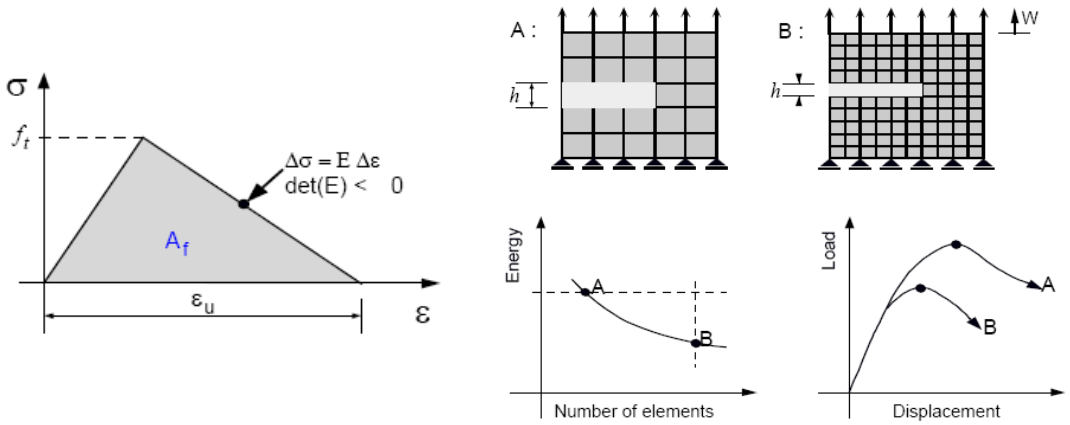


Figure 5.6 Dependency of local smeared crack finite element analysis on the size of finite elements (*Ožbolt, J. (1999b)* after *Bažant, Z.; Cedolin, L. (1979)*)

Therefore, a localisation limiter was implemented in the MASA code to regularise the total energy consumption capacity as an attempt to assure a mesh independent result. The main assumption of the crack band method used is that cracks are expressed as a material damage which is localised in a row of finite elements. To assure a constant and mesh independent concrete fracture energy $G_F$, the constitutive law needs to be modified such that $G_F = A_f h$ is constant, where $A_f$ is the area under the uniaxial tensile stress-strain curve and h is the average element size

and therefore the width of the crack band (Figure 5.6). Principally, the same relation is valid for uniaxial compression with the assumption that the concrete compressive fracture energy $G_C$ is a material constant. Therefore, also $G_C = A_{fc}h$ is assumed to be constant, where $A_{fc}$ is the area under the uniaxial compressive stress-strain curve. Although the crack band method provides results which are independent of the element size, they can still depend on the orientation with respect to the stress field and shape of the finite elements. This is particularly true for relatively coarse meshes. To reduce this dependency while keeping the simplicity and relatively low computational costs of the crack band method, an advanced stress relaxation method was developed and implemented in the MASA code.

#### 5.1.1.3 Modelling of bond

In engineering practice, the reinforcement slip is typically neglected, and a rigid connection between concrete and reinforcing bar is assumed for the finite element analyses of reinforced concrete. In the context of research on bond however, the bond characteristic has to be considered. For example, the calculated slip corresponding to the peak load of pullout tests on straight anchorages is doubled if realistic bond instead of perfect bond properties are considered (*Jendele, L.; Cervenka, J. (2006)*). *Shi, Y.-C.; Li, Z.-X. et al. (2009)* pointed out that realistic bond modelling is in particular important for seismic loading.

MASA features a discrete bond element to consider the bond realistically. The bond element essentially consists of non-linear springs (Figure 5.7). The spring characteristic is equivalent to the constitutive law of bond, i.e. the monotonic bond model (Section 2.2.4). The bond element serves as a means of connecting the one-dimensional reinforcing bar element to the surrounding three-dimensional concrete elements.

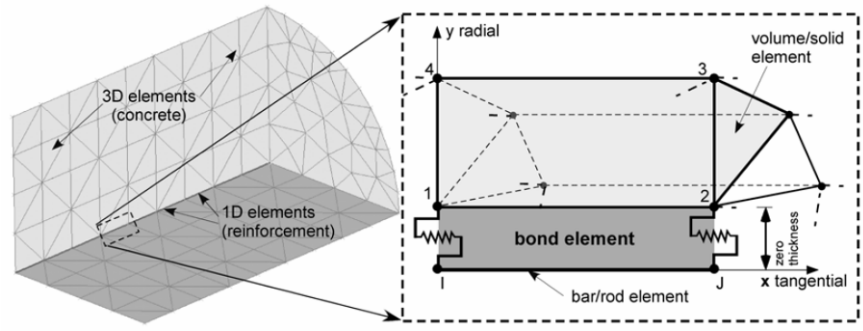


Figure 5.7 Bond element provided in MASA (*Lettow, S.; Eligehausen, R. et al. (2004)*)

The constitutive law of bond is defined according to *Lowes, L.; Moehle, J. et al. (2004)* employing a piecewise function on the basis of the studies presented in *Eligehausen, R.; Popov, E. et al. (1983)*. The ascending branch of the bond stress-slip curve is described corresponding to a function developed by *Menegotto, M.; Pinto, P. (1973)* to model the cyclic stress strain behaviour of reinforcing bars. The bond resistance is split into two components, namely a mechanical component $\tau_m$ and a frictional component $\tau_f$. Figure 5.8 shows the basic bond stress-slip curve.

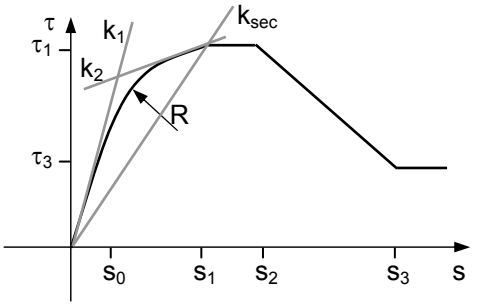


$$s \le s_1: \quad \tau = \left(\frac{s}{s_0}\right) \cdot \left[\left(\frac{k_2}{k_1}\right) + \left(1 - \left(\frac{k_2}{k_1}\right)\right) \cdot \left(\frac{1}{1 + \left(\frac{s}{s_0}\right)^R}\right)^{\frac{1}{R}}\right]$$

$$s_1 \le s \le s_2: \quad \tau = \tau_m + \tau_f$$

$$s_2 \le s \le s_3: \quad \tau = \tau_m \cdot \left(\frac{s_3 - s}{s_3 - s_2}\right) + \tau_f$$

$$s_3 \le s: \quad \tau = \tau_f$$

Figure 5.8 Basic bond stress-slip curve according to *Lowes, L.; Moehle, J. et al. (2004)* on the basis of *Eligehausen, R.; Popov, E. et al. (1983)*

*Lettow, S. (2007)* carried out a substantial literature review to determine realistic parameter values for the bond model for monotonic loading. The influence of the concrete strength on the bond was assumed to be proportional to the square root of the mean concrete compressive strength $f_{cm}$, the parameter $s_3$ was taken equal to the rib distance c, and the frictional bond was specified as $\tau_f = \tau_3 = 0.4\tau_1$. Table 5.1 gives an overview on the suggested functions and values.

Table 5.1 Functions and values suggested by *Lettow, S. (2007)* to define the parameters of the bond stress-slip curve according to *Lowes, L.; Moehle, J. et al. (2004)* on the basis of *Eligehausen, R.; Popov, E. et al. (1983)*

| Parameter | Function or value | Unit | Remark |
|---|---|---|---|
| $\tau_1$ = | $20f_R^{0.8} \cdot f_c^{0.5}$ | [N/mm$^2$] | ($f_c$ in MPa) |
| $\tau_3$ = | $0.4\tau_1$ | [N/mm$^2$] | ($0.3 \div 0.5\tau_1$) |
| $\tau_m$ = | $\tau_1 - \tau_f$ | [N/mm$^2$] | |
| $k_{sec}$ = | $120f_R + 0.23f_c$ | [(N/mm$^2$) / mm] | ($f_c$ in MPa) |
| $k_1$ = | $(0.8 + 20f_R) \cdot k_{secant}$ | [(N/mm$^2$) / mm] | |
| $k_2$ = | $(0.22 - 2f_R) \cdot k_{secant}$ | [(N/mm$^2$) / mm] | |
| $s_1$ = | $\tau_1 / k_{sec}$ | [mm] | |
| $s_2 - s_1$ = | 0.8 | [mm] | (0.6 ÷ 1.0) |
| $s_3$ = | c | [mm] | |
| R = | 5.0 | [-] | (1.0 ÷ 5.0) |

All parameter values are defined by the concrete strength $f_c$ and the reinforcing bar geometry in terms of related rib area $f_R$, rib height a, and rib distance c. The values proposed by *Lettow, S. (2007)* are given in Table 5.2.

Table 5.2 Geometric parameters of reinforcing bars suggested by *Lettow, S. (2007)* as being typical, with the addition of $\phi$ = 32 mm by the author

| $\phi$ | [mm] | 6 | 10 | 12 | 16 | 20 | 25 | 32 |
|---|---|---|---|---|---|---|---|---|
| $f_R$ | [-] | 0.050 | 0.060 | 0.070 | 0.080 | 0.085 | 0.090 | 0.094 |
| a | [mm] | 0.25 | 0.42 | 0.60 | 0.80 | 1.02 | 1.26 | 1.52 |
| c | [mm] | 5.0 | 7.0 | 8.5 | 10.0 | 12.0 | 14.0 | 15.4 |

The hysteretic energy model was implemented to account for the bond damage due to load cycling (Section 2.2.13). Further, the formulation of the bond element takes into consideration the influence of transverse concrete compression (Section 2.2.10) and inelastic steel strains (Section 2.2.11). The effects are taken into account by multiplying the basic bond stress-slip curve (Figure 5.8) by the factors $\Omega_c$, $\Omega_s$, and $\Omega_{cyc}$, yielding a factored bond stress-slip curve (Section 2.2.15). Concrete cracks are expressed by softened concrete elements (Section 5.1.1.2) which reduce the bond strength of bond elements situated in the crack. Reference is made to *Ožbolt, J.; Lettow, S. et al. (2002)* for further details regarding to the bond element and the equations used for its definition. The bond elements allow the simulation of reinforced

concrete structures realistically which was shown by numerous studies (e.g. *Sharma, A.; Ožbolt, J. et al. (2010)*).

### 5.1.2 FEMAP

The engineering analysis program FEMAP is used to create finite element models (pre-processing) and to visualise the computed results (post-processing). For pre-processing, FEMAP provides meshing tools helping to generate the numerical description of nodes, nodal connectivity, boundary conditions, material data, and loads. A tailor-made FEMAP application enables modelling the bond elements. The data transfer between FEMAP and MASA is realised through interface programs integrated in MASA. For post-processing, the analysis results are handled in the neutral file format (*.neu) ready for visual interpretation and readout in FEMAP.

### 5.1.3 Testing of bond element with respect to load cycling

Figure 5.9a shows a simple model employing 1 bar element (2) connected by means of 2 bond elements (3) to 4 solid elements (1) which was generated to demonstrate the functioning of the bond element. For this purpose, all outer nodes of solid elements were constrained by pin bearings.

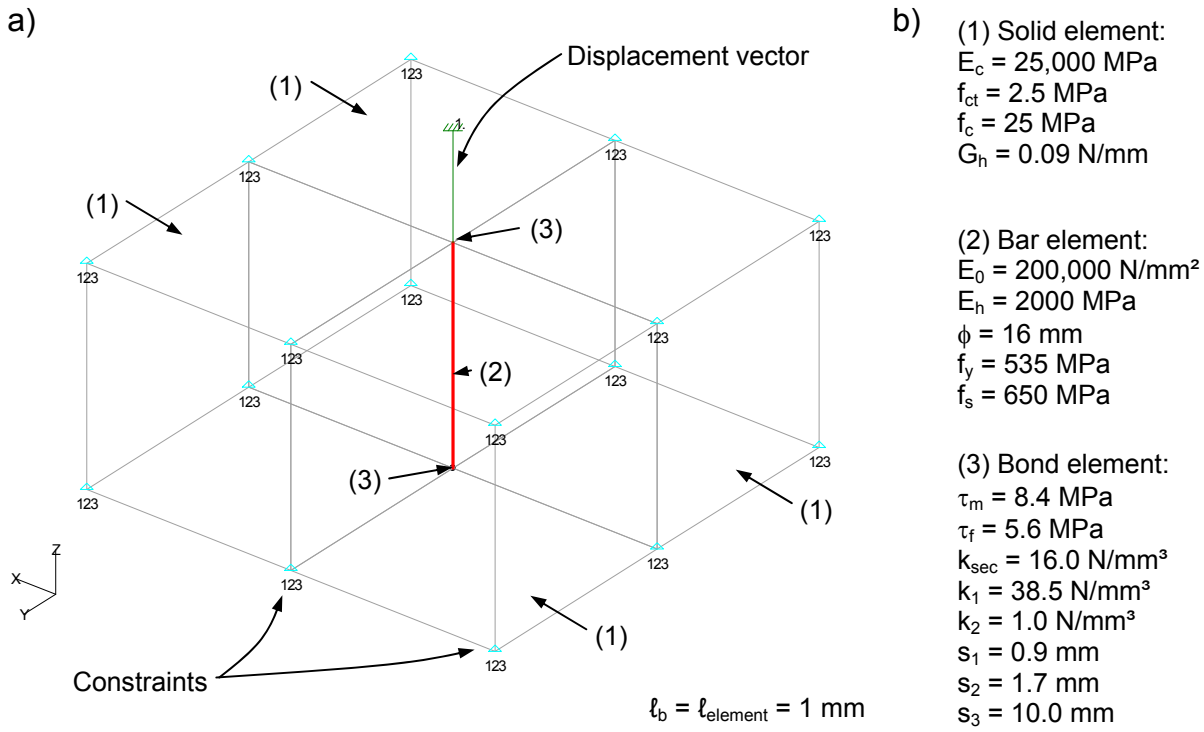


Figure 5.9 a) Model employing 1 bar element connected by means of 2 bond elements to 4 solid elements; b) Parameter used to define property of bar element, bond elements, and solid elements

The bar element was loaded monotonically and cyclically (10 cycles between the peak slips of 1 mm) by a displacement vector acting on the top node of the bar element. The finite element analysis provided the resulting force N. The bond stress was calculated by dividing the force N by the theoretical bond surface of the simulated bar, i.e. $\pi \cdot \phi \cdot \ell_b$. The monotonic bond stress-slip curve (Figure 5.10a) shows the characteristic points of the constitutive law of bond according to the parameters defining the material properties of concrete, reinforcing bar, and bond (Figure 5.9b). The cyclic bond stress-slip curves (Figure 5.10b) replicate the hysteretic energy model (Section 2.2.13).

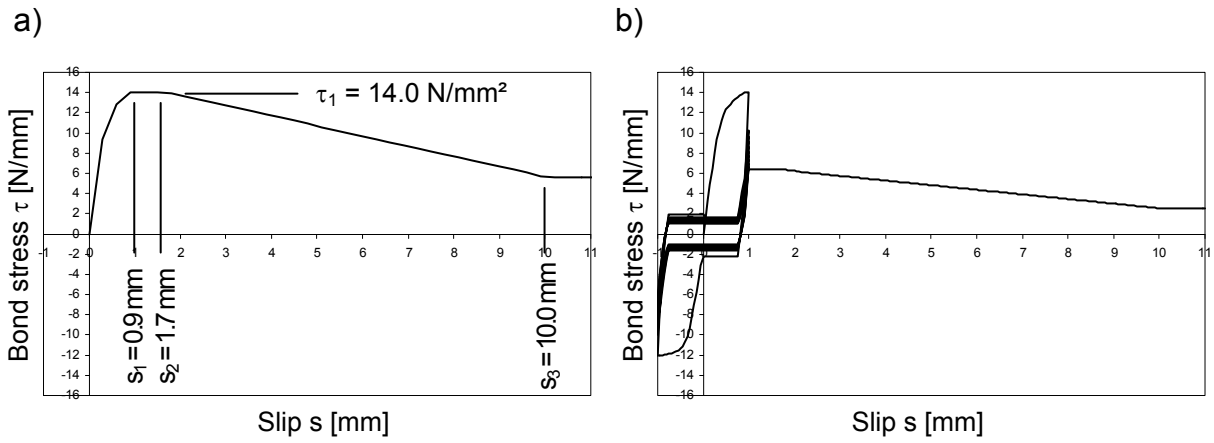


Figure 5.10 Bond stress-slip curve (*Mahrenholtz, C. (2011c)*): a) Monotonic loading b) Cyclic loading

## 5.2 Numerical Setup

### 5.2.1 Model

The model presented in the following is the first model to be developed to simulate the bond stress-slip behaviour of reinforcing bars in cracked concrete and the effect of crack cycling on the bond. Numerous pre-tests were carried out to optimise the detailing of the model and to identify a solution to apply the loading required to generate reinforcing bar slip and crack width according to the load protocol. The final solution presented in the following is a compromise of several requirements such as computational performance (keywords: element size, load steps, number of iterations), realistic simulation of tests (keywords: boundary conditions, state of stress, bar stiffness) and load control (keywords: crack width and bar slip during crack opening, cycling and pullout).

Figure 5.11 shows the developed model with outer dimensions of L / W / H = 240 mm / 240 mm / 240 mm. The elements were generated in a 10 mm by 10 mm grid. Only the bonded length of the reinforcing bar was modelled. Bar elements with fixed end rotations (Section 5.1.1.1) were used to avoid buckling of the

bars during the cyclic push-pull-loading. The concrete was modelled employing solid elements (Section 5.1.1.2). The solid elements were disconnected from each other above and below the bonded length. They were partly defined by linear-elastic properties to allow a gradual introduction of the strains which were generated by the displacement vectors controlling the concrete crack width. Bar and solid elements were connected by means of bond elements (Section 5.1.1.3). The displacement vector controlling the reinforcing bar slip loaded the central node of the bar elements. The model comprised 13,640 elements with 15,550 nodes.

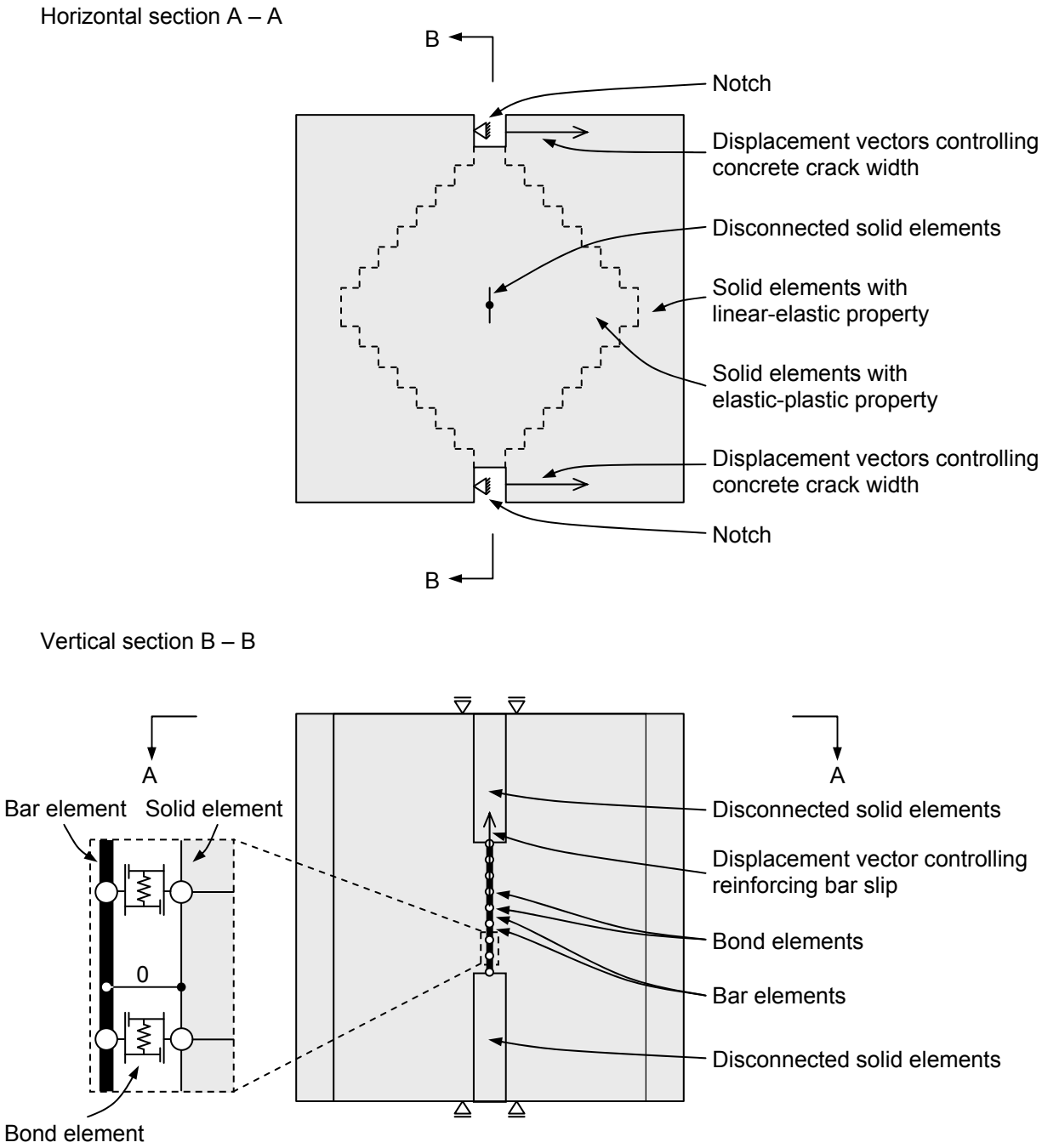


Figure 5.11 Finite element model

No attempts were made to tune the parameters of the element properties for each specimen separately in order to obtain the best possible agreement of the numerical and experimental bond stress-slip curves. Instead, a parameter set of intermediate values was used to guarantee the general significance of the results. In the following, the parameters are presented which were selected taking into account the material test results and the values given in the codes.

#### 5.2.1.1 Reinforcing bars

The specified key material parameters defining the reinforcing bar properties in MASA are given in Table 5.3. The exact strengths $f_y$ and $f_u$ were not critical, provided the steel remained in the elastic range to be in line with the experimental bond test. The steel stress-strain model is visualised in Figure 5.1.

Table 5.3 Key material parameters for reinforcing bars

| Diameter [mm] | Yield strength $f_y$ [MPa] | Tensile strength $f_u$ [MPa] | Modulus of elasticity $E_s$ [N/mm²] |
|---|---|---|---|
| 12<br>16<br>25 | 535 | 650 | 200,000 |

#### 5.2.1.2 Concrete

The key parameters defining the concrete properties in MASA are the compressive strength $f_c$, the tensile strength $f_{ct}$, the modulus of elasticity $E_c$, and the fracture energy $G_f$. The concrete members used for the experimental tests were cast in concrete class C20/25 according to *Eurocode 2 (2005)*. Therefore, the mean compressive strength $f_{cm}$ specified in *Eurocode 2 (2005)* for concrete class C20/25 was taken for the simulation. The experimentally tested compressive strengths $f_c$ are given in Table C.1 and C.2 of Appendix C: Bond Test Data.

The tensile strength $f_{ct}$ and modulus of elasticity $E_c$ were calculated on the basis of the mean compressive strength $f_{cm}$ according to *Eurocode 2 (2005)*:

$$f_{ctm} = 0.30 \cdot f_{ck}^{2/3} = 0.30 \cdot (f_{cm} - 8\,\text{MPa})^{2/3} \qquad \text{Equation 5.1}$$

$$E_{cm} = 22{,}000 \cdot (f_{cm}/10)^{0.3} \qquad \text{Equation 5.2}$$

Also the fracture energy $G_f$ was estimated on the basis of the mean compressive strength $f_{cm}$ according to *Karihaloo, B. (1994)*:

$$G_{fm} = 8 \cdot f_{cm}^{0.7} / 1000 \qquad \text{Equation 5.3}$$

The resulting key material parameters are compiled in Table 5.4 which also provides the values taken for the simulation of high strength concrete to extend the parametric range (Section 5.5).

Table 5.4 Key material parameters for concrete

| Concrete grade | Compress. strength $f_c$ [MPa] | Tensile strength $f_{ct}$ [MPa] | Modulus of elasticity $E_c$ [N/mm²] | Fracture energy $G_f$ [N/mm$^2$ · mm] |
|---|---|---|---|---|
| C20/25 | 28 | 2.2 | 30,000 | 0.08 |
| C50/60 | 58 | 4.1 | 37,000 | 0.14 |

#### 5.2.1.3 Bond

The parameters required to define the bond characteristics in MASA are explained in Section 5.1.1.3. The bond strength $\tau_1$ and its corresponding slip $s_1$ as well as the slip plateau $s_2 – s_2$ are the key parameters (Table 5.5). The slip values characterising the bond of cast-in-place and post-installed reinforcing bars were specified according to *Lettow, S. (2007)*. The bond strength $\tau_1$ was defined for all bar diameters on basis of the experimentally tested bond strengths $\tau_u$ which were approximately 8 N/mm² for reinforcing bars cast-in-place in uncracked concrete class C20/25. The experimentally tested bond strengths $\tau_u$ for post-installed reinforcing bars were close to 30 N/mm². It is noted that the tested cast-in-place and post-installed reinforcing bars were furnished with a debonded pre-length to eliminate the effect of confinement generated by the confined setup. The tested bond strengths are given in Table C.1 and C.2 of Appendix C: Bond Test Data.

Table 5.5 also provides the values taken for the simulation of bond tests in high strength concrete to extend the parametric range (Section 5.5). Due to the absence of relevant bond tests, the bond strength $\tau_1$ for concrete class C50/60 was taken as the bond strength $\tau_1$ for concrete class C20/25 multiplied by $(f_{ck,C50/60} / f_{ck,C20/25})^{0.5}$ which is a common approach (Section 2.2.6). Generally, the influence of the concrete strength on the bond strength of post-installed reinforcing bars is small or even insignificant (Section 2.2.5). Therefore, it is deemed to be acceptable to use identical bond material parameters for post-installed reinforcing bars irrespective of the concrete grade the bars are installed in.

Table 5.5 Key material parameters for bond

| Concrete grade | Installation method | Bond strength $\tau_1 = \tau_m + \tau_f$ [MPa] | Slip begin. plateau $s_1$ [mm] | Slip plateau $s_2 - s_1$ [mm] |
|---|---|---|---|---|
| C20/25 | cast-in-place | 8 | 0.9 | 0.8 |
| C50/60 | cast-in-place | 12 | 0.9 | 0.8 |
| C20/25 | post-installed | 30 | 0.9 | 0.8 |
| C50/60 | post-installed | 30 | 0.9 | 0.8 |

### 5.2.2 Boundary and loading conditions

The boundary and loading conditions of the model shown in Figure 5.11 were designed corresponding to the experimental tests (Chapter 4). The concrete was loaded by a series of displacement vectors acting along the notch to generate the crack width (Figure 5.11). The reinforcing bar was loaded by a displacement vector at its centre. The confined setup was simulated by a set of bearings at the top and bottom face while a series of bearings along the notches were required to satisfy the equilibrium in the other directions.

## 5.3 Numerical Procedure

### 5.3.1 Load protocol

In principal, the numerical tests were carried out corresponding to the procedures of the experimental tests. The proportionality of displacement vector controlling the reinforcing bar slip and the displacement vectors controlling the concrete crack width allowed the simultaneous load and crack cycling tests to be conducted in one run. The load cycling tests in constant cracks required two runs, one to open the crack while the displacement vector controlling the reinforcing bar slip was set to zero and another one to generate the reinforcing bar slip while the displacement vectors controlling the concrete crack width were set to zero which arrested the opened crack.

The secant stiffness method (SSM) was applied to allow subsequent runs. In consequence, the computation time accumulated to about 2 days per test (Resource: Quadcore, 2.66 GHz CPU, 8 GB RAM, 64-bit OS, MASA kernel 25.01.2011).

### 5.3.2 Test program

The primary program of the numerical tests partly mirrored the test program of the experimental tests (Table 4.2 and Table 4.3) comprising the same test parameters.

The program is given in Table 5.6 for tests on cast-in-place and and in Table 5.7 for tests on post-installed reinforcing bars.

Table 5.6 Numerical test program of tests on cast-in-place reinforcing bars

| Cast-in-place | Crack width $w_{max}$ [mm] | Bar diameter $\phi$ [mm] | Peak slip $s_{max}$ / $s_u$ $-s_{min}$ / $s_u$ [-] | Number of cycles $n_{cyc}$ [-] |
|---|---|---|---|---|
| Monotonic loading, compressed concrete | | | | |
| numCI20-w0.0-d16-com | – | 16 | – | – |
| Monotonic loading, uncracked concrete | | | | |
| numCI20-w0.0-d16-ucr | – | 16 | – | – |
| Monotonic loading, cracked concrete | | | | |
| numCI20-w0.1-d16-cr | 0.1 | 16 | – | 10 |
| numCI20-w0.4-d16-cr | 0.4 | 16 | – | 10 |
| numCI20-w0.8-d16-cr | 0.8 | 16 | – | 10 |
| Load cycling in constant cracks | | | | |
| numCI20-w0.4-d16-s0.5-con | 0.4 | 16 | 0.5 | 10 |
| numCI20-w0.4-d16-s1.0-con | 0.4 | 16 | 1.0 | 10 |
| numCI20-w0.4-d16-s2.0-con | 0.4 | 16 | 2.0 | 10 |
| Simultaneous load and crack cycling | | | | |
| numCI20-w0.1-d16-s0.5-cyc | 0.1 | 16 | 0.5 | 10 |
| numCI20-w0.1-d16-s1.0-cyc | 0.1 | 16 | 1.0 | 10 |
| numCI20-w0.4-d16-s0.5-cyc | 0.4 | 16 | 0.5 | 10 |
| numCI20-w0.4-d16-s1.0-cyc | 0.4 | 16 | 1.0 | 10 |
| numCI20-w0.4-d16-s2.0-cyc | 0.4 | 16 | 2.0 | 10 |
| numCI20-w0.8-d16-s0.5-cyc | 0.8 | 16 | 0.5 | 10 |
| numCI20-w0.8-d16-s1.0-cyc | 0.8 | 16 | 1.0 | 10 |
| numCI20-w0.4-d12-s0.5-cyc | 0.4 | 12 | 0.5 | 10 |
| numCI20-w0.4-d25-s0.5-cyc | 0.4 | 25 | 0.5 | 10 |

Table 5.7 Numerical test program of tests on post-installed reinforcing bars

| Post-installed | Crack width $w_{max}$ [mm] | Bar diameter $\phi$ [mm] | Peak slip $s_{max} / s_u$ $-s_{min} / s_u$ [-] | Number of cycles $n_{cyc}$ [-] |
|---|---|---|---|---|
| Monotonic loading, uncracked concrete | | | | |
| numPI20-w0.0-d16-ucr | – | 16 | – | – |
| Monotonic loading, cracked concrete | | | | |
| numPI20-w0.4-d16-cr | 0.4 | 16 | – | – |
| Load cycling in constant cracks | | | | |
| numCI20-w0.4-d16-s0.5-con | 0.4 | 16 | 0.5 | 10 |
| Simultaneous load and crack cycling | | | | |
| numPI20-w0.4-d16-s0.25-cyc | 0.4 | 16 | 0.25 | 10 |
| numPI20-w0.4-d16-s0.5-cyc | 0.4 | 16 | 0.5 | 10 |
| numPI20-w0.4-d12-s0.5-cyc | 0.4 | 12 | 0.5 | 10 |
| numPI20-w0.4-d25-s0.5-cyc | 0.4 | 25 | 0.5 | 10 |

It was discussed in Section 4.4.1 that the influence of the reinforcing bar diameter on the bond strength is secondary and overcast by scatter. Therefore, monotonic loading tests on various reinforcing bar diameters were not conducted numerically. Only a limited number of load cycling test on reinforcing bars in constant cracks were simulated numerically for reasons given in Section 5.4.1.1.

## 5.4 Results and Discussion

### 5.4.1 General behaviour

The primary numerical test results were the bond stress-slip curves to determine the simulated bond damage. Post-processing with FEMAP also allows the visualisation concrete strains in the test specimen as shown in Figure 5.12 for an example.

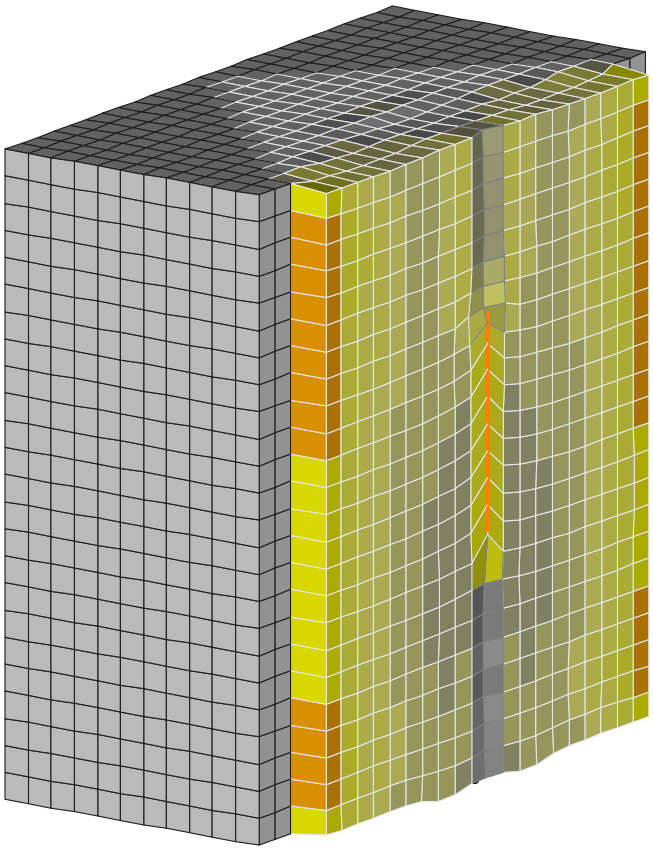

Figure 5.12 Example for visualisation of the simulation results (half model)

As for the experimental tests, the bar tension load taken from the finite element analyses is converted into bond stress according to the uniform bond model, i.e. num$\tau$ = N / ($\pi\phi\ell_b$). Therefore, the calculated ultimate bond strength num$\tau$ indicated in the plots shown in the following somewhat deviates from the ultimate bond strength $\tau_1$ specified for the bond element.

#### 5.4.1.1 Monotonic loading

Figure 5.13 shows the numerically determined bond stress-slip curves for the monotonic loading tests on 16 mm reinforcing bars in uncracked, cracked, and compressed concrete for cast-in-place and post-installed reinforcing bars.

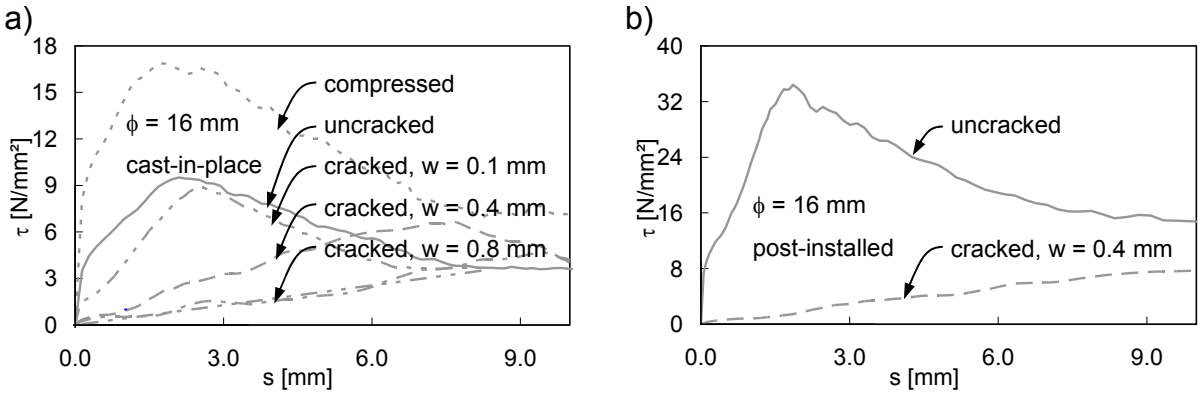


Figure 5.13 Bond stress-slip curves of numerical tests on a) cast-in-place and b) post-installed reinforcing bars subjected to monotonic loading

In general, the numerical analyses replicates the experimentally observed bond behaviour of cast-in-place and post-installed reinforcing bars subjected to monotonic loading realistically for uncracked as well as compressed concrete. However, the simulated bond stress-slip curves for cracked concrete show a softer behaviour if compared to the experiments (Figure 4.13 and Figure 4.14). This effect becomes increasingly pronounced with increased crack widths and is inevitable if the smeared crack approach (Section 5.1.1.2) is used in combination with bond elements (Section 5.1.1.3), which requires one-dimensional bar elements embedded in three-dimensional solid elements (*Ožbolt, J. (2011)*): The smeared crack damages the solid elements in which the bar elements are embedded, therefore initially reducing the pullout resistance of the connected bar elements. It requires pronounced slip before the load is gradually picked up by the adjacent solid elements. Figure 5.14 compares the situation of a reinforcing bar located in a crack for experimental and numerical tests.

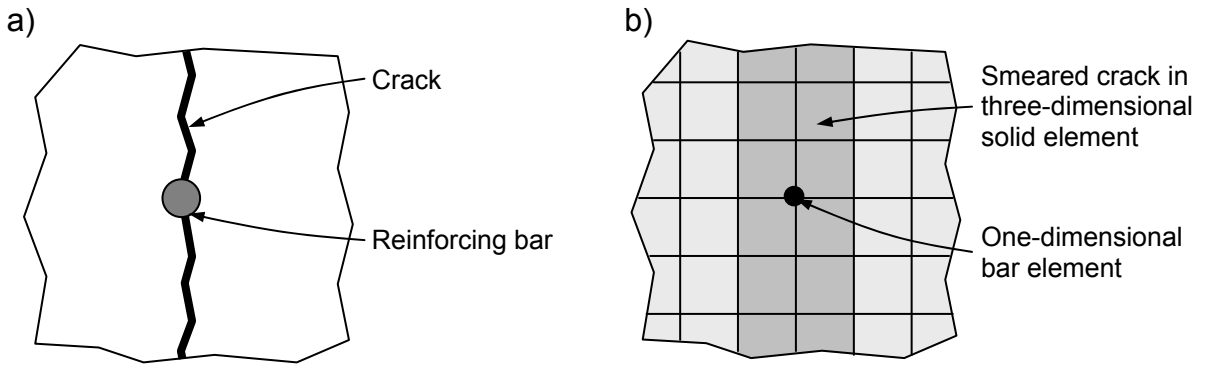


Figure 5.14 Reinforcing bar in crack: a) Experimental test; b) Numerical test

All plots of the numerical tests under monotonic loading are presented in *Mahrenholtz, C. (2011c)* and the key results can be found in Table C.3 and C.4 of Appendix C: Bond Test Data.

### 5.4.1.2 Simultaneous load and crack cycling

Figure 5.15 shows the numerically derived bond stress-slip curves for the simultaneous load and crack cycling tests on 16 mm cast-in-place and post-installed reinforcing bars. For better visualisation, only the first and the last cycle is plotted.

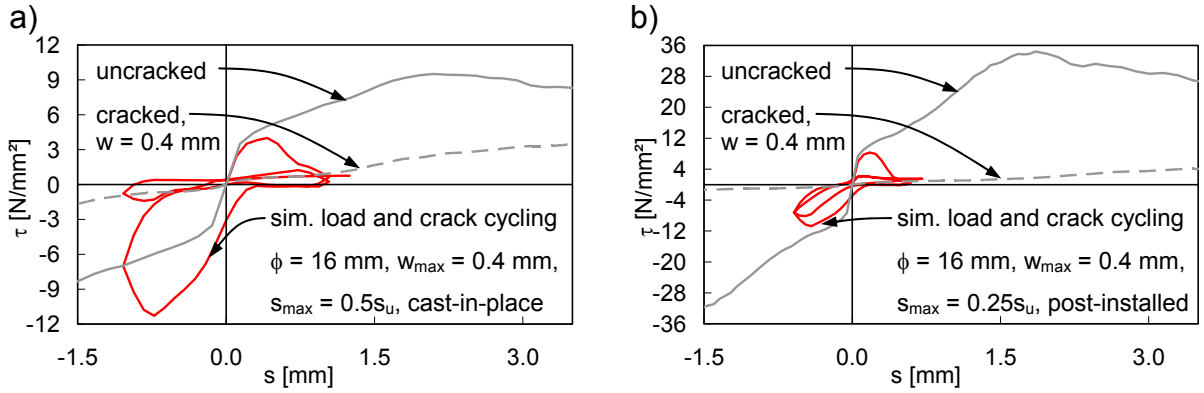


Figure 5.15 Bond stress-slip curves of numerical tests on a) cast-in-place and b) post-installed reinforcing bars subjected to simultaneous load and crack cycling

Numerical analyses of simultaneous load and crack cycling tests resulted in bond stress-slip curves which first follows the monotonic curve for uncracked concrete and is then gradually deviating towards the curve for cracked concrete. This is in line with the experimental test observations (Section 4.4.1). Because of the smeared crack approach, as discussed in Section 5.4.1.1, the bond stress-slip response of the numerical tests drops significantly which is in contrast to the experimentally derived curves. The corresponding reduction in energy consumption underestimates the damage during the cycling with positive slip values if compared to the experimental tests. However, the underestimated damage results in an increased bond response in compression. In consequence, the energy consumption is approximately balanced. A comparison of the numerical and experimetally determined bond damage is given in Section 5.4.3.

In the following Figure 5.16 and Figure 5.17 the bond stress-slip curves of simultaneous load and crack cycling tests are shown to demonstrate the influence of various parameters.

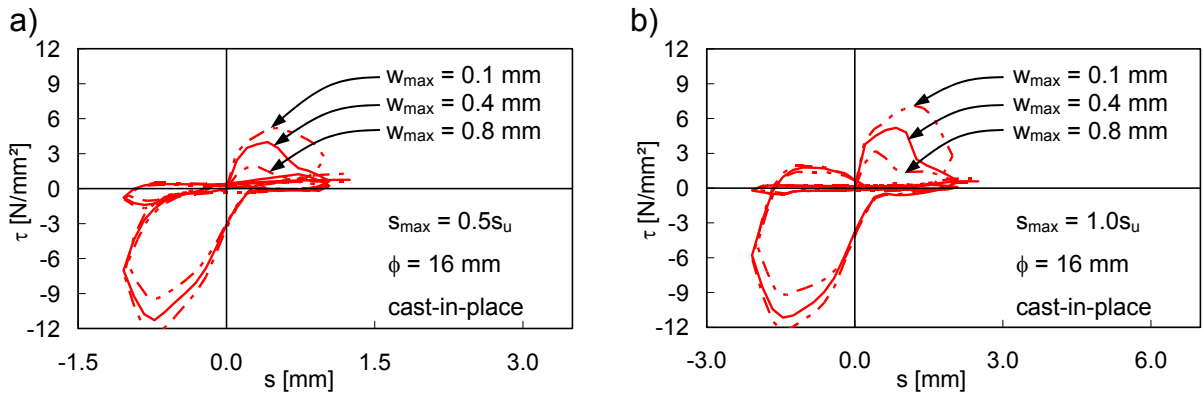


Figure 5.16 Bond stress-slip curves of numerical tests on cast-in-place reinforcing bars subjected to simultaneous load and crack cycling: Influence of maximum crack width $w_{max}$ for peak slip a) $s_{max} = 0.5s_u$ and b) $s_{max} = 1.0s_u$

In principle, the influence of the maximum crack width $w_{max}$ on the bond stress-slip curves of simultaneous load and crack cycling is realistically simulated, as illustrated in Figure 5.16a for peak slips $s_{max} = 0.5s_u$ and in Figure 5.16b for peak slips $s_{max} = 1.0s_u$. As for the experiments, larger maximum crack widths lead to smaller energy dissipation during the initial positive loop. Therefore, the corresponding initial negative loop shows larger bond strengths.

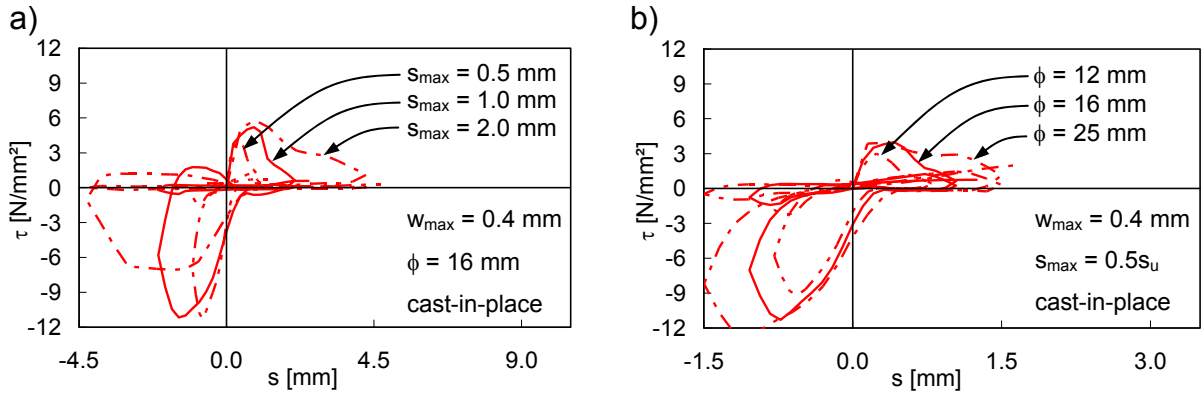


Figure 5.17 Bond stress-slip curves of numerical tests on cast-in-place reinforcing bars subjected to simultaneous load and crack cycling: Influence of a) peak slip $s_{max}$ and b) reinforcing bar diameter $\phi$ for maximum crack width $w_{max} = 0.4$ mm

Also as Figure 5.17a shows the influence of the peak slip $s_{max}$ on the bond stress-slip curves of simultaneous load and crack cycling is in principle realistically simulated. The influence of the initial positive hysteretic loop on the initial negative hysteretic loop is increasing with increasing peak slips. As for the experiments, the bond stress-slip curves of simultaneous load and crack cycling shown in Figure 5.17b do

not allow a meaningful discussion of the influence of the reinforcing bar diameter $\phi$ on the bond damage. Instead, the bond damage of the different reinforcing bar diameters is quantified in Section 5.4.2.

All plots of the numerical tests under simultaneous load and crack cycling are presented in *Mahrenholtz, C. (2011c)* and the key results can be found in Table C.3 and C.4 of Appendix C: Bond Test Data.

#### 5.4.1.3 Load cycling in constant cracks

The numerically derived bond stress-slip curves for the load cycling tests 16 mm diameter cast-in-place and post-installed reinforcing bars in cracked concrete on is shown in Figure 5.18. For the sake of better readability, only the first and last hystereses are plotted.

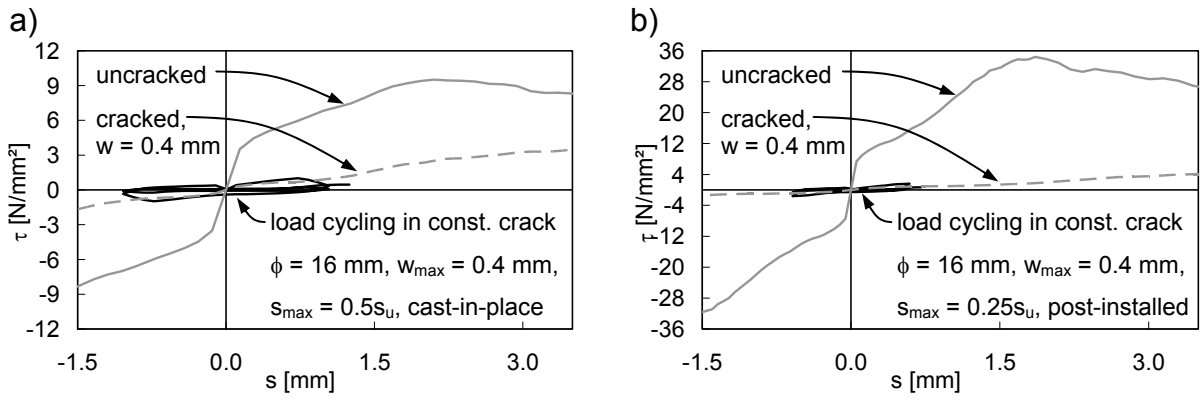


Figure 5.18 Bond stress-slip curves of numerical tests on a) cast-in-place and b) post-installed reinforcing bars subjected to load cycling in constant crack

Due to the difficulties discussed in Section 5.4.1.1, the simulation of tests on various reinforcing bar diameters under load cycling in constant cracks does not lead to satisfactory results as Figure 5.18 shows. Therefore, this loading type is not further discussed here.

All plots of the numerical tests under load cycling are presented in *Mahrenholtz, C. (2011c)* and the key results can be found in Table C.3 and C.4 of Appendix C: Bond Test Data.

### 5.4.2 Bond damage

Figure 5.19 illustrates the bond damage of cast-in-place reinforcing bars under simultaneous load and crack cycling for peak slips $s_{max} = 0.5s_u$ and $s_{max} = 1.0s_u$ for an example. The solid line represents the experimental and the dashed line the

numerical determined bond damage. Overall, the bond deterioration is realistically simulated although the accuracy is reduced with larger peak slip values. In the following section, the differences between experimentally and numerically calculated bond damage are given for all tests.

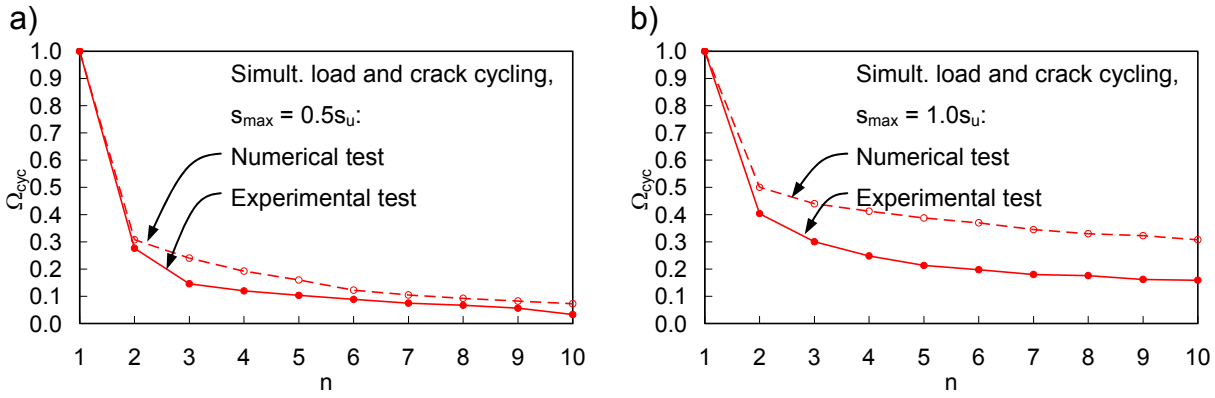


Figure 5.19 Factor $\Omega_{cyc}$ versus cycle n to describe the bond damage of cast-in-place reinforcing bars under simultaneous load and crack cycling for peak slips for the examples a) $s_{max} = 0.5s_u$ and b) $s_{max} = 1.0s_u$

### 5.4.3 Validation

The bond stress-slip curves for the monotonic loading tests on cast-in-place and post-installed reinforcing bars derived experimentally and numerically are superposed in Figure 5.20 as an example for the crack width 0.4 mm.

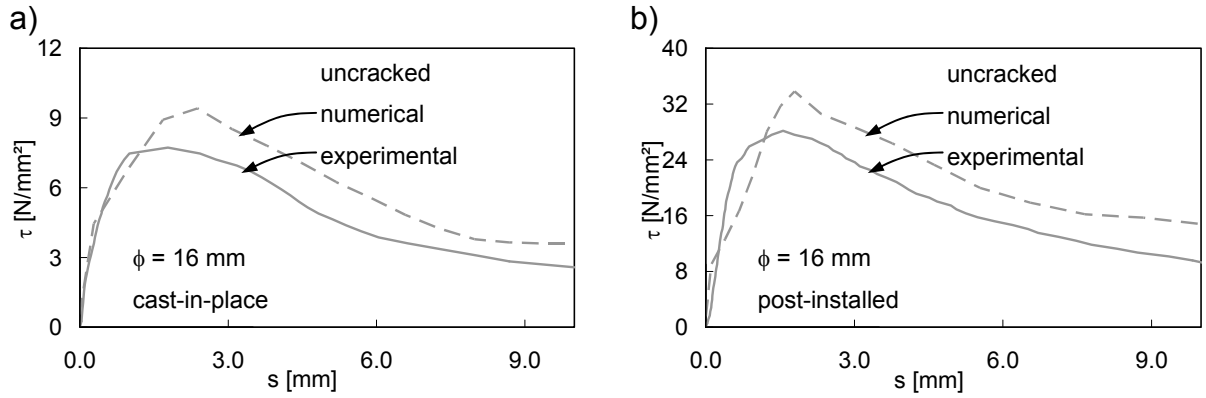


Figure 5.20 Bond stress-slip curves of tests on a) cast-in-place and b) post-installed reinforcing bars subjected to monotonic loading, uncracked concrete

The calculated bond strength num$\tau_u$ based on the numerical analyses is about 20 percent higher than the bond strength exp$\tau_u$ derived from the experiments and the bond strength $\tau_1$ specified for the bond element (Section 5.2.1.3). Similar finite

element models discussed in *Lettow, S. (2007)* showed the same behaviour. A possible explanation is the multiaxial state of stress caused by the confined setup who's influence may not have been totally eliminated by the debonded pre-length (Section 2.2.2). Most importantly, however, the numerically and experimentally tested ratios of the ultimate bond strengths for reinforcing bars situated in cracked and uncracked concrete are almost identical which will be shown in the following.

Table 5.8 and Table 5.9 list the ratios of bond strengths determined for experimental and numerical monotonic loading tests on cast-in-place and post-installed reinforcing bars in cracked concrete and compressed concrete, $\Omega_w = \tau_{u,cr} / \tau_{u,ucr}$ and $\Omega_c = \tau_{u,com} / \tau_{u,ucr}$, respectively. The factors $\Omega_w$ and $\Omega_c$ are discussed in Section 2.2.11 and Section 2.2.10, respectively. Table 5.10 gives the bond damage derived from experimental and numerical simultaneous load and crack cycling tests on cast-in-place and post-installed reinforcing bars after 10 cycles, $\Omega_{cyc(n=10)} = 1 - d_{(n=10)}$. The factor $\Omega_{cyc}$ is discussed in Section 2.2.13.

Table 5.8 Experimentally and numerically determined $\Omega_w$ for monotonic loading on cast-in-place bars and post-installed reinforcing bars in cracked concrete

| Cast-in-place | exp$\Omega_w$ [-] | num$\Omega_w$ [-] |
|---|---|---|
| Monotonic loading, cracked concrete | | |
| CI20-w0.1-d16-cr | 0.96 | 0.93 |
| CI20-w0.4-d16-cr | 0.75 | 0.69 |
| CI20-w0.8-d16-cr | 0.49 | 0.48 |
| Post-installed | exp$\Omega_w$ [-] | num$\Omega_w$ [-] |
| Monotonic loading, cracked concrete | | |
| PI20-w0.4-d16-cr | 0.82 | 0.59 |

Table 5.9 Experimentally and numerically determined $\Omega_c$ for monotonic loading on cast-in-place reinforcing bars in compressed concrete

| Cast-in-place | exp$\Omega_c$ [-] | num$\Omega_c$ [-] |
|---|---|---|
| Monotonic loading, compressed concrete | | |
| CI20-w0.0-d16-com | 1.70 | 1.77 |

Table 5.10 Experimentally and numerically determined $\Omega_{cyc(n=10)}$ for simultaneous load and crack cycling on cast-in-place bars and post-installed reinforcing bars

| Cast-in-place | $exp\Omega_{cyc(n=10)}$ [-] | $num\Omega_{cyc(n=10)}$ [-] |
|---|---|---|
| Simultaneous load and crack cycling | | |
| CI20-w0.1-d16-s0.5-cyc | 0.16 | 0.17 |
| CI20-w0.1-d16-s1.0-cyc | 0.06 | 0.05 |
| CI20-w0.4-d16-s0.5-cyc | 0.16 | 0.31 |
| CI20-w0.4-d16-s1.0-cyc | 0.03 | 0.07 |
| CI20-w0.4-d16-s2.0-cyc | 0.03 | 0.03 |
| CI20-w0.8-d16-s0.5-cyc | 0.14 | 0.29 |
| CI20-w0.8-d16-s1.0-cyc | 0.06 | 0.08 |
| CI20-w0.4-d12-s0.5-cyc | 0.17 | 0.30 |
| CI20-w0.4-d25-s0.5-cyc | 0.28 | 0.34 |
| Post-installed | $exp\Omega_{cyc(n=10)}$ [-] | $num\Omega_{cyc(n=10)}$ [-] |
| Simultaneous load and crack cycling | | |
| PI20-w0.4-d16-s0.25-cyc | 0.36 | 0.27 |

In general, the experimentally and numerically tested factors $\Omega_w$ (Table 5.8), $\Omega_c$ (Table 5.9), and $\Omega_{cyc(n=10)}$ (Table 5.10) show good agreement. Furthermore, the numerical monotonic loading tests on reinforcing bars generally yielded bond stress-slip curves which agree well with the experimental test results in particular for tests in uncracked and compressed concrete (Section 5.4.1.1). Also the overall hysteretic behaviour of the simultaneous load and crack cycling tests was simulated reasonably well (Section 5.4.1.2). In summary, the MASA bond element and its integrated hysteretic energy model were validated and proved fit for simulation of column-to-foundation connections under seismic loading conditions.

## 5.5 Extension of Parametric Range

The main objective of Chapter 5 is the validation of the bond element for seismic conditions, i.e. for large parallel cracks and transverse compression. Furthermore, the valid parametric range for the bond model is extended in the following.

The experimental and numerical studies gave evidence that the difference of the bond damage between various reinforcing bar diameters is negligible. Therefore, numerical studies of reinforcing bars in which diameters differ with respect to the experimentally tested diameters were deemed to be unnecessary.

To study the influence of concrete strength, the test program was amended by tests for which the material parameters were adapted to account for high strength concrete properties (Table 5.4 and Table 5.5).

Following, the suitability of the bond element for the simulation of tests in high strength concrete is evaluated. The increase of the bond strength due to higher concrete strength is estimated by raising the concrete compressive strength to the power of ½ (Section 2.2.6). Therefore, the bond element parameter for the bond strength $\tau_1$ to simulate C50/60 concrete was taken as the bond strength $\tau_1$ for C20/25 concrete multiplied by $(f_{ck,C50/60} / f_{ck,C20/25})^{0.5} = 1.58$ (Section 5.2.1.3). The resulting bond strengths determined by numerical tests on monotonically loaded reinforcing bars in C20/25 and C50/60 concrete test yields approximately the same value (Table 5.11).

Table 5.11 Ratio of bond strength for C20/25 and C50/60 concrete calculated by means of numerical tests and according to input parameters

| Cast-in-place | $num\tau_{u,C50/60} / num\tau_{u,C20/25}$ [-] | $\tau_{1,C50/60} / \tau_{1,C20/25}$ [-] |
|---|---|---|
| CI50-w0.0-d16-ucr<br>CI20-w0.0-d16-ucr | 1.48 | 1.58 |

The influence of the concrete strength on the bond damage, however, is virtually non-existent (Table 5.12). This is in line with the results presented in *Eligehausen, R.; Popov, E. et al. (1983)* (Figure 5.21) which showed that the concrete strength does not influence the bond deterioration.

Table 5.12 Ratio of bond damage for C20/25 and C50/60 concrete calculated by means of numerical tests and according to experimental tests conducted by *Eligehausen, R.; Popov, E. et al. (1983)*

| Cast-in-place | $num\Omega_{cyc(n=10),C50/60} / num\Omega_{cyc(n=10),C20/25}$ $exp\Omega_{cyc(n=10),C50/60} / exp\Omega_{cyc(n=10),C20/25}$ [-] | [-] |
|---|---|---|
| CI50-w0.4-d16-s0.5-cyc<br>CI20-w0.4-d16-s0.5-cyc | 1.03 | ≈ 1.0[1)] |

[1)] Assumed on the basis of *Eligehausen, R.; Popov, E. et al. (1983)*

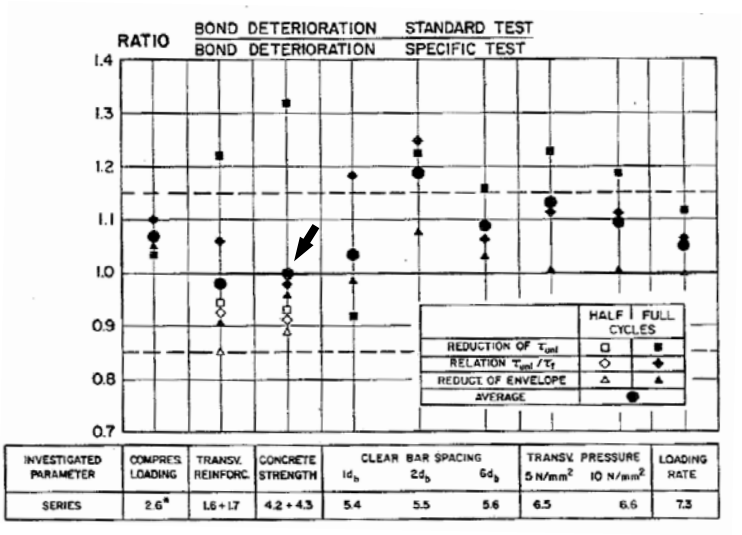


Figure 5.21 Influence of investigated parameters on bond behaviour during cyclic loading (*Eligehausen, R.; Popov, E. et al. (1983)*), arrow indicates the mean influence of concrete strength

In summary, the bond element was validated to simulate bond damage realistically at least for the concrete strength range between 20 MPa and 50 MPa. It is reasonable to assume that concrete strengths outside of this range are also realistically simulated.

## 5.6 Summary and Conclusions

The pre-processing program FEMAP was used to generate the finite element model, employing bond elements to link one-dimensional bar elements with three-dimensional solid elements simulating the bond interaction between reinforcement and concrete. The finite element program MASA, applying the smeared crack method, was then used to simulate the behaviour of monotonic and cyclic tests on cast-in-place reinforcing bars. To the knowledge of the author, these finite element analyses were the first numerical tests on reinforcing bars located in cracked concrete employing bond elements.

By comparison to the experimental observations, the overall hysteretic behaviour of seismically loaded reinforcing bars is well captured in the numerical simulations. However, if compared to the components of bond stress-slip curves of experimental tests, the bond response is underestimated for the positive and to approximately the same degree overestimated for the negative loop of the hysteresis response. The observed balancing of under- and overestimated bond response results in a similar energy consumption if compared to experimental test results.

This observation is confirmed by the evaluated damage factors which match well for experimental and numerical tests. In conclusion, the evaluated test data

demonstrates that the finite element model used including the bond element simulates simultaneous load and crack cycling tests reasonably closely for practical purposes. The parametric range was successfully extended for different concrete strength.

Therefore, the implemented bond element is validated and empowers the finite element program MASA to simulate realistically concrete member joints, e.g. column-to-foundation connections, under seismic loading.

Therefore, the implemented bond element used in the finite element program MASA is validated and allows the realistic simulation of concrete member joints (e.g. column-to-foundation connections) under seismic loading even if the connection relies solely on bond.

# 6 Experimental Studies on Column-to-Foundation Connections

In this chapter, the experimental tests on cast-in-place and post-installed column-to-foundation connections are presented. These were conducted at the Structural Laboratory of the University of Canterbury. The study allows evaluation of the influence of the anchorage detailing with and without hooks as well as the installation method on the seismic performance. First, the strain and its measurement along reinforcing bar anchorages is introduced in Section 6.1. The experimental setup of the column-to-foundation connection test is discussed in Section 6.2, and the experimental procedure including test program and load protocol is described in Section 6.3. Next, the test results are discussed in Section 6.4. Key findings are highlighted in Section 6.5. The complete experimental test program of the studies on cast-in-place and post-installed column-to-foundation connections is reported in detail in *Mahrenholtz, C. (2012a)*.

## 6.1 Basics

The bond stress distribution developing during experimental tests is determined by means of strain gauge measurements. For each increment, the averaged bond stress is calculated according to Equation 2.2. The sequence of incremental bond stresses allows approximating the bond stress distribution along the anchorage (Figure 6.1).

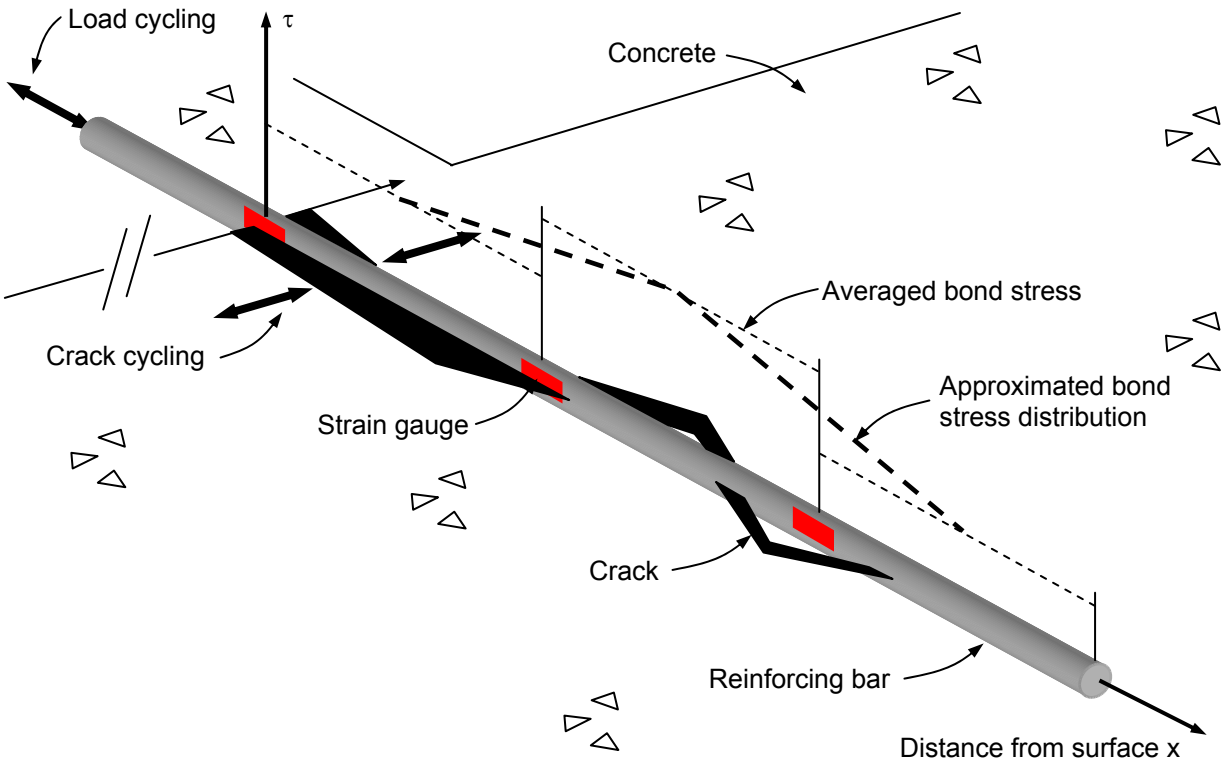


Figure 6.1 Schematic illustration of the experimental determination of the bond stress distribution along anchorage

### 6.1.1 Conventional strain gauge installation

The installation of strain gauges for measuring the strain at a selected point along a reinforcing bar (Figure 6.2a) is common practice and described in detail in various documents such as manufacturer's installation guidelines and manuals. On the contrary, the application of multiple strain gauges for measuring the strain continuously along the reinforcing bar (Figure 6.2b) is rather uncommon. Here, the close distance of the strain gauges turns out to be problematic as explained in the following.

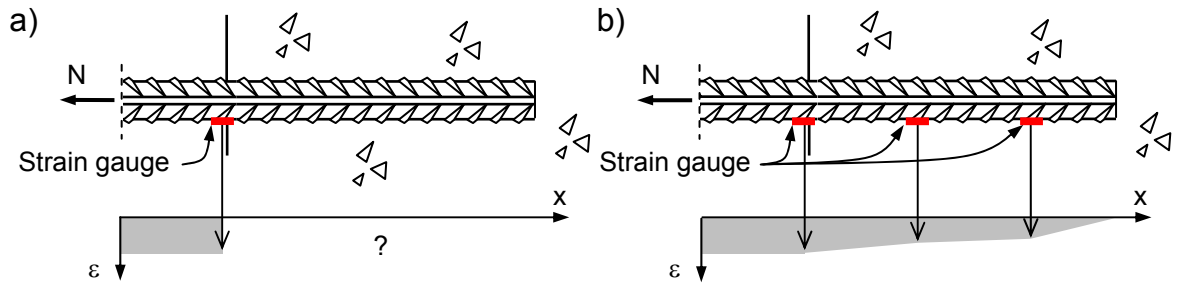


Figure 6.2 a) Selective strain measurement; b) Continuous strain measurement

Typically, the ribs are removed over a stretch of 50 mm and more to increase the workability and thus the quality of the strain gauge installation. After gluing the strain gauge, the stretch is covered by a mastic tape. The length affected by the strain gauge installation is relatively small compared to the total length if the strain has to be measured at a selected point only, e.g. at the beginning of an anchorage to determine the tensile stress (Figure 6.3a). On the contrary, when the strain has to be measured continuously along the reinforcing bar, e.g. to study the bond stress distribution of column-to-foundation connection anchorages, the above described installation method cannot be followed. The reinforcing bar would be almost totally covered by mastic tape (Figure 6.3b), thus compromising measurement of the bond transfer between concrete and reinforcing bar that the strain gauges were installed to
.

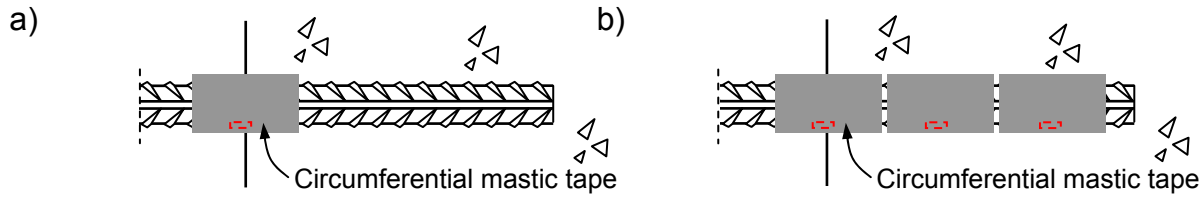


Figure 6.3 Conventional strain gauge installation for: a) Selective strain measurement; b) Continuous strain measurement

Two solutions of this problem are proposed in the literature:

- The reinforcing bar is longitudinally grooved and cut into two halves. The two halves are joined together after installation of the strain gauges on the cut surface. The cables are routed in the groove. This method is described in *Chung, L.; Shah, S. P. (1989)*.
- The reinforcing bar is longitudinally grooved. A fibre optical strain gauge is installed in the groove. Also, the fibre optical cable is routed in the groove. This method is described in *Kenek, A.; Martin, P. (2001)*.

Both existing solutions are elaborate and expensive, not user-friendly and rather impracticable if the number of tests is not limited to just a few. Therefore, an alternative method of strain gauge installation was developed which is reliable and practicable, using standard electrical strain gauges.

### 6.1.2 Alternative strain gauge installation

The alternative installation method was developed to minimise the disruption of the bond transfer between concrete and reinforcing bar. The method is suitable for selective strain measurement (Figure 6.4a) and particularly advantageous for continuous strain measurement (Figure 6.4b).

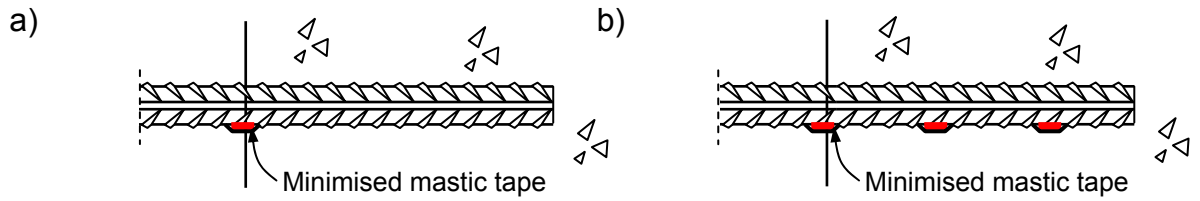


Figure 6.4 Alternative strain gauge installation for: a) Selective strain measurement; b) Continuous strain measurement

The key features of the alternative installation method are pointed out in the following:

- The size of the strain gauges used for the test was 5 mm x 2 mm. The carrier foils were slightly larger, about 7 mm x 3 mm. Therefore, the grinded and sandpapered areas are reduced to about 10 mm x 5 mm.
- After installation of the strain gauges, the application of epoxy coating layers ensures a good protection against corrosion. The coating engulfs reliably the uneven profile of cable, lead wire and strain gauge carrier foil.
- Finally, only a small piece of mastic tape, about 7 mm x 7 mm, is placed on top to protect the strain gauge against mechanical damage.
- Thin steel wires but not cable ties are used to reduce the interference of the bond stress transfer to a minimum.

The alternative method was verified by comparing the strain measurements of a mock-up test with a reference test which was carried out under identical conditions but employing the sophisticated strain gauge installation method as presented in *Chung, L.; Shah, S. P. (1989)* as discribed in Section 6.1.1. Figure 6.5 depicts the normal force distribution of a reinforcing bar anchorage under several load levels for the mock-up test and for the reference test. The comparison shows that the stress distribution is identical which verifies the alternative strain gauge installation method. Further details can be found in *Mahrenholtz, C. (2011d)*.

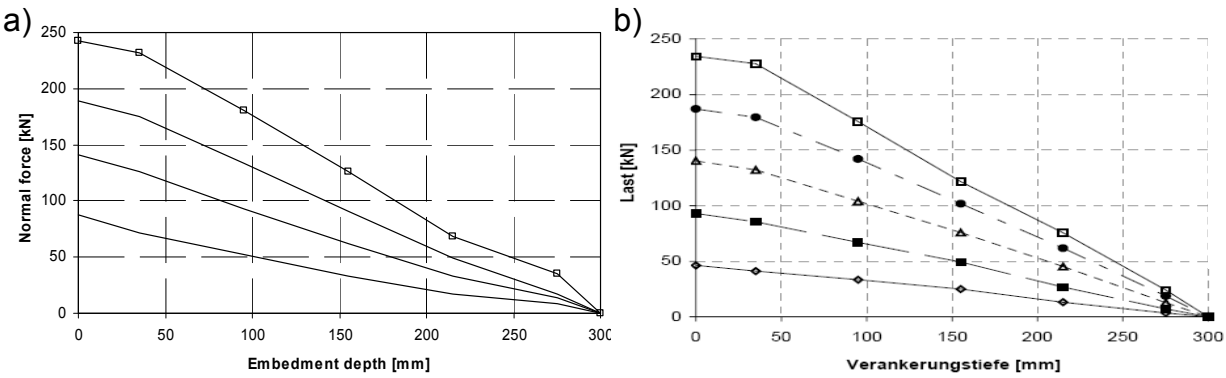


Figure 6.5 Normal force distribution over embedment depth for various load levels: a) Mock-up test (*Mahrenholtz, C. (2011e)*); b) Reference test (*Spieth, H. (2003)*)

Figure 6.6 shows the details of the strain gauge installation as it was carried out for the column-to-foundation connection tests described in the following.

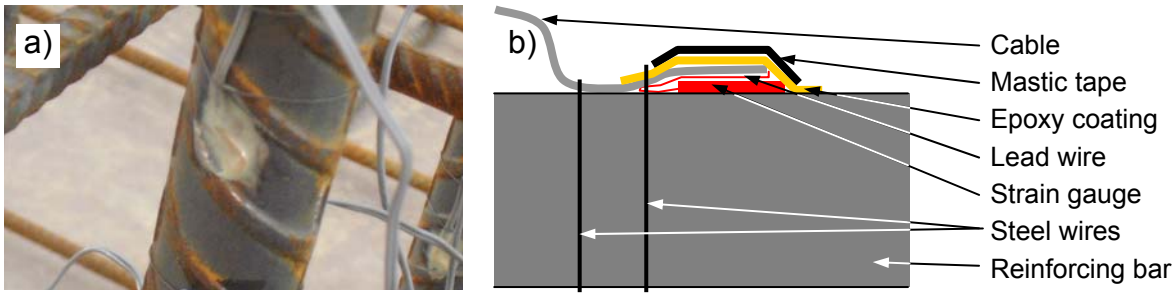


Figure 6.6 Detail of strain gauge installation: a) Photo of strain gauge after application of an epoxy coating layer and before sticking mastic tape; b) Schematic of alternative method

## 6.2 Experimental Setup

### 6.2.1 Test specimens

Foundations and columns were manufactured as precast elements. In order to study the stress distribution along the anchorage, two opposing corner starter bars were fitted with strain gauges, applying the installation method introduced in Section 6.1. Foundations and columns were either cast monolithically in two steps to investigate the behaviour of cast-in-place starter bars, or separately to test the behaviour of post-installed starter bars.

The columns (cross section 300 mm / 300 mm) were designed according to *Eurocode 2 (2005)*, Section 6.2.3 with stirrups at 150 mm spacing to avoid shear failure of the column prior to the failure of the connection. In order to investigate the influence of the column reinforcing bar diameter and cross section, different layouts

of four or eight longitudinal reinforcing bars were adapted. The foundation (slab thickness 300 mm and 500 mm) was designed without shear reinforcement. The top and bottom reinforcement was provided at 200 mm spacing and met the requirements of the minimum reinforcement according to *Eurocode 2 (2005)*, Section 7.3.2. Further structural analyses according to *Eurocode 2 (2005)*, Section 6.4.3 showed that punching failure of the foundation is not critical. Two foundation heights were tested to study the influence of different anchorage lengths. The proportional geometry of column and foundation as well as the reinforcement layout can be considered as being representative. Figure 6.7 shows the details of the tested specimens. The specimens were manufactured by the precast company Stahlton, Christchurch. Further details of the construction are given in *Mahrenholtz, C. (2012a)*.

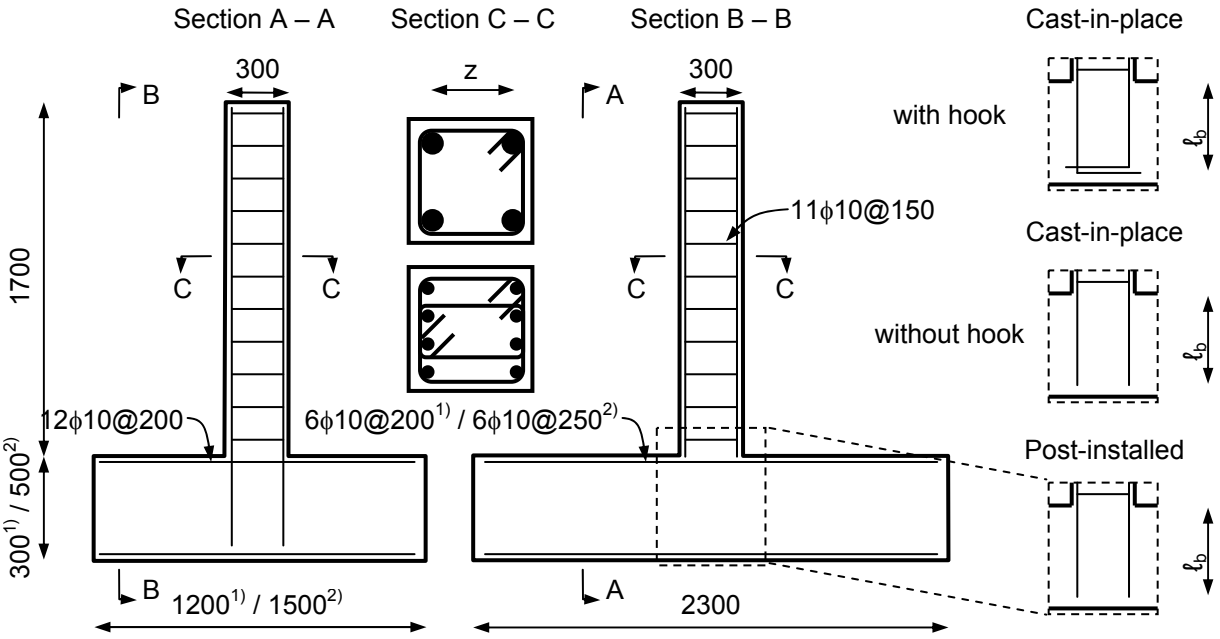


1) for tests on specimens detailed with starter bar anchorage length $\ell_b$ = 240 mm
2) for tests on specimens detailed with starter bar anchorage length $\ell_b$ = 420 mm

Figure 6.7 Layout of test specimens

### 6.2.1.1 Reinforcing bars

The Seismic 500E reinforcing bars used complied with *AS/NZS 4671 (1997)* which specifies a lower characteristic yield strength of $R_{ek,L} \geq 500$ MPa and an upper characteristic yield strength of $R_{ek,U} \leq 600$ MPa. Grade Seismic 500E was used because it is the most common type in New Zealand and Australia. The steel properties, however, are basically equivalent to a B500B steel according to *Eurocode 2 (2005)*. The characteristic yield strength $R_{ek}$ is in the following referred to as $f_{yk}$ for

the sake of consistency. The characteristic ultimate strength is specified as $R_m \geq 1.08R_e \geq 540$ MPa and is referred to as $f_{uk}$ in the following. The minimum uniform elongation, equivalent to $\varepsilon_u$, is $A_{gt} \geq 10.0$ %. The tested yield and tensile strengths were between $f_y = 534$ and 540 MPa and $f_u = 622$ and 676 MPa. The measured mean related rib areas are given in Table 6.1. Figure 6.8 shows a typical stress-strain diagram determined for a Seismic 500E reinfocing bar. The strengths of the individual specimens are given in Table D.1 of Appendix D: Column-to-Foundation Connection Test Data.

Table 6.1 Related rib area

| Diameter [mm] | Related rib area $f_R$ [-] |
|---|---|
| 16 | 0.06 |
| 25 | 0.06 |
| 32 | 0.06 |

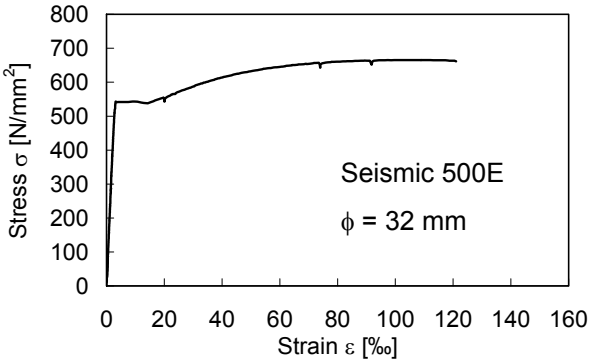

Figure 6.8 Typical stress-strain diagram

### 6.2.1.2 Concrete

Column and foundation were designed in different concrete strengths to mimic the common practice of constructing the column with a concrete strength higher than the foundation concrete strength. The columns and foundations were made of grade 50 and grade 20 concrete according to *NZS 3109 (1997)* with a target concrete compressive strength of $f_c' = 50$ MPa and $f_c' = 20$ MPa, respectively. The properties are approximately equivalent to the concrete classes C50/60 and C20/25 according to *Eurocode 2 (2005)*. The concrete compressive strength $f_c'$ is in the following referred to as $f_{ck}$ for the sake of consistency. The concrete elements were produced according to *NZS 3104 (2003)* and *NZS 3112 (1986)*. The columns and the foundations reached a mean tested concrete compressive strength between $f_c = 47.6$ and 73.5 MPa and $f_c = 20.4$ and 24.7 MPa, respectively. The strengths of the individual specimens are given in Table D.1 of Appendix D: Column-to-Foundation Connection Test Data.

### 6.2.1.3 Bond (spring)

The same mortar as for the bond tests was used for tests on post-installed column-to-foundation connections. Reference is made to Section 4.2.1.3 for further details. The drill bit diameters stipulated in the MPII were increased by 5 mm since

the circular gap between drill hole and reinforcing bar had to accommodate geometric tolerances of the prefabricated elements and the strain gauges including cables and mastic tape (bore hole diameters $d_0$ = 25 mm, 37 mm, 45 mm for reinforcing bar diameters $\phi$ = 16 mm, 25 mm, 32 mm). According to *Rößle, M.; Mészároš, J. (1998)*, the size of the annular gap which is filled by mortar after the installation has only a limited influence on the bond behaviour. The bond strength of the starter bars were tested in a confined test setup (Section 2.2.2) for every cyclically loaded test specimen. To eliminate the influence of confinement, the cast-in-place and post-installed test bars were furnished with a debonded pre-length of 5$\phi$. Thus, the tests were conducted exactly like the tests described in Section 4.2.1.3. The pullout tests are reported in detail in *Mahrenholtz, C. (2012a)*.

Figure 6.9 shows close ups of the confined test setup and pulled out reinforcing bar. The concrete consoles between the ribs of cast-in-place reinforcing bars have been crushed. The residual concrete was of powdery texture and could be easily removed by a brush with steel wirs. The post-installed reinforcing bars sheared off along the perimeter of the reinforcing bar. The mortar consoles remained between the ribs and could be easily removed as limited adhesion to the smooth surface of the reinforcing bar existed. The mean tested bond strengths were between $\tau_u$ = 13.9 and 16.7 MPa for cast-in-place bars and $\tau_u$ = 35.0 and 36.4 MPa for post-installed bars. The bond strengths determined for the individual specimens are summarised in Table D.1 of Appendix D: Column-to-Foundation Connection Test Data.

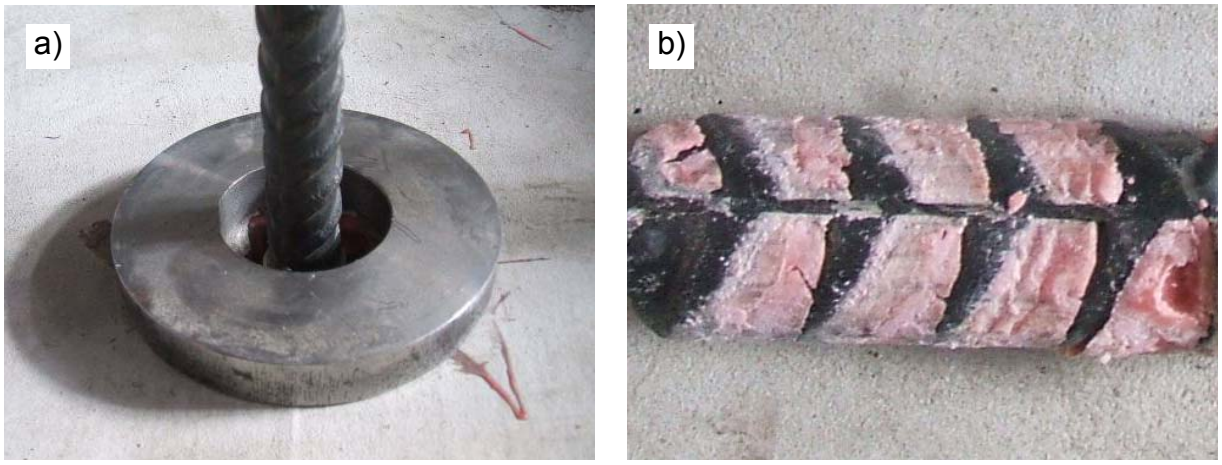


Figure 6.9 Close up of a) bearing plate for confined test setup and b) pulled out reinforcing bar (post-installed, as an example)

### 6.2.2 Test setup and erection sequence

To reasonably limit the number of influencing test parameters, the column was not axially loaded which is conservative since axial loads delay the strength degradation under cyclic loading (*Saatcioglu, M.; Ozcebe, G. (1989)*). Also, the omission of a continuous bedding of the foundation is deemed to be conservative because stiffer

beddings increase the column-to-foundation connection capacity (*Bruckner, M. (2006)*). The specimens were placed on line bearings and anchored to the strong floor, providing a bearing for vertical forces (Figure 6.10a). Props were used to carry the horizontal forces. A 500 kN actuator with load cell was placed between the reaction frame and the bearing plate connected to the column at y = 1500 mm above the foundation. The drift is derived by dividing the displacement $\Delta$ by the lever arm y. The drift $\theta$ of the tested sub-assemblage is equivalent to the story drift because the column height approximately equals the location of the point of contra-flexure of a real structure. Figure 6.10b shows the structural system of the sub-assemblage.

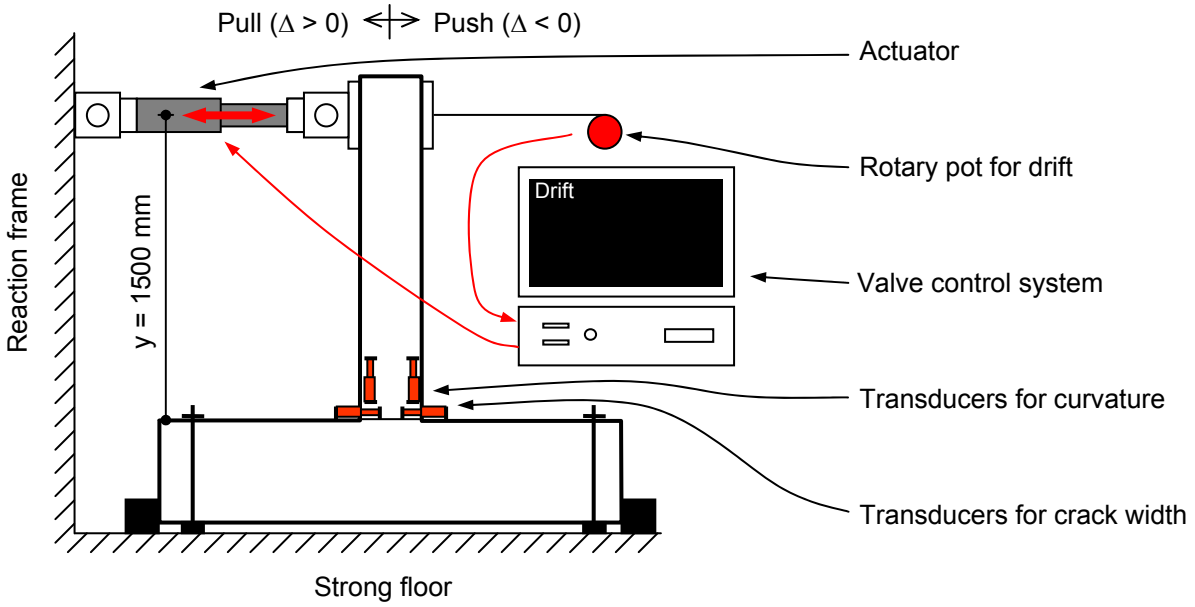


Figure 6.10 a) Schematic test setup

A rotary pot was installed to measure the displacement $\Delta$ resulting from the applied load F. Transducers were placed at the column base to measure the column curvature (Figure 6.11a). During testing, additional transducers measuring the crack widths in the foundation were installed as the cracks developed. Figure 6.11b shows the complete test setup.

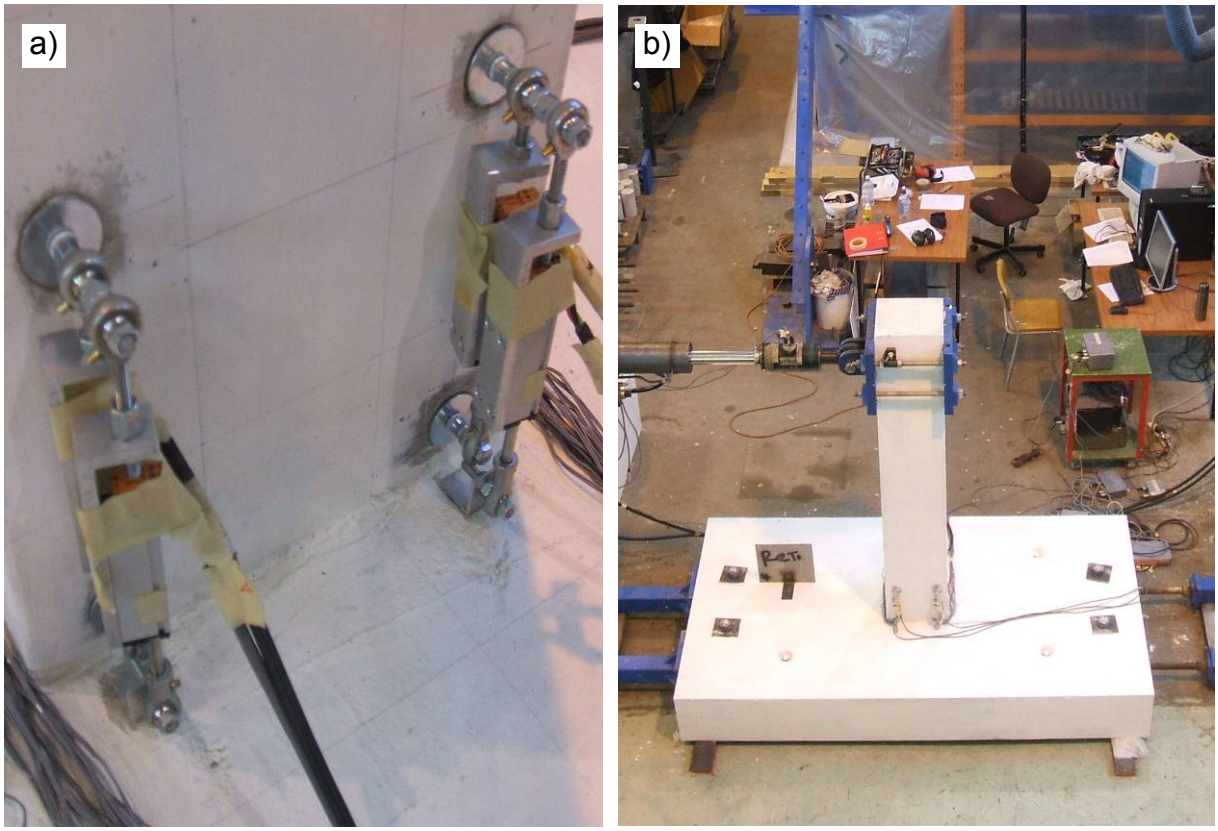


Figure 6.11 a) Close up of transducers; b) 500 kN actuator loading the tied-down and propped test specimen

Figure 6.10 shows the structural system of the sub-assemblage and the moment generated couple. The tension load capacity $T_{max}$ of the starter bar anchorage is equivalent to $N_R$ as the minimum of the failure loads corresponding to the different failure modes (Section 2.3.1.2). In the following, the bond strength is denoted $\tau_R$.

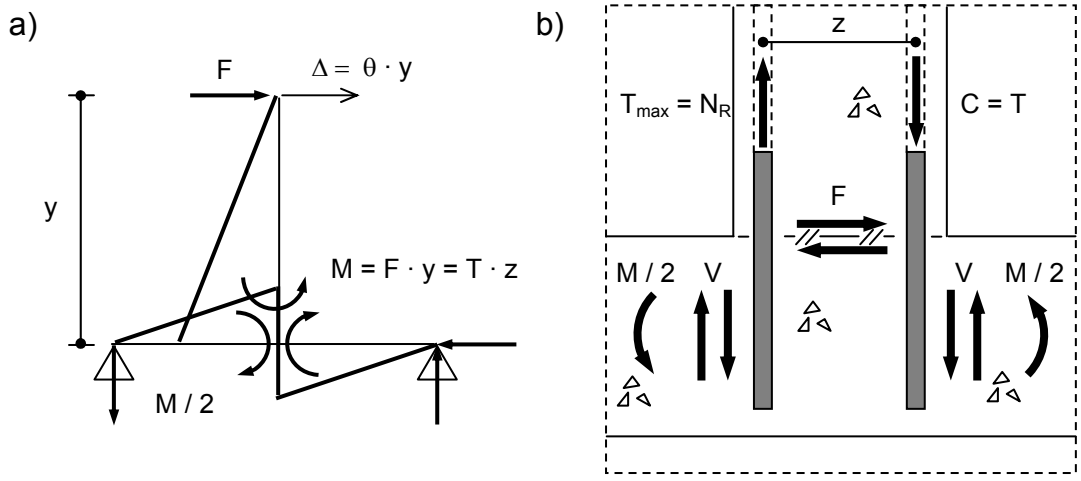


Figure 6.12 a) Structural system sub-assemblage; b) Loading of connection

## 6.3 Experimental Procedure

### 6.3.1 Load protocol

All tests were run at quasi-static loading rates (Section 2.2.7). The actuator was fitted with two hydraulic valves which were controlled by the valve control unit. Both, monotonic and cyclic tests started with thirty pre-loading cycles between the load $F_{pre}$ and $-F_{pre}$, to simulate the stiffness degradation due to service loads in reality. The pre-load $F_{pre}$ was calculated according to

$$F_{pre} = 1.3(M_y / y) \cdot 0.75 / 2.1 \qquad \text{Equation 6.1}$$

where 1.3 is a factor to cover uncertainties in the structural analysis potentially leading to overloading, $M_y$ is the connection bending moment capacity based on the mean yield strength, 0.75 equals the ratio of characteristic and mean capacity (Section 9.1), and $2.1 = 1.4 \cdot 1.5 \approx \gamma_F \cdot \gamma_M$ is the approximatede global safety factor. The pre-loading was carried out in force controlled mode.

The valve control program defined the load protocols for the monotonic and cyclic loading as shown schematically in Figure 6.13. Loading was terminated at 5 % drift. The cyclic load protocol is an adoption of the recommendations formulated in *ACI 374.1 (2005)* and includes 24 cycles which were split into 8 drift levels each comprising 3 cycles.

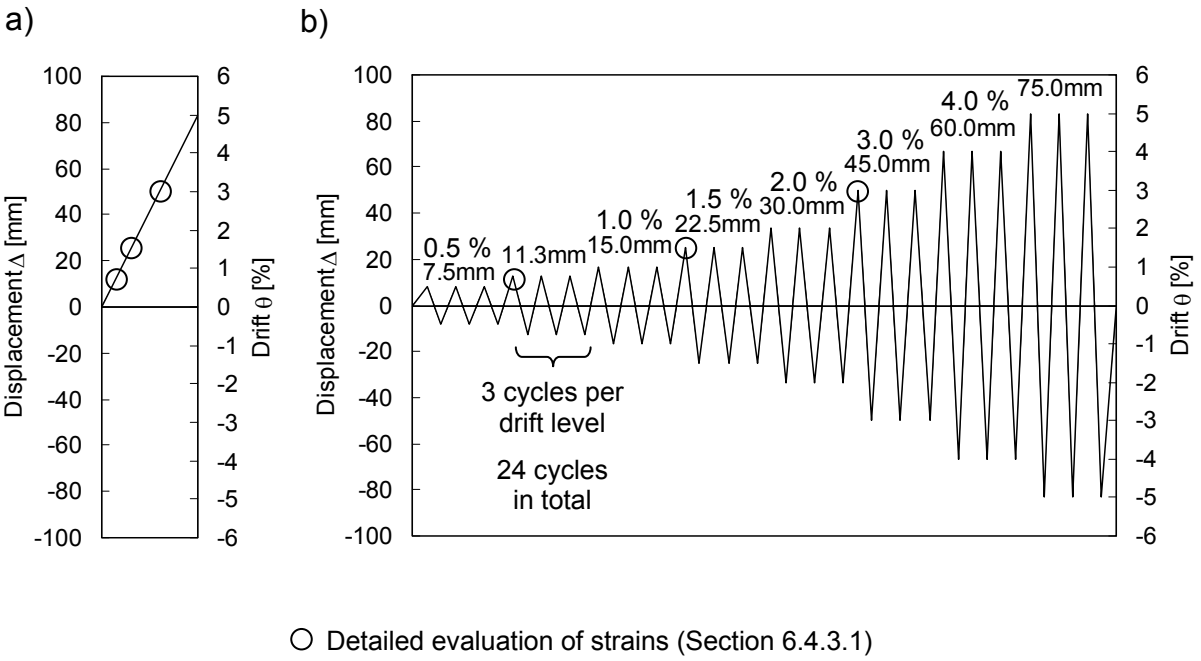


Figure 6.13 Load protocols: a) Monotonic; b) Cyclic

### 6.3.2 Test program

Table 6.2 shows the complete program for the tests on cast-in-place and post-installed column-to-foundation connections. The key test parameters are the anchorage detailing in terms of installation method and anchorage form as well as starter bar layout, starter bar diameter and length (Figure 6.7). Two of each type of test specimen were produced to carry out one monotonic (mon) and one cyclic (cyc) test. The table also provides the anchorage lengths $\ell_{b,rqd}$ in compliance with *Eurocode 2 (2005)*. The calculation of $\ell_{b,rqd}$ requires the estimation of the actual design strengths of the specimens which is explained in detail in Section 8.2. The low ratios of required anchorage length and provided anchorage length $\ell_b$ / $\ell_{b,rqd}$ demonstrate that all test specimens would allow only a low utilisation of the column bending moment capacity based on the yield strength. Moreover, anchoring only a fraction of the starter bar yield capacity is a violation of the provisions for seismic load cases stipulated in *Eurocode 8 (2006)*. For further details in this regard, reference is made to Section 2.3.1.1 and Appendix A: Conventional Anchorage Design.

Table 6.2 Experimental test program of tests on cast-in-place post-installed column-to-foundation connections

| Cast-in-place and Post-installed | Anchorage detailing | Starter bar layout | $\phi$ [1] $\ell_b$ [2] [mm] | $\alpha_1$ [3] $\alpha_2$ [4] [-] | $\ell_{b,rqd}$ [5] $\ell_b$ / $\ell_{b,rqd}$ [mm] |
|---|---|---|---|---|---|
| exp1mon | Cast-in-place | 4 bars | 16 | 0.7 | 525 |
| exp1cyc | w/ hook | per face | 240 | 1.0 | 0.46 |
| exp2mon | Cast-in-place | 4 bars | 16 | 1.0 | 656 |
| exp2cyc | w/o hook | per face | 240 | 0.9 | 0.37 |
| exp3mon | Post-installed | 4 bars | 16 | 1.0 | 656 |
| exp3cyc | w/o hook | per face | 240 | 0.9 | 0.37 |
| exp4mon | Post-installed | 2 bars | 25 | 1.0 | 821 |
| exp4cyc | w/o hook | per face | 240 | 0.7 | 0.29 |
| exp5mon | Cast-in-place | 2 bars | 32 | 0.7 | 1050 |
| exp5cyc | w/ hook | per face | 420 | 1.0 | 0.40 |
| exp6mon | Cast-in-place | 2 bars | 32 | 1.0 | 1107 |
| exp6cyc | w/o hook | per face | 420 | 0.7 | 0.38 |
| exp7mon | Post-installed | 2 bars | 32 | 1.0 | 1107 |
| exp7cyc | w/o hook | per face | 420 | 0.7 | 0.38 |
| exp8mon | Post-installed | 2 bars | 25 | 1.0 | 821 |
| exp8cyc | w/o hook | per face | 420 | 0.7 | 0.51 |

[1] Starter bar diameter

[2] Anchorage length

[3] $\alpha_1 = 1.0$ [$\alpha_1 = 0.7$] for anchorages without [with] hooks

[4] $\alpha_2 = 1 - 0.15\ ((a / 2) - \phi) / \phi$ [$\alpha_2 = 1 - 0.15\ ((a / 2 - 3\phi) / \phi$] for anchorages without [with] hooks

[5] $\ell_{b,rqd} = \phi f_{yd} / (4 f_{bd})$; $f_{yd}$, $f_{bd}$ see Table D.5 of Appendix D: Column-to-Foundation Connection Test Data

Notes: Half of the clear spacing between adjacent bars a / 2 is for anchorages of column-to-foundation connections generally smaller than the concrete covers c and $c_1$

### 6.3.3 Valve control

The specimens were tested displacement controlled according to the monotonic and cyclic load protocols shown schematically in Figure 6.13 at a quasi-static rate. The valve control unit followed the valve control program which was provided by a comma-separated values file (*.csv), storing tabular data in plain textual form (Figure

6.14). The valve control program for monotonic testing comprised 221, for cyclic testing 7981 displacement increments.

| step | Ram A (mm) | Ram A (mm) |
|---|---|---|
| | drift (%) | displacement A |
| 1 | 0 | 0 |
| 2 | 0.01 | 0.15 |
| 3 | 0.02 | 0.3 |
| 4 | 0.03 | 0.45 |
| 5 | 0.04 | 0.6 |
| 6 | 0.05 | 0.75 |
| 7 | 0.06 | 0.9 |
| 8 | 0.07 | 1.05 |
| 9 | 0.08 | 1.2 |
| 10 | 0.09 | 1.35 |
| 11 | | |
| 12 | | |

one drift increment

Figure 6.14 Valve control program

## 6.4 Results and Discussion

### 6.4.1 General behaviour

Figure 6.15 provides an overview of the monotonic and cyclic load-drift curves. For the sake of readability, only the first cycle of each drift level is shown. Figure 6.16 illustrates the observed crack patterns of all experimental tests for the drift level corresponding to the failure load which was defined according to Figure 6.17.

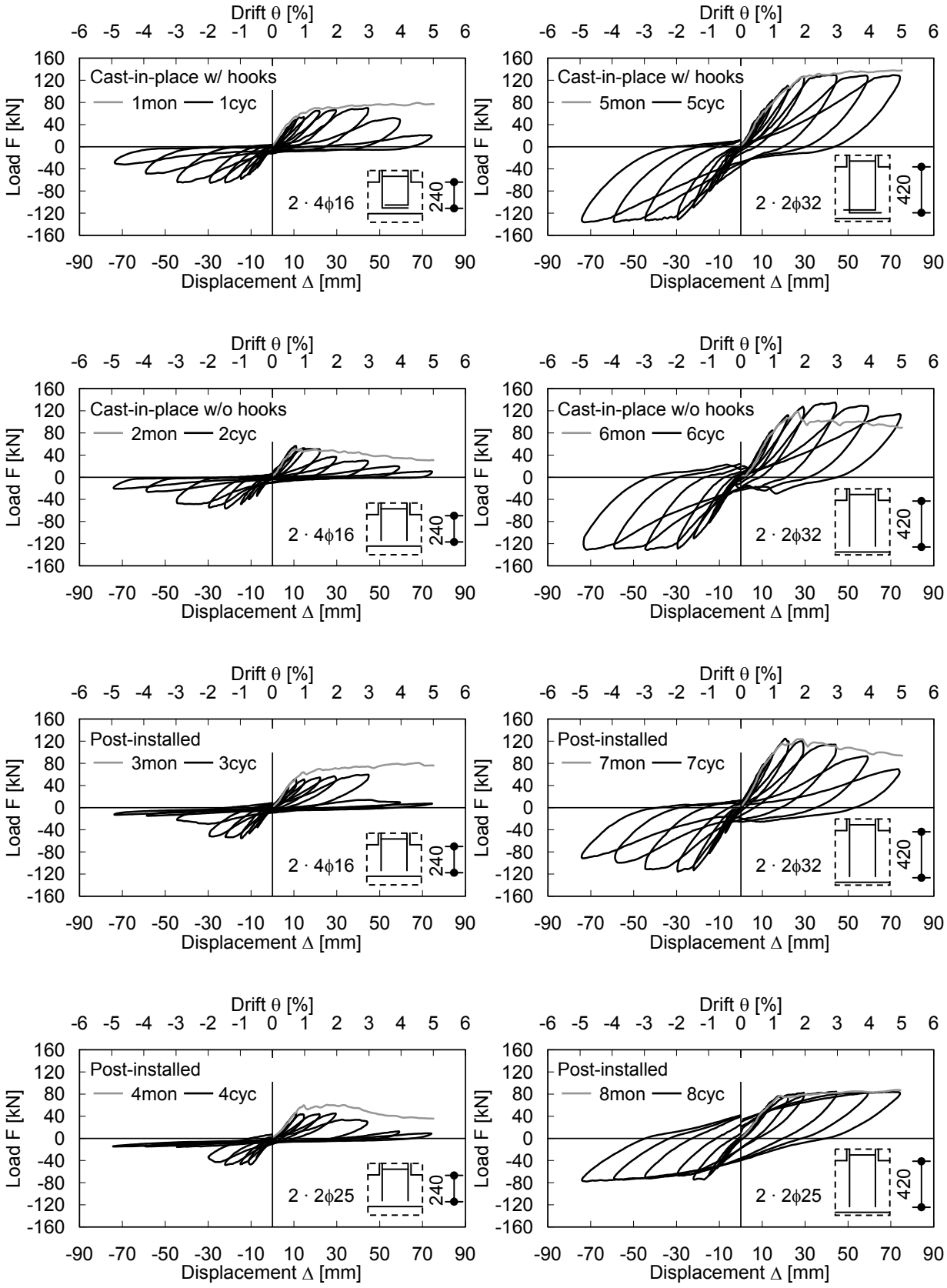


Figure 6.15 Overview of monotonic and cyclic load-drift curves of experimental tests

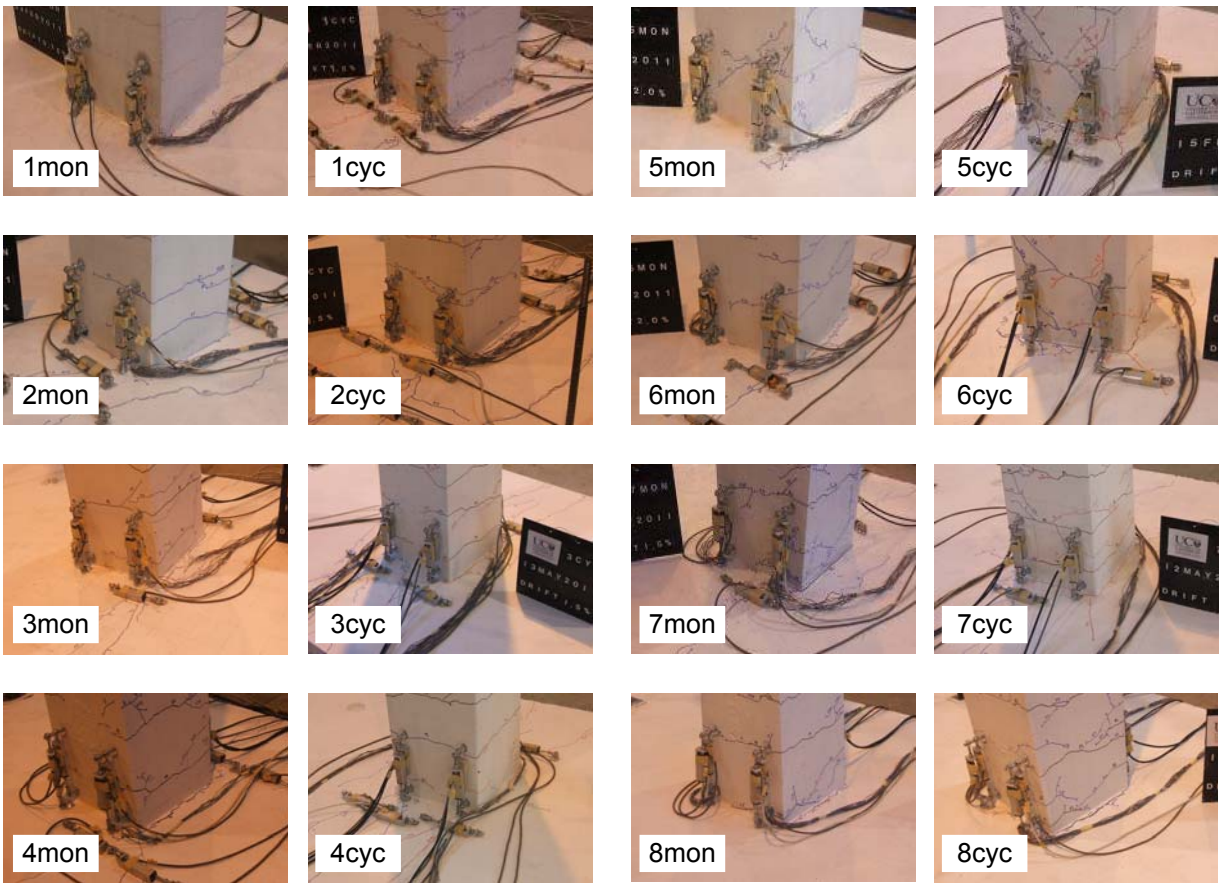


Figure 6.16 Observed crack patterns of experimental tests at failure load

The different anchorage failure modes as introduced in Section 2.3.1.2 do not appear as clear as shown in Figure 2.31 which makes pinpointing of the governing failure mode difficult. In the context of this thesis however, it is less important to differentiate between the pullout and the concrete breakout failure mode. The important thing for the development of the design concept (Chapter 9) is primarily the differentiation between the ductile yielding failure and the brittle pullout or concrete breakout failure. Therefore, the following two failure modes were identified:

- Yielding failure (mode Y), characterised by a constant F-$\Delta$ response above the yield capacity of the column.
- Pullout or concrete breakout failure (mode P/C), characterised by a declining or constant F-$\Delta$ response below the yield capacity of the column.

In the following, the global behaviour is described in brief for each specimen. A more detailed description of the global behaviour of the tested specimens including load-drift curves in which the sequence of cracks, pullout and concrete breakout or yield is indicated is given in Appendix D: Column-to-Foundation Connection Test Data.

During the monotonic and the cyclic tests on Specimen 1, 2 and 3 ($2 \cdot 4\phi16$, $\ell_b$ = 240 mm) cracks developed at approximately 1.0 % drift. While monotonic and cyclic loading caused Specimen 1 (cast-in-place with hook) to fail by yielding (mode Y) which was followed by strain hardening, Specimen 2 and 3 (cast-in-place without hook and post-installed) did not attain the yield moment capacity of the column during cyclic loading and failed by pullout and concrete breakout (mode P/C) at about 1.5 % drift.

Almost in parallel to the development of cracks at around 1.5 % drift, the monotonic and the cyclic tests on Specimen 5, 6 and 7 ($2 \cdot 2\phi32$, $\ell_b$ = 420 mm) caused yielding of the starter bars (mode Y). Only Specimen 5 (cast-in-place with hook) developed pronounced strain hardening characteristics whereas Specimen 6 and 7 (cast-in-place without hook and post-installed) displayed pinching behaviour during cyclic loading.

Specimen 4 ($2 \cdot 2\phi25$, $\ell_b$ = 240 mm, post-installed) performed poorly during both the monotonic and cyclic test. The strength deteriorated at 1.5 % drift, significantly below the yield moment capacity (mode P/C), accompanied by pronounced cracking. Testing ended in total destruction of the connection core. This behaviour is in strong contrast to the performance of Specimen 8 ($2 \cdot 2\phi25$, $\ell_b$ = 420 mm, post-installed) during monotonic and cyclic loading. Almost no cracks developed in the foundation and yielding of the column starter bars occurred just before 1.5 % drift (mode Y). The F-$\Delta$ diagram showed strain hardening and significant energy hysteresis, reflecting the development of the plastic hinge.

For most tested column-to-foundation connections, the load-drift curves reveal only limited influence of the cyclic loading on the pre-peak behaviour. In contrast, the post-peak behaviour clearly shows an accelerated strength reduction due to the cyclic loading. Specimen 4 as the connection with the smallest ratio of anchorage length and reinforcing bar diameter however, experienced a strength deterioration which is more pronounced for cyclic loading if compared to monotonic loading already for small drifts. On the contrary, the monotonic load-drift curve and the envelope of the cyclic load-drift curve of Specimen 8 perfectly match up to the ultimate drift.

For the following discussion, the failure load is defined as the maximum load, i.e. $F_{R,p/c} = F_{max}$, if failure mode P/C was governing (Figure 6.17a). For failure mode Y, the bilinear representation (Figure 6.17b) in accordance with *ATC-40 (1996)* was used to determine $F_{R,y}$ which is termed in the following also as the failure load for the sake of consistency.

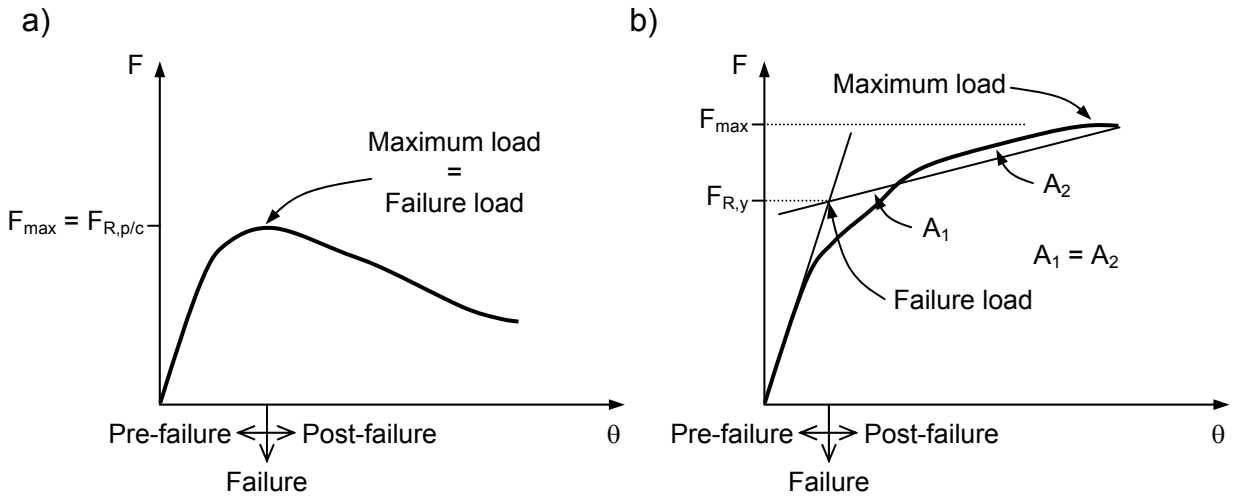


Figure 6.17 Connection capacity: a) Failure mode P and C; b) Failure mode Y, bilinear representation of yielding capacity after *ATC-40 (1996)*

The crack patterns are reported in detail in *Mahrenholtz, C. (2012a)*. In general, the primary crack in the foundation developed in the plane of the pulled starter bars. However, Figure 6.16 demonstrates that the crack pattern in particular of the secondary cracks experiences high variation. Reasoned engineering judgment was used to measure the crack widths where multiple closely spaced cracks were observed or where there was a variation in width in the same crack along its length: The crack width of adjacent cracks (Figure 6.18a) were added and the crack widths of opposing cracks averaged (Figure 6.18b).

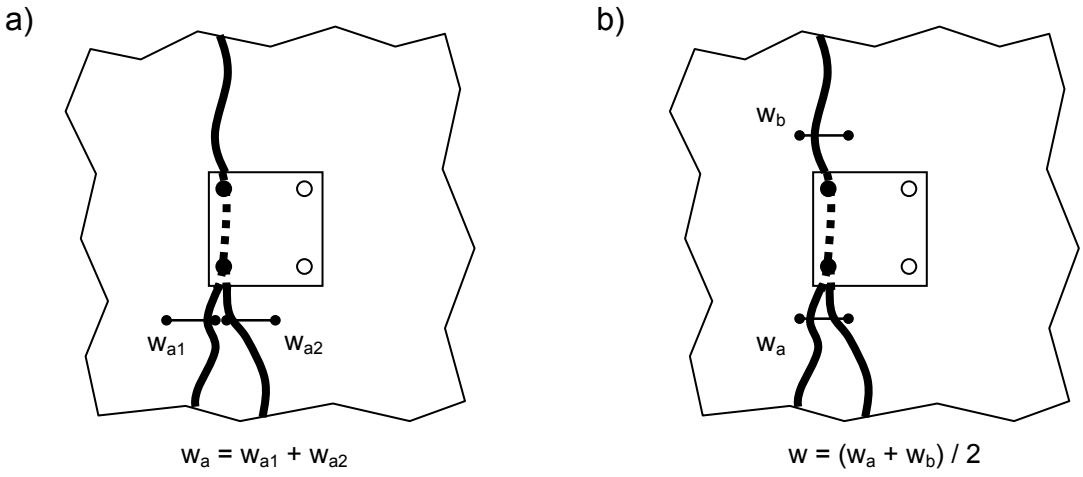


Figure 6.18 Crack width: a) Adding of adjacent cracks; b) Averaging of opposing cracks

Table 6.3 provides the tested maximum loads, the failure mode, and failure loads as well as corresponding drifts and crack widths.

Table 6.3 Maximum loads, failure modes, failure loads as well as corresponding drifts and crack widths experimentally tested

| Specimen ID | Maximum load[1] $expF_{max}$ [kN] | Failure mode[2] | Failure load[3] $expF_R$ [kN] | Drift[4] $\theta_R$ [%] | Crack width[5] $w_R$ [mm] |
|---|---|---|---|---|---|
| exp1mon | 79.4 | Y | 71.0 | 1.5 | 0.5 |
| exp1cyc | 70.0 | Y | 65.5 | 1.5 | 0.5 |
| exp2mon | 50.8 | P/C | 50.8 | 0.75 | 0.8 |
| exp2cyc | 56.7 | P/C | 56.7 | 0.75 | 0.8 |
| exp3mon | 80.8 | Y | 65.0 | 1.5 | 0.8 |
| exp3cyc | 59.6 | P/C | 59.6 | 1.5 | 0.8 |
| exp4mon | 60.7 | P/C | 60.7 | 1.5 | 0.8 |
| exp4cyc | 46.3 | P/C | 46.3 | 1.5 | 0.8 |
| exp5mon | 137.9 | Y | 129.5 | 2.0 | 0.1 |
| exp5cyc | 129.6 | Y | 128.0 | 2.0 | 0.1 |
| exp6mon | 118.5 | Y | 116.5 | 2.0 | 0.5 |
| exp6cyc | 135.1 | Y | 127.0 | 2.0 | 0.5 |
| exp7mon | 124.0 | Y | 119.0 | 1.5 | 0.5 |
| exp7cyc | 124.7 | Y | 119.0 | 1.5 | 0.5 |
| exp8mon | 84.4 | Y | 80.0 | 1.5 | 0.1 |
| exp8cyc | 83.9 | Y | 80.0 | 1.5 | 0.1 |

[1] Maximum load measured during complete loading up to 5.0 % drift

[2] Y: Yielding failure; P/C: Pullout or concrete failure

[3] Failure load as defined in Figure 6.17

[4] Drift corresponding to failure load

[5] Crack width corresponding to failure load

The majority of cyclic tests yielded failure loads which were larger than the failure loads of the corresponding monotonic tests. Exceptions were Specimen 2 and 6 (cast-in-place starter bars without hooks). The difference was less than 15 % and is ascribed to scatter. However, this fact is a clear indication that the adverse effect of cyclic loading on the connection capacity is probably secondary in comparison to the beneficial effect of moment loading.

The experimentally determined capacities are compared to the calculative capacities in Chapter 8 and Chapter 9.

### 6.4.2 Stiffness degradation and energy dissipation

For seismic engineering, the degradation of stiffness and dissipation of energy as a function of the cyclic loading is important. The stiffness degradation and energy dissipation of the test specimens under reversed cyclic loading are defined as the peak-to-peak stiffness (Figure 6.19a) and area enclosed by the load-drift hysteresis loops (Figure 6.19b), respectively. The following considerations are based onf the first cycle of each drift level.

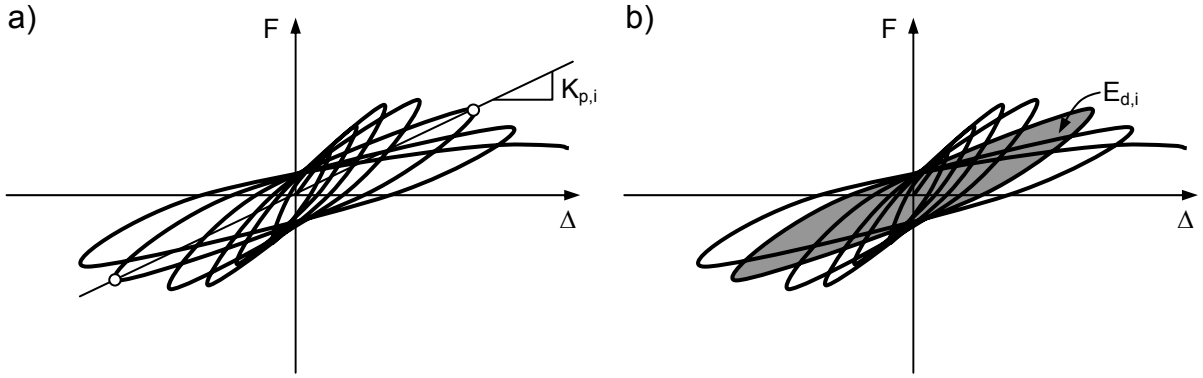


Figure 6.19 Definition of the sub-assemblage a) peak-to-peak stiffness $K_{p,i}$ and b) energy dissipation $E_{d,i}$ of the $i^{th}$ cycle (schemetic, only one cycle per drift level shown)

The degradation of concrete members is to a large degree expressed by the decrease in effective stiffness over cycles. Therefore, the behaviour of the stiffness $K_p$ as a function of the cyclic loading is an important property for seismic engineering (Figure 6.20a). The progress of stiffness degradation can be analysed best on the basis of Figure 6.20b for which the stiffness of the $i^{th}$ cycle was normalised with reference to the stiffness of the very $1^{st}$ cycle. For connections with 16 mm diameter starter bars and 240 mm anchorage length (Specimens 1 to 3), the stiffness of anchorages with hooks (Specimen 1) is larger than that of anchorages without hooks (Specimens 2 and 3). The stiffness of all connections with 32 mm diameter starter bars and 420 mm anchorage length (Specimens 5 to 7) are initially similar however, when the post-installed connection (Specimen 7) fails at 1.5 % drift, its stiffness drops considerably and lags behind the stiffness of the cast-in-place connections. The curve for the 240 mm long anchorages of Specimen 4 shows a significantly softer behaviour than the curve for the 420 mm long anchorages of Specimen 8 though both specimens have the same starter bar diameter of 25 mm.

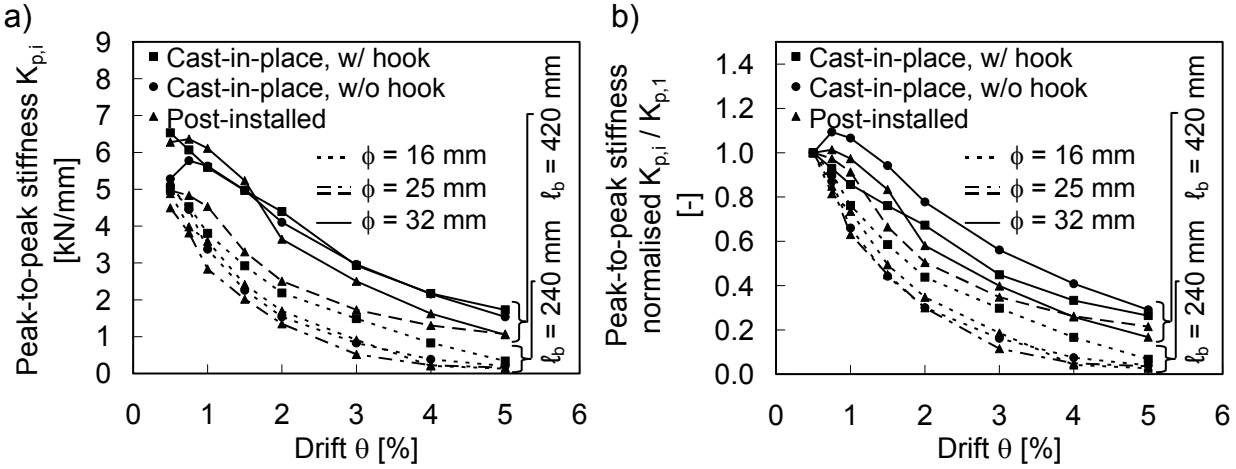


Figure 6.20 Peak-to-peak stiffness after first cycle of each drift level: a) Absolute; b) Normalised with reference to 1st cycle of drift level θ = 0.5 %

Also the ability to dissipate energy is an important seismic performance criterion for reinforced concrete structures. The absolute energy dissipation $E_d$ allows comparing the seismic performance of the different column-to-foundation configurations (Figure 6.21a). Cast-in-place column-to-foundation connections which anchorages were detailed with hooks (Specimens 1, $\ell_b$ = 240 mm and 5, $\ell_b$ = 420 mm) dissipated significantly more energy than cast-in-place column-to-foundation connections which anchorages provided the same anchorage length but were detailed without hooks (Specimens 2, $\ell_b$ = 240 mm and 6, $\ell_b$ = 420 mm). Notably, their post-installed counterparts (Specimens 3, $\ell_b$ = 240 mm and 7, $\ell_b$ = 420 mm) dissipated less energy. Possible explanations are scattering effects and that the bond of cast-in-place anchorages are more damaged if compared to post-installed anchorges. More pronounced bond damage, in turn, increases the energy dissipation. The post-installed column-to-foundation connection with 25 mm starter bars, anchorage length of 240 mm (Specimen 4) showed the poorest performance, consuming less than 14 kNm during cycling. The same connection configuration with an anchorage length of 420 mm (Specimen 8) developed a perfect plastic hinge, dissipating more than 51 kNm which was the maximum value of all tests. Figure 6.21b shows the relative energy dissipation, for which the energy dissipation of the $i^{th}$ cycle was normalised with reference to the energy dissipation of the very 1st cycle.

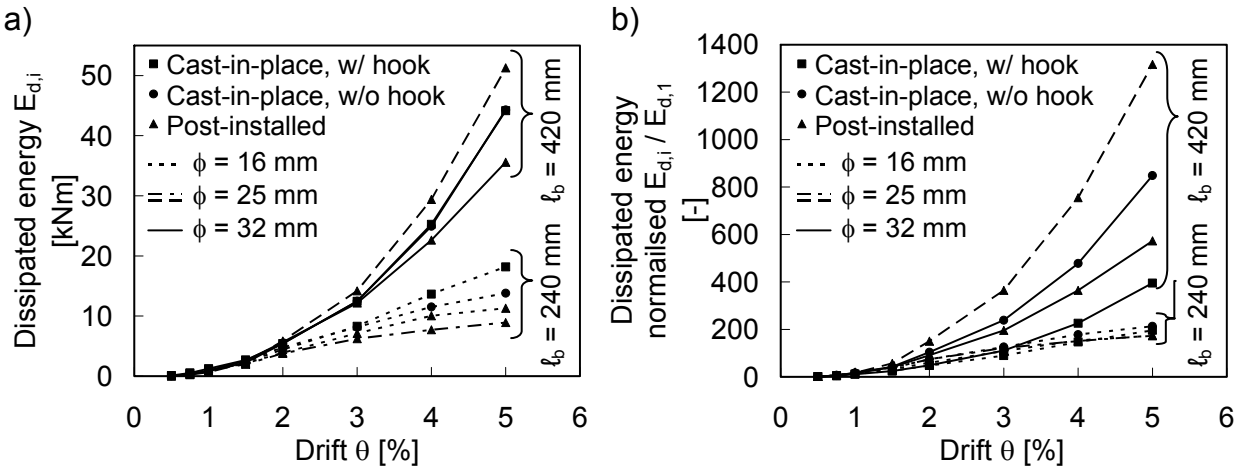


Figure 6.21 Dissipated energy of first cycle of each drift level: a) Absolute; b) Normalised with reference to 1st cycle of drift level $\theta$ = 0.5 %

To study the influence of cyclic loading further, also the stiffness degradation and energy dissipation during the three cycles of the representative drift level $\theta$ = 1.5 % were evaluated. The drift level $\theta$ = 1.5 % is most relevant since it is the drift level at which most specimens failed. The absolute values for the secant stiffness and dissipated energy of all tested specimens are plotted in Figure 6.22a and Figure 6.23a and the results normalised with reference to the first cycle of the drift level $\theta$ = 1.5 % in Figure 6.22b and Figure 6.23b. It is evident, that the differences between the various specimens are small. Therefore, the diagrams were split for the two anchorage lengths $\ell_b$ = 240 mm and $\ell_b$ = 420 mm, producing Figure 6.22c, Figure 6.22d, Figure 6.23c, and Figure 6.23d.

Clearly, the stiffness dagradation is more pronounced for the smaller anchorage length $\ell_b$ = 240 mm if compared to the larger anchorage length $\ell_b$ = 420 mm. Also, the attenuation of the energy dissipation is more pronounced for the smaller than for the larger anchorage length. Further interpretations of the evaluation with respect to the influence of the different detailing and installation method would be rather speculative.

The differences of the various specimens in terms of secant stiffness and dissipated energy become more pronounced for drift levels larger than $\theta$ = 1.5 %, however, are then progressively influenced by scattering effects, making a meaningful discussion impossible.

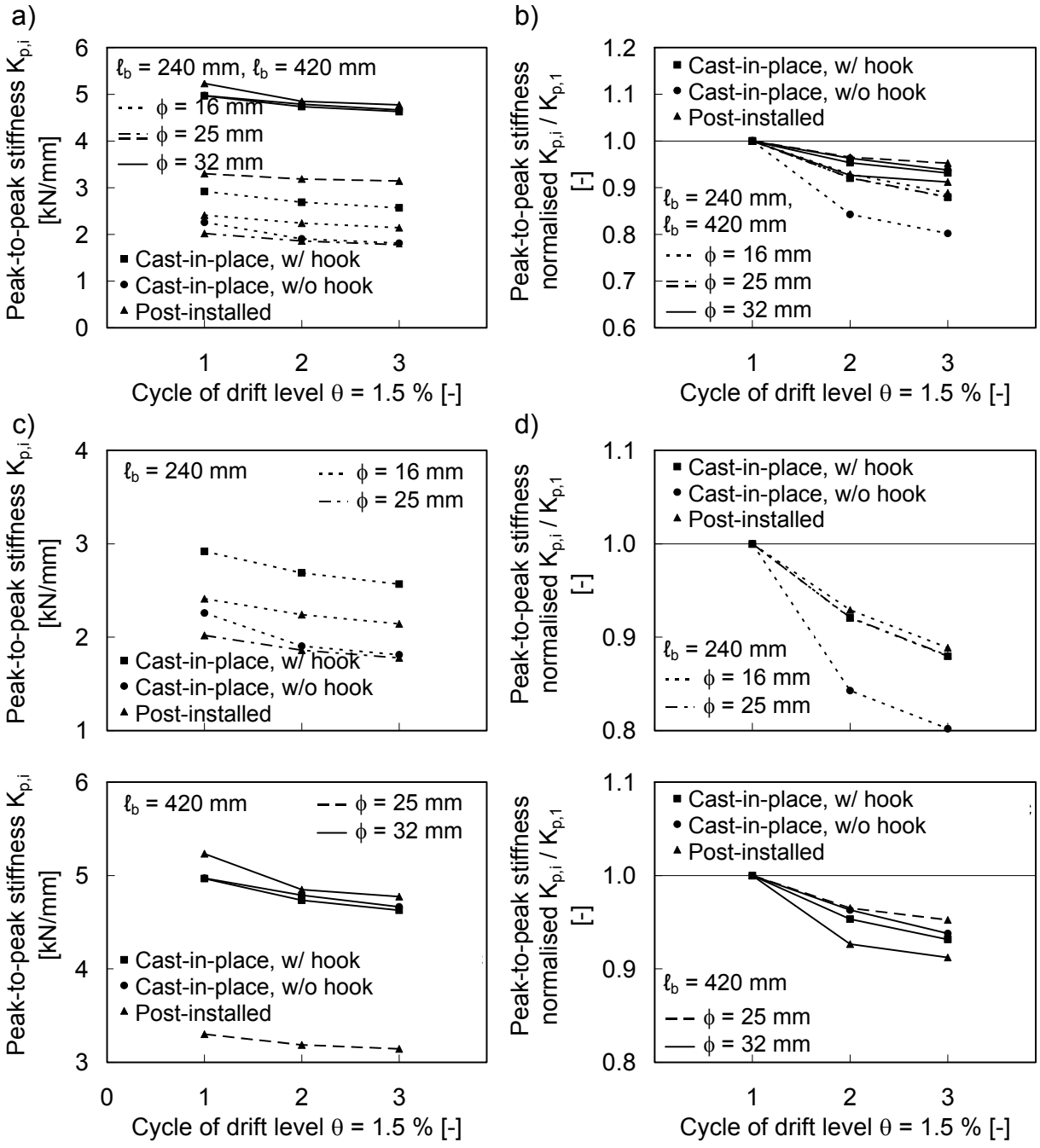


Figure 6.22 Peak-to-peak stiffness after each cycle of drift level $\theta$ = 1.5 %:
a) Absolute; b) Normalised with reference to 1st cycle of drift level $\theta$ = 1.5 %;
c) Absolute, separated for different anchorage lengths; d) Normalised with reference to 1st cycle of drift level $\theta$ = 1.5 %, separated for different anchorage lengths

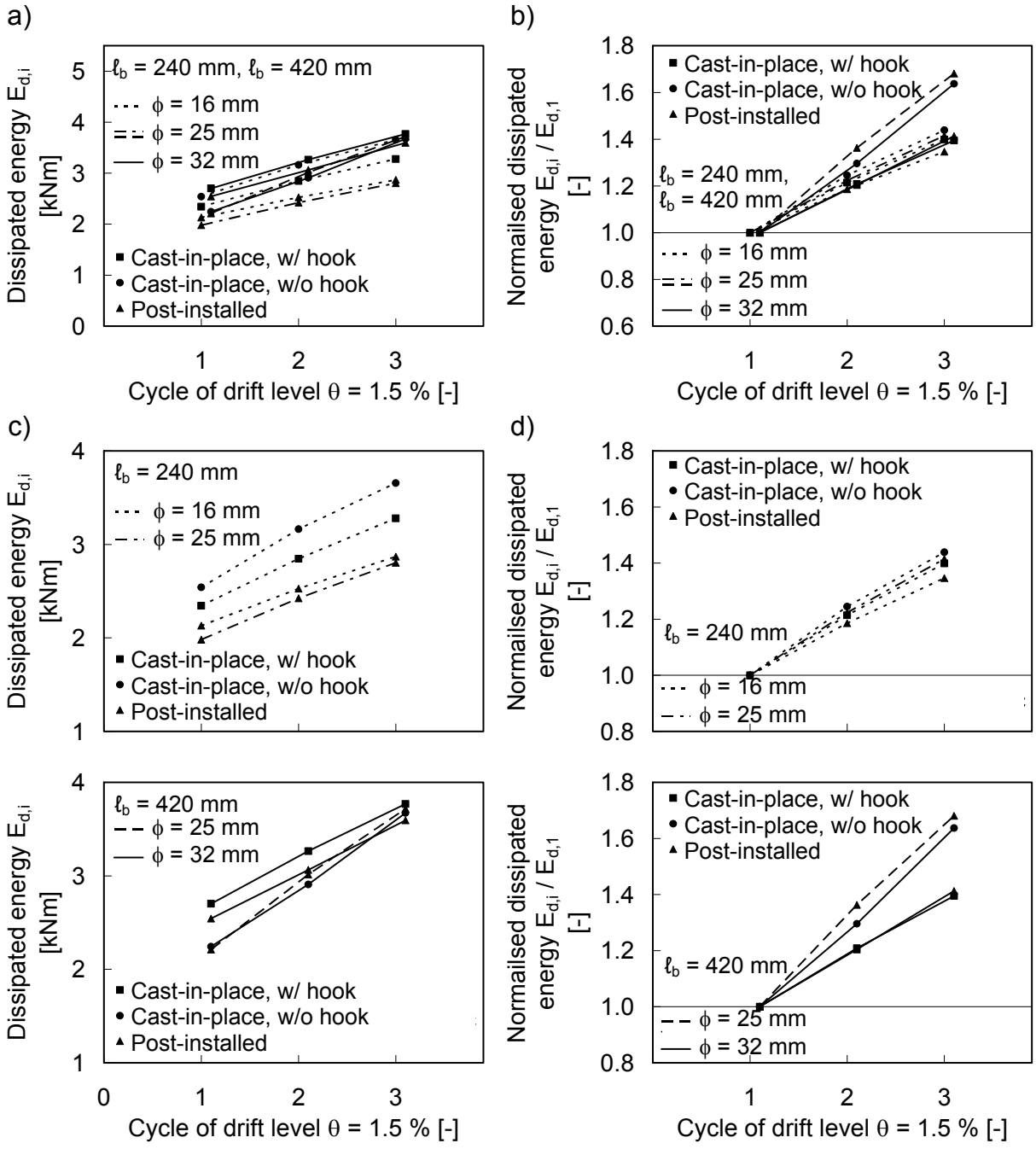


Figure 6.23 Dissipated energy of each cycle of drift level $\theta$ = 1.5 %: a) Absolute; b) Normalised with reference to 1st cycle of drift level $\theta$ = 1.5 %; c) Absolute, separated for different anchorage lengths; d) Normalised with reference to 1st cycle of drift level $\theta$ = 1.5 %, separated for different anchorage lengths

In summary, for identical column starter bar layouts and anchorage lengths, different anchorage detailing and installation methods had only comparatively small impact on the test results with respect to of stiffness degradation and energy dissipation. This is in particular true for the behaviour of stiffness degradation and energy dissipation during the three cycles representing a drift level. In contrast, the anchorage lengths

significantly influenced the overall static and seismic performance, as the response of Specimen 4 and 8 shows.

Furthermore, comparing the behaviour of Specimen 4 ($2 \cdot 2$ post-installed 25 mm reinforcing bars, $\ell_b$ = 240 mm) with Specimen 2 and 3 ($2 \cdot 4$ cast-in-place without hook and post-installed 16 mm reinforcing bars, $\ell_b$ = 240 mm) shows that the detailing of starter bars with smaller diameters is more favourable than the use of larger bar diameters: Though the reinforcing bar cross sections and therefore the moment capacity of these specimens are in the same order, however, Specimen 4 reveals a significant poorer performance than Specimen 2 and 3. Finally, the performance of Specimen 8 ($2 \cdot 2$ post-installed 25 mm reinforcing bars, $\ell_b$ = 420 mm) compared to Specimen 6 and 7 ($2 \cdot 4$ cast-in-place without hook and post-installed 32 mm reinforcing bars, $\ell_b$ = 420 mm) demonstrates the purpose of the general seismic design approach to localise plastification in controlled relatively weaker cross sections, i.e. plastic hinges: The moment capacity of Specimen 8 is about two third the moment capacity of Specimen 6 and 7 and therefore experiences pronounced yielding and strain hardening which leads to significant energy dissipation without jeopardising the stiffness.

In conlcusion, the relative anchorage length $\ell_b / \phi$ is a distinctive parameter which gives an indication for the connection performance. However, its dependency on the connection geometry in terms of starter bar layout, anchorage length, anchorage detailing and installation method is highly complex because of the effect of overlapping influencing area and the group effect (Section 2.3.1.2) and cannot be properly evaluated by means of the few experimentally conducted tests. More importantly, however, is the assessment of the stiffness degradation and energy dissipation together with other characteristics relevant for the evaluation of the seismic performance according to standardised assessment criteria which is presented in Section 6.4.4.

### 6.4.3 Detailed study of anchorage

#### 6.4.3.1 Distribution of tensile and bond stresses

The global F-$\Delta$ response is reflected by the strain distribution along the starter bar anchorage. According to the considerations made in Section 3.3, it was expected that the damage propagates from the loaded end towards the unloaded end of the anchorage. The strain gauges installed along the starter bar anchorage (Figure 6.24) provided the strain values during loading. The strain readings were then used to calculate the tensile and bond stresses in the starter bar anchorages according to the equations given in Section 2.2.1.

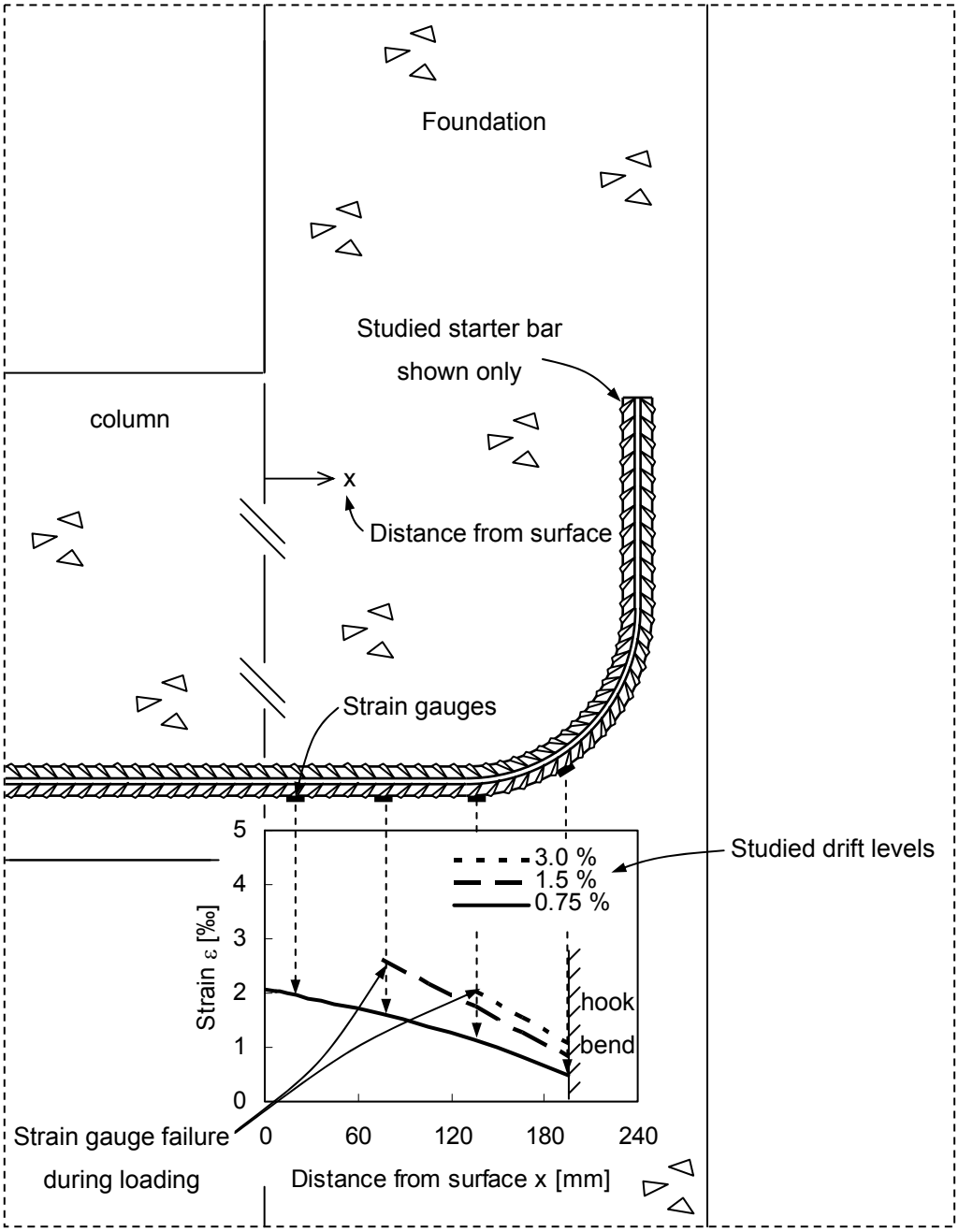


Figure 6.24 Explanation of strain reading for stress plots

For the following study, the stresses were calculated for the peak of the first cycle of three drift levels as indicated by the circles in Figure 6.13, i.e. 0.75 %, 1.5 % and 3.0 %. The following diagrams (Figure 6.25 to Figure 6.32) show the distribution of tensile stresses and bond stresses for all experimentally tested specimens. Black and gray curves indicate tensile stresses and bond stresses, respectively.

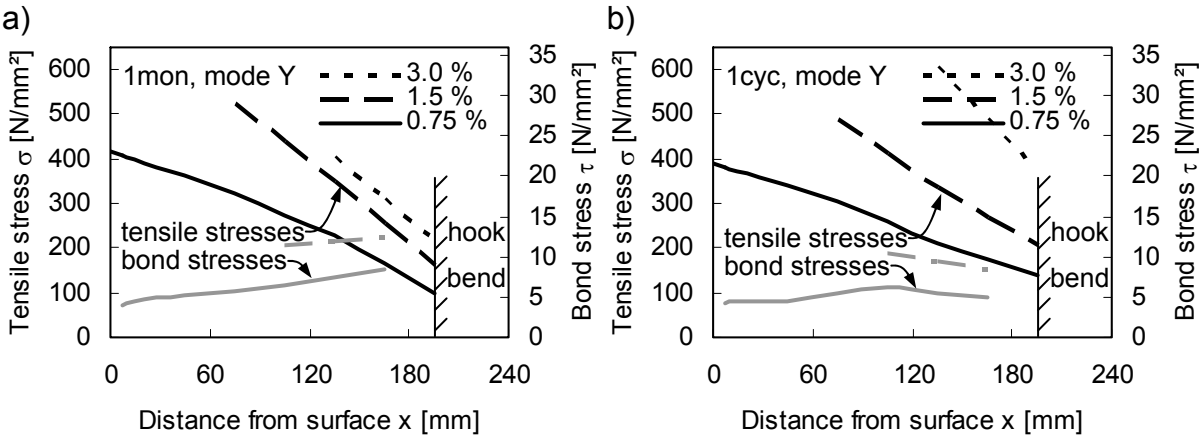


Figure 6.25 Reinforcing bar stress profiles along anchorage on the basis of strain gauge readings for a) monotonic and b) cyclic testing on Specimen 1 – $\ell_b$ = 240 mm, 2 · 4$\phi$16, cast-in-place with hooks

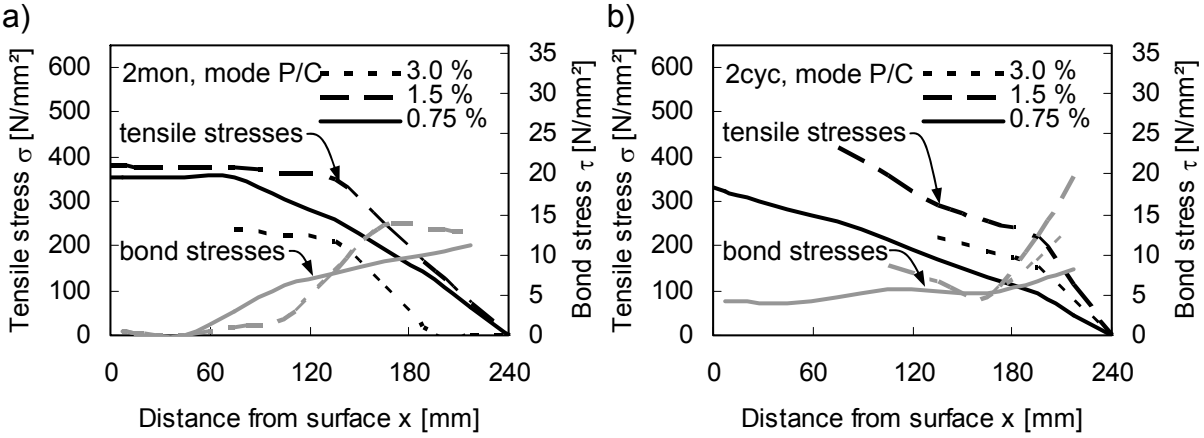


Figure 6.26 Reinforcing bar stress profiles along anchorage on the basis of strain gauge readings for a) monotonic and b) cyclic testing on Specimen 2 – $\ell_b$ = 240 mm, 2 · 4$\phi$16, cast-in-place without hooks

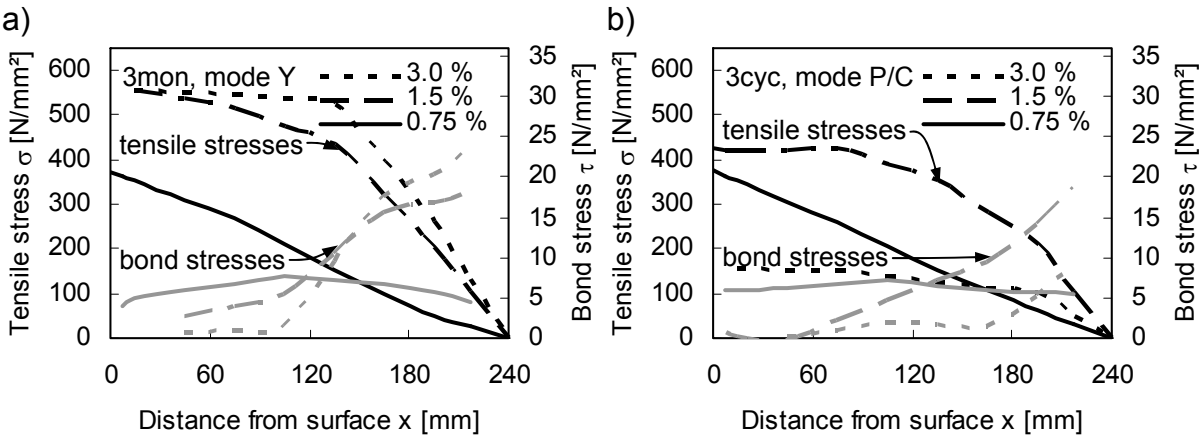


Figure 6.27 Reinforcing bar stress profiles along anchorage on the basis of strain gauge readings for a) monotonic and b) cyclic testing on Specimen 3 – $\ell_b$ = 240 mm, 2 · 4$\phi$16, post-installed

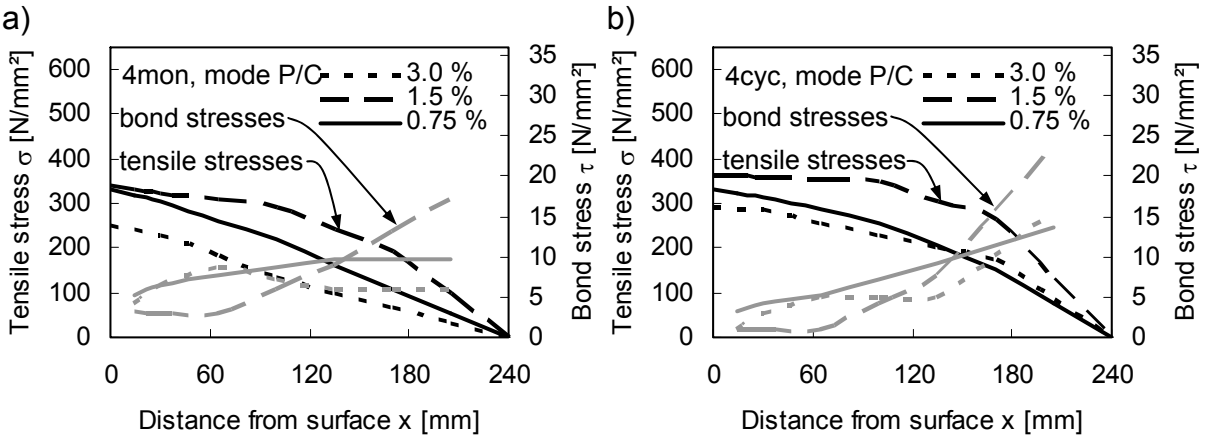


Figure 6.28 Reinforcing bar stress profiles along anchorage on the basis of strain gauge readings for a) monotonic and b) cyclic testing on Specimen 4 – $\ell_b$ = 240 mm, 2 · 2$\phi$25, post-installed

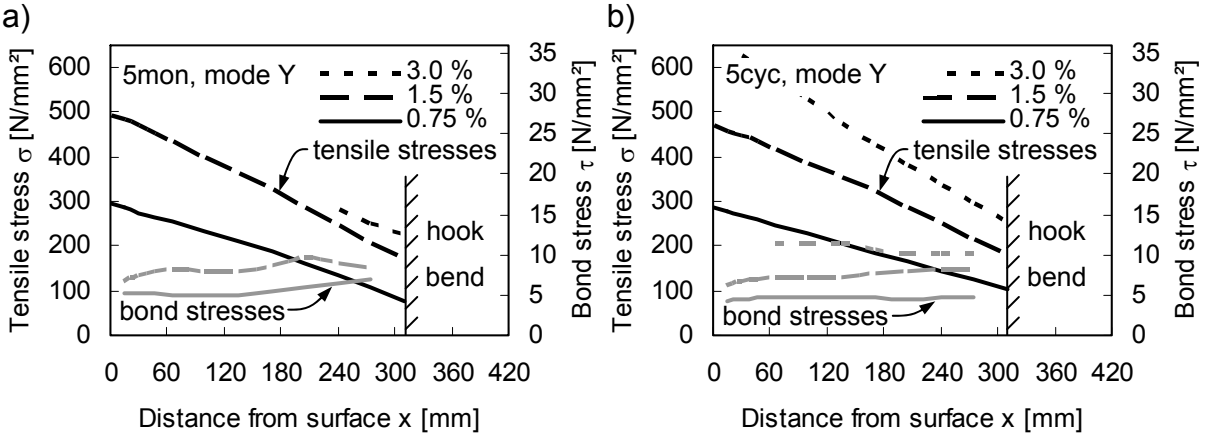


Figure 6.29 Reinforcing bar stress profiles along anchorage on the basis of strain gauge readings for a) monotonic and b) cyclic testing on Specimen 5 – $\ell_b$ = 420 mm, 2 · 2$\phi$32, cast-in-place with hooks

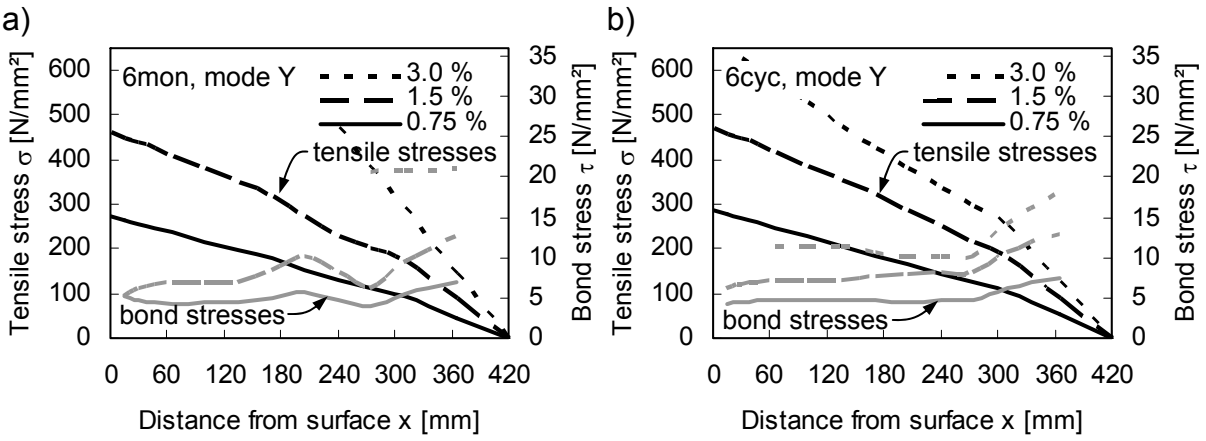


Figure 6.30 Reinforcing bar stress profiles along anchorage on the basis of strain gauge readings for a) monotonic and b) cyclic testing on Specimen 6 – $\ell_b$ = 420 mm, 2 · 2$\phi$32, cast-in-place without hooks

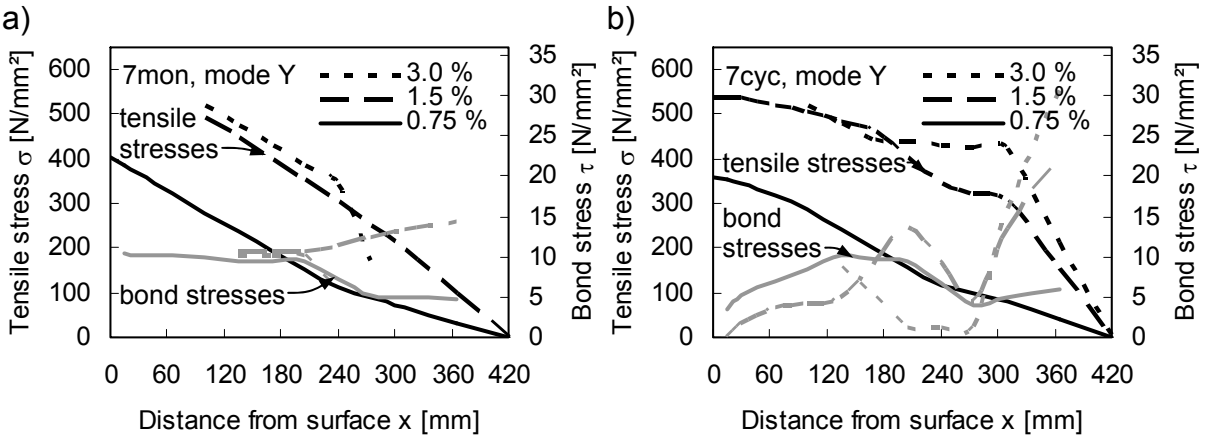


Figure 6.31 Reinforcing bar stress profiles along anchorage on the basis of strain gauge readings for a) monotonic and b) cyclic testing on Specimen 7 – $\ell_b$ = 420 mm, 2 · 2ϕ32, post-installed

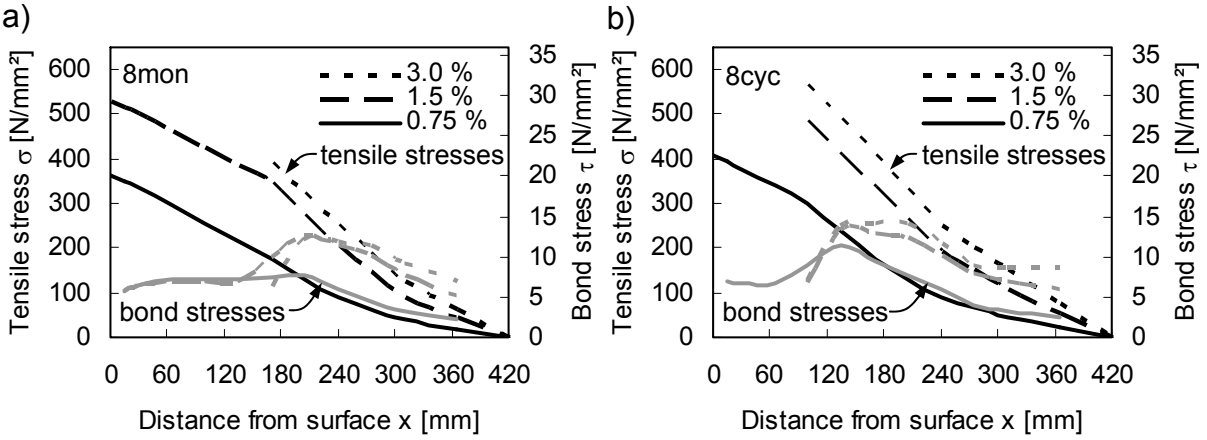


Figure 6.32 Reinforcing bar stress profiles along anchorage on the basis of strain gauge readings for a) monotonic and b) cyclic testing on Specimen 8 – $\ell_b$ = 420 mm, 2 · 2ϕ25, post-installed

Some strain gauges failed during loading, in particular when approaching the pullout or concrete cone capacity if the connection failed in mode P/C. The strain gauges also failed shortly after reaching yielding capacity ($\varepsilon_y \approx 4‰$) in case of a mode Y failure of the connection. In general, the derived stress curves have an inconsistent appearance which demonstrates the inhomogeneous damage in the anchorage zones: The stresses are influenced for example by loosened concrete parts which are jammed between the pulled starter bar and the intact concrete. Therefore, the curves of the tensile and bond stresses are very unsteady and difficult to interpret in detail.

By trend, however, the diagrams give evidence that the bond stresses are redistributed from the loaded end (x = 0 mm) towards the unloaded end (x = $\ell_b$ = 240 mm and 420 mm, respectively), regardless to the failure mode of the column-to-foundation connection. For specimens failing in the ductile mode Y, the

stress redistribution continues till the end of testing. On the contrary, strains are reduced and the redistribution halts as the strength of the column-to-foundation connection deteriorates for specimens failing in the brittle mode P/C.

In general, it is difficult to tell whether the stress redistribution is more pronounced for cyclic loading if compared to monotonic loading. However, the connection with the smallest ratio of anchorage length and diameter, Specimen 4, clearly shows that cyclic loading is fostering the redistribution if compared to the monotonic loading. On the contrary, monotonic and cyclic loading cause the same redistribution at Specimen 8 which has the largest ratio of anchorage length and diameter.

#### 6.4.3.2 Penetration of strain

In general, the maximum tensile stress of the starter bar develops at the column-to-foundation interface. For connections failing in yielding (mode Y), the loaded end of the anchorage is the starting point for the penetration of yielding which is triggered by the strain hardening in the previously yielded location. The penetration of yielding is accompanied by significant slip (Figure 6.33a). Specimen 8 is a prominent example where this phenomenon can be observed (Figure 6.32).

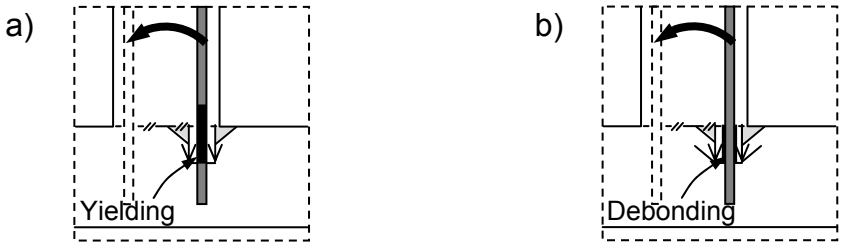


Figure 6.33 Column-to-foundation connection anchorages: a) Penetration of yielding; a) Penetration of debonding

For connections failing by pullout or concrete breakout (mode P/C), the debonding is initiated also at the loaded end of the starter bar anchorage and propagates towards the unloaded end. The anchorage develops excessive slip accompanied by the development of cracks and sequential concrete breakouts (Figure 6.33b). The phenomenon is termed in the following as penetration of debonding due to the similarity to the penetration of yielding. Specimen 4 is a prominent example where this phenomenon was observed (Figure 6.28).

The penetration of yielding and debonding is reflected in the profiles of tensile and bond stresses (Figure 6.25ff): For small drifts imposed on the sub-assemblage, the bond stress curves of the starter bar anchorages are almost constant over the distance from surface and the tensile stress curves are linearly decreasing. With increasing drifts, the tensile stresses become almost constant at the zone close to

the loaded end and experience a drop at the depth of yielding or debonding, respectively. At the same time, the bond stresses are redistributed to the unloaded end. In summary, both, penetration of yielding and penetration of debonding causes a disconnection of reinforcing bar and concrete. For this reason, the bond stresses diminish at the loaded end and concentrate increasingly at the unloaded end. The yield penetration has a positive contribution to the rotation capacity because of the accompanying inelastic strains (ductile failure mode Y), however it also reduces the bonded length which may cause a pullout in the aftermath. The debonding penetration is generally critical because the bond stress concentration at the unloaded end may cause the exceedance of the bond stresses, resulting in a pullout if not failed before due to concrete breakout (brittle failure mode P/C).

The design provisions of *NZS 3101 (2006)* define min{8$\phi$; h/2} which has to be disregarded when determining the anchorage length of starter bars to account for potential yield penetration. This is a good estimation for the ultimate penetration of both, yielding and debonding as the strain gauge measurement show (Section 6.4.3.1). Penetration of yielding and debonding at drift levels corresponding to the failure loads, however, is better estimated by means of the design provisions of *Eurocode 8 (2006)*, taking 5$\phi$ into account for the yield penetration. The design provisions stipulated in *Eurocode 8 (2006)* and *NZS 3101 (2006)* to account for the penetration of yielding are presented in Appendix A: Conventional Anchorage Design.

#### 6.4.3.3 Decomposition of bond and bearing

In the following, the development of the tensile stresses along the anchorage under monotonic and cyclic loading is evaluated in more detail. Contrary to anchorages without hooks transferring the complete load by bond, anchorages with hooks transfer only a portion by bond action and the remainder by bearing action of the hook. In fact, bond is transferred also along the tail of the hook which is neglected in the following evaluation for reasons of simplification. The definition of bond and bearing zone is schematically shown in Figure 6.34.

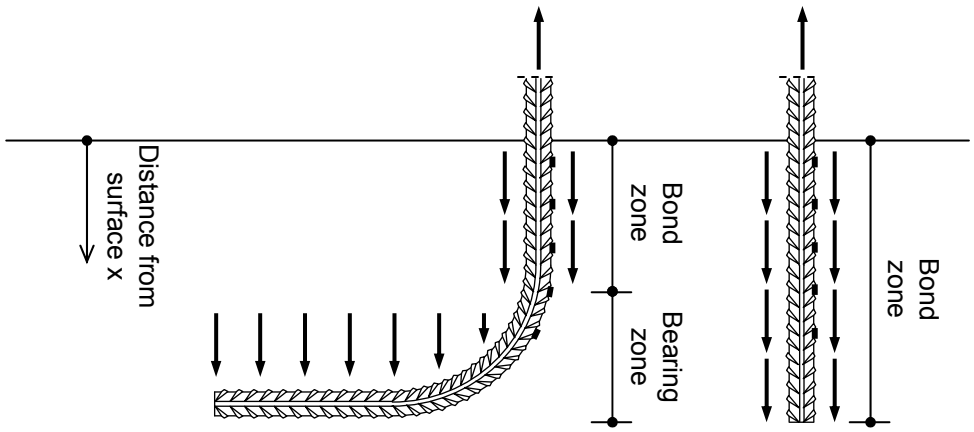


Figure 6.34 Simplified definition of bond and bearing zone and location of strain gauges

The decomposition of the tensile stresses in bond and bearing component is analysed for Specimen 1 and 5 which anchorages were detailed with hooks. The diagrams shown in Figure 6.35 plot the tensile stress versus drift for the monotonic and cyclic test at the beginning of the anchorage (x = 0 mm) and at the onset of the hook bend (x = 135 mm and 240 mm, respectively). The stress at the onset of the hook bend is the component which is transferred in the bearing zone mostly by mechanical interlock. The difference between the two curves is the component which is transferred by bond along the bond zone. The test data show that bond and bearing components each carried about half of the load. No significant difference between cyclic test and monotonic test can be detected.

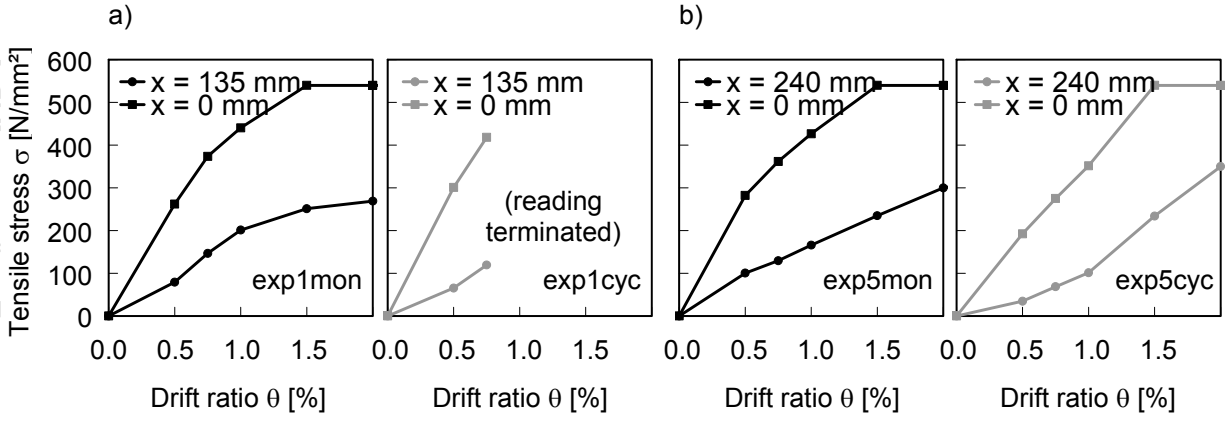


Figure 6.35 Decomposition of bond and bearing under monotonic an cyclic loading for monotonic and cyclic loading on a) Specimen 1 ($\ell_b$ = 240 mm, $\phi$ = 16 mm) and b) Specimen 1 ($\ell_b$ = 420 mm, $\phi$ = 32 mm)

### 6.4.4 Assessment of seismic performance

The performance of moment resisting frame concrete members is commonly assessed with reference to the acceptance criteria given in *ACI 374.1 (2005)*. For acceptance, the assessed sub-assemblage has to develop sufficient initial strength, must not exceed a known overstrength limit, and has to provide sufficient ductility, damping and stiffness. In the following, the criteria stipulated in Clauses 9.1.1, 9.1.2, and 9.1.3 of *ACI 374.1 (2005)* are applied on the tested column-to-foundation connection:

1. The column has to attain the lateral resistance $\exp M_{max}$ (tested maximum flexural capacity) equal to or greater than the nominal lateral resistance $\mathrm{cal}M_y$ (calculated nominal flexural capacity) before its drift exceeds the value consistent with the allowable story drift limitation (Figure 6.36b). The purpose of this criterion is to ensure sufficient initial strength before the drift exceeds the allowable story drift limitations.
2. The maximum lateral resistance $\exp M_{max}$ recorded in the test must not exceed $\lambda \mathrm{cal}M_y$, where $\lambda$ is the specified overstrength factor (Figure 6.36b). The purpose of this criterion is to avoid adverse overstrength effects which may change the aspired hierarchy of member capacity.
3. For cycling at the given drift $\theta_a$ at which acceptance is sought, but not less than a drift of 0.035, the characteristics of the third complete cycle has to satisfy the following:
   - The peak force $\exp M_{\theta a}$ for a given loading direction must not be less than $0.75 \exp M_{max}$ for the same loading direction (Figure 6.36b). This criterion excludes brittle members which strength deteriorates significantly after the peak.
   - The relative energy dissipation ratio $E_{d,\theta a} / E_{d\#,\theta a}$ must not be less than 0.125 (Figure 6.36a). This criterion excludes members with insufficient energy dissipation in order to avoid inadequate damping.
   - The secant stiffness $K_{p,\theta a}$ from a drift of $-\theta_a$ to a drift of $+\theta_a$ must not be less than 0.05 times the initial stiffness $K_{p,\theta i}$ for the initial drift $\theta_i$ (Figure 6.36c). This criterion excludes members which hysteresis have a pronounced pinching character and therefore would behave too softly.

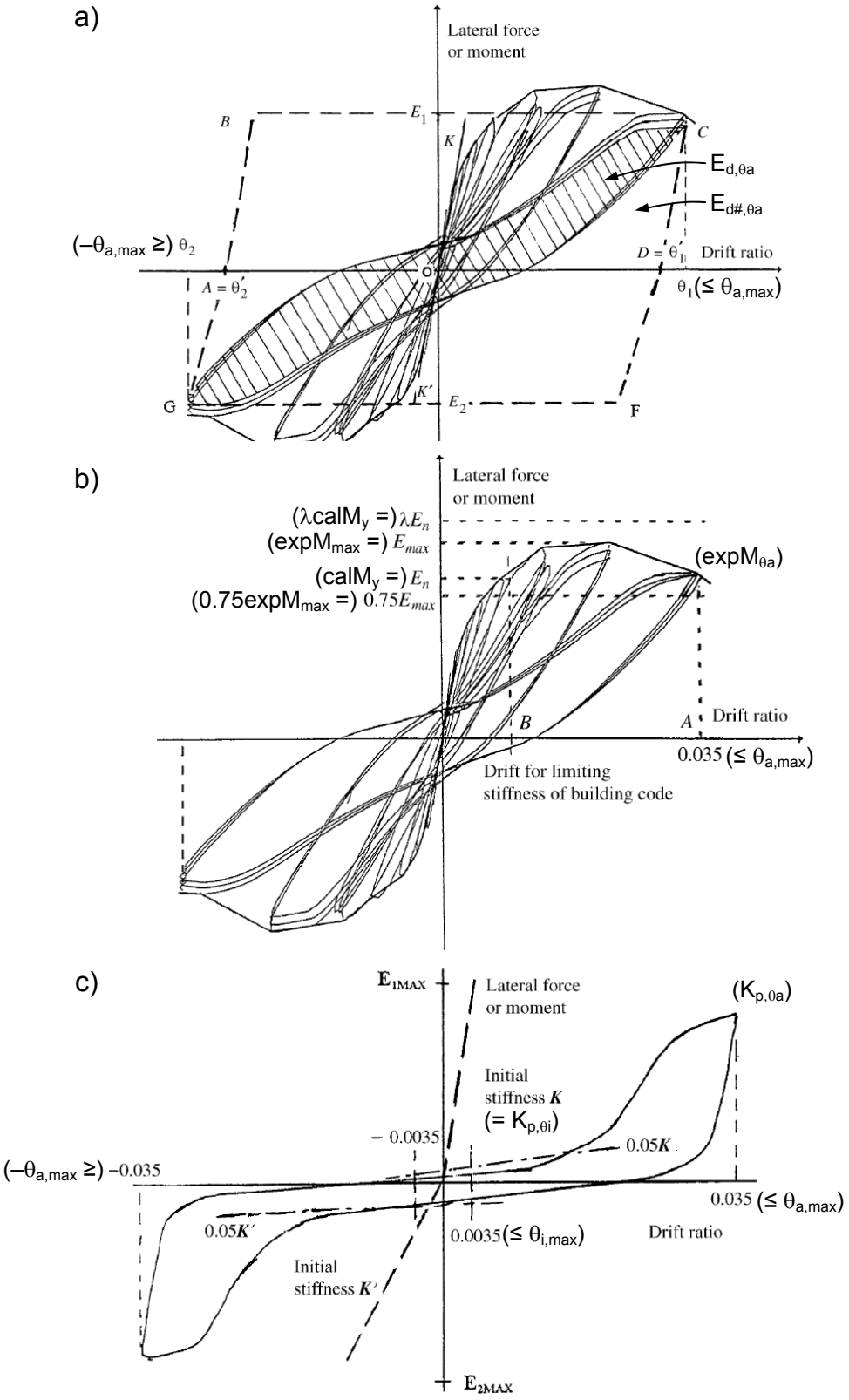


Figure 6.36 Assessment according to criteria stipulated in *ACI 374.1 (2005)*: a) Relative energy dissipation ratio; b) Quantities used in evaluating acceptance criteria, c) Unacceptable hysteretic behaviour

Further details and comments can be found in *ACI 374.1 (2005)*. It is noted that the current US-American building code *IBC (2006)* does not include values for the allowable story displacement $\Delta_a$ and deflection amplification factors $C_d$. Instead, values for both parameters can be found in US-American code for design loads *ASCE 7 (2005)* (Table 12.2-1 and Table 12.12-1).

The nominal lateral resistance calM$_y$ is determined using specified values for geometric properties of the test members, yield strength of reinforcement, and compressive strength of concrete, as well as a strain compatibility analysis for flexural capacity, and a reduction factor of 1.0.

It is evident that the performance of sub-assemblages has to evaluated on a case by case basis: The allowable story displacement $\Delta_a$ depends on the structure type, number of stories, and occupancy type. Also the deflection amplification factor $C_d$ is subject to the structure type. Therefore, the following assumptions were made for the evaluation of the tested column-to-foundation connections:

- An allowable story drift $\theta_{a,max} = \Delta_a / h$ of 0.035 and a deflection amplification factor of 2.5 based on *ASCE 7 (2005)* for moment resisting frame systems detailed as an ordinary reinforced concrete moment frame according to *ACI 318 (2011)*. Assuming a strength reduction factor of 0.9, the limiting initial drift $\theta_{i,max}$ equals to $\theta_{a,max} / (\phi C_d) = 0.035 / (0.9 \cdot 2.5) = 0.015$.
- The overstrength factor is a product of material safety factor, material overstrength factor, and a factor taking into account an existing reinforcement cross section larger than calculative required. Neglecting the latter factor and assuming 1.3 for both, the material safety factor as well as the material overstrength factor, yields a total overstrength factor of $\lambda = 1.7$.
- Due to the lack of 3.5 % drift cycles, a drift of 4.0 % is considered as the acceptance drift $\theta_a$ which is conservative. The initial drift $\theta_i$ is 0.5 %.

The result of the evaluation of the cyclic tests is given in Table 6.4. Only the positive domain of the cyclic tests was evaluated because of the specimen symmetry. For later discussion, the assessment criteria were also applied on the monotonic tests if applicable. Almost all specimens with 240 mm short anchorage length failed to comply with the criteria according to *ACI 374.1 (2005)*, whereas all specimens with 420 mm long anchorage length complied – even if detailed with substandard anchorage lengths without hooks. More details of the evaluation are provided in Table D.3 of Appendix D: Column-to-Foundation Connection Test Data.

Table 6.4 Performance assessment of experimental tests based on acceptance criteria stipulated in *ACI 374.1 (2005)* and the strain hardening criterion

| Monotonic loading: mon Cyclic loading: cyc | Anchorage detailing | Starter bar layout | 1. | 2. | 3. | | | ACI 374.1 compliant?[6] | Strain hardening?[7] |
|---|---|---|---|---|---|---|---|---|---|
| | | | Initial strength[1] | Over-strength[2] | Ductiility[3] | Damping[4] | Stiffness[5] | | |
| exp1mon | Cast-in-place | 4 bars | O | O | O | NA | NA | YES | YES |
| exp1cyc | w/ hook | per face | O | O | X | O | X | NO | NO |
| exp2mon | Cast-in-place | 4 bars | O | O | X | NA | NA | NO | NO |
| exp2cyc | w/o hook | per face | O | O | X | O | X | NO | NO |
| exp3mon | Post-installed | 4 bars | O | O | O | NA | NA | YES | YES |
| exp3cyc | w/o hook | per face | O | O | X | O | X | NO | NO |
| exp4mon | Post-installed | 2 bars | X | O | X | NA | NA | NO | NO |
| exp4cyc | w/o hook | per face | X | O | X | X | X | NO | NO |
| exp5mon | Cast-in-place | 2 bars | O | O | O | NA | NA | YES | YES |
| exp5cyc | w/ hook | per face | O | O | O | O | O | YES | YES |
| exp6mon | Cast-in-place | 2 bars | O | O | O | NA | NA | YES | NO |
| exp6cyc | w/o hook | per face | O | O | O | O | O | YES | NO |
| exp7mon | Post-installed | 2 bars | O | O | O | NA | NA | YES | NO |
| exp7cyc | w/o hook | per face | O | O | O | O | O | YES | NO |
| exp8mon | Post-installed | 2 bars | O | O | O | NA | NA | YES | YES |
| exp8cyc | w/o hook | per face | O | O | O | O | O | YES | YES |

[1] Acceptance criterion: $expM_{max} / calM_y > 1.00$

[2] Acceptance criterion: $expM_{max} / \lambda\ calM_y < 1.00$

[3] Acceptance criterion: $expM_{\theta a} / expM_{max} > 0.75$

[4] Acceptance criterion: $E_{d,\theta a} / E_{d\#,\theta a} > 0.125$

[5] Acceptance criterion: $K_{p,\theta a} / K_{p,\theta i} > 0.05$

[1) – 5)] Indication of compliance with acceptance criterion by 'O', indication of non-compliance by 'X'

[6] 'YES' if compliance with all acceptance criteria of ACI 374.1, else 'NO'

[7] 'YES' if strain hardening criterion is met, else 'NO'

In addition, the performance of the connection was assessed in regard of strain hardening. The performance of anchorages can be deemed to be adequate if the anchored starter bar develops pronounced strain hardening, irrespective whether detailed with or without hook. Therefore, a strain hardening criterion is proposed to

evaluate the seismic performance which compliance is much easier verified: The connection complies with the strain hardening criterion and therefore provides adequate performance if the anchored starter bars of the connection yield and do not fail by pullout or concrete breakout until the drift for which acceptance is sought, but not less than a drift of 0.035.

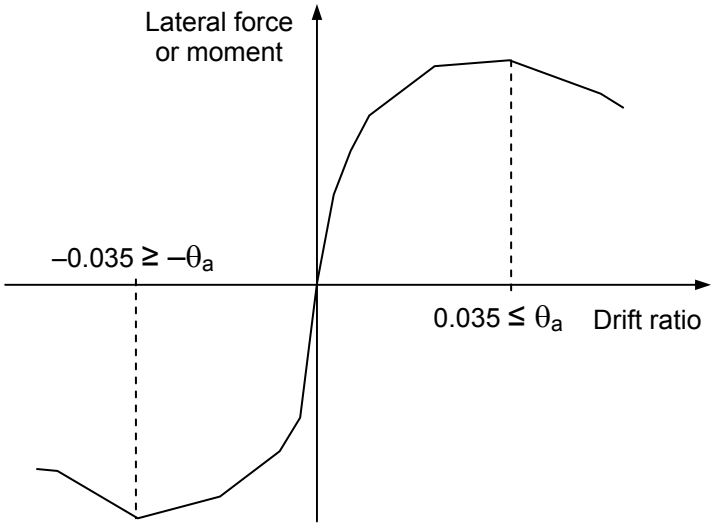


Figure 6.37 Assessment according to proposed strain hardening criterion

The results of the simplified assessment of the tested specimens according to the strain hardening criterion are also given in Table 6.4. Notably, the proposed criterion is more stringent for the experimentally tested specimens than the criteria according to *ACI 374.1 (2005)*.

## 6.5 Summary and Conclusions

Sixteen large scale tests conducted to study the behaviour of column-to-foundation connections with standard and substandard starter bar anchorages were presented in this chapter. The specimens were detailed with three different starter bar anchorage configurations, namely post-installed and cast-in-place anchorages with and without hooks. Three different column cross sections in terms of starter bar layouts and two different foundation dimensions were tested. One specimen of each type was tested to failure under monotonic loading, the other under cyclic loading. Load, drift, and cracking data were measured. These tests on column-to-foundation connections were the first ever focussing on the seismic performance of post-installed and cast-in-place substandard anchorages without hooks.

Significant influence of cyclic loading on connection capacities was observed for anchorages characterised by small ratios of anchorage lengths and reinforcing bar diameters. The influence is diminishing for larger anchorage lengths and is potentially overcast by scatter. In conclusion, the adverse effect of cyclic loading on

column-to-foundation connections capacities is rather small if compared to the beneficial effect of moment loading.

The general evaluation of stiffness degradation and energy dissipation provided an overview of the seismic performance and demonstrated that the anchorage length of the starter bar anchorages without hooks must provide sufficient lengths to achieve a similar behaviour as code conforming connections which are characterised by a more pronounced strain hardening.

Analyses of bond stress distributions along the anchorage length revealed that a significant and consistent influence of cyclic loading on bond stress redistributions towards the unloaded end is generally not significant. For anchorages characterised by very low $\ell_b$-$\phi$-ratios, however, the accelerated bond damage due to cyclic loading is relatively influential and more pronounced redistributions take place. This observation supports the general understanding of the bond behaviour of substandard anchorages.

The penetration of yielding was studied in detail and the similarities to the penetration of debonding were pointed out. Yielding and debonding penetrated ¼ to ½ of the anchorage length. It was shown that the provisions of the reinforced concrete design codes accounting for the penetration of yielding potentially overestimate the penetration for drift levels corresponding to the failure loads.

Detailed analyses of bearing and bond decomposition for anchorages detailed with hooks revealed that about half of the load is carried by the bearing of the hook and the other half by the bonding of the straight portion of the anchorage. No major differences between monotonic and cyclic loading were observed.

Analysing the load-drift curves according to the seismic assessment provisions of the *ACI 374.1 (2005)* allowed the standardised evaluation of the seismic performance. While connections with small anchorage lengths did not comply with the acceptance criteria, connections with large anchorage lengths were classified to have adequate seismic performance. This is a notable finding since pronounced strain hardening was observed only in two cases. Therefore, an alternative strain hardening criterion was proposed to assess the seismic performance of column-to-foundation connections. In general, assessments on the basis of the strain hardening criterion are more stringent but at the same time more meaningful and less tedious.

In conclusion, the tests allowed studying the failure mechanism and seismic performance of column-to-foundation connections which were detailed in eight different configurations. Evidence was given that substandard connections may allow the development of the full flexural column capacity despite their low calculated design utilisation ratio. Further tests are required to establish a sufficient large data base allowing the development of a sound design concept for column-to-foundation

connections. For this reason, numerical tests are presented in the following chapter which were benchmarked by the experimental test results.

# 7 Numerical Studies on Column-to-Foundation Connections

In this chapter, the numerical studies conducted on column-to-foundation connections are presented. The aim was to study the behaviour of connections under monotonic and cyclic loading in detail. Furthermore, the numerical studies allowed extending the parametric range. First, the modelling and analysing of anchorages employing bond elements is introduced in Section 7.1. The model is presented in Section 7.2, followed by the introduction of the simulation procedure in Section 7.3. Test results are discussed and the model validated in Section 7.4. Summarising and concluding remarks are given in Section 7.6. Reference is made to *Mahrenholtz, C. (2012b)* where further details of the complete numerical test program can be found.

## 7.1 Basics

The bond stress distribution which develops during numerical testing is determined by means of simulated elemental strains. For each bar element, the averaged bond stress is calculated according to Equation 2.2. The sequence of elemental bond stresses allows approximating the bond stress distribution along the anchorage (Figure 7.1).

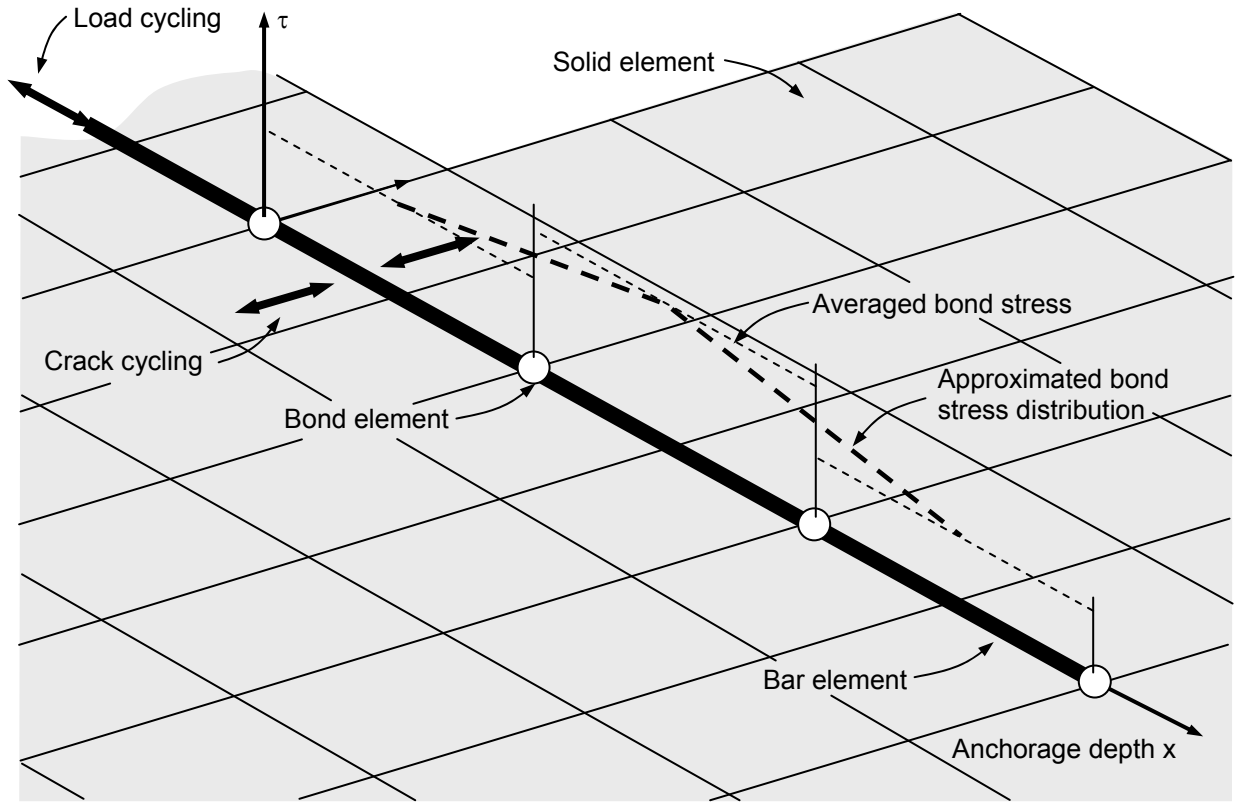


Figure 7.1 Schematic illustration of the numerical determination of the bond stress distribution along anchorage

The general background of the finite element program used, MASA is introduced in Section 5.1.1 and the pre- and post-processing program FEMAP in Section 5.1.2.

### 7.1.1 Calculating crack widths

When applying the smeared crack method (Section 5.2.1.2), cracking is expressed by the concrete simulating solid elements, in which strains exceed the concrete tensile strength. The crack width is determined on the basis of the calculated concrete strains $\varepsilon_c$.

The strain in the crack plane of the numerical bond tests were directly controlled by displacement vectors applied to the concrete (Section 5.2.2). Therefore, the crack width equalled the magnitude of the displacement vectors. In contrast, the numerical tests on the column-to-foundation connections required the strain values of the solid elements of the smeared crack to be extracted from the output data. The strains of these solid elements of the size $\ell_{element}$ correspond to crack widths of $w = \varepsilon_c \cdot \ell_{element}$. The cack widths given in Section 7.4.1 were derived by averaging the strains of two

elements adjoining the bar elements below the interface of column and foundation (Figure 7.2).

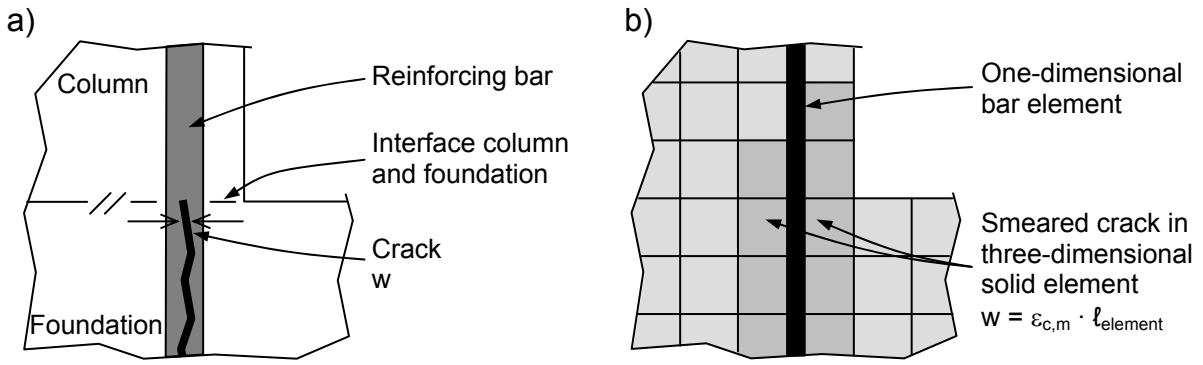


Figure 7.2 Determination of crack width: a) Experimental test; b) Numerical test

The maximum contour level of graphical outputs of finite element analyses is typically scaled to represent a defined maximum crack width $w_{max}$, i.e. $\varepsilon_c = w_{max} / \ell_{element}$.

## 7.2 Numerical Setup

### 7.2.1 Model

Figure 7.3 shows an example of a numerical model which renders the shape and dimensions of the experimental test specimen one-to-one. Utilising the symmetry, only one half of the specimen was modelled to speed up processing. Concrete and reinforcing bars were modelled by elements in a 30 mm by 30 mm grid to balance sufficiently accurate results against reasonable computation times. The bar elements (Section 5.1.1.1) modelling the column starter bars were linked with bond elements (Section 5.1.1.2) to the adjacent solid elements modelling the concrete (Section 5.1.1.3). All other reinforcing bars beside the starter bars were modelled by connecting bar elements and solid elements rigidly to save computational capacity. To reduce the work load of the computation further, the stirrups provided in the foundation and the upper part of the column were neglected since these do not have a significant influence on the result. Some zones of the concrete were assigned linear-elastic properties which additionally accelerates the computation. The largest model contained 28,870 elements with 32,425 nodes.

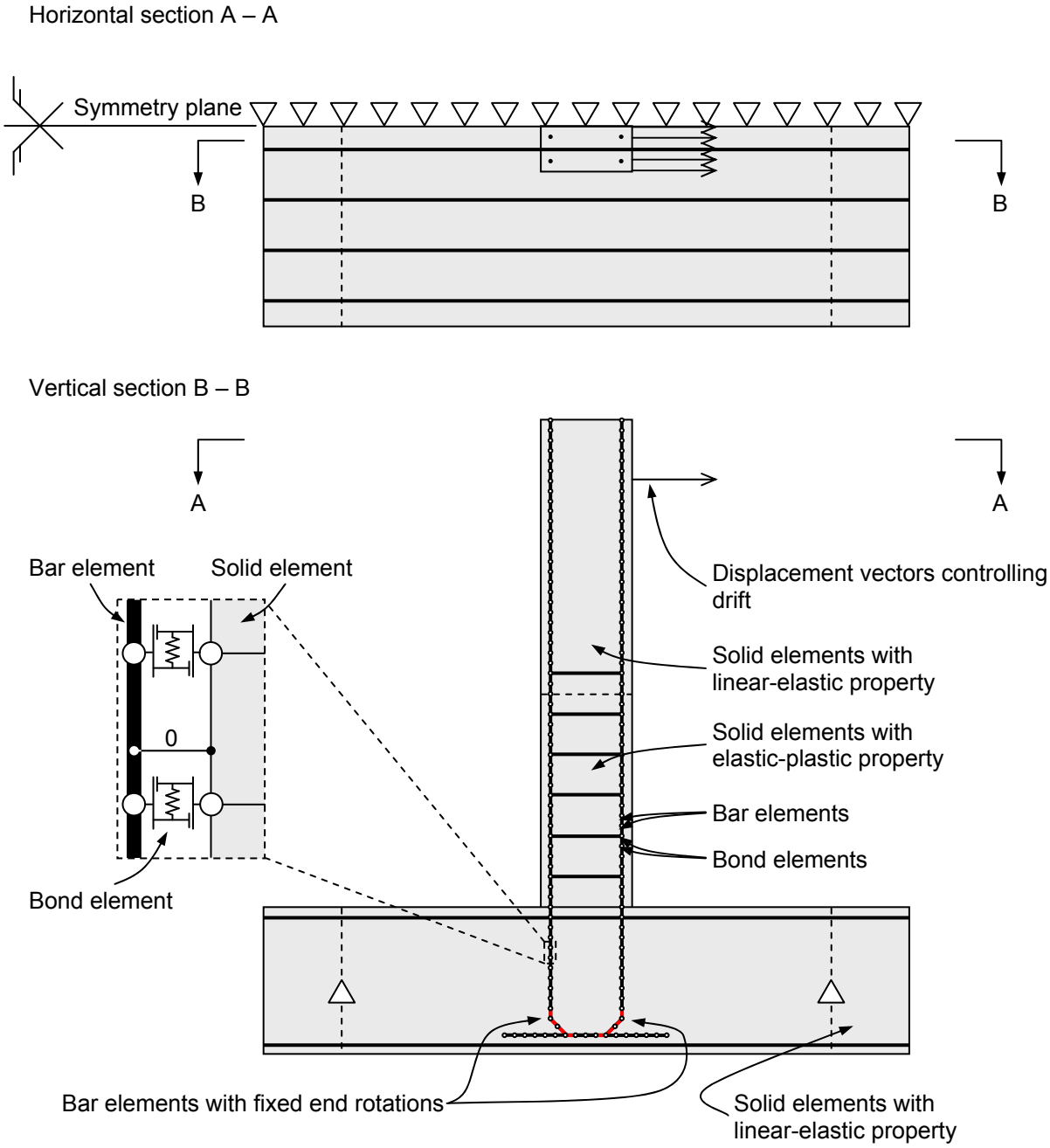


Figure 7.3 Finite element model

As discussed in Section 5.1.1.1, the finite element code MASA generally requires modelling the reinforcement by truss elements or bar elements with fixed end rotations because the element library does not include fully fledged bar elements. Pre-studies have shown that the quality of the simulation is not improved if the reinforcing bars are modelled using bar elements with tuned stiffness at the column-foundation interface (*Mahrenholtz, C. (2012a)*). Therefore, truss elements were generally employed to model the reinforcing bars. Consequently, the shear force at the column-foundation interface can be transferred across concrete in

compression only. An exception was the bend of the anchorages with hooks for which the hinging effect of the truss elements cannot be ignored. Therefore, the elements creating the bend of the hooks were designed with fixed end rotation bar elements.

The material parameters, in particular of concrete, tend to exhibit large scatter. Furthermore, the determination of fracture energies by means of material testing is very elaborate and the estimation of concete tensile strengths on the basis of concrete splitting tests often leads to questionable results. In addition, the properties derived from tests on concrete test samples describe the properties of the small concrete test cube which is inevitably different from the properties of the large concrete test specimen due to the differences in casting and curing. However, the aim of the numerical studies presented in this study was to develop a reasonably accurate finite element models based on standard material property values but not to tune the material property values for each finite element model individually for a best fit of experimentally and numerically tested load-drift curves. Therefore, the approach described in the following sections was made.

#### 7.2.1.1 Reinforcing bars

The material tests on the reinforcing bar samples yielded very similar results for all reinforcing bar diameters (*Mahrenholtz, C. (2012a)*). Therefore, the same parameter values were used for all reinforcing bar diameters to define the properties in MASA which are given in Table 7.1. The steel stress-strain model is visualised in Figure 5.1.

Table 7.1 Key material parameters for reinforcing bars

| Diameter [mm] | Yield strength $f_y$ [MPa] | Tensile strength $f_u$ [MPa] | Modulus of elasticity $E_s$ [N/mm²] |
|---|---|---|---|
| 16<br>25<br>32 | 535 | 650 | 200,000 |

#### 7.2.1.2 Concrete

The key parameters defining concrete properties in MASA are the compressive strength $f_c$, the tensile strength $f_{ct}$, the modulus of elasticity $E_c$, and the fracture energy $G_f$. Since the foundation and column of the experimentally tested subassemblages were designed with a concrete quality equalling class C20/25 and C50/60 according to *Eurocode 2 (2005)*, the mean compressive strength $f_{cm}$ specified in *Eurocode 2 (2005)* for concrete class C20/25 and C50/60 was taken for the

simulation. The same parameters values were used as for the simulation of the bond tests (Section 5.2.1) and are given in Table 7.2. The experimentally tested compressive strengths $f_c$ are given in Table D.1 of Appendix D: Column-to-Foundation Connection Test Data.

Table 7.2 Key material parameters for concrete

| Concrete grade | Compress. strength $f_c$ [MPa] | Tensile strength $f_{ct}$ [MPa] | Modulus of elasticity $E_c$ [N/mm²] | Fracture energy $G_f$ [N/mm] |
|---|---|---|---|---|
| C20/25 | 28 | 2.2 | 30,000 | 0.08 |
| C50/60 | 58 | 4.1 | 37,000 | 0.14 |

#### 7.2.1.3 Bond

The parameters required to define the bond characteristic in MASA are explained in Section 5.1.1.3. The bond strength $\tau_1$ and its corresponding slip $s_1$ as well as the slip plateau $s_2 – s_2$ are the key parameters (Table 7.3). The slip values were specified according to *Lettow, S. (2007)* and are the same as for the simulations of the bond tests (Section 5.2.1). The bond strength $\tau_1$ was defined for all bar diameters on the basis of the experimentally tested bond strengths $\tau_u$ (Section 6.2.1.3) which were approximately 14 N/mm² for cast-in-place reinforcing bars. The experimentally tested bond strengths $\tau_u$ for post-installed reinforcing bars were approximately 35 N/mm². It is noted that the tested cast-in-place and post-installed reinforcing bars were furnished with a debonded pre-length to eliminate the effect of confinement generated by the confined setup. The tested bond strengths are given in Table D.1 of Appendix D: Column-to-Foundation Connection Test Data.

Table 7.3 also provides the values taken for the simulation of concrete reinforcement in high strength concrete. Due to the absence of relevant bond tests, the bond strength $\tau_1$ for C50/60 concrete was based on the bond strength $\tau_1$ for C20/25 concrete multiplied by $(f_{ck,C50/60} / f_{ck,C20/25})^{0.5}$ which is a common approach (Section 2.2.6). In general, the influence of the concrete strength on the bond strength of post-installed reinforcing bars is small or even insignificant (Section 2.2.5). Therefore, the simplification to use identical bond material parameters for post-installed reinforcing bars irrespective of the concrete grade in which the bars are installed is justified.

Table 7.3 Key material parameters for bond

| Concrete grade | Installation method | Bond strength $\tau_1 = \tau_m + \tau_f$ [MPa] | Slip begin. plateau $s_1$ [mm] | Slip plateau $s_2 - s_1$ [mm] |
|---|---|---|---|---|
| C20/25 | cast-in-place | 14 | 0.9 | 0.8 |
| C50/60 | cast-in-place | 20 | 0.9 | 0.8 |
| C20/25 | post-installed | 35 | 0.9 | 0.8 |
| C50/60 | post-installed | 35 | 0.9 | 0.8 |

The model of Specimen 2 was generated without and with bond elements as an example demonstrating the necessity of bond elements for bond critical zones, i.e. the anchorage of the starter bar. Figure 7.4 illustrates the difference of the numerical results for both models. The monotonic tests are indicated in grey and the cyclic tests in black. Without bond elements, the strength of the column-to-foundation connection is overestimated.

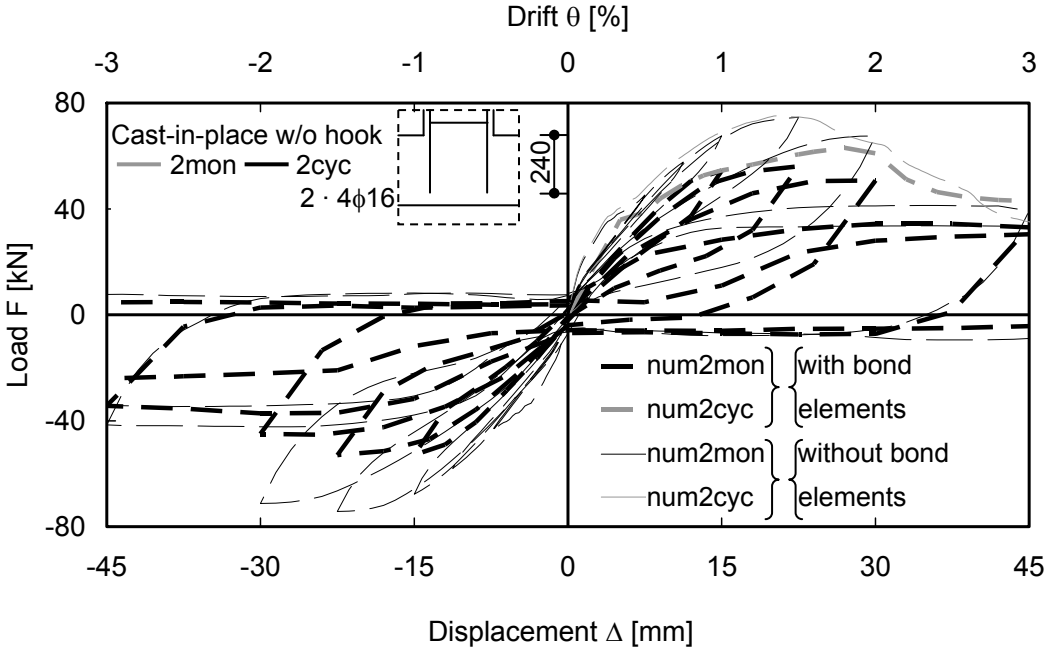


Figure 7.4 Influence of modelling with and without bond elements (example: Specimen 2, 2 · 4ϕ16, $\ell_b$ = 240 mm)

The capacities as a result of the numerical tests on column-to-foundation connections modelled without and with bond elements are compared in Table 7.4. Also for information, the experimentally tested column-to-foundation connection capacities for monotonic and cyclic loading are given. It is evident that the bond of the starter bars cannot be simplified by rigid connections between bar and concrete.

In particular connections with short starter bar anchorages solely relying on bond require the employment of bond elements to achieve realistic results.

Table 7.4 Comparison of connection capacities according to numerical and experimental tests without and with bond elements (example: Specimen 2, 2 · 4ϕ16, $\ell_b$ = 240 mm)

| Load protocol | $numF_{max}$ *starter bars without bond elements* [kN] | $numF_{max}$ *starter bars with bond elements* [kN] | $expF_{max}$ [kN] |
|---|---|---|---|
| Monotonic | 75.2 | 63.7 | 50.8 |
| Cyclic | 74.6 | 56.1 | 56.7 |

Furthermore, different tuning parameters for the hysteretic energy model implemented in the bond elements of Specimen 2 were used in order to demonstrate their influence on the load-drift behaviour of the column-to-foundation connection for an example. Figure 7.5 shows the numerical results for two different tuning parameter sets. The monotonic tests are indicated in grey and the cyclic tests in black. Using the tuning parameters $a_1$ = 1.2, $a_2$ = 1.1, $a_{1f}$ = 1.2 and $a_{2f}$ = 0.67 (*Eligehausen, R.; Popov, E. et al. (1983)*) underestimates the degradation of strength if compared to the tuning parameters $a_1 = a_{1f}$ = 2.5 and $a_2 = a_{2f}$ = 1.0 proposed in Section 4.4.2.

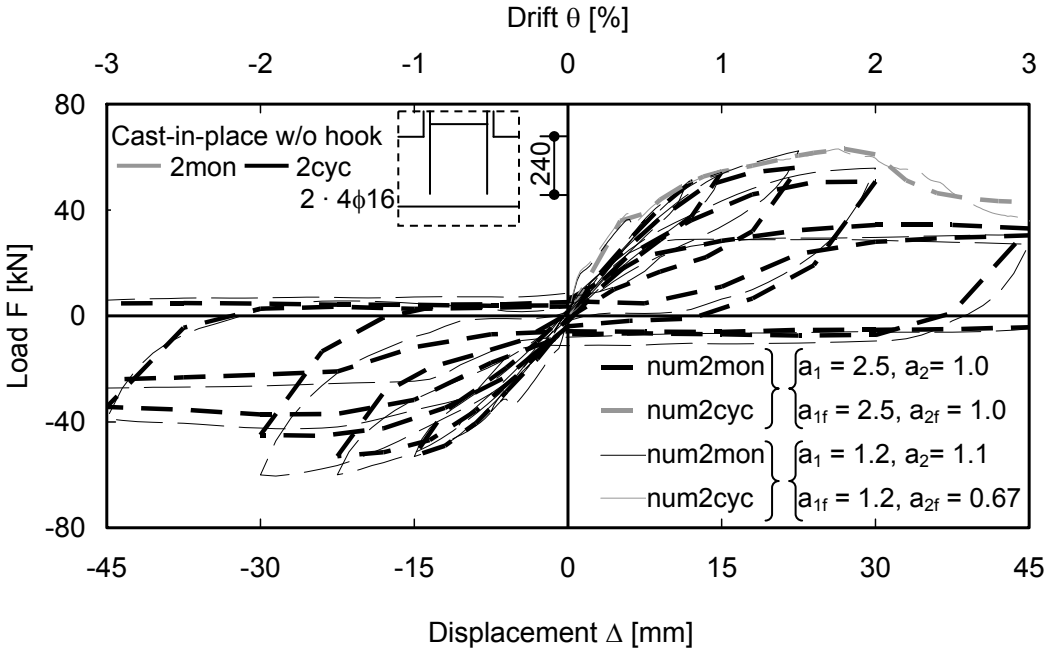


Figure 7.5 Influence of modelling with different tuning parameters (example: Specimen 2, 2 · 4ϕ16, $\ell_b$ = 240 mm)

The numerically tested connection capacities taking into account different tuning parameters are compared in Table 7.5. Also for information, the experimentally tested column-to-foundation connection capacities for monotonic and cyclic loading are given. In conclusion, using the tuning parameters $a_1 = a_{1f} = 2.5$ and $a_2 = a_{2f} = 1.0$ proposed in Section 4.4.2 lead to more realistic results. Reference is made to Section 4.4.2 where a possible explanation is discussed.

Table 7.5 Comparison of connection capacities according to numerical and experimental tests with different tuning parameters sets (example: Specimen 2, $2 \cdot 4\phi16$, $\ell_b$ = 240 mm)

| Load protocol | $numF_{max}$ $a_1 = a_{1f} = 1.2$ $a_2 = 1.1$, $a_{2f} = 0.67$ [kN] | $numF_{max}$ $a_1 = a_{1f} = 2.5$ $a_2 = a_{2f} = 1.0$ [kN] | $expF_{max}$ [kN] |
|---|---|---|---|
| Monotonic | 63.1 | 63.7 | 50.8 |
| Cyclic | 62.5 | 56.1 | 56.7 |

### 7.2.2 Boundary and loading conditions

The boundary and loading conditions of the model, shown in Figure 7.3, were designed analogous to the experimental tests (Chapter 6): Line bearings at both ends of the foundation counteracted the loads. Displacement vectors loaded the column 1500 mm above the top of foundation to control the drift.

## 7.3 Numerical Procedure

### 7.3.1 Load protocol

In principal, the numerical tests were carried out corresponding to the experimental tests. To reduce the required number of load steps to be calculated, the applied displacement increments were increased compared to those used in the experiments. The displacement increment for the lower drift levels was 0.3 mm (0.02 % drift) and was increased stepwise to 3.0 mm (0.2 % drift) for the last drift level.

The secant stiffness method (SSM) is generally preferred for the analyses because the stiffness matrix is permanently updated in the course of computation and therefore allows a higher accuracy of the simulation. However, trial runs showed that for the complex model and load protocol the SSM results in extreme computation times which were increased by the order of 10 or more compared to the constant stiffness method (CSM). Because the computation time already accounts for about 9 days for the CSM (Resource: Quadcore, 2.66 GHz CPU, 8 GB RAM, 64-bit OS, MASA kernel 25.01.2011), the unfavourably long computation times did not allow

using the SSM. However, the tests using the CSM yielded sufficiently accurate results as will be shown in the following sections.

### 7.3.2 Test program

The part of the numerical test program which is discussed in the following in detail was identical to the test program of the experimental tests. Each model was run twice to carry out one monotonic (mon) and one cyclic (cyc) type of loading. Table 7.6 comprises the numerical test program. The table also provides the anchorage lengths $\ell_{b,rqd}$ required according to *Eurocode 2 (2005)*. The remarks given in Section 6.3.2 apply.

Table 7.6 Numerical test program of tests on cast-in-place post-installed column-to-foundation connections

| Cast-in-place and Post-installed | Anchorage detailing | Starter bar layout | $\phi$ [1] $\ell_b$ [2] [mm] | $\alpha_1$ [3] $\alpha_2$ [4] [-] | $\ell_{b,rqd}$ [5] $\ell_b$ / $\ell_{b,rqd}$ [mm] |
|---|---|---|---|---|---|
| num1mon | Cast-in-place | 4 bars | 16 | 0.7 | 560 |
| num1cyc | w/ hook | per face | 240 | 1.0 | 0.43 |
| num2mon | Cast-in-place | 4 bars | 16 | 1.0 | 701 |
| num2cyc | w/o hook | per face | 240 | 0.9 | 0.34 |
| num3mon | Post-installed | 4 bars | 16 | 1.0 | 701 |
| num3cyc | w/o hook | per face | 240 | 0.9 | 0.34 |
| num4mon | Post-installed | 2 bars | 25 | 1.0 | 876 |
| num4cyc | w/o hook | per face | 240 | 0.7 | 0.27 |
| num5mon | Cast-in-place | 2 bars | 32 | 0.7 | 1121 |
| num5cyc | w/ hook | per face | 420 | 1.0 | 0.38 |
| num6mon | Cast-in-place | 2 bars | 32 | 1.0 | 1181 |
| num6cyc | w/o hook | per face | 420 | 0.7 | 0.36 |
| num7mon | Post-installed | 2 bars | 32 | 1.0 | 1181 |
| num7cyc | w/o hook | per face | 420 | 0.7 | 0.36 |
| num8mon | Post-installed | 2 bars | 25 | 1.0 | 876 |
| num8cyc | w/o hook | per face | 420 | 0.7 | 0.27 |

[1] Starter bar diameter

[2] Anchorage length

[3] $\alpha_1 = 1.0$ [$\alpha_1 = 0.7$] for anchorages without [with] hooks

[4] $\alpha_2 = 1 - 0.15\ ((a / 2) - \phi) / \phi$ [$\alpha_2 = 1 - 0.15\ ((a / 2 - 3\phi) / \phi$] for anchorages without [with] hooks

[5] $\ell_{b,rqd} = \phi f_{yd} / (4 f_{bd})$; $f_{yd}$, $f_{bd}$ see Table D.5 of Appendix D: Column-to-Foundation Connection Test Data

Notes: Half of the clear spacing between adjacent bars a / 2 is for anchorages of column-to-foundation connections generally smaller than the concrete covers c and $c_1$

## 7.4 Results and Discussion

### 7.4.1 General behaviour

Figure 7.6 shows the concrete strains as an example for the visualisation of the simulation results.

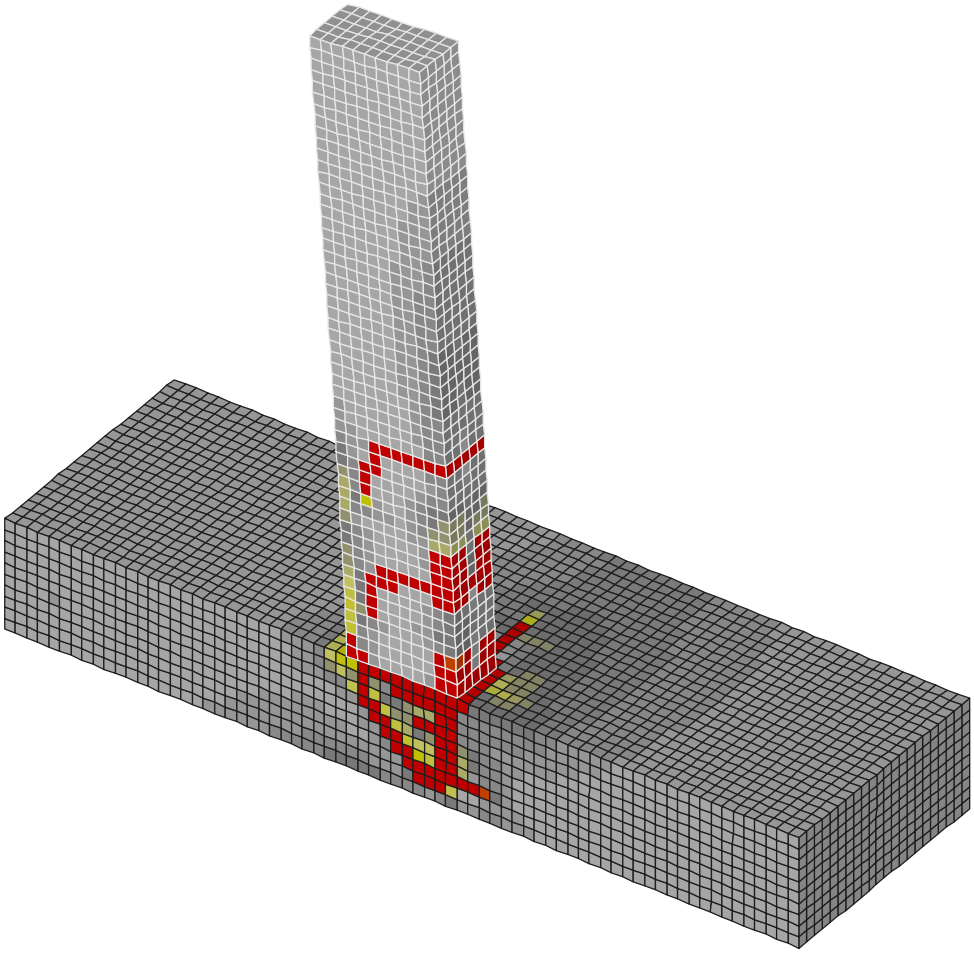

Figure 7.6 Example for graphical output of a numerical test

Figure 7.7 provides an overview of the monotonic and cyclic load-drift curves. For the sake of readability, only the first cycle of each drift level is shown. The dashed curves stand for the numerical tests and the solid curves for the experimental tests. The monotonic tests are indicated in grey and the cyclic tests in black. Figure 7.8 illustrates the observed crack patterns of the numerical tests for the drift level corresponding to the failure load which was defined according to Figure 6.17.

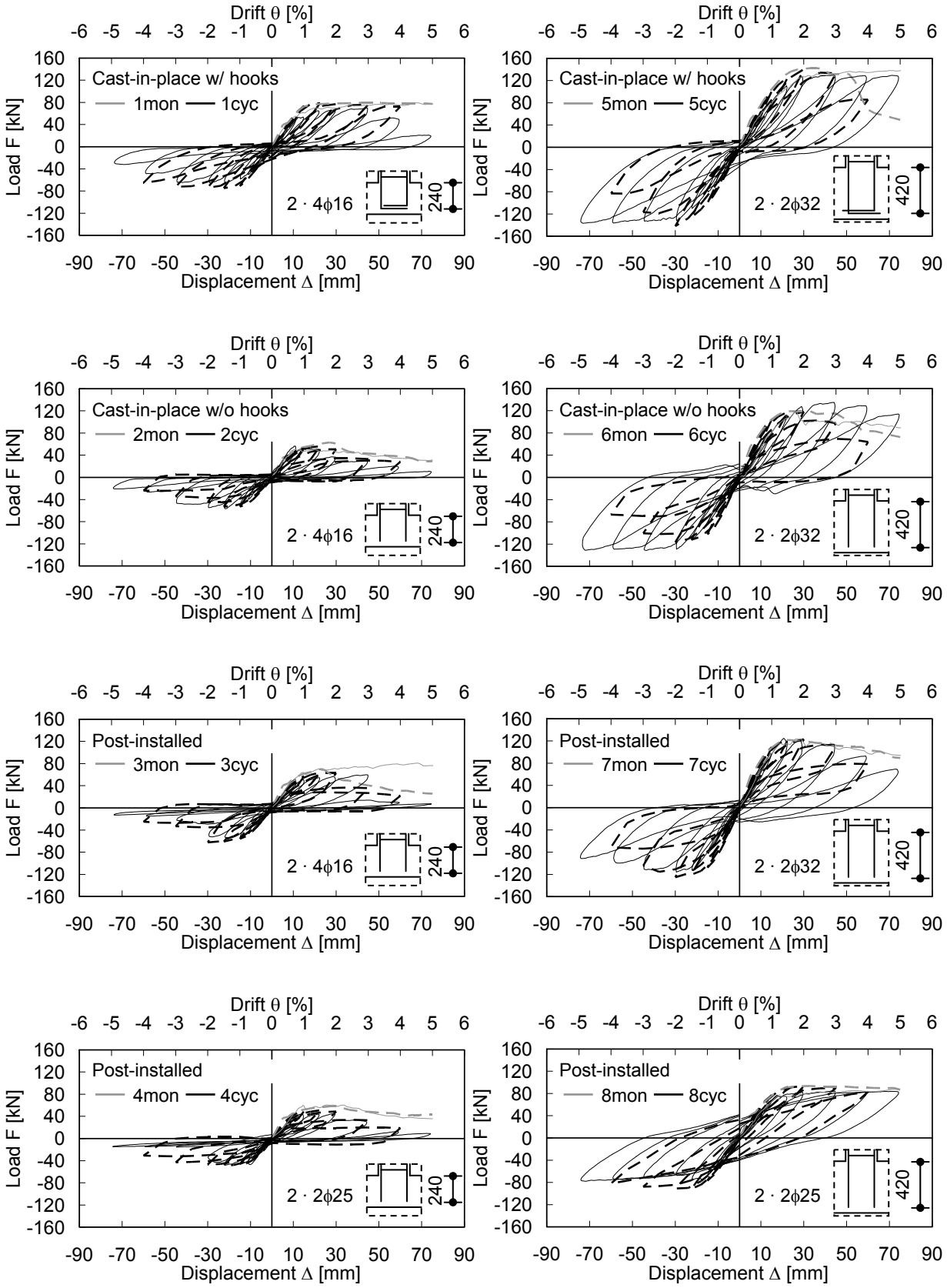


Figure 7.7 Overview of monotonic and cyclic load-drift curves of numerical tests

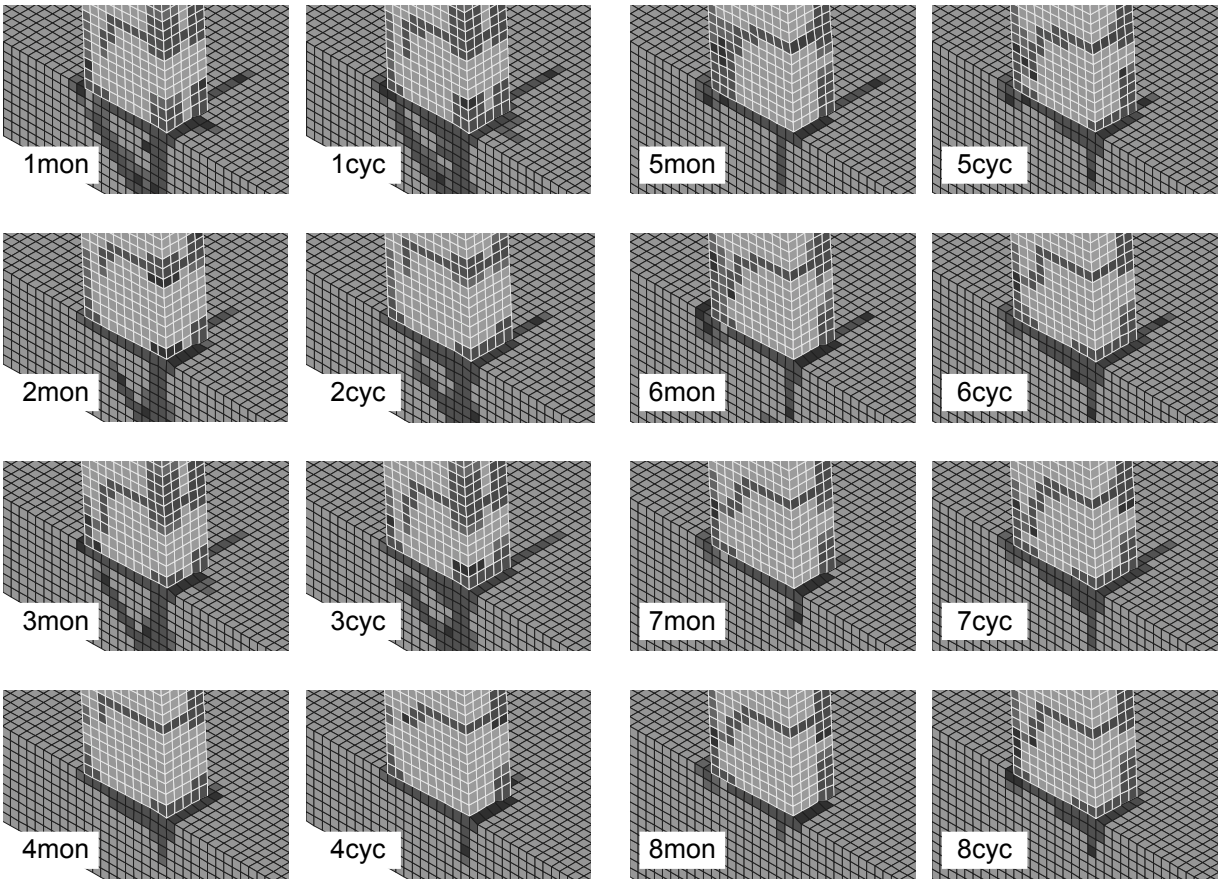


Figure 7.8 Observed crack patterns of numerical tests at failure load

Further details including concrete stress and strain plots can be found in Appendix D: Column-to-Foundation Connection Test Data.

In summary, the hysteretic load-drift behaviour of the column-to-foundation connections was realistically simulated. The curves confirm the observation made for experimental tests that cyclic loading mainly affects the post-failure behaviour whereas the pre-failure domain is only affected for very small ratios of anchorage length and diameter, i.e. Specimen 4. The load-drift curves of Specimen 8 show a perfect match of numerical and experimental test results. This is typical for the simulation of reinforced concrete elements for which failure is predominantly driven by yielding. Concrete damage effects such as cracks and concrete breakout, as well as bond damage effects causing exsessive slip and pullout, are considerably more difficult to simulate.

Table 7.7 provides the tested maximum loads, the failure modes, failure loads as well as corresponding drifts and crack widths. The pinpointing of failure mode and determination of failure load were made in accordance with Section 6.4.1. The crack

width was calculated as discussed in Section 7.1.1. Benchmarking for the validation of the model is conducted in Section 7.4.2

Table 7.7 Maximum loads, failure modes, failure loads as well as corresponding drifts and crack widths numerically tested

| Specimen ID | Maximum load[1] $numF_{max}$ [kN] | Failure mode[2] | Failure load[3] $numF_R$ [kN] | Drift[4] $\theta_R$ [%] | Crack width[5] $w_R$ [mm] |
|---|---|---|---|---|---|
| num1mon | 79.6 | Y | 73.5 | 1.5 | 0.3 |
| num1cyc | 78.7 | Y | 72.5 | 1.5 | 0.3 |
| num2mon | 63.8 | P/C | 63.8 | 1.5 | 0.7 |
| num2cyc | 56.1 | P/C | 56.1 | 1.5 | 0.7 |
| num3mon | 71.0 | P/C | 71.0 | 1.5 | 0.7 |
| num3cyc | 64.8 | P/C | 64.8 | 1.5 | 0.7 |
| num4mon | 58.6 | P/C | 58.6 | 1.5 | 1.0 |
| num4cyc | 50.9 | P/C | 50.9 | 1.5 | 0.8 |
| num5mon | 142.3 | Y | 132.5 | 2.0 | 0.4 |
| num5cyc | 142.2 | Y | 131.0 | 2.0 | 0.4 |
| num6mon | 119.5 | P/C | 119.5 | 2.0 | 0.5 |
| num6cyc | 118.0 | P/C | 118.0 | 2.0 | 0.5 |
| num7mon | 122.0 | P/C | 109.5 | 1.5 | 0.5 |
| num7cyc | 123.2 | P/C | 111.0 | 1.5 | 0.5 |
| num8mon | 93.4 | Y | 86.0 | 1.5 | 0.4 |
| num8cyc | 93.3 | Y | 86.0 | 1.5 | 0.4 |

[1] Maximum load measured during complete loading up to 5.0 % drift

[2] Y: Yielding failure; P/C: Pullout or concrete failure

[3] Failure load as defined in Figure 6.17

[4] Drift corresponding to failure load

[5] Crack width corresponding to failure load

The numerically determined capacities are compared to the calculative capacities in Chapter 8 and Chapter 9.

### 7.4.2 Validation

Load-drift curves of experimentally and numerically tested specimens were considered to validate the finite element model. Table 7.8 compares the experimentally and numerically tested maximum loads, their ratio and the experimentally and numerically tested failure modes.

Table 7.8 Experimentally and numerically tested maximum loads, their ratio and the failure modes

| Specimen ID | $expF_{max}$ [kN] | $numF_{max}$ [kN] | $expF_{max}$ / $numF_{max}$ [-] | Failure mode exp. tested | Failure mode num. tested |
|---|---|---|---|---|---|
| 1mon | 79.4 | 79.6 | 1.00 | Y | Y |
| 1cyc | 70.0 | 78.7 | 0.89 | Y | Y |
| 2mon | 50.8 | 63.8 | 0.80 | P/C | P/C |
| 2cyc | 56.7 | 56.1 | 1.01 | P/C | P/C |
| 3mon | 80.8 | 71.0 | 1.14 | Y | P/C |
| 3cyc | 59.6 | 64.8 | 0.92 | P/C | P/C |
| 4mon | 60.7 | 58.6 | 1.04 | P/C | P/C |
| 4cyc | 46.3 | 50.9 | 0.91 | P/C | P/C |
| 5mon | 137.9 | 142.3 | 0.97 | Y | Y |
| 5cyc | 129.6 | 142.2 | 0.91 | Y | Y |
| 6mon | 118.5 | 119.5 | 0.99 | Y | P/C |
| 6cyc | 135.1 | 118.0 | 1.14 | Y | P/C |
| 7mon | 124.0 | 122.0 | 1.02 | Y | P/C |
| 7cyc | 124.7 | 123.2 | 1.01 | Y | P/C |
| 8mon | 84.4 | 93.4 | 0.90 | Y | Y |
| 8cyc | 83.9 | 93.3 | 0.90 | Y | Y |

In the light of complexity and available resources, the agreement of the maximum loads numerically and experimentally tested is good. The variation can be partly ascribed to the inevitable scatter immanent to experimental tests on reinforced concrete elements which is particularly pronounced for connections failing in bond.

The failure modes were correctly predicted for the majority of the specimens with three exceptions. While the monotonic experimental test on Specimen 3 is considered to be an outlier, the design of Specimen 6 and 7 is putting the failure mode at the transition zone between failure mode P/C and mode Y: The starter bars of the experimental tests just reached the yield strength whereas the starter bars of the numerical tests just remained elastic. Generally, MASA predicts a more brittle behaviour which is also confirmed by the failure progress in the post-peak region of several specimens. The reason could be according to *Eligehausen, R.; Ožbolt, J. et al. (2006)* that the bars are modelled by truss elements, whereas in reality the bending stiffness of the bars contributes to a more ductile behaviour (*Randl, N. (2007)*, *Tanaka, Y.; Murakoshi, J. (2011)*).

The overall load-drift responses (Section 7.4.1) show a good agreement of the numerically and experimentally tested column-to-foundation connections, in particular

for pre-peak drifts. The post-peak strength degradation is reproduced as well as a more pronounced pinching behaviour for increasing drifts.

### 7.4.3 Detailed study of anchorage

#### 7.4.3.1 Tensile and bond stress in column starter bar

The distribution of tensile and bond stress is needed for the study of the progressive strain penetration and for the evaluation of the structural behaviour after exceedance of the connection capacity. The determination of the strains during the experimental tests turned out to be difficult in particular after substantial damage of the column-to-foundation connection core in terms of cracks and spalling concrete pieces (Section 6.3.1). Numerical tests help to mitigate this deficiency as shown in the following.

The post-processing program FEMAP (Section 5.1.2) provides beam diagrams allowing reading the analysed tensile stresses (Figure 7.9). Approximately constant tensile stresses indicate insignificant bond stresses and progressively decreasing tensile stress represent progressively incresasing bond stresses. The tensile stresses were readout for every drift level separately to calculate the corresponding the bond stresses according to the equations given in Section 2.2.1.

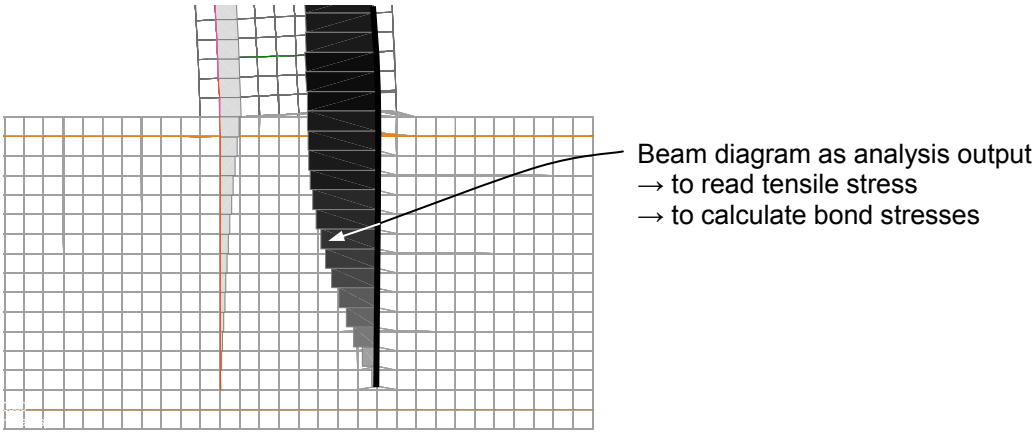


Figure 7.9 Example plot showing the steel tensile stresses in the column starter bar

The following diagrams (Figure 7.10 to Figure 7.17) show the distribution of tensile stresses and bond stresses which were numerically determined for the peak of the first cycle of the 0.75 % drift level, the drift level corresponding to the failure of the connection, and the drift level 4.0 %. Black and grey curves indicate tensile stresses and bond stresses, respectively.

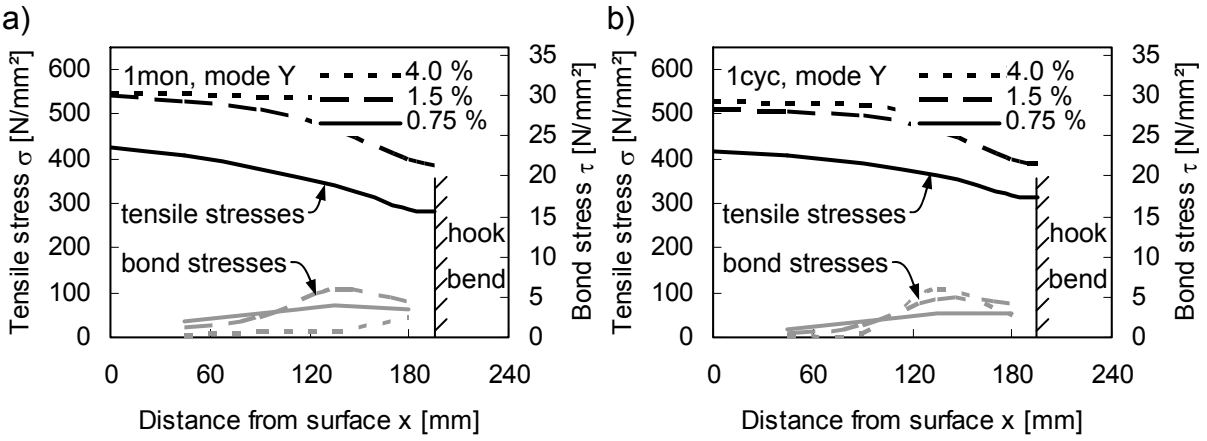


Figure 7.10 Reinforcing bar stress profiles along anchorage for a) monotonic and b) cyclic simulation of Specimen 1 – $\ell_b$ = 240 mm, 2 · 4$\phi$16, cast-in-place with hooks

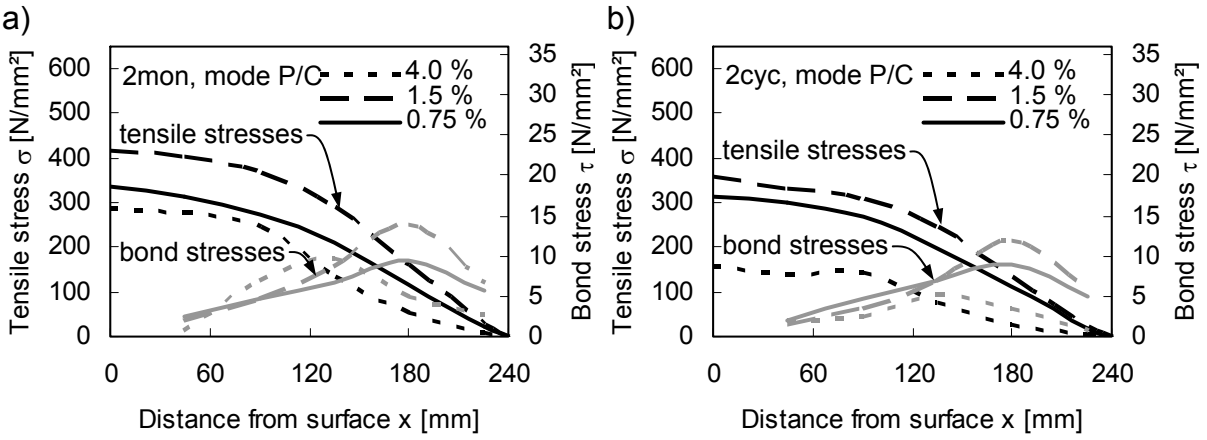


Figure 7.11 Reinforcing bar stress profiles along anchorage for a) monotonic and b) cyclic simulation of Specimen 2 – $\ell_b$ = 240 mm, 2 · 4$\phi$16, cast-in-place without hooks

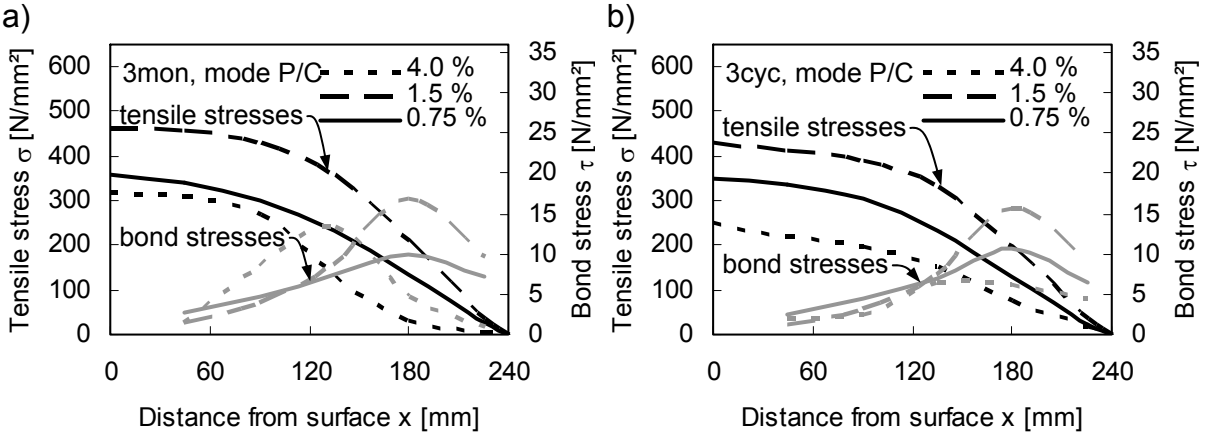


Figure 7.12 Reinforcing bar stress profiles along anchorage for a) monotonic and b) cyclic simulation of Specimen 3 – $\ell_b$ = 240 mm, 2 · 4$\phi$16, post-installed

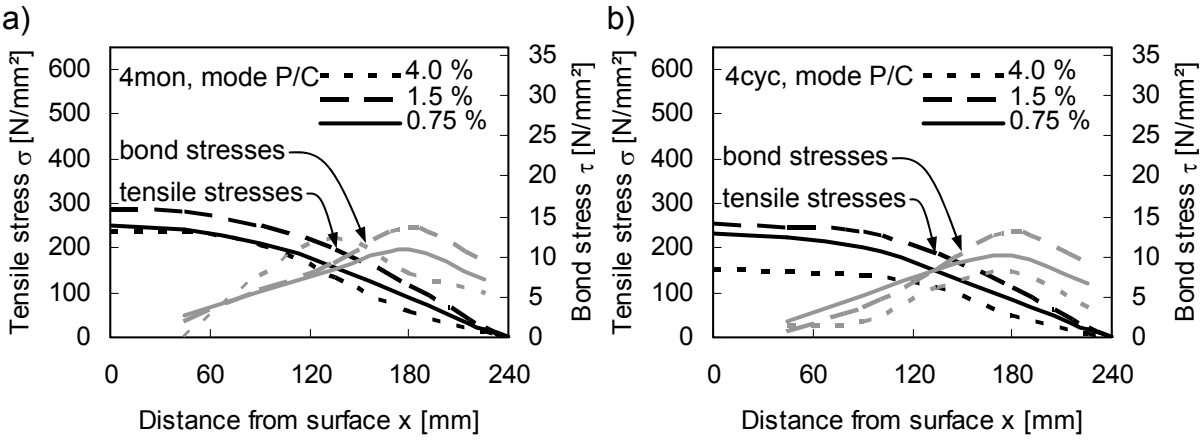


Figure 7.13 Reinforcing bar stress profiles along anchorage for a) monotonic and b) cyclic simulation of Specimen 4 – $\ell_b$ = 240 mm, 2 · 2$\phi$25, post-installed

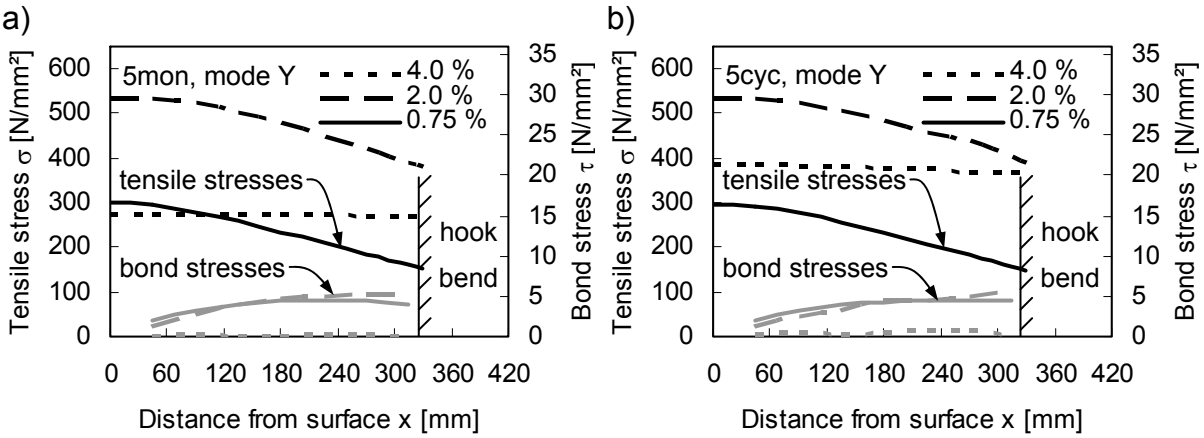


Figure 7.14 Reinforcing bar stress profiles along anchorage for a) monotonic and b) cyclic simulation of Specimen 5 – $\ell_b$ = 420 mm, 2 · 2$\phi$32, cast-in-place with hooks

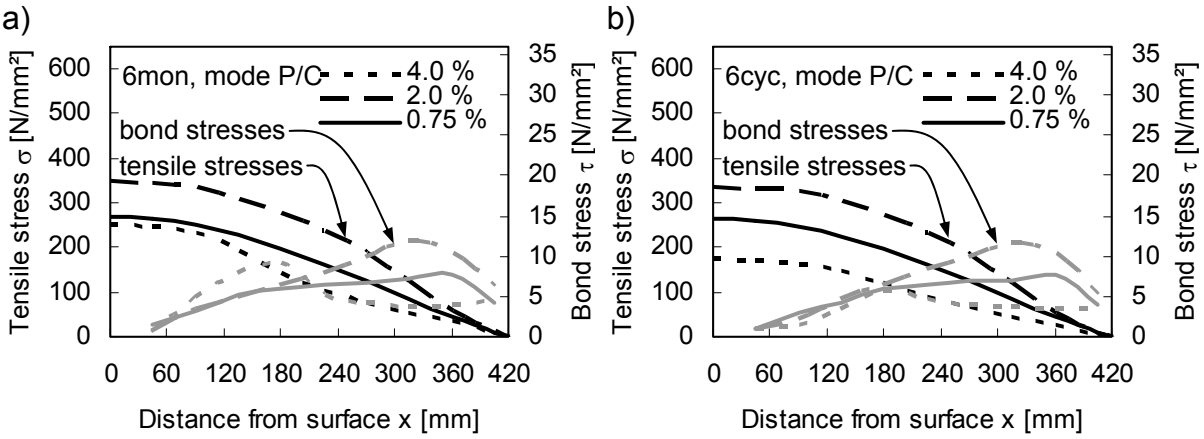


Figure 7.15 Reinforcing bar stress profiles along anchorage for a) monotonic and b) cyclic simulation of Specimen 6 – $\ell_b$ = 420 mm, 2 · 2$\phi$32, cast-in-place without hooks

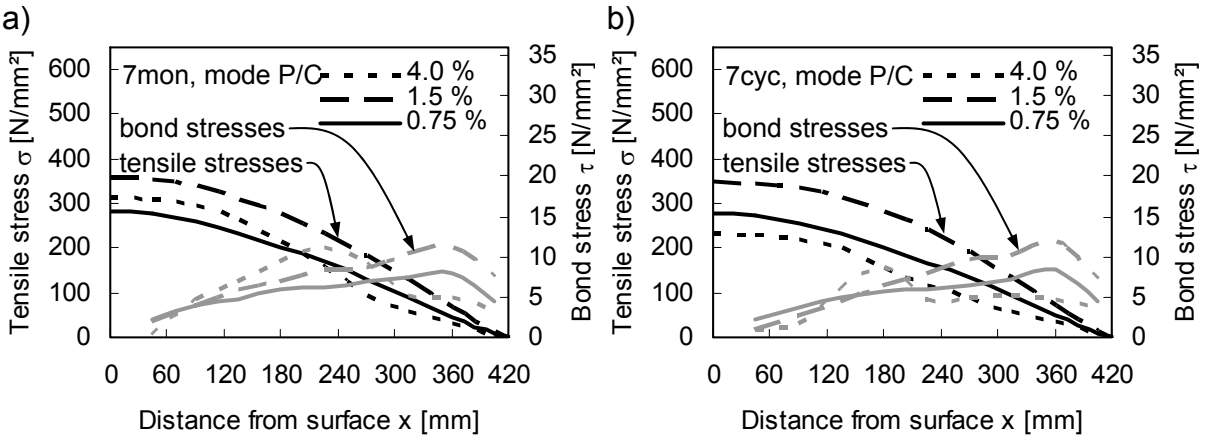


Figure 7.16 Reinforcing bar stress profiles along anchorage for a) monotonic and b) cyclic simulation of Specimen 7 – $\ell_b$ = 420 mm, 2 · 2$\phi$32, post-installed

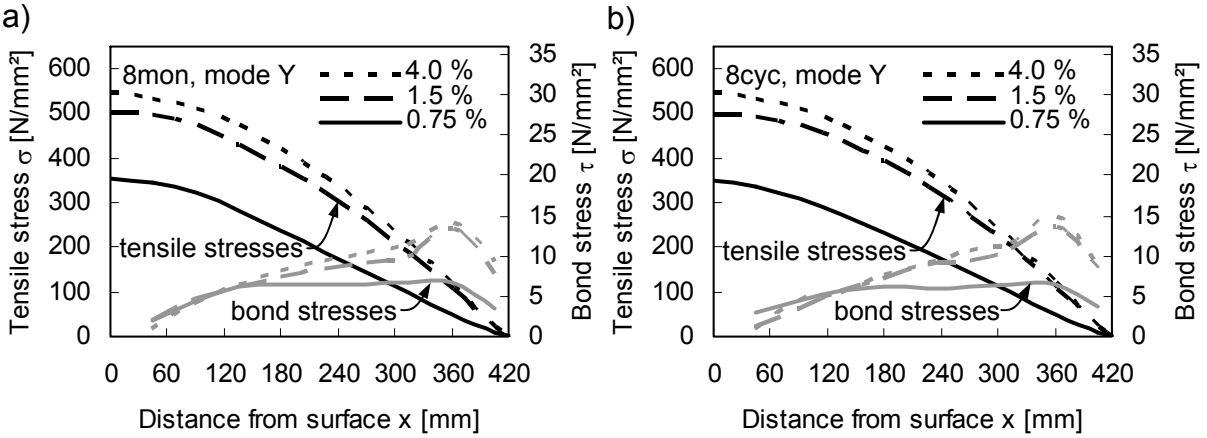


Figure 7.17 Reinforcing bar stress profiles along anchorage for a) monotonic and b) cyclic simulation of Specimen 8 – $\ell_b$ = 420 mm, 2 · 2$\phi$25, post-installed

The cast-in-place anchorages with hook, i.e. Specimen 1 and Specimen 5, allow the development of pronounced yielding with continuous penetration after the failure load is surpassed (Figure 7.10 and Figure 7.14). No significant differences between monotonic and cyclic loading can be observed even for short starter bar anchorages. The yielding penetrates down to where the hook bend starts. The post-failure retraction of stresses below the yielding strength leads to a constant tensile stress distribution along the complete anchorage length and diminishing bond stresses. The simulation of connections in which starter bar anchorages are detailed with hooks yielded stress profiles which differ significantly from the stress profiles derived from the strain gauge reading (Section 6.4.3.1). A possible reason could be the simplification to replicate the bending stiffness of the hook by means of bar elements with fixed end rotation (Section 7.2.1).

Post-installed and cast-in-place starter bar anchorages without hooks show a redistribution to the unloaded end which is most pronounced at the moment of failure.

This phenomenon is more significant for relatively short starter bar anchorages, i.e. Specimen 2, 3, and 4 (Figure 7.11, Figure 7.12, Figure 7.13), compared to longer starter bar anchorages, i.e. Specimen 6, 7, and 8 (Figure 7.15, Figure 7.16, Figure 7.17). The stress profiles derived from the simulation of connections in which starter bar anchorages are detailed without hooks, qualitatively match well with the stress profiles on the basis of strain gauge reading (Section 6.4.3.1).

The stress profiles for Specimen 7 (post-installed, $\ell_b$ = 420 mm, 2 · 2$\phi$32, Figure 7.16) appear to be absolutely identical to those of Specimen 6 (cast-in-place, $\ell_b$ = 420 mm, 2 · 2$\phi$32, Figure 7.15). This observation match with the failure loads which are almost the same for Specimen 6 and 7. In conclusion, the influence of bond strength becomes less significant for larger anchorage lengths. On the contrary, smaller anchorage lengths benefit from higher bond strengths as the stress profiles for Specimen 2 (cast-in-place, $\ell_b$ = 240 mm, 2 · 4$\phi$16, Figure 7.11) and 3 (post-installed, $\ell_b$ = 420 mm, 2 · 4$\phi$16, Figure 7.12) show.

The diagrams for Specimen 4 (post-installed, $\ell_b$ = 240 mm, 2 · 2$\phi$25, Figure 7.13), characterised by a small ratio of starter bar anchorage length and diameter, illustrate best that the tensile stresses decrease not linearly but progressively towards the unloaded end during low drift levels. Furthermore, the redistribution of the bond stresses to the unloaded end can be observed already at drift levels corresponding pre-failure loads. This penetration of debonding is significantly more pronounced for the cyclic test if compared to the monotonic test.

In contrast, a large ratio of starter bar anchorage length and diameter reveals an almost linear distribution of tensile stresses in particular for low drift levels which is demonstrated best by the diagrams for Specimen 8 (post-installed, $\ell_b$ = 420 mm, 2 · 2$\phi$25, Figure 7.17). Despite the substandard detailing of the anchorage, penetration of yielding does not putting the capacity of the anchorage at risk. In this regard, virtually no difference between the cyclic and monotonic test can be determined even at drift levels corresponding to post-failure loads.

#### 7.4.3.2 Concrete compressive stresses in the foundation

In this section, the advantage of finite element analyses to provide concrete compressive stress plots as shown in Figure 7.18 was used to localise the compression strut in the core of the column-to-foundation connection. Furthermore, the plots indicate where the bond stresses are transferred from reinforcing bar to concrete by means of concrete compressive stresses which can be understood as local struts (Figure 2.29a). The contour levels go from light grey to black. Black corresponds to the concrete compression strength $f_c$. The tensioned starter bar is sketched for better visualisation.

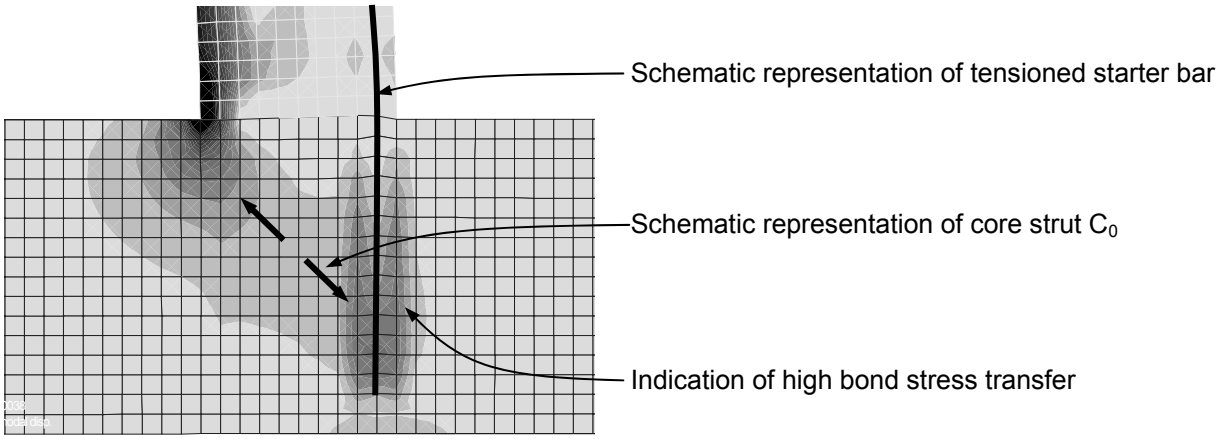


Figure 7.18 Example plots showing the concrete compressive stresses in the foundation

The following plots (Figure 7.19 to Figure 7.26) show the distribution of concrete compressive stresses which were numerically determined for the peak of the first cycle of the 0.75 % drift level, the drift level corresponding to the failure of the connection, and the drift level 4.0 %.

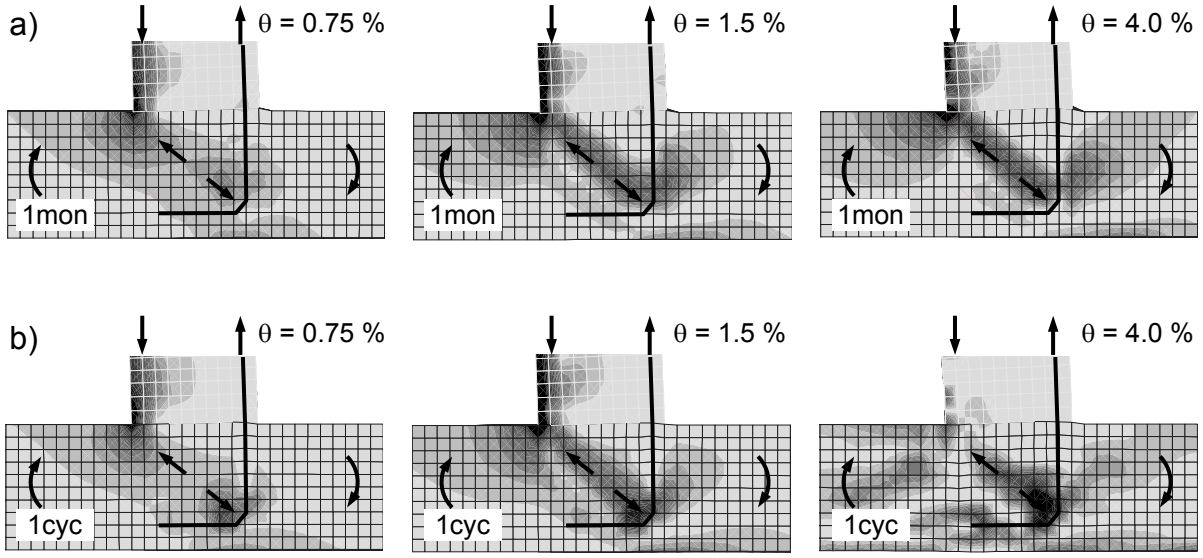


Figure 7.19 Development of concrete compressive stresses for a) monotonic and b) cyclic simulation of Specimen 1 – $\ell_b$ = 240 mm, 2 · 4$\phi$16, cast-in-place with hooks

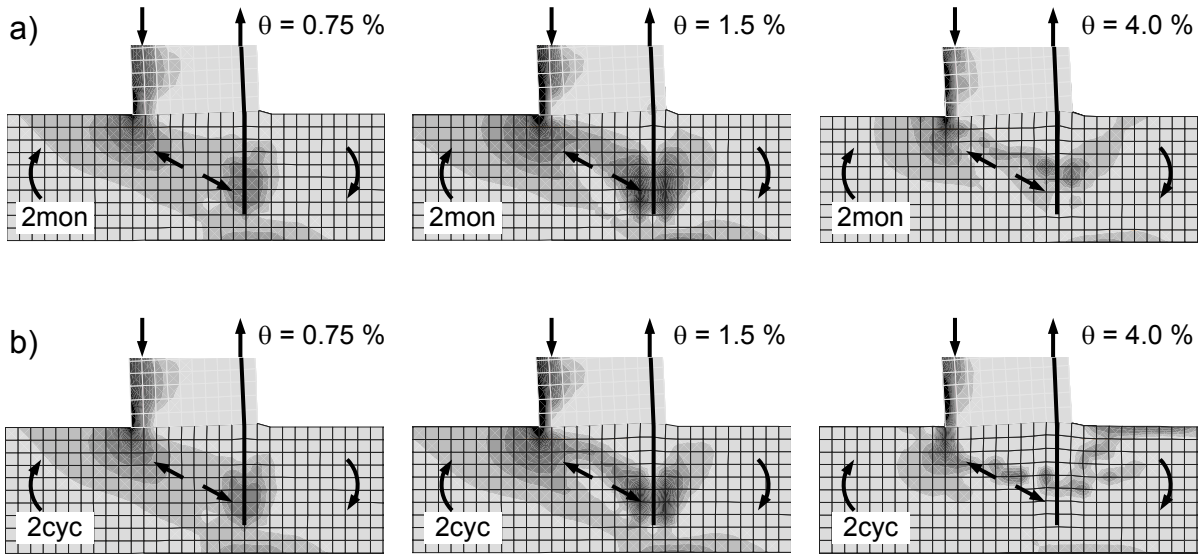


Figure 7.20 Development of concrete compressive stresses for a) monotonic and b) cyclic simulation of Specimen 2 – $\ell_b$ = 240 mm, 2 · 4$\phi$16, cast-in-place without hooks

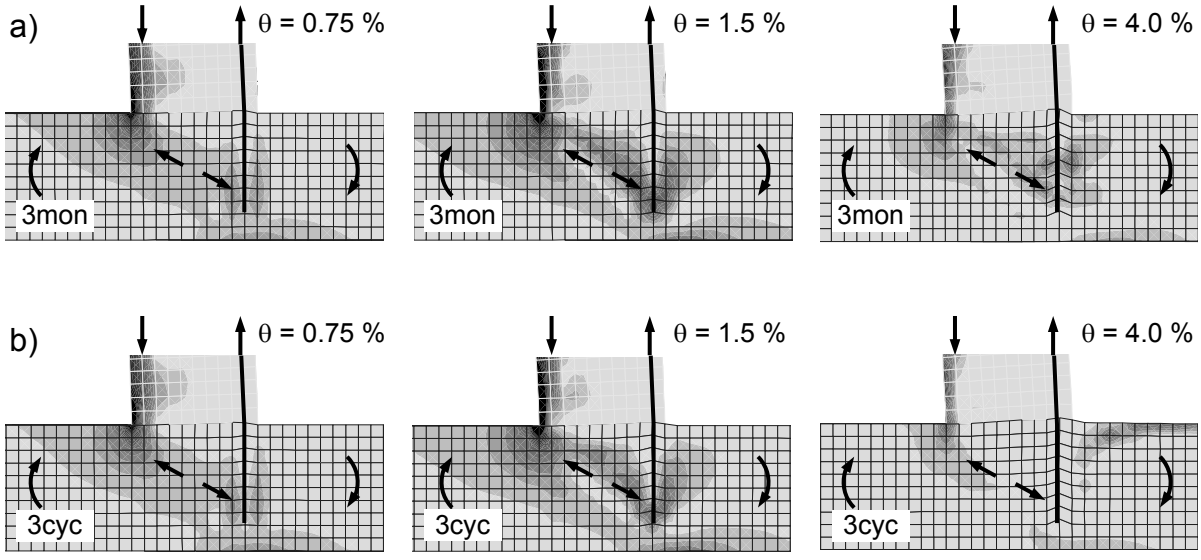


Figure 7.21 Development of concrete compressive stresses for a) monotonic and b) cyclic simulation of Specimen 3 – $\ell_b$ = 240 mm, 2 · 4$\phi$16, post-installed

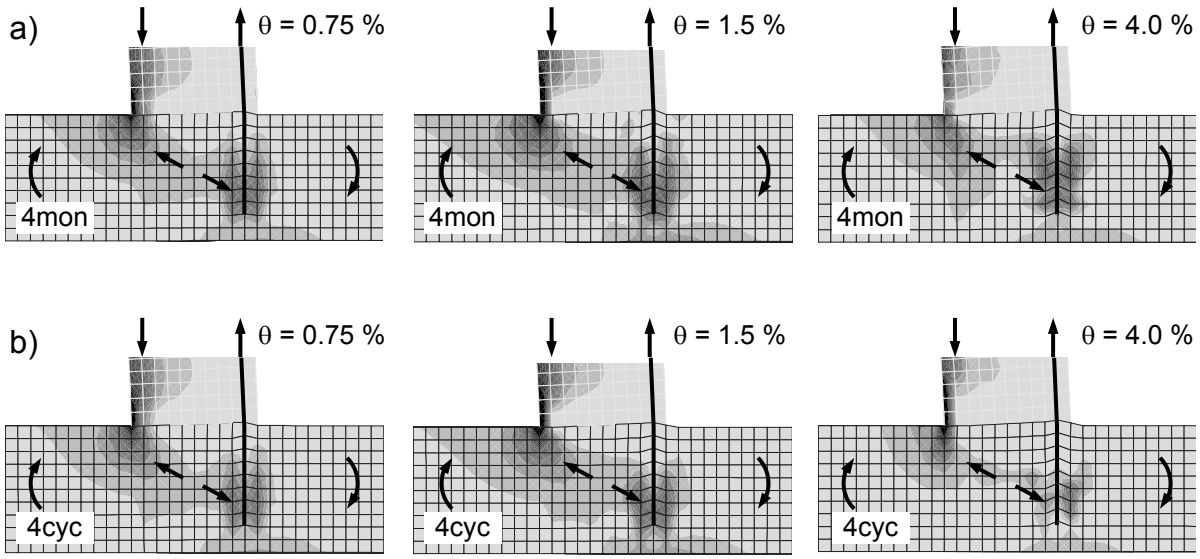


Figure 7.22 Development of concrete compressive stresses for a) monotonic and b) cyclic simulation of Specimen 4 – $\ell_b$ = 240 mm, 2 · 2$\phi$25, post-installed

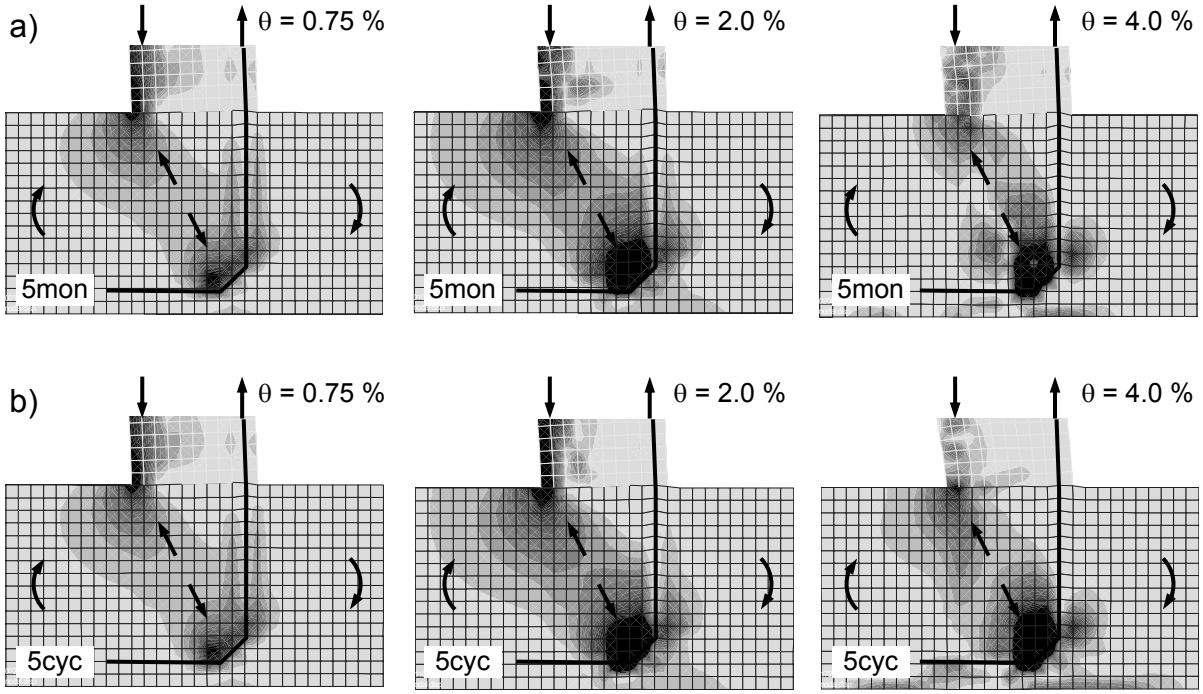


Figure 7.23 Development of concrete compressive stresses for a) monotonic and b) cyclic simulation of Specimen 5 – $\ell_b$ = 420 mm, 2 · 2$\phi$32, cast-in-place with hooks

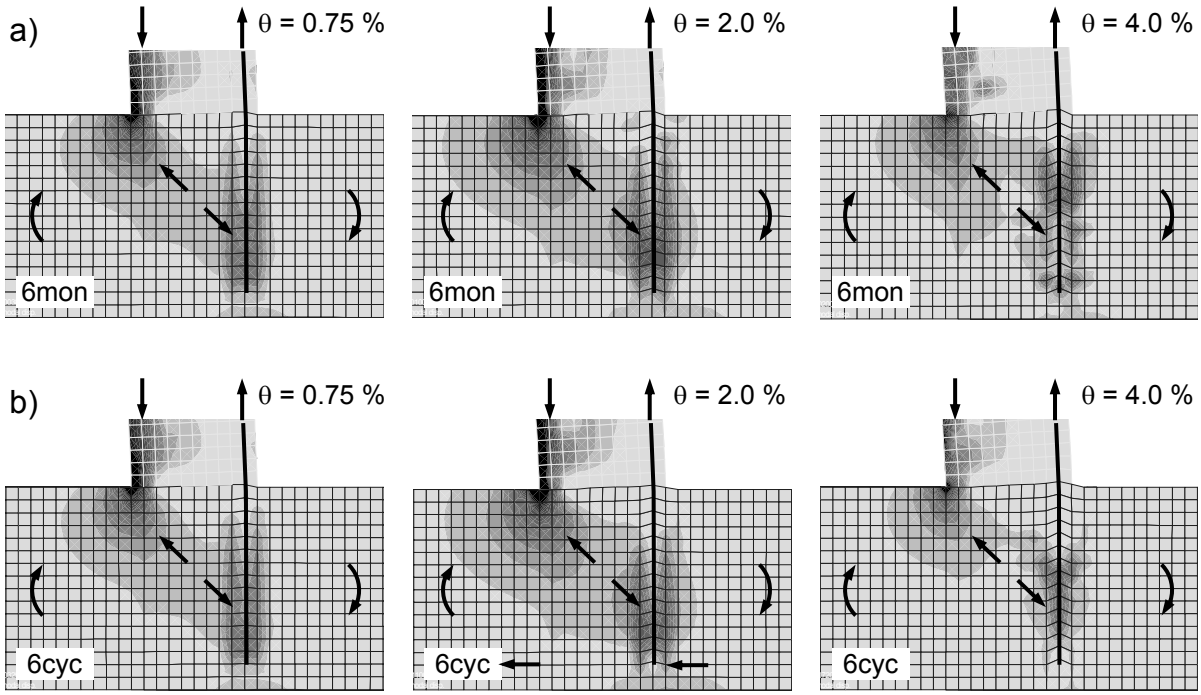


Figure 7.24 Development of concrete compressive stresses for a) monotonic and b) cyclic simulation of Specimen 6 – $\ell_b$ = 420 mm, 2 · 2$\phi$32, cast-in-place without hooks

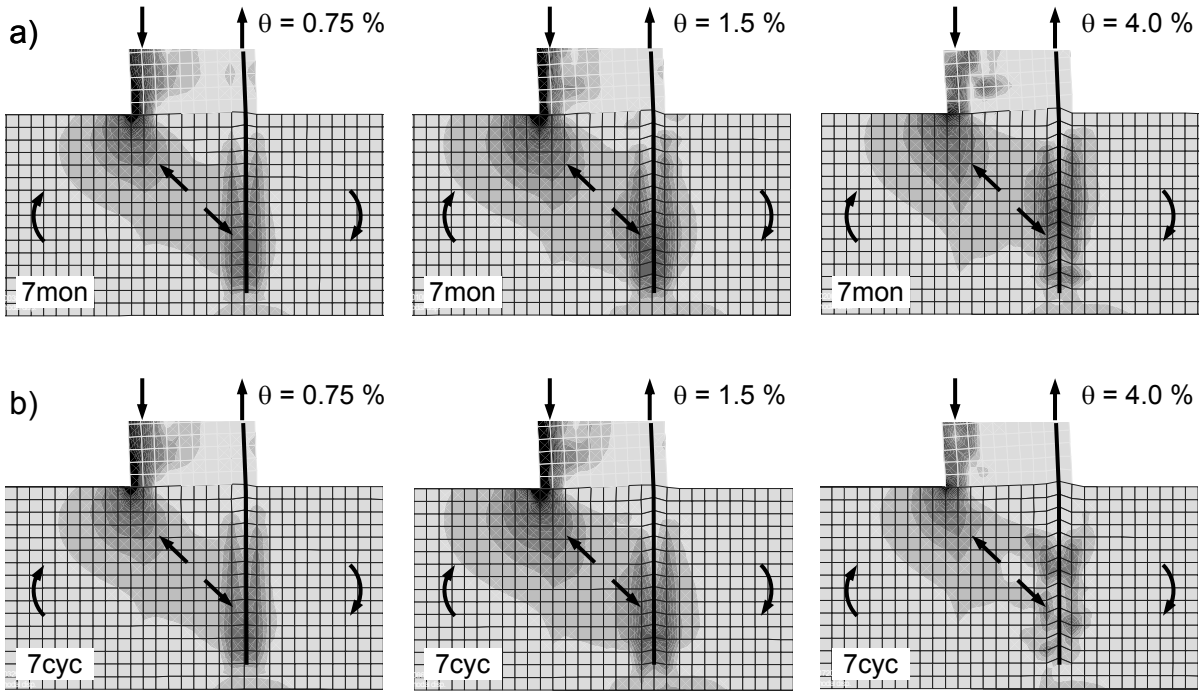


Figure 7.25 Development of concrete compressive stresses for a) monotonic and b) cyclic simulation of Specimen 7 – $\ell_b$ = 420 mm, 2 · 2$\phi$32, post-installed

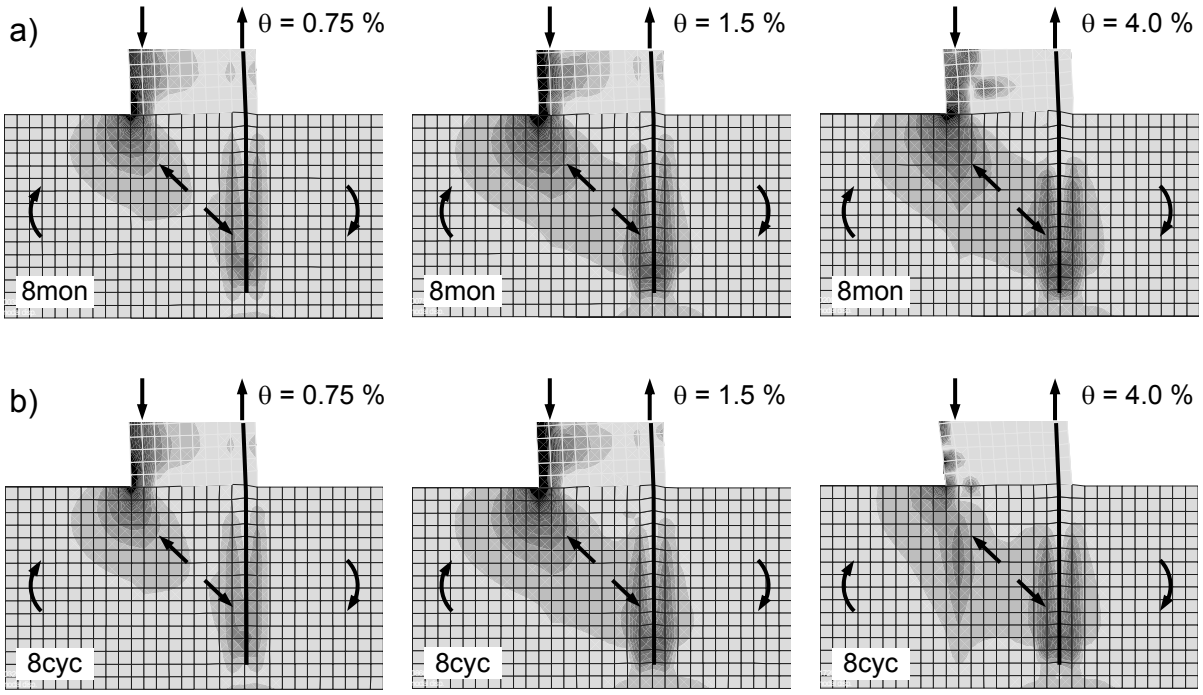


Figure 7.26 Development of concrete compressive stresses for a) monotonic and b) cyclic simulation of Specimen 8 – $\ell_b$ = 420 mm, 2 · 2$\phi$25, post-installed

The above diagrams visualising the concrete compressive stresses do not show any conclusive difference between monotonic and cyclic loading. The compressive stresses concentrate at the interface between column and foundation, i.e. where the compression load is induced, and the anchorage, i.e. where the strut is supported. This can be explained by the three-dimensional shape of the strut orthogonal to the section plane. The bottle shaped strut distributes and therefore reduces the compressive stresses.

For column-to-foundation connections in which starter bar anchorages are detailed with hooks, the strut is supported at the bend of the hook. For column-to-foundation connections in which starter bar anchorage is detailed without a hook, the strut load is transferred along the anchorage close to the unloaded end where the activated bond agglomerates. For column-to-foundation connections detailed with relatively short starter bar anchorage lengths, e.g. Specimen 4 (Figure 7.22), the strut in the core is shallow and attacks at the lower end of the anchorage. In column-to-foundation connections characterised by large starter bar anchorage lengths, e.g. Specimen 8 (Figure 7.35), the strut in the core is steeper and attacks at the middle of the anchorage.

#### 7.4.3.3 Concrete tensile stresses in the foundation

In the following, the concrete tensile stress plots of finite element analyses as shown in Figure 7.27 was used to visualise splitting forces generated by the pulling of the starter bar. Also, high concrete tensile stresses along the starter bar demonstrate the bond stresses transfer because the circumferrential tensile stresses are a reaction to the induced compressive stresses (Figure 2.8b). Moreover, the plots allowed us to look for the concrete tensile stresses of some distance from the anchorage predicted as by *Kupfer, H.; Münger, F. et al. (2003)* for wall-to-foundation connections (Section 2.3.2). The contour levels go from light grey to black. Black corresponds to the concrete tensile strength $f_{ct}$. The tensioned starter bar is sketched for better visualisation.

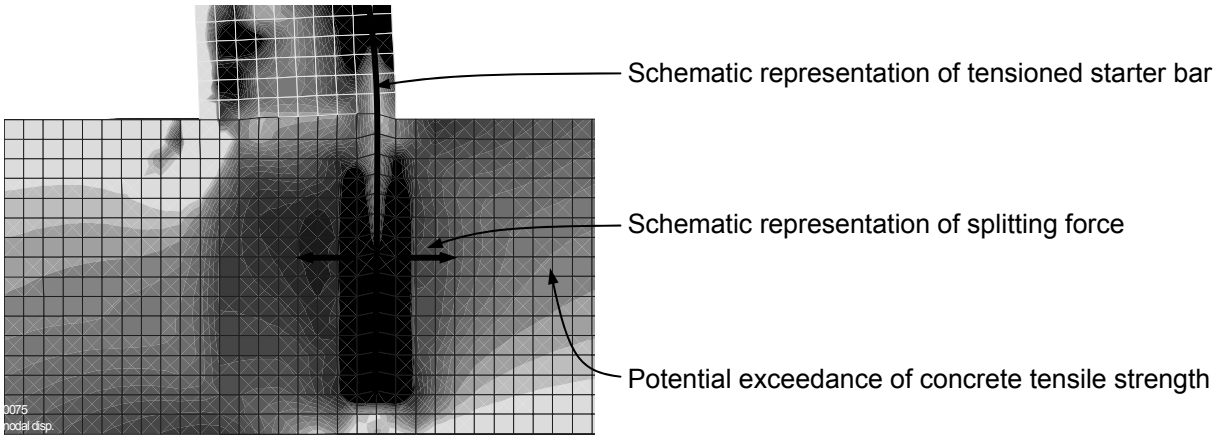


Figure 7.27 Example plot showing the concrete tensile stresses in the foundation

The following plots (Figure 7.28 to Figure 7.35) show the distribution of concrete tensile stresses which were numerically determined for the peak of the first cycle of the 0.75 % drift level, the drift level corresponding to the failure of the connection, and the drift level 4.0 %.

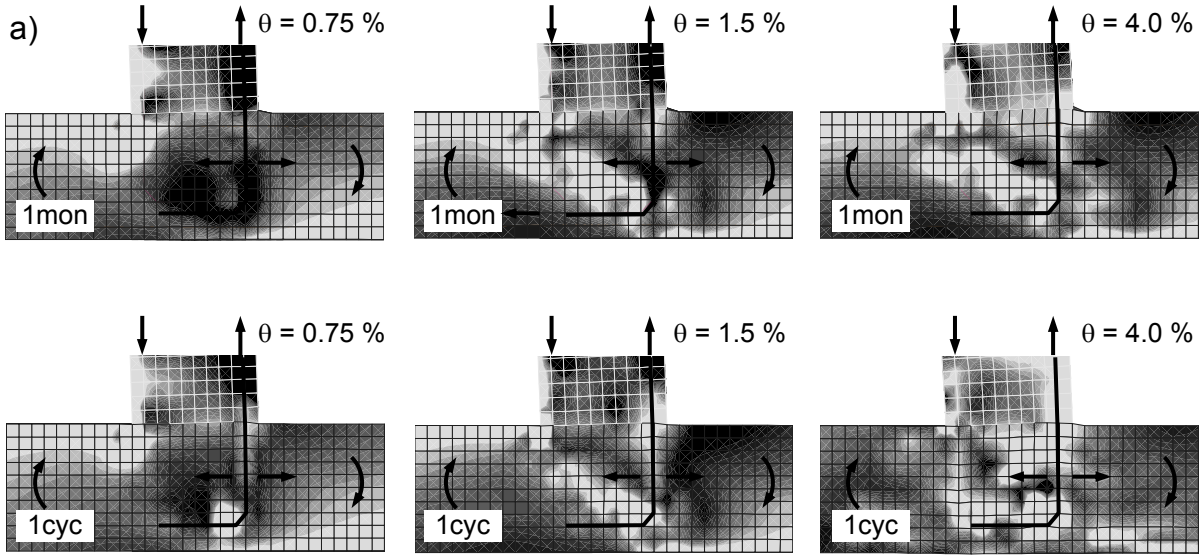


Figure 7.28 Development of concrete tensile stresses for a) monotonic and b) cyclic simulation of Specimen 1 – $\ell_b$ = 240 mm, 2 · 4$\phi$16, cast-in-place with hooks

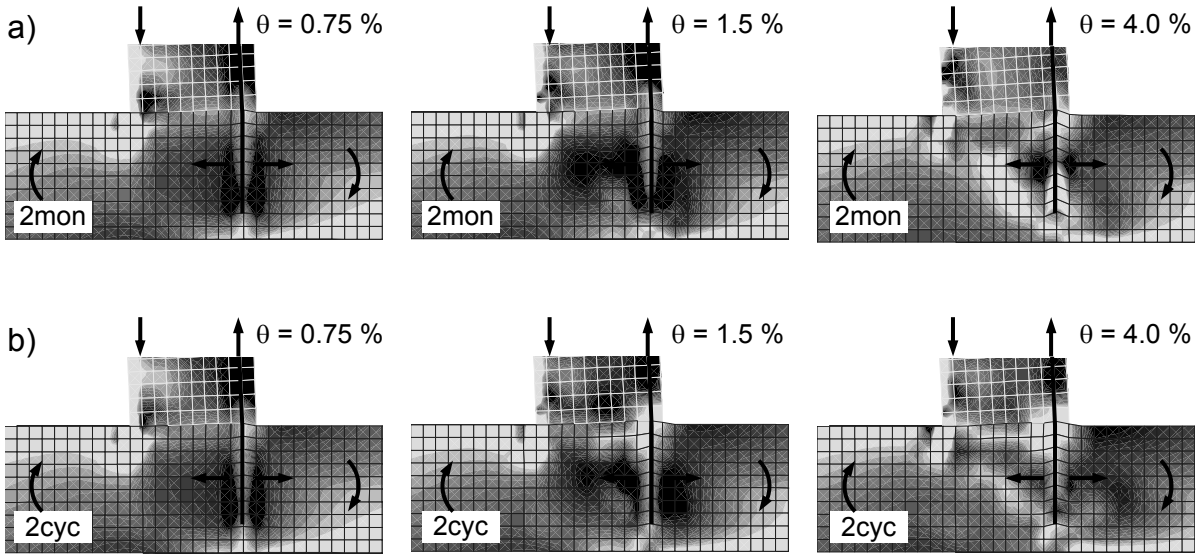


Figure 7.29 Development of concrete tensile stresses for a) monotonic and b) cyclic simulation of Specimen 2 – $\ell_b$ = 240 mm, 2 · 4$\phi$16, cast-in-place without hooks

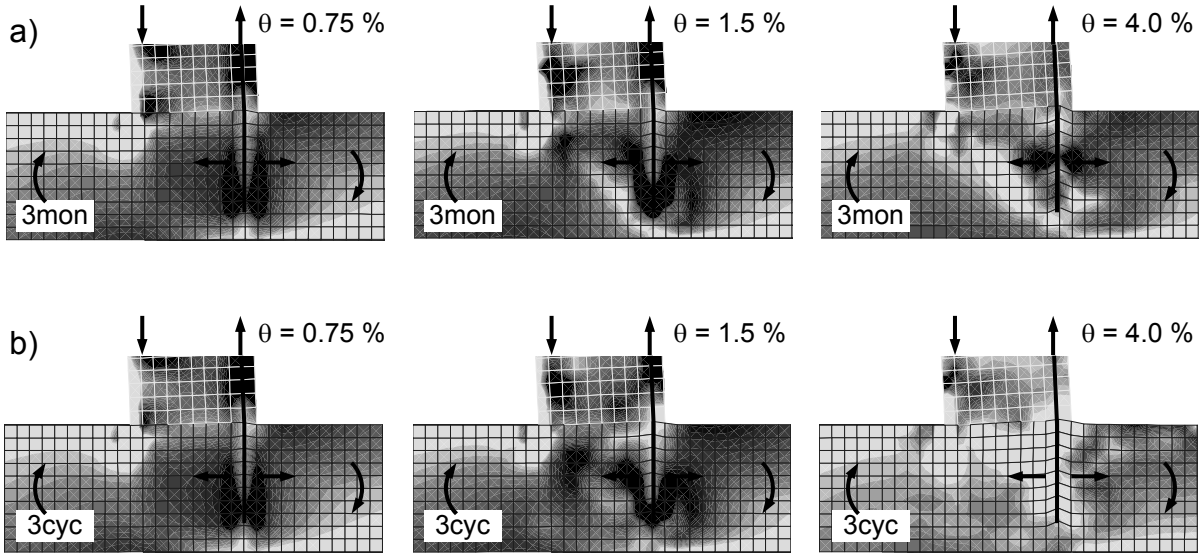


Figure 7.30 Development of concrete tensile stresses for a) monotonic and b) cyclic simulation of Specimen 3 – $\ell_b$ = 240 mm, 2 · 4$\phi$16, post-installed

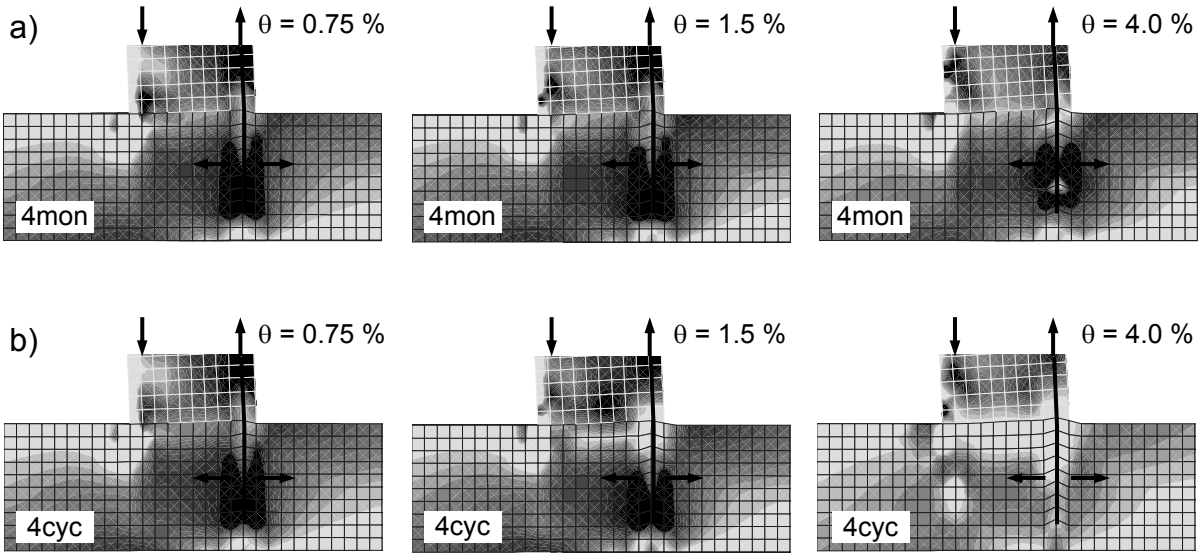


Figure 7.31 Development of concrete tensile stresses for a) monotonic and b) cyclic simulation of Specimen 4 – $\ell_b$ = 240 mm, 2 · 2$\phi$25, post-installed

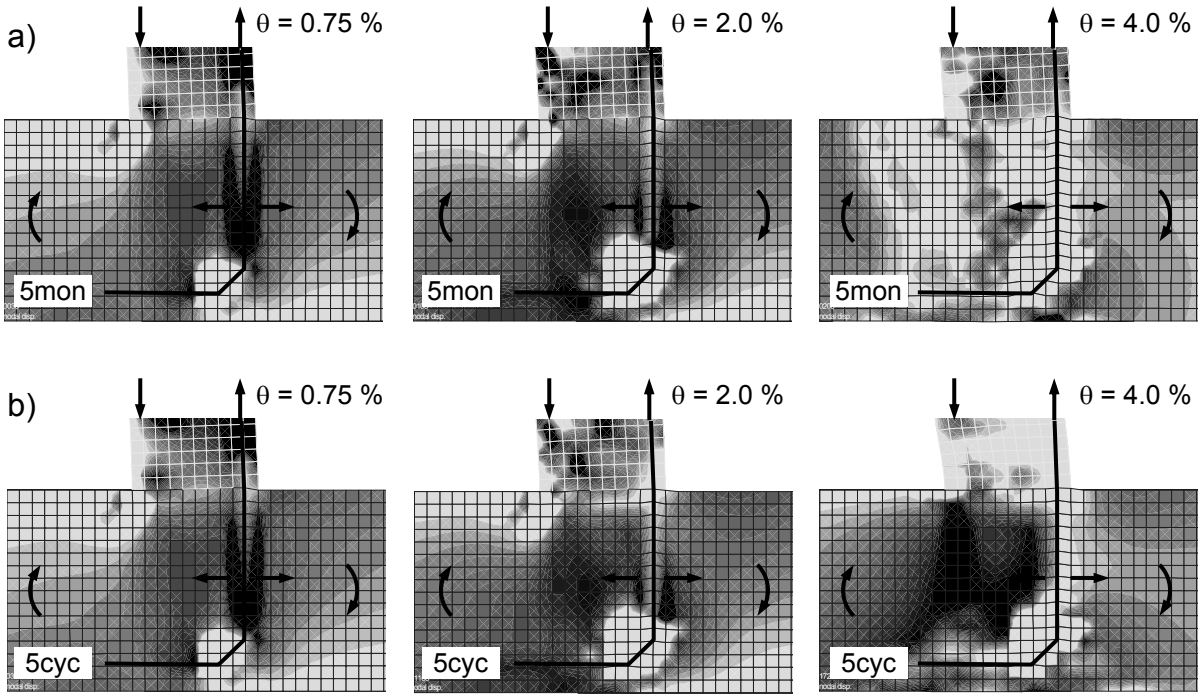


Figure 7.32 Development of concrete tensile stresses for a) monotonic and b) cyclic simulation of Specimen 5 – $\ell_b$ = 420 mm, 2 · 2$\phi$32, cast-in-place with hooks

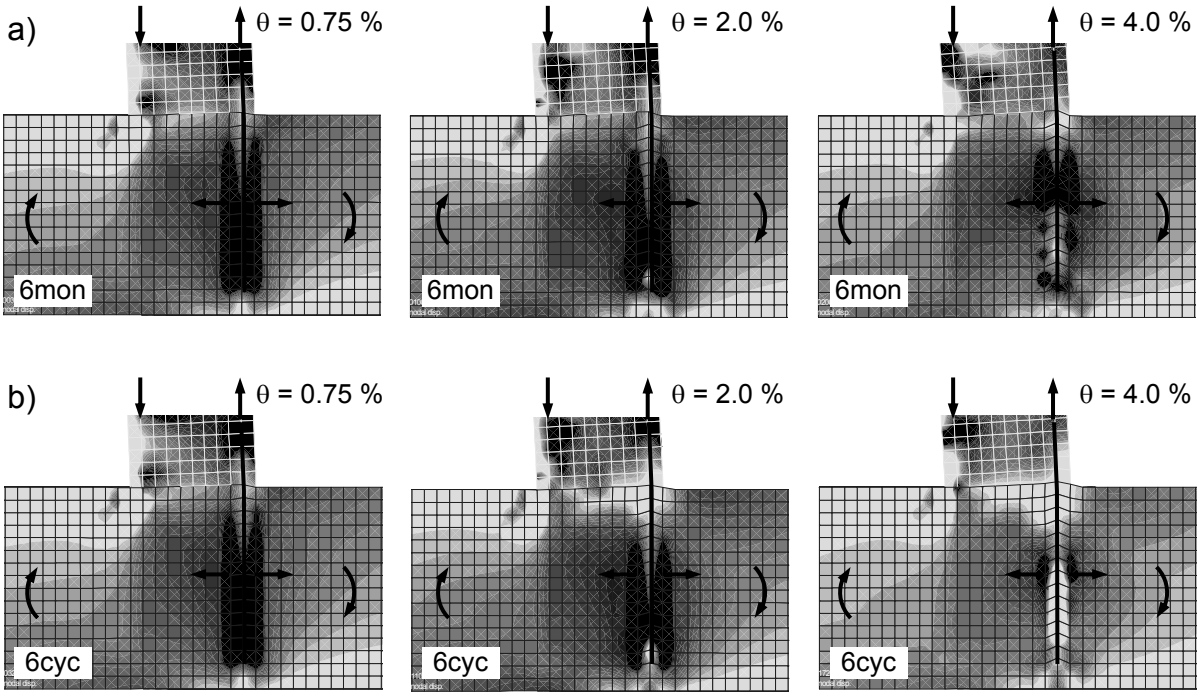


Figure 7.33 Development of concrete tensile stresses for a) monotonic and b) cyclic simulation of Specimen 6 – $\ell_b$ = 420 mm, 2 · 2$\phi$32, cast-in-place without hooks

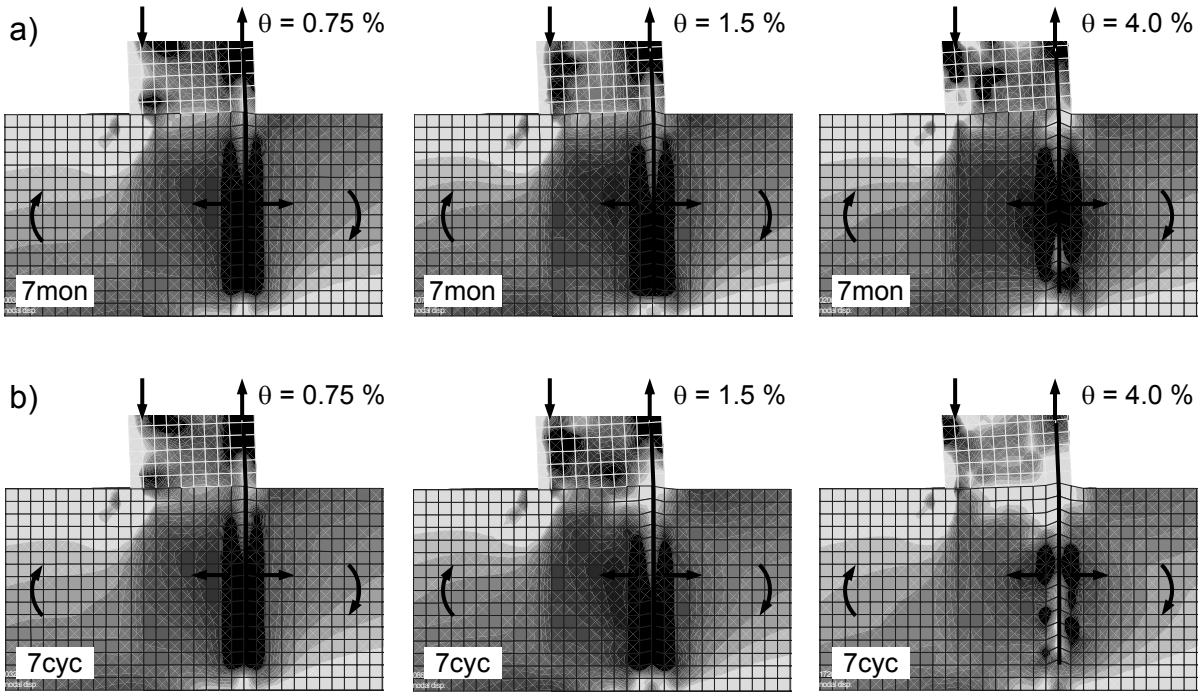


Figure 7.34 Development of concrete tensile stresses for a) monotonic and b) cyclic simulation of Specimen 7 – $\ell_b$ = 420 mm, 2 · 2$\phi$32, post-installed

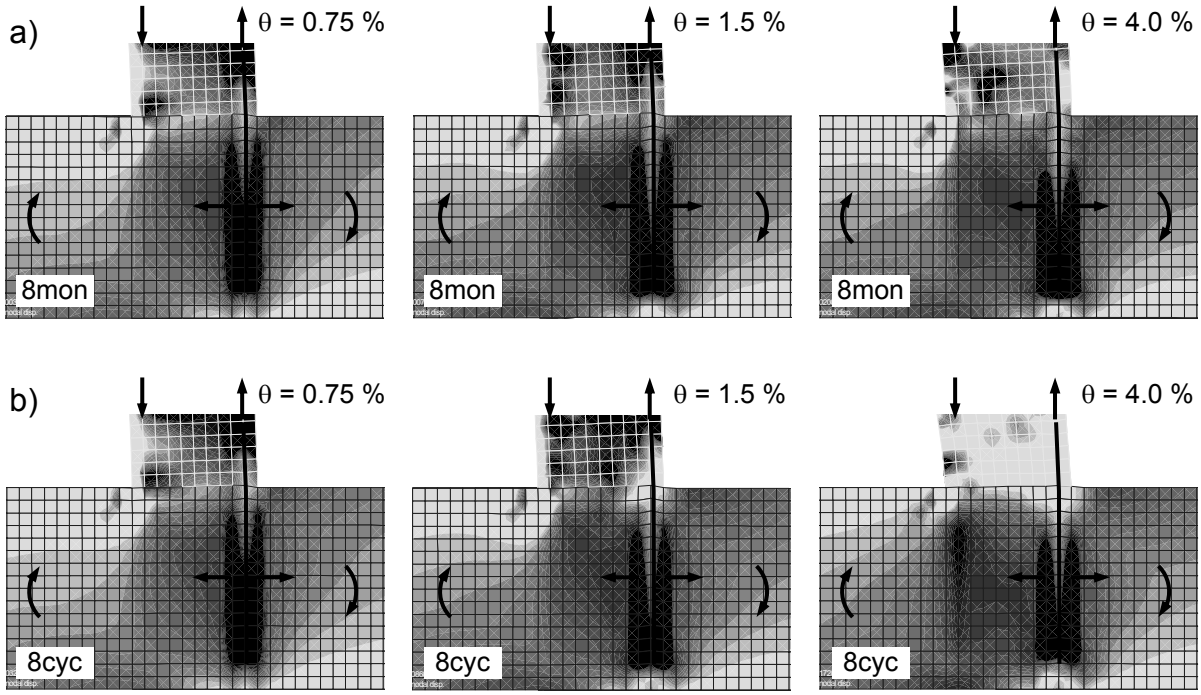


Figure 7.35 Development of concrete tensile stresses for a) monotonic and b) cyclic simulation of Specimen 8 – $\ell_b$ = 420 mm, 2 · 2$\phi$25, post-installed

The plots of the concrete tensile stresses for Specimen 4 (post-installed, $\ell_b$ = 240 mm, 2 · 2$\phi$25, Figure 7.31) clearly demonstrate the difference in response of

montonic and cyclic loading on the column-to-foundation connection in which starter bar anchorage is characterized by small ratios of anchorage length and diameter: The tensile stresses progressively concentrate at the unloaded end of the starter bar anchorage. The difference is secondary at smaller drifts but pronounced for the drift corresponding to the failure of the connection. For larger drifts, the bond is destroyed and therefore no significant concrete tensile stresses develop in the vicinity of the starter bar anchorage.

In contrast, the plots of the concrete tensile stresses for Specimen 8 (post-installed, $\ell_b$ = 420 mm, 2 · 2$\phi$25, Figure 7.35) at the drift corresponding to the failure of the connection shows that there is virtually no difference between montonic and cyclic loading on the column-to-foundation connection in which starter bar anchorages are detailed with large ratios of anchorage length and diameter.

Moreover, it is noteworthy that significant concrete tensile stresses develop only within the potential concrete breakout cone. The strut-and-tie model presented in *Kupfer, H.; Münger, F. et al. (2003)* includes a concrete tie adjacent to the starter bar anchorage as indicated in Figure 7.27. A possible explanation is that the support of the concrete strut (Figure 7.18) is distributed over almost the entire length of the anchorage which therefore also reduces the tensile stresses close to the starter bar anchorage. Furthermore, the three-dimensional load transfer in column-to-foundation connections is reducing the stresses.

#### 7.4.3.4 Steel tensile stresses in the foundation

The output of the finite element analyses was also used to evaluate the steel tensile stresses in the longitudinal reinforcement of the foundation as shown in Figure 7.36.

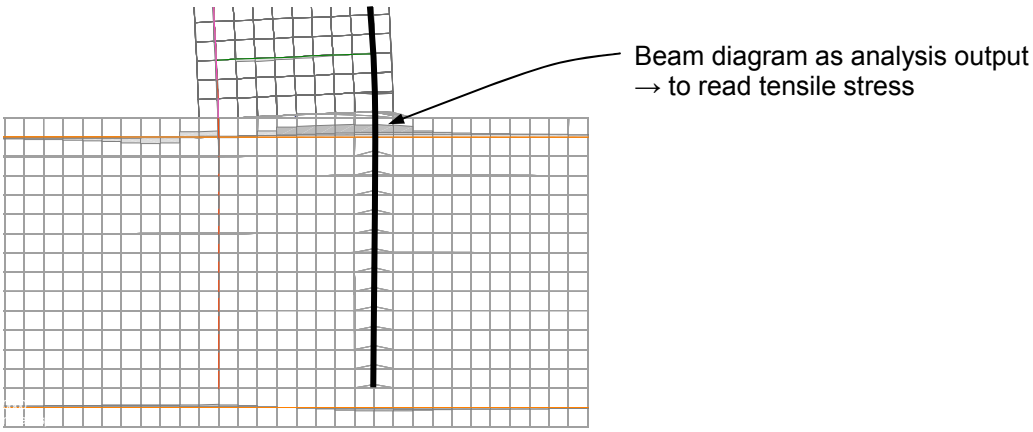


Figure 7.36 Example plot showing the steel tensile stresses in the foundation

The plots showed low stresses in the foundation reinforcement for drift levels corresponding to the failure of the column-to-foundation connection, and only in rare

cases stresses above 100 N/mm². This was surprising because the analysis of a simple mechanical approach would estimate significantly higher tensile stresses in the upper foundation reinforcement as will be shown in the following.

The longitudinal reinforcement of the foundation is stressed due to the moment loading of the connection, causing the steel tensile stress $\sigma'_{s,ben}$ (Figure 7.37a), and the splitting force induced by the pulled anchorage, causing the steel tensile stress $\sigma'_{s,spl}$ (Figure 7.37b).

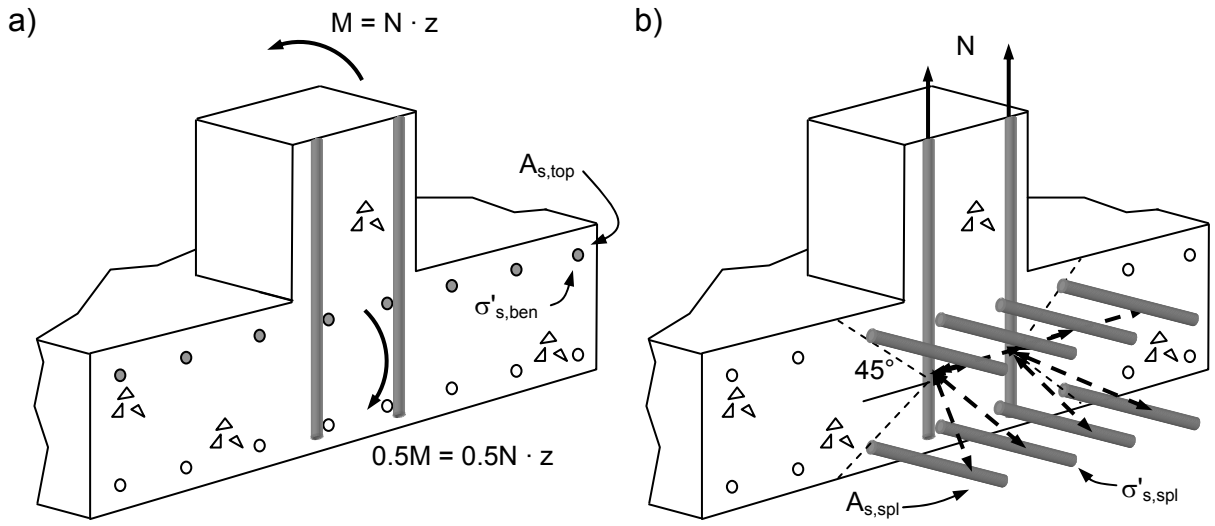


Figure 7.37 Detail of connection illustrating the generation of steel tensile stresses $\sigma_{Ts}$ due to a) bending and b) splitting

The tensile steel stress $\sigma'_{s,ben}$ resulting from the foundation moment (Figure 6.12b) equals

$$\sigma'_{s,ben} = \frac{0.5M}{A_{s,top} \cdot z'} = \frac{0.5N \cdot z}{A_{s,top} \cdot z'} \qquad \text{Equation 7.1}$$

where $A_{s,top}$ is the cross section of the upper foundation reinforcement and z' the internal lever arm of the foundation. For individual pad foundations, the complete width of the foundation is assumed to be effective. If the foundation is detailed as a raft foundation, the use of effective beam models (e.g. *Grasser, E.; Thielen, G. (1972)*, *Fraser, D. (1983)*) should be considered.

The splitting force is a function of the tension load N pulling the anchored starter bar and is conservatively estimated asccording to *EOTA TR 029 (2010)* to be equivalent to 0.5N. However, for the following equations the less conservative value of 0.25N proposed in *Leonhardt, F.; Mönnig, E. (1977)* is used. The splitting forces have to be taken up by the foundation reinforcement $A_{s,spl}$ in the vicinity. Tentatively it is assumed that the upper and lower reinforcement within a 45° angle starting at the

centroid of the anchorage is activated (Figure 7.37b). Therefore, the steel tensile stress $\sigma'_{s,spl}$ is derived by

$$\sigma'_{s,spl} = \frac{0.25N}{(A_{s,top} + A_{s,bot})(b_{col} + \ell_b) / b_{fdn}} \qquad \text{Equation 7.2}$$

where $A_{s,top}$ and $A_{s,bot}$ is the cross section of the upper und lower foundation reinforcement and $b_{col}$ and $b_{fdn}$ is the width of column and foundation.

The total steel tensile stress $\sigma'_s$ must not exceed the steel yield strength $f_y$:

$$\sigma'_s = \sigma'_{s,ben} + \sigma'_{s,spl} = N \cdot \left( \frac{0.5z}{A_{s,top} z'} + \frac{0.25 b_{fdn}}{(A_{s,top} + A_{s,bot})(b_{col} + \ell_b)} \right) \leq f_y \qquad \text{Equation 7.3}$$

For foundations with symmetric top and bottom reinforcement ($A_{s,top} = A_{s,bot}$), the equation is simplified to:

$$\sigma'_s = \sigma'_{s,ben} + \sigma'_{s,spl} = \frac{N}{A_{s,top}} \cdot \left( \frac{0.5z}{z'} + \frac{0.125 b_{fdn}}{b_{col} + \ell_b} \right) \leq f_y \qquad \text{Equation 7.4}$$

The tensile loading of the lower foundation reinforcement is not governing, since it can be assumed that its cross section is larger than the cross section of the upper reinforcement. In addition, only bending action is loading the lower reinforcement but no splitting action. It is reasonable to assume that the bending compressive stresses in foundations are generally not governing since the reinforcement ratios of foundations are commonly low, making yielding of the reinforcement critical.

The comparison of the steel tensile stresses $\sigma'_s$ derived by means of the finite element analyses and according to above given equations showed that the steel tensile stresses in the upper reinforcement of the foundation are strongly overestimated when applying the above presented simple mechanical model. For the example shown in Figure 7.36 (Specimen num7cyc, $N_R$ = 288 kN, $\ell_b$ = 420 mm, $A_{s,top} = A_{s,bot}$ = 679 mm², $z$ = 208 mm, $z'$ = 418 mm, $b_{col}$ = 300 mm, $b_{fdn}$ = 1500 mm), the mechanical model predicts tensile stresses of $\sigma'_{s,ben} + \sigma'_{s,spl}$ = 105 N/mm² + 109 N/mm² = 241 N/mm², whereas the numerical analysis show tensile stresses of only 92 N/mm². Since the steel tensile stresses generated by bending inevitably develop, the splitting forces have to be negligible.

The finding that the steel tensile stresses generated in the upper reinforcement of the foundation is comparatively low is reasonable since the splitting forces are generated were the bond stresses of the starter bar anchorage concentrates. As shown in Section 7.4.3.1, the bond transfer mainly takes place in the zone closer to the unloaded end of the anchorage. Furthermore, the three-dimensional load transfer in column-to-foundation connections is reducing the stresses. In conclusion, the

tensioning of the foundation reinforcement is not critical and needs no additional design check.

### 7.4.4 Assessment of seismic performance

Analogous to Section 6.4.4, the performance of the numerically tested specimens was assessed according to the criteria stipulated in *ACI 374.1 (2005)*. The preliminary analysis revealed that some numerically tested connections violated the ductility criterion for the drift $\theta_a$ = 4.0 % cycles, although the experimentally tested counterparts developed pronounced strain hardening, e.g. Specimen 5. As pointed out in Section 7.4.2 and explained in Section 5.1.1.1, simulations employing truss elements to model reinforcing bars generally tend to overestimate the strength degradation (*Eligehausen, R.; Ožbolt, J. et al. (2006)*). Therefore, the assessment according to the criteria stipulated in *ACI 374.1 (2005)* and the strain hardening criterion was conducted for the drift of $\theta_a$ = 3.0 % instead of 4.0 %. The key results of the assessment are given in Table 7.9. Apart from the monotonic test on Specimen 3, the evaluation of experimental tests and numerical tests yielded the same results (compare Table 6.4 and Table 7.9). This is true for both the *ACI 374.1 (2005)* criteria and the strain hardening criterion. Since the experimental monotonic test on Specimen 3 can be considered to be an outlier, the notable agreement of seismic perfomance assessment for experimental and numerical tests is a further verification of the finite element approach used. More details of the evaluation are provided in Table D.4 of Appendix D: Column-to-Foundation Connection Test Data.

Table 7.9 Performance assessment of numerical tests based on acceptance criteria stipulated in *ACI 374.1 (2005)* and the strain hardening criterion

| Monotonic loading: mon<br>Cyclic loading: cyc | Anchorage detailing | Starter bar layout | 1. | 2. | 3. | | | ACI 374.1 compliant?[6] | Strain hardening?[7] |
|---|---|---|---|---|---|---|---|---|---|
| | | | Initial strength[1] | Over-strength[2] | Ductiility[3] | Damping[4] | Stiffness[5] | | |
| num1mon | Cast-in-place | 4 bars | O | O | O | NA | NA | YES | YES |
| num1cyc | w/ hook | per face | O | O | O | O | X | NO | YES |
| num2mon | Cast-in-place | 4 bars | O | O | X | NA | NA | NO | NO |
| num2cyc | w/o hook | per face | O | O | X | O | O | NO | NO |
| num3mon | Post-installed | 4 bars | O | O | X | NA | NA | NO | NO |
| num3cyc | w/o hook | per face | O | O | X | O | O | NO | NO |
| num4mon | Post-installed | 2 bars | X | O | O | NA | NA | NO | NO |
| num4cyc | w/o hook | per face | X | O | X | O | X | NO | NO |
| num5mon | Cast-in-place | 2 bars | O | O | O | NA | NA | YES | NO |
| num5cyc | w/ hook | per face | O | O | O | O | O | YES | NO |
| num6mon | Cast-in-place | 2 bars | O | O | O | NA | NA | YES | NO |
| num6cyc | w/o hook | per face | O | O | O | O | O | YES | NO |
| num7mon | Post-installed | 2 bars | O | O | O | NA | NA | YES | NO |
| num7cyc | w/o hook | per face | O | O | O | O | O | YES | NO |
| num8mon | Post-installed | 2 bars | O | O | O | NA | NA | YES | YES |
| num8cyc | w/o hook | per face | O | O | O | O | O | YES | YES |

[1] Acceptance criterion: $numM_{max} / calM_y > 1.00$

[2] Acceptance criterion: $numM_{max} / \lambda\ calM_y < 1.00$

[3] Acceptance criterion: $numM_{\theta a} / numM_{max} > 0.75$

[4] Acceptance criterion: $E_{d,\theta a} / E_{d\#,\theta a} > 0.125$

[5] Acceptance criterion: $K_{p,\theta a} / K_{p,\theta i} > 0.05$

[1) – 5)] Indication of compliance with acceptance criterion by 'O', indication of non-compliance by 'X'

[6] 'YES' if compliance with all acceptance criteria of ACI 374.1, else 'NO'

[7] 'YES' if strain hardening criterion is met, else 'NO'

## 7.5 Extension of Parametric Range

In order to provide a sound data basis for the quantification of the beneficial and adverse effect of moment loading and cyclic loading on the connection capacity, the

parametric range was extended. For this purpose, additional column-to-foundation connections were numerically tested for which the diameter of the column starter bars as well as the reinforcement ratio and concrete strength of the foundation was varied:

- The column reinforcing bars were modelled with diameters between $\phi$ = 12 mm and $\phi$ = 40 mm, resulting in reinforcement ratios between 1.0 % and 5.6 % for the columns and 0.2 % and 1.0 % for the foundations.
- Besides the simulation of the foundation concrete with low strength concrete of a compressive strength of $f_c$ = 28 MPa, the foundation concrete was redefined as high strength concrete with a compressive strength of $f_c$ = 58 MPa.

The complete numerical test program comprised 106 monotonic and cyclic test runs and is given in Table D.2 and the evaluation of the seismic performance analogous to Section 7.4.4 is provided in Table D.4 of Appendix D: Column-to-Foundation Connection Test Data.

The evaluation of the conducted numerically tests showed that generally the assessment according to the criteria of *ACI 374.1 (2005)* and according to the strain hardening criterion have almost the same result. In rare cases, connections detailed with a starter bar diameter of 12 mm did not meet the overstrength or stiffness criteria of *ACI 374.1 (2005)* which, however, can be neglected since such small starter bar diameters are not generally relevant for seismic engineering. Taken as a whole, assessing column-to-foundation connections according to the strain hardening criterion can be deemed to be an adequate approach. The advantage of the strain hardening criterion is the much easier and faster handling if compared to the assessment according to *ACI 374.1 (2005)*.

The evaluation further revealed that for low strength concrete ($f_c$ = 28 MPa) anchorage lengths larger than about 20$\phi$ and for high strength concrete ($f_c$ = 58 MPa) larger than approximately 15$\phi$ are required to achieve adequate seismic performance. These anchorage lengths are small compared to those in accordance with *Eurocode 2 (2005)*. Further detailed analyses of the exact anchorage lengths necessary to achieve an adequate seismic performance were not conducted because probabilistic considerations of ductile and brittle failure modes tend to govern in respect of minimum required anchorage lengths as will be shown in Section 9.2.3. However, it can be concluded that the adverse effect of cyclic loading on the connection capacity is secondary in comparison to the beneficial effect of moment loading as already pointed out in Section 6.4.1. Another interesting observation was that some connection geometries which just failed in mode Y under monotonic loading, failed in mode P/C under cyclic loading.

A detailed evaluation of the tests is made in Section 8.1.1 and Section 8.1.2. All values of the assessment for all experimental tests and numerical tests are given in Table D.4 of Appendix D: Column-to-Foundation Connection Test Data.

## 7.6 Summary and Conclusions

The finite element method was used to simulate the behaviour of monotonic and cyclic tests on post-installed and cast-in-place column-to-foundation connections in which starter bars were detailed with and without hooks. The finite element program, MASA, employed applies the smeared crack method. The model was generated using bond elements to link one-dimensional bar elements with three-dimensional solid elements in order to simulate the bond interaction between reinforcing bars and concrete. The finite element models were loaded analogous to the experimental test specimens. These numerical tests were the first ever to simulate the behaviour of reinforced concrete members which were connected by starter bars without hooks and therefore required simulation of the bond.

The use of bond elements suitable to simulate realistic bond behaviour under seismic loading yielded load-drift curves which coincided well with the load-drift curves of the experiments. The post-failure behaviour was also well predicted, however some specimens behaved in a more brittle manner than the experimental results suggested. This phenomenon was also observed by *Eligehausen, R.; Ožbolt, J. et al. (2006)* who ascribed the differences to the modelling of the reinforcement by truss elements. The model is able to replicate the distribution of steel stresses and concrete strains and furthermore to capture different failure modes. The detailed study of the bond stress distribution of the starter bar anchorage showed that cyclic loading accelerates bond stress redistribution to the unloaded end of anchorages which are characterised by small ratios of anchorage length and bar diameter. This effect is accompanied by decreased failure loads if compared to monotonic loading. Significant concrete tensile stresses outside the potential concrete breakout cone of the starter bar anchorage were not observed.

To account for the unrealistic overestimation of post-failure strength degradation, the following relaxation of the acceptance criteria according to *ACI 374.1 (2005)* was deemed to be acceptable for assessment of numerical tests: The ductility, damping, and stiffness of the numerical tests were evaluated for 3.0 % instead of 3.5 % drift as stipulated in *ACI 374.1 (2005)*. The assessment of the numerically tested column-to-foundation connections yielded almost the same results as the experimentally tested connections. It was shown that for column-to-foundation connections a newly introduced acceptance criterion on the basis of the strain hardening evaluation is less elaborative yet provides the same significance as the acceptance criteria according to *ACI 374.1 (2005)*.

The finite element models were used to extend the parametric range of column-to-foundation connections. For this reason, the reinforcing bar diameters and concrete strengths were varied. It turned out that assessing column-to-foundation connections on the basis of the proposed strain hardening criterion is an adequate method for which application is simpler if compared to the assessment according to *ACI 374.1 (2005)*.

The results of the simulations are used in the following chapter to develop models accounting for the beneficial effect of moment loading and the adverse effect of cyclic loading on the connection capacity.

# 8 Enhanced Bonded Anchor Model

The numerical studies on column-to-foundation connections were conducted for an extended parametric range establishing together with the experimental test results an extensive data base. The data base is used in Section 8.1 to develop additional factors to take into account the beneficial effect of moment loading and adverse effect of cyclic loading on the connection capacity. These additional factors are used for the enhancement of the bonded anchor model which is introduced and verified in Section 8.2. Summary and conclusion is provided in Section 8.3.

## 8.1 Factors Accounting for Beneficial Effect and Adverse Effect

### 8.1.1 Beneficial effect of moment loading on connection capacity

In the following, the factor $\psi_M$ replicating the beneficial effect of moment loading on the connection capacity is studied. According to Section 2.3.3, the factor $\psi_M$ is defined as the ratio of the tested connection capacity and calculated concrete breakout capacity (Figure 8.1). The calculated pullout capacity is likewise taken into account for column-to-foundation connections in which starter bar anchorages are detailed without hooks, because concrete breakout and pullout capacity respond similarly with respect to the beneficial effect of moment loading: With increasing compression stresses the capacity is increased and with increasing crack widths the capacity is reduced for both, the concrete breakout and pullout failure mode. Therefore, the concrete breakout and the pullout capacity of the connection is considered jointly for the following evaluation. The steel capacity is not influenced by the moment loading. Therefore, the anchor group capacity $N_R$ is calculated according to the minimum of Equation 2.16 and 2.17, taking into account the effects of overlapping influencing areas and the group (Table 2.3). The tested anchor group capacity $N_{R,p/c}$ equals $F_{max} \cdot y / z$ (Figure 6.12).

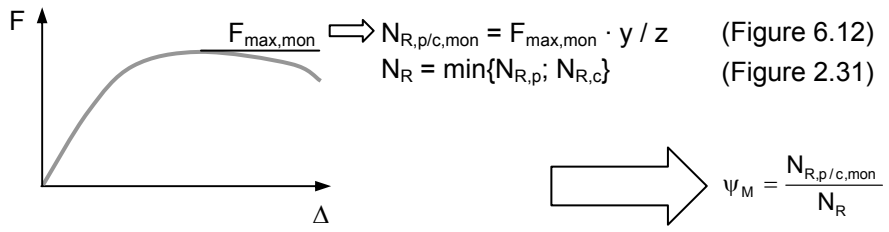


Figure 8.1 Schematic of $\psi_M$ determination

The result for the evaluation of $\psi_M$ is shown in Figure 8.2 as a function of the normalised internal lever arm. The results for experimental tests are indicated by hollow data points and the results for numerical tests by solid data points. The evaluation comprised only the connections failing in mode P or mode C. By trend, the factors $\psi_M$ corresponding to the calculative mode P are larger if compared to those corresponding to mode C.

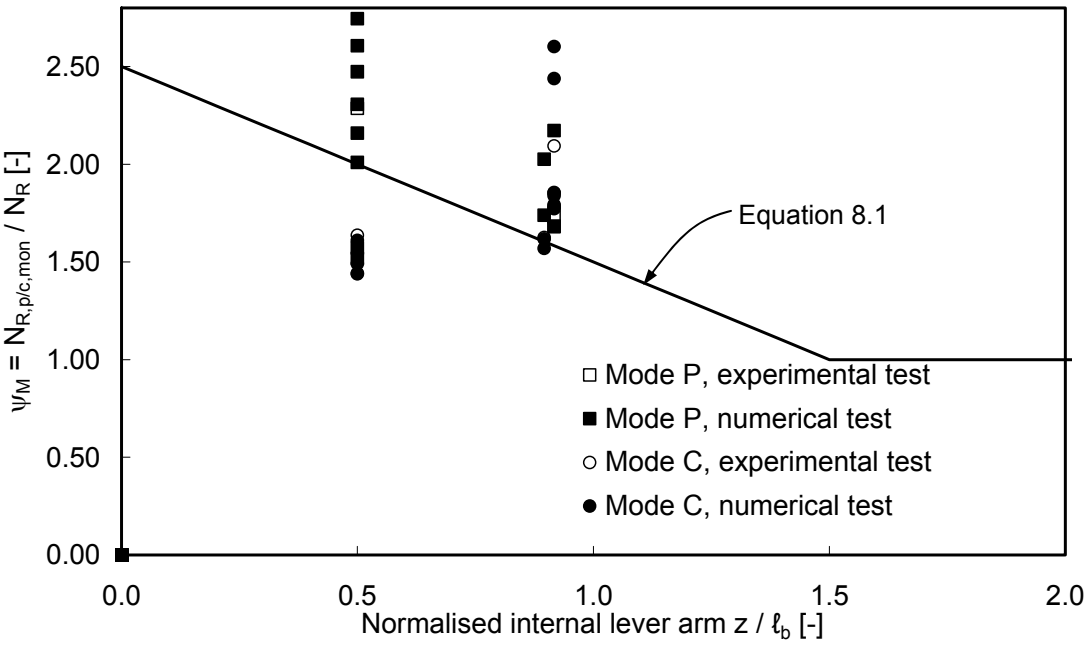


Figure 8.2 Influence of internal lever arm on factor $\psi_M$ (solid data points: numerical tests; hollow data points: experimental tests) and proposed Equation 8.1

Based on the studies on cast-in-place and post-installed column-to-foundation connections presented in *Herzog, M. (2010)*, it is suggested to use the equation

$$\psi_{M,N} = 2.5 - \frac{z}{\ell_b} \geq 1.0 \qquad \text{Equation 8.1}$$

to describe the beneficial effect of moment loading. The graphical representation of Equation 8.1 is also plotted in Figure 8.2. The distribution of the ratios of tested and calculated beneficial effect due to moment loading is shown in Figure 8.3 as relative frequency (bars) and normal distribution (curve). The mean value and CV are in the same order as for the equations proposed in *Fichtner, S. (2011)* and *Herzog, M. (2010)* (Section 2.3.3). Further details in respect of the beneficial effect of moment loading on the connection capacity will be provided in *Herzog, M. (2012)*.

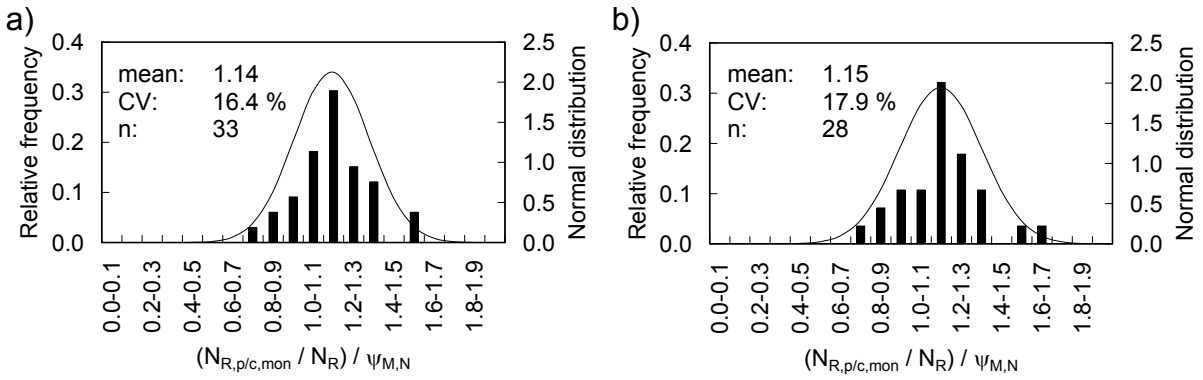


Figure 8.3 Distribution of ratios tested and calculated reduction due to moment loading a) for experimental and numerical tests as well as b) for numerical tests

### 8.1.2 Adverse effect of cyclic loading on connection capacity

In this section, the factor $\psi_{cyc}$ expressing the adverse effect of cyclic loading on the connection capacity is studied. The factor $\psi_{cyc}$ is determined as the ratio of the cyclically tested and monotonically tested connection capacity (Figure 8.4). The cyclic loading does not affect the failure load corresponding to the yield failure mode. Therefore, only the concrete breakout and the pullout capacity of the connection is considered. The tested anchor group capacity $N_{R,p/c}$ equals to $F_{max} \cdot y / z$ (Figure 6.12). Because column-to-foundation connections comprise multiple anchorages, the factors taking into account the effect of overlapping influencing areas and group are considered (Table 2.3).

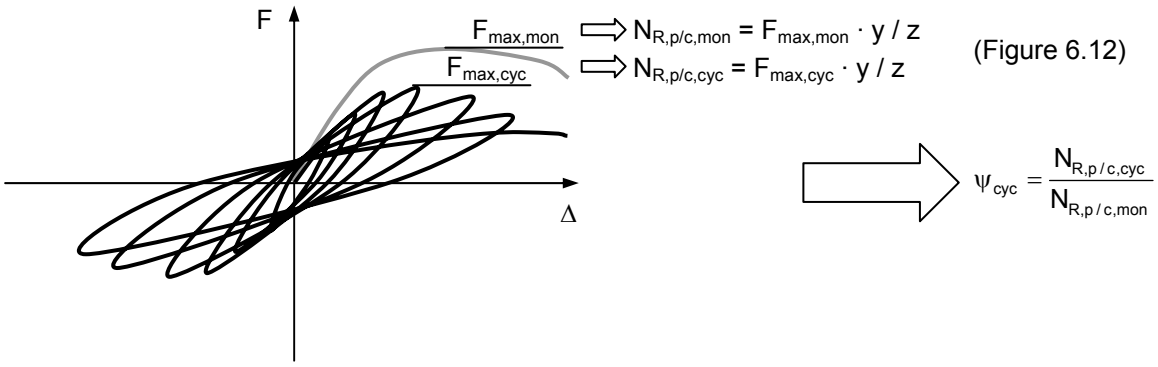


Figure 8.4 Schematic of $\psi_{cyc}$ determination

The result for the evaluation of $\psi_{cyc}$ is shown in Figure 8.5 as a function of the normalised anchorage length. For information only, the values for tests failing in mode Y are plotted in the diagram, which have factors $\psi_{cyc}$ of about 1.0. The results for experimental tests are indicated by hollow data points and the results for numerical tests by solid data points. The evaluation comprised only the connections failing in mode P or mode C. The factors corresponding to the calculative mode P and mode C are in the same band of scatter.

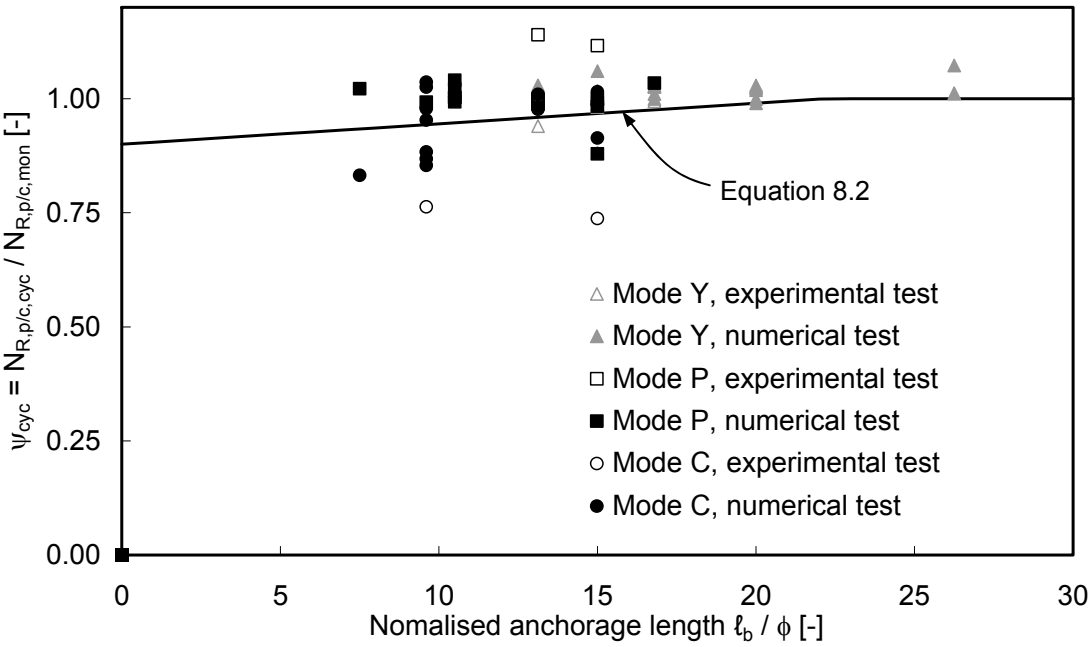


Figure 8.5 Influence of anchorage length on factor $\psi_{cyc}$ (solid, hollow data points: numerical, experimental tests, respectively) and proposed Equation 8.2

It is proposed to use the equation

$$\psi_{cyc,N} = 0.9\left(1+\frac{\ell_b}{200\phi}\right) \leq 1.0 \qquad \text{Equation 8.2}$$

to describe the adverse effect of cyclic loading. The graphical representation of Equation 8.2 is also plotted in Figure 8.5. The distribution of the ratios of tested and calculated reductions due to cyclic loading are presented in Figure 8.6. The mean value and CV are in the same order as for the equation proposed to decribe the beneficial effect (Section 2.3.3 and Section 8.1.1).

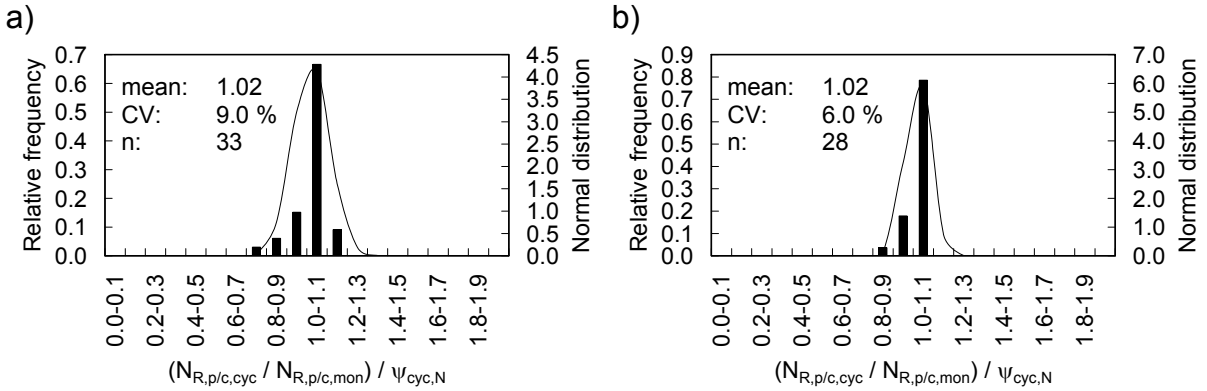


Figure 8.6 Distribution of ratios tested and calculated reduction due to cyclic loading a) for experimental and numerical tests as well as b) for numerical tests

## 8.2 Proposed Enhanced Bonded Anchor Model

### 8.2.1 Capacity according to enhanced bonded anchor model

The equations given in the following Section 8.2.1.1, Section 8.2.1.2, and Section 8.2.1.3 to determine the yield, concrete breakout, and pullout capacity, respectively, describe the bonded anchor model which serves as the basis for the bonded anchor design provisions according to the *CEN/TS 1992-4 (2009)*. Therefore, the concept and the denominations comply with *CEN/TS 1992-4 (2009)*, e.g. the bond strength is denoted $\tau_R$. The provisions of the *CEN/TS 1992-4 (2009)* are cited in detail in Appendix B: Bonded Anchor Design.

The verification of a model requires the consideration of mean values. Therefore, the equations partly differ from those given in *CEN/TS 1992-4 (2009)*, e.g. the definition of the k factor to calculate the concrete breakout capacity or the critical centre-to-centre distance $s_{cr,Np}$ to calculate the pullout capacity.

Further, the factors taking into account the group effect have to be reconsidered as pointed out in the following:

- The increased failure surface of anchor groups increases the pullout capacity if compared to single anchors (Figure 8.7a).
- The influence of the increase in failure surface on the pullout capacity decreases with increasing bond strengths and increasing spacing between the bonded anchorages, making the concrete breakout capacity governing. The current equation describing the increased failure load of anchor groups was developed for tightly arranged anchors, e.g. anchor pairs or quadruple anchor groups (Figure 8.7b).
- In contrast, the tensioned starter bars of column-to-foundation connections have linear arrangement which has an impact on the failure surface. *Herzog, M. (2010)* studied the behaviour of column-to-foundation connections under static loading and developed an equation taking into account the increased failure load of linear arranged bonded starter bars (Figure 8.7c).

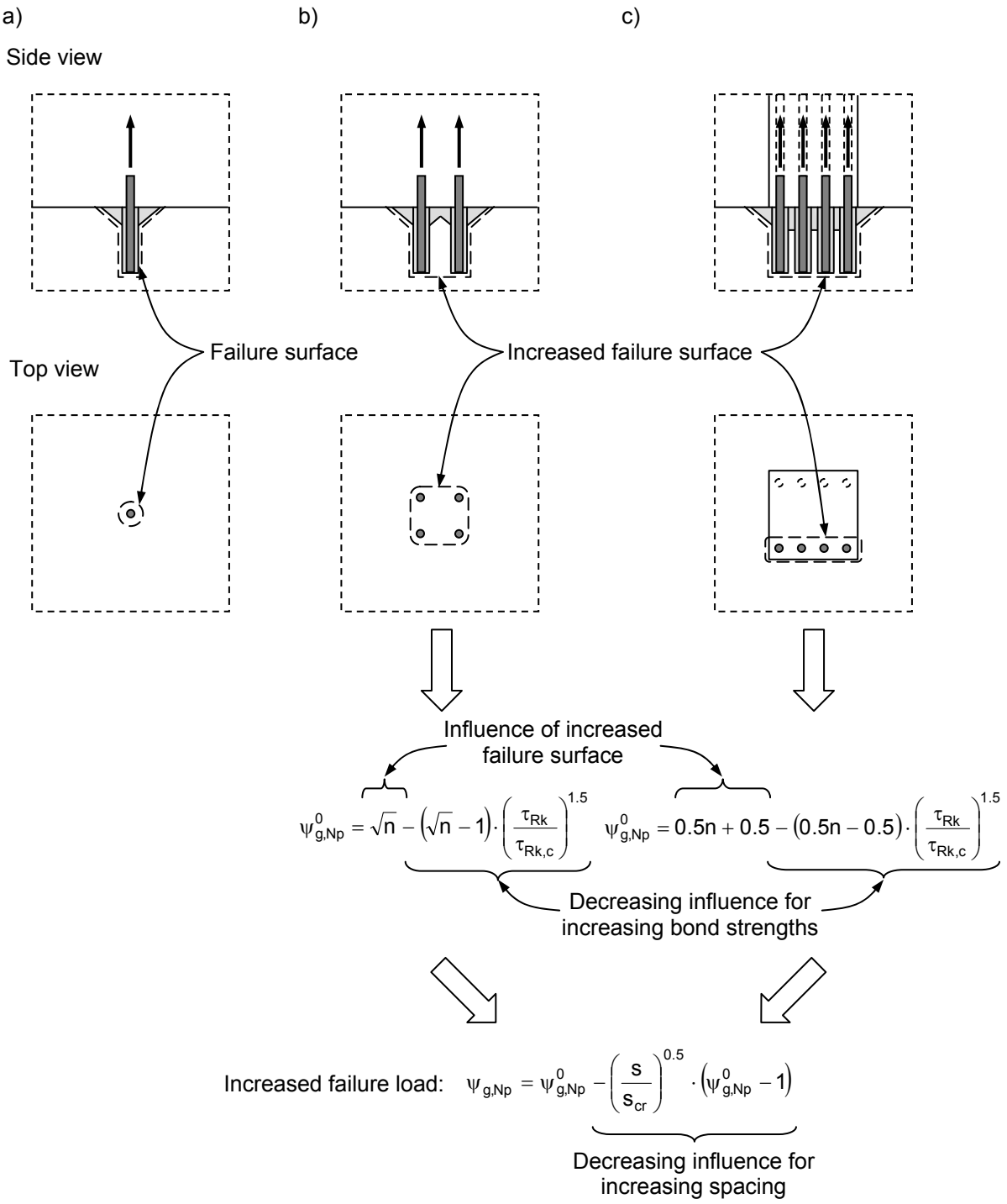


Figure 8.7 a) Failure surface for single anchor as well as increase of failure surface and failure load for b) tightly arranged anchor group after *Eligehausen, R.; Cook, R. et al. (2006)* and c) linear arranged anchor group of column-to-foundation connection after *Herzog, M. (2010)*

Studying the limiting behaviour of the two equations given for $\psi^0_{g,Np}$ given in Figure 8.7b and Figure 8.7c for anchor pairs (n = 2) shows a maximum difference of 6 % between the two equations if the extreme case of $\tau_R$ / $\tau_{R,c}$ = 0 is assumed, where $\tau_{R,c}$

is the upper limit of bond strength that can be utilised which is determined by the concrete breakout strength (Section 8.2.1.3). Since the difference is deemed to be negligable it is recommended to use the equation proposed by *Herzog, M. (2010)* for any column-to-foundation connection including layouts where only two starter bar per face are detailed.

Finally, the proposed factors $\psi_{M,N}$ and $\psi_{cyc,N}$ to account for the beneficial effect of moment loading on the connection capacity (Section 8.1.1) and adverse effect of cyclic loading on the connection capacity (Section 8.1.2), respectively, are amended to the bonded anchor model as shown in the Sections 8.2.1.2 and 8.2.1.3.

The background of the following presented approach for the analytical calculation of yield, concrete breakout, and pullout capacity to determine the resulting anchorage capacity is discussed in Section 2.3.1.2. As briefly discussed in Section 2.3.1.2, models are developed on the basis of mean values. Therefore, actual material strengths and connection capacities are considered to verify the enhanced bonded anchor model in the following: The tested mean material strengths (Section 6.2.1) are used for the analytical calculation of capacities if compared with experimentally determined capacities. The material strengths defined for the finite element model (Section 7.2.1) are used for the analytical calculation of capacities if compared with numerically determined capacities.

#### 8.2.1.1 Yield capacity

The yield capacity of the anchor group in the context of column-to-foundation connections is calculated on the basis of the total cross section of the starter bars and yield strength:

$$N_{R,y} = A_s \cdot f_y \qquad \text{Equation 8.3}$$

where

$A_s$ stressed cross section of steel

$$A_s = n \cdot \pi \cdot \phi^2 / 4$$

- $n$ number of starter bars per face
- $\phi$ nominal diameter of starter bars

$f_y$ yield strength derived from material tests (Section 6.2.1.1).

Figure 8.8 shows the cross section $A_s$ for linear arranged starter bar anchorages of column-to-foundation connections.

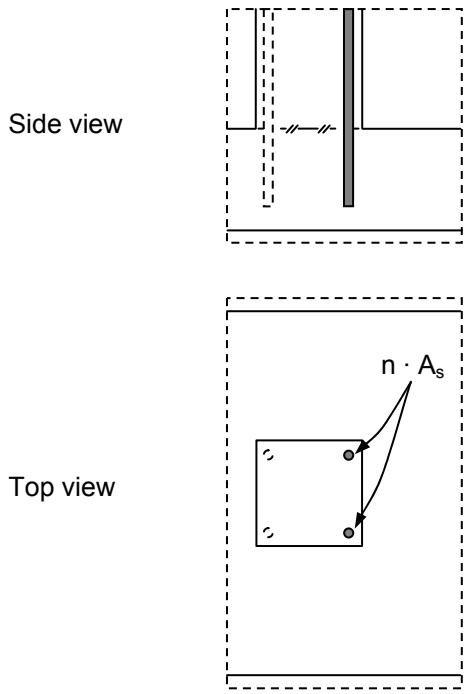


Figure 8.8 Cross section area $A_s$ for linear arranged starter bar anchorages of column-to-foundation connections

### 8.2.1.2 Concrete breakout capacity

The concrete breakout capacity of the anchor group in the context of column-to-foundation connections is calculated according to:

$$N_{R,c} = N^0_{R,c} \cdot \frac{A_{c,N}}{A^0_{c,N}} \cdot \psi_{s,N} \cdot \psi_{M,N} \cdot \psi_{cyc,N} \qquad \text{Equation 8.4}$$

where

$N^0_{R,c}$ initial value of the resistance

$$N^0_{R,c} = k \cdot \sqrt{f_c[\text{MPa}]} \cdot \ell_b[\text{mm}]^{1.5}$$

- k $k_{cr}$ = 10.2 for cracked concrete to be assumed for column-to-foundation connections
- $f_c$ concrete cylinder strength derived from material tests (Section 6.2.1.2)
- $\ell_b$ anchorage length

$A^0_{c,N}$ reference cone base area of an individual starter bar without the influence of adjoining starter bars and foundation edges, idealising the activated concrete as a pyramid with an edge length of

$$s_{cr,N} = 2c_{cr,N} = 3\ell_b$$

$A_{c,N}$ actual cone base area, limited by overlapping areas of adjoining starter bars and foundation edges

$\psi_{s,N}$ factor taking into account the disturbance of the stress distribution due to foundation edges, with the smallest edge distance is considered in

$$\psi_{s,N} = 0.7 + 0.3 \cdot \frac{c}{c_{cr,N}} \leq 1.0 .$$

The background of the above equations is provided in *Fuchs, W.; Eligehausen, R. et al. (1995)*. The factors given in the following are based on the findings described in Section 8.1.1 and Section 8.1.2.

$\psi_{M,N}$ factor taking into account the beneficial effect of moment loading on the capacity of column-to-foundation connections (for any load case)

$$\psi_{M,N} = 2.5 - \frac{z}{\ell_b} \geq 1.0$$

$\psi_{cyc,N}$ factor taking into account the adverse effect of cyclic loading on the capacity of column-to-foundation connections (for seismic load case)

$$\psi_{cyc,N} = 0.9\left(1 + \frac{\ell_b}{200\phi}\right) \leq 1.0$$

Figure 8.9 shows the idealised area $A_{c,N}$ for linear arranged starter bar anchorages of column-to-foundation connections. It is conservative to use the above equations also to calculate the concrete breakout capacity for column-to-foundation connections in which starter bars are detailed with hooks because hooks generate larger concrete breakouts compared to the theoretical assumption of a conical concrete breakout.

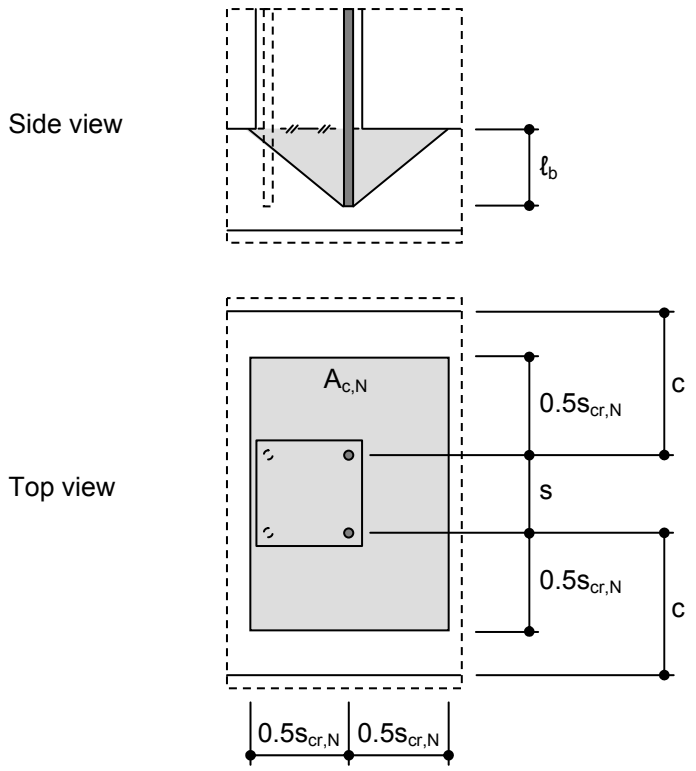


Figure 8.9 Idealised area $A_{c,N}$ for linear arranged starter bar anchorages of column-to-foundation connections

Regarding factor $\psi_{N,cyc}$, reference is made to the discussion on the bidirectional loading in Section 9.2.4.

### 8.2.1.3 Pullout capacity

The pullout capacity of the anchor group in the context of column-to-foundation connections is calculated according to:

$$N_{R,p} = N^0_{R,p} \cdot \frac{A_{p,N}}{A^0_{p,N}} \cdot \psi_{s,Np} \cdot \psi_{g,Np} \cdot \psi_{M,N} \cdot \psi_{cyc,N} \qquad \text{Equation 8.5}$$

where

$N^0_{R,p}$ initial value of the resistance

$$N^0_{R,p} = n \cdot \pi \cdot \phi \cdot \ell_b \cdot \tau_R$$

n number of starter bars per face

$\phi$ nominal diameter of starter bars

$\ell_b$ anchorage length

$\tau_R$ bond strength

$A^0_{p,N}$ reference influence base area of an individual starter bar without the influence of adjoining starter bars and foundation edges, idealising the activated concrete as a prism with an edge length of

$$s_{cr,Np} = 20 \cdot \phi \cdot \left( \frac{\tau_R[\text{MPa}]}{10} \right)^{0.5} = 6.3 \cdot \phi \cdot \sqrt{\tau_R[\text{MPa}]} = 2c_{cr,Np}$$

according to *Eligehausen, R.; Cook, R. et al. (2006)*

$\tau_R$ $\tau_R = \tau_{R,ucr}$ bond strength in uncracked concrete

$A_{p,N}$ actual influence base area, limited by overlapping areas of adjoining starter bars and foundation edges

$\psi_{s,Np}$ factor taking into account the disturbance of the stress distribution due to foundation edges, with the smallest edge distance is considered in

$$\psi_{s,Np} = 0.7 + 0.3 \cdot \frac{c}{c_{cr,Np}} \leq 1.0$$

$\psi_{g,Np}$ factor taking into account the failure surface of starter bar group

$$\psi_{g,Np} = \psi^0_{g,Np} - \left( \frac{s}{s_{cr,Np}} \right)^{0.5} \cdot \left( \psi^0_{g,Np} - 1 \right) \geq 1.0$$

$$\psi^0_{g,Np} = 0.5n + 0.5 - (0.5n - 0.5) \cdot \left( \frac{\tau_R}{\tau_{R,c}} \right)^{1.5} \begin{cases} \geq 1.0 \\ \leq n \end{cases}$$

according to *Herzog, M. (2010)* for linear arranged bonded starter bars

$\tau_R$ $\tau_R = \tau_{R,cr}$ bond strength in cracked concrete

$$\tau_{R,c} = \frac{k}{\pi \cdot \phi} \sqrt{\ell_b[\text{mm}] \cdot f_c[\text{MPa}]}$$

k $k = k_{cr} = 10.2$ for applications in cracked concrete to be assumed for column-to-foundation connections

$f_c$ concrete cylinder strength derived from material tests (Section 6.2.1.2)

n number of starter bars

s spacing, in case of multiple spacings the mean value of the spacings should be used.

The background of above given equations is provided in *Eligehausen, R.; Mallée, R. et al. (2006)* and *Eligehausen, R.; Cook, R. et al. (2006)*. The equation for the upper limit of bond strength $\tau_{R,c}$ that can be utilised without exceeding the concrete breakout strength was developed by equating Equation 2.16 with Equation 2.17. The factors given in the following are based on the findings described in Section 8.1.1 and Section 8.1.2.

$\psi_{M,N}$ factor taking into account the beneficial effect of moment loading on the capacity of column-to-foundation connections (for any load case)

$$\psi_{M,N} = 2.5 - \frac{z}{\ell_b} \geq 1.0$$

$\psi_{cyc,N}$ factor taking into account the adverse effect of cyclic loading on the capacity of column-to-foundation connections (for seismic load case)

$$\psi_{cyc,N} = 0.9\left(1 + \frac{\ell_b}{200\phi}\right) \leq 1.0$$

Figure 8.10 shows the idealised area $A_{p,N}$ for linear arranged starter bar anchorages of column-to-foundation connections. The pullout capacity is not relevant for column-to-foundation connections in which starter bars are detailed with hooks as the mechanical interlock of the hook prevents the pullout.

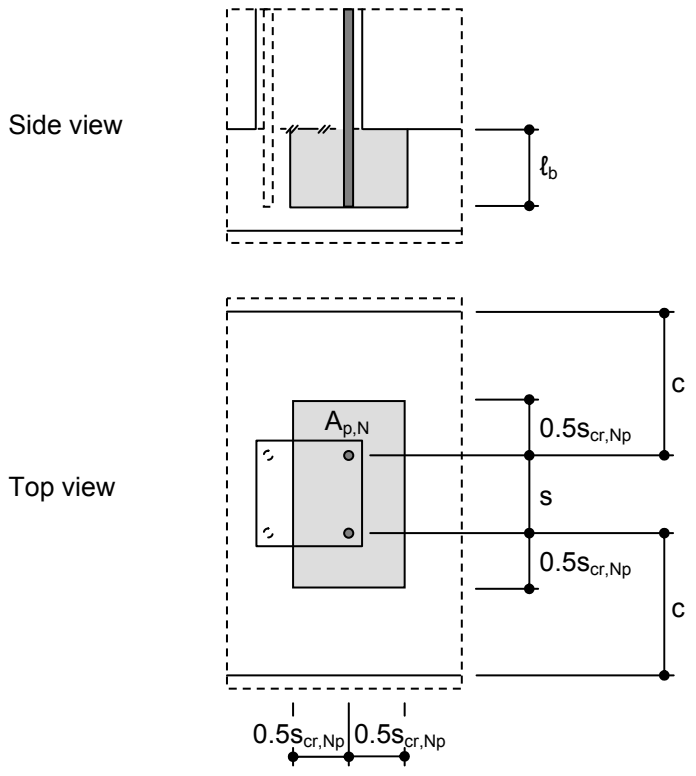


Figure 8.10 Idealised area $A_{p,N}$ for linear arranged starter bar anchorages of column-to-foundation connections

According to *Herzog, M. (2010)*, cracked concrete is assumed for starter bar anchorages of column-to-foundation connections. Based on the discussion presented in Section 2.2.11, $\tau_{R,cr}$ for cracked concrete is taken as $0.5\tau_u$ derived from the bond tests carried out using the tested specimens. The bond tests were conducted without influence of confinement and are described in Section 6.2.1.3. Regarding the factor $\psi_{N,cyc}$, reference is made to the discussion on the bidirectional loading in Section 9.2.4.

### 8.2.2 Capacity according to conventional anchorage model

As discussed in Section 2.3.1.1, the conventional anchorage design approach according to *Eurocode 2 (2005)* defines required anchorage lengths $\ell_{b,rqd}$ on the basis of *design* bond strengths $f_{bd}$. For anchorage lengths $\ell_b$ smaller than the required anchorage lengths $\ell_{b,rqd}$, the design tension stress has to be reduced below the design yield strength by the ratio of $\ell_b$ / $\ell_{b,rqd}$.

To compare the ultimate capacity calculated according enhanced bonded anchor design approach and according to the conventional anchorage design approach on the basis of mean strength values, the following differentiation became necessary for the conventional anchorage design approach:

- Yielding capacity (mode Y): The reinforcing bar yields. The yielding capacity of the bar with a stressed cross section $A_s$ is based on the yield strength:
  $N_{R,y} = A_s \cdot f_y$ Equation 8.6
- Pullout capacity (mode P): The bond fails and the bar is pulled out. The pullout capacity is based on the uniform bond design model:
  $N_{R,p} = \pi \cdot \phi \cdot \ell_b \cdot f_b / (\alpha_1 \cdot \alpha_2)$ Equation 8.7

The background of the conventional anchorage design including the definition of the coefficients $\alpha_1$ and $\alpha_2$ taking into account the effect of the anchorage form (with or without hook) and the confinement (concrete cover) is given in Section 2.3.1.1. For starter bar anchorages of column-to-foundation connections, half of the clear spacing between adjacent bars a / 2 is generally smaller than the concrete covers c and $c_1$, therefore, the equations given in Table 8.2 of *Eurocode 2 (2005)* for $\alpha_1$ and $\alpha_2$ are simplified to:

$$\alpha_1 = \begin{cases} 1.0 & \text{for anchorages without hooks} \\ 0.7 & \text{for anchorages with hooks} \end{cases}$$

$$\alpha_2 = \begin{cases} 1 - 0.15\,((a / 2 - \phi) / \phi & \text{for anchorages without hooks} \\ 1 - 0.15\,((a / 2 - 3\phi) / \phi & \text{for anchorages with hooks} \end{cases}$$

According to the consideratons presented later in Section 9.1, the bond strength analogous to *Eurocode 2 (2005)* is estimated on the basis of design bond strength $f_b = f_{bk} / 0.75 = f_{bd} \cdot \gamma_c / 0.75$. In order to consider the actual strengths of the tested specimens, the design bond strengths are determined on the basis of the tested concrete compressive strengths $f_c$. As a common approach it is assumed for the experimental tests that the tested mean concrete strength $f_{c,mean}$ is equivalent to the characteristic concrete strength $f_{ck}$ in the context of the properties defined in Table 3.1 of *Eurocode 2 (2005)* which is justified by the good testing conditions in the test laboratories. The same was assumed for the steel yield strength $f_{y,mean}$ and $f_{yk}$. The procedure is illustrated step by step in Figure 8.11. For the evaluation of numerical tests, the defined concrete compressive strength $f_c$ and steel yield strength $f_y$ was taken as $f_{ck}$ and $f_{yk}$, respectively.

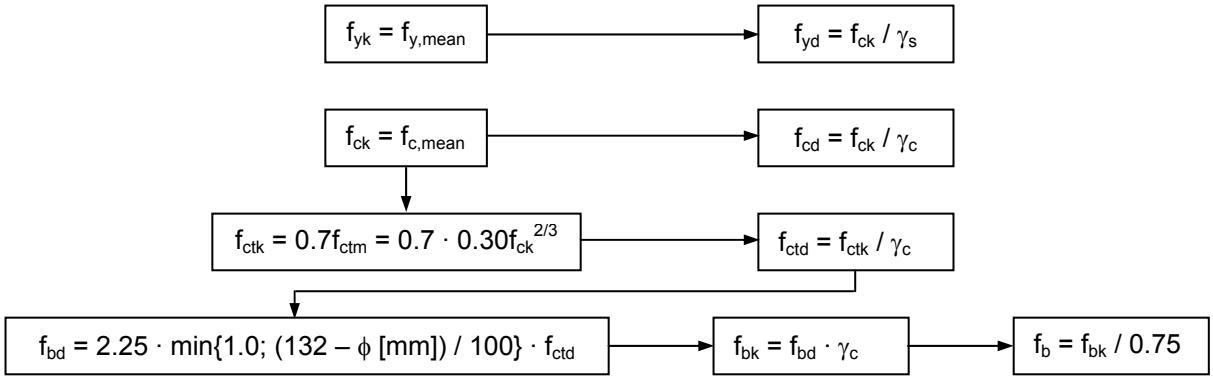


Figure 8.11 Procedure to determine bond strength $f_b$ on the basis of concrete strength $f_c$ analogous to Eurocode 2 (2005)

The material safety factors for steel and concrete, $\gamma_s$ and $\gamma_c$, given in the national annexes of the *Eurocode 2 (2005)* and *Eurocode 8 (2006)*, i.e. *Eurocode 2 / NA (2009)* and *Eurocode 8 / NA (2009)* were used as follows:

$$\gamma_c = \begin{cases} 1.5 \text{ for fundamental load case (monotonically loaded specimens)} \\ 1.3 \quad \text{for seismic load case (cyclically loaded specimens)} \end{cases}$$

$$\gamma_s = \begin{cases} 1.15 \text{ for fundamental load case (monotonically loaded specimens)} \\ 1.0 \quad \text{for seismic load case (cyclically loaded specimens)} \end{cases}$$

The derived strengths are summarised in Table D.5 and Table D.6 of Appendix D: Column-to-Foundation Connection Test Data.

### 8.2.3 Validation of enhanced bonded anchor model

In the following, the validity of the enhanced bonded anchor model is verified and compared to the conventional anchorage model. For this reason, the experimentally or numerically tested column-to-foundation connection capacities ($expM_R$ and $numM_R$), each equalling either the yield capacity $M_{R,y}$ or the minimum of pullout and concrete breakout capacity $M_{R,p/c}$ (Figure 6.17), are compared to the capacities $calM_R = N_R \cdot z$ which are calculated according to

- the current bonded anchor model, where $N_R$ was determined without taking into account the factors $\psi_{cyc,N}$ and $\psi_{M,N}$,
- the enhanced bonded anchor model, where $N_R$ was determined taking into account the factors $\psi_{cyc,N}$ and $\psi_{M,N}$ as shown in Section 8.2.1, and
- the enhanced bonded anchor model, where $N_R$ was determined taking into account the factors $\psi_{cyc,N}$ only for the calculation of the pullout capacity (mode P) and $\psi_{M,N}$ only for the calculation of the concrete breakout capacity (mode C).

Furthermore, the experimentally or numerically tested column-to-foundation connection capacities ($expM_R$ and $numM_R$) are compared to the capacities $calM_R = N_R \cdot z$ which are calculated according to

- the conventional anchorage model, where $N_R$ was determined on the basis of the *Eurocode 2 (2005)* (Section 8.2.2).

Analyses presented in *Mahrenholtz, C. (2012a)* allow the simplifying estimate of z as the centre-to-centre distance of the starter bars (Figure 6.7). As pointed out in Section 8.2.1, the material strengths tested and defined for the experimental and numerical studies, respectively, were used for the validation. The tested and defined concrete strengths $f_c$, yield strengths $f_y$, and bond strengths $\tau_u$ are given in Table D.1 and Table D.2 of Appendix D: Column-to-Foundation Connection Test Data.

Figure 8.12 shows the legend which is used for the following diagrams showing the comparison of mean column-to-foundation connection capacities tested and calculated according to the current bonded anchor model, enhanced bonded anchor model, and conventional anchorage model as well as the corresponding statistical distribution of the ratios of tested and calculated mean connection capacities.

| Anchorage detailing | Installation method | Monotonic | | Cyclic | |
|---|---|---|---|---|---|
| | | experimental | numerical | experimental | numerical |
| without hook | cast-in-place | □ | ■ | □ | ■ |
| with hook | cast-in-place | ○ | ● | ○ | ● |
| | post-installed | △ | ▲ | △ | ▲ |

Figure 8.12 Legend for diagrams

The diagrams of Figure 8.13a and Figure 8.14a show that the enhanced bonded anchor model predicts the capacities of column-to-foundation connections more realistically than the bonded anchor model without considering the beneficial effect of moment loading and the adverse effect of cyclic loading on the capacity. Furthermore, taking into account the penetration of yielding and debonding does not improve the accuracy of the predicted capacity. Therefore, the approach without taking into account the strain penetration is proposed as the enhanced bonded anchor model to be used for column-to-foundation connections.

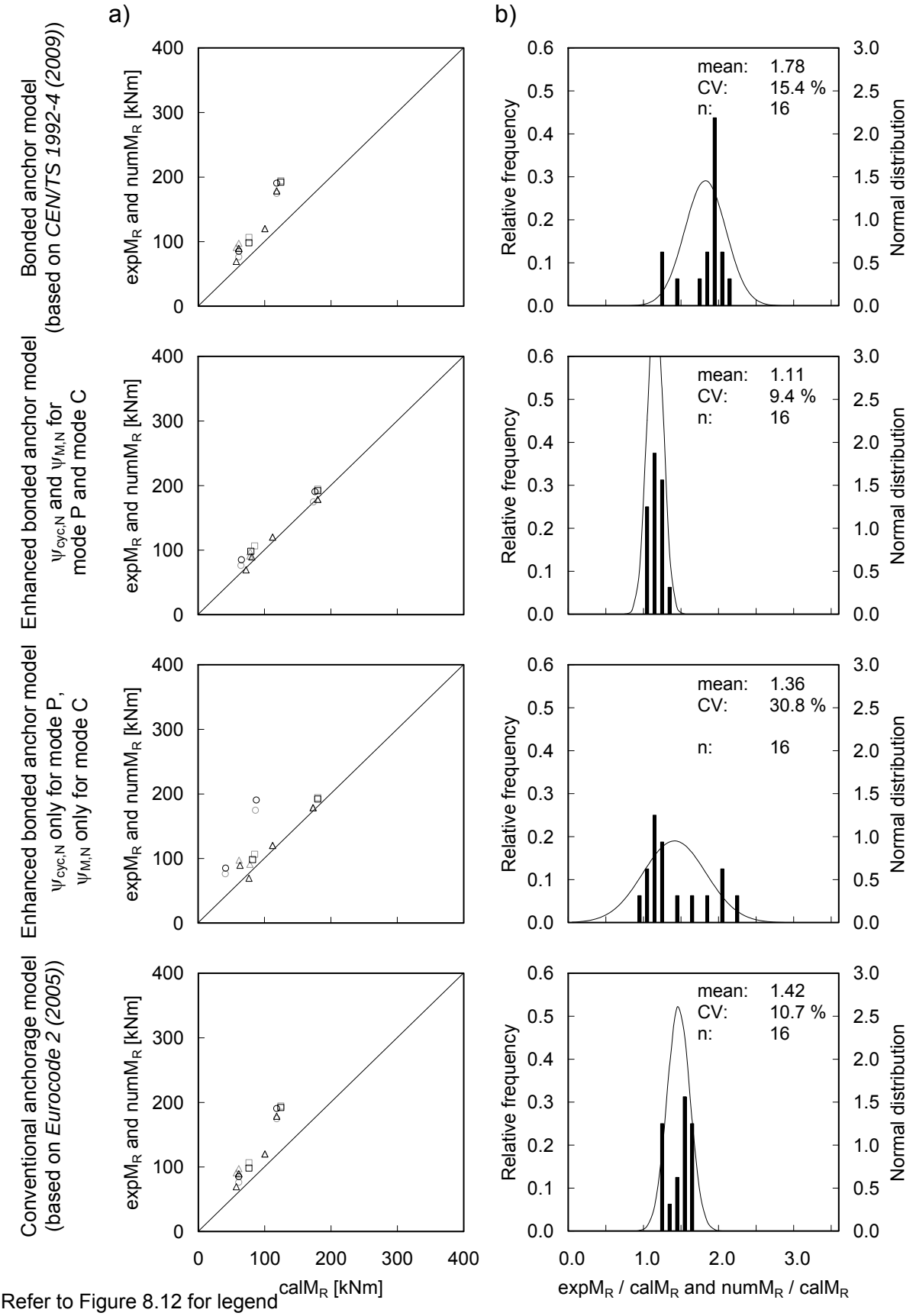


Refer to Figure 8.12 for legend

Figure 8.13 Mean column-to-foundation connection capacities: a) Comparison of capacities experimentally tested and calculated; b) Corresponding statistical distribution of the ratios of experimentally tested and calculated capacities

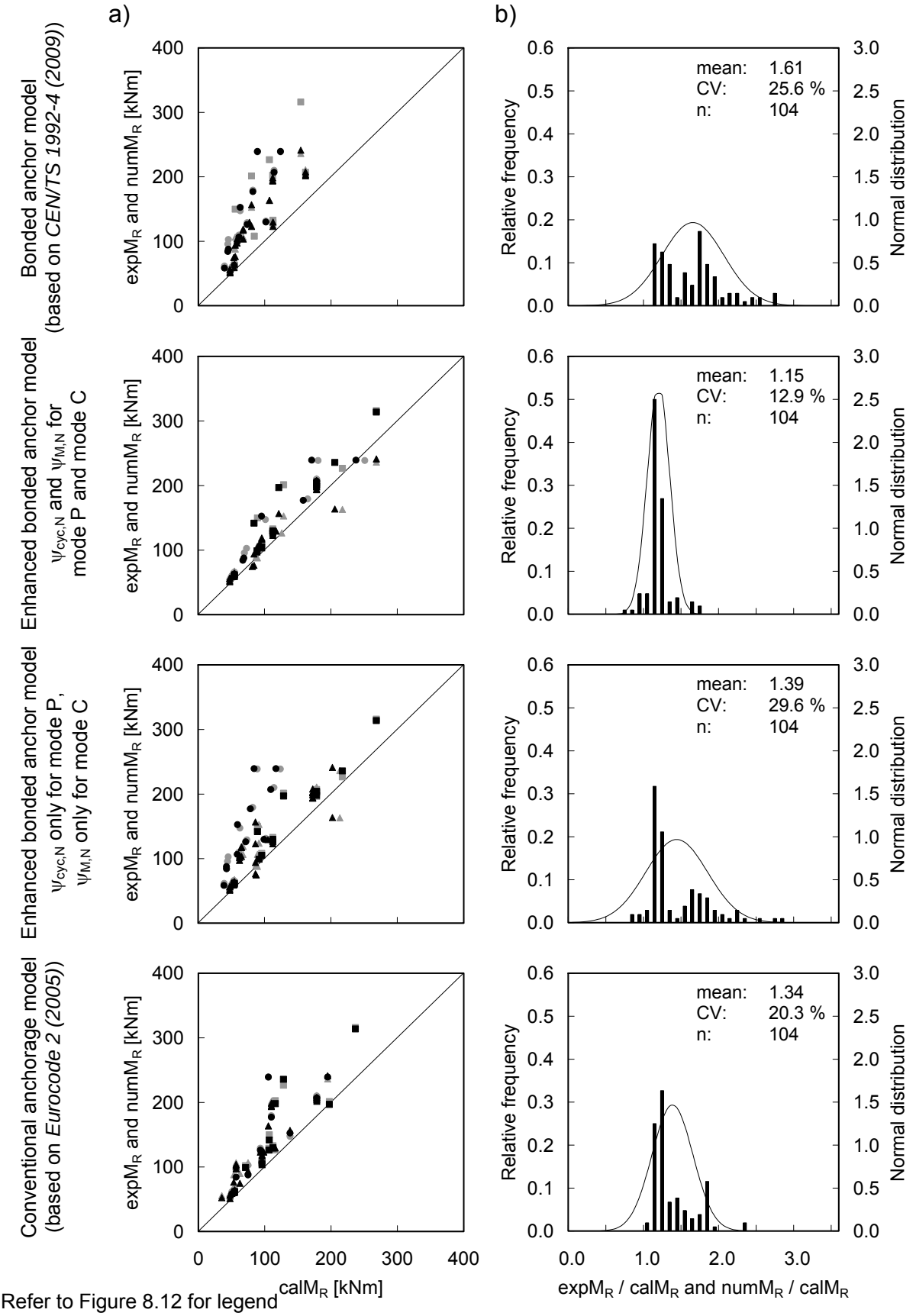


Refer to Figure 8.12 for legend

Figure 8.14 Mean column-to-foundation connection capacities: a) Comparison of capacities numerically tested and calculated; b) Corresponding statistical distribution of the ratios of numerically tested and calculated capacities

The statistical distribution of the ratio of tested and calculated column-to-foundation connection capacities is given in Figure 8.13b and Figure 8.14b. The smallest coefficient of variation (CV) is achieved for the enhanced bonded anchor model taking into account both factors $\psi_{cyc,n}$ and $\psi_{M,N}$ for the pullout mode and concrete breakout mode. Furthermore, a CV below 15 % is generally understood as a verification of a structural model in the context of reinforced concrete design. Therefore, the CV of 13 % underlines the soundness of the suggested enhanced bonded anchor model disregarding the penetration of yielding and debonding.

Table 8.1 compares the frequency of appearance of the failure mode determined by experimental or numerical tests and the predicted failure mode according to the calculation of capacities based on mean material strengths. It is evident that the accuracy in terms of the correct failure mode prediction is higher for the enhanced bonded anchor model if compared to the conventional anchorage model.

Table 8.1 Frequency of appearance of tested failure mode and predicted failure mode, calculated on the basis of mean strengths

| Tested failure mode | Predicted failure mode | Enhanced bonded anchor model | | Conventional anchorage model | |
|---|---|---|---|---|---|
| | | Experimental | Numerical | Experimental | Numerical |
| Y | Y | 8 | 56 | – | 34 |
| P/C | Y | – | 14 | – | 4 |
| Y | P/C | 3 | 2 | 11 | 24 |
| P/C | P/C | 5 | 32 | 5 | 42 |

Also Figure 8.15 and Figure 8.16 demonstrate that the influence of various parameters are better captured by the proposed enhanced bonded anchor model if compared to the conventional anchorage model. In Figure 8.15, the ratios of the experimentally tested column-to-foundation connection capacities $expM_R$ and calculated capacities $calM_R$ applying the enhanced bonded anchor model (Figure 8.15a) and conventional anchorage model (Figure 8.15b) are plotted as a function of various parameters $\ell_b / \phi$, $z / \ell_b$, $\rho / \rho_{min}$, and $f_{ck}$. Figure 8.16 shows the same diagrams using numerically tested column-to-foundation connection capacities $numM_R$. Figure 8.15 and Figure 8.16 also show the least square fit trend line. The influence of the particular parameter is well taken into account if the trend line is constant and close to $expM_R / calM_R = 1.0$ or $numM_R / calM_R = 1.0$.

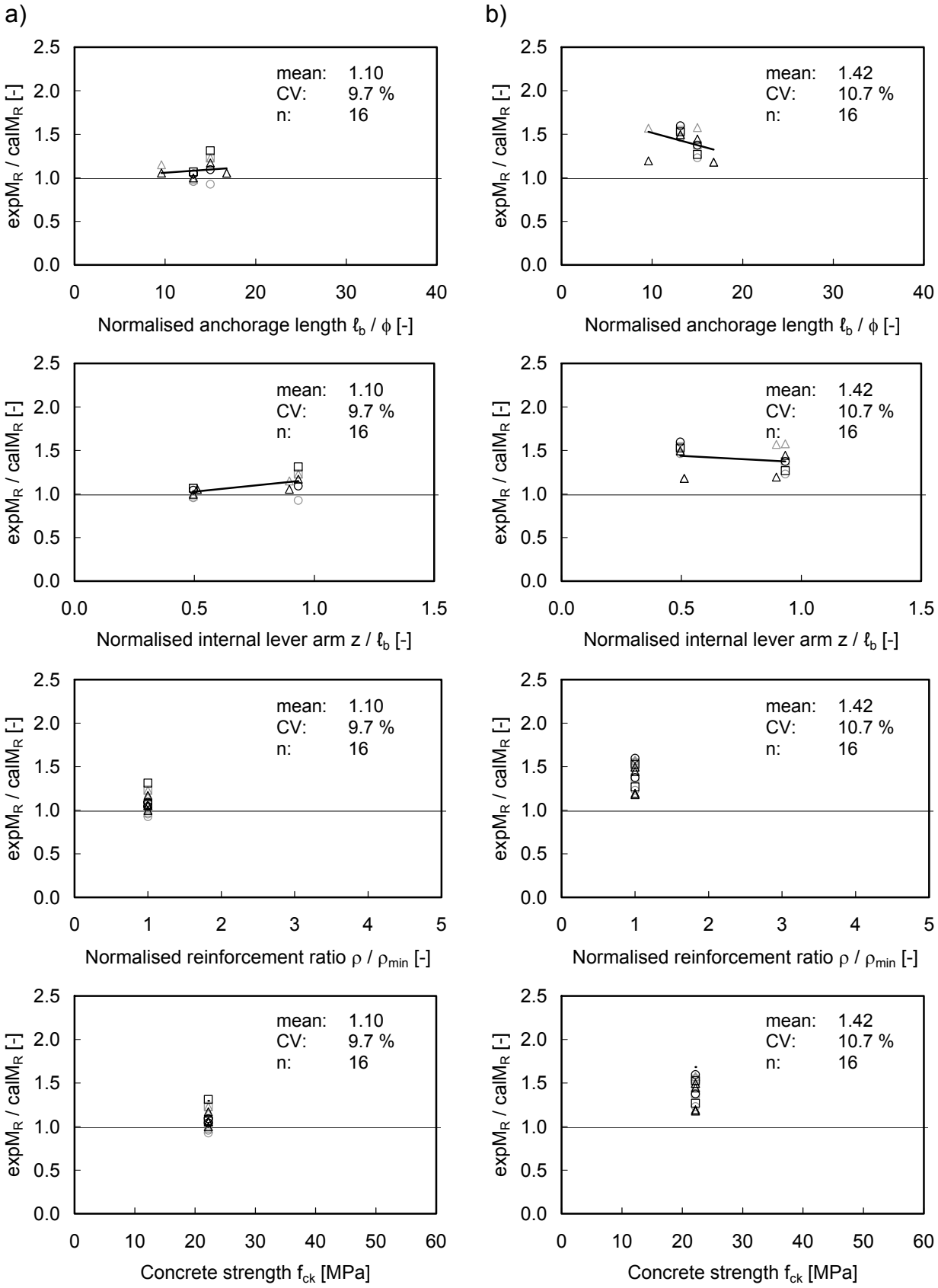


Refer to Figure 8.12 for legend

Figure 8.15 Ratios of experimentally tested column-to-foundation connection capacities and calculated capacities applying the a) enhanced bonded anchor model and b) conventional anchorage model as a function of $\ell_b / \phi$, $z / \ell_b$, $\rho / \rho_{min}$, and $f_{ck}$

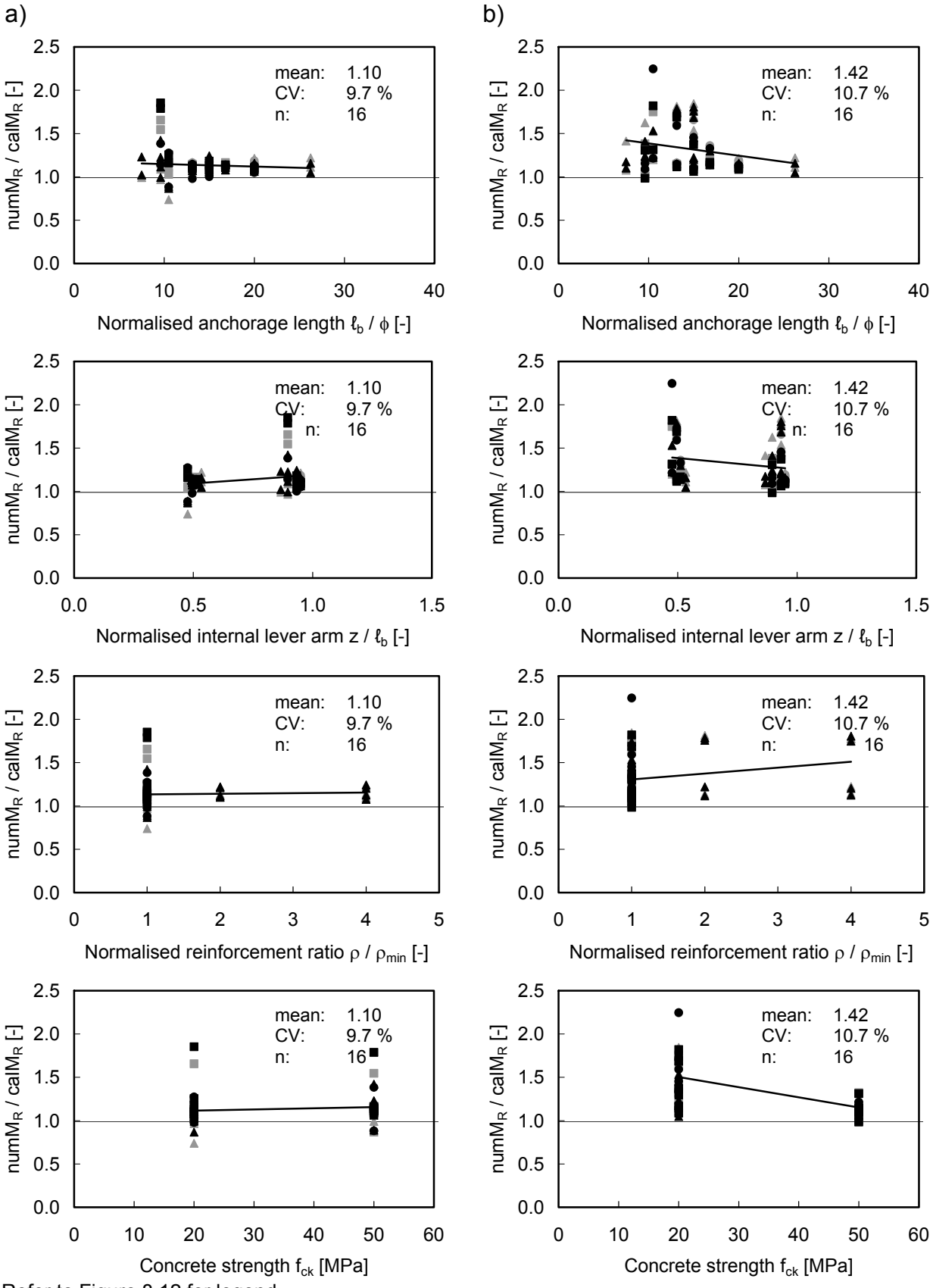


Refer to Figure 8.12 for legend

Figure 8.16 Ratios of numerically tested column-to-foundation connection capacities and calculated capacities applying the a) enhanced bonded anchor model and b) conventional anchorage model as a function of $\ell_b / \phi$, $z / \ell_b$, $\rho / \rho_{min}$, and $f_{ck}$

In summary, the column-to-foundation connection capacity is accurately predicted if calculated on the basis of the proposed enhanced bonded anchor model. Only the actual capacity of connections detailed with hooks is significantly underestimated which gives evidence that the advanced approach could be further improved. For this purpose, the increased concrete breakout capacity anchorages with hooks could be taken into account by an additional factor. However, this further enhancement appears to be unnecessary, since the proposed enhanced bonded anchor model was mainly developed for column-to-foundation connection anchorages without hooks.

The compiled data of calculated mean capacities and corresponding failure modes for experimentally and numerically tested column-to-foundation connections are given in Table D.7 and Table D.8, respectively, of Appendix D: Column-to-Foundation Connection Test Data.

## 8.3 Summary and Conclusions

Based on experimental and numerical test data covering a meaningful parametric range, equations to define factors accounting for the beneficial effect of moment loading and the adverse effect of cyclic loading are proposed. Particular focus was put on the simplicity of the equations since the main objective of this thesis is to provide a practicable design concept which can be easily adapted by practitioners.

The factors taking into account beneficial and adverse effects allowed enhancing the bonded anchor model. The proposed enhanced bonded anchor model was validated by comparing tested connection capacities and connection capacities calculated on the basis of the enhanced bonded anchor model. The accurate prediction of the column-to-foundation connection capacities was demonstrated. The ratio of tested connection capacities and capacities calculated according to the enhanced bonded anchor model showed a remarkably low scatter. The influence of the various parameters were captured, allowing a realistic prediction of the connection capacities. Only the capacity of column-to-foundation connections detailed with hooked anchorages were underestimated. This can be explained by the activation of larger concrete parts if compared to anchorages without hooks which remains unconsidered in the proposed enhanced bonded anchor model.

The enhanced bonded anchor model serves as the basis for the design concept for cast-in-place and post-installed column-to-foundation connections introduced in the following chapter.

# 9 Design Concept for Column-to-Foundation Connections

First, the conceptual approach of designing in accordance with the Eurocode suite is briefly explained in Section 9.1. The concept to design column-to-foundation connection anchorages on the basis of enhanced bonded anchor design provisions and the suitability of post-installation systems for seismic applications is discussed in Section 9.2. The flowchart of the complete design concept is shown in Section 9.3 which may be used as a guideline for the design of column-to-foundation connections on the basis of enhanced bonded anchor design provisions, potentially allowing shortened anchorage lengths without hooks. Summary and conclusion is provided in Section 9.4.

## 9.1 Introduction of the Safety Concept for Designing

### 9.1.1 General safety concept of partial safety factors

The European civil engineering design codes (Eurocode suite) use the safety concept of partial safety factors (PSF), in the US also known as load and resistance factor design (LRFD), to consider aspects of scatter and safety. Figure 9.1 illustrates the relationship of load and resistance as a general probabilistic consideration. The y-coordinate represents the frequency of occurrence and the x-coordinate the strength.

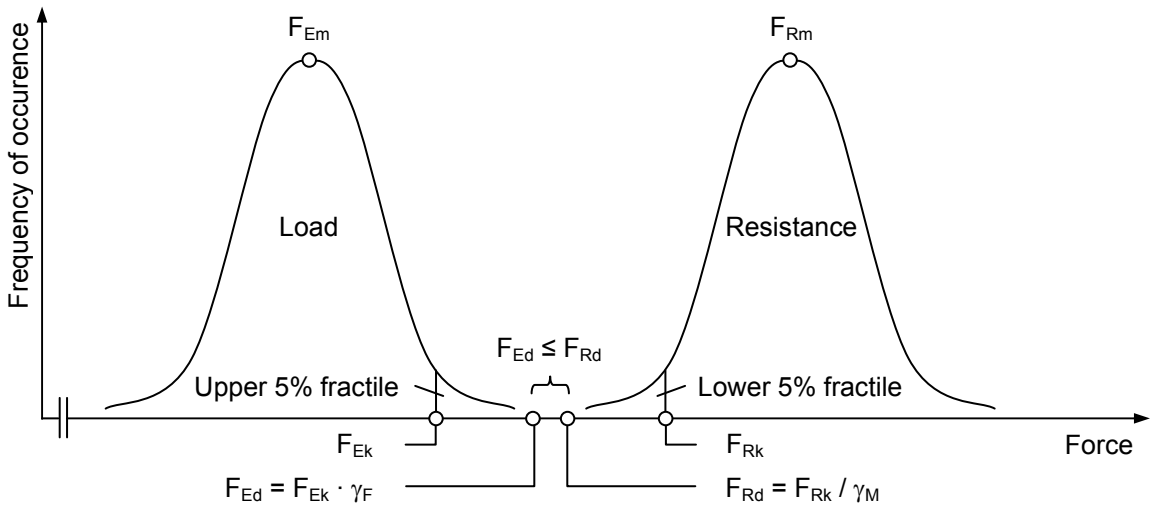


Figure 9.1 General probabilistic consideration of load and resistance as a frequency distribution

The actual resistance $F_{Rm}$ is taken as the tested arithmetic mean:

$$F_{Rm} = \frac{1}{n}\sum_{i=1}^{n} F_{Ri} \qquad \text{Equation 9.1}$$

In civil engineering, it is common to define characteristic strengths $F_{Rk}$ as the lower 5 % fractile

$$F_{Rk} = F_{R,5\%} = F_{R,0.05} = F_{Rm}(1 - k \cdot CV) \qquad \text{Equation 9.2}$$

where factor k can be found in tables (e.g. *Wesche, K. (1973)*) and CV is the coefficient of variation (CV = $\sigma$ / $\mu$). Mostly, a normal distribution is assumed and 75 % is typically used as the coefficient of confidence in the context of reinforced concrete (*Eurocode 0 (2002)*), whereas anchorages are evaluated assuming 90 % as the coefficient of confidence (*ETAG 001 (2006)*).

The basis of the partial safety factor design approach is that the design load $F_{Ed}$ has to be smaller or equal to the design resistance $F_{Rd}$:

$$F_{Ed} \leq F_{Rd} \qquad \text{Equation 9.3}$$

The maximum allowable design load is derived by multiplying the characteristic load $F_{Ek}$ by the safety factor $\gamma_F$ and the design resistance by dividing the characteristic resistance $F_{Rk}$ by the material safety factor $\gamma_M$:

$$(F_{Ed} = F_{Ek} \cdot \gamma_F) \leq (F_{Rk} / \gamma_M = F_{Rd}) \qquad \text{Equation 9.4}$$

Further details with respect to stochastic evaluation within the scope of structural engineering can be found e.g. in *Fischer, L. (1995)* and *Zehn, M. (2007)*. The load safety factor for most seismic load cases equals $\gamma_F$ = 1.0. For fundamental load cases, the load safety factor is often estimated by an averaged factor of $\gamma_F$ = 1.4. The definition of the material safety factors for anchorages designed according to *CEN/TS 1992-4 (2009)* can be found in Appendix B: Bonded Anchor Design.

### 9.1.2 Safety concept for seismic anchorages

#### 9.1.2.1 Conservatism for brittle failure

*CEN/TS 1992-4 (2009)* stipulates the general seismic strength reduction factor of $\alpha_{eq}$ = 0.75 as a multiplyer for the design capacity corresponding to concrete related, i.e. brittle failure modes (Clause 8.4.2). This factor is often referred to as ‘seismic factor’ and is intended to provide additional conservatism for seismic load cases to cover adverse seismic influences on the capacity of the anchorage which are still under investigation. Details are given in Section B.1.1 of Appendix B: Bonded Anchor Design.

### 9.1.2.2 Ensurement of ductile failure

In particular in the context of seismic engineering, the brittle failure mode P/C is deemed to be unacceptable (Figure 9.2a). Therefore, an important design goal in seismic engineering is that the ductile failure mode Y is governing (Figure 9.2b). Consequently, a margin of safety between the two failure modes is essential. Since material strengths scatter, the margin of safety between mode Y and mode P/C determines the probability of their occurrence.

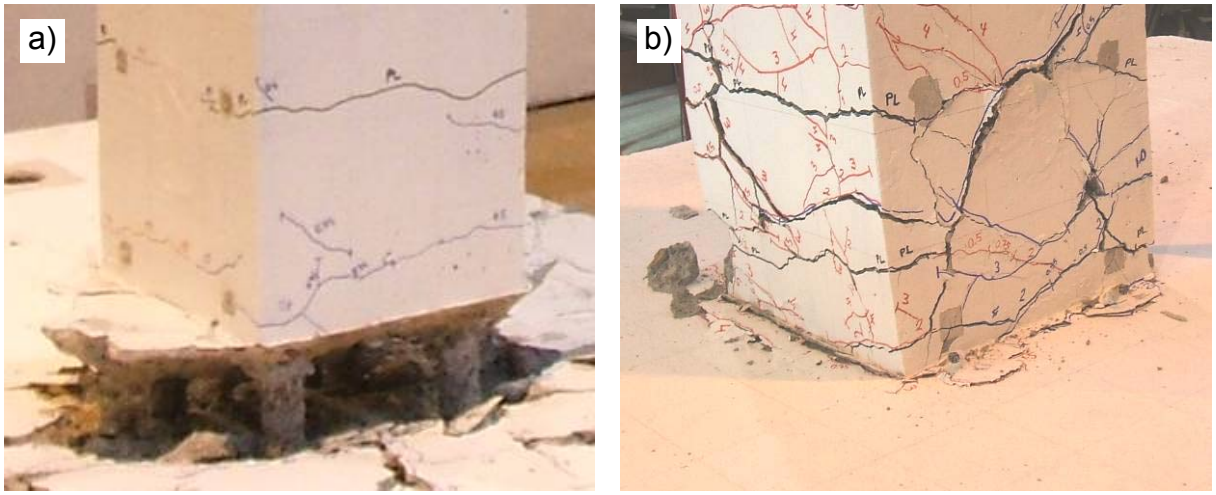


Figure 9.2 a) Brittle failure mode P/C: Structural disintegration of Specimen 4;
b) Ductile failure mode Y: Plastic hinging of Specimen 8

The study presented in *Hoehler, M. (2006)* is instructive for the understanding of the evaluation of the test data in respect to reliable ductile failure. *Hoehler, M. (2006)* studied the probability of the governing failure mode for anchors based on a method formulated by *Cornell, A. (1967)*. The ductile steel failure (index 's') and the brittle concrete failure (index 'c') were considered. The mean failure loads $\mu_m$, its standard deviation $\sigma_m$, the safety index $\beta$, and the probability of failure $p_f$ were defined as follows:

$$\mu_m = \mu_c - \mu_s \qquad \text{Equation 9.5}$$

$$\sigma_m = \sqrt{\sigma_c{}^2 + \sigma_s{}^2} \qquad \text{Equation 9.6}$$

$$\beta = \frac{\mu_m}{\sigma_m} \qquad \text{Equation 9.7}$$

$$p_f = \int_{-\infty}^{-\beta} \frac{1}{\sqrt{2\pi}} \cdot \exp\left(-\frac{1}{2}x^2\right) dx \qquad \text{Equation 9.8}$$

Further, it was assumed that the analytical models (Section 2.3.1.2) can predict the mean failure loads for steel and concrete failure accurately (neglecting model uncertainty) and that all variables are normally distributed. If no margin of safety between the failure modes is prescribed, i.e. $\beta = 0$, both failure modes are equally likely. To ensure that the ductile failure mode is more likely than the brittle failure mode, a safety index $\beta > 1$ is required. The schematic representation of the method is shown in Figure 9.3.

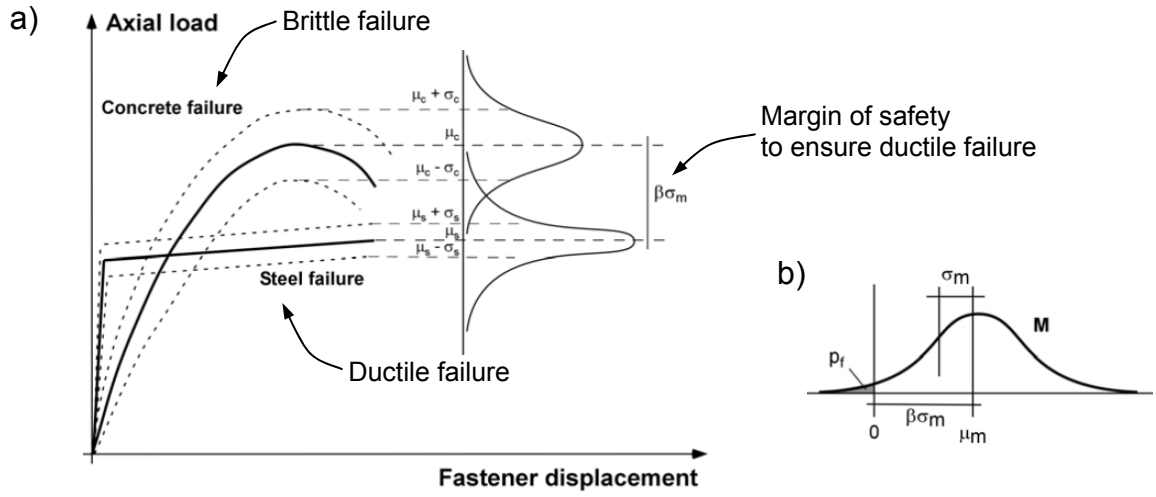


Figure 9.3 Schematic representation of the method used to determine the probability of brittle failure: a) Distributions of the normalised variables; b) Probability density function for the margin of safety (*Hoehler, M. (2006)*)

The method was used to study the probability of failure modes numerically. For steel failure mode a scatter of 5 % and an overstrength factor of 1.10 was assumed and for concrete failure mode a scatter of 15 % and a conservative understrength factor of 0.85. The numerical study allowed determining the relationship between the ratio of failure loads (anchorage capacities) and failure mode probabilities. *Hoehler, M. (2006)* concluded that the following ratio is required to reduce the probability of a brittle failure to 1 % which was tentatively taken as a minimum requirement:

$$N_{Rd,s} \leq 0.7 N_{Rd,c} \qquad \text{Equation 9.9}$$

The requirement of ductile failure for seismic load cases is also stipulated in *CEN/TS 1992-4 (2009)* (Clause 8.4.3) where all brittle failure modes are taken into account, e.g. pullout and concrete breakout. The ratio of the failure loads is described by a slightly different factor, i.e. 0.6 instead of 0.7, because the design provision is based on the characteristic values which also allows the consideration of the partial factor $\gamma_{inst}$. Details are given in Section B.1.1 of Appendix B: Bonded Anchor Design.

### 9.1.3 Suitability of Post-installation System for Seismic Applications

The system used for the post-installation of column starter bars in the foundation has to be qualified for seismic applications. Since the design concept is based on the bonded anchor design provisions, the technical approval for bonded anchors according to the approval guideline *ETAG 001 (2006)* is required (Section 2.3.1.2). The seismic amendment of *ETAG 001 (2006)* is currently under preparation (*Proposal for ETAG 001 Seismic Amendment (2012)*). In addition, the technical approval for post-installed reinforcing bars according to *EOTA TR 023 (2006)* is needed (Section 2.3.1.1) to show that the post-installed reinforcing bars develop bond characteristics similar to cast-in-place reinforcing bars. This requirement ensures that the proposed design concept is valid for any post-installed reinforcing bars for which performance is at least equivalent to cast-in-place reinforcing bars. The equivalence, however, has to be shown also for seismic loading. Therefore, *EOTA TR 023 (2006)* has to be amended accordingly. For the time being, simultaneous load and crack cycling tests as presented in Chapter 4 would serve the purpose.

## 9.2 Proposed design concept for column-to-foundation connections

### 9.2.1 Capacity according to enhanced bonded anchor design provisions

The enhanced bonded anchor model provides the basis for the design concept of column-to-foundation connections which is proposed as an alternative approach to the conventional anchorage design (Section 2.3.1.1). To demonstrate compliance with the safety concept of PSF and thus to ensure conservative predictions of capacities, the adaption of the enhanced bonded anchor model as design provisions is verified in Section 9.2.3 by comparing tested and calculated characteristic capacities.

The equations given in the following Section 9.2.1.1, Section 9.2.1.2, and Section 9.2.1.3 to calculate the characteristic yield, concrete breakout, and pullout capacity, respectively, represent the enhanced bonded anchor design provisions which are proposed as an addendum to the *CEN/TS 1992-4 (2009)*. The proposed factors $\psi_{M,N}$ and $\psi_{cyc,N}$ accounting for the beneficial effect of moment loading and adverse effect cyclic loading on the connection capacity (Section 8.1.1 and Section 8.1.2), respectively, were implemented. The approach is based on the assumption that the post-installation system used is suitable for seismic applications.

In general, the equations given in the following for the calculation of the capacities are given in line with *CEN/TS 1992-4 (2009)*. However, the k factors suitable for concrete compressive strengths derived from 150 mm diameter testing cylinders is applied to comply with future revisions of *CEN/TS 1992-4 (2009)* and *Eurocode 2*

*(2005)*. For the sake of clarity, the provisions for the calculation of the characteristic capacities are presented unshortened, though the formulas are partly repetitive to those already discussed in Section 8.2.1.

#### 9.2.1.1 Yield capacity

The yield capacity of anchor groups in the context of a column-to-foundation connection design is calculated based on the total cross section of the starter bars and yield strength:

$$N_{Rk,y} = A_s \cdot f_{yk} \qquad \text{Equation 9.10}$$

where

$A_s$ stressed cross section of steel

$$A_s = n \cdot \pi \cdot \phi^2 / 4$$

- $n$ number of starter bars per face
- $\phi$ nominal diameter of starter bars

$f_{yk}$ characteristic yield strength.

Figure 8.8 shows the cross section $A_s$ for the linear arranged starter bar anchorages of column-to-foundation connections.

#### 9.2.1.2 Concrete breakout capacity

The concrete breakout capacity of column-to-foundation connection starter bar anchorages designed as an anchor group is determined by:

$$N_{Rk,c} = N^0_{Rk,c} \cdot \frac{A_{c,N}}{A^0_{c,N}} \cdot \psi_{s,N} \cdot \psi_{M,N} \cdot \psi_{cyc,N} \qquad \text{Equation 9.11}$$

where

$N^0_{Rk,c}$ initial value of the characteristic resistance

$$N^0_{Rk,c} = k_3 \cdot \sqrt{f_{ck}[\text{MPa}]} \cdot \ell_b[\text{mm}]^{1.5}$$

- $k_3$ $k_3 = k_{cr} = 7.7$ for cracked concrete to be assumed for column-to-foundation connections
- $f_{ck}$ characteristic concrete cylinder strength according to the *Eurocode 2 (2005)*
- $\ell_b$ anchorage length

$A^0_{c,N}$ reference cone base area of an individual starter bar without the influence of adjoining starter bars and foundation edges, idealising the activated concrete as a pyramid with an edge length of

$$s_{cr,N} = 2c_{cr,N} = 3\ell_b$$

$A_{c,N}$ actual cone base area, limited by overlapping areas of adjoining starter bars and foundation edges

$\psi_{s,N}$ factor taking into account the disturbance of the stress distribution due to foundation edges, with the smallest edge distance is considered in

$$\psi_{s,N} = 0.7 + 0.3 \cdot \frac{c}{c_{cr,N}} \leq 1.0$$

$\psi_{M,N}$ factor taking into account the beneficial effect of moment loading on the capacity of column-to-foundation connections (for any load case)

$$\psi_{M,N} = 2.5 - \frac{z}{\ell_b} \geq 1.0$$

$\psi_{cyc,N}$ factor taking into account the adverse effect of cyclic loading on the capacity of column-to-foundation connections (for seismic load case)

$$\psi_{cyc,N} = 0.9\left(1 + \frac{\ell_b}{200\phi}\right) \leq 1.0$$

.

Figure 8.9 shows the idealised area $A_{c,N}$ for linear arranged starter bar anchorages of column-to-foundation connections. Regarding factor $\psi_{N,cyc}$, reference is made to the discussion on the bidirectional loading in Section 9.2.4.

#### 9.2.1.3 Pullout capacity

The pullout capacity of the column-to-foundation connection starter bar anchorages designed as an anchor group is determined by:

$$N_{Rk,p} = N^0_{Rk,p} \cdot \frac{A_{p,N}}{A^0_{p,N}} \cdot \psi_{s,Np} \cdot \psi_{g,Np} \cdot \psi_{M,N} \cdot \psi_{cyc,N} \qquad \text{Equation 9.12}$$

where

$N^0_{Rk,p}$ initial value of the characteristic resistance

$$N^0_{Rk,p} = n \cdot \pi \cdot \phi \cdot \ell_b \cdot \tau_{Rk}$$

n number of starter bars per face

$\phi$ nominal diameter of starter bars

$\ell_b$ anchorage length

$\tau_{Rk}$ characteristic bond strength

$A^0_{p,N}$ reference influence base area of an individual starter bar without the influence of adjoining starter bars and foundation edges, idealising the activated concrete as a prism with an edge length of

$$s_{cr,Np} = 20 \cdot \phi \cdot \left( \frac{\tau_{Rk}[\text{MPa}]}{7.5} \right)^{0.5} = 7.3 \cdot \phi \cdot \sqrt{\tau_{Rk}[\text{MPa}]} = 2c_{cr,Np} \leq 3\ell_b$$

$\tau_{Rk}$ $\tau_{Rk} = \tau_{Rk,ucr}$ characteristic bond strength in uncracked concrete

$A_{p,N}$ actual influence base area, limited by overlapping areas of adjoining starter bars and foundation edges

$\psi_{s,Np}$ factor taking into account the disturbance of the stress distribution due to foundation edges, with the smallest edge distance is considered in

$$\psi_{s,Np} = 0.7 + 0.3 \cdot \frac{c}{c_{cr,Np}} \leq 1.0$$

$\psi_{g,Np}$ factor taking into account the failure surface of starter bar group

$$\psi_{g,Np} = \psi^0_{g,Np} - \left( \frac{s}{s_{cr,Np}} \right)^{0.5} \cdot \left( \psi^0_{g,Np} - 1 \right) \geq 1.0$$

$$\psi^0_{g,Np} = 0.5n + 0.5 - (0.5n - 0.5) \cdot \left( \frac{\tau_{Rk}}{\tau_{Rk,c}} \right)^{1.5} \begin{cases} \geq 1.0 \\ \leq n \end{cases}$$

according to *Herzog, M. (2010)* for linear arranged starter bars

$\tau_{Rk}$ $\tau_{Rk} = \tau_{Rk,cr}$ characteristic bond strength in cracked concrete

$$\tau_{Rk,c} = \frac{k_2}{\pi \cdot \phi} \sqrt{\ell_b[\text{mm}] \cdot f_{ck}[\text{MPa}]}$$

$k_2$ $k_2 = k_{cr} = 7.7$ for cracked concrete to be assumed for column-to-foundation connections

$f_{ck}$ characteristic concrete cylinder strength according to the *Eurocode 2 (2005)*

n number of starter bars

s spacing, in case of multiple spacings the mean value of the spacings should be used

$\psi_{M,N}$ factor taking into account the beneficial effect of moment loading on the capacity of column-to-foundation connections (for any load case)

$$\psi_{M,N} = 2.5 - \frac{z}{\ell_b} \geq 1.0$$

$\psi_{cyc,N}$ factor taking into account the adverse effect of cyclic loading on the capacity of column-to-foundation connections (for seismic load case)

$$\psi_{cyc,N} = 0.9\left(1 + \frac{\ell_b}{200\phi}\right) \leq 1.0$$

.

Figure 8.10 shows the idealised area $A_{p,N}$ for linear arranged starter bar anchorages of column-to-foundation connections. Regarding factor $\psi_{N,cyc}$, reference is made to the discussion on the bidirectional loading in Section 9.2.4.

Since the foundation experiences pronounced cracking which significantly reduces the column starter bar anchorage capacities, the material strengths corresponding to cracked concrete have to be taken into account (*Herzog, M. (2010)*). Therefore, the characteristic bond strength for cracked concrete $\tau_{Rk,cr}$ given in the approval document of the mortar (ETA) for post-installed bonded anchors is used for the capacity calculation of post-installed starter bars according to the proposed enhanced bonded anchor design provisions, where factor $\psi_c$ takes into account the influence of concrete strength:

$$\tau_{Rk,PI} = \tau_{Rk,cr} \cdot \psi_c \qquad \text{Equation 9.13}$$

Similarly for bonded anchors, the installation safety has to be taken into account by means of an installation safety factor when determining the design bond strength of post-installed starter bars:

$$\tau_{Rd,PI} = \tau_{Rk,PI} / (\gamma_c \cdot \gamma_{inst}) \qquad \text{Equation 9.14}$$

Without taking the negligible influence of reinforcing bar diameter into account, the characteristic bond strength according to the approval document (ETA) of the used mortar is 7 MPa. Moreover, the factor $\psi_c$ can be expressed as $0.94 + f_{ck} \cdot 0.09 / 30$ MPa and $\psi_{inst}$ is taken as 1.4. It is noteworthy that the tested bond strengths were approximately $\tau_u = 35.0$ MPa (Section 6.2.1.3) promising a characteristic bond strength much higher than 7 MPa. No apparent reasons such as concrete strength or testing setup can be identified for this discrepancy. Since the characteristic bond strengths were determined by means of assessment tests

(Section 2.3.1.2) which are confidential and unknown to the author, the true reasons can only be guessed and are therefore not discussed here.

In the context of cast-in-place anchorages, the *Eurocode 2 (2005)* does not distinguish between cracked and uncracked concrete and provides only the generally valid design bond strength $f_{bd}$ (Section 2.3.1.1). Furthermore, no approval document is available for 'cast-in-place bonded anchors'. Taking the small crack widths at the moment of the connection failure into account (Table 6.3 and Table 7.7), it is assumed that the bond strength of reinforcing bars analogous to the *Eurocode 2 (2005)* is the equivalent to the bond strength of post-installed bars in cracked concrete according to the approval document. Applying Equation 2.11 and the equations given in Table 3.1 of the *Eurocode 2 (2005)*, the equation $f_{bk} = 2.25 \cdot \eta_1 \cdot \eta_2 \cdot f_{ctd} / \gamma_c = 2.25 \cdot \eta_1 \cdot \eta_2 \cdot 0.7 \cdot 0.30 f_{ck}^{2/3} = \eta_1 \cdot \eta_2 \cdot 0.473 f_{ck}^{2/3}$ is deduced to define the characteristic bond strength. For the capacity calculation of cast-in-place starter bars according to the proposed enhanced bonded anchor design provisions, the characteristic bond strength is therefore taken as:

$$\tau_{Rk,CI} = f_{bk} = (132 - \phi\,[\text{mm}]) / 100 \cdot 0.473 f_{ck}^{2/3} \qquad \text{Equation 9.15}$$

The relationship between characteristic and design bond strengths of cast-in-place reinforcing bars according to *Eurocode 2 (2005)* is illustrated in Figure 8.11. The characteristic concrete strength $f_{ck}$ and the characteristic steel yield strength $f_{yk}$ was defined as described in Section 8.2.2.

In contrast to bonded anchors, installation safety has not to be taken into account when calculating the design bond strength cast-in-place starter bars:

$$\tau_{Rd,CI} = \tau_{Rk,CI} / \gamma_M \qquad \text{Equation 9.16}$$

The *CEN/TS 1992-4 (2009)* specifies the material safety factor $\gamma_{Mc}$ to be considered for the concrete breakout capacity on the basis of the material safety factor for concrete $\gamma_c$ given in the Eurocode suite as follows:

$$\gamma_{Mc} = \gamma_c \cdot \gamma_{inst} = \begin{cases} 1.5 \cdot \gamma_{inst} & \text{for fundamental load case (monotonically loaded specimens)} \\ 1.3 \cdot \gamma_{inst} & \text{for seismic load case (cyclically loaded specimens)} \end{cases}$$

For the pullout capacity, the following material safety factor $\gamma_{Mp}$ is suggested:

$$\gamma_{Mp} = \gamma_{Mc}$$

In the context of column-to-foundation design where only the utilisation of yield strength but not the ultimate strength is allowed (Section 2.3.1.2), the material safety factor for steel $\gamma_s$ given in the Eurocode suite is applied as follows:

$$\gamma_{Ms} = \gamma_s = \begin{cases} 1.15 & \text{for fundamental load case (monotonically loaded specimens)} \\ 1.0 & \text{for seismic load case (cyclically loaded specimens)} \end{cases}$$

For further details in regard of partial safety factors, refer to Appendix B: Bonded Anchor Design.

The characteristic material strengths and resulting design material strengths of the experimentally and numerically tested specimens used for the following validation of the enhanced bonded anchor design provisions are summarised in Table D.5 and D.6, respectively, of Appendix D: Column-to-Foundation Connection Test Data.

Clearly, the approach to use the bond strength defined by Equation 9.16 to validate the enhanced bonded anchor design provisions in the following is somewhat tentative, however it leads to reasonable results for cast-in-place column-to-foundation connections as will be shown in Section 9.2.3. The following sections provide the design provisions to determine the yield, concrete breakout and pullout capacities of post-installed and cast-in-place anchorages for column-to-foundation connections.

#### 9.2.1.4 Brittle failure mode

As explained in Section 9.1.2.1, extra conservatism is used for seismic design in regard of the anchorage capacity corresponding to brittle failure modes. The corresponding equation given in Clause 8.4.2 of *CEN/TS 1992-4 (2009)* introduces a 'seismic factor' of $\alpha_{eq} = 0.75$ and can be rewritten for the design of column-to-foundation connection starter bars as follows:

$$N_{Rd,p/c} = 0.75 \cdot \min \begin{cases} \dfrac{N_{Rk,p}}{\gamma_c \cdot \gamma_{inst}} \\ \dfrac{N_{Rk,c}}{\gamma_c} \end{cases} \qquad \text{Equation 9.17}$$

For column-to-foundation connections under seismic loading, however, ductile failure has to be ensured which is addressed in the following section. Therefore, the 'seismic factor' does not play a role in the final design concept for column-to-foundation connection but is only used for the studies presented in Section 9.2.2, e.g. to plot Figure 9.8 and Figure 9.9.

#### 9.2.1.5 Ductile failure mode

As pointed out in Section 9.1.2.1, seismic design of anchorages requires the ensurement of ductile failure behaviour. Rewriting the corresponding equation given in Clause 8.4.3 of *CEN/TS 1992-4 (2009)* for the design of column-to-foundation connection starter bars yields:

$$N_{Rk,s} \leq 0.6 \frac{N_{Rk,p/c}}{\gamma_{inst}}$$ Equation 9.18

The partial factor $\gamma_{inst}$ takes into account the installation safety of the post-installed starter bar and is given in the approval document (ETA) of the post-installation system. For cast-in-place starter bars, the installation factor does not apply or is taken as 1.0. Details on the partial safety factors for post-installed anchorages according to *CEN/TS 1992-4 (2009)* including the installation safety factor $\gamma_{inst}$ can be found in Appendix B: Bonded Anchor Design.

### 9.2.2 Capacity according to conventional anchorage design provisions

As in Section 8.2.3, the tested and calculated characteristic capacities resulting from the proposed enhanced bonded anchor design provisions and the conventional anchorage design provisions are compared in the following Section 9.2.3. To allow a meaningful comparison and as discussed in Section 8.2.2, the following two failure modes are taken into account for the conventional anchorage design provisions:

- Yielding capacity (mode Y): The reinforcing bar yields. The yielding capacity of the bar with a stressed cross section $A_s$ is based on the yield strength:
  $N_{Rk,y} = A_s \cdot f_{yk}$ Equation 9.19
- Pullout capacity (mode P): The bond fails and the bar is pulled out. The pullout capacity is based on the uniform bond design model:
  $N_{Rk,p} = \pi \cdot \phi \cdot \ell_b \cdot f_{bk} / (\alpha_1 \cdot \alpha_2)$ Equation 9.20

The coefficients $\alpha_1$ and $\alpha_2$, the derivation of the bond strength $f_{bk}$ analogous to *Eurocode 2 (2005)*, as well as the safety factors $\gamma_c$ and $\gamma_s$ used to determine the design capacities are explained in Section 8.2.2.

### 9.2.3 Validation of design concept for column-to-foundation connections

According to the safety concept of PSF design (Section 9.1), the proposed design provisions are conservative if for any column-to-foundation anchorage detailing the calculated capacity is smaller than the 5 % fractile value of the tested capacity. For this reason, the experimentally or numerically tested column-to-foundation connection capacity ($expM_R$ and $numM_R$), equalling either the yield capacity $M_{R,y}$ or the minimum of pullout and concrete breakout capacity $M_{R,p/c}$ (Figure 6.17), is compared with the capacity $calM_{Rk} = N_{Rk} \cdot z$ which is calculated according to

- the enhanced bonded anchor design provisions where $N_{Rk}$ was determined considering the factors $\psi_{cyc,N}$ and $\psi_{M,N}$ (Section 8.2.1) and

- the conventional anchorage design provisions, where $N_R$ was determined analogous to *Eurocode 2 (2005)* (Section 8.2.2).

As pointed out in Section 9.2.1, the characteristic material strengths are used for the validation of the proposed design provisions. The characteristic concrete strengths $f_{ck}$, yield strengths $f_{yk}$, and bond strengths $\tau_{Rk}$ are given in Table D.5 and Table D.6 of Appendix D: Column-to-Foundation Connection Test Data.

Figure 9.4 shows the legend used for the following diagrams which show the comparison of characteristic column-to-foundation connection capacities tested and calculated according to the proposed enhanced bonded anchor design provisions and conventional anchorage design provisions as well as the corresponding statistical distribution of the ratios of tested and calculated characteristic connection capacities.

| Anchorage detailing | Installation method | Monotonic | | Cyclic | |
|---|---|---|---|---|---|
| | | experimental | numerical | experimental | numerical |
| without hook | cast-in-place | □ | ■ | □ | ■ |
| with hook | cast-in-place | ○ | ● | ○ | ● |
| | post-installed | △ | ▲ | △ | ▲ |

Figure 9.4 Legend for diagrams

The diagrams of Figure 9.5 and Figure 9.6 show that the characteristic connection capacity is conservatively predicted by the enhanced bonded anchor design provisions.

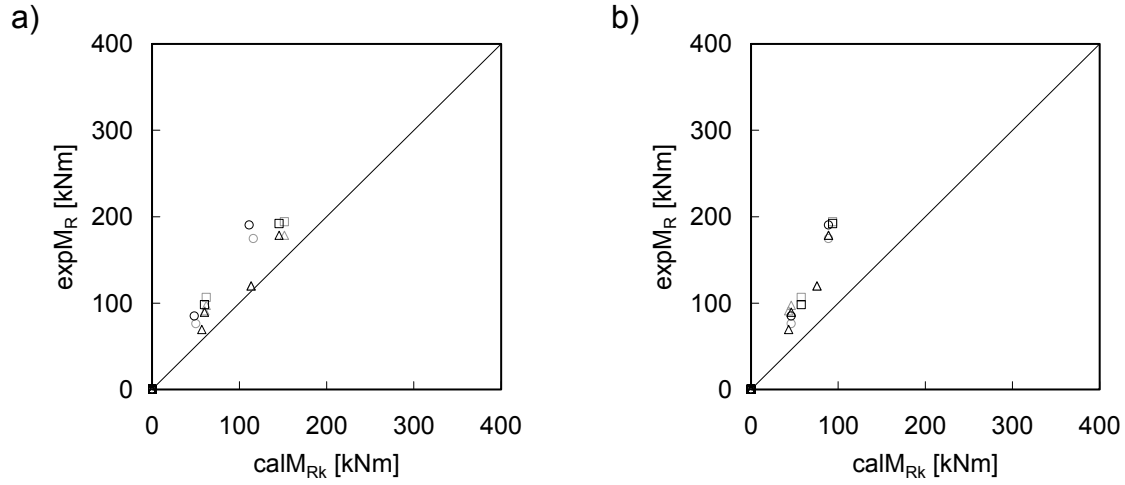


Refer to Figure 9.4 for legend

Figure 9.5 Comparison of experimentally tested and calculated characteristic column-to-foundation connection capacities applying the a) enhanced bonded anchor design provisions (*CEN/TS 1992-4 (2009)* enhanced) and b) conventional anchorage design provisions (*Eurocode 2 (2005)*)

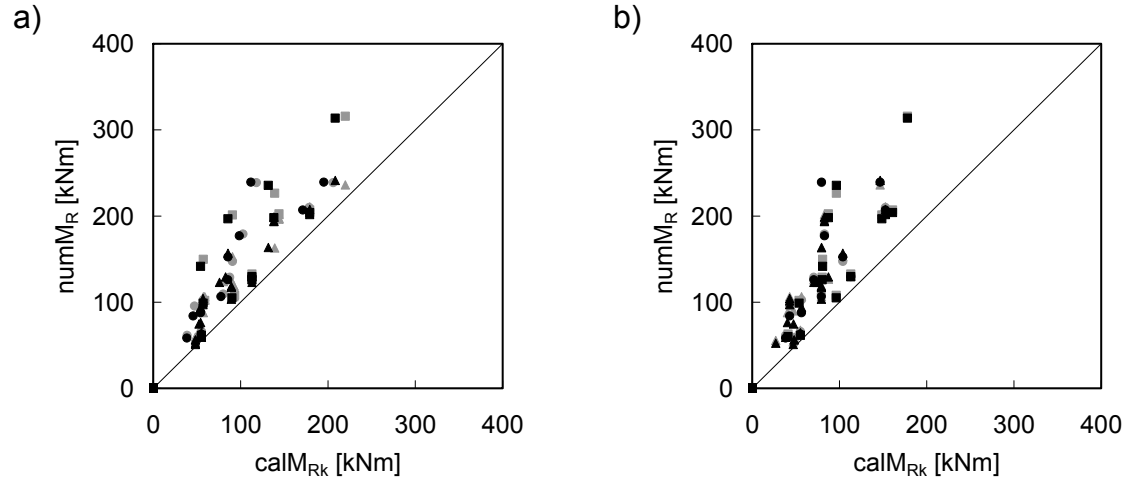


Refer to Figure 9.4 for legend

Figure 9.6 Comparison of numerically tested and calculated characteristic column-to-foundation connection capacities applying the a) enhanced bonded anchor design provisions (*CEN/TS 1992-4 (2009)* enhanced) and b) conventional anchorage design provisions (*Eurocode 2 (2005)*)

Table 9.1 compares the frequency of appearance of the failure mode determined by experimental or numerical tests and the predicted failure mode according to the calculation of capacities based on characteristic material strengths. Both, the enhanced bonded anchor design provisions and the conventional anchorage design provisions predict the failure mode of the connection conservatively: No column-to-foundation connection failed in a brittle failure mode if not predicted. Moreover, ductile mode Y is determined to be the governing failure mode only for specimens developing pronounced strain hardening, as the detailed evaluation of the load-drift curves show (*Mahrenholtz, C. (2012a)*, *Mahrenholtz, C. (2012b)*).

Table 9.1 Frequency of appearance of tested failure mode and predicted failure mode, calculated on the basis of characteristic strengths

| Tested failure mode | Predicted failure mode | Enhanced bonded anchor model | | Conventional anchorage model | |
|---|---|---|---|---|---|
| | | Experimental | Numerical | Experimental | Numerical |
| Y | Y | 2 | 36 | – | 18 |
| P/C | Y | – | – | – | – |
| Y | P/C | 9 | 22 | 11 | 40 |
| P/C | P/C | 5 | 46 | 5 | 46 |

In Figure 9.7 the ratio of tested and calculated capacities of column-to-foundation connections is statistically evaluated. As discussed in Section 9.1.2, only the ductile

failure mode Y is acceptable for seismic applications. Therefore, cases for which failure mode P or C was calculated according to the enhanced bonded anchor design provisions or the conventional anchorage design provisions were excluded for this statistical evaluation. Because the enhanced bonded anchor design provisions and conventional anchorage design provisions predict yielding of the starter bar anchorage conservatively (Table 9.1) the statistical distribution shows for both approaches small CVs (3.5 % and 3.4 %) and 5 % fractile values larger than 1.0.

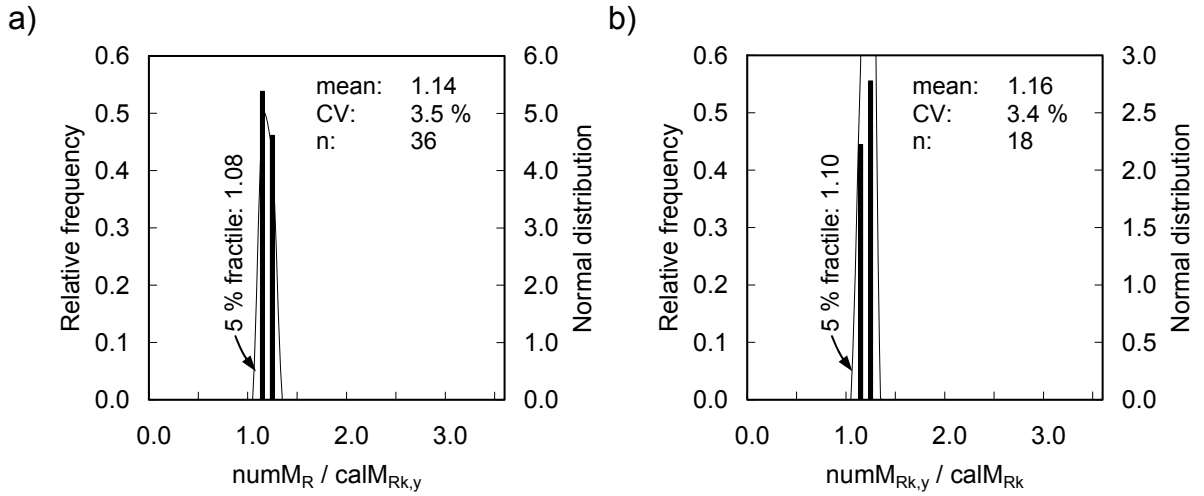


Figure 9.7 Statistical distribution of ratios of numerically tested and calculated characteristic column-to-foundation connection capacities applying the a) enhanced bonded anchor design provisions (*CEN/TS 1992-4 (2009)* enhanced) and b) conventional anchorage design provisions (*Eurocode 2 (2005)*)

On the basis of the above presented studies, the proposed enhanced bonded anchor design provisions are deemed to be validated. The overview of calculated characteristic capacities and corresponding failure modes for experimentally and numerically tested column-to-foundation connections are given in Table D.7 and Table D.8, respectively, of Appendix D: Column-to-Foundation Connection Test Data.

It is instructive to compare also the tested column-to-foundation connection capacity with the calculated design capacity of the connection as shown in the diagrams of Figure 9.8 and Figure 9.9. It is evident, that the benefit of the enhanced bonded anchor design provisions is jeopardized by the increased safety factor for pullout failure.

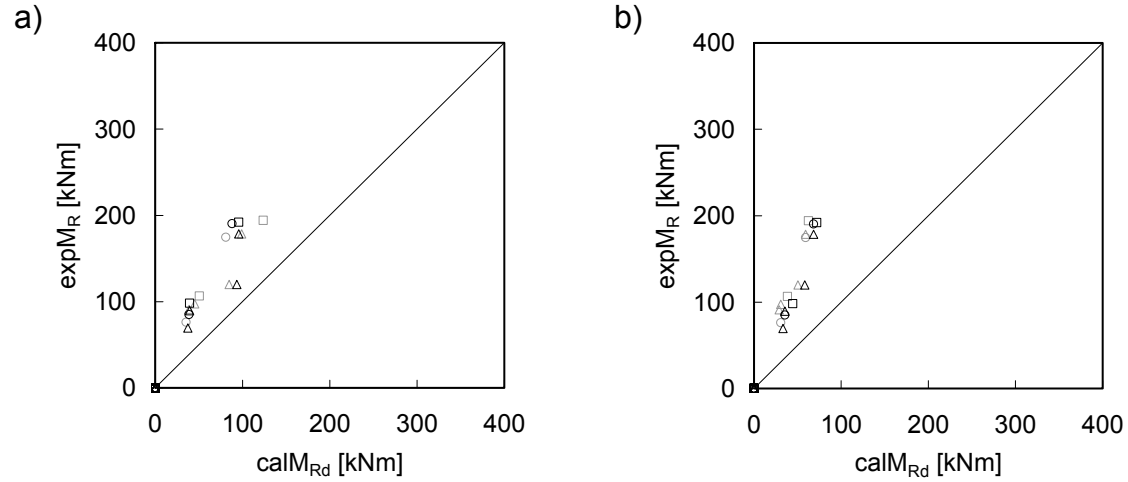


Refer to Figure 9.4 for legend

Figure 9.8 Comparison of experimentally tested and calculated design column-to-foundation connection capacities applying the a) enhanced bonded anchor design provisions (*CEN/TS 1992-4 (2009)* enhanced) and b) conventional anchorage design provisions (*Eurocode 2 (2005)*)

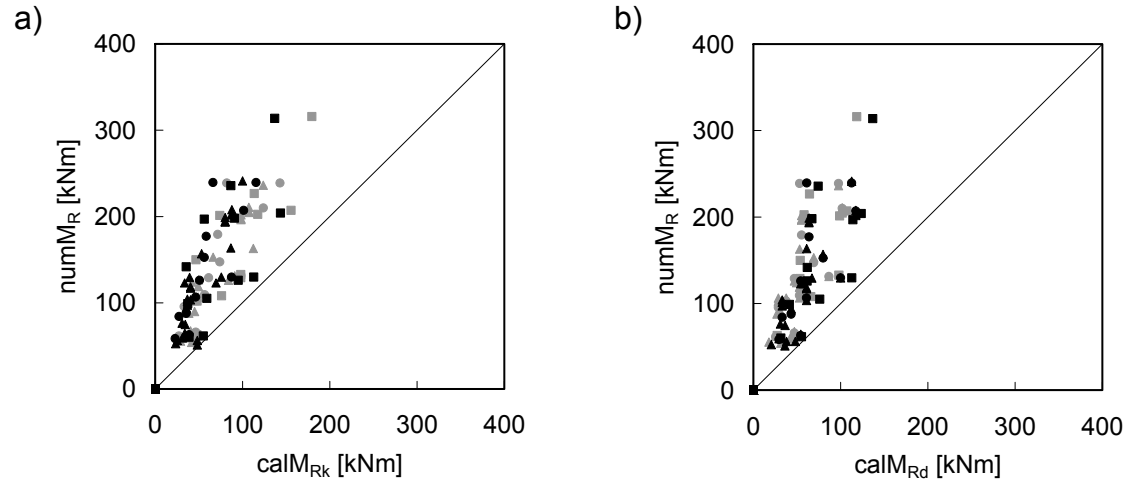


Refer to Figure 9.4 for legend

Figure 9.9 Comparison of numerically tested and calculated design column-to-foundation connection capacities applying the a) enhanced bonded anchor design provisions (*CEN/TS 1992-4 (2009)* enhanced) and b) conventional anchorage design provisions (*Eurocode 2 (2005)*)

However, no experimentally or numerically tested specimen complies with the requirement of ductile failure (Section 9.2.1.5) since the ratio of the ductile and brittle anchorage capacity is for all cases larger than 0.6 as shown in the last column of Table D.7 and Table D.8 in Appendix D: Column-to-Foundation Connection Test Data.

In Section 9.2.5, the requirement to ensure ductile failure is studied in detail in order to determine the anchorage lengths necessary according to the proposed column-to-foundation design provisions.

### 9.2.4 Bidirectional loading

Chapter 6 and Chapter 7 presented experimental and numerical studies on column-to-foundation connections where seismic loading was simulated by monodirectional, quasi-static loads according to a defined load protocol. The load protocol was based on *ACI 374.1 (2005)* and it is reasonable to assume its adequateness to simulate seismic loading realistically. Furthermore, the use of quasi-static loading rates is a common approach for testing and is deemed to be sufficiently accurate also for column-to-foundation connections according to the considerations discussed in Section 2.2.7. Earthquakes, however, load the structure not only in one direction but consecutively in various directions.

It is assumed that the beneficial effect of moment loading is not affected by the bidirectional loading because the loading history does not influence the beneficial effect and the factor

$$\psi_{M,N} = 2.5 - \frac{z}{\ell_b} \geq 1.0 \qquad \text{Equation 9.21}$$

takes the influence of the geometry directly into account as illustrated schematically in Figure 9.10a: The shown column-to-foundation connection experiences the beneficial effect only when loaded in the weak direction of the column (Figure 9.10b). In contrast, the effect disappears when loaded in the strong direction of the column (Figure 9.10c) as the influence of the compression strut on the anchorage capacity deminishes with larger ratios of inner lever arm z and anchorage length $\ell_b$. According to *Herzog, M. (2010)*, the effect disappears for ratios of z : $\ell_b$ larger than 1.5 : 1.0.

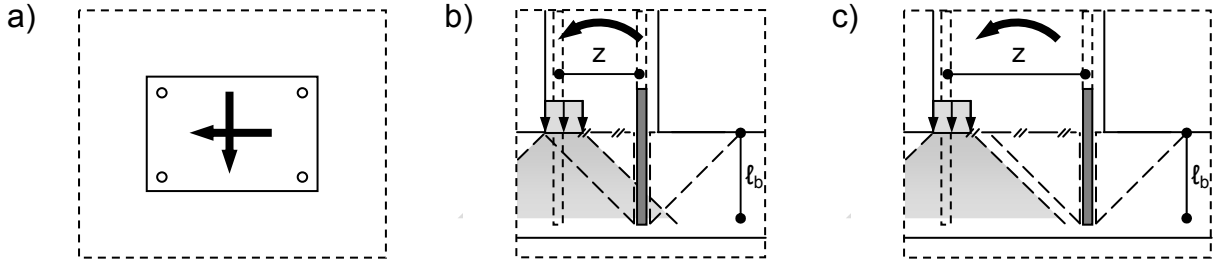


Figure 9.10 Beneficial effect depends on loading direction of a) rectangular columns (top view): b) Significant effect when loaded in the weak direction (side view); c) No effect when loaded in the strong direction (side view)

In contrast, the bidirectional loading history influences the adverse effect of cyclic loading which leads to a chequered crack pattern as schematically illustrated by the sequence shown in Figure 9.11.

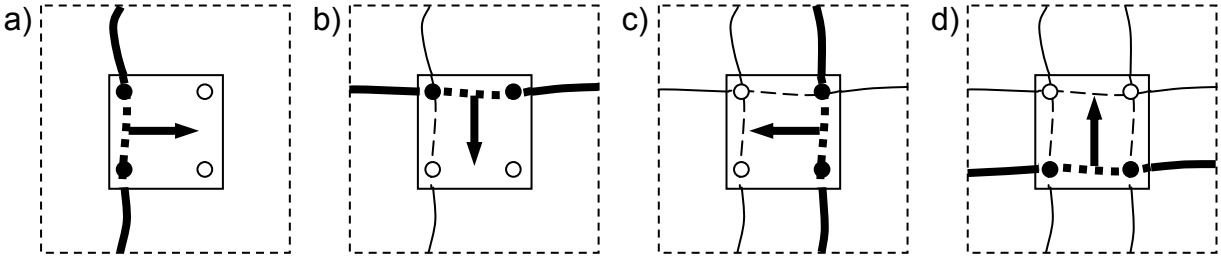


Figure 9.11 Bidirectional loading on column-to-foundation connection and resulting crack pattern (top view)

As a result of the bidirectional loading, the starter bars may be situated in the junction of two intersecting cracks, leading to a more pronounced bond damage. For the sake of simplicity and due to lack of tests on bidirectional loaded column-to-foundation connections, it is therefore proposed to use the factor

$$\psi_{cyc,N} = \left(0.9\left(1+\frac{\ell_b}{200\phi}\right)\right)^2 \leq 1.0 \qquad \text{Equation 9.22}$$

to take the effect of cyclic loading into account.

### 9.2.5 Finally required related anchorage length

The general parametric study presented in the following demonstrates the effect of the stipulated ductile failure for column-to-foundation connections designed according to the enhanced bonded anchor design provisions. For this reason, the capacities of cast-in-place and post-installed connections are evaluated with respect to Equation 9.18, assuming the post-installation system used for the tested column-to-foundation connections. The characteristic bond strengths for the post-installed and cast-in-place starter bars are calculated according to Equation 9.11 and Equation 9.12 assuming the seismic load case. Therefore, not only factor $\psi_{M,N}$ but also factor $\psi_{cyc,N}$ is applied. Two different concrete strengths ($f_{ck}$ = 20 MPa, $f_{ck}$ = 50 MPa) and three different starter bar diameters ($\phi$ = 16 mm, $\phi$ = 25 mm, $\phi$ = 32 mm, $f_{uk}$ = 600 MPa) in two different layouts (two and four starter bars per column face) were evaluated. The same column dimensions were assumed as used for the conducted tests ($h_{col}$ = $b_{col}$ = 300 mm). The material strengths used for the example are summarised in Table 9.2.

Table 9.2 Material strengths used for examples

| Concrete strength $f_{ck}$ [MPa] | Bond strength $\tau_{Rk}$ [MPa] | | Steel strength $f_{uk}$ [MPa] |
|---|---|---|---|
| | cast-in-place | post-installed | |
| 20 | 3.5[1)] | 7.0[2)] | 600 |
| 50 | 6.4[1)] | 7.6[2)] | |

[1)] According to Equation 9.15

[2)] According to Equation 9.13

To conveniently evaluate the enhanced bonded anchor design provisions in respect to Equation 9.18, the calculated anchorage capacities $N_{Rk,p/c} = \min\{N_{Rk,p}; N_{Rk,c}\}$ and $N_{Rk,s}$ were normalised with reference to $N_{Rk,s} \cdot \gamma_{inst} / 0.6$ and plotted against the related anchorage length $\ell_b / \phi$. Normalised anchorage capacities corresponding to the failure mode P/C equal to 1.0 identify the anchorage length needed to achieve reliably ductile failure. Figure 9.12 provides explanations of the conceptual representation provided in the following. Reference is also made to Section 2.3.1.2 where the anchorage capacity as the minimum of the capacities $N_{Rk,p}$, $N_{Rk,c}$ and $N_{Rk,y}$ is discussed.

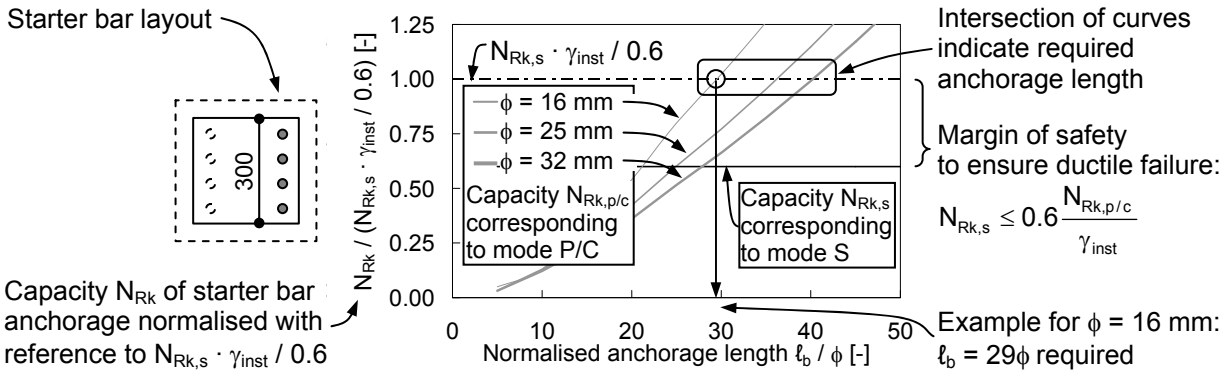


Figure 9.12 Explanation of conceptual representation of cast-in-place and post-installed starter bar capacities $N_{Rk,p/c}$ and $N_{Rk,s}$ to determine minimum anchorage length required to reliably achieve ductile failure

The conceptual representations shown in Figure 9.13 for cast-in-place and in Figure 9.14 for post-installed column-to-foundation connections demonstrate that the enhanced bonded anchor design concept for column-to-foundation connections is most advantageous for columns reinforced by four corner starter bars and high foundation concrete strengths.

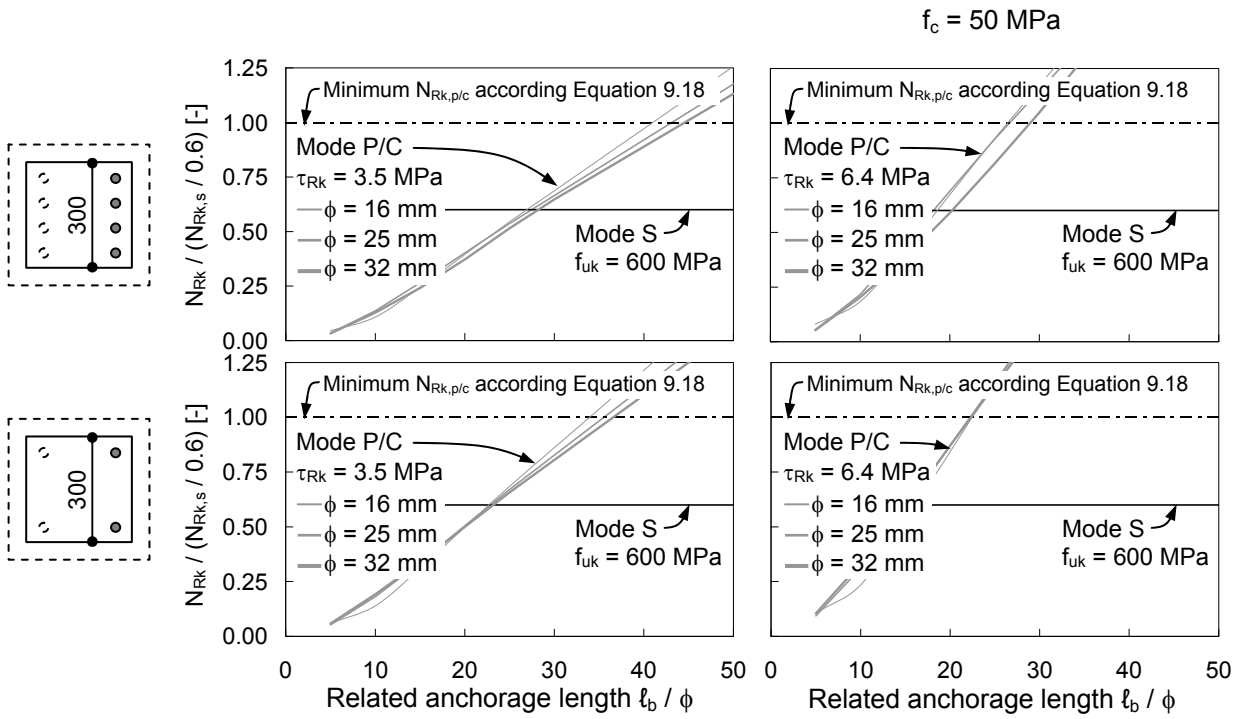


Figure 9.13 Conceptual representation of cast-in-place starter bar capacities $N_{Rk,p/c}$ and $N_{Rk,s}$ to determine minimum anchorage length required to reliably achieve ductile failure, two example configurations

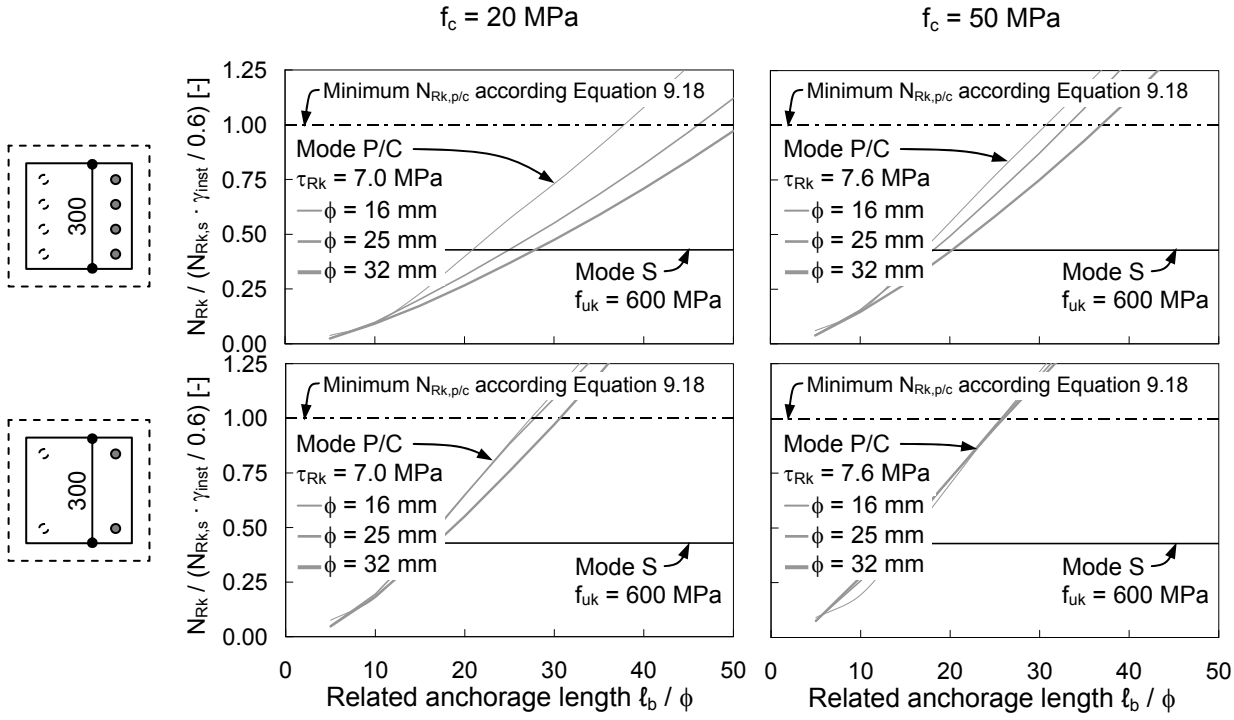


Figure 9.14 Conceptual representation of post-installed starter bar capacities $N_{Rk,p/c}$ and $N_{Rk,s}$ to determine minimum anchorage length required to reliably achieve ductile failure, two example configurations, $\gamma_{inst}$ = 1.4

In addition, conceptual representations are shown for post-installed starter bars in Figure 9.15 where an installation safety factor of $\gamma_{inst}$ = 1.0 (high installation safety) was assumed. Here, an anchorage length of about 20$\phi$ is sufficient to reliably achieve ductile failure of the column-to-foundation connection, if four corner starter bars are post-installed in foundations which concrete strengths are $f_{ck}$ = 50 MPa.

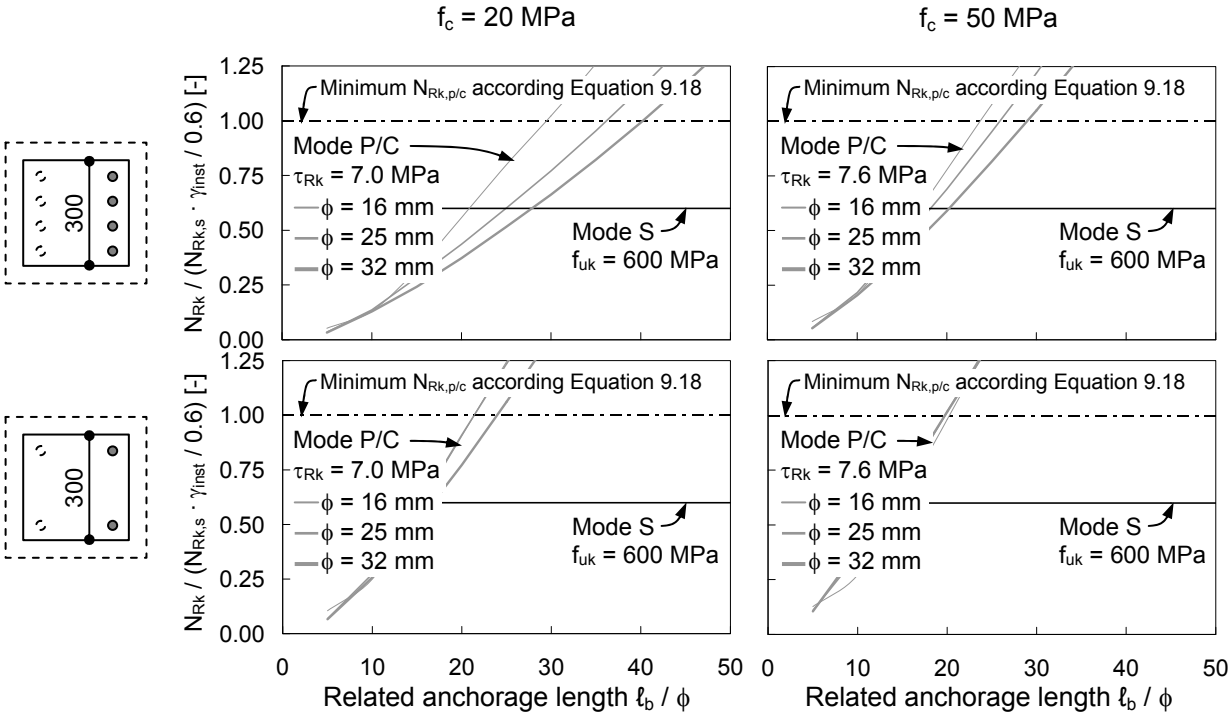


Figure 9.15 Conceptual representation of post-installed starter bar capacities $N_{Rk,p/c}$ and $N_{Rk,s}$ to determine minimum anchorage length required to reliably achieve ductile failure, two example configurations, $\gamma_{inst}$ = 1.0

Table 9.3 provides an overview of the related anchorage lengths of starter bars cast-in-place and post-installed in grade 20 and 50 concrete which are required to ensure ductile failure.

Table 9.3 Required related anchorage length to ensure ductile failure

| Starter bar layout | Foundation concrete strength $f_{ck}$ [MPa] | Column starter bar diameter $\phi$ [mm] | Required related anchorage length $\ell_b / \phi$ [-] | | |
|---|---|---|---|---|---|
| | | | Cast-in-place | Post-installed | |
| | | | | $\gamma_{inst}$ = 1.4 | $\gamma_{inst}$ = 1.0 |
| 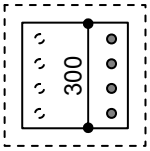  | 20 | 16 | 41 | 38 | 30 |
| | | 25 | 43 | 46 | 37 |
| | | 32 | 45 | 51 | 41 |
| | 50 | 16 | 27 | 31 | 24 |
| | | 25 | 27 | 34 | 26 |
| | | 32 | 29 | 37 | 29 |
| 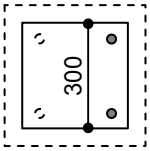  | 20 | 16 | 34 | 28 | 22 |
| | | 25 | 36 | 28 | 22 |
| | | 32 | 37 | 31 | 24 |
| | 50 | 16 | 23 | 26 | 21 |
| | | 25 | 22 | 26 | 20 |
| | | 32 | 23 | 26 | 20 |

In Section 7.5 it was concluded that for low strength concrete ($f_{ck}$ = 20 MPa) anchorage lengths larger than 20$\phi$ and for high strength concrete ($f_{ck}$ = 50 MPa) anchorage lengths larger than 15$\phi$ are required to achieve adequate seismic performance according to the criteria stipulated in the *ACI 374.1 (2005)* or according to the strain hardening criterion. In the light of above presented parametric study it is evident that the satisfaction of the requirement regarding reliable ductile failure expressed in Equation 9.18 is governing in respect of the anchorage length. Therefore, the seismic performance of individual column-to-foundation connections do not have to be assessed according to *ACI 374.1 (2005)*.

## 9.3 Complementary Retrofitting Works, Flowchart and Conditions of Use

### 9.3.1 Complementary retrofitting works to upgrade the existing structure

As pointed out in *Priestley, N.; Seible, F. et al. (2007)* for bridge column concrete jacketing anchored to the foundation by means of post-installed reinforcing bars, column retrofit measures which generate additional loading to the foundation may have to be accompanied by foundation retrofit measures. *Priestley, N.; Seible, F. et al. (2007)* recommend the construction of reinforced concrete overlays which are

connected by means of long dowels to enhance flexural and shear strength of the foundation of the bridge.

In the following two sections alternative complementary retrofitting measures are suggested which appear more suitable for moment resisting frame structures and may be sufficient to upgrade the capacity of existing foundations in order to shift the column to the first position of the hierarchy of failure. Depending on the individual design requirements, the complementary retrofit measures for flexuaral enhancement and shear enhancement may also be applied jointly.

#### 9.3.1.1 Post-installed near-surface reinforcement

Post-installed near-surface reinforcement is suitable to enhance the foundation flexural strength. Figure 9.16a demonstrates the installation sequence: First, grooves are cut parallel to the direction of loading. Following, the grooves are filled with mortar and near-surface reinforcement is placed. Crosswise application of near-surface reinforcement is required for bidirectionally loaded columns-to-foundation connections.

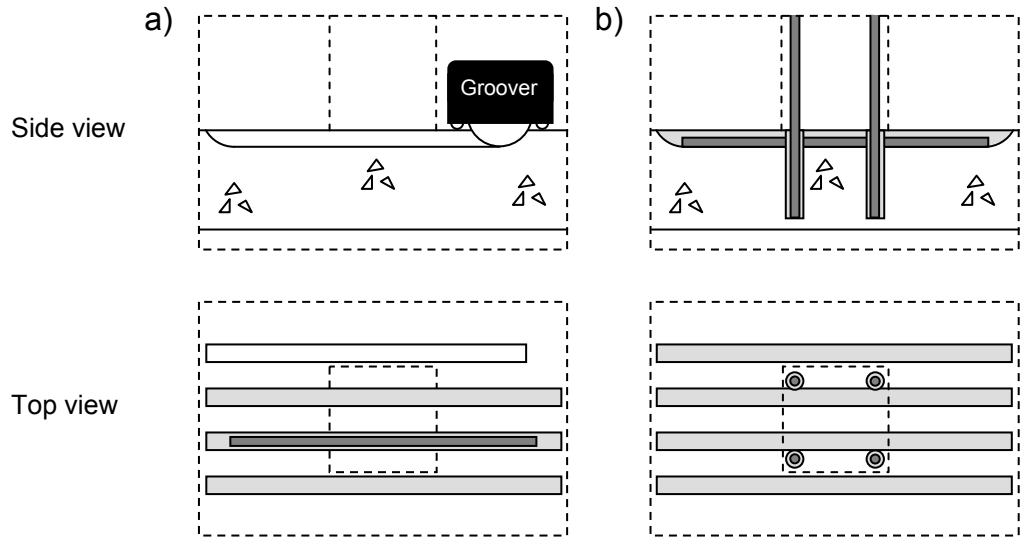


Figure 9.16 a) Post-installation of near-surface reinforcement; b) Post-installation of column starter bars

Standard steel reinforcing bars may be used though near-surface reinforcement typically involves bars made of fibre reinforced polymers (FRP) to reduce the required cross section as described e.g. in *De Lorenzis, L.; Teng, J.-G. (2006)*. The post-installation of the column starter bars (Figure 9.17b) is carried out subsequently since grooving is impossible once the starter bars are installed.

#### 9.3.1.2 Post-installed dowel reinforcement

Post-installed dowel reinforcement is recommended to enhance the foundation shear strength. The installation sequence is shown in Figure 9.17a: First, holes are drilled in the foundation. Next, mortar is injected and dowel reinforcement placed. Installation of dowel reinforcement in all directions is required for bidirectionally loaded columns-to-foundation connections.

`

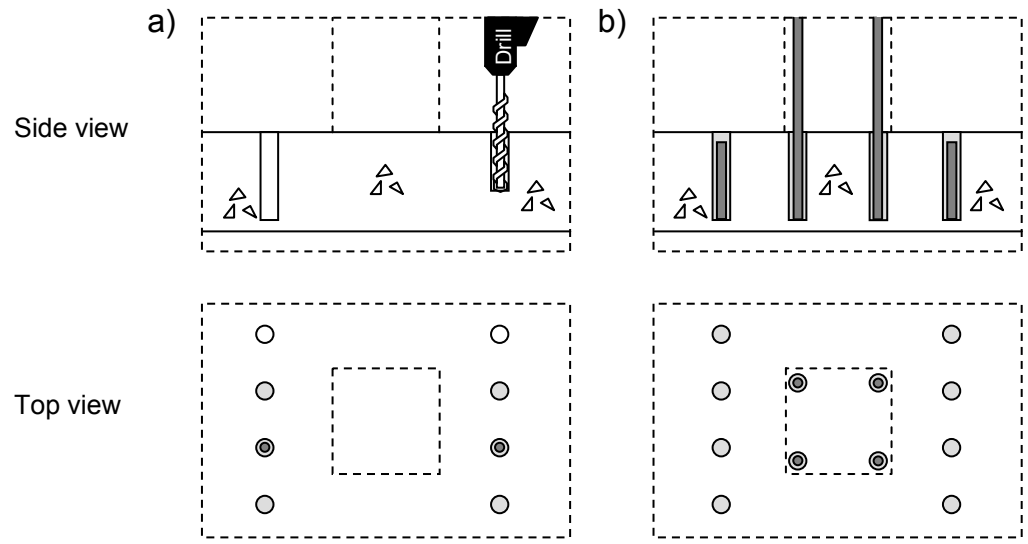


Figure 9.17 a) Post-installation of dowel reinforcement; b) Post-installation of column starter bars

Headed reinforcing bars should be used because of the limited available development length for the dowel reinforcement. A similar approach to strengthen slabs against punching shear is suggested in *Ruiz, M.; Muttoni, A. et al. (2010)*. The effectiveness of the post-installed dowels is further improved if the holes are drilled with an undercut at the bottom and a countersunk hole at the top. The post-installation of the column starter bars (Figure 9.17b) may be carried out at the same time. Installation should be carried out successively if different post-installation systems for column starter bars and dowel reinforcement are used.

### 9.3.2 Flowchart

Figure 9.18 illustrates the flowchart of the complete design concept. The structured flowchart may serve as a guideline for practitioners.

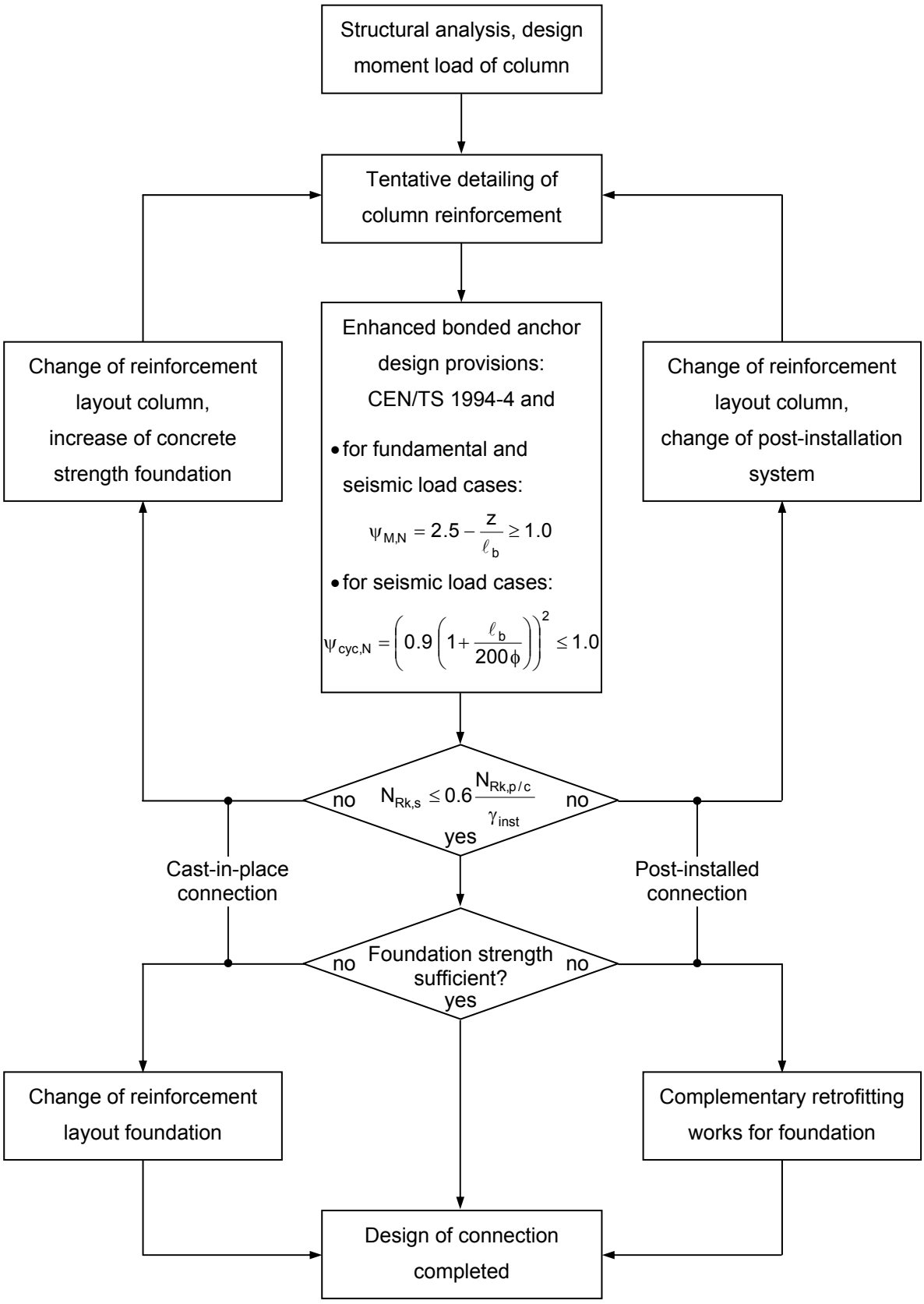


Figure 9.18 Flowchart of design concept

### 9.3.3 Conditions of use

Attention was paid on a simple, yet universally valid design concept for designing post-installed and cast-in-place column-to-foundation connections detailed with reduced anchorage lengths without hooks. However, the proposed design concept was studied and developed under the assumptions that

- the column starter bar anchorage length reaches close to the total depth of the foundation,
- the starter bar layout is symmetric in respect of the loading direction,
- the concrete strength is between $f_{ck}$ = 20 MPa and $f_{ck}$ = 50 MPa,
- post-installed starter bars are not loaded permanently to exclude adverse sustained loading effects (Section 2.2.8),
- the column is axially not loaded or in compression but not tension,.
- post-installed starter bars are installed at normal ambient temperatures to exclude adverse temperature effects (Section 2.2.9), and
- the post-installation system is qualified for seismic applications (Section 9.1.3).

Moreover, the evaluation of the adequate seismic performance on the basis of *ACI 374.1 (2005)* was conducted assuming that the allowable story displacement $\Delta_a$ is limited to 3.5 %, the deflection amplification factor $C_d$ and the total overstrength factor $\lambda$ equals 2.5 and 1.7 (Section 6.4.4 and Section 7.4.4), respectively, and that the moment resisting frame system is detailed as an ordinary reinforced concrete moment frame according to *ACI 318 (2011)*. However, the safety concept for seismic anchorages turned out to be decisive with regard to the required anchorage lengths by a large margin (Section 9.1.2). Therefore, the assumption of the general validity of the proposed design concept for column-to-foundation connections of moment resisting frames is reasonable.

## 9.4 Summary and Conclusions

The general safety concept on the basis of partial safety factors was briefly introduced to point out the context of mean, characteristic, and design values for load and resistance. The conversatism for brittle failure and ensurement of ductile failure as the safety concept for seismic anchorages was outlined. The suitability assessment of post-installation systems was discussed.

Following, the capability of the developed enhanced bonded anchor design provisions to generate conservative characteristic values for the capacity of column-to-foundation connections was shown, validating the proposed approach. Furthermore, the evaluation of design values for the capacity of column-to-foundation

connections clearly demonstrated that the application of the enhanced bonded anchor design provisions allow achieving significantly higher utilisation ratios if compared to the conventional anchorage design.

The evaluation of the proposed enhanced bonded anchor provisions showed that anchorage lengths of $15\phi$ are sufficient to reliably achieve yielding as the governing failure mode, a four corner column starter bar layout, high foundation concrete strengths, and a high performance mortar rated for high installation safety provided. Larger anchorage lengths are required for different starter bar layouts and lower concrete strengths. The satisfaction of the requirement to provide sufficient safety margin between ductile and brittle failure of the anchorage also ensures an adequate seismic performance of the column-to-foundation connection.

The provided flowchart gives guidance for practitioners to design column-to-foundation connections on the basis of enhanced bonded anchor design provisions. Finally, the conditions of use are listed which have to be obeyed when applying the developed design concept.

# 10 Summary and Open Questions

The main objective of the thesis was to overcome the knowledge deficits in seismic bond behaviour of cast-in-place and post-installed concrete reinforcement, and to develop a design concept for column-to-foundation connections which allows the reduction of the anchorage length to the extent that hooks can be omitted. In the following, the key points of every chapter are summarised (Section 10.1) and open questions outlined (Section 10.2) which can be understood as a recommendation for successive studies.

## 10.1 Summary

Lessons learnt from recent earthquakes include the knowledge that many existing buildings require seismic retrofitting, calling for innovative retrofit solutions where the outcome is economic and fast. For reinforced concrete buildings, additional columns are a first-grade retrofit solution. However, the connection to the existing building requires the column starter bars to be post-installed in the foundation. To date a design concept for post-installed column-to-foundation connections which allows the reduction of column starter bar anchorage lengths to the extent that the anchorage can be accommodated in the foundation has not been realised. Such a design concept, however, would be interesting also for cast-in-place column-to-foundation connections.

For short anchorage lengths without hook, the bond behaviour is of paramount importance. In the past, many effects which influence the bond behaviour of concrete reinforcement have been studied and models developed to describe the effects analytically. The superpositioning of the models allows consideration of several effects which occur at the same time. However, the effect of crack cycling under seismic conditions has not been studied to date. Crack cycling is in particular relevant for starter bar anchorages without hooks which load transfer solely rely on bond. The two coexisting design approaches available for the design of anchorages, namely the conventional anchorage design and the bonded anchor design, were discussed and an overview of the key points presented. In comparison to the conventional anchorage design resulting in anchorage lengths of $40\phi$, the bonded anchor design potentially allows shorter anchorage lengths and therefore provides the basis for a retrofit design concept employing additional columns.

The quantification of the beneficial effect of moment loading on the starter bar anchorage capacity is essential in developing an economic design concept on the basis of bonded anchor design provisions. Since post-installed anchorages rely on bond which is sensitive to load and crack cycling, also the adverse effect of cyclic loading on the anchorage capacity needs to be considered carefully. Exploratory tests on bond behaviour during seismic crack cycling showed that the bond strength deterioration is potentially more pronounced for crack cycling if compared to load cycling. The close examination of column-to-foundation connections under seismic excitation revealed that load and crack cycling act simultaneously.

Four investigative steps were identified to be required for the development of a sound design concept for substandard column-to-foundation connections in which starter bars are detailed without hooks and/or with reduced anchorage lengths:

- Experimentally conducted simultaneous load and crack cycling tests on cast-in-place and post-installed reinforcing bars which were the first of its kind and yielded a number of conclusive results. Evidence was given that simultaneous load and crack cycling generates a more pronounced bond damage if compared to load cycling tests in cracked concrete. This can be explained by the increased energy hysteresis since the dissipated energy is partly converted in bond damage. Notably, the hysteretic energy model (*Eligehausen, R.; Popov, E. et al. (1983)*) is capable to reflect the accelerated bond damage under seismic conditions because the effects of transverse compression and longitudinal cracks which occurred during the crack cycling are directly taken into account by means of the modified energy dissipation involved.
- Numerically conducted simultaneous load and crack cycling tests were conducted by means of a non-linear finite element program which simulates the cast-in-place and post-installed reinforcing bars by one-dimensional bar elements, connected by means of bond elements to three-dimensional solid elements representing the concrete. These tests were the first ever using bond elements in cracks and verified the bond element implemented in the finite element program used. By the hysteretic energy model and further algorithms implemented in the used finite elements to model the effects of transverse compression and parallel cracks, the accelerated damage effect was realistically taken into account.
- Experimental tests on column-to-foundation connections were carried out to study their seismic performance and the influence of differently detailed anchorages. The monotonic and cyclic tests delivered unprecedented data for substandard column-to-foundation connections. These experimental tests on column-to-foundation connections were the first ever focussing on the seismic

performance of post-installed and cast-in-place substandard anchorages without hooks. The similarities of debonding and yielding penetrating from the loaded end of the anchorage towards the unloaded end were described. The most important finding was that only for anchorage characterised by very low ratios of anchorage length and diameter the cyclic loading significantly accelerates the bond stress redistribution to the unloaded end. In contrast, connections detailed with sufficiently long anchorages developed a seismic performance which is rated as being adequate according to *ACI 374.1 (2005)* even though the anchorage length was substantially reduced if compared to the anchorage length stipulated in reinforced concrete design codes.

- Numerical tests on column-to-foundation connections were carried out and the capability of the finite element program employed to simulate seismically loaded structural connections by means of bond elements linking one-dimensional bar elements and three-dimensional solid elements was shown. To the knowledge of the author, these were the first numerical studies on reinforced concrete joints, where short starter bar anchorages solely rely on bond, potentially failing by concrete breakout or pullout. The overall load-drift behaviour was realistically simulated for all failure modes. The graphic output of stresses and strains allowed extended studies and enabled for example the analysis of the penetration of strain. After the successful benchmarking, a parametric study established a sound data base for further investigations. It was confirmed that only anchorages characterised by very low ratios of anchorage length and diameter develop significant differences between monotonic and cyclic loading.

The data base facilitated the confirmation of a factor $\psi_M$ taking into account the beneficial effect of moment loading on the connection capacity and the development of a new factor $\psi_{cyc}$ taking into account the adverse effect of cyclic loading on the connection capacity. Equations were developed to define the factors $\psi_{M,N}$ and $\psi_{cyc,N}$ which were then used to enhance the bonded anchor model. The enhancement of the bonded anchor model was validated using the experimental and numerical test results. It was shown that the column-to-foundation connection capacities are more accurately predicted by the enhanced bonded anchor model if compared to the conventional anchorage model. Therefore, the factors describing the beneficial effect and adverse effect are proposed to be added to the current bonded anchor design provisions given in *CEN/TS 1992-4-5 (2009)*.

It was shown that the bonded anchor design provisions enhanced by the factors $\psi_{M,N}$ and $\psi_{cyc,N}$ are in line with the safety concept of partial safety factor design, validating the application of the factors describing the beneficial effect of moment loading and adverse effect of cyclic loading. Moreover, it was shown that connections designed according to the enhanced bonded anchor design provisions yield higher utilisation

ratios if compared to the conventional anchorage design provisions. The required margin of safety between the ductile yielding failure mode and the brittle failure modes comprising concrete breakout and pullout inhibits very short anchorage lengths. Therefore, the resulting moderate anchorage lengths guarantee the compliance with the seismic performance assessment criteria stipulated in *ACI 374.1 (2005)*. High concrete grades of the foundation and high performance mortars with high installation safety allow short cast-in-place and post-installed column starter bar anchorage lengths of $20\phi$. The required anchorage lengths are increased for lower grade concretes and mortars with low installation safety.

## 10.2 Open Question

If applied on post-installed starter bars, the proposed design concept for column-to-foundation connections on the basis of enhanced bonded anchor design provisions requires qualified post-installation systems. The future seismic qualification guidelines for post-installed anchorages (*Proposal for ETAG 001 Seismic Amendment (2012)*) studies the influence of load and crack cycling in separate tests: Load cycling tests on anchorages located in constantly opened cracks and crack cycling tests on anchorages constantly loaded. The current definition of the constant load during crack cycling is conservative and may jeopardize economical qualification of post-installed reinforcing bars for seismic applications. Further studies on the correlation of load and crack width for structural connections potentially allows reducing the constant load applied during crack cycling qualification tests and are therefore recommended. Moreover, the qualification scheme to show the equivalence of post-installed and cast-in-place reinfrocing bars *EOTA TR 023 (2006)* currently does not include seismic loading. Research is recommended allowing the simplification of simultaneous load and crack cycling tests before stipulating these as an additional qualification test. For example, using the residual bond strength as an performance indicator to avoid the tedious analyses of the hystereses.

If the proposed design concept for column-to-foundation connections on the basis of enhanced bonded anchor design provisions is applied on cast-in-place starter bars, characteristic bond strengths $\tau_R$ according to *CEN/TS 1992-4-5 (2009)* are required. Generally, these characteristic bond strengths are derived by pullout tests with confined setup on the basis of the bonded anchor qualification guideline (*ETAG 001 (2006)*, Part 5). In contrast, the reinforced concrete design code *Eurocode 2 (2005)* specifies universally valid design bond strengths $f_{bd}$. It would be reasonable, therefore, to conduct research allowing the development of a general relationship between $f_{bd}$ and $\tau_R$. The bond strengths for concrete reinforcement specified in *CEB-FIP Model Code 1990 (1993)*, Table 3.1.1 may serve as a basis.

The tests on column-to-foundation connections were conducted without axial loading on the column and neglected the elastic bedding of the foundation. Additional studies to evaluate the positive influence of axial compressive loading on the column and elastic bedding of the foundation are recommended, potentially allowing further enhancement of the bonded anchor design provisions (Figure 10.1a). Also the influence of axial tensile loading on the column could be investigated to extend the range of application to corner columns in tension. Furthermore, specially manufactured starter bars which anchorage length is detailed with a staggered conical geometry similar to bonded expansion anchors develop an improved bond behaviour which may also allow reducing the anchorage length of starter bars (Figure 10.1b).

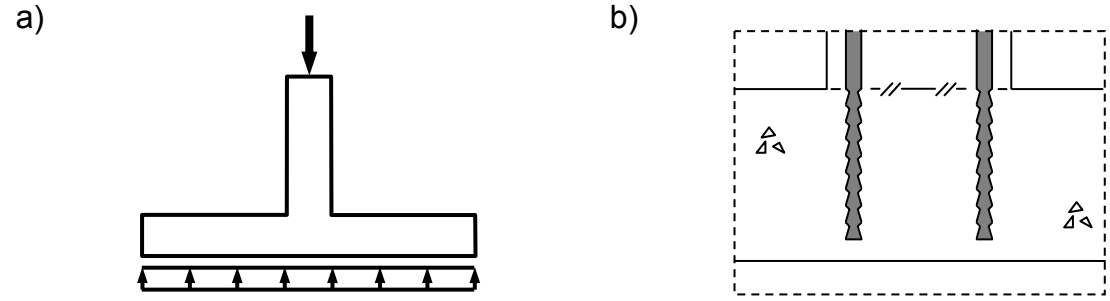


Figure 10.1 Further enhancement of bonded anchor design provisions imaginable if a) axial loading on column and elastic bedding of foundation is taken into account or b) specially manufactured starter bars are used

In order to take maximum advantage of the enhanced bonded anchor design provisions, high installation safety ratings of the used post-installation systems are important. Therefore, special attention should be paid on installation techniques to reduce the scatter of tested bond strengths and to achieve high installation safety ratings in the course of qualification testing. This would require special attention to be payed to the moisture sensitivity of the mortar. In addition, a concept of mandatory installation trainings and its certifications by authorities would lead to more consistent installation outcomes and potentially allow reducing the installation safety factors stipulated in the technical specification of post-installation systems.

Post-earthquake fires are frequently experienced in the wake of earthquake disasters which may influence the structural and non-structural building system performance (*Wang, X.; M. Chen; et al. (2011)*). Post-earthquake fires are also relevant for post-installed reinforcing bar anchorages since common epoxy resin based mortars are potentially sensitive to fire (*Pinoteau, N.; Guillet, T. et al. (2011)*). It is reasonable to assume that the influence is small for post-installed column starter bars because of the large concrete covers provided by the foundation concrete. However, research is required to substantiate this assumption.

The studies were conducted at quasi-static loading rates which is conservative according to the current experience (Section 2.2.7). However, research is needed to determine beyond doubt the influence of increased strain rates on the performance of column-to-foundation connections which were detailed according to the enhanced bonded anchor design provisions. The observation of a positive influence would help to make the enhanced bonded anchor design provisions for column-to-foundation connections less conservative.

Finally, the proposed enhanced bonded anchor design provisions for column-to-foundation connections are valid only if the anchorage length reaches over almost the total depth of the foundation (Figure 10.2a). The format of the equations describing the beneficial effect of moment loading and adverse effect of cyclic loading takes into account the negative influence of shorter embedment depths: Both factors $\psi_{M,N}$ and $\psi_{cyc,N}$ attain smaller values for shorter anchorage lengths, provided the geometry beside the anchorage length remains unchanged. However, research is required to substantiate the assumption that the proposed enhanced bonded anchor design provisions for column-to-foundation connections are valid also if the anchorage length is shorter than the total depth (Figure 10.2b). In particular, the influence of the splitting forces (Section 7.4.3.4) has to be re-evaluated.

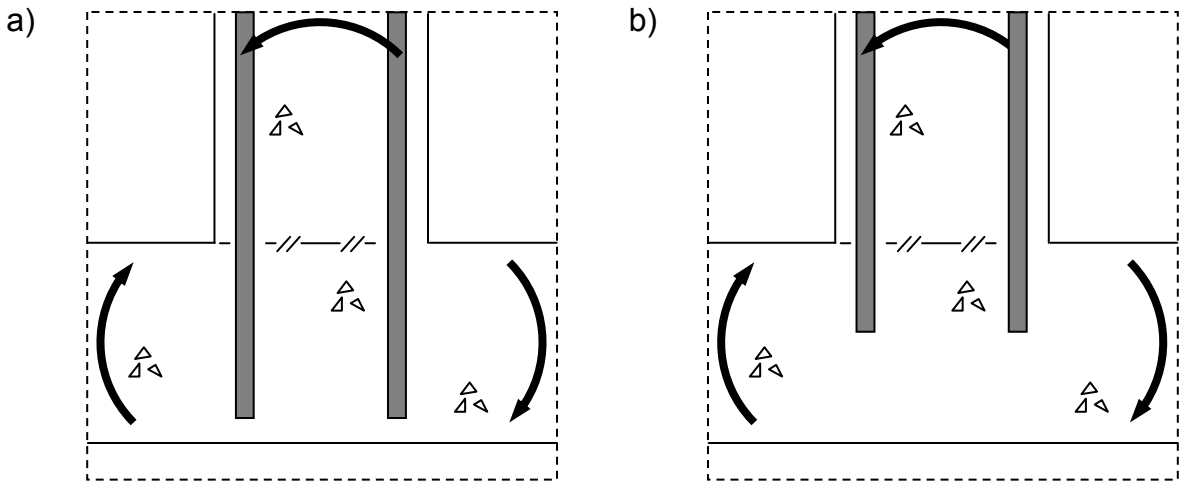


Figure 10.2 Column-to-foundation connections: a) Anchorage length of the column starter bars reaches over almost the total depth of the foundation; b) Anchorage length of the column starter bars is shorter than the total depth of the foundation

# Zusammenfassung (German Summary)

## Model für den Verbund zwischen Bewehrungsstahl und Beton unter seismischer Beanspruchung und seine Anwendung für Stützen-Fundament-Anschlüsse

### Kapitel 1 – Einleitung

In ländlichen Gegenden fordern Erdbeben nur wenige Opfer, meist verursacht durch Steinschlag und Hangrutschungen. In städtischen Gebieten verursachen Erdbeben jedoch Katastrophen, denen jedes Jahr wegen einstürzender Gebäude Zehntausende zum Opfer fallen. In vielen Teilen der Welt ist die städtische Bebauung von Stahlbetongebäuden geprägt. Stahlbeton gilt als ein für Erdbebengebiete geeignetes Baumaterial, jedoch haben mehrere starke Erdbeben in den letzten Jahren gezeigt, dass nicht nur Gebäude aus älteren Beständen anfällig für Erdbebenschäden sind. Die Ursache ist darin zu suchen, dass entweder die Gebäude schlecht konstruiert oder die Erdbebenbeschleunigung höher als erwartet waren. Insbesondere strukturell zu schwach ausgebildete Erdgeschosse verursachen Totaleinstürze. Der Bestand nicht erdbebensicher ausgeführter Gebäude ist erheblich. Da Stahlbetonbauwerke eine lange Lebensdauer haben, löst sich das Problem nicht von selbst. Deshalb sind in der letzten Zeit Erdbeben-ertüchtigungsmaßnahmen in den Fokus gerückt.

Erdbebenertüchtigungen werden entweder als Vorsichtsmaßnahmen durchgeführt, oder um während eines Erdbeben entstandene moderate Schäden zu beheben. Die meisten Erdbebenertüchtigungen erfordern die Verwendung von nachträglich installierten Verankerungen oder Anschlussbewehrungen. Für letzteres werden im bestehenden Stahlbetontragwerk Löcher gebohrt, in die spezieller Mörtel injiziert wird. Dann werden Anschlussbewehrungsstäbe eingesetzt. Nach dem Erhärten des Mörtels kann ein neues Stahlbetonbauteil anbetoniert werden. Insbesondere zusätzliche Stützen im Erdgeschoss sind eine geeignete Erdbeben-ertüchtigungsmaßnahme, um strukturell zu schwach ausgeführte Erdgeschosse zu verstärken: Im Vergleich zu Wänden sind Stützen platzsparend, haben eine hohe Duktilität und können unabhängig von der Belastungsrichtung plastische Gelenke ausbilden. Die Herausforderung ist hierbei der Stützen-Fundament-Anschluss. Es gibt zwar Untersuchungen, die die Gleichwertigkeit von einbetonierten und

nachträglich eingemörtelten Bewehrungsstäben gezeigt haben. Jedoch ist die Fundamentabmessung im Allgemeinen nicht groß genug, um die erforderliche Verankerungslänge der Stützenanschlussbewehrung auszuführen, die den Bemessungsvorschriften der Stahlbetonnorm für gerade Verankerungen entspricht.

Ziel dieser Dissertation ist es daher, das Verhalten von einbetonierten und nachträglich eingemörtelten Bewehrungsstäben unter Erdbebenbelastungen zu untersuchen und ein Bemessungskonzept für nachträglich installierte Stützen-Fundament-Anschlüsse zu entwickeln. Das Bemessungskonzept muss hierbei ermöglichen, die Verankerungslänge so sehr zu reduzieren, dass die Stützenanschlussbewehrung in gewöhnlichen Fundamentabmessungen verankert werden kann.

**Kapitel 2 – Stand der Technik**

Für die angestrebten kurzen Verankerungslängen ohne Haken ist das Verbundverhalten von größter Wichtigkeit. Viele Effekte, die die Verbundfestigkeit von Betonstabstählen beeinflussen, wurden in der Vergangenheit untersucht. Das Grundgesetz des Verbundes beschreibt die Verbundspannungs-Schlupf-Beziehung zwischen Bewehrungsstahl und Beton. Das Grundgesetz des Verbundes wird von konstanten und veränderlichen Parametern beeinflusst. Zu den konstanten Parametern gehören die Eigenschaften des

- Bewehrungsstahls, hierbei insbesondere die bezogene Rippenfläche, und des
- Betons, hierbei insbesondere die Betonfestigkeit.

Die wichtigsten veränderlichen Parameter im Zusammenhang von Stützen-Fundament-Anschlüssen sind

- inelastische Stahldehnung,
- Betonquerdruck,
- Längsriss,
- Verbundschädigung aus zyklischer Last und
- Verbundschädigung aus zyklischen Rissen.

Für viele Effekte wurden Modelle zur analytischen Beschreibung entwickelt. Der Schädigungseffekt aus zyklischen Rissen unter Erdbebenrandbedingungen wurde hingegen noch nicht beschrieben. Die Superposition der einzelnen Modelle ermöglicht es, mehrere Effekte zu berücksichtigen, die zeitgleich wirken. Die komponentenweise Beschreibung der Effekte ist auch für numerische Herangehensweisen geeignet.

Prinzipiell bestehen zwei Möglichkeiten, Verankerungen von Bewehrungsstäben zu bemessen. Zum einen die konventionelle Bemessung der Verankerung, deren Ergebnis eine Verankerungslänge ist, die unabhängig von konkreten Einbausituationen gültig ist. Hierbei werden Bemessungsverbundspannungen angesetzt, die so niedrig sind, dass ein Spalten des Betons selbst bei geringen Betondeckungen ausgeschlossen werden kann und somit die Fließspannung des Stahls ausgenutzt werden kann. Dieser Ansatz ist nicht nur für einbetonierte, sondern auch für nachträglich einbetonierte Bewehrung anzuwenden, vorausgesetzt, das verwendete System ist hierzu nachweislich geeignet. Hierbei ergeben sich jedoch Verankerungslängen von über 40$\phi$. Zum anderen erlaubt die Verbundankerbemessung, die Zugfestigkeit des Betons auszunutzen. Folglich wird zwischen den Versagensmodi Stahlversagen, Betonausbruch und Herausziehen unterschieden. Ursprünglich für Verbundanker entwickelt, kann dieser Ansatz auch für einbetonierte und nachträglich einbetonierte Bewehrung verwendet werden, da der Tragmechanismus identisch ist. Somit ist dieser Ansatz auch auf Stützen-Fundament-Anschlüsse übertragbar, deren gezogene Anschlussbewehrung einer Verbundankergruppe entspricht. Dieser Ansatz scheint für den Anschluss von Stützenanschlussbewehrung besonders geeignet zu sein, da das Fundament große Betondeckungen jedoch nur kurze Verankerungslängen ermöglicht. Um eine wirtschaftliche Bemessung des Anschlusses als Verbundankergruppe zu ermöglichen, muss der Einfluss der Momentenbelastung auf den Anschluss berücksichtigt werden, der sich günstig auf den Traglastwiderstandes des Betonausbruchs und des Herausziehens wirkt. Da das angestrebte Bemessungskonzept auch für Erdbebenlastfälle geeignet sein soll, muss jedoch auch der ungünstig wirkende Einfluss aus zyklischer Belastung berücksichtigt werden.

**Kapitel 3 – Hintergründe des Forschungsansatzes**

Die aus der Erdbebenbeanspruchung resultierenden zyklischen Belastungen bewirken nicht nur zyklische Lasten, sondern auch zyklische Risse, die in Stahlbetonanschlüssen entlang der Verankerungen verlaufen können. Der Einfluss zyklischer Risse ist insbesondere für Verankerungen ohne Haken relevant, da hier die Lasten allein durch Verbundspannungen eingeleitet werden. Bei einem Erdbeben kommt es bei der Rissöffnung zu großen Rissweiten und bei der Rissschließung zu hohen Betonquerdrücken.

Tastversuche mit einbetonierten und nachträglich eingemörtelten Bewehrungsstäben haben gezeigt, dass zyklische Risse bei den für Erdbeben zu erwartenden großen Rissweiten und Betonquerdrücken eine ausgeprägtere Verbundschädigung hervorrufen als zyklische Lasten.

Eine genauere Betrachtung des Stützen-Fundament-Anschlusses zeigt, dass zyklische Lasten und zyklische Risse gleichzeitig und in Phase auf die Verankerungen wirken. Daher ist bei Erdbebenlastfällen von einer beschleunigten Umlagerung der Verbundspannungen vom belasteten Ende der Verankerung am Anschlusspunkt Stütze-Fundament zum unbelasteten Ende auszugehen. Die veränderliche Verteilung der Verbundspannung in Abhängigkeit von Verankerungstiefe, Spannungszustand und Belastungsgeschichte erfordert eine inkrementelle Untersuchung entlang der Einbindetiefe.

Als Vorraussetzung eines verlässlichen Bemessungskonzeptes für Stützen-Fundament-Anschlüsse auf Basis des Verbundankermodells wurden vier Untersuchungsschritte identifiziert, die in den folgenden Kapiteln diskutiert werden.

**Kapitel 4 – Experimentelle Untersuchungen des Verbundes**

Um den Einfluss von gleichzeitig wirkenden zyklischen Lasten und zyklischen Rissen mit der erforderlichen Genauigkeit experimentell untersuchen zu können, wurde ein spezieller Versuchskörper und Versuchsaufbau entwickelt. Als Versuchskörper wurde ein Stahlbetonkörper verwendet, in dem die zu untersuchenden Bewehrungsstäbe einbetoniert oder nachträglich eingemörtelt wurden. Zwei Servo-Hydraulikzylinder kamen zum Einsatz, um den Bewehrungsstab zu belasten und den Riss zu generieren. Beide Servo-Hydraulikzylinder wurden über eine zweiaxiale Servo-Steuerung angesprochen, um eine Synchronisierung von Last und Riss zu ermöglichen. Die Last wurde hierbei über den gemessenen Schlupf des Bewehrungsstabes und der Riss über die gemessene Rissweite gesteuert.

Mit den experimentellen Versuchen wurde erstmalig der Einfluss von gleichzeitig wirkender zyklischer Last und zyklischem Riss auf einbetonierte und nachträglich eingemörtelte Bewehrungsstäbe untersucht. Es wurde nachgewiesen, dass gleichzeitig wirkende zyklische Lasten und zyklische Risse zu einer Verbundschädigung führen, die im Vergleich zu der bei reinen zyklischen Lasten ausgeprägter ist. Dies kann mit der erhöhten Energiehysterese erklärt werden, da die verbrauchte Energie teilweise in Verbundschädigung umgewandelt wird. Ein auf dem Energieverbrauch basierendes Verbundschädigungsmodell (*Eligehausen, R.; Popov, E. et al. (1983)*) ist jedoch geeignet, die beschleunigte Verbundschädigung zu erfassen, da die vom zyklischen Riss resultierenden Effekte Betonquerdruck und Längsriss direkt durch den damit einhergehenden veränderten Energieverbrauch berücksichtigt wird. Die Gültigkeit des auf dem Energieverbrauch basierenden Verbundschädigungsmodell wurde für den maßgebenden Bereich von Rissweite and Bewehrungsstabdurchmesser nachgewiesen.

**Kapitel 5 – Numerische Untersuchungen des Verbundes**

Um den Einfluss von gleichzeitig wirkenden zyklischen Lasten und zyklischen Rissen numerisch untersuchen zu können, wurde ein nicht-lineares Finites Element Programm eingesetzt, das ein Verbundelement zur Simulation des Verbundes zur Verfügung stellt. Das Verbundelement, in dem Verbundmodelle zur Simulation der Effekte aus inelastischer Stahldehnung, Betonquerdruck und Verbundschädigung aus zyklischer Belastung integriert wurden, verbindet Volumenelemente und Stabelemente, die zur Simulation von Beton and Bewehrungsstab verwendet werden. Risse werden als verschmiertes Rissband dargestellt, bei dem geschädigten Volumenelementen eine verminderte Festigkeit zugeordnet werden.

Die mit dem Finiten Element Programm durchgeführten numerischen Versuche sind die ersten, die den Verbund im gerissenen Beton mittels eines Verbundelements simulieren, das eindimensionale Stabelemente und dreidimensionale Volumenelemente verbindet. Die Untersuchungen ermöglichten die Verifizierung der numerischen Herangehensweise für die Simulation von Stahlbetonelementen, in denen die Bewehrungsstäbe gleichzeitig durch zyklische Lasten und zyklische Risse beansprucht werden. Wegen des auf dem Energieverbrauch basierenden Verbundschädigungsmodells (*Eligehausen, R.; Popov, E. et al. (1983)*) und anderer, in den Finiten Elementen integrierten Algorithmen, die den Einfluss von Betonquerdruck und Längsrissen modellieren, wurde die beschleunigte Verbundschädigung realistisch berücksichtigt.

**Kapitel 6 – Experimentelle Untersuchungen von Stützen-Fundament-Anschlüssen**

Zur experimentellen Untersuchung von Stützen-Fundament-Anschlüssen unter seismischer Belastung wurden sechzehn Großversuche durchgeführt. Die Versuchskörper wurden mit acht unterschiedlichen Verankerungsdetails ausgeführt, um den Einfluss von Verankerungslänge und Verankerungsform ebenso wie den der Installationsart, d.h. einbetoniert oder nachträglich eingemörtelt, untersuchen zu können. Jede Konfiguration wurde sowohl monoton als auch zyklisch getestet. Mit diesen experimentellen Versuchen wurde erstmals das seismische Verhalten von einbetonierten und nachträglich eingemörtelten Anschlussbewehrungen untersucht, deren gerade Verankerungslängen im Vergleich zu den nach konventionellen Bemessungsvorschriften erforderlichen Verankerungslängen stark verkürzt waren.

Die Ausführungsart der Verankerung bei ansonsten gleicher Ausführung der Stützenbewehrung hatte einen geringen Einfluss auf die Steifigkeitsabnahme und den Energieverbrauch der Stützen-Fundament-Anschlüsse während der zyklischen Versuche. Im Gegensatz hierzu hatte die Verankerungslänge einen großen Einfluss auf das statische und seismische Tragverhalten. Die entlang der Verankerung

gemessenen Stahldehnungen ermöglichten die Beschreibung der Ähnlichkeit zwischen dem Eindringen von Stahlfließen und Verbundversagen. Die wichtigste Erkenntnis war, dass nur bei sehr kleinen Verhältnissen von Verankerungslänge und Durchmesser die zyklische Belastung die Verbundspannungsumlagerung signifikant beeinflusst und somit die Traglast im vorkritischen Beanspruchungsbereich reduziert. Im Gegensatz hierzu entwickelten mit ausreichend langen Verankerungslängen konstruierte Stützen-Fundament-Anschlüsse ein Tragverhalten, das gemäß *ACI 374.1 (2005)* als erdbebentauglich zu bewerten ist, selbst wenn die Verankerungslängen erheblich reduziert waren im Vergleich zu denen, die in den Stahlbetonnormen definiert werden.

**Kapitel 7 – Numerische Untersuchungen von Stützen-Fundament-Anschlüssen**

Zur numerischen Untersuchung von Stützen-Fundament-Anschlüssen unter seismischer Belastung wurden zunächst die Versuche simuliert, die auch experimentell getestet wurden. Die Eignung des eingesetzten Finite Element Programms, das Tragverhalten von Stahlbetonanschlüssen mittels Verbundelementen zur Verbindung von eindimensionalen Stabelementen und dreidimensionalen Volumenelementen, wurde nachgewiesen. Nach Kenntnis des Autors waren dies die ersten numerischen Untersuchungen an Stahlbetonanschlüssen, deren kurzen Bewehrungsverankerung über reinen Verbund erfolgten und durch Betonausbruch bzw. Herausziehen versagen können.

Das Last-Verschiebungs-Verhalten wurde realistisch für alle Versagensmodi simuliert. Die graphische Auswertung der Betondruckspannungen im Knoten ermöglichte die graphische Auswertung der Stahldehnungen die Analyse des Eindringens der Stahldehnung. Nach erfolgreichem Benchmarking ermöglichte die Durchführung einer Parameterstudie den Aufbau einer Datenbank für weitere Untersuchen. Es konnte bestätigt werden, dass sich nur bei sehr kleinen Verhältnissen von Verankerungslänge und Durchmesser signifikante Unterschiede zwischen monotoner und zyklischer Belastung entwickeln.

**Kapitel 8 – Weiterentwickelte Verbundankermodel**

Die Datenbank ermöglichte die Bestätigung eines Faktors $\psi_M$, der den günstigen Einfluss der Momentenbelastung auf den Traglastwiderstand des Anschlusses berücksichtigt und die Entwicklung eines neuen Faktors $\psi_{cyc}$, der den ungünstigen Einfluss der zyklischen Belastung auf den Traglastwiderstand des Anschlusses erfasst. Zur Definition der Faktoren $\psi_{M,N}$ und $\psi_{cyc,N}$ wurden Gleichungen hergeleitet, die dazu verwendet wurden, um das Verbundankerbemessungsmodell weiterzuentwickeln. Die Weiterentwicklung wurde anhand der experimentellen und

numerischen Versuchsergebnisse validiert. Die Verhältniswerte aus Versuch und Modellvorhersage weist eine geringe Streuung auf. Zudem ist die Modellvorhersage nach dem weiterentwickeltem Verbundankerbemessungsmodell genauer als nach der konventionellen Bemessung der Verankerung. Daher werden die Faktoren zur Berücksichtigung des günstigen Einfluss der Momentenbelastung und des ungünstigen Einfluss der zyklischen Belastung auf den Traglastwiderstand des Anschlusses als Erweiterung der bestehenden Verbundankerbemessungs-vorschriften nach *CEN/TS 1992-4-5 (2009)* vorgeschlagen.

**Kapitel 9 – Bemessungskonzept für Stütze-Fundament-Anschlüsse**

Die erweiterten Verbundankerbemessungsvorschriften stehen im Einklang mit dem Sicherheitskonzept der Teilsicherheitsbeiwerte. Somit wurde die Anwendung der vorgeschlagenen Faktoren zur Berücksichtigung des günstigen Einflusses der Momentenbelastung und des ungünstigen Einflusses der zyklischen Belastung auf den Traglastwiderstand des Anschlusses als Bemessungsvorschrift validiert. Zudem wurde gezeigt, dass nach den erweiterten Verbundankerbemessungsvorschriften ausgeführte Verankerungen von Stützen-Fundament-Anschlüssen einen höheren Ausnutzungsgrad ermöglichen als Verankerungen, die nach der konventionellen Bemessung ausgeführt wurden.

Der erforderliche Sicherheitsabstand zwischen duktilem Stahlversagensmodus und sprödem Versagensmodi in Form von Betonausbruch and Herausziehen, schließt sehr kurze Verankerungslängen aus. Die sich aus dieser Anforderung ergebenen moderaten Verankerungslängen garantieren die Erfüllung der Bewertungskriterien für seismische Tragverhalten gemäß *ACI 374.1 (2005)*. Für hochfesten Fundamentbeton und Hochleistungsmörtel mit hoher Installationssicherheit ergeben sich Verankerungslängen für einbetonierte und nachträglich eingemörtelte Stützenanschlussbewehrungen von $20\phi$. Die erforderlichen Verankerungslängen vergrößern sich für niederfestere Betone und Mörtel mit niedrigerer Installations-sicherheit oder Verbundfestigkeit.

**Kapitel 10 – Zusammenfassung und offene Fragen**

Die im Zusammenhang dieser Dissertation durchgeführten Versuche haben das Verbundverhalten von einbetonierten und nachträglich eingemörtelten Bewehrungsstäben unter seismischer Beanspruchung umfassend untersucht. Diese Grundlagenforschung ermöglichte eine fundierte Untersuchung des Tragverhaltens von Stützen-Fundament-Anschlüssen unter gewöhnlichen und seismischen Lastfällen. Die wichtigsten Ergebnisse und Rückschlüsse der Untersuchungen sind in Kapitel 10 zusammengefasst.

Zudem führt Kapitel 10 noch offene Fragestellungen auf, im Zuge derer Beantwortung noch interessante Erkenntnisgewinne erwartet werden können:

- Bei der Anwendung des vorgeschlagenen Bemessungskonzept für Stützen-Fundament-Anschlüsse auf Basis der erweiterten Verbundankerbemessungs-vorschriften für nachträglich installierte Bewehrungsanschlüsse werden zugelassene Systeme benötigt. Die zukünftige Zulassungsrichtlinie für nachträglich installierte Verankerungen unter seismischer Beanspruchung (*Proposal for ETAG 001 Seismic Amendment (2012)*) untersucht den Einfluss von zyklischer Last und zyklischem Riss in getrennten Tests: Zyklische Lastversuche von Ankern, die in einem konstant geöffneten Riss installiert wurden und zyklische Rissversuche von Ankern, die von einer konstanten Last belastet werden. Die derzeitige Definition der konstanten Last, die während der zyklischen Riss aufgebracht wird, ist konservativ und gefährdet eine wirtschaftliche Zulassung von Bewehrungsstäben für seismische Anwendungen. Weitere Untersuchungen über die Korrelation zwischen Last und Rissweite bei Anschlussknoten führen potentiell zu einer Reduktion der konstanten Last, die während der Zulassungsversuche im zyklischen Riss angesetzt wird und werden daher empfohlen.
- Falls das vorgeschlagene Bemessungskonzept für Stützen-Fundament-Anschlüsse auf Basis der erweiterten Verbundankerbemessungsvorschriften für einbetonierte Bewehrungsanschlüsse angewendet wird, werden charakteristische Verbundspannungen $\tau_R$ gemäß *CEN/TS 1992-4-5 (2009)* benötigt. Diese charakteristische Verbundspannungen werden im Allgemeinen anhand von Auszugsversuchen mit naher Abstützung gemäß der Zulassungsrichtlinie für Verbundanker (*ETAG 001 (2006)*, Teil 5) ermittelt. Im Gegensatz hierzu wird in der Stahlbetonnorm *Eurocode 2 (2005)* für die verschiedenen Betonfestigkeitsklassen allgemeingültige Bemessungsverbund-spannungen $f_{bd}$ definiert. Es wäre daher sinnvoll Untersuchungen durchzuführen, die die Entwicklung einer allgemeingültigen Beziehung zwischen $f_{bd}$ und $\tau_R$ ermöglichen. Die im *CEB-FIP Model Code 1990 (1993)*, Tabelle 3.1.1 angegebenen Verbundspannungen könnten als Basis dienen.
- Die Versuche mit Stützen-Fundament-Anschlüssen wurden ohne axiale Druckbelastung der Stütze und ohne elastische Bettung des Fundaments durchgeführt. Zusätzliche Untersuchungen zum Bestimmen des positiven Einflusses von axialer Belastung und elastischer Bettung werden empfohlen, die potentiell eine Weiterentwicklung der Verbundankerbemessungsrichtlinien ermöglichen. Desweiteren ist ein verbessertes Verbundverhalten durch die Verwendung von speziell hergestellten Verankerungsstäben zu erwarten, die eine abgestufte, konische Geometrie ähnlich derer von Verbundspreizankern

haben, was ebenfalls eine Reduzierung der Verankerungslänge von Anschlussbewehrungen ermöglichen könnte.

- Um die Vorteile der erweiterten Verbundankerbemessungsvorschriften maximal auszunutzen, ist die Installationssicherheitseinstufung der Systeme für nachträgliche Bewehrungsanschlüsse wichtig. Deshalb sollte das Augenmerk auf die Installationstechnik gerichtet werden, um die Streuung der ermittelten Verbundfestigkeiten zu reduzieren und um eine hohe Installationssicherheits-einstufung im Zuge des Zulassungsverfahrens zu erreichen. Besondere Beachtung erfordert hierbei die Feuchteempfindlichkeit des Mörtels. Zudem könnte ein Konzept aus verpflichtendem Installationstraining und dessen behördliche Zertifizierung eine Reduzierung der in den Zulassungen angegebenen Installationssicherheitsbeiwerte ermöglichen.
- Brände sind ein häufiges Folgeereignis von Erdbebenkatastrophen, die das Verhalten von tragenden und nichttragenden Tragwerksteilen beeinflussen können (*Wang, X.; M. Chen; et al. (2011)*). Folgebrände sind auch relevant für nachträglich installierte Bewehrungsanschlüsse, da die für gewöhnlich verwendeten, auf Epoxydharz basierenden Systeme potentiell empfindlich auf Brandbeanspruchungen reagieren (*Pinoteau, N.; Guillet, T. et al. (2011)*). Es ist sinnvoll anzunehmen, dass der Einfluss für nachträglich installierte Stützenanschlussbewehrung wegen der vom Fundament gebildeten Betondeckung klein ist. Dennoch sind Untersuchungen erforderlich, um diese Annahme zu bestätigen.
- Die Untersuchungen wurden mit quasi-statischen Belastungsgeschwindigkeiten durchgeführt was nach den bisherigen Erfahungen eine konservative Herangehensweise ist (Section 2.2.7). Dennoch sind Untersuchungen erforderlich, um den Einfluss von erhöhten Dehnungsgeschwindigkeiten auf das Verhalten von Stützen-Fundament-Anschlüssen, die gemäß den weiter-entwickelten Verbundankerbemessungsvorschriften konstruiert wurden, zweifelsfrei festzustellen. Die Beobachtung eines positiven Einflusses könnte dazu genutzt werden, die weiterentwickelten Verbundankerbemessungs-vorschriften für Stützen-Fundament-Anschlüssen weniger konservativ auszugestalten.
- Die weiterentwickelten Verbundankerbemessungsvorschriften für Stützen-Fundament-Anschlüsse sind nur gültig, wenn die Stützenanschlussbewehrung über fast die ganze Fundamenttiefe ausgeführt wird. Das Format der Formeln, die den günstigen Effekt aus der Momentenbelastung und den ungünstigen Effekt aus der zyklischen Belastung beschreiben, berücksichtigt den negativen Einfluss von kürzeren Verankerungslängen: Beide Faktoren $\psi_{M,N}$ und $\psi_{cyc,N}$ nehmen bei kürzeren Verankerungslängen bei ansonsten gleichbleibender

Geometrie niedrigere Werte an. Trotzdem sind Untersuchungen notwendig, um die Annahme zu untermauern, dass die weiterentwickelten Verbundanker-bemessungsvorschriften für Stützen-Fundament-Anschlüssen auch gültig sind, wenn die Stützenanschlussbewehrung kürzer als die Fundamenttiefe ausgeführt ist.

## Literature

*DIN 1045 (2001)*: Tragwerke aus Beton, Stahlbeton und Spannbeton: Teil 1 Bemessung und Konstruktion; Teil 2 Festlegung, Eigenschaften, Herstellung und Konformität (Concrete, reinforced concrete and prestressed concrete structures: Part 1, design and construction; Part 2, regulation, properties, production and conformity). Deutsches Institut für Normung (in German)

*DIN 1048 (1991)*: Prüfverfahren für Beton (Test methods for concrete). Deutsches Institut für Normung (in German)

*DIN 4149 (2005)*: Bauten in deutschen Erdbebengebieten: Lastannahmen, Bemessung and Ausführung üblicher Hochbauten, (Construction in German earthquake regions: Loading assumptions, design and execution of typical tall structures). Deutsches Institut für Normung (in German)

*DIN 488-1 (1986)*: Betonstahl – Sorten, Eigenschaften, Kennzeichen (Reinforcing steel – Types, properties, identification). Deutsches Institut für Normung (in German)

*Aboutaha, R. et al. (1994)*: Seismic retrofit of R/C columns with inadequate lap splices. Proceedings of the ASCE '94 Structural Congress, Atlanta

*ACI 224 (2001)*: Control of Cracking in Concrete Structures (ACI 224-01) and commentary (ACI 224R-01), American Concrete Institute, Farmington Hills, Michigan

*ACI 318 (2011)*: Building code requirements for structural concrete (ACI 318-11) and commentary (ACI 318R-11), American Concrete Institute, Farmington Hills, Michigan

*ACI 355.2 (2007)*: Qualification of post-installed mechanical anchors in concrete (ACI 355.2-07) and commentary, American Concrete Institute (ACI), Farmington Hills, Michigan

*ACI 355.4 (2010)*: Acceptance criteria for qualification of post-installed adhesive anchors in concrete (ACI 355.4-10) and commentary (ACI 355.4R-10) (Provisional Standard), American Concrete Institute (ACI), Farmington Hills, Michigan

*ACI 374.1 (2005)*: Acceptance criteria for moment frames based on structural testing and commentary, American Concrete Institute (ACI), Farmington Hills, Michigan

*Alexander, S.; Simmonds, S. (1987)*: Ultimate Strength of Slab-Column Connections. ACI Structural Journal, May-June 1987, Vol. 84, No. 3, 255-261

*Alsiwat, J.; Saatcioglu, M. (1992)*: Reinforcement anchorage slip under monotonic loading. ASCE Journal of Structural Engineering, September 1992, Vol. 118, No. 9, 2421-2438

*Appl, J. (2009)*: Tragverhalten von Verbunddübeln unter Zugbelastung (Behaviour of bonded anchors under tensilion loading). Dissertation, University of Stuttgart, 2009 (in German)

*AS/NZS 4671 (1997)*: Steel reinforcing materials. New Zealand Standard Council, Wellington

*ASCE 7 (2005)*: Minimum design loads for buildings and other structures: Revision of ANSI/ASCE 7-05, American Society of Civil Engineers (ASCE), Reston, Virginia

*ASTM A615 (2004)*: Standard specification for deformed and plain carbon steel bars for concrete reinforcement. American Society for Testing and Materials (ASTM), ASTM International, West Conshohocken, PA

*ASTM A944 (2010)*: Standard test method for comparing bond strength of steel reinforcing bars to concrete using beam-end specimens. American Society for Testing and Materials (ASTM), ASTM International, West Conshohocken, PA

*ATC-40 (1996)*: Seismic evaluation and retrofit of concrete buildings: Volumes 1; 2, Applied Technology Council (ATC)

*Bažant, Z.; Cedolin, L. (1979)*: Blunt crack band propagation in finite element analysis. ASCE Journal of Engineering Mechanics, March 1979, Vol. 105, No. 2, 297-315

*Bažant, Z.; Ožbolt, J. (1990)*: Nonlocal microplane model for fracture, damage, and size effect in structures. ASCE Journal of Engineering Mechanics, Vol. 116, No. 11, 2485-2496

*Bischoff, P.; Perry, S. (1991)*: Compressive behaviour of concrete at high strain rates. Materials and Structures, Vol. 24, No. 6, 1991, 425-450

*Bousias, S.; Verzeletti, G.; Fardis, M. (1995)*: Load-path effects in column biaxial bending with axial force. ASCE Journal of Engineering Mechanics, Vol. 121, No. 5, 596-605

*Bradley, A.; Cubrinovski, M. (2011)*: Near-source strong ground motions observed in the 22 February 2011 Christchurch Earthquake. Bulletin of the New Zealand Society for Earthquake Engineering, Vol. 44, No. 4, 181-194, 2011

*Bruckner, M. (2006)*: Anwendung von Ankerstäben in Rahmenecken, Rahmenendknoten und Stütze-Fundament-Verbindungen (Application of headed bars in external beam-column joints and column-to-foundation connections). Dissertation, University of Stuttgart (in German)

*Bruckner, M.; Eligehausen, R.; Ožbolt, J. (2001)*: Influence of bending compressive stresses on the concrete cone capacity. Proceedings of the Symposium on Connections between Steel and Concrete, Stuttgart

*Fib Bulletin No. 10 (2003)*: Bond of reinforcement in concrete. State-of-art report. Bulletin No. 10, Fédération International du Béton (fib)

*Fib Bulletin No. 24 (2003)*: Seismic assessment and retrofit of reinforced concrete buildings. Bulletin No. 24, Fédération International du Béton (fib)

*Fib Bulletin No. 58 (2011)*: Design of anchorages in concrete. Guide to good practice. Bulletin No. 58, Fédération International du Béton (fib)

*CEB Bulletin d'information No. 120 (1991)*: Behavior and analysis of reinforced concrete structures under alternate actions inducing inelastic response. Bulletin d'information Nr. 210, Comité Euro-International du Béton (CEB), London

*CEB Bulletin d'information No. 131 (1979)*: Structural concrete under seismic action. Bulletin d'information Nr. 131, Comité Euro-International du Béton (CEB), Paris

*CEB Bulletin d'information No. 132 (1981)*: Bond and splices in reinforced concrete for seismic loading. Bulletin d'information Nr. 132, Comité Euro-International du Béton (CEB), Rome

*CEB Bulletin d'information No. 151 (1981)*: Bond action and bond behaviour of reinforcement. Bulletin d'information Nr. 151, Comité Euro-International du Béton (CEB), Paris

*CEB Bulletin d'information No. 158 (1984)*: CEB-Manual Cracking and Deformation. Bulletin d'information Nr. 158, Comité Euro-International du Béton (CEB), London

*CEB Bulletin d'information No. 187 (1988)*: Concrete structures under impact and impulsive loading. Bulletin d'information Nr. 187, Comité Euro-International du Béton (CEB), London

*CEB Bulletin d'information No. 216 (1994)*: Fastenings to concrete and masonry structures. Bulletin d'information Nr. 216, Comité Euro-International du Béton (CEB), London

*CEB Bulletin d'information No. 226 (1995)*: Design of fastenings in concrete, Draft CEB Guide - Part 1 to 3 and Fastenings for seismic retrofitting, State-of-the-art report on Design and application, Bulletin d'information Nr. 226, Comité Euro-International du Béton (CEB), London

*CEB Bulletin d'information No. 230 (1996)*: RC elements under cyclic loading. Bulletin d'information Nr. 230, (state-of-the-art report, printed revised hardbound edition of Bulletin 210), Comité Euro-International du Béton (CEB), London

*CEB Bulletin d'information Nr. 213/214 (1993)*: CEB-FIP Model Code 1990. Bulletin d'information Nr. 213/214, Comité Euro-International du Béton (CEB), London

*CEB State of the Art Report (1996)*: Fastenings for seismic retrofitting, State-of-the-art report on design and application, Comité Euro-International du Béton (CEB), London

*CEB-FIP Model Code 1990 (1993)*: Design Code, Comite Euro-International du Beton, American Society of Civil Engineers

*CEN/TS 1992-4 (2009)*: Design of fastenings for use in concrete – Part 4-1 – 4-5. Technical Specification, European Committee for Standardization (CEN), Brussels

*CEN/TS 1992-4-5 (2009)*: Design of fastenings for use in concrete – Part 4-5: Post-installed fasteners – Chemical systems. Technical Specification, European Committee for Standardization (CEN), Brussels

*Chun, S.-C.; Oh, B.; Lee, S.-H.; Kang, H.-K.; Wallace, J. W. (2009)*: Mechanical anchorage in exterior beam-column joints subjected to cyclic loading. ACI Structural Journal, January-February 2009, Vol. 104, No. 1, 102-112

*Chun, S.-C.; Oh, B.; Lee, S.-H.; Naito, C.-J. (2009)*: Anchorage strength and behavior of headed bars in exterior beam-column joints. ACI Structural Journal, September-October 2009, Vol. 106, No. 5, 579-590

*Chung, L.; Shah, S. P. (1989)*: Effect of loading rate on anchorage bond and beam-column joints. ACI Structural Journal, March-April 1989, Vol. 86, No. 2, 132-142

*Ciampi, V.; Eligehausen, R.; Bertero, V.; Popov, E. (1982)*: Analytical model for concrete anchorages of reinforcing bars under generalized excitations. Report No. UCB/EERC 82-23, Earthquake Engineering Research Center, University of California, Berkeley, California, Nov. 1982

*Cook, R.; Collins, D.; Klingner, R.; Polyzois, D. (1992)*: Load-deflection behavior of cast-in-place and retrofit concrete anchors. ACI Structural Journal, November-December 1992, Vol. 89, No. 6, 639-649

*Cook, R.; Konz, R. (2001)*: Factors influencing bond strength of adhesive anchors. ACI Structural Journal, January-February 2001, Vol. 98, No. 1, 76-86

*Cook, R.; Kunz, J.; Fuchs, W.; Konz, R. (1998)*: Behavior and design of single adhesive anchors under tensile load in uncracked concrete, ACI Structural Journal, Januar-February 1998, Vol. 95, No. 1, 9-26

*Cornell, A. (1967)*: Bounds on the reliability of structural systems. ASCE Journal of the Structural Division, June 1967, Vol. 93, No. 1, 171-200

*Curbach, M. (1987)*: Festigkeitssteigerung von Beton bei hohen Belastungsgeschwindigkeiten (Strength increase of concrete at high loading rates). Dissertation, IMB, Universität Karlsruhe (TH) (in German)

*Dallner, C. (2008)*: Thermomechanische Einsatzgrenzen von Kunststoffen (Thermo-mechanical operating limits of plastics). Dissertation, Universität Erlangen-Nürnberg

*Dhakal, R.; Pan, T.-C. (2003)*: Characteristics of high-speed cyclic test of beam-column joints. ACI Structural Journal, March-April 2003, Vol. 100, No. 2, 188-196

*DIBt KKW Leitfaden (2010)*: Leitfaden für Dübelbefestigungen in Kernkraftwerken und anderen kerntechnischen Anlagen (Guideline for fastenings in nuclear power plants and other nuclear technical facilities), Deutsches Institut für Bautechnik (DIBt), Berlin (in German)

*Dörr, K. (1980)*: Ein Beitrag zur Bemessung von Stahlbetonscheiben unter besonderer Berücksichtigung des Verbundverhaltens (A contribution to the design concept for reinforced concrte slab loaded in plane under particular consideration of the bond behaviour). Dissertation, TH Darmstadt (in German)

*Dutta, A.; Mander, J. (2001)*: Energy based methodology for ductile design of concrete columns. ASCE Journal of Structural Engineering, December 2001, Vol. 127, No. 12, 1374-1381

*EERI SER Chi-Chi (1999)*: The Chi-Chi, Taiwan Earthquake of September 21, 1999. Special Earthquake Report, Earthquake Engineering Research Institute (EERI), Oakland, California

*EERI SER Christchurch (2011)*: The M 6.3 Christchurch, New Zealand, Earthquake of February 22. Special Earthquake Report, Earthquake Engineering Research Institute (EERI), Oakland, California

*EERI SER Kobe (1996)*: Kobe eight months after: Images of the “Interim City”. Learning from Earthquakes, Earthquake Engineering Research Institute (EERI), Oakland, California

*EERI SER Maule (2010)*: The Mw 8.8 Chile Earthquake of February 27, 2010. Special Earthquake Report, Earthquake Engineering Research Institute (EERI), Oakland, California

*Eibl, J.; Curbach, M. (1989)*: An attempt to explain strength increase due to high loading rates. Nuclear Engineering and Design, Vol. 112, 45-50

*Eibl, J.; Idda, K.; Lucero-Cimas, H.-N. (1997)*: Verbundverhalten bei Querzug (Bond behaviour under shear load). Forschungsbericht, IMB, Universität Karlsruhe (TH) (in German)

*Eibl, J.; Keintzel, E. (1989)*: Zur Beanspruchung von Befestigungsmitteln bei dynamischen Lasten (Loading of fastenings under dynamic loads). IMB, Universität Karlsruhe (TH) (in German)

*Eligehausen, R.; Cook, R.; Appl, J. (2006)*: Behavior and design of adhesive bonded anchors. ACI Structural Journal, November-December 2006, Vol. 103, No. 6, 822-830

*Eligehausen, R.; Herzog, M. (2008)*: Bemessung – Vereinheitlichung Stahlbeton- und Dübeltheorie (Design – Unifying reinforced concrete methoid and anchor method). University of Stuttgart, not published (in German)

*Eligehausen, R.; Herzog, M.; Mahrenholtz, C. (2012)*: Bridging the gap between design provisions for connections using anchorage models and reinforced concrete Models. ACI Spring Convention 2012, Texas

*Eligehausen, R.; Lettow, S.; Ožbolt, J.; Mayer, U. (2003)*: Bond of RC members using nonlinear 3D FE Analysis. Proceedings of the Conference on Fracture Mechanics of Concrete Structures (FraMCoS 5), Volume 2, Vail

*Eligehausen, R.; Mallée, R.; Silva, J. (2006)*: Anchorage in concrete construction. Ernst & Sohn, Berlin

*Eligehausen, R.; Ožbolt, J.; Genesio, G.; Hoehler, M.; Pampanin, S. (2006)*: Three-dimensional modelling of poorly detailed RC frame joints. Proceedings for the Conference of the New Zealand Society for Earthquake Engineering (NZSEE 2006), Napier

*Eligehausen, R.; Popov, E.; Bertero, V. (1983)*: Local bond stress-slip relations of deformed bars under generalized excitations. Report No. UCB/EERC 83-23, Earthquake Engineering Research Center, University of California, Berkeley, California, Oct. 1983

*Engström, B. (1992)*: Ductility of tie connections in precast structures. Chalmers University of Technology, Göteborg

*Engström, B.; Magnusson, J.; Huang, A. (1998)*: Pull-out behavior of ribbed bars in normal and high-strength concrete with various confinements. Proceedings of Bond and development of reinforcement: a tribute to Dr. Peter Gergely. ACI Special Publication 180, 215-242

*EOTA TR 023 (2006)*: Assessment of post-installed rebar connections. Technical Report 023

*EOTA TR 029 (2010)*: Design of bonded anchors. Technical Report 029

*ETAG 001 (2006)*: Guideline for European technical approval of metal anchors for use in concrete, Parts 1 – 6. European Organization of Technical Approvals (EOTA), Brussels

*Eurocode 0 (2002)*: Basis of structural design. European Committee for Standardization (CEN); DIN EN 1990-: 2002

*Eurocode 2 (2005)*: Design of concrete structures. European Committee for Standardization (CEN); DIN EN 1992: 2005

*Eurocode 2 / NA (2009)*: Design of concrete structures – National Annex. European Committee for Standardization (CEN); DIN EN 1992: 2009/NA (draft)

*Eurocode 8 (2006)*: Design of structures for earthquake resistance. European Committee for Standardization (CEN); DIN EN 1998: 2006

*Eurocode 8 / NA (2009)*: Design of structures for earthquake resistance – National Annex. European Committee for Standardization (CEN); DIN EN 1998: 2009/NA (draft)

*Feistel, G. (2012)*: Aktueller Stand der Europäischen Regelungen für Befestigungssysteme (Update of the European standards for fastening systems). Beton-Kalender 2012, Part 2, 1-11, Ernst & Sohn, Berlin

*Fellinger, M. (2009)*: Difference and Similarities of 'Anchor' and 'Rebar' connections. 5th Central European Congress on Concrete Engineering, Baden

*Fichtner, S. (2011)*: Untersuchungen zum Tragverhalten von Gruppenbefestigungen unter Berücksichtigung der Ankerplattendicke und einer Mörtelschicht (Investigation on the behaviour of anchor groups under consideration of anchor plate thickness and mortar layer). Dissertation, University of of Stuttgart, 2011 (in German)

*Fischer, L. (1995)*: Bestimmung des 5%-Quantils im Zuge der Bauwerksprüfung – Bezugnahme auf DIN-Normen und Eurocodes (Evaluation of 5%-Quantile in the course of Structural Inspection. Reference to DIN-Standards and EURO-Codes). Bautechnik 72, Heft 11, 712-722

*Franchi, A.; Rosati, G.; Cattaneo, S.; Crespi, P.; Muciaccia, G. (2009)*: Experimental investigation on post-installed metal anchors subjected to seismic loading in R/C members. Studi e ricerche - Politecnico di Milano. Scuola di specializzazione in construzioni in cemento armato, Volume 29

*Fraser, D. (1983)*: Elastic Analysis of Laterally Loaded Frames. J. Struct. Eng. 109, 1479 (1983)

*Fu, H.; Erki, M.; Seckin, M. (1991)*: Review of effects of loading rate on reinforced concrete. ASCE Journal of Structural Engineering, September 1991, Vol. 117, No. 12, 3660-3679

*Fuchs, W. (2007)*: The human factor in fastening technology-a force to be reckoned with. Proceedings of the 2nd RILEM International Symposium on Connections between Steel and Concrete, Stuttgart

*Fuchs, W.; Eligehausen, R.; Breen, J. (1995)*: Concrete Capacity Design (CCD) Approach for fastening to concrete. ACI Structural Journal, January-February 1995, Vol. 92, No. 6, 73-94

*Gambarova, P.; Rosati, G. (1996)*: Bond and splitting in bar pull-out: behavioural laws and concrete cover role. Magazine of Concrete Research, Volume 49, Issue 179, 99-110

*Gambarova, P.; Rosati, G.; Zasso, B. (1989)*: Steel-to-concrete bond after concrete splitting: Test Results. Materials and Structures, Vol. 22, No. 127, 1989, 35-47

*Grasser, E.; Thielen, G. (1972)*: Hilfsmittel zur Berechnung der Schnittgrößen und Formänderungen von Stahlbetontragwerken (Tools to determine forces and deformations of reinforced concrete structures). Schriftenreihe DAfStb, No. 240 (in German)

*Gutierrez, E.; Magonette, G.; Verzeletti, G. (1993)*: Experimental studies of loading rate effects on reinforced concrete columns. ASCE Journal of Engineering Mechanics, Vol. 119, No. 1, 887-904

*Hahn, C. (2008)*: Approval tests according to ETAG and AC 308 on the adhesive anchors consisting of the deformed rebar #4 (1/2 in) and the reaction resin mortar X. Report No. Y (confidential, not published)

*Hamad, B.; Hammoud, A.; Kunz, J. (2006)*: Evaluation of bond strength of bonded-in or post-installed reinforcement. ACI Structural Journal, March-April 2006, Vol. 103, No. 2, 207-218

*Harajli, M.; Mabsout, M. (2002)*: Evaluation of bond strength of steel reinforcing bars in plain and fiber-reinforced concrete. ACI Structural Journal, July-August 2002, Vol. 99, No. 4, 509-517

*Haskett, M.; Oehlers, D.; Mohamed Ali, M. (2008)*: Local and global bond characteristics of steel reinforcing bars. Engineering Structures 30, 376-383

*Hawkins, N.; Lin, I.; Ueda, T. (1986)*: Beam bar anchorage in exterior column-beam connections. ACI Journal Proceedings, May 1986, Vol. 83, No. 3, 412-422

*Hawkins, N.; Lin, I.-J.; Jeang, F.-L. (1982)*: Local bond strength of concrete for cyclic reversed actions. Proceedings of Bond in Concrete, Applied Science Publishers, London, 151-161

*Henry, R.; Ingham, J. (2011)*: Behaviour of tilt-up precast concrete buildings during the 2010/2011 Christchurch earthquakes. Structural Concrete, Vol. 12, No. 4

*Herzog, M. (2008)*: Harmonization of design in reinforced concrete and fastening technology. Proceedings of the 7th fib International PhD Symposium in Civil Engineering, Stuttgart

*Herzog, M. (2010)*: Experimentelle Untersuchungen zum Tragverhalten von eingemörtelter Bewehrung in Rahmenknoten (Experimental studies on the behaviour of post-installed anchorages in joints). Internal Presentation Institute für Befestigungstechnik, not published (in German)

*Herzog, M. (2012)*: Vereinheitlichung der Bemessung im Stahlbetonbau und der Befestigungstechnik (Design concept unification for reinforced concrete and concrete anchors). Dissertation, University of Stuttgart, 2012 (in German, in preparation)

*Hjorth, C. (1979)*: Ein Beitrag zur Frage der Festigkeiten und des Verbundverhaltens von Stahl und Beton bei hohen Dehngeschwindigkeiten (A contribution to the bond problem of steel and concrete under high strain rates). Dissertation, Technische Universität Braunschweig (in German)

*Hoehler, M. (2006)*: Behavior and testing of fastenings to concrete for use in seismic applications. Dissertation, University of Stuttgart, 2006

*Hülder, G. (2008)*: Zur Aushärtung kalthärtender Reaktionsharzsysteme für tragende Anwendungen im Bauwesen (Curing of cold-hardening reaction resin systems for structural applications in construction). Dissertation, Universität Erlangen-Nürnberg

*Hwang, S.-J.; Kuo, W.-W. (2007)*: Recent advances in seismic retrofit of RC structures in Taiwan. Proceedings of the Indonesia International Cement and Concrete Forum, 366-379, Jakarta

*IBC (2006)*: International Building Code (IBC). International Code Council (ICC), 2006

*Idda, K. (1999)*: Verbundverhalten von Betonrippenstählen bei Querzug (Bond behaviour of deformed reinforcing bars considering transverse tension). Dissertation, IMB, Universität Karlsruhe (TH) (in German)

*ISE (2012)*: The Mw9.0 Tōhoku Earthquake and Tsunami of 11th March 2011. Field Report of Earthquake Engineering Field Investigation Team (EEFIT), The Institution of Structural Engineers (ISE), London, UK

*Jagfeld, P. (1980)*: Langzeituntersuchungen an epoxidharzverklebten Zementmörtelprismen (Long-term tests with cement specimen glued together with epoxy resin). Schriftenreihe DAfStb, No. 309 (in German)

*Jendele, L.; Cervenka, J. (2006)*: Finite element modelling of reinforcement with bond. Computers and Structures 84, 1780–1791

*Jirsa, J.; Breen, J.; Luke, J.; Hamad, B. (1982)*: Effect of casting position on bond. Proceedings of Bond in Concrete, 1982

*Jones, E.; Jirsa, J. (1986)*: Seismic strengthening of a reinforced concrete frame using structural steel bracing. Structural Laboratory Report 86-5, The University of Texas at Austin

*Kang, H.-K.; Shin, M.; Mitra, N.; Bonacci, J. (2009)*: Seismic design of reinforced concrete beam-column joints with headed bars. ACI Structural Journal, November-December 2009, Vol. 106, No. 6, 868-877

*Karihaloo, B. (1994)*: Fracture mechanics and structural concrete. Longman Concrete Design and Construction Series

*Kenek, A.; Martin, P. (2001)*: Faseroptische Dehnungsmessungen an einbetonierten Bewehrungsstäben (Fibre optical strain measurement of cast in situ reinforcing bars). Institut für Baustatik und Konstruktion, ETH, Zürich (in German)

*Kobarg, J. (1986)*: Ein inkrementelles Stahl-Betonverbundgesetz unter Berücksichtigung von Stahldehnung und Querdruck (Incremental steel concrete bond model considering steel strain and lateral pressure). Dissertation, IMB, Universität Karlsruhe (TH) (in German)

*Kreuser, R.; Purainer, R. (2003)*: Zur wirklichkeitsnahen Berechnung von Tragwerken aus Stahlbeton (Realistic analysis of reinforced concrete structures). Bauingenieur, 2003, Volume 78 (in German)

*Kulkarni, S.; Shah, S. (1998)*: Response of reinforced concrete beams at high strain rates. ACI Structural Journal, November-December 1998, Vol. 95, No. 6, 705-715

*Kunnath, S.; Chai, Y.-H. (2004)*: Cumulative damage-based inelastic cyclic demand spectrum. Earthquake Engineering and Structural Dynamics, Vol. 33, No. 4, 499-520

*Kunz, J.; Cook, R.; Fuchs, W.; Spieth, H. (1998)*: Tragverhalten und Bemessung von chemischen Befestigungen (Load behaviour and design of chemical fastenings). Beton- und Stahlbetonbau 93, Heft 1 (in German)

*Kupfer, H.; Münger, F.; Kunz, J.; Jährig, A. (2003)*: Nachträglich verankerte gerade Bewehrungsstäbe bei Rahmenknoten (Post-installed straight reinforcingbars for moment frame joints). Bauingenieur, 2003, Volume 78 (in German)

*Lee, G.-C.; Loh, C.-H. (1999)*: Preliminary report from MCEER-NCREE workshop on the 921 Taiwan earthquake. A summary report of earthquake reconnaissance efforts of the multidisciplinary center for earthquake engineering research, Buffalo

*Lee, H.-J.; Yu, S.-Y. (2009)*: Cyclic response of exterior beam-column joints with different anchorage methods. ACI Structural Journal, May-June 2009, Vol. 106, No. 3, 329-339

*Lee, J.-H. (2008)*: Damage analysis of reinforced concrete columns under cyclic loading. KCI Concrete Journal (July 2001 Vol. I 3 No. 2)

*Leonhardt, F.; Mönnig, E. (1977)*: Vorlesungen über Massivbau. Teil 3: Grundlagen zum Bewehren im Stahlbetonbau (Reinforced concrete lecture. Part 3: Basics for reinforcement detailing). 3. Auflage, Springer, Berlin (in German)

*Lettow, S. (2007)*: Ein Verbundelement für nichtlineare Finite Elemente Analysen – Anwendung auf Übergreifungsstößen (A bond element for non-linear finite element analysis – Applied on splices). Dissertation, University of Stuttgart (in German)

*Lettow, S.; Eligehausen, R.; Ožbolt, J. (2004)*: The simulation of bond between concrete and reinforcement in nonlinear threedimensional finite element analysis. Proceedings of the 5th fib International PhD Symposium in Civil Engineering, Stuttgart

*Liao, Y.-H. et al. (2005)*: Deaths related to housing in 1999 Chi-Chi, Taiwan, earthquake. Safety Science 43

*Lindorf, A.; Lemnitzer, L.; Curbach, M. (2009)*: Experimental investigations on bond behaviour of reinforced concrete under transverse tension and repeated loading. Engineering Structures 31, 1469-1476

*De Lorenzis, L.; Teng, J.-G. (2006)*: Near-surface mounted FRP reinforcement: An emerging technique for strengthening structures. Composites Part B: Engineering, Vol. 38, 119-143

*Lowes, L.; Moehle, J.; Govindjee, S. (2004)*: Concrete-steel bond model for use in finite element modeling of reinforced concrete structures. ACI Structural Journal, July-August 2004, Vol. 101, No. 4, 501-511

*Mahrenholtz, C. (2008)*: European approvals of concrete anchors: Qualification procedures and tests. Workshop on Concrete for Coastal Environment, NIT Mangalore, India

*Mahrenholtz, C. (2009a)*: Eingemörtelte Bewehrungsstäbe im sich zyklisch öffnenden und schließenden Riss (Post-installed reinforcing bars subjected to crack cycling). Report WS 222/10-08/06 of the Institut für Werkstoffe im Bauwesen (IWB), Universität Stuttgart, not published (in German)

*Mahrenholtz, C. (2009b)*: Handout DIBt AK KKW: Äquivalenz Rissprüfung mit vergrößerten Riss und zusammengedrückten Riss (Handout DIBt WG NNP: Equivalence of crack test with enlarged crack and compressed crack). Presentation to meeting 26.06.2009, Berlin, not published

*Mahrenholtz, C. (2009c)*: Cyclic crack tests on Hilti KB-TZ, Hilti HSL-3-G, Hilti HUS-H, Hilti HDA-T, Hilti HIT-RE500SD, Hilti HIT-HY150 MAX, Simpson StrongBolt, Simpson SET-XP; Headed Bolts – Test and summary report. HS II/09-09/06, Institut für Werkstoffe im Bauwesen, Universität Stuttgart, not published

*Mahrenholtz, C. (2009d)*: Eingemörtelte Bewehrungsstäbe im sich zyklisch öffnenden und schließenden Riss, Weiteres Vorgehen (Post-installed reinforcing bars subjected to crack cycling, Next steps). Presentation WS 222/12-09/10 of the Institut für Werkstoffe im Bauwesen (IWB), Universität Stuttgart, not published (in German)

*Mahrenholtz, C. (2009e)*: Cyclic crack tests on post-installed and cast-in anchors – Test and summary report. HS II/09-09/06, Institut für Werkstoffe im Bauwesen, Universität Stuttgart, not published

*Mahrenholtz, C. (2009f)*: Cyclic crack tests on single anchors. Workshop, Seismic Testing Criteria, Stuttgart, July 6

*Mahrenholtz, C. (2010)*: Guidance for testing on anchors in cycled concrete cracks. E10/12-Bft/12, Institut für Werkstoffe im Bauwesen, Universität Stuttgart, not published

*Mahrenholtz, C. (2011a)*: Displacement-controlled tests on monotonically and cyclically loaded reinforcing bars installed in constant and cycled cracks, analytical studies. E11/02-R/06, Institut für Werkstoffe im Bauwesen, Universität Stuttgart, not published

*Mahrenholtz, C. (2011b)*: Displacement-controlled tests on monotonically and cyclically loaded reinforcing bars installed in constant and cycled cracks, experimental studies. E11/02-R/02, Institut für Werkstoffe im Bauwesen, Universität Stuttgart, not published

*Mahrenholtz, C. (2011c)*: Displacement-controlled tests on monotonically and cyclically loaded reinforcing bars installed in constant and cycled cracks, numerical studies. E11/02-R/05, Institut für Werkstoffe im Bauwesen, Universität Stuttgart, not published

*Mahrenholtz, C. (2011d)*: An alternative method of strain gauge application for measuring strains continuously along a reinforcing bar. Annual Report 2008/10, 69-76 of the Institut für Werkstoffe im Bauwesen (IWB), Universität Stuttgart

*Mahrenholtz, C. (2011e)*: Strain gauge application for measuring strains continuously along reinforcing bar. Institut für Werkstoffe im Bauwesen, Universität Stuttgart, not published

*Mahrenholtz, C. (2012a)*: Column-to-foundation connections under monotonic and cyclic loading, experimental studies. E11/02-R/07, Institut für Werkstoffe im Bauwesen, Universität Stuttgart, not published

*Mahrenholtz, C. (2012b)*: Column-to-foundation connections under monotonic and cyclic loading, numerical studies. E11/02-R/08, Institut für Werkstoffe im Bauwesen, Universität Stuttgart, not published

*Mahrenholtz, C.; Eligehausen, R.; Hofmann, J. (2011)*: Behavior and design of connections with post-installed reinforcing bars under seismic loading. Presentation to fib SAG Fastening Meeting 2011, Berlin, not published

*Mahrenholtz, C.; Eligehausen, R.; Hofmann, J. (2012)*: Seismic bond model for cast-in-place and post-installed reinforcing bars. Proceedings of the Conference on Bond in Concrete (BIC), Brescia

*Mahrenholtz, C.; Eligehausen, R.; Hofmann, J.; Fuchs, W. (2012)*: Post-installed bars under low installation temperatures. Proceedings of the 3rd International Conference on Concrete Repair, Rehabilitation and Retrofitting (ICCRRR), Cape Town

*Mahrenholtz, C.; Eligehausen, R.; Hofmann, J.; Pampanin, S. (2011)*: Bond deterioration of between reinforcing bars and concrete subject to cyclic loads and cracks. Proceedings of the Conference on Advances in Concrete through Science and Engineering (RILEM PRO 79), Hongkong

*Mahrenholtz, C.; Eligehausen, R.; Sharma, A. (2010)*: Behavior of post-installed concrete undercut anchors subjected to high loading rate and crack cycling frequency. Proceedings of the 9th U.S. National and 10th Canadian Conference on Earthquake Engineering, Paper No 1589, Toronto

*Mahrenholtz, C.; Sharma, A. (2010)*: Influence of High Rate on Hilti HDA – Final Report with Test Protocols. AF09/03-RWE07/03, Institut für Werkstoffe im Bauwesen, Universität Stuttgart

*Mahrenholtz, C.; Silva, J.; Eligehausen, R.; Hofmann, J. (2012)*: Testing anchors in cyclic cracks: Guidance for testing laboratories on how to generate cracks and cycle crack widths. Concrete International (in preparation)

*Mahrenholtz, P. (2010)*: Cyclic shear and cyclic crack tests on undercut anchors, expansion anchors, and headed bolts – Test and Summary Report. HS II/14-10/05, Institut für Werkstoffe im Bauwesen, Universität Stuttgart, not published

*Mahrenholtz, P. (2012)*: Experimental performance and recommendations for qualification of post-installed anchors for seismic applications. Dissertation, University of Stuttgart, 2012

*Mahrenholtz, P.; Mahrenholtz, C.; Eligehausen, R. (2013)*: Behavior of headed bolts during load and crack cycling. Engineering Structures (in preparation)

*Mahrenholtz, P.; Mahrenholtz, C.; Sharma, A.; Eligehausen, R. (2012)*: Concrete undercut anchors: Performance under dynamic actions in the context of qualification for use in NPP. Engineering Structures (in preparation)

*Mainz, J. (1993)*: Modellierung des Verbundtragverhaltens von Betonrippenstahl (Modelling of the bond behaviour of deformed reinforcing bars). Berichte aus dem Konstruktiven Ingenieurbau, TU München (in German)

*Malhotra, P. (2002)*: Cyclic-demand spectrum. Earthquake Engineering and Structural Dynamics, Vol. 31, No. 7, 1441-1457

*Malvar, L. (1992)*: Bond of reinforcement under controlled confinement. ACI Materials Journal, November-December 1992, Vol. 89, No. 6, 593-601

*Malvar, L.; Ross, C. (1998)*: Review of strain rate effects for concrete in tension. ACI Materials Journal, November-December 1992, Vol. 95, No. 6, 735-739

*Martin, H. (1973)*: Zusammenhang zwischen Oberflächenbeschaffenheit, Verbund und Sprengwirkung von Bewehrungsstählen unter Kurzzeitbelastung (Dependency of reinforcing bars on surface, bond, and wediging effect under short term loading). Schriftenreihe DAfStb, No. 228 (in German)

*Martin, H.; Noakowski, P. (1981)*: Verbundverhalten von Betonstählen – Untersuchung auf der Grundlage von Ausziehversuchen (Bond behaviour of reinforcing bars – Study based on bond tests). Schriftenreihe DAfStb, No. 319 (in German)

*Matthews, P. (2011)*: Death Zone. The Press, New Zealand, 10.04.2011

*Mazzarolo, E.; Scotta, R.; Berto, L.; Saetta, A. (2012)*: Long anchorage bond-slip formulation for modeling of r.c. elements and joints. Engineering Structures 34, 330–341

*Mazzolani, F.; Della Corte, G.; D'Aniello, M. (2009)*: Experimental analysis of steel dissipative bracing systems for seismic upgrading. Journal of Civil Engineering and Management, Vol. 15, No. 1, 7-19

*Menegotto, M.; Pinto, P. (1973)*: Method of analysis of cyclically loaded reinforced concrete plane frames including changes in geometry and nonelastic behaviour of elements under combined normal geometry and nonelastic behaviour of elements under combined normal force and bending. Proceedings of the IABSE Symposium on the Resistance and Ultimate Deformability of Structures Acted on by Well-defined Repeated Loads, Lisbon

*Menzel, C. (1939)*: Some factors influencing results of pull-out bond tests. ACI Journal, May-June 1939, Vol. 35, No. 6, 517-544

*Mészáro š , J. (2002)*: Tragverhalten von Einzelverbunddübeln unter zentrischer Kurzzeitbelastung (Short-term load behavior of adesive anchors under tension). Dissertation, University of Stuttgart (in German)

*Monti, G.; Spacone, E.; Filippou, F. (1993)*: Model for anchored reinforcing bars under seismic excitations. Report No. UCB/EERC 93-08, Earthquake Engineering Research Center, University of California, Berkeley, California, Dec. 1993

*Morita, S.; Kaku, T. (1973)*: Local bond stress-slip relationship under repeated loading. Proceedings of the IABSE Symposium on the resistance and ultimate deformability of structures acted on by well-defined repeated loads, Lisbon

*Mullapudi, T. (2004)*: Monotonic and cyclic behaviour of headed anchors with cracked and uncracked concrete. Master Thesis, IWB, Universität Stuttgart

*Noakowski, P.; Janovic, K. (1978)*: Vorschlag für ein allgemeingültiges Verbundprüfverfahren (Proposal for gerneric bond test). Institutsbericht, Lehrstuhl für Massivbau, TU München (in German)

*Nuti, C.; Santini, S. (2008)*: Fastening technique in seismic areas: A critical review. Proceedingof the Conference on Tailor Made Concrete Structures, 899-905, Roma

*NZS 1170.5 (2004)*: Structural design actions. Part 5: Earthquake actions. New Zealand Standard Council, Wellington

*NZS 3101 (2006)*: Concrete structures standard. Part 1: The Design of Concrete Structure. Part 2: Commentary on the Design of Concrete Structures. New Zealand Standard Council, Wellington

*NZS 3104 (2003)*: Specification for Concrete Production. New Zealand Standard Council, Wellington

*NZS 3109 (1997)*: Concrete Construction. New Zealand Standard Council, Wellington

*NZS 3112 (1986)*: Specification for Methods of Tests of Concrete. Part 1: Tests relating to fresh concrete. Part 2: Tests relating to determination of strength of concrete. New Zealand Standard Council, Wellington

*Ožbolt, J. (1999a)*: Finite element program for 3D nonlinear analysis of concrete and reinforced concrete structures. Institut für Werkstoffe im Bauwesen, Universität Stuttgart, Germany

*Ožbolt, J. (1999b)*: Masa Manual.

*Ožbolt, J. (2011)*: Personal communication, September 19, 2011

*Ožbolt, J.; Lettow, S.; Kozar, I. (2002)*: Discrete bond element for 3D finite lement analysis of reinforced concrete structures. Proceedings of Bond in concrete - from research to standards, University of Technology and Economics, Budapest

*Ožbolt, J.; Li, Y.-J.; Kozar, I. (2001)*: Microplane model for concrete with relaxed kinematic constraint. International Journal of Solids and Structures, 38, 2683-2711

*Paulay, T.; Priestley, N. (1992)*: Seismic design of reinforced concrete and masonry buildings. John Wiley & Sons, Inc.

*Pinoteau, N.; Guillet, T.; Pimienta, P.; Rivillon, P.; Rémond, S. (2011)*: Fire resistance of post-installed rebars. Presentation to fib SAG Fastening Meeting 2011, Berlin, not published

*Pochanart, S.; Harmon, T. (1989)*: Bond-slip model for generalized excitations including fatigue. ACI Materials Journal, September-October 1989, Vol. 86, No. 5, 465-476

*Priestley, N.; Seible, F.; Calvi, G. (2007)*: Seismic design and retrofit of bridges. John Wiley & Sons, Inc.

*Proposal for ETAG 001 Seismic Amendment (2012)*: Guideline for European Technical Approval of metal anchors for use in concrete - Annex E: Assessment of metal anchors under seismic actions. Draft April 2012

*Randl, N. (2007)*: Load bearing behaviour of cast-in shear dowels. Beton- und Stahlbeton, Vol. 102, Special Edition, 2007, 31-37

*Rehm, G. (1958)*: Über die Grundlagen des Verbundes zwischen Stahl und Beton (Basic principles of the bond between steel and concrete). Dissertation, Technische Universität München, Schriftenreihe DAfStb, No. 138 (in German)

*Rehm, G.; Eligehausen, R. (1979)*: Bond of ribbed bars under repeated loads. Journal of the American Concrete Institute, Vol. 76, Nr. 2, Feb. 1979, 297-309

*Rehm, G.; Franke, L. (1978)*: Verankerungen von Betonrippenstählen in Kunstharzmörtel und Kunstharzbeton (Anchorage of ribbed rebars in resin mortar and resin concrete). Bauingenieur, 1978, Volume 53 (in German)

*Rehm, G.; Franke, L. (1982)*: Kleben im konstruktiven Ingenieurbau (Bonding in structural engineering). Schriftenreihe DAfStb, No. 321 (in German)

*Rehm, G.; Franke, L.; Zeus, K. (1980)*: Kunstharzmörtel und Kunstharzbetone unter Kurzzeit- und Dauerstandbelastung (Resin mortars and resin concrete under short- and long-term loading). Schriftenreihe DAfStb, No. 309 (in German)

*RILEM/CEB/FIP (1982)*: RC5 Bond test for reinforcement steel. 1. Beam test. RC6 Bond test for reinforcement steel. 1. Pull-out test.

*Riva, P. (2006)*: Seismic behaviour of precast colum-to-foundation grouted sleeve connections. Advances in Engineering Structures, Mechanics & Construction, 121-128

*RMS (2000)*: Event Report: Chi-Chi, Taiwan Earthquake. Risk Management Solutions

*Rodriguez, M.; Muttoni, A.; Gambarova, P. (2007)*: Analytical modeling of the pre- and postyield behavior of bond in reinforced concrete. ASCE Journal of Structural Engineering, October 2007, Vol. 133, No. 10, 1364-1372

*Rodriguez, M.; Zhang, Y.-G.; Lotez, D.; Graves, H.; Klingner, R. (1995)*: Dynamic behaviour of anchors in cracked and uncracked concrete: a progress report. Nuclear Engineering and Design, Vol. 168, 23-34

*Rößle, M.; Mészáro š , J. (1998)*: Ausziehversuche an Einzelbefestigungen mit Injektionsdübeln M16: Einfluss von Bohrlochdurchmesser und Lage der Ankerstange im Bohrloch (Pullout tests on single connections with adhesive anchors M16: Influence of drill hole diameter and position of metal part in the drill hole).Bericht Nr. 98/8-2/5, IWB, Universität Stuttgart, not published (in German)

*Rostasy, F.; Scheuermann, J. (1987)*: Verbundverhalten einbetonierten Betonrippenstahls bei extrem tiefer Temperatur (Bond behaviour of cast-in ribbed reinforcing bars at extreme low temperatures). Schriftenreihe DAfStb, No. 380 (in German)

*Royles, R.; Morley, P.; Khan, M. (1982)*: The behaviour of reinforced concrete at elevated temperatures with particular reference to bond strength. Proceedings of Bond in Concrete, 1982

*Ruiz, M.; Muttoni, A.; Kunz, J. (2010)*: Strengthening of flat slabs against punching shear using post-installed shear reinforcement. ACI Structural Journal, July-August 2010, Vol. 107 No. 4, 434-442

*Russo, G.; Pauletta, M. (2006)*: A simple method for evaluating the maximum slip of anchorages. Materials and Structures, Vol. 39, No. 5, 2006, 533-546

*Russwurm, D.; Martin, H. (1993)*: Betonstähle für den Stahlbetonbau (Reinforcing bars for reinforced concrete structures). Institut für Stahlbetonbewehrung e.V., München

*Saatcioglu, M.; Ozcebe, G. (1989)*: Response of reinforced concrete columns to simulated seismic loading. ACI Structural Journal, January-February 1989, Vol. 86, No. 1, 3-12

*Sasani, M.; Bazan, M.; Sagiroglu, S. (2007)*: Experimental and analytical progressive collapse evaluation of actual reinforced concrete structure. ACI Structural Journal, November-December 2007, Vol. 104, No. 6, 731-739

*Schlaich, J.; Schäfer, K. (2001)*: Konstruieren im Stahlbetonbau (Designing of reinforced concrete). Beton-Kalender 2001, 341-395, Part 2, Ernst & Sohn, Berlin.

*SESOC (2011)*: Christchurch Seismic Design Load Levels Interim Advice

*Shakya, K.; Matsumoto, K.; Watanabe, K.; Niwa, J. (2012)*: Cyclic response of beam-column joints of RC bridges upon partial replacement of steel rebars with steel

fibers. Proceedings of the 9th CUEE and 4th ACEE Joint Conference, Tokyo, 947-954

*Sharma, A. (2008)*: Investigation on inelastic behavior of non-seismically detailed reinforced concrete beam-column joints under cyclic excitations, Visiting Researcher Report, IWB, Universität Stuttgart, not published

*Sharma, A.; Ožbolt, J.; Reddy, G.; Vaze, K.; Ghosh, A.; Kushwawa, H. (2010)*: Effect of loading rate on load-deflection behavior and failure mode of plain concrete slabs – 3D finite element analysis approach. International Journal of Earth Sciences and Engineering, Vol. 3, No. 4, 812-822

*Shi, Y.-C.; Li, Z.-X.; Hao, H. (2009)*: Bond slip modelling and its effect on numerical analysis of blast-induced responses of RC columns. Journal of Structural Engineering and Mechanics, Vol. 32, No.2, 2009

*Shima, H.; Chou, L.-L.; Okamura, H. (1987)*: Micro and macro models for bond in reinforced concrete. Journal of the Faculty of Engineering, Vol. XXXIX, No. 2, 133-194, University of Tokyo

*Shiohara, H. et al. (1986)*: Study on seisic retrofitting of existing reinforced concrete frames using post-cast shear walls. Aoyama Laboratory, Department of Architecture, Faculty of Engineering, University of Tokyo

*Simons, I. (2007)*: Verbundverhalten von eingemörtelten Bewehrungsstäben unter zyklischer Beanspruchung (Bond behaviour of post-installed reinforcing bars subjected to cyclic loading). Dissertation, University of Stuttgart (in German)

*Simons, I.; Eligehausen, R. (2008)*: Tragverhalten und Bemessung von eingemörtelten Bewehrungsstäben unter zyklischer Beanspruchung im ungerissenen und gerissenen Beton (Behavior and design of reinforcing bars under cyclic loading post-installed in uncracked and cracked concrete). Beton- und Stahlbetonbau 103, Heft 9 (in German)

*Sippel, T. (1996)*: Zum Trag- und Verformungsverhalten von Stahlbetontragwerken unter Betriebsbelastung (Load bearing and displacement behaviour of reinforced concrete structures under service loads). Dissertation, University of Stuttgart (in German)

*Souroushian, P.; Choi, K.-B. (1989)*: Local bond of deformed bars with different diameters in confined concrete. ACI Structural Journal, March-April 1989, Vol. 86, No. 2, 217-222

*Souroushian, P.; Choi, K.-B.; Park, G.-H.; Aslani, F. (1991)*: Bond of deformed bars to concrete: Effects of confinement and strengths of concrete. ACI Materials Journal, May-June 1991, Vol. 88, No. 3, 227-232

*Spieth, H. (2003)*: Tragverhalten und Bemessung von eingemörtelten Bewehrungsstäben (Behaviour of post-installed reinforcing bars). Dissertation, University of Stuttgart

*Spieth, H.; Eligehausen, R. (2002)*: Bewehrungsanschlüsse mit nachträglich eingemörtelten Bewehrungsstäben (Reinforcement connections with post-installed reinforcing bars). Beton- und Stahlbetonbau 97, Heft 9 (in German)

*Stempniewski, L.; Urban, M.; Münich, C.; Zangani, D.; Messervey, T.; Sasek, S.; Liehr, S. (2010)*: Shaking table test of a two-storey stone masonry building reinforced with multifunctional textiles – 3rd International Workshop on Conservation of Heritage Structures using FRM und SHM, August 2010.

*Strang, G.; Fix, G. (2008)*: An analysis of the finite element method. Wellesley-Cambridge Press

*Su, Y.-P.; Tian, Y.; Song, X.-S. (2009)*: Progressive collapse resistance of axially-restrained frame beams. ACI Structural Journal, Journal/September-October 2009, Vol. 106, No. 5, 600-607

*Sugano, S. (1992)*: Research and design for seismic retrofit of existing buildings in Japan.

*Tanaka, R.; Oba, K. (2001)*: Experimental study on seismic performance of beam members connected with post-installed anchors. Proceedings of the Symposium on Connections between Steel and Concrete, Stuttgart

*Tepfers, R. (1973)*: A theory of bond applied to overlapped tensile reinforcement for deformed bars. Chalmers University of Technology, Göteborg

*Tsai, K.-C.; Hwang, S.-J. (2008)*: Seismic retrofit program for Taiwan school buildings after 1999 Chi-Chi earthquake. Proceedings of 14th World Conference on Earthquake Engineering, Beijing

*Tsonos, A. (2003)*: Post-earthquake repair and strengthening of reinforced concrete beam-column connections (theoretical & experimental investigation). Bulletin of the New Zealand Society for Earthquake Eingineering, Vol. 36, No. 2, 73-93, 2003

*Varga, J. (1995)*: Test program for fastenings with headed studs. Test report No. Te 696/1-95/4, Institute of Construction Materials, Universität Stuttgart, not published (in German)Report No. 1/49A-91/1A, Institut für Werkstoffe im Bauwesen, Universität Stuttgart (in German)

*Varga, J. (1996)*: Report on tests with headed anchors. Tensile and shear capacity of headed anchors with ribbed shafts. Report No. 696/03-96/05, Institute of Construction Materials, University of Stuttgart, not published (in German)

*Verderame, G.; De Carlo, G.; Ricci, P.; Fabbrocino, G. (2009)*: Cyclic bond behaviour of plain bars. Part II: Analytical investigation. Construction and Building Materials 23, 3512-3522

*Viwathanatepa, S.; Popov, E.; Bertero, V. (1979)*: Effects of generalized loadings on bond of reinforced bars embedded in confined concrete blocks. Report No. UCB/EERC 79-22, Earthquake Engineering Research Center, University of California, Berkeley, California, Nov. 1979

*Vos, E.; Reinhardt, H.-W. (1982)*: Influence of loading rate on bond behaviour of reinforcing steel and prestressing strands. Matériaux et Construction (RILEM), No. 85, 1982

*Wallace, J.; McConnell, S.; Gupta, P.; Cote, P. (1998)*: Use of headed reinforcement in beam-column joints subjected to earthquake loads. ACI Structural Journal, September-October 1998, Vol. 95, No. 5, 590-602

*Wang, X.; M. Chen; Hutchinson, T. (2011)*: Full-scale structural and nonstructural building system performance during earthquakes. JSOE Poster Presentation

*Weathersby, J. (2003)*: Investigation of bond slip between concrete and steel reinforcement under dynamic loading conditions. Dissertation at The Department of Civil and Environmental Engineering, Louisiana State University

*Wesche, K. (1973)*: Baustoffe für tragende Bauteile – Band 1: Eigenschaften, Meßtechnik, Statistik (Construction materials for structural elements – Volume 1: Properties, method of measurement, statistics). Bauverlag (in German)

*Wollmershauser, R.; Lee, M. (2008)*: Adhesive anchor installation and inspection. Concrete International, December 2008, 36-40

*Yamamoto, Y.; Hattori, Y.; Koh, T.; Kato, M. (2001)*: Shallow shear anchor bolts for structural seismic strengthening of columns with wing wall. Proceedings of the Symposium on Connections between Steel and Concrete, Stuttgart

*Yi, W.-J.; He, Q.-F.; Xiao, Y.; Kunnath, S. (2008)*: Experimental study on progressive collapse-resistant behavior of reinforced concrete frame structures. ACI Structural Journal, July-August 2008, Vol. 105, No. 4, 433-439

*Zahn, F. (2012)*: Bauwerksschäden infolge Erdbebens – Das M 6,3-Erdbeben am 22.2.2011 in Christchurch, Neuseeland(Structural earthquake damage – The M 6.3-Earthquake 22.2.2011 in Christchurch, New Zealand). Bautechnik 88, Heft 12, 836-847 (in German)

*Zareian, F.; Sampere, C.; Sandoval, V.; McCormick, D.; Moehle, J.; Leon, R. (2012)*: Reconnaissance of the Chilean wine industry affected by the 2010 Chile Offshore Maule Earthquake. Earthquake Spectra, Vol. 28, No. S1, S503-S512

*Zehn, M. (2007)*: Sicherheitstheorie in der Ingenieurpraxis (Safety theory in engineering practice). Skript 2007, Institut für Mechanik Konstruktionsberechnung, TU Berlin (in German)

*Zhao, G.-C. (1993)*: Tragverhalten von randfernen Kopfbolzenverankerungen bei Betonausbruch (Behaviour of headed bolt connections without edge influences). Dissertation, University of Stuttgart, 1993 (in German)

*Zielinski, A. (1982)*: Fracture of concrete and mortar under uniaxial impact tensile loading. Dissertation, Delft University of Technology

# Appendix A: Conventional Anchorage Design

Reinforcing bar anchorages conventionally designed fail in one of the following modes:

- Steel failure
- Bond (pullout) failure
- Splitting failure

The objective of conventional anchorage design is to fully utilise the steel strength due to economic reasons and to favour the ductile failure mode in particular for seismic load cases. For this reason, the anchorage length is defined sufficiently long to exclude bond (pullout) and splitting failure. The provisions for the determination of the anchorage length are given in the following. Some coefficients irrelevant in the context of this thesis were omitted.

## A.1 Eurocode 2 (2005), Eurocode 8 (2006)

The design bond strength $f_{bd}$ is determined in *Eurocode 2 (2005)* according to Clause 8.4.2 by

$$f_{bd} = 2.25 \cdot \eta_1 \cdot \eta_2 \cdot f_{ctd}$$

where

$f_{ctd}$ design concrete tensile strength

$\eta_1$ factor taking into account the position of the reinforcing bar during casting
$\eta_1$ = 1.0 for good bond conditions, $\eta_1$ = 0.7 for all other bond conditions

$\eta_2$ factor taking into account the diameter of reinforcing bar
$\eta_2$ = 1.0 for $\phi \leq 32$ mm, $\eta_2 = (132 - \phi\,[\text{mm}]) / 100$ for $\phi > 32$ mm.

The basic anchorage length $\ell_{b,rqd}$ required to transfer the tensile stress of a reinforcing bar without causing splitting failure is determined according to Clause 6.9.4 by

$$\ell_{b,rqd} = \frac{\phi \sigma_{sd}}{4 f_{bd}}$$

where

$\phi$ reinforcing bar diameter

$\sigma_{sd}$ design stress at the beginning of anchorage.

The design anchorage length $\ell_{bd}$ is determined according to Clause 6.9.5 by

$$\ell_{bd} = \alpha_1 \cdot \alpha_2 \cdot \ell_{b,rqd} \geq \ell_{b,min}$$

where

$\alpha_1$ coefficient taking into account the form of the bar
$\alpha_1$ = 1.0 for straight bars, $\alpha_1$ = 0.7 for bent and looped bars in tension
$\alpha_1$ = 1.0 for straight bars, $\alpha_1$ = 1.0 for bent and looped bars in compression

$\alpha_2$ coefficient taking into account the confinement of the concrete cover if $c_d > 3\phi$
$\alpha_2 = 1 - 0.15 (c_d - k\phi) / \phi$, k = 1 for straight bars, k = 3 for bent and looped bars, and $0.7 \leq \alpha_2 \leq 1.0$ for bars in tension ($c_d$ is the minimum of concrete cover and half the clearance between adjacent bars)

$\alpha_2$ = 1.0 for bars in compression

$\ell_{b,min}$ minimum anchorage length
$\ell_{b,min} > \max\{0.3\ell_b; 10\phi; 100 \text{ mm}\}$ for bars in tension
$\ell_{b,min} > \max\{0.6\ell_b; 10\phi; 100 \text{ mm}\}$ for bars in compression.

The use of an equivalent anchorage length $\ell_{b,eq}$ is suggested as a simplification for anchorages loaded in tension (Figure A.1):

$$\ell_{b,eq} = \alpha_1 \cdot \ell_{b,rqd}$$

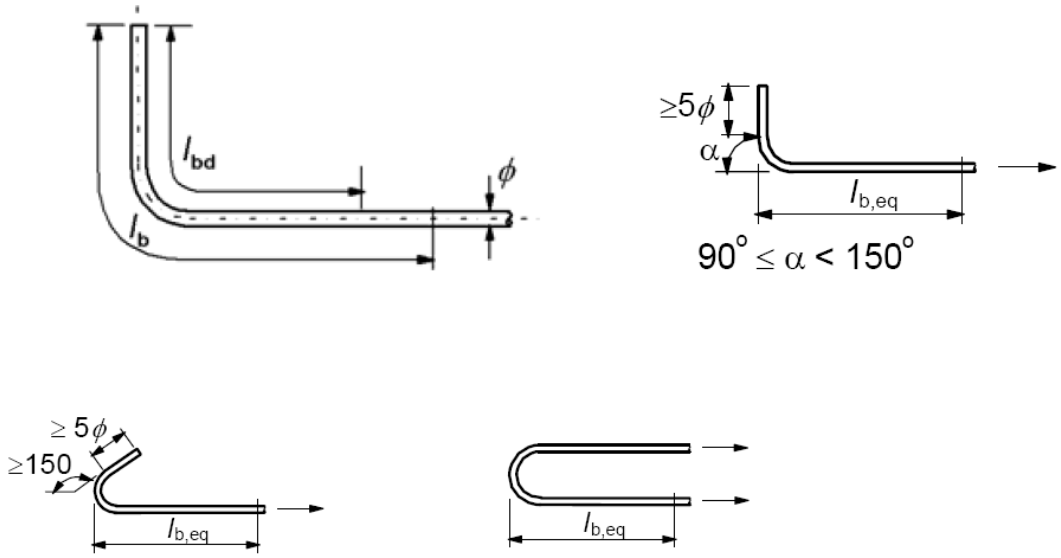


Figure A.1 Definition of $\ell_{bd}$ according to *Eurocode 2 (2005)*, Figure 8.1

The minimum inner bending diameter $\phi_{m,min}$ is $7\phi$ for bar diameters larger than 16 mm, else $5\phi$.

### A.1.1 Additional Seismic Design Provisions

In Clause 5.6.1 and 5.6.2 of *Eurocode 8 (2006)* two seismic design provision relevant in the context of the studied column-to-foundation connections are given: In contrast to low ductility class (DCL) structures, a potential yield penetration has to be considered for high ductility class (DCH) structures by disregarding the first $5\phi$ of the anchorage length (Figure A.2). Furthermore, the anchorage length has to be increased by additional 50 % if the column is loaded in tension.

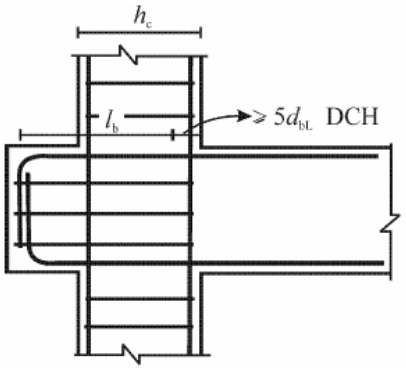


Figure A.2 Definition of $\ell_{bd}$ according to *Eurocode 8 (2006)*, Figure 5.13

For anchorages of column reinforcing bars $\sigma_{sd} / f_{yd}$ has to be assumed for seismic load cases when determining the anchorage length $\ell_{b,rqd}$. If the steel strength is fully utilised, the anchorage length is identical for seismic and fundamental load cases, because the ratio of the material safety factors for steel and concrete according to *Eurocode 2 / NA (2009)* and *Eurocode 8 / NA (2009)* remains unchanged:

$$\ell_{b,rqd} = \frac{\phi f_{yd}}{4 f_{bd}} = \frac{\phi f_{yk} / \gamma_s}{4 \cdot 2.25 \cdot f_{ctk} / \gamma_c} \text{ and } \frac{\gamma_c}{\gamma_s} = \frac{1.5}{1.15} \approx 1.3 = \frac{1.3}{1.0} = \frac{\gamma_{c,eq}}{\gamma_{s,eq}}$$

### A.1.2 Partial Safety Factors

The material safety factors $\gamma_s$ and $\gamma_c$ are given in the national annexes of the *Eurocode 2 (2005)* and *Eurocode 8 (2006)*, i.e. *Eurocode 2 / NA (2009)* Clause 2.4.2.4 and *Eurocode 8 / NA (2009)* Clause 5.2.4 as:

$\gamma_c$ = 1.5 (1.3) for concrete, fundamental (seismic) load case

$\gamma_s$ = 1.15 (1.0) for reinforcement steel, fundamental (seismic) load case

### A.1.3 Interrelationship between Mean and Design Bond Strength

Some reinforced concrete codes, e.g. *ACI 318 (2011)* and *NZS 3101 (2006)*, use the concrete compressive strength as the input parameter for the definition of the anchorage length, while other codes, e.g. *Eurocode 2 (2005)* and *DIN1045 (2001)*, use a design bond strength $f_{bd}$ as a basis. The design bond strength of cast-in-place reinforcing bars defined in *Eurocode 2 (2005)* for concrete classes between C20/25 and C50/60 is boiled down to a mere:

$f_{bd} = 2.25 f_{ctk,0.05} / \gamma_M = 2.25 \cdot (0.7 f_{ctm}) / \gamma_M = 2.25 \cdot (0.7 \cdot 0.30 f_{ck}^{2/3}) / \gamma_M = 0.473 f_{ck}^{2/3} / \gamma_M$

The factor 2.25 equals to the design bond strength anticipated for concrete class C20/25 which serves as a pivot point. The mean and characteristic bond strength is not required for the conventional reinforced concrete design and therefore not defined in the *Eurocode 2 (2005)*. In the context of this thesis, however, the characteristic bond strength is derived as follows:

$f_{bk} = f_{bd} \gamma_M = 0.473 f_{ck}^{2/3}$

Assuming a variation in bond strength of CV = 15 % and a k value of k = 1.645, which is generally accepted because of the substantial experience and knowledge of anchorages in concrete constructions ($n \rightarrow \infty$), the mean bond strength is defined as:

$f_{bm} = f_{bk} / (1 - k \cdot CV) = 0.473 f_{ck}^{2/3} / (1 - 1.645 \cdot 0.15) \approx 0.473 f_{ck}^{2/3} / 0.75$

The background for the statistical considerations is given in Section 9.1. For the assessment of post-installed reinforcing bars according to the *EOTA TR 023 (2006)*, the mean bond strength is determined by unconfined pullout tests using short anchorage lengths between 7$\phi$ and 10$\phi$. Consequently, the tested bond strengths are increased with reference to the general bond strength of cast-in-place reinforcing bars given in the *Eurocode 2 (2005)* due to confinement effect and therefore cannot directly related to the bond strengths given in the *Eurocode 2 (2005)*. To allow a performance comparison of post-installed reinforcing bars and cast-in-place reinforcing bars, the mean bond strength is increased by the factor 2.0 to consider the confinement effect and the factor 1 / 0.9 to account for the uniform distribution of the bond strength in the tests (*Spieth, H. (2003)*):

$$f_{bm} = \frac{2.0 \cdot 0.473 f_{ck}^{2/3}}{0.9 \cdot 0.75} = 1.4 f_{ck}^{2/3}$$

The function is plotted as a conceptual representation in *EOTA TR 023 (2006)* (Figure A.5) and allows a comparison of the bond strengths of post-installed reinforcing bars tested in confined test setup and the bond strengths of cast-in-place reinforcing bars determined analogous to *Eurocode 2 (2005)*.

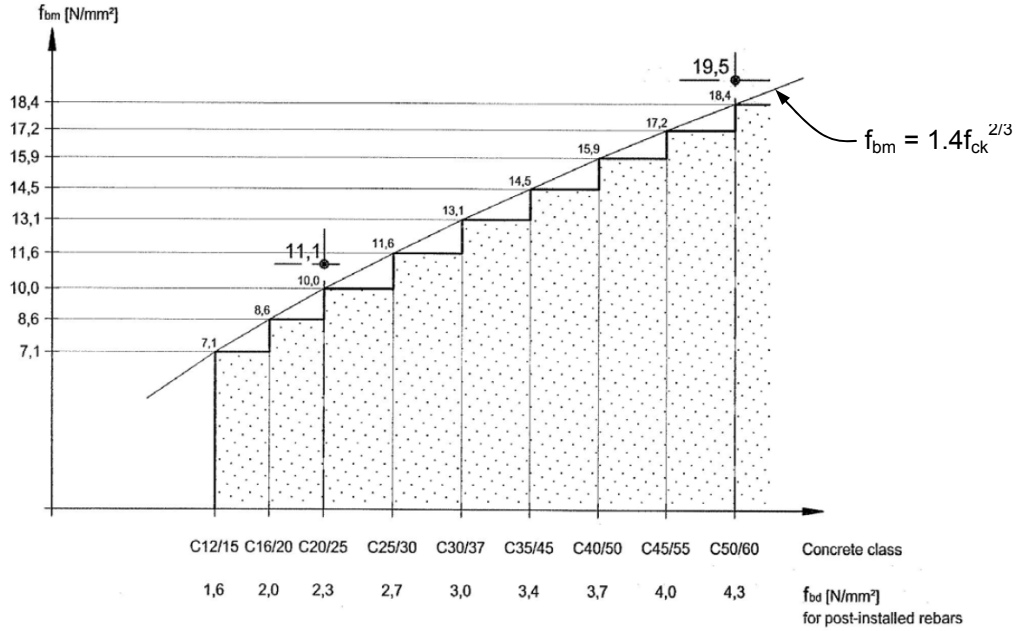


Figure A.5 Mean bond strengths $f_{bm}$ to be achieved in bond tests on post-installed reinforcing bars to allow a design analogous to cast-in-place reinforcing bars according to *Eurocode 2 (2005)* without limitation (*EOTA TR 023 (2006)*)

## A.2 ACI 318 (2011)

### Straight anchorage in compression according to Clause 12.3

The development length $\ell_{dc}$ of straight bars in compression is determined according to *ACI 318 (2011)*, Clause 12.3.2 by

$$\ell_{dc} = \max\left\{\left(\frac{0.24 f_y}{\sqrt{f_c'}}\right) d_b ; 0.043 f_y d_b\right\} \geq 200 \text{ mm}$$

where

$f_y$ specified yield strength

$f_c'$ specified compressive strength of concrete

$d_b$ nominal diameter of bar.

### Straight anchorage in tension according to Clause 12.2

The development length $\ell_d$ of straight bars in tension is determined according to Clause 12.2.2 or 12.2.3 by

$$\ell_d = \left\{\left(\frac{f_y \psi_t}{2.1\sqrt{f_c'}}\right) d_b \text{ for } d_b \leq 19 \text{ mm}; \quad \ell_d = \left(\frac{f_y \psi_t}{1.7\sqrt{f_c'}}\right) d_b \text{ for } d_b \geq 22 \text{ mm}\right.$$

$$\text{or } \ell_d = \left(\frac{f_y}{1.1\sqrt{f_c'}} \frac{\psi_t \psi_s}{\left(\frac{c_b + K_{tr}}{d_b}\right)}\right) d_b \geq 300 \text{ mm}$$

where

$\psi_t$ factor taking into account the position of reinforcing bar during casting
$\psi_t$ = 1.3 for poor bond conditions, $\psi_t$ = 1.0 for all other bond conditions

$\psi_s$ factor taking into account the diameter of reinforcing bar
$\psi_s$ = 0.8 for $d_b \leq 19$ mm, $\psi_s$ = 1.0 for $d_b \geq 22$ mm

$f_y$ specified yield strength

$f_c'$ specified compressive strength of concrete

$c_b$ minimum of the distance from centre of a bar to nearest concrete surface and one-half the centre-to-centre spacing of bars being developed

$d_b$ nominal diameter of bar

$K_{tr}$ term to consider confinement of transverse reinforcement, permitted to use $K_{tr} = 0$ as a design simplification.

The product of $\psi_t$ and $\psi_s$ must not be larger than 1.7 and the quotient of $(c_b + K_{tr})$ and $d_b$ not larger than 2.5.

**Hooked anchorage in compression according to Clause 12.5**

Hooks shall not be considered effective in developing bars in compression.

**Hooked anchorage in tension according to Clause 12.5**

The development length $\ell_{dh}$ of hooked bars in tension is determined according to Clause 12.5.2 by

$$\ell_{dh} = \left( \frac{0.24 f_y}{\sqrt{f_c'}} \right) d_b \geq 150 \text{ mm}$$

where

$f_y$ specified yield strength

$f_c'$ specified compressive strength of concrete

$d_b$ nominal diameter of bar.

The length $\ell_{dh}$ is permitted to be multiplied by 0.7 for $d_b \leq 36$ mm if the side cover is not less than 65 mm, and for 90° hooks if the cover on bar extension beyond hook is ≥ 50 mm.

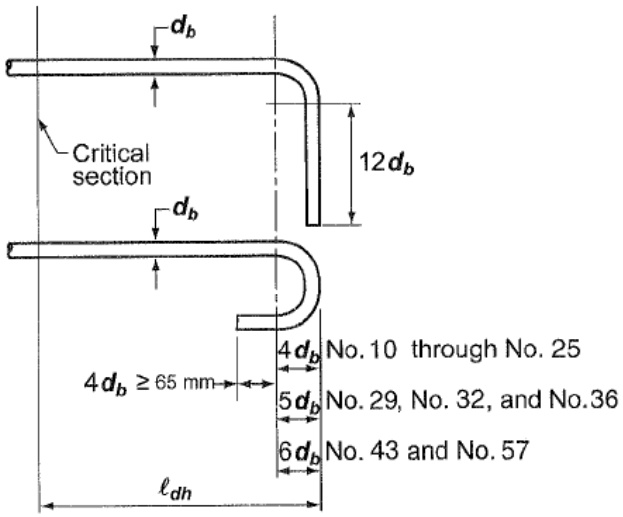


Figure A.3 Hooked bar details for development of standard hooks according to *ACI 318 (2011)*, Figure R12.5

The minimum inner bending diameter is $6d_b$ for bar diameters smaller than 25 mm, $10d_b$ for bar diameters larger than 45 mm, else $8d_b$.

### A.2.1 Additional Seismic Design Provisions

The only seismic design provision relevant in the context of the studied column-to-foundation connections is the ban of excess reinforcement for flexural members of structures belonging to the Seismic Design Category, D to F, strong ground shaking.

## A.3 NZ 3101 (2006)

**Straight anchorage in compression according to Clause 8.6.5**

The basic development length $L_{db}$ of straight bars in compression is determined according to *NZS 3101 (2006)*, Clause 8.6.5.1ff by

$$L_{db} = \max\left\{\left(\frac{0.22}{\sqrt{f_c'}}\right); 0.040\right\} f_y \cdot d_b \geq 200 \text{ mm}$$

where

$f_y$ lower characteristic yield strength of flexural reinforcement

$f_c'$ specified compressive strength of concrete

$d_b$ nominal diameter of bar.

The refined development length $L_d$ is determined by

$$L_d = \alpha_b \cdot \alpha_e \cdot \max\left\{\left(\frac{0.22}{\sqrt{f_c'}}\right); 0.040\right\} f_y \cdot d_b$$

where

$\alpha_b$ factor taking into account excess reinforcement as the ratio of required and provided flexural reinforcement, $\alpha_b = A_{sr} / A_{sp}$

$\alpha_e$ factor taking into account transverse reinforcement, $\alpha_b = 0.75$ if at least three bars and $A_{tr} / s \geq A_b / 600$, else $\alpha_b = 1.0$.

$A_{sr}$ area of flexural reinforcement required

$A_{sp}$ area of flexural reinforcement provided

$A_{tr}$ area of transverse reinforcement

s spacing of transverse reinforcement

$A_b$ area of developed reinforcement

For the column-to-foundation connections in context of this thesis, the refined development length $L_d$ yields the identical anchorage length as the basic development length $L_{db}$.

**Straight anchorage in tension according to Clause 8.6.2**

The basic development length $L_{db}$ of straight bars in tension is determined according to Clause 8.6.3.1ff by

$$L_{db} = 0.5 \cdot \alpha_a \cdot \frac{f_y}{\sqrt{f_c'}} \cdot d_b \geq 300 \text{ mm}$$

where

$\alpha_a$ factor taking into account position of reinforcing bar during casting, $\alpha_a = 1.3$ for poor bond conditions, $\alpha_a = 1.0$ for all other bond conditions

$f_y$ lower characteristic yield strength of flexural reinforcement

$f_c'$ specified compressive strength of concrete

$d_b$ nominal diameter of bar.

The refined development length $L_d$ is determined by

$$L_{db} = 0.5 \cdot \frac{\alpha_b}{\alpha_c \cdot \alpha_d} \cdot \frac{f_y}{\sqrt{f_c'}} \cdot d_b \geq 300 \text{ mm}$$

where

$\alpha_b$ factor taking into account excess reinforcement as the ratio of required and provided flexural reinforcement, $\alpha_b = A_{sr} / A_{sp}$

$\alpha_c$ factor taking into account the confinement, $\alpha_c = 1 + 0.5(c_m / d_b - 1.5)$ with the limitation of $1.0 \leq \alpha_c \leq 1.5$

$\alpha_d$ factor taking into account transverse reinforcement, $\alpha_d = 1 + ((A_{tr} / s)(f_{yt} / 80nd_b))^{0.5}$ with the limitation of $1.0 \leq \alpha_d \leq 1.5$ if at least three bars spaced less than $8d_b$, else $\alpha_d = 1.0$

$A_{sr}$ area of flexural reinforcement required

$A_{sp}$ area of flexural reinforcement provided

$c_m$ lesser of the concrete cover or the clear distance between bars.

$A_{tr}$ area of transverse reinforcement

s spacing of transverse reinforcement

$f_{yt}$ lower characteristic yield strength of transverse reinforcement

For the column-to-foundation connections in context of this thesis, the refined development length $L_d$ yields the identical anchorage length as the basic development length $L_{db}$.

**Hooked anchorage in compression according to Clause 8.6.10**

Hooks shall not be considered effective in developing bars in compression.

**Hooked anchorage in tension according to Clause 8.6.10**

The development length $\ell_{dh}$ is determined according to Clause 8.10.6.3ff by

$$L_{dh} = 0.24 \cdot \alpha_1 \cdot \frac{f_y}{\sqrt{f_c'}} \cdot d_b \geq 8d_b$$

where

$f_y$ lower characteristic yield strength of flexural reinforcement

$f_c'$ specified compressive strength of concrete.

$\alpha_1$ 0.7 for $d_b \leq 32$ mm, side cover not less than 60 mm, and for 90° hook with cover on bar extension beyond hook ≥ 40 mm

$d_b$ nominal diameter of bar.

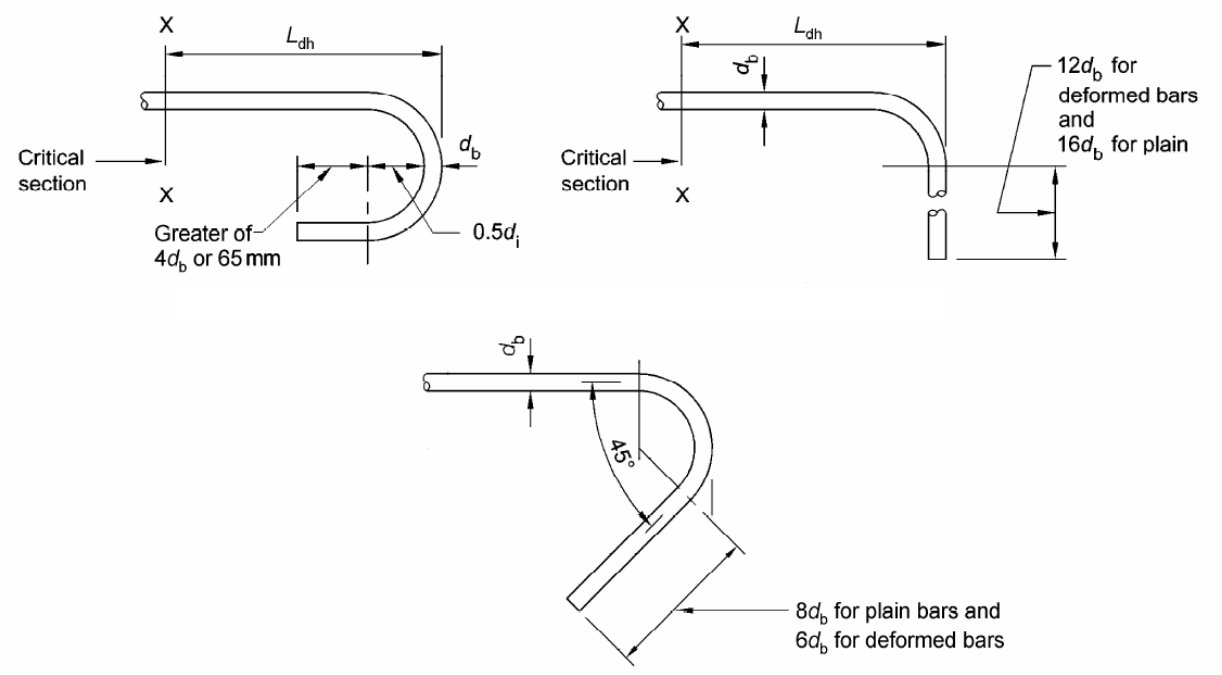


Figure A.4 Hooked bar details for development of standard hooks according to *NZS 3101 (2006)*, Figure 8.1

The minimum inner bending diameter $d_i$ is the minimum of

$$d_i \geq 0.92\left(0.5 + \frac{d_b}{s_b}\right)\frac{f_s d_b}{f_c'}$$

and $5d_b$ for bar diameters smaller than 20 mm, or $6d_b$ for bar diameters larger than 24 mm. $s_b$ is the centre-to-centre distance or, measured perpendicular to the plane of the bend, to the adjacent bar or group of bars or, for a bar or group of bars adjacent to the face of the member, the cover plus one half of $d_b$.

### A.3.1 Additional Seismic Design Provisions

Besides taking $\alpha_b$ as being equal to 1.0 for the determination of the development length, the only seismic design provision relevant in the context of the studied column-to-foundation connections is to consider the yield penetration by disregarding half the column depth or $8d_b$, whichever is less. The requirement is stipulated for beam-column joints, however, it is deemed to be applicable also for studied column-to-foundation connections.

## A.4 Comparison of Different Reinforced Concrete Codes

It is evident that the design provisions with respect to the anchorage detailing differ between the various reinforced concrete codes *Eurocode 2 (2005)* and *Eurocode 8 (2006)* as well as *ACI 318 (2011)* and *NZS 3101 (2006)*. This is owed to the fact that the load transfer of anchorages is very complex, preventing a simple yet universally valid solution. Table A.1 provides an overview of the most relevant aspects concerning anchorage lengths of tension reinforcing bars for the seismic load case, adapted to the situation of a column-to-foundation connection. For the sake of clarity, the denomination follows the definitions according to the Eurocode suite, i.e. anchorage length is denoted as $\ell_b$, reinforcing bar diameter as $\phi$, the nominal steel yield and concrete compressive stress as $f_{yk}$ and $f_{ck}$.

Table A.1 Comparison of code provisions relevant for column-to-foundation connection for seismic load case

| | EC 2 / EC 8<br>Section 8.4 | ACI 318<br>Section 12 | NZ 3101<br>Section 8.6 |
|---|---|---|---|
| Anchorage length without hooks | $\ell_b = \frac{\phi\sigma_{sd}}{4f_{bd}}$ | $\ell_b = \frac{f_{yk}}{1.1\sqrt{f_{ck}}}\phi$ [1)] | $\ell_b = 0.5\frac{f_{yk}}{\sqrt{f_{ck}}}\phi$ |
| Anchorage length with hooks | – | $\ell_b = 0.24\frac{f_{yk}}{\sqrt{f_{ck}}}\phi$ | $\ell_b = 0.24\frac{f_{yk}}{\sqrt{f_{ck}}}\phi$ |
| Minimum tail length | $5\phi$ | $12\phi$ | $12\phi$ |
| Minimum straight length | – | $8\phi$ > 150 mm | $8\phi$ |
| Minimum total length | max{$0.6\ell_b$; $10\phi$; 100 mm} | 300 mm | 200 mm |
| Minimum total length includes tail length | Yes | No | No |
| Length to be disregarded due to yield penetration | $5\phi$ | – | min{$8\phi$;$0.5h_c$ [2)]} |
| Bending diameter | $5\phi$ – $7\phi$ | $6\phi$ – $10\phi$ | $5\phi$ – $6\phi$ |
| Reduction factor[3)] taking into account... | | | |
| ... hooks | 0.7 | Additional 0.7 for $\phi \le 36$ mm | Additional 0.7 for $\phi \le 32$ mm |
| ... confinement of the concrete cover | 0.7 | 1 / 2.5 = 0.4 | 1 / 1.5 ≈ 0.7 |
| ... excess reinforcement | Allowed outside column[5)] | Only allowed for SDC[4)] A to C | Not allowed for seismic load |

[1)] for $\phi \ge 22$ mm, to be multiplied by 0.8 for $\phi \le 19$ mm

[2)] $h_c$: column depth, in the context of column-to-foundation connections the height of foundation

[3)] Maximum reduction factor imaginable for column-to-foundation connections given

[4)] According to 21.1.1.6; SDC: Seismic Design Category, D to F for strong ground shaking

[5)] $\sigma_{sd} = f_{yd}$ assumed when determining. $\ell_{b,rqd}$ for columns required for flexural strength in relevant zones of the structure (Clause 5.6.2.1)

It is important to note that *ACI 318 (2011)* and *NZS 3101 (2006)* do not consider the tail length as being a part of the anchorage length. Therefore, small member depths potentially make a reduction of the required anchorage length by means of excess reinforcement necessary. On the contrary, *Eurocode 2 (2005)* and *Eurocode 8 (2006)* takes the tail length into account.

## A.5 Minimum Related Rib Area

As already shown by *Rehm, G. (1958)*, the governing parameter for bond is the specific projected rib area $f_R$, also known as related rib area, which is defined as

$$f_R = \frac{k \cdot F_R \cdot \sin\beta}{\pi \cdot \phi \cdot c}$$

where

k number of ribs around perimeter,

$F_R$ area of one transverse rib,

$\beta$ angle between rib and longitudinal axis of bar,

$\phi$ nominal diameter of bar,

c distance between transverse ribs.

An economic design of the reinforcing bars is calling for small ribs, resulting in low values for the related rib area. Therefore, the codes stipulate minimum related rib areas given in Table A.2 to ensure sufficient bond strengths.

Table A.2 Comparison of code provisions with respect to the related rib area

| | EC 2 / EC 8[1)] | ACI 318[2)] | NZ 3101[3)] |
|---|---|---|---|
| Minimum related rib area, all bar diameters | 0.035 – 0.056 | 0.043 – 0.054 | 0.036 – 0.056 |
| Minimum related rib area for bar diameters 16 mm or larger | 0.056 | 0.048 | 0.056 |

[1)] In conjunction with *DIN 488-1 (1986)*

[2)] In conjunction with *ASTM A615 (2004)*

[3)] In conjunction with *AS/NZS 4671 (1997)*

## A.6 Crack Width Limits

Cracks cannot be avoided in reinforced concrete structures. However, appropiate reinforcement is limiting the crack widths. Larger crack widths put the reinforcement at corrosion risk. Therefore, reinforced concrete codes provide limits which depend

on the exposure condition and partly on the loading condition. Typical crack width limits are around 0.3 mm. The range of crack width limits is given in Table A.3.

Table A.3 Comparison of crack width limits

| | EC 2 / EC 8 | ACI 318[1)] | NZ 3101 |
|---|---|---|---|
| Maximum crack width | 0.2 mm – 0.4 mm | 0.10 mm – 0.41 mm | 0.2 mm – 0.5 mm |

[1)] In conjunction with *ACI 224 (2001)*

# Appendix B: Bonded Anchor Design

Reinforcing bar anchorages designed as bonded anchors fail in one of the following modes when loaded in tension:

- Steel failure
- Pullout (bond) failure
- Concrete breakout failure
- Splitting failure

Which failure mode is governing depends on the anchorage length, in the following termed embedment depth as well as the steel, concrete, and bond strength. In the following, the provisions for bonded anchor design are presented.

## B.1 CEN/TS 1992-4 (2009)

Currently, the design concept of concrete anchors is described in Annex C of *ETAG 001 (2006)* and specifically for bonded anchors in *EOTA TR 029 (2010)*. Both documents are incorporated in *CEN/TS 1992-4 (2009)* which design concept is introduced in the following. Eventually, this pre-norm will become the Part 4 of the *Eurocode 2 (2005)*. In order to provide the most updated information, the given equations are based on the latest available draft of the *CEN/TS 1992-4 (2009)* revision which uses concrete compressive stresses determined by means of test cylinders instead of test cubes.

The capacity of the anchor is determined by the minimum of the characteristic resistance corresponding to the different failure modes according to the following equations:

The steel stress is not limited to yielding but to the ultimate strength which determines the characteristic resistance corresponding to the steel failure mode:

$$N_{Rk,s} = A_s \cdot f_{uk}$$

where

$A_s$ stressed cross section of steel

$f_{uk}$ characteristic ultimate tensile strength, use of characteristic yield strength $f_{yk}$ is recommended for post-installed reinforcing bars in analogy to *Eurocode 2 (2005)*.

The characteristic resistance corresponding to the combined pullout and concrete failure mode is calculated according to the uniform bond model, assuming uniform bond stress distribution along the embedment depth:

$$N_{Rk,p} = N^0_{Rk,p} \cdot \frac{A_{p,N}}{A^0_{p,N}} \cdot \psi_{s,Np} \cdot \psi_{g,Np} \cdot \psi_{ec,Np} \cdot \psi_{re,Np}$$

where

$N^0_{Rk,p}$ initial value of the characteristic resistance

$$N^0_{Rk,p} = \pi \cdot d \cdot h_{ef} \cdot \tau_{Rk}$$

$\tau_{Rk}$ characteristic bond resistance, depending on the concrete strength, product-specific values given for uncracked ($\tau_{Rk,ucr}$) and cracked concrete ($\tau_{Rk,cr}$) in the corresponding approval document (ETA)

d stressed diameter of steel

$h_{ef}$ effective embedment depth

$A^0_{p,N}$ influence area of an individual anchor without the influence of adjoining anchors and concrete member edges, idealising the activated concrete as a prism (Figure B.1) with an edge length of

$$s_{cr,Np} = 20 \cdot d \cdot \left( \frac{\tau_{Rk}[MPa]}{7.5} \right)^{0.5} = 7.3 \cdot d \cdot \sqrt{\tau_{Rk}[MPa]} = 2c_{cr,Np} \le 3h_{ef}$$

$\tau_{Rk}$ $\tau_{Rk} = \tau_{Rk,ucr}$ characteristic bond strength in uncracked concrete

$A_{p,N}$ actual area, limited by overlapping areas of adjoining anchors ($s \le s_{cr,Np}$) and concrete member edges ($c \le c_{cr,Np}$) (Figure B.2)

$\psi_{s,Np}$ factor taking into account the disturbance of the stress distribution due to concrete member edges, where the smallest edge distance is considered in

$$\psi_{s,Np} = 0.7 + 0.3 \cdot \frac{c}{c_{cr,Np}} \le 1.0$$

$\psi_{g,Np}$ factor taking into account the failure surface of anchor groups

$$\psi_{g,Np} = \psi^0_{g,Np} - \left(\frac{s}{s_{cr,Np}}\right)^{0.5} \cdot \left(\psi^0_{g,Np} - 1\right) \geq 1.0$$

$$\psi^0_{g,Np} = \sqrt{n} - \left(\sqrt{n} - 1\right) \cdot \left(\frac{\tau_{Rk}}{\tau_{Rk,c}}\right)^{1.5} \geq 1.0$$

$\tau_{Rk}$ $\tau_{Rk} = \tau_{Rk,cr}$ characteristic bond strength in cracked concrete,
$\tau_{Rk} = \tau_{Rk,ucr}$ characteristic bond strength in uncracked concrete

$$\tau_{Rk,c} = \frac{k_2}{\pi \cdot d} \sqrt{h_{ef}[mm] \cdot f_{ck}[MPa]}$$

$k_2$ $k_2 = k_{cr} = 7.7$ for applications in cracked concrete,
$k_2 = k_{ucr} = 11.0$ for applications in uncracked concrete

$f_{ck}$ characteristic concrete cylinder strength

n number of anchors in a group

s spacing, in case of multiple spacings the mean value of the spacings should be used

$\psi_{ec,Np}$ factor taking into account load eccentricity, resulting in different loads on the individual anchor of an anchor groups

$$\psi_{ec,Np} = \frac{1}{1 + 2e_N / s_{cr,Np}} \leq 1.0$$

$e_N$ eccentricity of the resulting tensile load on the tensioned anchors

$\psi_{re,Np}$ factor taking into account the effect of dense reinforcement for embedment depths $h_{ef} < 100$ mm if reinforcement of anz diameter is present at a spacing ≥ 150 mm or reinforcement of 10 mm or less is present at a spacing ≥ 100 mm

$$\psi_{re,Np} = 0.5 + \frac{h_{ef}[mm]}{200} \leq 1.0$$

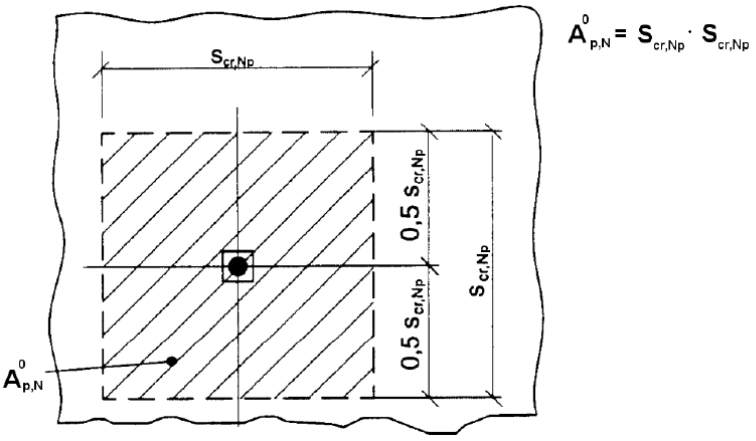


Figure B.1 Idealised influence area $A^0_{p,N}$ of an individual anchor after *EOTA TR 029 (2010)*

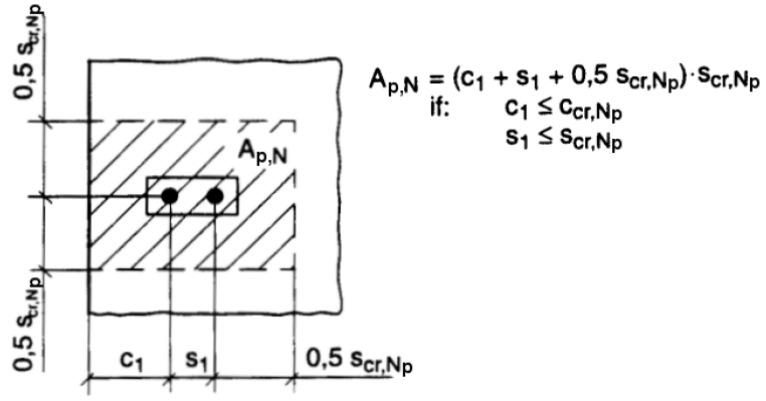


Figure B.2 Idealised actual area $A_{p,N}$ of a group of two anchors near the edge of concrete member after *EOTA TR 029 (2010)*

The concrete capacity method is used to calculate the characteristic resistance corresponding to the concrete breakout failure mode:

$$N_{Rk,c} = N^0_{R,c} \cdot \frac{A_{c,N}}{A^0_{c,N}} \cdot \psi_{s,N} \cdot \psi_{re,N} \cdot \psi_{ec,N}$$

where

$N^0_{Rk,c}$ initial value of the characteristic resistance

$$N^0_{Rk,c} = k_3 \cdot \sqrt{f_{ck}[\text{MPa}]} \cdot h_{ef}[\text{mm}]^{1.5}$$

$k_3$ $k_3 = k_{cr} = 7.7$ for applications in cracked concrete
$k_3 = k_{ucr} = 11.0$ for applications in uncracked concrete

$f_{ck}$ characteristic concrete cylinder strength

$A^0_{c,N}$ influence area of an individual anchor without the influence of adjoining anchors and concrete member edges, idealising the activated concrete as a prism (Figure B.2) with an edge length of

$$s_{cr,N} = 2c_{cr,N} = 3h_{ef}$$

$A_{c,N}$ actual area, limited by overlapping areas of adjoining anchors ($s \le s_{cr,N}$) and concrete member edges ($c \le c_{cr,N}$) (Figure B.4)

$\psi_{s,N}$ factor taking into account the disturbance of the stress distribution due to concrete member edges, with the smallest edge distance is considered in

$$\psi_{s,N} = 0.7 + 0.3 \cdot \frac{c}{c_{cr,N}} \le 1.0$$

$\psi_{re,N}$ factor taking into account the effect of dense reinforcement

$$\psi_{re,N} = 0.5 + \frac{h_{ef}\,[mm]}{200} \le 1.0$$

$\psi_{ec,N}$ factor taking into account load eccentricity, resulting in different loads on the individual anchor of an anchor groups

$$\psi_{ec,N} = \frac{1}{1 + 2e_N / s_{cr,N}} \le 1.0$$

$e_N$ eccentricity of the resulting tensile load on the tensioned anchors

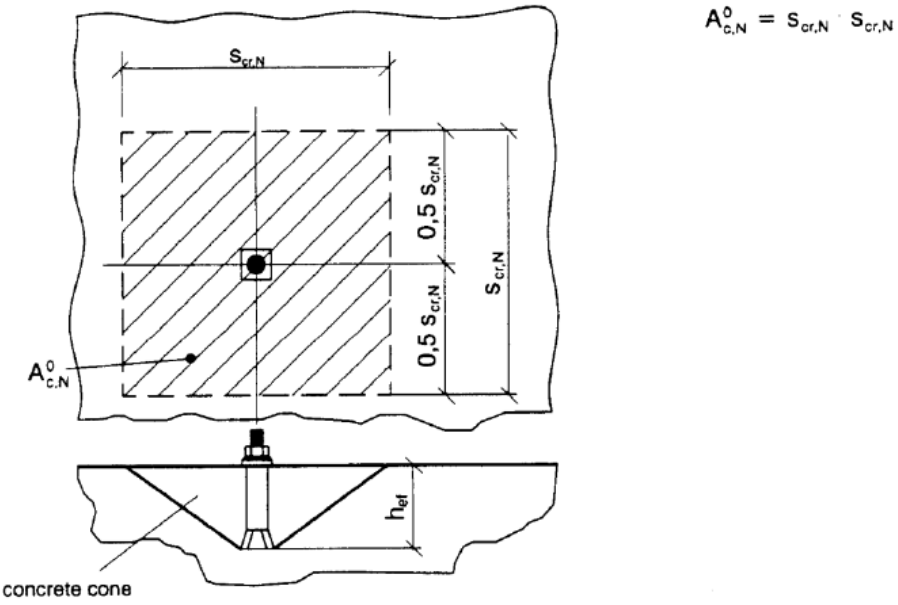


Figure B.3 Idealised influence area $A^0_{c,N}$ of an individual anchor after *EOTA TR 029 (2010)*

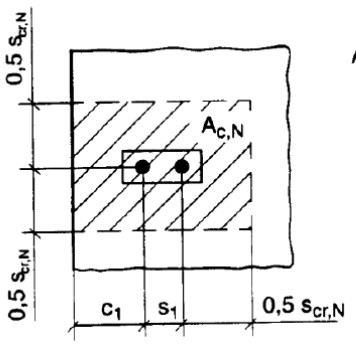


$A_{c,N} = (c_1 + s_1 + 0{,}5\, s_{cr,N}) \cdot s_{cr,N}$
if: $c_1 \le c_{cr,N}$
$s_1 \le s_{cr,N}$

Figure B.4 Idealised actual area $A_{c,N}$ of a group of two anchors at the edge of concrete member after *EOTA TR 029 (2010)*

The capacity in case of splitting failure is determined by:

$$N_{Rk,sp} = N^0_{R,c} \cdot \frac{A_{c,N}}{A^0_{c,N}} \cdot \psi_{s,N} \cdot \psi_{re,N} \cdot \psi_{ec,N} \cdot \psi_{h,sp}$$

where

$\psi_{sp,N}$ factor taking into account the actual concrete member depth h on the splitting resistance

$$\psi_{sp,N} = \left(\frac{h}{h_{min}}\right)^{2/3} \le \max\left\{1; \left(\frac{h_{ef} + 1.5c_1}{h_{min}}\right)^{2/3}\right\} \le 2$$

$h_{min}$ minimum thickness of concrete member

### B.1.1 Additional Seismic Design Provisions

In Section 8.4 of *CEN/TS 1992-4 (2009)* two seismic design provision relevant in the context of the studied column-to-foundation connections are given, both favouring the ductile steel failure.

First, the general seismic strength reduction factor $\alpha_{eq} = 0.75$ is stipulated in Clause 8.4.2 of *CEN/TS 1992-4 (2009)* for all concrete related, i.e. brittle failures such as concrete breakout and pullout failure. This factor is often referred to as 'seismic factor' and is intended to provide additional conservatism for seismic load cases:

$$R_{d,eq} = \alpha_{eq} \cdot \frac{R_{k,eq}}{\gamma_M}$$

$\alpha_{eq} = 0.75$ for concrete related failure modes

= 1.0 for steel failure

$R_{k,eq}$ characteristic seismic resistance for a given failure mode

Second, Clause 8.4.3 requires to design anchorages for structural connections for steel failure. To ensure ductile steel failure of the anchorage itself, the following equation has to be satisfied:

$$R_{k,s,eq} \leq 0.6 \cdot \frac{R_{R,conc,eq}}{\gamma_{inst}}$$

$R_{k,s,eq}$ characteristic seismic resistance for steel failure mode

$R_{k,conc,eq}$ characteristic seismic resistance for all non-steel modes

$\gamma_{inst}$ installation safety factor according to the corresponding approval document (ETA)

The installation safety factor $\gamma_{inst}$ is explained in the following section.

### B.1.2 Partial Safety Factors

The *CEN/TS 1992-4 (2009)* specifies the material safety factors for tension loaded bonded anchors as follows:

$\gamma_{Ms}$ Material safety factor for steel failure, where $\gamma_{Ms} = 1.2 f_{uk} / f_{yk} \geq 1.4$; in the context of column-to-foundation design where it is more meaningful to define the steel capacity using the yield strength $f_y$, $\gamma_{Ms} = \gamma_s$

$\gamma_{Mc}$ Material safety factor for concrete breakout failure, where $\gamma_{Mc} = \gamma_c \cdot \gamma_{inst}$

$\gamma_{Mp}$ Material safety factor for concrete breakout failure, where $\gamma_{Mp} = \gamma_{Mc}$ is recommended

The material safety factors $\gamma_s$ and $\gamma_c$ are given in the national annexes of the *Eurocode 2 (2005)* and *Eurocode 8 (2006)*, i.e. *Eurocode 2 / NA (2009)* and *Eurocode 8 / NA (2009)* as:

$\gamma_c$ = 1.5 (1.3) for concrete, fundamental (seismic) load case

$\gamma_s$ = 1.15 (1.0) for reinforcement steel, fundamental (seismic) load case

The installation safety factor $\gamma_{inst}$ takes into account that the attainable bond strength of bonded anchors is sensitive to the installation procedure. In particular poor cleaning of the drilled hole and wet concrete reduce the bond strength significantly.

The installation safety factor is defined according to one of the following three categories:

$\gamma_{inst}$ = 1.0 for systems with high installation safety

$\gamma_{inst}$ = 1.2 for systems with normal installation safety

$\gamma_{inst}$ = 1.4 for systems with low installation safety

The installation sensitivity depends on the used post-installation system. Therefore, the installation safety factor $\gamma_{inst}$ is determined by means of assessment tests in the course of prequalification of the post-installation system and is given in the approval document (ETA).

## B.2 ACI 318 (2011)

The Appendix D of the latest edition ACI 318 includes design provisions for bonded anchors which are almost identical to *CEN/TS 1992-4 (2009)*. Therefore, Appendix D of *ACI 318 (2011)* is not discussed here.

## B.3 NZ 3101 (2006)

Section 17, Clause 17.5.5 of *NZS 3101 (2006)* refers to ACI 318 Appendix D. Only mechanical anchors are addressed. However, it may be assumed that the following edition of NZ 3101 will also allow bonded anchors to be designed according to Appendix D of ACI 318.

# Appendix C: Bond Test Data

## C.1 Experimental Tests

The following tables show the program and summarise the factors $\Omega_i$ evaluated for the experimental tests on cast-in-place and post-installed reinforcing bars.

Table C.1 Program and factors $\Omega_i$ for the experimental tests on cast-in-place reinforcing bars (1/3)

| Cast-in-place | Crack width $w_{max}$ [mm] | Bar diameter $\phi$ [mm] | Concrete strength $f_c$ [3] [MPa] | Peak slip $s_u$ [1]; $s_{max} = -s_{min}$ [2] [mm] | Initial bond strength $\tau_u$ [1]; $\tau_1$ [2] [N/mm²] | 10th cycle bond strength $\tau^+_{1(n=10)}$ [N/mm²] | Residual bond strength $\tau_{u,res}$ [N/mm²] | Relative energy dissipation $E / E_0$ [-] | Damage effect cycling $\Omega_{cyc(n=10)}$ [-] | Effect of compression $\Omega_c$ [-] | Effect of crack $\Omega_w$ [-] |
|---|---|---|---|---|---|---|---|---|---|---|---|
| Monotonic loading, compressed concrete | | | | | | | | | | | |
| expCI20-w0.0-d16-com-1 | – | 16 | 20.4 | 1.94 | 12.90 | – | – | – | – | 1.70 | – |
| expCI20-w0.0-d16-com-2 | – | 16 | 20.4 | 2.05 | 13.43 | – | – | | | | |
| Monotonic loading, uncracked concrete | | | | | | | | | | | |
| expCI20-w0.0-d16-ucr-1 | – | 16 | 19.2 | 2.20 | 7.69 | – | – | – | – | – | – |
| expCI20-w0.0-d16-ucr-2 | – | 16 | 19.2 | 1.36 | 7.77 | – | – | – | – | – | – |
| Monotonic loading, cracked concrete | | | | | | | | | | | |
| expCI20-w0.1-d16-cr-1 | 0.1 | 16 | 19.2 | 2.20 | 7.69 | – | – | – | – | – | 0.96 |
| expCI20-w0.1-d16-cr-2 | 0.1 | 16 | 19.2 | 2.37 | 7.13 | – | – | | | | |
| expCI20-w0.4-d16-cr-1 | 0.4 | 16 | 23.7 | 1.71 | 5.41 | – | – | – | – | – | 0.75 |
| expCI20-w0.4-d16-cr-2 | 0.4 | 16 | 23.7 | 2.21 | 6.22 | – | – | | | | |
| expCI20-w0.8-d16-cr-1 | 0.8 | 16 | 19.2 | 2.51 | 3.21 | – | – | – | – | – | 0.49 |
| expCI20-w0.8-d16-cr-2 | 0.8 | 16 | 19.2 | 1.96 | 4.38 | – | – | | | | |
| expCI20-w0.8-d16-cr-3 | 0.8 | 16 | 19.2 | 1.75 | 3.59 | – | – | | | | |
| expCI20-w0.4-d12-cr-1 | 0.4 | 12 | 19.4 | 1.63 | 7.83 | – | – | – | – | – | – |
| expCI20-w0.4-d12-cr-2 | 0.4 | 12 | 19.4 | 1.52 | 7.46 | – | – | | | | |
| expCI20-w0.4-d25-cr-1 | 0.4 | 25 | 19.4 | 3.71 | 7.61 | – | – | – | – | – | – |
| expCI20-w0.4-d25-cr-2 | 0.4 | 25 | 19.4 | 2.22 | 6.92 | – | – | | | | |

Table C.1 Program and factors $\Omega_i$ for the experimental tests on cast-in-place reinforcing bars (2/3)

| Cast-in-place | Crack width $w_{max}$ [mm] | Bar diameter $\phi$ [mm] | Concrete strength $f_c$ [3)] [MPa] | Peak slip $s_u$ [1)]; $s_{max} = -s_{min}$ [2)] [mm] | Initial bond strength $\tau_u$ [1)];$\tau_1$ [2)] [N/mm²] | 10th cycle bond strength $\tau^+_{1(n=10)}$ [N/mm²] | Residual bond strength $\tau_{u,res}$ [N/mm²] | Relative energy dissipation $E / E_0$ [-] | Damage effect cycling $\Omega_{cyc(n=10)}$ [-] | Effect of compression $\Omega_c$ [-] | Effect of crack $\Omega_w$ [-] |
|---|---|---|---|---|---|---|---|---|---|---|---|
| Load cycling in constant cracks | | | | | | | | | | | |
| expCI20-w0.1-d16-s1.0-con-1 | 0.1 | 16 | 24.1 | 1.98 | 7.28 | 1.00 | 2.77 | 0.86 | 0.11 | – | – |
| expCI20-w0.1-d16-s1.0-con-2 | 0.1 | 16 | 24.1 | 1.98 | 6.83 | 0.54 | 2.09 | | | | |
| expCI20-w0.4-d16-s0.5-con-1 | 0.4 | 16 | 23.7 | 1.06 | 5.43 | 1.06 | 4.11 | 0.52 | 0.23 | – | – |
| expCI20-w0.4-d16-s0.5-con-2 | 0.4 | 16 | 23.7 | 1.06 | 5.87 | 1.50 | 5.06 | | | | |
| expCI20-w0.4-d16-s1.0-con-1 | 0.4 | 16 | 24.1 | 2.12 | 5.14 | 0.22 | 1.30 | 0.68 | 0.06 | – | – |
| expCI20-w0.4-d16-s1.0-con-2 | 0.4 | 16 | 24.1 | 2.12 | 5.82 | 0.41 | 2.17 | | | | |
| expCI20-w0.4-d16-s2.0-con-1 | 0.4 | 16 | 20.4 | 4.24 | 4.96 | 0.36 | 1.09 | 1.53 | 0.07 | – | – |
| expCI20-w0.8-d16-s0.5-con-1 | 0.8 | 16 | 24.1 | 1.04 | 2.88 | 0.57 | 2.78 | 0.45 | 0.19 | – | – |
| expCI20-w0.8-d16-s0.5-con-2 | 0.8 | 16 | 24.1 | 1.04 | 3.17 | 0.60 | 2.85 | | | | |
| expCI20-w0.8-d16-s1.0-con-1 | 0.8 | 16 | 24.1 | 2.07 | 3.17 | 0.36 | 1.43 | 0.71 | 0.09 | – | – |
| expCI20-w0.8-d16-s1.0-con-2 | 0.8 | 16 | 24.1 | 2.07 | 4.01 | 0.30 | 1.10 | | | | |
| expCI20-w0.4-d12-s0.5-con-1 | 0.4 | 12 | 19.4 | 0.79 | 7.10 | 1.71 | 5.67 | 0.39 | 0.23 | – | – |
| expCI20-w0.4-d12-s0.5-con-2 | 0.4 | 12 | 19.4 | 0.79 | 6.20 | 1.31 | 5.83 | | | | |

Table C.1 Program and factors $\Omega_i$ for the experimental tests on cast-in-place reinforcing bars (3/3)

| Cast-in-place | Crack width $w_{max}$ [mm] | Bar diameter $\phi$ [mm] | Concrete strength $f_c$ [3] [Mpa] | Peak slip $s_u$ [1], $s_{max} = -s_{min}$ [2] [mm] | Initial bond strength $\tau_u$ [1]; $\tau_1$ [2] [N/mm²] | 10th cycle bond strength $\tau^+_{1(n=10)}$ [N/mm²] | Residual bond strength $\tau_{u,res}$ [N/mm²] | Relative energy dissipation $E / E_0$ [-] | Damage effect cycling $\Omega_{cyc(n=10)}$ [-] | Effect of compression $\Omega_c$ [-] | Effect of crack $\Omega_w$ [-] |
|---|---|---|---|---|---|---|---|---|---|---|---|
| Simultaneous load and crack cycling | | | | | | | | | | | |
| expCI20-w0.1-d16-s0.5-cyc-1 | 0.1 | 16 | 21.6 | 0.99 | 5.91 | 1.32 | 4.27 | 0.74 | 0.16 | – | – |
| expCI20-w0.1-d16-s0.5-cyc-2 | 0.1 | 16 | 21.6 | 0.99 | 5.56 | 0.54 | 5.02 | | | | |
| expCI20-w0.1-d16-s1.0-cyc-1 | 0.1 | 16 | 24.1 | 1.98 | 8.81 | 0.53 | 2.11 | 1.19 | 0.06 | – | – |
| expCI20-w0.1-d16-s1.0-cyc-2 | 0.1 | 16 | 24.1 | 1.98 | 7.28 | 0.38 | 1.44 | | | | |
| expCI20-w0.4-d16-s0.5-cyc-1 | 0.4 | 16 | 23.7 | 1.06 | 4.48 | 0.56 | 1.22 | 0.82 | 0.16 | – | – |
| expCI20-w0.4-d16-s0.5-cyc-2 | 0.4 | 16 | 23.7 | 1.06 | 5.32 | 1.01 | 2.07 | | | | |
| expCI20-w0.4-d16-s1.0-cyc-1 | 0.4 | 16 | 24.1 | 2.12 | 5.74 | 0.22 | 0.82 | 1.07 | 0.03 | – | – |
| expCI20-w0.4-d16-s1.0-cyc-2 | 0.4 | 16 | 24.1 | 2.12 | 5.77 | 0.16 | 0.97 | | | | |
| expCI20-w0.4-d16-s2.0-cyc-1 | 0.4 | 16 | 20.4 | 4.24 | 6.52 | 0.19 | 0.53 | 0.84 | 0.17 | – | – |
| expCI20-w0.8-d16-s0.5-cyc-1 | 0.8 | 16 | 24.1 | 1.04 | 2.11 | 0.30 | 1.82 | 0.95 | 0.14 | – | – |
| expCI20-w0.8-d16-s0.5-cyc-2 | 0.8 | 16 | 24.1 | 1.04 | 1.91 | 0.25 | 1.54 | | | | |
| expCI20-w0.8-d16-s1.0-cyc-1 | 0.8 | 16 | 24.3 | 2.07 | 3.79 | 0.20 | 0.65 | 1.82 | 0.06 | – | – |
| expCI20-w0.8-d16-s1.0-cyc-2 | 0.8 | 16 | 24.3 | 2.07 | 3.63 | 0.22 | 0.44 | | | | |
| expCI20-w0.4-d12-s0.5-cyc-1 | 0.4 | 12 | 19.4 | 0.79 | 4.92 | 0.31 | 3.74 | 0.84 | 0.17 | – | – |
| expCI20-w0.4-d12-s0.5-cyc-2 | 0.4 | 12 | 19.4 | 0.79 | 8.99 | 2.56 | 5.73 | | | | |
| expCI20-w0.4-d25-s0.5-cyc-1 | 0.4 | 25 | 19.4 | 1.48 | 6.43 | 1.86 | 4.26 | 0.61 | 0.28 | – | – |
| expCI20-w0.4-d25-s0.5-cyc-2 | 0.4 | 25 | 19.4 | 1.48 | 5.87 | 1.55 | 4.94 | | | | |

[1] Monotonic tests

[2] Cyclic tests

[3] $f_c = 0.8 f_{c,cube}$

Table C.2 Program and factors $\Omega_i$ for the experimental tests on post-installed reinforcing bars

| Post-installed | Crack width $w_{max}$ [mm] | Bar diameter $\phi$ [mm] | Concrete strength $f_c$ [3)] [Mpa] | Peak slip $s_u$ [1)]; $s_{max} = -s_{min}$ [2)] [mm] | Initial bond strength $\tau_u$ [1)];$\tau_1$ [2)] [N/mm²] | 10th cycle bond strength $\tau^+_{1(n=10)}$ [N/mm²] | Residual bond strength $\tau_{u,res}$ [N/mm²] | Relative energy dissipation $E / E_0$ [-] | Damage effect cycling $\Omega_{cyc(n=10)}$ [-] | Effect of compression $\Omega_c$ [-] | Effect of crack $\Omega_w$ [-] |
|---|---|---|---|---|---|---|---|---|---|---|---|
| Monotonic loading, uncracked concrete | | | | | | | | | | | |
| expPI20-w0.0-d16-ucr-1 | – | 16 | 20.2 | 1.56 | 30.10 | – | – | – | – | – | – |
| expPI20-w0.0-d16-ucr-2 | – | 16 | 20.2 | 1.61 | 26.19 | – | – | | | | |
| Monotonic loading, cracked concrete | | | | | | | | | | | |
| expPI20-w0.4-d16-cr-1 | 0.4 | 16 | 24.1 | 2.50 | 21.99 | – | – | – | – | – | 0.82 |
| expPI20-w0.4-d16-cr-2 | 0.4 | 16 | 24.1 | 2.23 | 24.38 | – | – | | | | |
| Load cycling in constant cracks | | | | | | | | | | | |
| expPI20-w0.4-d16-s0.25-con-1 | 0.4 | 16 | 18.7 | 0.59 | 15.92 | 6.38 | 22.3 | 0.33 | 0.40 | – | – |
| Simultaneous load and crack cycling | | | | | | | | | | | |
| expPI20-w0.4-d16-s0.25-cyc-1 | 0.4 | 16 | 18.7 | 0.59 | 14.52 | 5.17 | 23.6 | 0.30 | 0.36 | – | – |

[1)] Monotonic tests

[2)] Cyclic tests

[3)] $f_c = 0.8 f_{c,cube}$

## C.2 Numerical Tests

The following tables show the program and summarise the factors $\Omega_l$ evaluated for the numerical tests on cast-in-place and post-installed reinforcing bars.

Table C.3 Program and factors $\Omega_i$ for the numerical tests of cast-in-place reinforcing bars (1/2)

| Cast-in-place | Crack width $w_{max}$ [mm] | Bar diameter $\phi$ [mm] | Concrete strength $f_c$ [Mpa] | Peak slip $s_u$ [1]; $s_{max} = -s_{min}$ [2] [mm] | Initial bond strength $\tau_u$ [1]; $\tau_1$ [2] [N/mm²] | 10th cycle bond strength $\tau^+_{1(n=10)}$ [N/mm²] | Residual bond strength $\tau_{u,res}$ [N/mm²] | Relative energy dissipation $E / E_0$ [-] | Damage effect cycling $\Omega_{cyc(n=10)}$ [-] | Effect of compression $\Omega_c$ [-] | Effect of crack $\Omega_w$ [-] |
|---|---|---|---|---|---|---|---|---|---|---|---|
| Monotonic loading, compressed concrete | | | | | | | | | | | |
| numCI20-w0.0-d16-com | – | 16 | 28.0 | 1.75 | 16.95 | – | – | – | – | 1.77 | |
| Monotonic loading, uncracked concrete | | | | | | | | | | | |
| numCI20-w0.0-d16-ucr | – | 16 | 28.0 | 2.17 | 9.55 | – | – | – | – | – | – |
| numCI50-w0.0-d16-ucr | – | 16 | 58.0 | 2.73 | 14.10 | – | – | – | – | – | – |
| Monotonic loading, cracked concrete | | | | | | | | | | | |
| numCI20-w0.1-d16-cr | 0.1 | 16 | 28.0 | 2.55 | 8.87 | – | – | – | – | – | 0.93 |
| numCI20-w0.4-d16-cr | 0.4 | 16 | 28.0 | 7.65 | 6.65 | – | – | – | – | – | 0.69 |
| numCI20-w0.8-d16-cr | 0.8 | 16 | 28.0 | 9.40 | 4.65 | – | – | – | – | – | 0.48 |
| Load cycling in constant cracks | | | | | | | | | | | |
| numCI20-w0.4-d16-s0.5-con | 0.4 | 16 | 28.0 | 1.06 | 1.00 | 0.07 | – | 0.21 | 0.21 | – | – |
| numCI20-w0.4-d16-s1.0-con | 0.4 | 16 | 28.0 | 2.12 | 1.87 | 0.16 | – | 0.17 | 0.09 | – | – |
| numCI20-w0.4-d16-s2.0-con | 0.4 | 16 | 28.0 | 4.24 | 2.94 | 1.06 | – | 0.09 | 0.02 | – | – |

Table C.3 Program and factors $\Omega_i$ for the numerical tests of cast-in-place reinforcing bars (2/2)

| Cast-in-place | Crack width $w_{max}$ [mm] | Bar diameter $\phi$ [mm] | Concrete strength $f_c$ [MPa] | Peak slip $s_u$ [1]; $s_{max} = -s_{min}$ [2] [mm] | Initial bond strength $\tau_u$ [1]; $\tau_1$ [2] [N/mm²] | 10th cycle bond strength $\tau^+_{1(n=10)}$ [N/mm²] | Residual bond strength $\tau_{u,res}$ [N/mm²] | Relative energy dissipation $E / E_0$ [-] | Damage effect cycling $\Omega_{cyc(n=10)}$ [-] | Effect of compression $\Omega_c$ [-] | Effect of crack $\Omega_w$ [-] |
|---|---|---|---|---|---|---|---|---|---|---|---|
| Simultaneous load and crack cycling | | | | | | | | | | | |
| numCI20-w0.1-d16-s0.5-cyc | 0.1 | 16 | 28.0 | 0.99 | 5.21 | 0.94 | – | 0.93 | 0.17 | – | – |
| numCI20-w0.1-d16-s1.0-cyc | 0.1 | 16 | 28.0 | 1.98 | 7.09 | 0.38 | – | 0.35 | 0.05 | – | – |
| numCI20-w0.4-d16-s0.5-cyc | 0.4 | 16 | 28.0 | 1.06 | 4.01 | 1.23 | – | 1.23 | 0.31 | – | – |
| numCI20-w0.4-d16-s1.0-cyc | 0.4 | 16 | 28.0 | 2.12 | 5.19 | 0.31 | – | 0.29 | 0.07 | – | – |
| numCI20-w0.4-d16-s2.0-cyc | 0.4 | 16 | 28.0 | 4.24 | 5.83 | 0.13 | – | 0.15 | 0.03 | – | – |
| numCI50-w0.4-d16-s0.5-cyc | 0.4 | 16 | 58.0 | 1.06 | 8.68 | 2.88 | – | 2.80 | 0.32 | – | – |
| numCI20-w0.8-d16-s0.5-cyc | 0.8 | 16 | 28.0 | 1.04 | 1.93 | 0.58 | – | 0.56 | 0.29 | – | – |
| numCI20-w0.8-d16-s1.0-cyc | 0.8 | 16 | 28.0 | 2.07 | 3.24 | 0.26 | – | 0.24 | 0.08 | – | – |
| numCI20-w0.4-d12-s0.5-cyc | 0.4 | 12 | 28.0 | 0.79 | 3.01 | 1.09 | – | 0.90 | 0.30 | – | – |
| numCI20-w0.4-d25-s0.5-cyc | 0.4 | 25 | 28.0 | 1.48 | 3.92 | 1.46 | – | 1.33 | 0.34 | – | – |

[1] Monotonic tests

[2] Cyclic tests

Table C.4 Program and factors $\Omega_i$ evaluated for the numerical tests of post-installed reinforcing bars

| Post-installed | Crack width $w_{max}$ [mm] | Bar diameter $\phi$ [mm] | Concrete strength $f_c$ [MPa] | Peak slip $s_u$ [1]; $s_{max} = -s_{min}$ [2] [mm] | Initial bond strength $\tau_u$ [1]; $\tau_1$ [2] [N/mm²] | 10th cycle bond strength $\tau^+_{1(n=10)}$ [N/mm²] | Residual bond strength $\tau_{u,res}$ [N/mm²] | Relative energy dissipation $E / E_0$ [-] | Damage effect cycling $\Omega_{cyc(n=10)}$ [-] | Effect of compression $\Omega_c$ [-] | Effect of crack $\Omega_w$ [-] |
|---|---|---|---|---|---|---|---|---|---|---|---|
| Monotonic loading, uncracked concrete | | | | | | | | | | | |
| numPI20-w0.0-d16-ucr | – | 16 | 28.0 | 1.85 | 34.40 | – | – | – | – | – | – |
| Monotonic loading, cracked concrete | | | | | | | | | | | |
| numPI20-w0.4-d16-cr | 0.4 | 16 | 28.0 | 7.65 | 6.65 | – | – | – | – | – | 0.29 |
| Load cycling in constant cracks | | | | | | | | | | | |
| numPI20-w0.4-d16-s0.5-con | 0.4 | 16 | 28.0 | 0.59 | 1.63 | 0.56 | – | – | – | – | – |
| Simultaneous load and crack cycling | | | | | | | | | | | |
| numPI20-w0.4-d16-s0.25-cyc | 0.4 | 16 | 28.0 | 0.59 | 8.29 | 2.20 | – | 2.12 | 0.27 | – | – |
| numPI20-w0.4-d16-s0.5-cyc | 0.4 | 16 | 28.0 | 1.18 | 9.82 | 3.25 | – | 3.12 | 0.32 | – | – |
| numPI50-w0.4-d16-s0.5-cyc | 0.4 | 16 | 58.0 | 1.06 | 12.46 | 3.52 | – | 3.48 | 0.28 | – | – |
| numPI20-w0.4-d12-s0.5-cyc | 0.4 | 12 | 28.0 | 0.79 | 9.42 | 2.64 | – | 2.61 | 0.28 | – | – |
| numPI20-w0.4-d25-s0.5-cyc | 0.4 | 25 | 28.0 | 1.48 | 10.09 | 3.73 | – | 3.73 | 0.37 | – | – |

[1] Monotonic tests

[2] Cyclic tests

# Appendix D: Column-to-Foundation Connection Test Data

## D.1 Experimental Tests

The following table shows the program and summarises the tested strengths of the experimental tests on cast-in-place and post-installed column-to-foundation connections.

Table D.1 Experimental test program of tests on cast-in-place post-installed column-to-foundation connections

| Monotonic loading: mon<br>Cyclic loading: cyc | Anchorage detailing | Starter bar layout | Starter bar diameter $\phi$ [mm] | Anchorage length $\ell_b$ [mm] | Concrete strength[1] $f_c$ [MPa] | Yield strength[2] $f_y$ [MPa] | Bond strength[3] $\tau_u$ [MPa] | Maximum load num$F_{max}$ [kN] | Failure mode |
|---|---|---|---|---|---|---|---|---|---|
| exp1mon | Cast-in-place | 4 bars | 16 | 240 | 24.1 | 537 | 15.4 | 79.4 | Y |
| exp1cyc | w/ hook | per face | | | 22.4 | 537 | 14.8 | 70.0 | Y |
| exp2mon | Cast-in-place | 4 bars | 16 | 240 | 21.7 | 537 | 13.2 | 50.8 | P/C |
| exp2cyc | w/o hook | per face | | | 24.1 | 537 | 13.9 | 56.7 | P/C |
| exp3mon | Post-installed | 4 bars | 16 | 240 | 20.4 | 537 | 33.2 | 80.8 | Y |
| exp3cyc | w/o hook | per face | | | 23.2 | 537 | 35.4 | 59.6 | P/C |
| exp4mon | Post-installed | 2 bars | 25 | 240 | 21.3 | 534 | 37.1 | 60.7 | P/C |
| exp4cyc | w/o hook | per face | | | 20.6 | 534 | 36.4 | 46.3 | P/C |
| exp5mon | Cast-in-place | 2 bars | 32 | 420 | 23.0 | 540 | 16.7 | 137.9 | Y |
| exp5cyc | w/ hook | per face | | | 22.5 | 540 | 16.5 | 129.6 | Y |
| exp6mon | Cast-in-place | 2 bars | 32 | 420 | 21.9 | 540 | 15.7 | 118.5 | Y |
| exp6cyc | w/o hook | per face | | | 24.7 | 540 | 16.7 | 135.1 | Y |
| exp7mon | Post-installed | 2 bars | 32 | 420 | 20.5 | 540 | 33.7 | 124.0 | Y |
| exp7cyc | w/o hook | per face | | | 22.2 | 540 | 35.1 | 124.7 | Y |
| exp8mon | Post-installed | 2 bars | 25 | 420 | 21.8 | 534 | 36.0 | 84.4 | Y |
| exp8cyc | w/o hook | per face | | | 20.7 | 534 | 35.0 | 83.9 | Y |

[1] Foundation concrete; [2] Column starter bar; [3] Between foundation concrete and column starter bar, $\tau_{u,mon} = \tau_{u,cyc} (f_{c,mon} / f_{c,cyc})^{0.5}$

In the following, the monotonic and cyclic load-drift curves of the experimental tests are presented. The sequence of cracks, pullout and concrete breakout or yield is indicated in the diagrams. In addition, the photos taken after the termination of testing at are shown to illustrate the damage pattern.

### D.1.1 Specimen 1 – $\ell_b$ = 240 mm, 2 · 4$\phi$16, cast-in-place with hooks

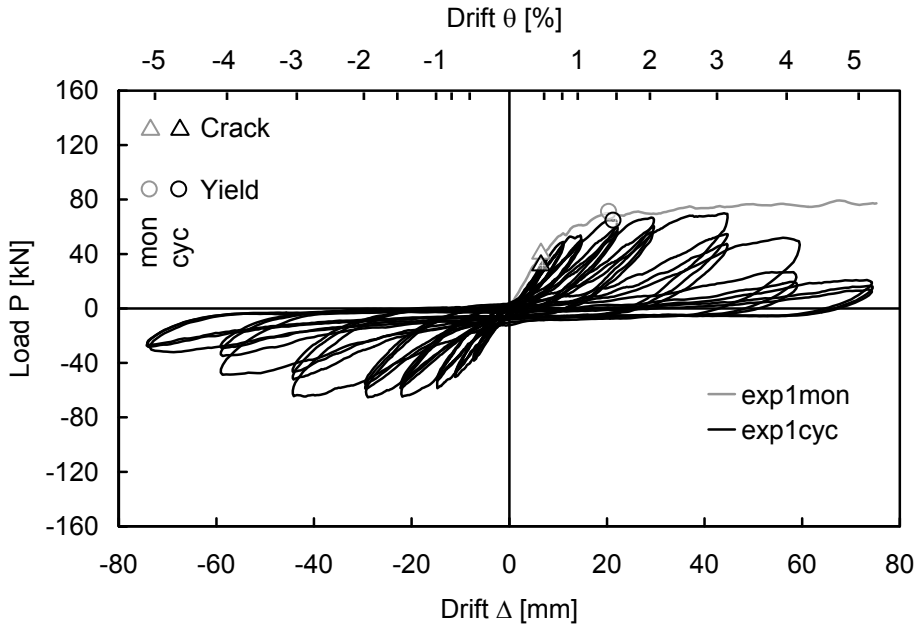


Figure D.1 Monotonic and cyclic test on Specimen 1: Experimentally determined load-drift curves

The monotonic and the cyclic test on Specimen 1 (cast-in-place with hooks) showed similar behaviour. Cracks appeared at 0.5 % drift and starter bars yielded at about 1.5 % drift (failure mode Y). Concrete breakout was observed at 3.0 % drift, however, the capacity was not decreasing. The monotonic test showed pronounced strain hardening whereas the strength of the cyclic test significantly decreased during the cycles at 3.0 % and 4.0 % drift levels, accompanied by the development of concrete breakouts.

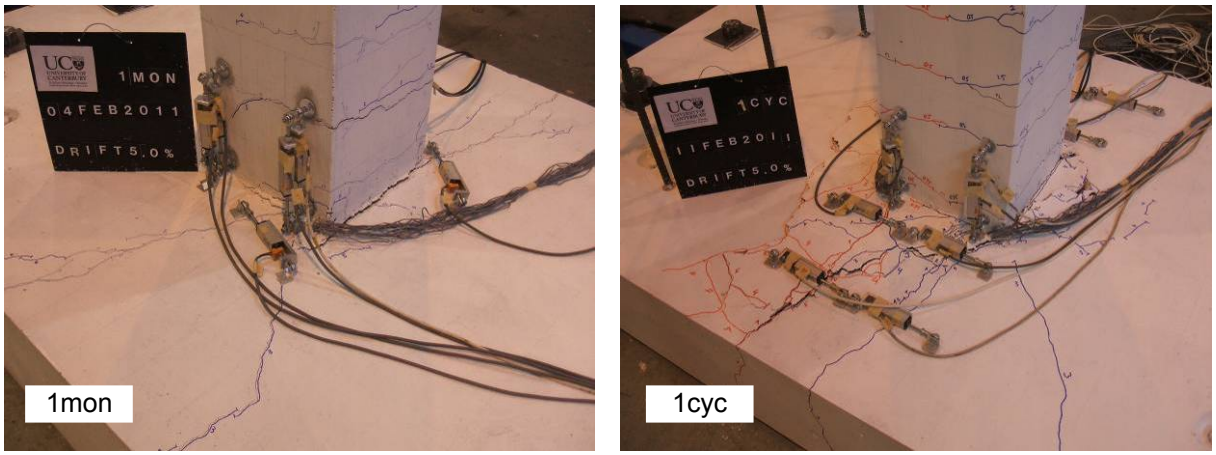


Figure D.2 Monotonic and cyclic test on Specimen 1: Damage pattern after testing

### D.1.2 Specimen 2 – $\ell_b$ = 240 mm, 2 · 4$\phi$16, cast-in-place without hooks

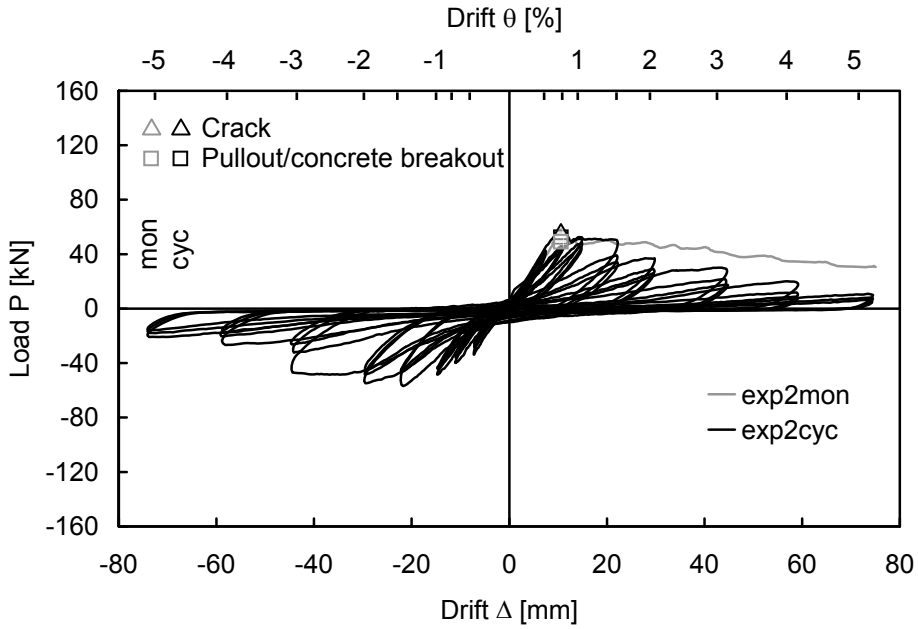


Figure D.3 Monotonic and cyclic test on Specimen 2: Experimentally determined load-drift curves

During the monotonic and cyclic test on Specimen 2 (cast-in-place without hooks) cracks developed at 0.75 % drift and the maximum load was reached before utilising the flexural capacity of the column. The failure mode is therefore categorised as failure mode P/C. The strength steadily decreased and concrete breakouts appeared at 1.5 % drift. The strength degradation of the cyclic test was slightly more pronounced if compared to the degradation of the monotonic test.

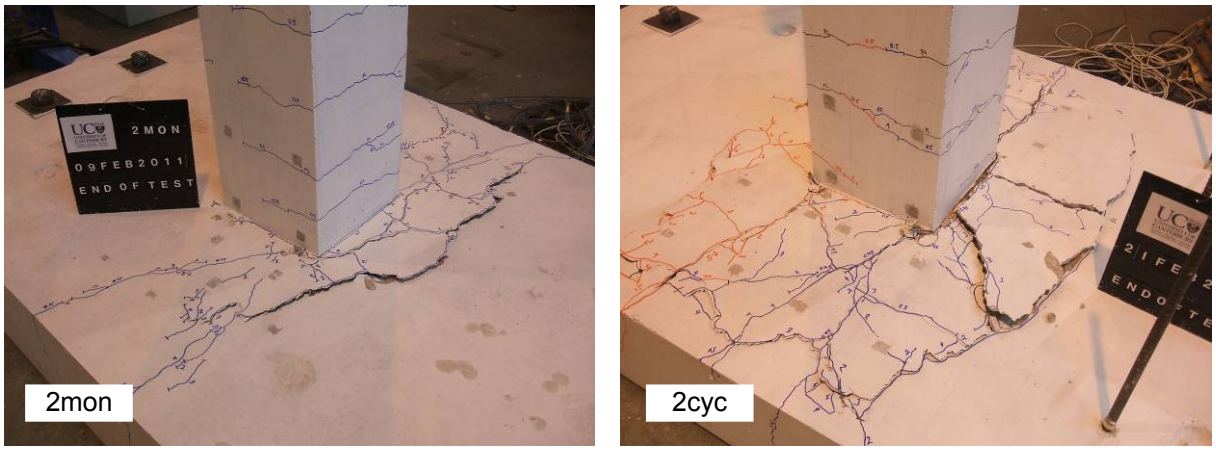


Figure D.4 Monotonic and cyclic test on Specimen 2: Damage pattern after testing

### D.1.3 Specimen 3 – $\ell_b$ = 240 mm, 2 · 4$\phi$16, post-installed

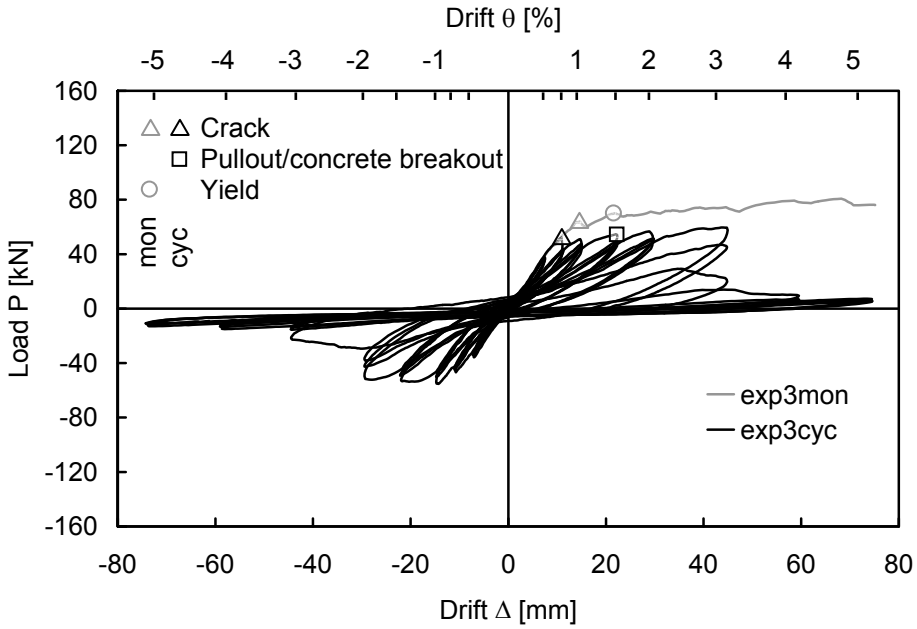


Figure D.5 Monotonic and cyclic test on Specimen 3: Experimentally determined load-drift curves

The monotonic test on Specimen 3 (post-installed) showed yielding of the starter bars at 1.5 % drift (failure mode Y). In parallel to the yielding failure, cracks and concrete breakouts occurred. The steady increase of the strength indicated strain hardening. The maximum load was reached at 4.0 % drift. On the contrary, the cyclic test exhibited failure mode P/C at 1.5 % drift. However, a negligible increase in strength was observed up to 3.0 % drift. The load-drift behaviour indicates that the failure of this specimen design is in the transition zone of failure mode Y and P/C.

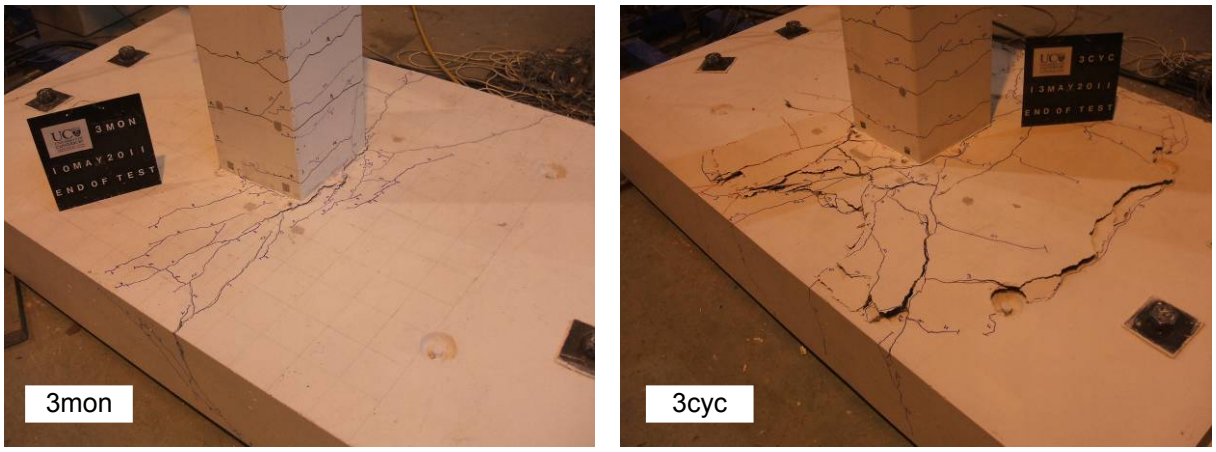


Figure D.6 Monotonic and cyclic test on Specimen 3: Damage pattern after testing

### D.1.4 Specimen 4 – $\ell_b$ = 240 mm, 2 · 2$\phi$25, post-installed

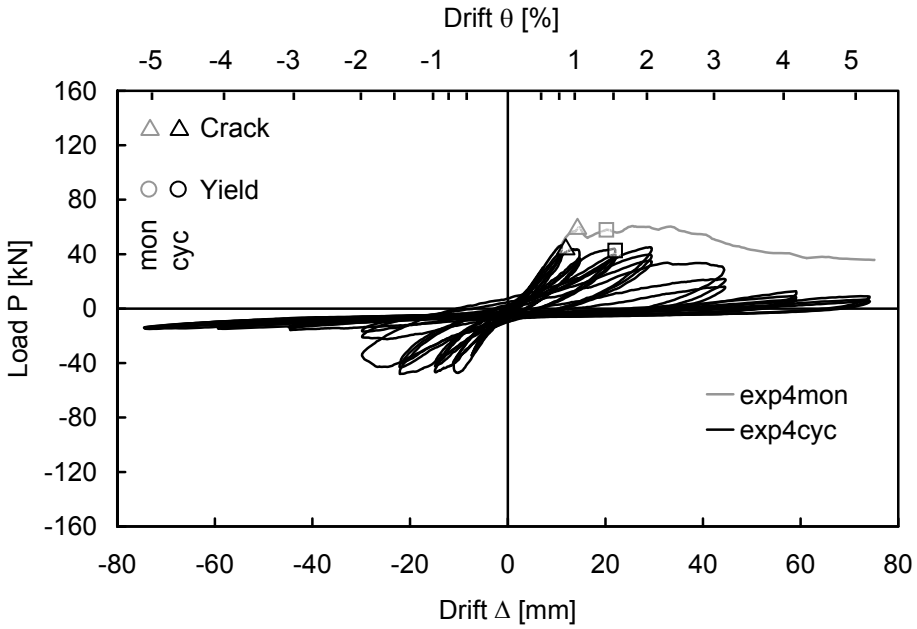


Figure D.7 Monotonic and cyclic test on Specimen 4: Experimentally determined load-drift curves

Specimen 4 (post-installed) performed poorly during the monotonic and cyclic test. Cracks were observed at 1.0 % drift, marking the onset of a plateau. The plateau ended with the development of concrete breakouts at 1.5 % drift, and the strength deteriorated thereafter (failure mode P/C). For the monotonic test, the strength deterioration was less pronounced than for the cyclic test.

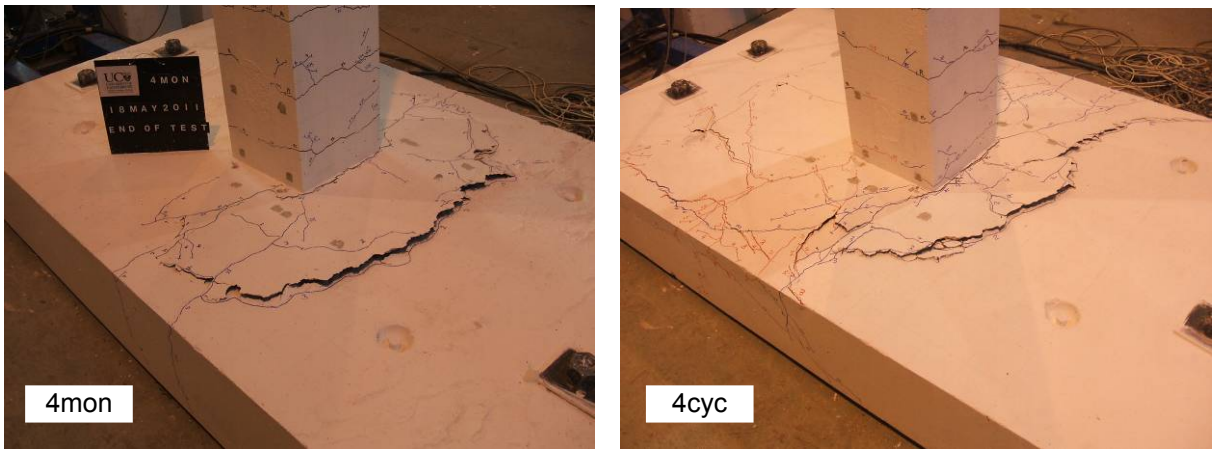


Figure D.8 Monotonic and cyclic test on Specimen 4: Damage pattern after testing

### D.1.5 Specimen 5 – $\ell_b$ = 420 mm, 2 · 2$\phi$32, cast-in-place with hooks

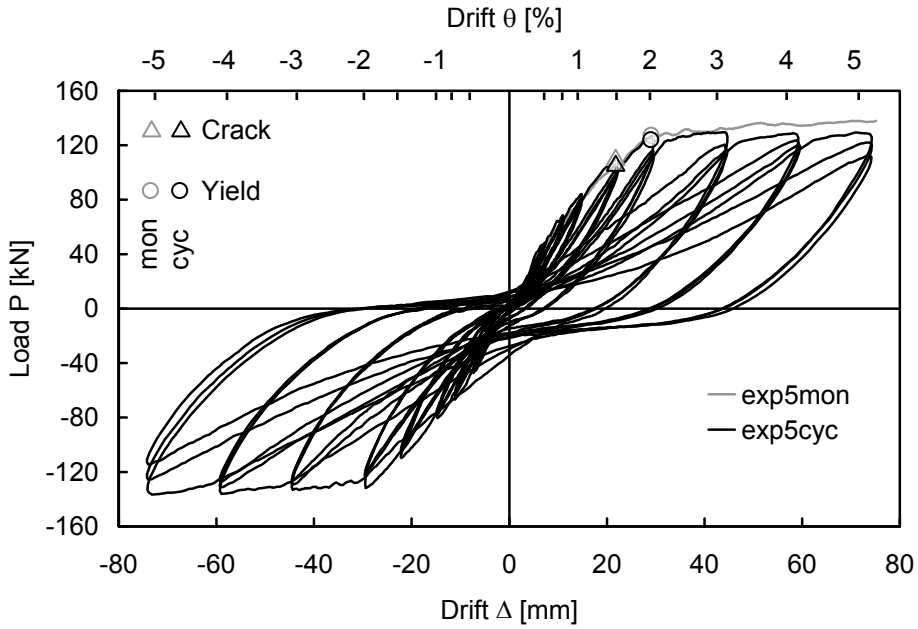


Figure D.9 Monotonic and cyclic test on Specimen 5: Experimentally determined load-drift curves

The monotonic and the cyclic test on Specimen 5 (cast-in-place with hooks) showed a similar behaviour. Cracks formed next to the column at around 1.5 % drift, almost simultaneously with yielding of the starter bars (failure mode Y). Both specimens failed by steel yielding, however, the monotonic test showed a more pronounced strain hardening and only the cyclic test developed concrete breakouts at 5.0 % drift.

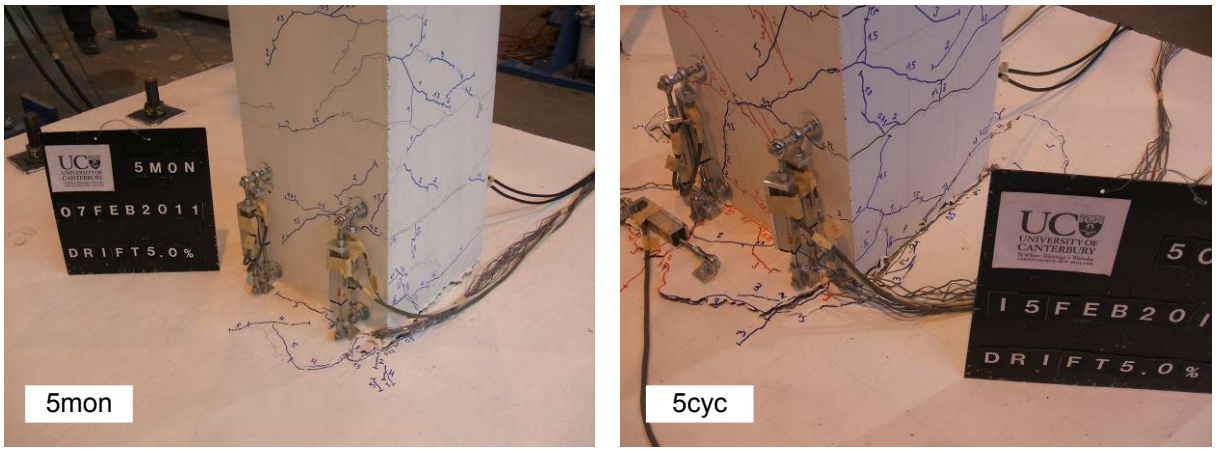


Figure D.10 Monotonic and cyclic test on Specimen 5: Damage pattern after testing

### D.1.6 Specimen 6 – $\ell_b$ = 420 mm, 2 · 2$\phi$32, cast-in-place without hooks

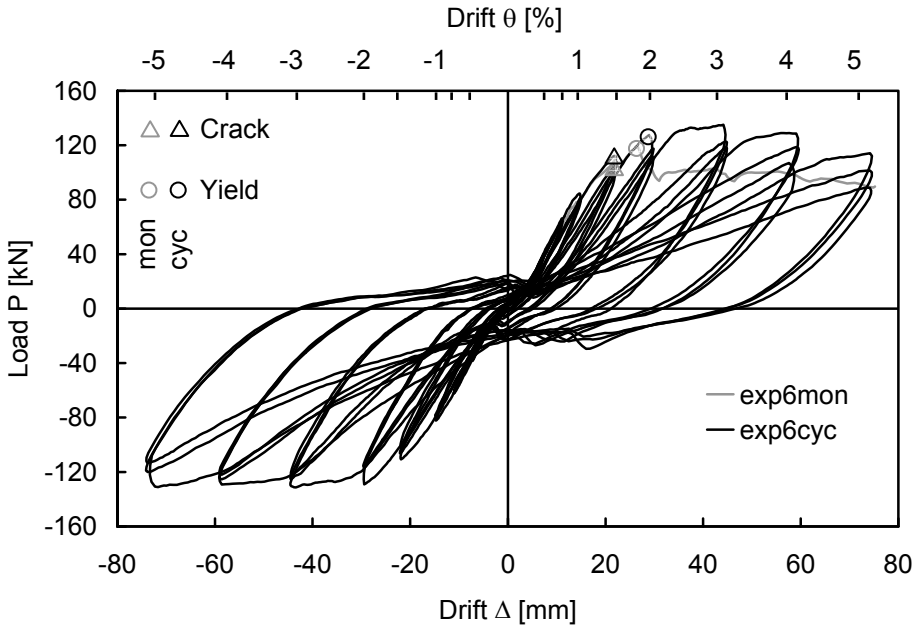


Figure D.11 Monotonic and cyclic test on Specimen 6: Experimentally determined load-drift curves

For the monotonic and cyclic test on Specimen 6 (cast-in-place without hooks) cracks were observed at 1.5 % drift and yielding of the starter bars occurred at 2.0 % drift (failure mode Y). The following behaviour of the monotonic and cyclic tests differed slightly: The strength of the monotonically tested specimen decreased with a small jump accompanied by a progressive cracking. Concrete breakouts developed at 3.0 % drift. The strength of the specimen tested cyclically reached the peak at 3.0 % drift and thereafter decreased similar to the monotonic test.

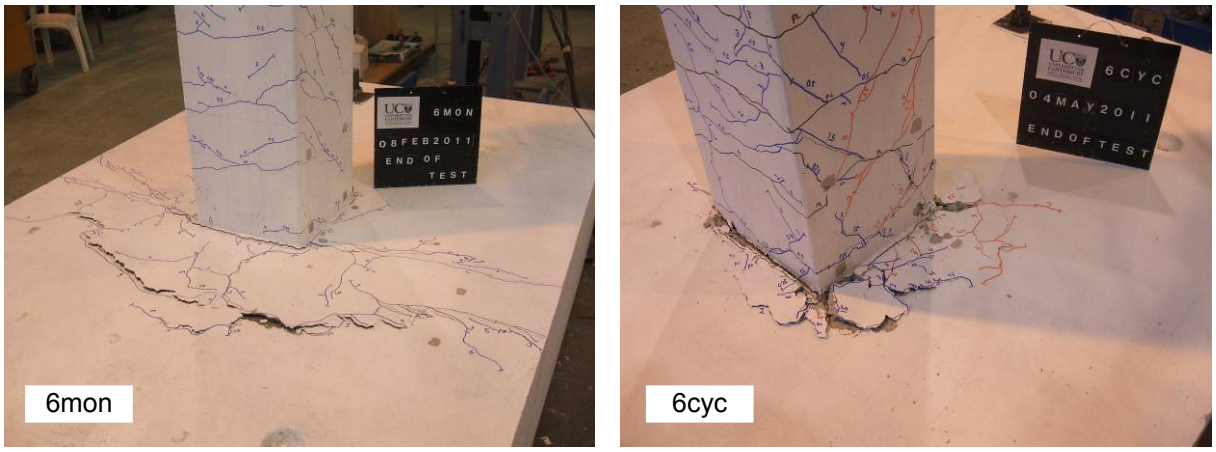


Figure D.12 Monotonic and cyclic test on Specimen 6: Damage pattern after testing

### D.1.7 Specimen 7 – $\ell_b$ = 420 mm, 2 · 2$\phi$32, post-installed

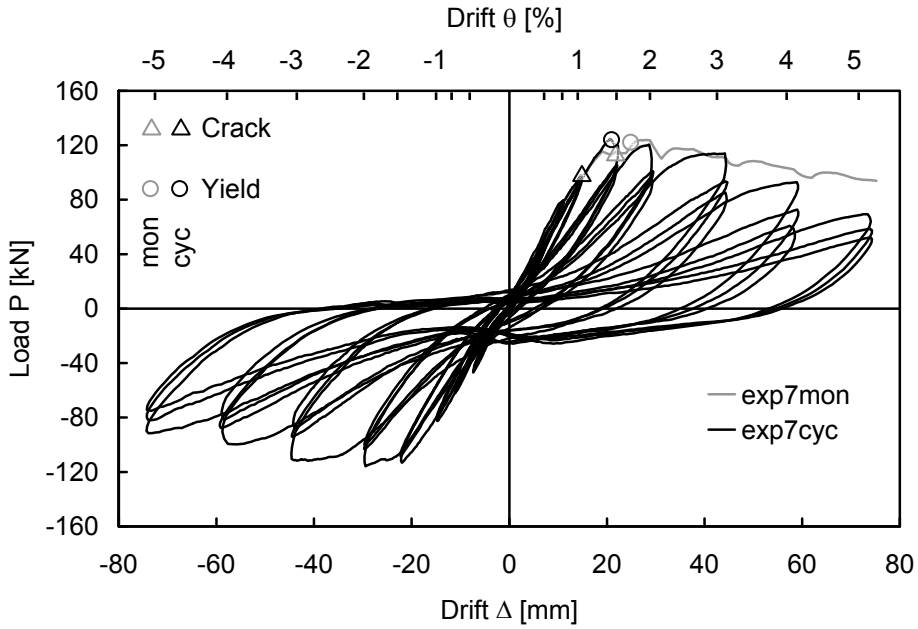


Figure D.13 Monotonic and cyclic test on Specimen 7: Experimentally determined load-drift curves

First cracks appeared already at 1.0 % drift for the monotonic and cyclic test on Specimen 7 (post-installed). Yielding of the column starter bars developed at around 1.5 % drift in parallel to the formation of concrete breakouts (failure mode Y). Although the following progressive decrease in strength was more pronounced than for Specimen 6, the overall behaviour was similar. More concrete damage was observed for the cyclic test than for the monotonic test.

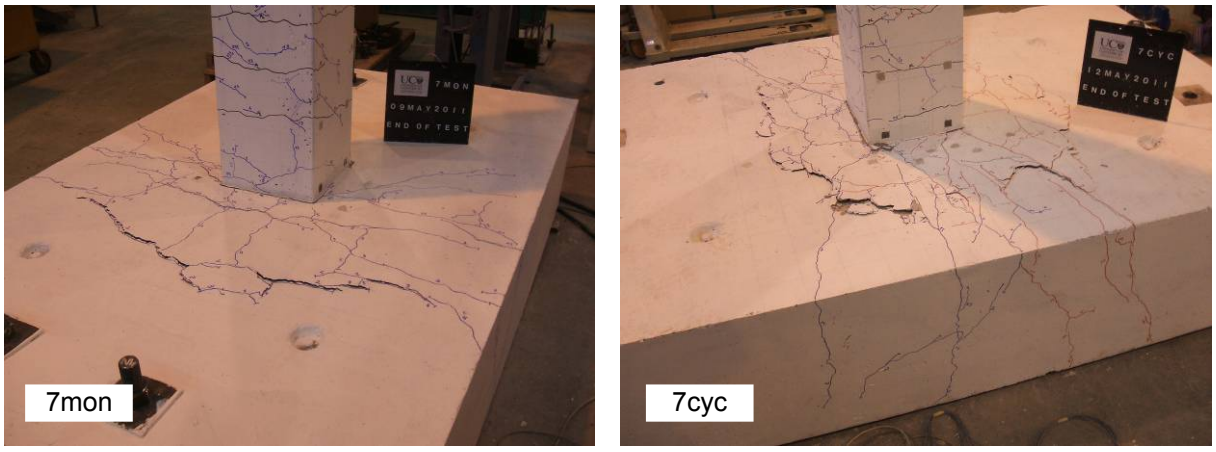


Figure D.14 Monotonic and cyclic test on Specimen 7: Damage pattern after testing

### D.1.8 Specimen 8 – $\ell_b$ = 420 mm, 2 · 2$\phi$25, post-installed

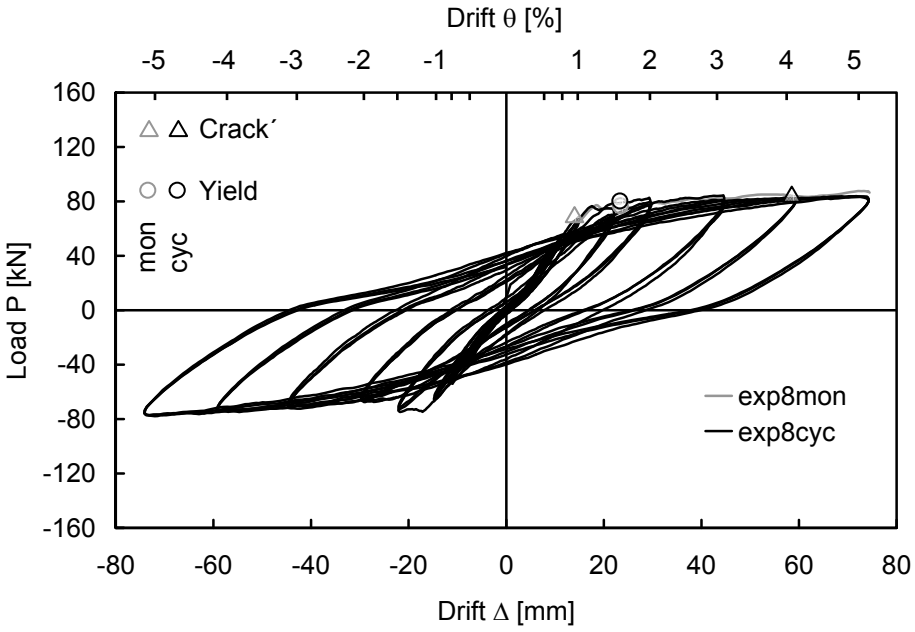


Figure D.15 Monotonic and cyclic test on Specimen 8: Experimentally determined load-drift curves

Almost no cracks developed in the foundation during the monotonic and cyclic test on Specimen 8 (post-installed). Yielding of the column starter bars occurred just before 1.5 % drift (failure mode Y). The strength remained constant thereafter. Failure was not located in the foundation but in the column where a pronounced plastic hinging was observed.

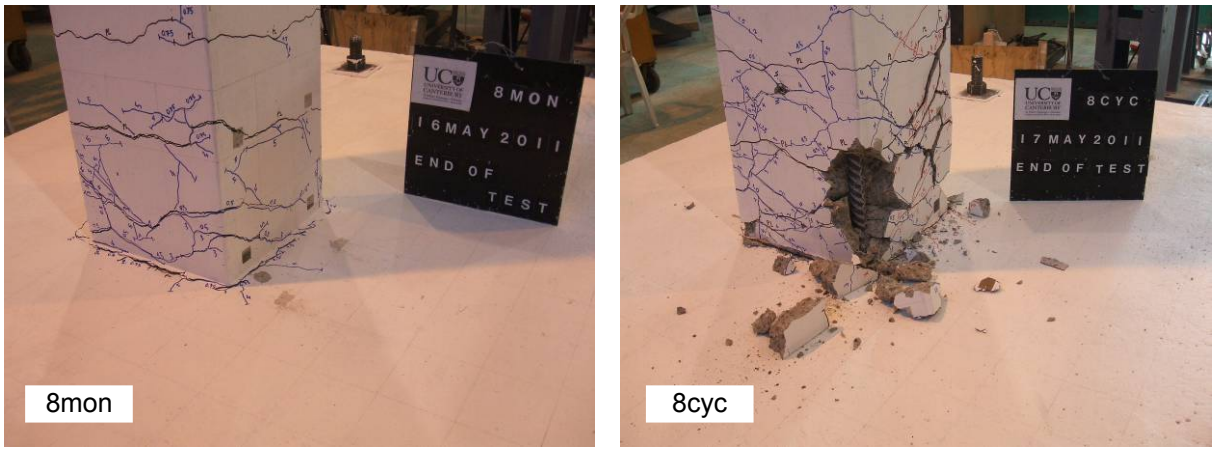


Figure D.16 Monotonic and cyclic test on Specimen 8: Damage pattern after testing

## D.2 Numerical Tests

The following table shows the program and summarises the defined strengths for the numerical tests on cast-in-place and post-installed column-to-foundation connections.

Table D.2 Numerical test program of tests on cast-in-place post-installed column-to-foundation connections (1/8)

| Monotonic loading: mon<br>Cyclic loading: cyc | Anchorage detailing | Starter bar layout | Starter bar diameter $\phi$ [mm] | Anchorage length $\ell_b$ [mm] | Concrete strength[1] $f_c$ [MPa] | Yield strength[2] $f_y$ [MPa] | Bond strength[3] $\tau_u$ [MPa] | Maximum load num$F_{max}$ [kN] | Failure mode |
|---|---|---|---|---|---|---|---|---|---|
| num1mon | Cast-in-place | 4 bars | 16 | 240 | 28.0 | 535 | 14.0 | 79.6 | Y |
| num1cyc | w/ hook | per face | | | 28.0 | 535 | 14.0 | 78.7 | Y |
| num1mon-CI20-d12-h | Cast-in-place | 4 bars | 12 | 240 | 28.0 | 535 | 14.0 | 49.4 | Y |
| num1cyc-CI20-d12-h | w/ hook | per face | | | 28.0 | 535 | 14.0 | 49.4 | Y |
| num1mon-CI20-d25-h | Cast-in-place | 4 bars | 25 | 240 | 28.0 | 535 | 14.0 | 99.8 | P/C |
| num1cyc-CI20-d25-h | w/ hook | per face | | | 28.0 | 535 | 14.0 | 94.5 | P/C |
| num2mon | Cast-in-place | 4 bars | 16 | 240 | 28.0 | 535 | 14.0 | 63.8 | P/C |
| num2cyc | w/o hook | per face | | | 28.0 | 535 | 14.0 | 56.1 | P/C |
| num2mon-CI20-d12-s | Cast-in-place | 4 bars | 12 | 240 | 28.0 | 535 | 14.0 | 48.5 | Y |
| num2cyc-CI20-d12-s | w/o hook | per face | | | 28.0 | 535 | 14.0 | 48.0 | Y |
| num2mon-CI20-d25-s | Cast-in-place | 4 bars | 25 | 240 | 28.0 | 535 | 14.0 | 68.5 | P/C |
| num2cyc-CI20-d25-s | w/o hook | per face | | | 28.0 | 535 | 14.0 | 58.5 | P/C |

[1] Foundation concrete; [2] Column starter bar; [3] Between foundation concrete and column starter bar

Table D.2 Numerical test program of tests on cast-in-place post-installed column-to-foundation connections (2/8)

| Monotonic loading: mon<br>Cyclic loading: cyc | Anchorage detailing | Starter bar layout | Starter bar diameter $\phi$ [mm] | Anchorage length $\ell_b$ [mm] | Concrete strength[1] $f_c$ [MPa] | Yield strength[2] $f_y$ [MPa] | Bond strength[3] $\tau_u$ [MPa] | Maximum load num$F_{max}$ [kN] | Failure mode |
|---|---|---|---|---|---|---|---|---|---|
| num3mon | Post-installed | 4 bars | 16 | 240 | 28.0 | 535 | 35.0 | 71.0 | P/C |
| num3cyc | w/o hook | per face | | | 28.0 | 535 | 35.0 | 64.8 | P/C |
| num3mon-PI20-d12-s | Post-installed | 4 bars | 12 | 240 | 28.0 | 535 | 35.0 | 48.0 | Y |
| num3cyc-PI20-d12-s | w/o hook | per face | | | 28.0 | 535 | 35.0 | 49.3 | Y |
| num3mon-PI20-d25-s | Post-installed | 4 bars | 25 | 240 | 28.0 | 535 | 35.0 | 70.9 | P/C |
| num3cyc-PI20-d25-s | w/o hook | per face | | | 28.0 | 535 | 35.0 | 62.6 | P/C |
| num3mon-PI20-d16-s-d[4] | Post-installed | 4 bars | 16 | 240 | 28.0 | 535 | 35.0 | 68.5 | P/C |
| num3cyc-PI20-d16-s-d[4] | w/o hook | per face | | | 28.0 | 535 | 35.0 | 67.6 | P/C |
| num3mon-PI20-d16-s-q[5] | Post-installed | 4 bars | 16 | 240 | 28.0 | 535 | 35.0 | 68.4 | P/C |
| num3cyc-PI20-d16-s-q[5] | w/o hook | per face | | | 28.0 | 535 | 35.0 | 69.4 | P/C |
| num4mon | Post-installed | 2 bars | 25 | 240 | 28.0 | 535 | 35.0 | 58.6 | P/C |
| num4cyc | w/o hook | per face | | | 28.0 | 535 | 35.0 | 50.9 | P/C |
| num4mon-PI20-d16-s | Post-installed | 2 bars | 16 | 240 | 28.0 | 535 | 35.0 | 44.3 | Y |
| num4cyc-PI20-d16-s | w/o hook | per face | | | 28.0 | 535 | 35.0 | 44.9 | Y |
| num4mon-PI20-d32-s | Post-installed | 2 bars | 32 | 240 | 28.0 | 535 | 35.0 | 59.9 | P/C |
| num4cyc-PI20-d32-s | w/o hook | per face | | | 28.0 | 535 | 35.0 | 49.9 | P/C |

[1] Foundation concrete; [2] Column starter bar; [3] Between foundation concrete and column starter bar; [4] Foundation reinforcement doubled; [5] Foundation reinforcement quadrupled

Table D.2 Numerical test program of tests on cast-in-place post-installed column-to-foundation connections (3/8)

| Monotonic loading: mon<br>Cyclic loading: cyc | Anchorage detailing | Starter bar layout | Starter bar diameter $\phi$ [mm] | Anchorage length $\ell_b$ [mm] | Concrete strength[1] $f_c$ [MPa] | Yield strength[2] $f_y$ [MPa] | Bond strength[3] $\tau_u$ [MPa] | Maximum load num$F_{max}$ [kN] | Failure mode |
|---|---|---|---|---|---|---|---|---|---|
| num5mon | Cast-in-place | 2 bars | 32 | 420 | 28.0 | 535 | 14.0 | 142.3 | Y |
| num5cyc | w/ hook | per face | | | 28.0 | 535 | 14.0 | 142.2 | Y |
| num5mon-CI20-d25-h | Cast-in-place | 2 bars | 25 | 420 | 28.0 | 535 | 14.0 | 93.5 | Y |
| num5cyc-CI20-d25-h | w/ hook | per face | | | 28.0 | 535 | 14.0 | 94.5 | Y |
| num5mon-CI20-d40-h | Cast-in-place | 2 bars | 40 | 420 | 28.0 | 535 | 14.0 | 151.0 | P/C |
| num5cyc-CI20-d40-h | w/ hook | per face | | | 28.0 | 535 | 14.0 | 157.1 | P/C |
| num6mon | Cast-in-place | 2 bars | 32 | 420 | 28.0 | 535 | 14.0 | 119.5 | P/C |
| num6cyc | w/o hook | per face | | | 28.0 | 535 | 14.0 | 118.0 | P/C |
| num6mon-CI20-d25-s | Cast-in-place | 2 bars | 25 | 420 | 28.0 | 535 | 14.0 | 93.3 | Y |
| num6cyc-CI20-d25-s | w/o hook | per face | | | 28.0 | 535 | 14.0 | 96.5 | Y |
| num6mon-CI20-d40-s | Cast-in-place | 2 bars | 40 | 420 | 28.0 | 535 | 14.0 | 159.2 | P/C |
| num6cyc-CI20-d40-s | w/o hook | per face | | | 28.0 | 535 | 14.0 | 159.6 | P/C |

[1] Foundation concrete; [2] Column starter bar; [3] Between foundation concrete and column starter bar

Table D.2 Numerical test program of tests on cast-in-place post-installed column-to-foundation connections (4/8)

| Monotonic loading: mon<br>Cyclic loading: cyc | Anchorage detailing | Starter bar layout | Starter bar diameter $\phi$ [mm] | Anchorage length $\ell_b$ [mm] | Concrete strength[1] $f_c$ [MPa] | Yield strength[2] $f_y$ [MPa] | Bond strength[3] $\tau_u$ [MPa] | Maximum load num$F_{max}$ [kN] | Failure mode |
|---|---|---|---|---|---|---|---|---|---|
| num7mon | Post-installed | 2 bars | 32 | 420 | 28.0 | 535 | 35.0 | 122.0 | Y |
| num7cyc | w/o hook | per face | | | 28.0 | 535 | 35.0 | 123.2 | Y |
| num7mon-PI20-d25-s | Post-installed | 2 bars | 25 | 420 | 28.0 | 535 | 35.0 | 44.9 | Y |
| num7cyc-PI20-d25-s | w/o hook | per face | | | 28.0 | 535 | 35.0 | 45.5 | Y |
| num7mon-PI20-d40-s | Post-installed | 2 bars | 40 | 420 | 28.0 | 535 | 35.0 | 108.6 | P/C |
| num7cyc-PI20-d40-s | w/o hook | per face | | | 28.0 | 535 | 35.0 | 109.0 | P/C |
| num7mon-PI20-d32-s-d[4] | Post-installed | 2 bars | 32 | 420 | 28.0 | 535 | 35.0 | 109.0 | Y |
| num7cyc-PI20-d32-s-d[4] | w/o hook | per face | | | 28.0 | 535 | 35.0 | 107.1 | Y |
| num7mon-PI20-d32-s-q[5] | Post-installed | 2 bars | 32 | 420 | 28.0 | 535 | 35.0 | 112.9 | Y |
| num7cyc-PI20-d32-s-q[5] | w/o hook | per face | | | 28.0 | 535 | 35.0 | 110.3 | Y |
| num8mon | Post-installed | 2 bars | 25 | 420 | 28.0 | 535 | 35.0 | 112.9 | Y |
| num8cyc | w/o hook | per face | | | 28.0 | 535 | 35.0 | 110.3 | Y |

[1] Foundation concrete; [2] Column starter bar; [3] Between foundation concrete and column starter bar; [4] Foundation reinforcement doubled; [5] Foundation reinforcement quadrupled

Table D.2 Numerical test program of tests on cast-in-place post-installed column-to-foundation connections (5/8)

| Monotonic loading: mon<br>Cyclic loading: cyc | Anchorage detailing | Starter bar layout | Starter bar diameter $\phi$ [mm] | Anchorage length $\ell_b$ [mm] | Concrete strength[1] $f_c$ [MPa] | Yield strength[2] $f_y$ [MPa] | Bond strength[3] $\tau_u$ [MPa] | Maximum load num$F_{max}$ [kN] | Failure mode |
|---|---|---|---|---|---|---|---|---|---|
| num1mon-CI50-d16-h | Cast-in-place | 4 bars | 16 | 240 | 58.0 | 535 | 20.0 | 79.9 | Y |
| num1cyc-CI50-d16-h | w/ hook | per face | | | 58.0 | 535 | 20.0 | 78.5 | Y |
| num1mon-CI50-d12-h | Cast-in-place | 4 bars | 12 | 240 | 58.0 | 535 | 20.0 | 49.7 | Y |
| num1cyc-CI50-d12-h | w/ hook | per face | | | 58.0 | 535 | 20.0 | 50.6 | Y |
| num1mon-CI50-d25-h | Cast-in-place | 4 bars | 25 | 240 | 58.0 | 535 | 20.0 | 134.2 | P/C |
| num1cyc-CI50-d25-h | w/ hook | per face | | | 58.0 | 535 | 20.0 | 131.2 | P/C |
| num2mon-CI50-d16-s | Cast-in-place | 4 bars | 16 | 240 | 58.0 | 535 | 20.0 | 78.3 | Y |
| num2cyc-CI50-d16-s | w/o hook | per face | | | 58.0 | 535 | 20.0 | 79.6 | Y |
| num2mon-CI50-d12-s | Cast-in-place | 4 bars | 12 | 240 | 58.0 | 535 | 20.0 | 49.6 | Y |
| num2cyc-CI50-d12-s | w/o hook | per face | | | 58.0 | 535 | 20.0 | 51.0 | Y |
| num2mon-CI50-d25-s | Cast-in-place | 4 bars | 25 | 240 | 58.0 | 535 | 20.0 | 98.2 | P/C |
| num2cyc-CI50-d25-s | w/o hook | per face | | | 58.0 | 535 | 20.0 | 101.7 | P/C |

[1] Foundation concrete; [2] Column starter bar; [3] Between foundation concrete and column starter bar

Table D.2 Numerical test program of tests on cast-in-place post-installed column-to-foundation connections (6/8)

| Monotonic loading: mon<br>Cyclic loading: cyc | Anchorage detailing | Starter bar layout | Starter bar diameter $\phi$ [mm] | Anchorage length $\ell_b$ [mm] | Concrete strength[1] $f_c$ [MPa] | Yield strength[2] $f_y$ [MPa] | Bond strength[3] $\tau_u$ [MPa] | Maximum load num$F_{max}$ [kN] | Failure mode |
|---|---|---|---|---|---|---|---|---|---|
| num3mon-PI50-d16-s | Post-installed | 4 bars | 16 | 240 | 58.0 | 535 | 35.0 | 78.9 | Y |
| num3cyc-PI50-d16-s | w/o hook | per face | | | 58.0 | 535 | 35.0 | 77.8 | Y |
| num3mon-PI50-d12-s | Post-installed | 4 bars | 12 | 240 | 58.0 | 535 | 35.0 | 49.6 | Y |
| num3cyc-PI50-d12-s | w/o hook | per face | | | 58.0 | 535 | 35.0 | 50.7 | Y |
| num3mon-PI50-d25-s | Post-installed | 4 bars | 25 | 240 | 58.0 | 535 | 35.0 | 101.9 | P/C |
| num3cyc-PI50-d25-s | w/o hook | per face | | | 58.0 | 535 | 35.0 | 104.5 | P/C |
| num3mon-PI50-d16-s-d[4] | Post-installed | 4 bars | 16 | 240 | 58.0 | 535 | 35.0 | 79.1 | P/C |
| num3cyc-PI50-d16-s-d[4] | w/o hook | per face | | | 58.0 | 535 | 35.0 | 79.0 | P/C |
| num3mon-PI50-d16-s-q[5] | Post-installed | 4 bars | 16 | 240 | 58.0 | 535 | 35.0 | 79.3 | P/C |
| num3cyc-PI50-d16-s-q[5] | w/o hook | per face | | | 58.0 | 535 | 35.0 | 78.0 | P/C |
| num4mon-PI50-d25-s | Post-installed | 2 bars | 25 | 240 | 58.0 | 535 | 35.0 | 82.7 | P/C |
| num4cyc-PI50-d25-s | w/o hook | per face | | | 58.0 | 535 | 35.0 | 82.0 | P/C |
| num4mon-PI50-d16-s | Post-installed | 2 bars | 16 | 240 | 58.0 | 535 | 35.0 | 44.6 | Y |
| num4cyc-PI50-d16-s | w/o hook | per face | | | 58.0 | 535 | 35.0 | 47.3 | Y |
| num4mon-PI50-d32-s | Post-installed | 2 bars | 32 | 240 | 58.0 | 535 | 35.0 | 84.4 | P/C |
| num4cyc-PI50-d32-s | w/o hook | per face | | | 58.0 | 535 | 35.0 | 86.3 | P/C |

[1] Foundation concrete; [2] Column starter bar; [3] Between foundation concrete and column starter bar; [4] Foundation reinforcement doubled; [5] Foundation reinforcement quadrupled

Table D.2 Numerical test program of tests on cast-in-place post-installed column-to-foundation connections (7/8)

| Monotonic loading: mon<br>Cyclic loading: cyc | Anchorage detailing | Starter bar layout | Starter bar diameter $\phi$ [mm] | Anchorage length $\ell_b$ [mm] | Concrete strength[1] $f_c$ [MPa] | Yield strength[2] $f_y$ [MPa] | Bond strength[3] $\tau_u$ [MPa] | Maximum load num$F_{max}$ [kN] | Failure mode |
|---|---|---|---|---|---|---|---|---|---|
| num5mon-CI50-d32-h | Cast-in-place | 2 bars | 32 | 420 | 58.0 | 535 | 20.0 | 143.4 | Y |
| num5cyc-CI50-d32-h | w/ hook | per face | | | 58.0 | 535 | 20.0 | 147.6 | Y |
| num5mon-CI50-d25-h | Cast-in-place | 2 bars | 25 | 420 | 58.0 | 535 | 20.0 | 93.8 | Y |
| num5cyc-CI50-d25-h | w/ hook | per face | | | 58.0 | 535 | 20.0 | 96.4 | Y |
| num5mon-CI50-d40-h | Cast-in-place | 2 bars | 40 | 420 | 58.0 | 535 | 20.0 | 210.7 | P/C |
| num5cyc-CI50-d40-h | w/ hook | per face | | | 58.0 | 535 | 20.0 | 209.1 | P/C |
| num6mon-CI50-d32-s | Cast-in-place | 2 bars | 32 | 420 | 58.0 | 535 | 20.0 | 142.6 | Y |
| num6cyc-CI50-d32-s | w/o hook | per face | | | 58.0 | 535 | 20.0 | 142.1 | Y |
| num6mon-CI50-d25-s | Cast-in-place | 2 bars | 25 | 420 | 58.0 | 535 | 20.0 | 93.9 | Y |
| num6cyc-CI50-d25-s | w/o hook | per face | | | 58.0 | 535 | 20.0 | 96.5 | Y |
| num6mon-CI50-d40-s | Cast-in-place | 2 bars | 40 | 420 | 58.0 | 535 | 20.0 | 159.2 | P/C |
| num6cyc-CI50-d40-s | w/o hook | per face | | | 58.0 | 535 | 20.0 | 159.6 | P/C |

[1] Foundation concrete; [2] Column starter bar; [3] Between foundation concrete and column starter bar; [4] Foundation reinforcement doubled; [5] Foundation reinforcement quadrupled

Table D.2 Numerical test program of tests on cast-in-place post-installed column-to-foundation connections (8/8)

| Monotonic loading: mon<br>Cyclic loading: cyc | Anchorage detailing | Starter bar layout | Starter bar diameter $\phi$ [mm] | Anchorage length $\ell_b$ [mm] | Concrete strength[1] $f_c$ [MPa] | Yield strength[2] $f_y$ [MPa] | Bond strength[3] $\tau_u$ [MPa] | Maximum load num$F_{max}$ [kN] | Failure mode |
|---|---|---|---|---|---|---|---|---|---|
| num7mon-CI50-d32-s | Post-installed | 2 bars | 32 | 420 | 58.0 | 535 | 35.0 | 142.7 | Y |
| num7cyc-CI50-d32-s | w/o hook | per face | | | 58.0 | 535 | 35.0 | 142.9 | Y |
| num7mon-PI50-d25-s | Post-installed | 2 bars | 25 | 420 | 58.0 | 535 | 35.0 | 44.9 | Y |
| num7cyc-PI50-d25-s | w/o hook | per face | | | 58.0 | 535 | 35.0 | 48.2 | Y |
| num7mon-PI50-d40-s | Post-installed | 2 bars | 40 | 420 | 58.0 | 535 | 35.0 | 157.5 | P/C |
| num7cyc-PI50-d40-s | w/o hook | per face | | | 58.0 | 535 | 35.0 | 160.9 | P/C |
| num7mon-PI50-d32-s-d[4] | Post-installed | 2 bars | 32 | 420 | 58.0 | 535 | 35.0 | 142.8 | Y |
| num7cyc-PI50-d32-s-d[4] | w/o hook | per face | | | 58.0 | 535 | 35.0 | 143.1 | Y |
| num7mon-PI50-d32-s-q[5] | Post-installed | 2 bars | 32 | 420 | 58.0 | 535 | 35.0 | 143.0 | Y |
| num7cyc-PI50-d32-s-q[5] | w/o hook | per face | | | 58.0 | 535 | 35.0 | 144.1 | Y |
| num8mon-PI50-d25-s | Post-installed | 2 bars | 25 | 420 | 28.0 | 535 | 35.0 | 112.9 | Y |
| num8cyc-PI50-d25-s | w/o hook | per face | | | 28.0 | 535 | 35.0 | 110.3 | Y |

[1] Foundation concrete; [2] Column starter bar; [3] Between foundation concrete and column starter bar; [4] Foundation reinforcement doubled; [5] Foundation reinforcement quadrupled

In the following, the monotonic and cyclic load-drift curves of the numerical tests are presented. The sequence of cracks, pullout and concrete breakout or yield is indicated in the diagrams. In addition, the graphical output of the tensile strain distribution in the column-to-foundation connection core is shown for the drift corresponding to the failure load. The plots of concrete tensile strains demonstrate the concrete damage, i.e. cracks and shear failures. The contour levels go from light grey to black. Black corresponds to the exceedance of the elastic range of concrete tensile strain $f_{ct} / E_c$. For better visualisation, the tensioned starter bar is sketched in the following diagrams.

### D.2.1 Specimen 1 – $\ell_b$ = 240 mm, 2 · 4$\phi$16, cast-in-place with hooks

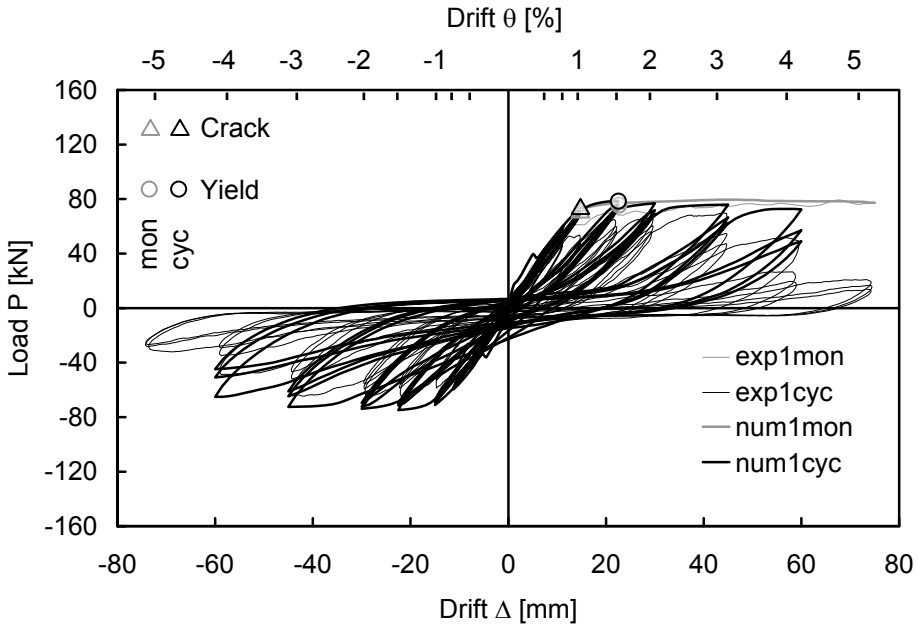


Figure D.17 Monotonic and cyclic test on Specimen 1: Numerically (and experimentally) determined load-drift curves

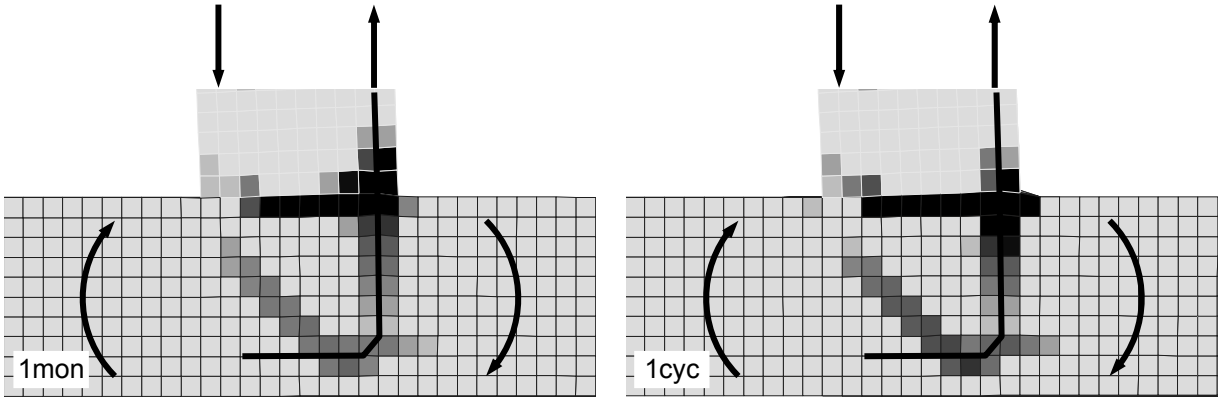


Figure D.18 Monotonic and cyclic simulation of Specimen 1: Tensile strain at drift corresponding to failure load

### D.2.2 Specimen 2 – $\ell_b$ = 240 mm, 2 · 4$\phi$16, cast-in-place without hooks

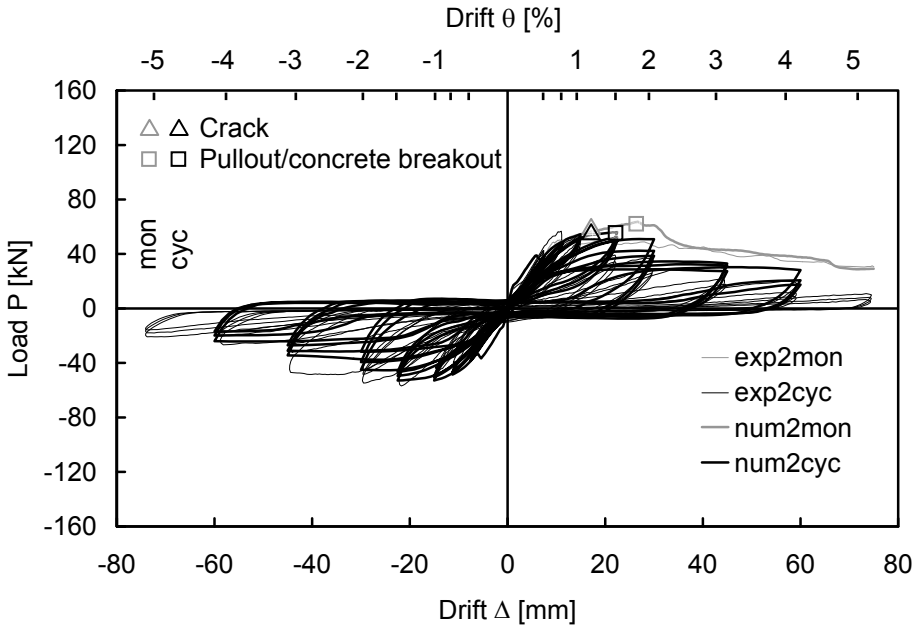


Figure D.19 Monotonic and cyclic test on Specimen 2: Numerically (and experimentally) determined load-drift curves

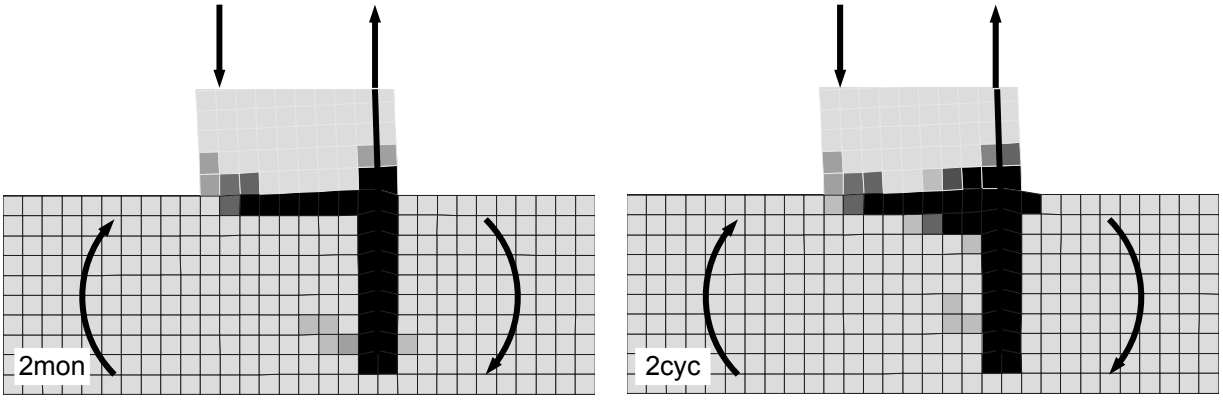


Figure D.20 Monotonic and cyclic simulation of Specimen 2: Tensile strain at drift corresponding to failure load

### D.2.3 Specimen 3 – $\ell_b$ = 240 mm, 2 · 4$\phi$16, post-installed

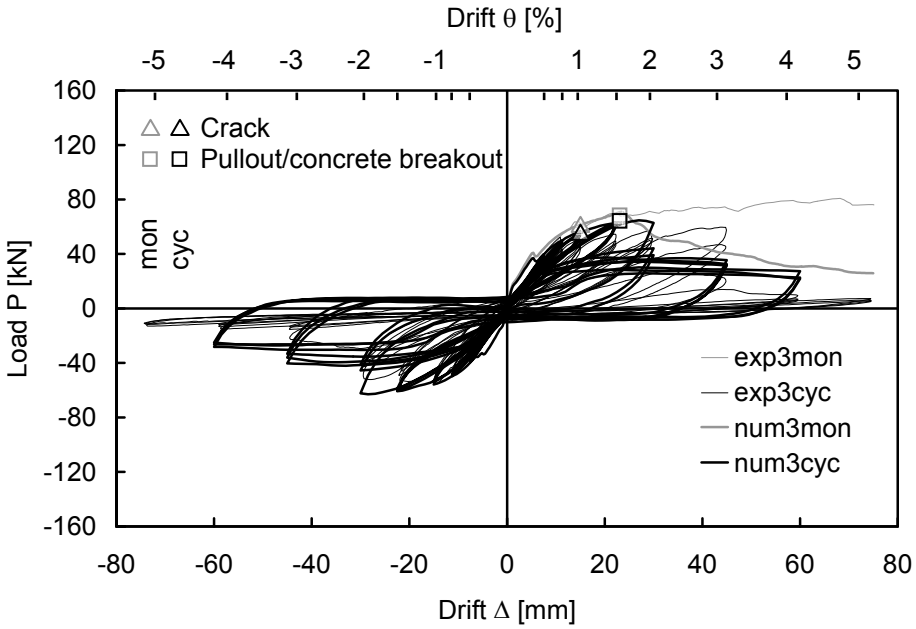


Figure D.21 Monotonic and cyclic test on Specimen 3: Numerically (and experimentally) determined load-drift curves

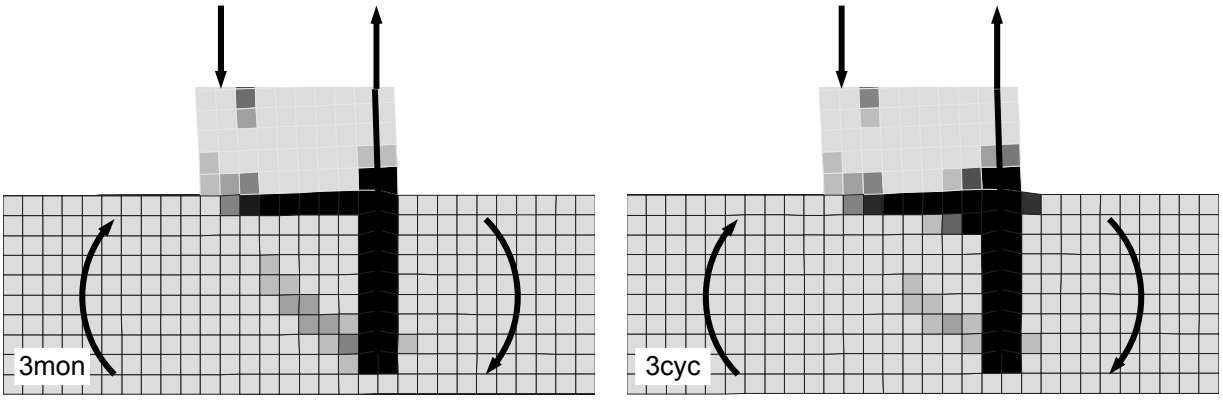


Figure D.22 Monotonic and cyclic simulation of Specimen 3: Tensile strain at drift corresponding to failure load

### D.2.4 Specimen 4– $\ell_b$ = 240 mm, 2 · 2ϕ25, post-installed

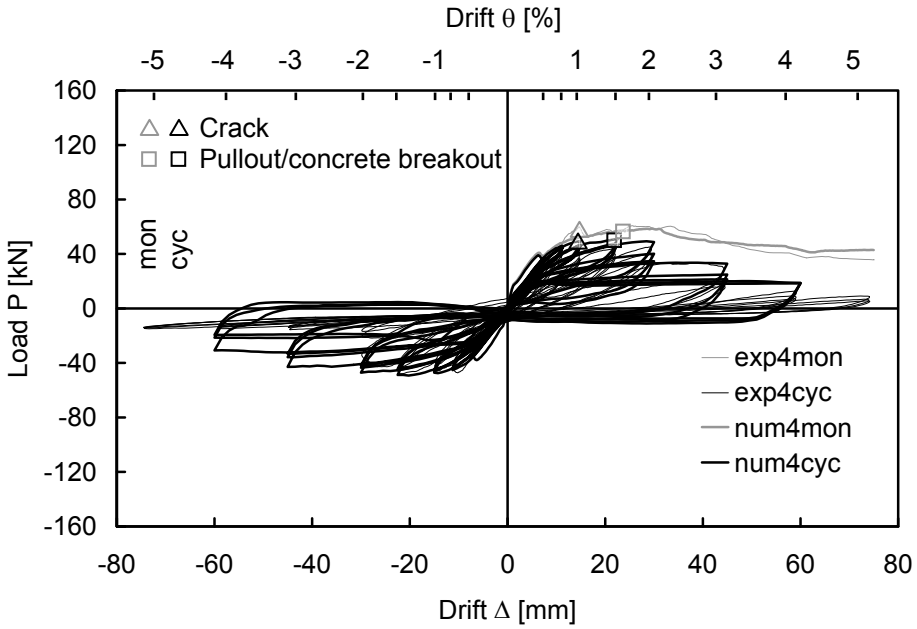


Figure D.23 Monotonic and cyclic test on Specimen 4: Numerically (and experimentally) determined load-drift curves

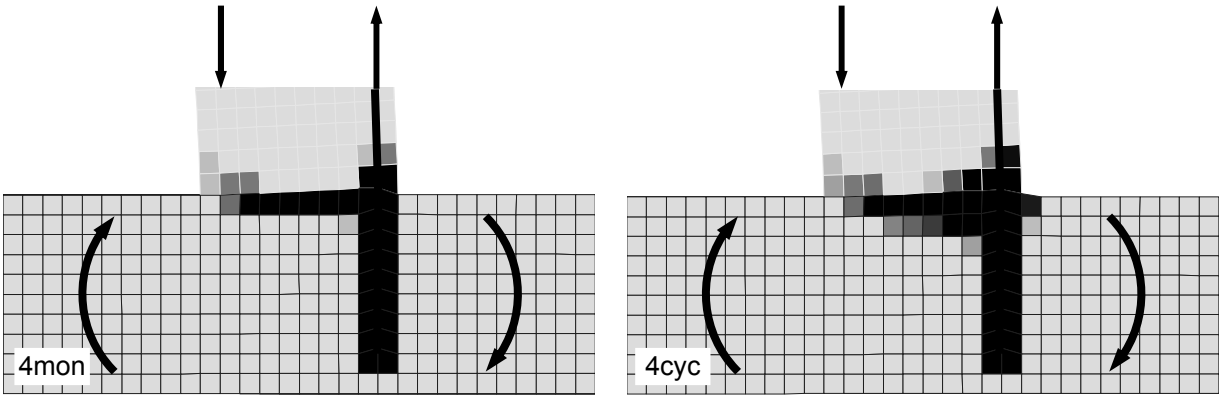


Figure D.24 Monotonic and cyclic simulation of Specimen 4: Tensile strain at drift corresponding to failure load

### D.2.5 Specimen 5 – $\ell_b$ = 420 mm, 2 · 2$\phi$32, cast-in-place with hooks

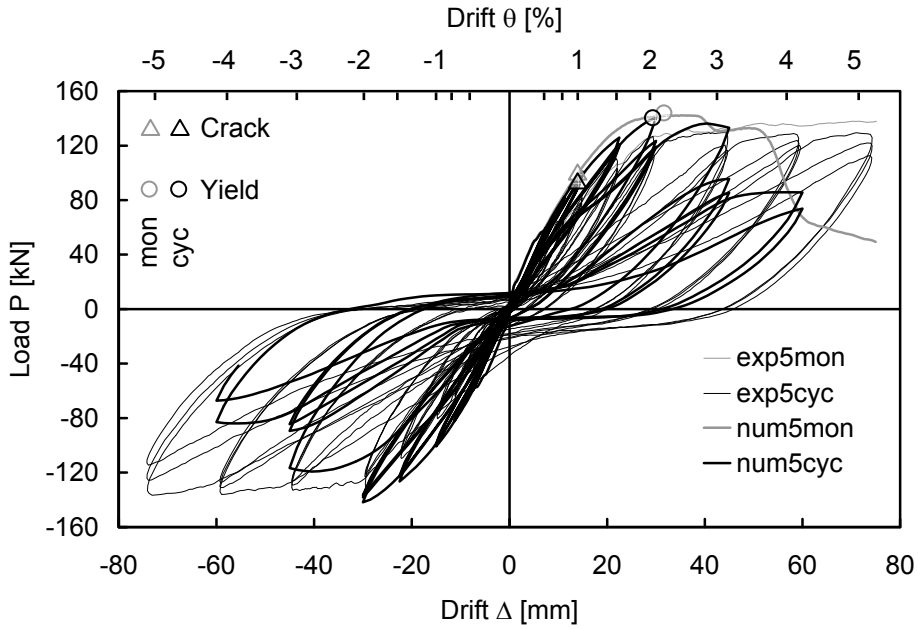


Figure D.25 Monotonic and cyclic test on Specimen 5: Numerically (and experimentally) determined load-drift curves

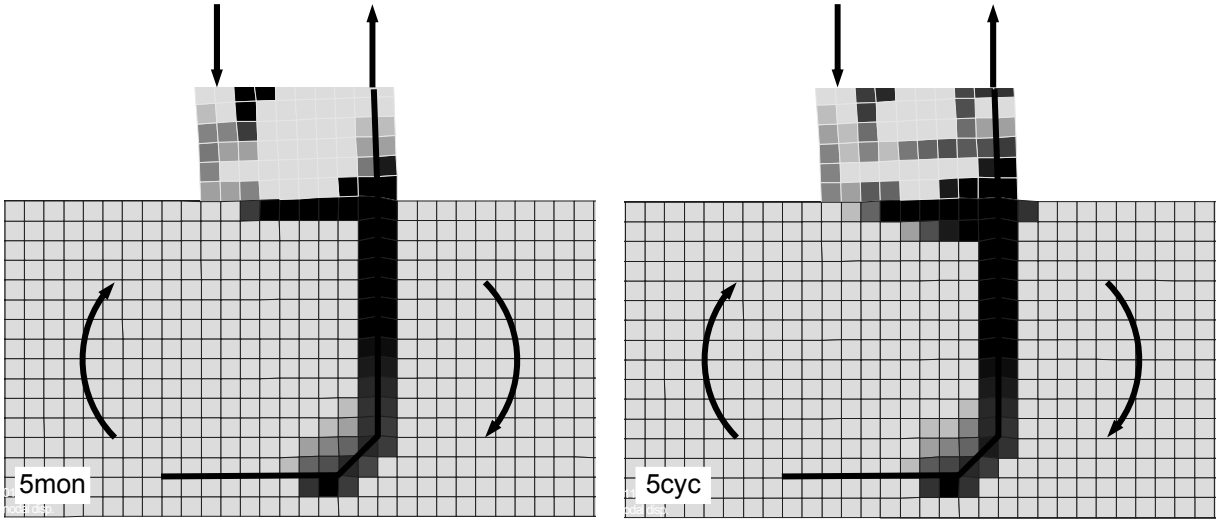


Figure D.26 Monotonic and cyclic simulation of Specimen 5: Tensile strain at drift corresponding to failure load

### D.2.6 Specimen 6 – $\ell_b$ = 420 mm, 2 · 2$\phi$32, cast-in-place without hooks

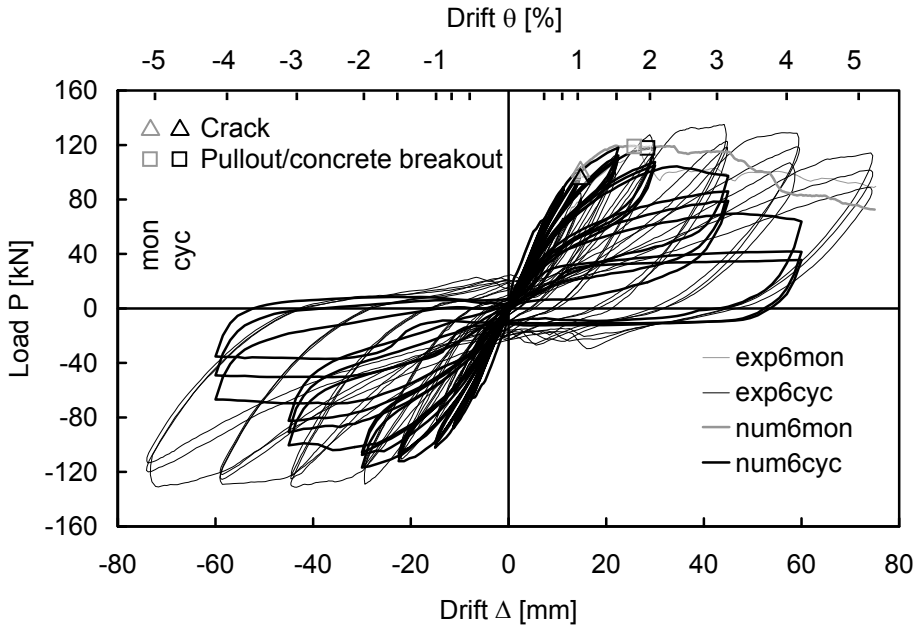


Figure D.27 Monotonic and cyclic test on Specimen 6: Numerically (and experimentally) determined load-drift curves

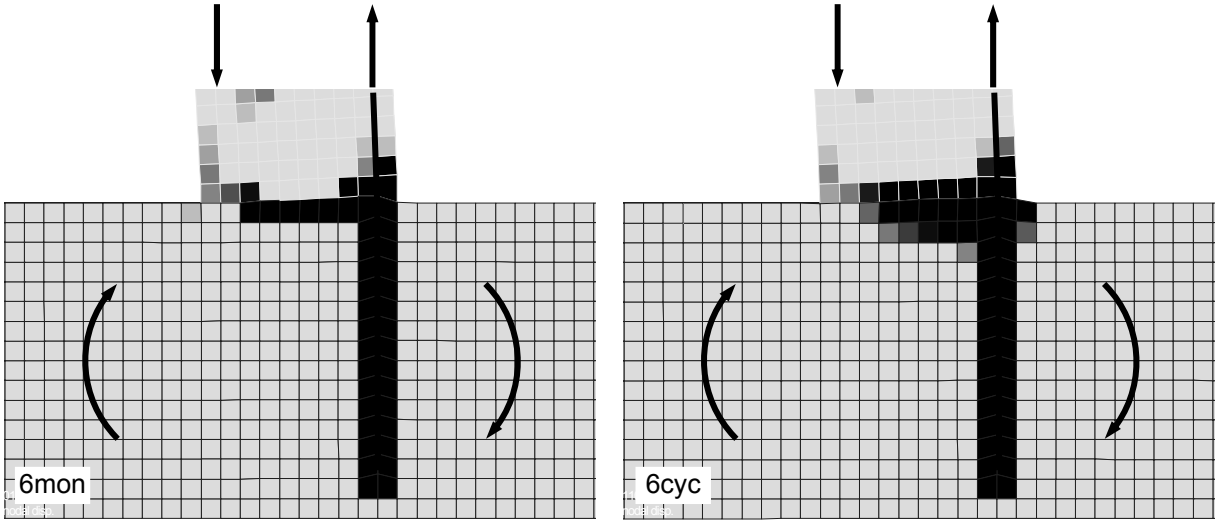


Figure D.28 Monotonic and cyclic simulation of Specimen 6: Tensile strain at drift corresponding to failure load

### D.2.7 Specimen 7 – $\ell_b$ = 420 mm, 2 · 2$\phi$32, post-installed

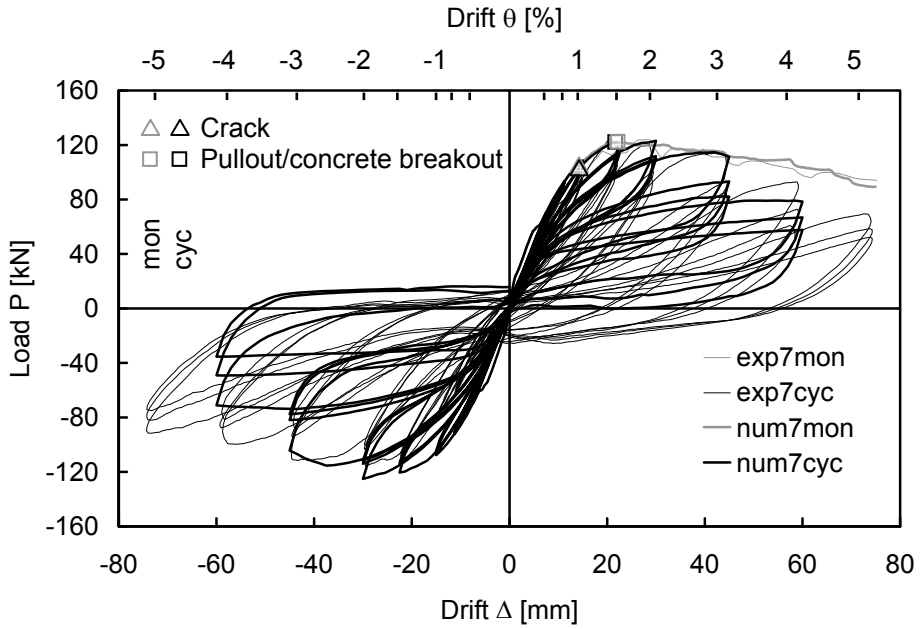


Figure D.29 Monotonic and cyclic test on Specimen 7: Numerically (and experimentally) determined load-drift curves

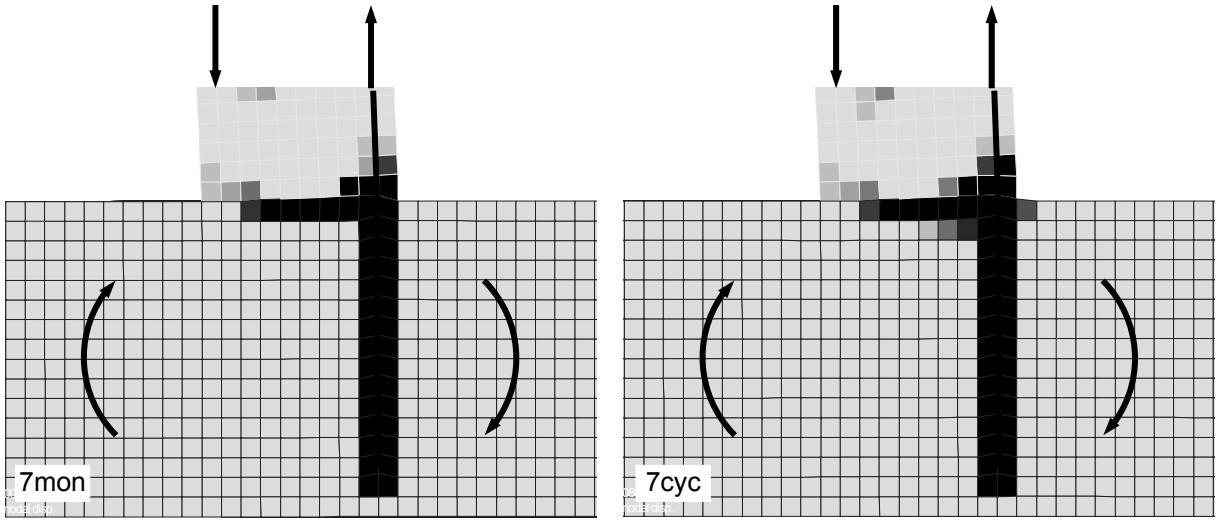


Figure D.30 Monotonic and cyclic simulation of Specimen 7: Tensile strain at drift corresponding to failure load

### D.2.8 Specimen 8 – $\ell_b$ = 420 mm, 2 · 2$\phi$25, post-installed

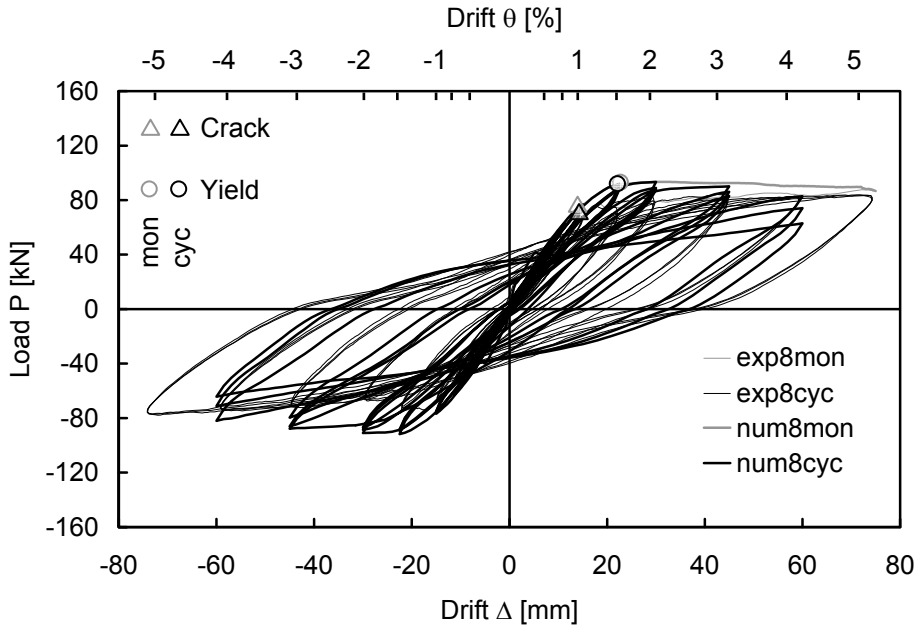


Figure D.31 Monotonic and cyclic test on Specimen 8: Numerically (and experimentally) determined load-drift curves

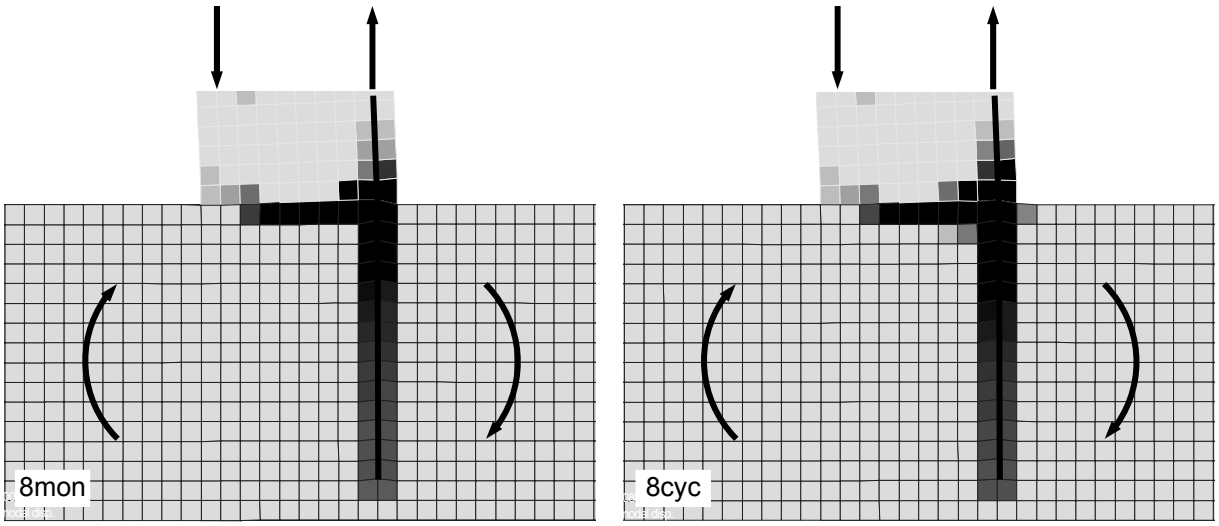


Figure D.32 Monotonic and cyclic simulation of Specimen 8: Tensile strain at drift corresponding to failure load

## D.3 Assessment of Seismic Performance

Table D.3 summarises the assessment of the seismic performance for the experimental tests and Table D.4 the assessment of the seismic performance for the numerical tests.

Table D.3 Assessment of performance based on acceptance criteria given in *ACI 374.1 (2005)* and the strain hardening criterion

| Monotonic loading: mon<br>Cyclic loading: cyc | Anchorage detailing | Starter bar layout | $\phi$[1]; $\ell_b$[2] [mm]<br>$f_c$[3] [MPa] | 1.<br>Initial strength<br>$expM_{max}$ / $calM_y$ > 1.00 | 2.<br>Overstrength<br>$expM_{max}$ / $\lambda$ $calM_y$ < 1.00 | 3.<br>Ductility<br>$expM_{\theta a}$ / $expM_{max}$ > 0.75 | Damping<br>$E_{d,\theta a}$ / $E_{d\#,\theta a}$ > 0.125 | Stiffness<br>$K_{p,\theta a}$ / $K_{p,\theta i}$ > 0.05 | ACI 374.1 compliant? | Strain hardening? |
|---|---|---|---|---|---|---|---|---|---|---|
| exp1mon | Cast-in-place | 4 bars | 16; 240 | 1.41 | 0.96 | 0.94 | NA | NA | YES | YES |
| exp1cyc | w/ hook | per face | 24.1, 22.4 | 1.34 | 0.85 | 0.28 | 0.16 | 0.01 | NO | NO |
| exp2mon | Cast-in-place | 4 bars | 16; 240 | 1.05 | 0.61 | 0.68 | NA | NA | NO | NO |
| exp2cyc | w/o hook | per face | 21.7, 24.1 | 1.17 | 0.69 | 0.35 | 0.14 | 0.00 | NO | NO |
| exp3mon | Post-installed | 4 bars | 16; 240 | 1.44 | 0.98 | 0.96 | NA | NA | YES | YES |
| exp3cyc | w/o hook | per face | 20.4, 23.2 | 1.11 | 0.72 | 0.22 | 0.11 | 0.00 | NO | NO |
| exp4mon | Post-installed | 2 bars | 25; 240 | 0.98 | 0.60 | 0.62 | NA | NA | NO | NO |
| exp4cyc | w/o hook | per face | 21.3, 20.6 | 0.78 | 0.46 | 0.28 | 0.09 | 0.00 | NO | NO |
| exp5mon | Cast-in-place | 2 bars | 32; 420 | 1.16 | 0.89 | 0.98 | NA | NA | YES | YES |
| exp5cyc | w/ hook | per face | 23.0, 22.5 | 1.19 | 0.84 | 0.99 | 0.16 | 0.15 | YES | YES |
| exp6mon | Cast-in-place | 2 bars | 32; 420 | 1.17 | 0.76 | 0.80 | NA | NA | YES | NO |
| exp6cyc | w/o hook | per face | 21.9, 24.7 | 1.22 | 0.87 | 0.95 | 0.21 | 0.05 | YES | NO |
| exp7mon | Post-installed | 2 bars | 32; 420 | 1.26 | 0.80 | 0.79 | NA | NA | YES | NO |
| exp7cyc | w/o hook | per face | 20.5, 22.2 | 1.33 | 0.80 | 0.75 | 0.18 | 0.06 | YES | NO |
| exp8mon | Post-installed | 2 bars | 25; 420 | 1.26 | 0.84 | 0.99 | NA | NA | YES | YES |
| exp8cyc | w/o hook | per face | 21.8, 20.7 | 1.28 | 0.83 | 0.98 | 0.33 | 0.20 | YES | YES |

[1] Starter bar diameter; [2] Anchorage length; [3] Compressive strength of foundation concrete (monotonically tested specimen, cyclically tested specimen)

Table D.4 Assessment of performance based on acceptance criteria given in *ACI 374.1 (2005)* and the strain hardening criterion (1/8)

| Monotonic loading: mon<br>Cyclic loading: cyc | Anchorage detailing | Starter bar layout | $\phi$[1]; $\ell_b$[2] [mm]<br>$f_c$[3] [MPa] | 1. | 2. | 3. | | | ACI 374.1 compliant? | Strain hardening? |
|---|---|---|---|---|---|---|---|---|---|---|
| | | | | Initial strength<br>$numM_{max}$ / $calM_y > 1.00$ | Overstrength<br>$numM_{max}$ / $\lambda\ calM_y < 1.00$ | Ductility<br>$numM_{\theta a}$ / $numM_{max} > 0.75$ | Damping<br>$E_{d,\theta a}$ / $E_{d\#,\theta a} > 0.125$ | Stiffness<br>$K_{p,\theta a}$ / $K_{p,\theta i} > 0.05$ | | |
| num1mon | Cast-in-place | 4 bars | 16; 240 | 1.58 | 0.96 | 1.00 | NA | NA | YES | YES |
| num1cyc | w/ hook | per face | 28.0 | 1.55 | 0.95 | 0.89 | 0.15 | 0.04 | YES | YES |
| num1mon-CI20-d12-h | Cast-in-place | 4 bars | 12; 240 | 1.71 | 0.95 | 1.00 | NA | NA | YES | YES |
| num1cyc-CI20-d12-h | w/ hook | per face | 28.0 | 1.53 | 0.95 | 0.83 | 0.18 | 0.01 | NO | YES |
| num1mon-CI20-d25-h | Cast-in-place | 4 bars | 25; 240 | 1.08 | 0.69 | 0.82 | NA | NA | YES | NO |
| num1cyc-CI20-d25-h | w/ hook | per face | 28.0 | 1.14 | 0.71 | 0.58 | 0.32 | 0.07 | NO | NO |
| num2mon | Cast-in-place | 4 bars | 16; 240 | 1.25 | 0.77 | 0.67 | NA | NA | NO | NO |
| num2cyc | w/o hook | per face | 28.0 | 1.07 | 0.68 | 0.51 | 0.57 | 0.13 | NO | NO |
| num2mon-CI20-d12-s | Cast-in-place | 4 bars | 12; 240 | 1.69 | 1.03 | 1.00 | NA | NA | NO | YES |
| num2cyc-CI20-d12-s | w/o hook | per face | 28.0 | 1.62 | 1.02 | 0.67 | 0.47 | 0.02 | NO | NO |
| num2mon-CI20-d25-s | Cast-in-place | 4 bars | 25; 240 | 0.48 | 0.38 | 0.57 | NA | NA | NO | NO |
| num2cyc-CI20-d25-s | w/o hook | per face | 28.0 | 0.41 | 0.32 | 0.42 | 0.69 | 0.16 | NO | NO |

[1] Starter bar diameter; [2] Anchorage length; [3] Compressive strength of foundation concrete

Table D.4 Assessment of performance based on acceptance criteria given in *ACI 374.1 (2005)* and the strain hardening criterion (2/8)

| Monotonic loading: mon<br>Cyclic loading: cyc | Anchorage detailing | Starter bar layout | $\phi$[1]; $\ell_b$[2] [mm]<br>$f_c$[3] [MPa] | 1.<br>Initial strength<br>num$M_{max}$ / cal$M_y$ > 1.00 | 2.<br>Overstrength<br>num$M_{max}$ / $\lambda$ cal$M_y$ < 1.00 | 3.<br>Ductility<br>num$M_{\theta a}$ / num$M_{max}$ > 0.75 | 3.<br>Damping<br>$E_{d,\theta a}$ / $E_{d\#,\theta a}$ > 0.125 | 3.<br>Stiffness<br>$K_{p,\theta a}$ / $K_{p,\theta i}$ > 0.05 | ACI 374.1 compliant? | Strain hardening? |
|---|---|---|---|---|---|---|---|---|---|---|
| num3mon | Post-installed | 4 bars | 16; 240 | 1.44 | 0.86 | 0.57 | NA | NA | NO | NO |
| num3cyc | w/o hook | per face | 28.0 | 1.29 | 0.78 | 0.53 | 0.50 | 0.12 | NO | NO |
| num3mon-PI20-d12-s | Post-installed | 4 bars | 12; 240 | 1.67 | 1.02 | 0.99 | NA | NA | NO | YES |
| num3cyc-PI20-d12-s | w/o hook | per face | 28.0 | 1.67 | 1.05 | 0.91 | 0.32 | 0.22 | NO | YES |
| num3mon-PI20-d25-s | Post-installed | 4 bars | 25; 240 | 0.50 | 0.39 | 0.56 | NA | NA | NO | NO |
| num3cyc-PI20-d25-s | w/o hook | per face | 28.0 | 0.34 | 0.34 | 0.40 | 0.42 | 0.01 | NO | NO |
| num3mon-PI20-d16-s-d[3] | Post-installed | 4 bars | 16; 240 | 1.41 | 0.83 | 0.53 | NA | NA | NO | NO |
| num3cyc-PI20-d16-s-d[3] | w/o hook | per face | 28.0 | 1.38 | 0.82 | 0.61 | 0.54 | 0.22 | NO | NO |
| num3mon-PI20-d16-s-q[4] | Post-installed | 4 bars | 16; 240 | 1.40 | 0.83 | 0.65 | NA | NA | NO | NO |
| num3cyc-PI20-d16-s-q[4] | w/o hook | per face | 28.0 | 1.42 | 0.84 | 0.56 | 0.54 | 0.09 | NO | NO |
| num4mon | Post-installed | 2 bars | 25; 240 | 0.96 | 0.58 | 0.82 | NA | NA | NO | NO |
| num4cyc | w/o hook | per face | 28.0 | 0.80 | 0.51 | 0.51 | 0.45 | 0.00 | NO | NO |
| num4mon-PI20-d16-s | Post-installed | 2 bars | 16; 240 | 1.56 | 0.95 | 0.99 | NA | NA | YES | YES |
| num4cyc-PI20-d16-s | w/o hook | per face | 28.0 | 1.57 | 0.97 | 0.94 | 0.18 | 0.30 | YES | YES |
| num4mon-PI20-d32-s | Post-installed | 2 bars | 32; 240 | 0.65 | 0.39 | 0.83 | NA | NA | NO | NO |
| num4cyc-PI20-d32-s | w/o hook | per face | 28.0 | 0.46 | 0.32 | 0.48 | 0.57 | 0.20 | NO | NO |

[1] Starter bar diameter; [2] Anchorage length; [3] Compressive strength of foundation concrete

Table D.4 Assessment of performance based on acceptance criteria given in *ACI 374.1 (2005)* and the strain hardening criterion (3/8)

| Monotonic loading: mon<br>Cyclic loading: cyc | Anchorage detailing | Starter bar layout | $\phi$[1]; $\ell_b$[2] [mm]<br>$f_c$[3] [MPa] | 1. | 2. | 3. | | | ACI 374.1 compliant? | Strain hardening? |
|---|---|---|---|---|---|---|---|---|---|---|
| | | | | Initial strength<br>$numM_{max}$ / $calM_y > 1.00$ | Overstrength<br>$numM_{max}$ / $\lambda\ calM_y < 1.00$ | Ductility<br>$numM_{\theta a}$ / $numM_{max} > 0.75$ | Damping<br>$E_{d,\theta a}$ / $E_{d\#,\theta a} > 0.125$ | Stiffness<br>$K_{p,\theta a}$ / $K_{p,\theta i} > 0.05$ | | |
| num5mon | Cast-in-place | 2 bars | 32; 420 | 1.45 | 0.92 | 0.92 | NA | NA | YES | NO |
| num5cyc | w/ hook | per face | 28.0 | 1.42 | 0.92 | 0.77 | 0.26 | 0.20 | YES | NO |
| num5mon-CI20-d25-h | Cast-in-place | 2 bars | 25; 420 | 1.56 | 0.93 | 0.99 | NA | NA | YES | YES |
| num5cyc-CI20-d25-h | w/ hook | per face | 28.0 | 1.53 | 0.94 | 0.96 | 0.25 | 0.23 | YES | YES |
| num5mon-CI20-d40-h | Cast-in-place | 2 bars | 40; 420 | 1.12 | 0.66 | 0.68 | NA | NA | NO | NO |
| num5cyc-CI20-d40-h | w/ hook | per face | 28.0 | 1.10 | 0.69 | 0.68 | 0.20 | 0.03 | NO | NO |
| num6mon | Cast-in-place | 2 bars | 32; 420 | 1.30 | 0.77 | 0.96 | NA | NA | YES | NO |
| num6cyc | w/o hook | per face | 28.0 | 1.23 | 0.76 | 0.77 | 0.43 | 0.36 | YES | NO |
| num6mon-CI20-d25-s | Cast-in-place | 2 bars | 25; 420 | 1.52 | 0.93 | 1.00 | NA | NA | YES | NO |
| num6cyc-CI20-d25-s | w/o hook | per face | 28.0 | 1.54 | 0.96 | 0.98 | 0.39 | 0.18 | YES | NO |
| num6mon-CI20-d40-s | Cast-in-place | 2 bars | 40; 420 | 1.17 | 0.70 | 0.65 | NA | NA | NO | NO |
| num6cyc-CI20-d40-s | w/o hook | per face | 28.0 | 1.15 | 0.70 | 0.37 | 0.40 | 0.03 | NO | NO |

[1] Starter bar diameter; [2] Anchorage length; [3] Compressive strength of foundation concrete

Table D.4 Assessment of performance based on acceptance criteria given in *ACI 374.1 (2005)* and the strain hardening criterion (4/8)

| Monotonic loading: mon<br>Cyclic loading: cyc | Anchorage detailing | Starter bar layout | $\phi$[1]; $\ell_b$[2] [mm]<br>$f_c$[3] [MPa] | 1.<br>Initial strength<br>num$M_{max}$ / cal$M_y$ > 1.00 | 2.<br>Overstrength<br>num$M_{max}$ / $\lambda$ cal$M_y$ < 1.00 | 3.<br>Ductility<br>num$M_{\theta a}$ / num$M_{max}$ > 0.75 | 3.<br>Damping<br>$E_{d,\theta a}$ / $E_{d\#,\theta a}$ > 0.125 | 3.<br>Stiffness<br>$K_{p,\theta a}$ / $K_{p,\theta i}$ > 0.05 | ACI 374.1 compliant? | Strain hardening? |
|---|---|---|---|---|---|---|---|---|---|---|
| num7mon | Post-installed | 2 bars | 32; 420 | 1.33 | 0.79 | 0.92 | NA | NA | YES | NO |
| num7cyc | w/o hook | per face | 28.0 | 1.25 | 0.79 | 0.79 | 0.25 | 0.50 | YES | NO |
| num7mon-PI20-d25-s | Post-installed | 2 bars | 25; 420 | 1.56 | 0.97 | 0.98 | NA | NA | YES | YES |
| num7cyc-PI20-d25-s | w/o hook | per face | 28.0 | 1.47 | 0.98 | 0.87 | 0.40 | 0.26 | YES | YES |
| num7mon-PI20-d40-s | Post-installed | 2 bars | 40; 420 | 0.80 | 0.48 | 0.92 | NA | NA | NO | NO |
| num7cyc-PI20-d40-s | w/o hook | per face | 28.0 | 0.75 | 0.48 | 0.67 | 0.43 | 0.32 | NO | NO |
| num7mon-PI20-d32-s-d[3] | Post-installed | 2 bars | 32; 420 | 1.19 | 0.70 | 0.95 | NA | NA | YES | NO |
| num7cyc-PI20-d32-s-d[3] | w/o hook | per face | 28.0 | 1.11 | 0.69 | 0.75 | 0.26 | 0.49 | YES | NO |
| num7mon-PI20-d32-s-q[4] | Post-installed | 2 bars | 32; 420 | 1.21 | 0.73 | 0.89 | NA | NA | YES | NO |
| num7cyc-PI20-d32-s-q[4] | w/o hook | per face | 28.0 | 1.11 | 0.71 | 0.78 | 0.28 | 0.51 | YES | NO |
| num8mon-PI20-d25-s | Post-installed | 2 bars | 25; 420 | 1.54 | 0.93 | 0.99 | NA | NA | YES | YES |
| num8cyc-PI20-d25-s | w/o hook | per face | 28.0 | 1.51 | 0.93 | 0.97 | 0.22 | 0.26 | YES | YES |

[1] Starter bar diameter; [2] Anchorage length; [3] Compressive strength of foundation concrete

Table D.4 Assessment of performance based on acceptance criteria given in *ACI 374.1 (2005)* and the strain hardening criterion (5/8)

| Monotonic loading: mon<br>Cyclic loading: cyc | Anchorage detailing | Starter bar layout | $\phi$[1]; $\ell_b$[2] [mm]<br>$f_c$[3] [MPa] | 1.<br>Initial strength<br>$numM_{max}$ / $calM_y$ > 1.00 | 2.<br>Overstrength<br>$numM_{max}$ / $\lambda\ calM_y$ < 1.00 | 3.<br>Ductility<br>$numM_{\theta a}$ / $numM_{max}$ > 0.75 | Damping<br>$E_{d,\theta a}$ / $E_{d\#,\theta a}$ > 0.125 | Stiffness<br>$K_{p,\theta a}$ / $K_{p,\theta i}$ > 0.05 | ACI 374.1 compliant? | Strain hardening? |
|---|---|---|---|---|---|---|---|---|---|---|
| num1mon-CI50-d16-h | Cast-in-place | 4 bars | 16; 240 | 1.60 | 0.97 | 1.00 | NA | NA | YES | YES |
| num1cyc-CI50-d16-h | w/ hook | per face | 58.0 | 1.52 | 0.95 | 0.91 | 0.40 | 0.12 | YES | YES |
| num1mon-CI50-d12-h | Cast-in-place | 4 bars | 12; 240 | 1.71 | 0.99 | 1.00 | NA | NA | YES | YES |
| num1cyc-CI50-d12-h | w/ hook | per face | 58.0 | 1.56 | 1.00 | 0.89 | 0.46 | 0.03 | NO | YES |
| num1mon-CI50-d25-h | Cast-in-place | 4 bars | 25; 240 | 1.37 | 0.90 | 0.97 | NA | NA | YES | NO |
| num1cyc-CI50-d25-h | w/ hook | per face | 58.0 | 1.46 | 0.94 | 0.79 | 0.25 | 0.12 | YES | NO |
| num2mon-CI50-d16-s | Cast-in-place | 4 bars | 16; 240 | 1.58 | 0.95 | 1.00 | NA | NA | YES | YES |
| num2cyc-CI50-d16-s | w/o hook | per face | 58.0 | 1.62 | 0.96 | 0.90 | 0.31 | 0.21 | YES | YES |
| num2mon-CI50-d12-s | Cast-in-place | 4 bars | 12; 240 | 1.71 | 0.99 | 1.00 | NA | NA | YES | YES |
| num2cyc-CI50-d12-s | w/o hook | per face | 58.0 | 1.63 | 1.00 | 0.86 | 0.50 | 0.23 | YES | YES |
| num2mon-CI50-d25-s | Cast-in-place | 4 bars | 25; 240 | 0.91 | 0.54 | 0.87 | NA | NA | NO | NO |
| num2cyc-CI50-d25-s | w/o hook | per face | 58.0 | 0.90 | 0.56 | 0.42 | 0.59 | 0.24 | NO | NO |

[1] Starter bar diameter; [2] Anchorage length; [3] Compressive strength of foundation concrete

Table D.4 Assessment of performance based on acceptance criteria given in *ACI 374.1 (2005)* and the strain hardening criterion (6/8)

| Monotonic loading: mon<br>Cyclic loading: cyc | Anchorage detailing | Starter bar layout | $\phi$[1]; $\ell_b$[2] [mm]<br>$f_c$[3] [MPa] | 1.<br>Initial strength<br>num$M_{max}$ / cal$M_y$ > 1.00 | 2.<br>Overstrength<br>num$M_{max}$ / $\lambda$ cal$M_y$ < 1.00 | 3.<br>Ductility<br>num$M_{\theta a}$ / num$M_{max}$ > 0.75 | 3.<br>Damping<br>$E_{d,\theta a}$ / $E_{d\#,\theta a}$ > 0.125 | 3.<br>Stiffness<br>$K_{p,\theta a}$ / $K_{p,\theta i}$ > 0.05 | ACI 374.1 compliant? | Strain hardening? |
|---|---|---|---|---|---|---|---|---|---|---|
| num3mon-PI50-d16-s | Post-installed | 4 bars | 16; 240 | 1.58 | 0.95 | 1.00 | NA | NA | YES | YES |
| num3cyc-PI50-d16-s | w/o hook | per face | 58.0 | 1.54 | 0.94 | 0.96 | 0.31 | 0.19 | YES | YES |
| num3mon-PI50-d12-s | Post-installed | 4 bars | 12; 240 | 1.71 | 1.05 | 1.00 | NA | NA | NO | YES |
| num3cyc-PI50-d12-s | w/o hook | per face | 58.0 | 1.60 | 1.08 | 0.90 | 0.89 | 0.10 | NO | YES |
| num3mon-PI50-d25-s | Post-installed | 4 bars | 25; 240 | 0.95 | 0.56 | 0.67 | NA | NA | NO | NO |
| num3cyc-PI50-d25-s | w/o hook | per face | 58.0 | 0.85 | 0.58 | 0.43 | 0.46 | 0.25 | NO | NO |
| num3mon-PI50-d16-s-d[3] | Post-installed | 4 bars | 16; 240 | 1.59 | 0.96 | 1.00 | NA | NA | YES | NO |
| num3cyc-PI50-d16-s-d[3] | w/o hook | per face | 58.0 | 1.56 | 0.96 | 0.94 | 0.33 | 0.15 | YES | NO |
| num3mon-PI50-d16-s-q[4] | Post-installed | 4 bars | 16; 240 | 1.59 | 0.96 | 1.00 | NA | NA | YES | NO |
| num3cyc-PI50-d16-s-q[4] | w/o hook | per face | 58.0 | 1.54 | 0.94 | 0.94 | 0.35 | 0.14 | YES | NO |
| num4mon-PI50-d25-s | Post-installed | 2 bars | 25; 240 | 1.32 | 0.82 | 0.73 | NA | NA | NO | NO |
| num4cyc-PI50-d25-s | w/o hook | per face | 58.0 | 1.34 | 0.82 | 0.66 | 0.30 | 0.56 | NO | NO |
| num4mon-PI50-d16-s | Post-installed | 2 bars | 16; 240 | 1.56 | 0.96 | 0.99 | NA | NA | YES | YES |
| num4cyc-PI50-d16-s | w/o hook | per face | 58.0 | 1.54 | 1.00 | 0.88 | 0.42 | 0.24 | YES | YES |
| num4mon-PI50-d32-s | Post-installed | 2 bars | 32; 240 | 0.92 | 0.54 | 0.80 | NA | NA | NO | NO |
| num4cyc-PI50-d32-s | w/o hook | per face | 58.0 | 0.90 | 0.56 | 0.35 | 0.96 | 0.23 | NO | NO |

[1] Starter bar diameter; [2] Anchorage length; [3] Compressive strength of foundation concrete

Table D.4 Assessment of performance based on acceptance criteria given in *ACI 374.1 (2005)* and the strain hardening criterion (7/8)

| Monotonic loading: mon<br>Cyclic loading: cyc | Anchorage detailing | Starter bar layout | $\phi^{1)}$; $\ell_b^{2)}$ [mm]<br>$f_c^{3)}$ [MPa] | 1.<br>Initial strength<br>num$M_{max}$ / cal$M_y$ > 1.00 | 2.<br>Overstrength<br>num$M_{max}$ / $\lambda$ cal$M_y$ < 1.00 | 3.<br>Ductility<br>num$M_{\theta a}$ / num$M_{max}$ > 0.75 | Damping<br>$E_{d,\theta a}$ / $E_{d\#,\theta a}$ > 0.125 | Stiffness<br>$K_{p,\theta a}$ / $K_{p,\theta i}$ > 0.05 | ACI 374.1 compliant? | Strain hardening? |
|---|---|---|---|---|---|---|---|---|---|---|
| num5mon-CI50-d32-h | Cast-in-place | 2 bars | 32; 420 | 1.55 | 0.92 | 0.99 | NA | NA | YES | YES |
| num5cyc-CI50-d32-h | w/ hook | per face | 58.0 | 1.55 | 0.95 | 0.76 | 0.60 | 0.26 | YES | YES |
| num5mon-CI50-d25-h | Cast-in-place | 2 bars | 25; 420 | 1.57 | 0.93 | 0.99 | NA | NA | YES | YES |
| num5cyc-CI50-d25-h | w/ hook | per face | 58.0 | 1.56 | 0.96 | 0.95 | 0.32 | 0.17 | YES | YES |
| num5mon-CI50-d40-h | Cast-in-place | 2 bars | 40; 420 | 1.39 | 0.92 | 0.89 | NA | NA | YES | NO |
| num5cyc-CI50-d40-h | w/ hook | per face | 58.0 | 1.38 | 0.92 | 0.53 | 0.93 | 0.02 | NO | NO |
| num6mon-CI50-d32-s | Cast-in-place | 2 bars | 32; 420 | 1.50 | 0.92 | 0.99 | NA | NA | YES | YES |
| num6cyc-CI50-d32-s | w/o hook | per face | 58.0 | 1.51 | 0.92 | 0.92 | 0.41 | 0.17 | YES | YES |
| num6mon-CI50-d25-s | Cast-in-place | 2 bars | 25; 420 | 1.57 | 0.93 | 0.99 | NA | NA | YES | YES |
| num6cyc-CI50-d25-s | w/o hook | per face | 58.0 | 1.54 | 0.96 | 0.98 | 0.39 | 0.18 | YES | YES |
| num6mon-CI50-d40-s | Cast-in-place | 2 bars | 40; 420 | 1.17 | 0.70 | 0.65 | NA | NA | NO | NO |
| num6cyc-CI50-d40-s | w/o hook | per face | 58.0 | 1.15 | 0.70 | 0.37 | 0.38 | 0.03 | NO | NO |

[1)] Starter bar diameter; [2)] Anchorage length; [3)] Compressive strength of foundation concrete

Table D.4 Assessment of performance based on acceptance criteria given in *ACI 374.1 (2005)* and the strain hardening criterion (8/8)

| Monotonic loading: mon<br>Cyclic loading: cyc | Anchorage detailing | Starter bar layout | $\phi$[1]; $\ell_b$[2] [mm]<br>$f_c$[3] [MPa] | 1. Initial strength<br>num$M_{max}$ / cal$M_y$ > 1.00 | 2. Overstrength<br>num$M_{max}$ / $\lambda$ cal$M_y$ < 1.00 | 3. Ductility<br>num$M_{\theta a}$ / num$M_{max}$ > 0.75 | 3. Damping<br>$E_{d,\theta a}$ / $E_{d\#,\theta a}$ > 0.125 | 3. Stiffness<br>$K_{p,\theta a}$ / $K_{p,\theta i}$ > 0.05 | ACI 374.1 compliant? | Strain hardening? |
|---|---|---|---|---|---|---|---|---|---|---|
| num7mon-PI50-d32-s | Post-installed | 2 bars | 32; 420 | 1.51 | 0.92 | 0.99 | NA | NA | YES | YES |
| num7cyc-PI50-d32-s | w/o hook | per face | 58.0 | 1.54 | 0.92 | 0.81 | 0.42 | 0.09 | YES | YES |
| num7mon-PI50-d25-s | Post-installed | 2 bars | 25; 420 | 1.57 | 0.97 | 0.99 | NA | NA | YES | YES |
| num7cyc-PI50-d25-s | w/o hook | per face | 58.0 | 1.55 | 1.00 | 0.86 | 0.46 | 0.12 | YES | YES |
| num7mon-PI50-d40-s | Post-installed | 2 bars | 40; 420 | 1.17 | 0.69 | 0.61 | NA | NA | NO | NO |
| num7cyc-PI50-d40-s | w/o hook | per face | 58.0 | 1.14 | 0.71 | 0.56 | 0.49 | 0.34 | NO | NO |
| num7mon-PI50-d32-s-d[3] | Post-installed | 2 bars | 32; 420 | 1.53 | 0.92 | 0.99 | NA | NA | YES | YES |
| num7cyc-PI50-d32-s-d[3] | w/o hook | per face | 58.0 | 1.53 | 0.92 | 0.76 | 0.54 | 0.11 | YES | YES |
| num7mon-PI50-d32-s-q[4] | Post-installed | 2 bars | 32; 420 | 1.54 | 0.92 | 0.99 | NA | NA | YES | YES |
| num7cyc-PI50-d32-s-q[4] | w/o hook | per face | 58.0 | 1.55 | 0.93 | 0.75 | 0.44 | 0.08 | YES | YES |
| num8mon-PI50-d25-s | Post-installed | 2 bars | 25; 420 | 1.57 | 0.93 | 0.99 | NA | NA | YES | YES |
| num8cyc-PI50-d25-s | w/o hook | per face | 58.0 | 1.54 | 0.96 | 0.97 | 0.78 | 0.16 | YES | YES |

[1] Starter bar diameter; [2] Anchorage length; [3] Compressive strength of foundation concrete

## D.4 Material strength for Comparison of Coexisting Design Approaches

The Table D.5 gives the material strengths used for the comparison of the experimentally tested and Table D.6 the material strengths used for the comparison of the numerically simulated column-to-foundation connection capacities with the calculated column-to-foundation connection capacities.

Table D.5 Characteristic and design material strengths of experimentally tested specimens used for the validation of the enhanced bonded anchor design provisions

| Monotonic loading: mon<br>Cyclic loading: cyc | Anchorage detailing | Starter bar layout | $\phi$[1]; $\ell_b$[2] [mm]<br>$f_c$[3] [MPa] | $f_{yk}$[4] [MPa] | $f_{yd}$[5] [MPa] | $f_{ck}$[6] [MPa] | $f_{cd}$[7] [MPa] | $f_{ctk}$[8] [MPa] | $f_{ctd}$[9] [MPa] | $f_{bd}$[10] [MPa] | $f_{bk}$[11] [MPa] | $f_b$[12] [MPa] | $\tau_{Rk}$[13] [MPa] | $\tau_{Rd}$[14] [MPa] | $\gamma_{inst}$[15] [-] |
|---|---|---|---|---|---|---|---|---|---|---|---|---|---|---|---|
| exp1mon | Cast-in-place | 4 bars | 16; 240 | 537 | 467 | 22.2 | 14.8 | 1.7 | 1.1 | 2.5 | 3.7 | 5.0 | 3.7 | 2.5 | – |
| exp1cyc | w/ hook | per face | 24.1, 22.4 | 537 | 537 | 22.2 | 17.1 | 1.7 | 1.3 | 2.9 | 3.7 | 5.0 | 3.7 | 2.9 | – |
| exp2mon | Cast-in-place | 4 bars | 16; 240 | 537 | 467 | 22.2 | 14.8 | 1.7 | 1.1 | 2.5 | 3.7 | 5.0 | 3.7 | 2.5 | – |
| exp2cyc | w/o hook | per face | 21.7, 24.1 | 537 | 537 | 22.2 | 17.1 | 1.7 | 1.3 | 2.9 | 3.7 | 5.0 | 3.7 | 2.9 | – |
| exp3mon | Post-installed | 4 bars | 16; 240 | 537 | 467 | 22.2 | 14.8 | 1.7 | 1.1 | 2.5 | 3.7 | 5.0 | 7.0 | 3.4 | 1.4 |
| exp3cyc | w/o hook | per face | 20.4, 23.2 | 537 | 537 | 22.2 | 17.1 | 1.7 | 1.3 | 2.9 | 3.7 | 5.0 | 7.0 | 3.9 | 1.4 |
| exp4mon | Post-installed | 2 bars | 25; 240 | 537 | 467 | 22.2 | 14.8 | 1.7 | 1.1 | 2.5 | 3.7 | 5.0 | 7.0 | 3.4 | 1.4 |
| exp4cyc | w/o hook | per face | 21.3, 20.6 | 537 | 537 | 22.2 | 17.1 | 1.7 | 1.3 | 2.9 | 3.7 | 5.0 | 7.0 | 3.9 | 1.4 |
| exp5mon | Cast-in-place | 2 bars | 32; 420 | 537 | 467 | 22.2 | 14.8 | 1.7 | 1.1 | 2.5 | 3.7 | 5.0 | 4.0 | 2.7 | – |
| exp5cyc | w/ hook | per face | 23.0, 22.5 | 537 | 537 | 22.2 | 17.1 | 1.7 | 1.3 | 2.9 | 3.7 | 5.0 | 4.0 | 3.1 | – |
| exp6mon | Cast-in-place | 2 bars | 32; 420 | 537 | 467 | 22.2 | 14.8 | 1.7 | 1.1 | 2.5 | 3.7 | 5.0 | 4.0 | 2.7 | – |
| exp6cyc | w/o hook | per face | 21.9, 24.7 | 537 | 537 | 22.2 | 17.1 | 1.7 | 1.3 | 2.9 | 3.7 | 5.0 | 4.0 | 3.1 | – |
| exp7mon | Post-installed | 2 bars | 32; 420 | 537 | 467 | 22.2 | 14.8 | 1.7 | 1.1 | 2.5 | 3.7 | 5.0 | 7.0 | 3.4 | 1.4 |
| exp7cyc | w/o hook | per face | 20.5, 22.2 | 537 | 537 | 22.2 | 17.1 | 1.7 | 1.3 | 2.9 | 3.7 | 5.0 | 7.0 | 3.9 | 1.4 |
| exp8mon | Post-installed | 2 bars | 25; 420 | 537 | 467 | 22.2 | 14.8 | 1.7 | 1.1 | 2.5 | 3.7 | 5.0 | 7.0 | 3.4 | 1.4 |
| exp8cyc | w/o hook | per face | 21.8, 20.7 | 537 | 537 | 22.2 | 17.1 | 1.7 | 1.3 | 2.9 | 3.7 | 5.0 | 7.0 | 3.9 | 1.4 |

[1] Starter bar diameter; [2] Anchorage length; [3] Compressive strength of foundation concrete (monotonically tested specimen, cyclically tested specimen) [4] $f_{yk} = f_{y,mean}$; [5] $f_{ck} = f_{c,mean}$; [6] $f_{yd} = f_{ck} / \gamma_s$; [7] $f_{cd} = f_{ck} / \gamma_c$; [8] $f_{ctk} = 0.7 f_{ctm} = 0.7 \cdot 0.30 f_{ck}^{2/3}$; [9] $f_{ctd} = f_{ctk} / \gamma_c$; [10] $f_{bd} = 2.25 \cdot \min\{1.0; (132 - \phi\ [\text{mm}]) / 100\} \cdot f_{ctd}$ (starter bars have vertical orientation during casting); [11] $f_{bk} = f_{bd} \cdot \gamma_c$; [12] $f_b = f_{bk} / 0.75$; [13] $\tau_{Rk,PI} = \tau_{Rk,cr} \cdot \psi_c$ [$\tau_{Rk,CI} = f_{bk} = 0.473 f_{ck}^{2/3}$] for post-installed [cast-in-place] bars; [14] $\tau_{Rd,PI} = \tau_{Rk,PI} / (\gamma_M \cdot \gamma_{inst})$ [$\tau_{Rd,CI} = \tau_{Rk,CI} / \gamma_M$] for post-installed [cast-in-place] bars; Notes: Material safety factors $\gamma_c = \gamma_{Mc} = 1.5$ [1.3] and $\gamma_s = \gamma_{Ms} = 1.15$ [1.0] for fundamental [seismic] load case was assumed for monotonic [cyclic] testing; Installation safety factor $\gamma_{inst} = 1.4$ [1.0] was assumed for post-installed [cast-in-place] bars irrespective of bar diameter; [15] Installation safety factor

Table D.6 Characteristic and design material strengths of numerically tested specimens used for the validation of the enhanced bonded anchor design provisions (1/8)

| Monotonic loading: mon<br>Cyclic loading: cyc | Anchorage detailing | Starter bar layout | $\phi$ [1]; $\ell_b$ [2] [mm]<br>$f_c$ [3] [MPa] | $f_{yk}$ [4] [MPa] | $f_{yd}$ [5] [MPa] | $f_{ck}$ [6] [MPa] | $f_{cd}$ [7] [MPa] | $f_{ctk}$ [8] [MPa] | $f_{ctd}$ [9] [MPa] | $f_{bd}$ [10] [MPa] | $f_{bk}$ [11] [MPa] | $f_b$ [12] [MPa] | $\tau_{Rk}$ [13] [MPa] | $\tau_{Rd}$ [14] [MPa] | $\gamma_{inst}$ [15] [-] |
|---|---|---|---|---|---|---|---|---|---|---|---|---|---|---|---|
| num1mon | Cast-in-place | 4 bars | 16; 240 | 535 | 465 | 20.0 | 13.3 | 1.5 | 1.0 | 2.3 | 3.5 | 4.6 | 3.5 | 2.3 | – |
| num1cyc | w/ hook | per face | 28 | 535 | 535 | 20.0 | 15.4 | 1.5 | 1.2 | 2.7 | 3.5 | 4.6 | 3.5 | 2.7 | – |
| num1mon-CI20-d12-h | Cast-in-place | 4 bars | 12; 240 | 535 | 465 | 20.0 | 13.3 | 1.5 | 1.0 | 2.3 | 3.5 | 4.6 | 3.5 | 2.3 | – |
| num1cyc-CI20-d12-h | w/ hook | per face | 28 | 535 | 535 | 20.0 | 15.4 | 1.5 | 1.2 | 2.7 | 3.5 | 4.6 | 3.5 | 2.7 | – |
| num1mon-CI20-d25-h | Cast-in-place | 4 bars | 25; 240 | 535 | 465 | 20.0 | 13.3 | 1.5 | 1.0 | 2.3 | 3.5 | 4.6 | 3.5 | 2.3 | – |
| num1cyc-CI20-d25-h | w/ hook | per face | 28 | 535 | 535 | 20.0 | 15.4 | 1.5 | 1.2 | 2.7 | 3.5 | 4.6 | 3.5 | 2.7 | – |
| num2mon | Cast-in-place | 4 bars | 16; 240 | 535 | 465 | 20.0 | 13.3 | 1.5 | 1.0 | 2.3 | 3.5 | 4.6 | 3.5 | 2.3 | – |
| num2cyc | w/o hook | per face | 28 | 535 | 535 | 20.0 | 15.4 | 1.5 | 1.2 | 2.7 | 3.5 | 4.6 | 3.5 | 2.7 | – |
| num2mon-CI20-d12-s | Cast-in-place | 4 bars | 12; 240 | 535 | 465 | 20.0 | 13.3 | 1.5 | 1.0 | 2.3 | 3.5 | 4.6 | 3.5 | 2.3 | – |
| num2cyc-CI20-d12-s | w/o hook | per face | 28 | 535 | 535 | 20.0 | 15.4 | 1.5 | 1.2 | 2.7 | 3.5 | 4.6 | 3.5 | 2.7 | – |
| num2mon-CI20-d25-s | Cast-in-place | 4 bars | 25; 240 | 535 | 465 | 20.0 | 13.3 | 1.5 | 1.0 | 2.3 | 3.5 | 4.6 | 3.5 | 2.3 | – |
| num2cyc-CI20-d25-s | w/o hook | per face | 28 | 535 | 535 | 20.0 | 15.4 | 1.5 | 1.2 | 2.7 | 3.5 | 4.6 | 3.5 | 2.7 | – |

[1] Starter bar diameter; [2] Anchorage length; [3] Compressive strength of foundation concrete (monotonically tested specimen, cyclically tested specimen) [4] $f_{yk} = f_y$; [5] $f_{ck} = f_c$; [6] $f_{yd} = f_{ck} / \gamma_s$; [7] $f_{cd} = f_{ck} / \gamma_c$; [8] $f_{ctk} = 0.7 f_{ctm} = 0.7 \cdot 0.30 f_{ck}^{2/3}$; [9] $f_{ctd} = f_{ctk} / \gamma_c$; [10] $f_{bd} = 2.25 \cdot \min\{1.0; (132 - \phi\ [\text{mm}]) / 100\} \cdot f_{ctd}$ (starter bars have vertical orientation during casting); [11] $f_{bk} = f_{bd} \cdot \gamma_c$; [12] $f_b = f_{bk} / 0.75$; [13] $\tau_{Rk,PI} = \tau_{Rk,cr} \cdot \psi_c$ [$\tau_{Rk,CI} = f_{bk} = 0.473 f_{ck}^{2/3}$] for post-installed [cast-in-place] bars; [14] $\tau_{Rd,PI} = \tau_{Rk,PI} / (\gamma_M \cdot \gamma_{inst})$ [$\tau_{Rd,CI} = \tau_{Rk,CI} / \gamma_M$] for post-installed [cast-in-place] bars; Notes: Material safety factors $\gamma_c = \gamma_{Mc} = 1.5$ [1.3] and $\gamma_s = \gamma_{Ms} = 1.15$ [1.0] for fundamental [seismic] load case was assumed for monotonic [cyclic] testing; Installation safety factor $\gamma_{inst} = 1.4$ [1.0] was assumed for post-installed [cast-in-place] bars irrespective of bar diameter; [15] Installation safety factor

Table D.6 Characteristic and design material strengths of numerically tested specimens used for the validation of the enhanced bonded anchor design provisions (2/8)

| Monotonic loading: mon<br>Cyclic loading: cyc | Anchorage detailing | Starter bar layout | $\phi$[1]; $\ell_b$[2]<br>[mm]<br>$f_c$[3]<br>[MPa] | $f_{yk}$[4]<br>[MPa] | $f_{yd}$[5]<br>[MPa] | $f_{ck}$[6]<br>[MPa] | $f_{cd}$[7]<br>[MPa] | $f_{ctk}$[8]<br>[MPa] | $f_{ctd}$[9]<br>[MPa] | $f_{bd}$[10]<br>[MPa] | $f_{bk}$[11]<br>[MPa] | $f_b$[12]<br>[MPa] | $\tau_{Rk}$[13]<br>[MPa] | $\tau_{Rd}$[14]<br>[MPa] | $\gamma_{inst}$[15]<br>[-] |
|---|---|---|---|---|---|---|---|---|---|---|---|---|---|---|---|
| num3mon | Post-installed | 4 bars | 16; 240 | 535 | 465 | 20.0 | 13.3 | 1.5 | 1.0 | 2.3 | 3.5 | 4.6 | 7.0 | 3.3 | 1.4 |
| num3cyc | w/o hook | per face | 28.0 | 535 | 535 | 20.0 | 15.4 | 1.5 | 1.2 | 2.7 | 3.5 | 4.6 | 7.0 | 3.8 | 1.4 |
| num3mon-PI20-d12-s | Post-installed | 4 bars | 12; 240 | 535 | 465 | 20.0 | 13.3 | 1.5 | 1.0 | 2.3 | 3.5 | 4.6 | 7.0 | 3.3 | 1.4 |
| num3cyc-PI20-d12-s | w/o hook | per face | 28.0 | 535 | 535 | 20.0 | 15.4 | 1.5 | 1.2 | 2.7 | 3.5 | 4.6 | 7.0 | 3.8 | 1.4 |
| num3mon-PI20-d25-s | Post-installed | 4 bars | 25; 240 | 535 | 465 | 20.0 | 13.3 | 1.5 | 1.0 | 2.3 | 3.5 | 4.6 | 7.0 | 3.3 | 1.4 |
| num3cyc-PI20-d25-s | w/o hook | per face | 28.0 | 535 | 535 | 20.0 | 15.4 | 1.5 | 1.2 | 2.7 | 3.5 | 4.6 | 7.0 | 3.8 | 1.4 |
| num3mon-PI20-d16-s-d[3] | Post-installed | 4 bars | 16; 240 | 535 | 465 | 20.0 | 13.3 | 1.5 | 1.0 | 2.3 | 3.5 | 4.6 | 7.0 | 3.3 | 1.4 |
| num3cyc-PI20-d16-s-d[3] | w/o hook | per face | 28.0 | 535 | 535 | 20.0 | 15.4 | 1.5 | 1.2 | 2.7 | 3.5 | 4.6 | 7.0 | 3.8 | 1.4 |
| num3mon-PI20-d16-s-q[4] | Post-installed | 4 bars | 16; 240 | 535 | 465 | 20.0 | 13.3 | 1.5 | 1.0 | 2.3 | 3.5 | 4.6 | 7.0 | 3.3 | 1.4 |
| num3cyc-PI20-d16-s-q[4] | w/o hook | per face | 28.0 | 535 | 535 | 20.0 | 15.4 | 1.5 | 1.2 | 2.7 | 3.5 | 4.6 | 7.0 | 3.8 | 1.4 |
| num4mon | Post-installed | 2 bars | 25; 240 | 535 | 465 | 20.0 | 13.3 | 1.5 | 1.0 | 2.3 | 3.5 | 4.6 | 7.0 | 3.3 | 1.4 |
| num4cyc | w/o hook | per face | 28.0 | 535 | 535 | 20.0 | 15.4 | 1.5 | 1.2 | 2.7 | 3.5 | 4.6 | 7.0 | 3.8 | 1.4 |
| num4mon-PI20-d16-s | Post-installed | 2 bars | 16; 240 | 535 | 465 | 20.0 | 13.3 | 1.5 | 1.0 | 2.3 | 3.5 | 4.6 | 7.0 | 3.3 | 1.4 |
| num4cyc-PI20-d16-s | w/o hook | per face | 28.0 | 535 | 535 | 20.0 | 15.4 | 1.5 | 1.2 | 2.7 | 3.5 | 4.6 | 7.0 | 3.8 | 1.4 |
| num4mon-PI20-d32-s | Post-installed | 2 bars | 32; 240 | 535 | 465 | 20.0 | 13.3 | 1.5 | 1.0 | 2.3 | 3.5 | 4.6 | 7.0 | 3.3 | 1.4 |
| num4cyc-PI20-d32-s | w/o hook | per face | 28.0 | 535 | 535 | 20.0 | 15.4 | 1.5 | 1.2 | 2.7 | 3.5 | 4.6 | 7.0 | 3.8 | 1.4 |

[1] Starter bar diameter; [2] Anchorage length; [3] Compressive strength of foundation concrete (monotonically tested specimen, cyclically tested specimen)
[4] $f_{yk} = f_y$; [5] $f_{ck} = f_c$; [6] $f_{yd} = f_{ck} / \gamma_s$; [7] $f_{cd} = f_{ck} / \gamma_c$; [8] $f_{ctk} = 0.7 f_{ctm} = 0.7 \cdot 0.30 f_{ck}^{2/3}$; [9] $f_{ctd} = f_{ctk} / \gamma_c$; [10] $f_{bd} = 2.25 \cdot \min\{1.0; (132 - \phi\ [\text{mm}]) / 100\} \cdot f_{ctd}$ (starter bars have vertical orientation during casting); [11] $f_{bk} = f_{bd} \cdot \gamma_c$; [12] $f_b = f_{bk} / 0.75$; [13] $\tau_{Rk,PI} = \tau_{Rk,cr} \cdot \psi_c$ [$\tau_{Rk,CI} = f_{bk} = 0.473 f_{ck}^{2/3}$] for post-installed [cast-in-place] bars; [14] $\tau_{Rd,PI} = \tau_{Rk,PI} / (\gamma_M \cdot \gamma_{inst})$ [$\tau_{Rd,CI} = \tau_{Rk,CI} / \gamma_M$] for post-installed [cast-in-place] bars; Notes: Material safety factors $\gamma_c = \gamma_{Mc} = 1.5$ [1.3] and $\gamma_s = \gamma_{Ms} = 1.15$ [1.0] for fundamental [seismic] load case was assumed for monotonic [cyclic] testing; Installation safety factor $\gamma_{inst} = 1.4$ [1.0] was assumed for post-installed [cast-in-place] bars irrespective of bar diameter; [15] Installation safety factor

Table D.6 Characteristic and design material strengths of numerically tested specimens used for the validation of the enhanced bonded anchor design provisions (3/8)

| Monotonic loading: mon<br>Cyclic loading: cyc | Anchorage detailing | Starter bar layout | $\phi$ [1]; $\ell_b$ [2] [mm]<br>$f_c$ [3] [MPa] | $f_{yk}$ [4] [MPa] | $f_{yd}$ [5] [MPa] | $f_{ck}$ [6] [MPa] | $f_{cd}$ [7] [MPa] | $f_{ctk}$ [8] [MPa] | $f_{ctd}$ [9] [MPa] | $f_{bd}$ [10] [MPa] | $f_{bk}$ [11] [MPa] | $f_b$ [12] [MPa] | $\tau_{Rk}$ [13] [MPa] | $\tau_{Rd}$ [14] [MPa] | $\gamma_{inst}$ [15] [-] |
|---|---|---|---|---|---|---|---|---|---|---|---|---|---|---|---|
| num5mon | Cast-in-place | 2 bars | 32; 420 | 535 | 465 | 20.0 | 13.3 | 1.5 | 1.0 | 2.3 | 3.5 | 4.6 | 3.5 | 2.3 | – |
| num5cyc' | w/ hook | per face | 28.0 | 535 | 535 | 20.0 | 15.4 | 1.5 | 1.2 | 2.7 | 3.5 | 4.6 | 3.5 | 2.7 | – |
| num5mon-CI20-d25-h | Cast-in-place | 2 bars | 25; 420 | 535 | 465 | 20.0 | 13.3 | 1.5 | 1.0 | 2.3 | 3.5 | 4.6 | 3.5 | 2.3 | – |
| num5cyc-CI20-d25-h | w/ hook | per face | 28.0 | 535 | 535 | 20.0 | 15.4 | 1.5 | 1.2 | 2.7 | 3.5 | 4.6 | 3.5 | 2.7 | – |
| num5mon-CI20-d40-h | Cast-in-place | 2 bars | 40; 420 | 535 | 465 | 20.0 | 13.3 | 1.5 | 1.0 | 2.1 | 3.2 | 4.3 | 3.5 | 2.3 | – |
| num5cyc-CI20-d40-h | w/ hook | per face | 28.0 | 535 | 535 | 20.0 | 15.4 | 1.5 | 1.2 | 2.5 | 3.2 | 4.3 | 3.5 | 2.7 | – |
| num6mon | Cast-in-place | 2 bars | 32; 420 | 535 | 465 | 20.0 | 13.3 | 1.5 | 1.0 | 2.3 | 3.5 | 4.6 | 3.5 | 2.3 | – |
| num6cyc | w/o hook | per face | 28.0 | 535 | 535 | 20.0 | 15.4 | 1.5 | 1.2 | 2.7 | 3.5 | 4.6 | 3.5 | 2.7 | – |
| num6mon-CI20-d25-s | Cast-in-place | 2 bars | 25; 420 | 535 | 465 | 20.0 | 13.3 | 1.5 | 1.0 | 2.3 | 3.5 | 4.6 | 3.5 | 2.3 | – |
| num6cyc-CI20-d25-s | w/o hook | per face | 28.0 | 535 | 535 | 20.0 | 15.4 | 1.5 | 1.2 | 2.7 | 3.5 | 4.6 | 3.5 | 2.7 | – |
| num6mon-CI20-d40-s | Cast-in-place | 2 bars | 40; 420 | 535 | 465 | 20.0 | 13.3 | 1.5 | 1.0 | 2.1 | 3.2 | 4.3 | 3.5 | 2.3 | – |
| num6cyc-CI20-d40-s | w/o hook | per face | 28.0 | 535 | 535 | 20.0 | 15.4 | 1.5 | 1.2 | 2.5 | 3.2 | 4.3 | 3.5 | 2.7 | – |

[1] Starter bar diameter; [2] Anchorage length; [3] Compressive strength of foundation concrete (monotonically tested specimen, cyclically tested specimen) [4] $f_{yk} = f_y$; [5] $f_{ck} = f_c$; [6] $f_{yd} = f_{ck} / \gamma_s$; [7] $f_{cd} = f_{ck} / \gamma_c$; [8] $f_{ctk} = 0.7 f_{ctm} = 0.7 \cdot 0.30 f_{ck}^{2/3}$; [9] $f_{ctd} = f_{ctk} / \gamma_c$; [10] $f_{bd} = 2.25 \cdot \min\{1.0; (132 - \phi\ [\text{mm}]) / 100\} \cdot f_{ctd}$ (starter bars have vertical orientation during casting); [11] $f_{bk} = f_{bd} \cdot \gamma_c$; [12] $f_b = f_{bk} / 0.75$; [13] $\tau_{Rk,PI} = \tau_{Rk,cr} \cdot \psi_c$ [$\tau_{Rk,CI} = f_{bk} = 0.473 f_{ck}^{2/3}$] for post-installed [cast-in-place] bars; [14] $\tau_{Rd,PI} = \tau_{Rk,PI} / (\gamma_M \cdot \gamma_{inst})$ [$\tau_{Rd,CI} = \tau_{Rk,CI} / \gamma_M$] for post-installed [cast-in-place] bars; Notes: Material safety factors $\gamma_c = \gamma_{Mc} = 1.5$ [1.3] and $\gamma_s = \gamma_{Ms} = 1.15$ [1.0] for fundamental [seismic] load case was assumed for monotonic [cyclic] testing; Installation safety factor $\gamma_{inst} = 1.4$ [1.0] was assumed for post-installed [cast-in-place] bars irrespective of bar diameter; [15] Installation safety factor

Table D.6 Characteristic and design material strengths of numerically tested specimens used for the validation of the enhanced bonded anchor design provisions (4/8)

| Monotonic loading: mon<br>Cyclic loading: cyc | Anchorage detailing | Starter bar layout | $\phi$[1]; $\ell_b$[2]<br>[mm]<br>$f_c$[3]<br>[MPa] | $f_{yk}$[4]<br>[MPa] | $f_{yd}$[5]<br>[MPa] | $f_{ck}$[6]<br>[MPa] | $f_{cd}$[7]<br>[MPa] | $f_{ctk}$[8]<br>[MPa] | $f_{ctd}$[9]<br>[MPa] | $f_{bd}$[10]<br>[MPa] | $f_{bk}$[11]<br>[MPa] | $f_b$[12]<br>[MPa] | $\tau_{Rk}$[13]<br>[MPa] | $\tau_{Rd}$[14]<br>[MPa] | $\gamma_{inst}$[15]<br>[-] |
|---|---|---|---|---|---|---|---|---|---|---|---|---|---|---|---|
| num7mon | Post-installed | 2 bars | 32; 420 | 535 | 465 | 20.0 | 13.3 | 1.5 | 1.0 | 2.3 | 3.5 | 4.6 | 7.0 | 3.3 | 1.4 |
| num7cyc | w/o hook | per face | 28.0 | 535 | 535 | 20.0 | 15.4 | 1.5 | 1.2 | 2.7 | 3.5 | 4.6 | 7.0 | 3.8 | 1.4 |
| num7mon-PI20-d25-s | Post-installed | 2 bars | 25; 420 | 535 | 465 | 20.0 | 13.3 | 1.5 | 1.0 | 2.3 | 3.5 | 4.6 | 7.0 | 3.3 | 1.4 |
| num7cyc-PI20-d25-s | w/o hook | per face | 28.0 | 535 | 535 | 20.0 | 15.4 | 1.5 | 1.2 | 2.7 | 3.5 | 4.6 | 7.0 | 3.8 | 1.4 |
| num7mon-PI20-d40-s | Post-installed | 2 bars | 40; 420 | 535 | 465 | 20.0 | 13.3 | 1.5 | 1.0 | 2.1 | 3.2 | 4.3 | 7.0 | 3.3 | 1.4 |
| num7cyc-PI20-d40-s | w/o hook | per face | 28.0 | 535 | 535 | 20.0 | 15.4 | 1.5 | 1.2 | 2.5 | 3.2 | 4.3 | 7.0 | 3.8 | 1.4 |
| num7mon-PI20-d32-s-d[3] | Post-installed | 2 bars | 32; 420 | 535 | 465 | 20.0 | 13.3 | 1.5 | 1.0 | 2.3 | 3.5 | 4.6 | 7.0 | 3.3 | 1.4 |
| num7cyc-PI20-d32-s-d[3] | w/o hook | per face | 28.0 | 535 | 535 | 20.0 | 15.4 | 1.5 | 1.2 | 2.7 | 3.5 | 4.6 | 7.0 | 3.8 | 1.4 |
| num7mon-PI20-d32-s-q[4] | Post-installed | 2 bars | 32; 420 | 535 | 465 | 20.0 | 13.3 | 1.5 | 1.0 | 2.3 | 3.5 | 4.6 | 7.0 | 3.3 | 1.4 |
| num7cyc-PI20-d32-s-q[4] | w/o hook | per face | 28.0 | 535 | 535 | 20.0 | 15.4 | 1.5 | 1.2 | 2.7 | 3.5 | 4.6 | 7.0 | 3.8 | 1.4 |
| num8mon | Post-installed | 2 bars | 25; 420 | 535 | 465 | 20.0 | 13.3 | 1.5 | 1.0 | 2.3 | 3.5 | 4.6 | 7.0 | 3.3 | 1.4 |
| num8cyc | w/o hook | per face | 28.0 | 535 | 535 | 20.0 | 15.4 | 1.5 | 1.2 | 2.7 | 3.5 | 4.6 | 7.0 | 3.8 | 1.4 |

[1] Starter bar diameter; [2] Anchorage length; [3] Compressive strength of foundation concrete (monotonically tested specimen, cyclically tested specimen) [4] $f_{yk} = f_y$; [5] $f_{ck} = f_c$; [6] $f_{yd} = f_{ck} / \gamma_s$; [7] $f_{cd} = f_{ck} / \gamma_c$; [8] $f_{ctk} = 0.7 f_{ctm} = 0.7 \cdot 0.30 f_{ck}^{2/3}$; [9] $f_{ctd} = f_{ctk} / \gamma_c$; [10] $f_{bd} = 2.25 \cdot \min\{1.0; (132 - \phi\ [\text{mm}]) / 100\} \cdot f_{ctd}$ (starter bars have vertical orientation during casting); [11] $f_{bk} = f_{bd} \cdot \gamma_c$; [12] $f_b = f_{bk} / 0.75$; [13] $\tau_{Rk,PI} = \tau_{Rk,cr} \cdot \psi_c$ [$\tau_{Rk,CI} = f_{bk} = 0.473 f_{ck}^{2/3}$] for post-installed [cast-in-place] bars; [14] $\tau_{Rd,PI} = \tau_{Rk,PI} / (\gamma_M \cdot \gamma_{inst})$ [$\tau_{Rd,CI} = \tau_{Rk,CI} / \gamma_M$] for post-installed [cast-in-place] bars; Notes: Material safety factors $\gamma_c = \gamma_{Mc} = 1.5$ [1.3] and $\gamma_s = \gamma_{Ms} = 1.15$ [1.0] for fundamental [seismic] load case was assumed for monotonic [cyclic] testing; Installation safety factor $\gamma_{inst} = 1.4$ [1.0] was assumed for post-installed [cast-in-place] bars irrespective of bar diameter; [15] Installation safety factor

Table D.6 Characteristic and design material strengths of numerically tested specimens used for the validation of the enhanced bonded anchor design provisions (5/8)

| Monotonic loading: mon<br>Cyclic loading: cyc | Anchorage detailing | Starter bar layout | $\phi$[1]; $\ell_b$[2] [mm]<br>$f_c$[3] [MPa] | $f_{yk}$[4] [MPa] | $f_{yd}$[5] [MPa] | $f_{ck}$[6] [MPa] | $f_{cd}$[7] [MPa] | $f_{ctk}$[8] [MPa] | $f_{ctd}$[9] [MPa] | $f_{bd}$[10] [MPa] | $f_{bk}$[11] [MPa] | $f_b$[12] [MPa] | $\tau_{Rk}$[13] [MPa] | $\tau_{Rd}$[14] [MPa] | $\gamma_{inst}$[15] [-] |
|---|---|---|---|---|---|---|---|---|---|---|---|---|---|---|---|
| num1mon-CI50-d16-h | Cast-in-place | 4 bars | 16; 240 | 535 | 465 | 50.0 | 33.3 | 2.9 | 1.9 | 4.3 | 6.4 | 8.6 | 6.4 | 4.3 | – |
| num1cyc-CI50-d16-h | w/ hook | per face | 58.0 | 535 | 535 | 50.0 | 38.5 | 2.9 | 2.2 | 4.9 | 6.4 | 8.6 | 6.4 | 4.9 | – |
| num1mon-CI50-d12-h | Cast-in-place | 4 bars | 12; 240 | 535 | 465 | 50.0 | 33.3 | 2.9 | 1.9 | 4.3 | 6.4 | 8.6 | 6.4 | 4.3 | – |
| num1cyc-CI50-d12-h | w/ hook | per face | 58.0 | 535 | 535 | 50.0 | 38.5 | 2.9 | 2.2 | 4.9 | 6.4 | 8.6 | 6.4 | 4.9 | – |
| num1mon-CI50-d25-h | Cast-in-place | 4 bars | 25; 240 | 535 | 465 | 50.0 | 33.3 | 2.9 | 1.9 | 4.3 | 6.4 | 8.6 | 6.4 | 4.3 | – |
| num1cyc-CI50-d25-h | w/ hook | per face | 58.0 | 535 | 535 | 50.0 | 38.5 | 2.9 | 2.2 | 4.9 | 6.4 | 8.6 | 6.4 | 4.9 | – |
| num2mon-CI50-d16-s | Cast-in-place | 4 bars | 16; 240 | 535 | 465 | 50.0 | 33.3 | 2.9 | 1.9 | 4.3 | 6.4 | 8.6 | 6.4 | 4.3 | – |
| num2cyc-CI50-d16-s | w/o hook | per face | 58.0 | 535 | 535 | 50.0 | 38.5 | 2.9 | 2.2 | 4.9 | 6.4 | 8.6 | 6.4 | 4.9 | – |
| num2mon-CI50-d12-s | Cast-in-place | 4 bars | 12; 240 | 535 | 465 | 50.0 | 33.3 | 2.9 | 1.9 | 4.3 | 6.4 | 8.6 | 6.4 | 4.3 | – |
| num2cyc-CI50-d12-s | w/o hook | per face | 58.0 | 535 | 535 | 50.0 | 38.5 | 2.9 | 2.2 | 4.9 | 6.4 | 8.6 | 6.4 | 4.9 | – |
| num2mon-CI50-d25-s | Cast-in-place | 4 bars | 25; 240 | 535 | 465 | 50.0 | 33.3 | 2.9 | 1.9 | 4.3 | 6.4 | 8.6 | 6.4 | 4.3 | – |
| num2cyc-CI50-d25-s | w/o hook | per face | 58.0 | 535 | 535 | 50.0 | 38.5 | 2.9 | 2.2 | 4.9 | 6.4 | 8.6 | 6.4 | 4.9 | – |

[1] Starter bar diameter; [2] Anchorage length; [3] Compressive strength of foundation concrete (monotonically tested specimen, cyclically tested specimen) [4] $f_{yk} = f_y$; [5] $f_{ck} = f_c$; [6] $f_{yd} = f_{ck} / \gamma_s$; [7] $f_{cd} = f_{ck} / \gamma_c$; [8] $f_{ctk} = 0.7 f_{ctm} = 0.7 \cdot 0.30 f_{ck}^{2/3}$; [9] $f_{ctd} = f_{ctk} / \gamma_c$; [10] $f_{bd} = 2.25 \cdot \min\{1.0; (132 - \phi\ [\text{mm}]) / 100\} \cdot f_{ctd}$ (starter bars have vertical orientation during casting); [11] $f_{bk} = f_{bd} \cdot \gamma_c$; [12] $f_b = f_{bk} / 0.75$; [13] $\tau_{Rk,PI} = \tau_{Rk,cr} \cdot \psi_c$ [$\tau_{Rk,CI} = f_{bk} = 0.473 f_{ck}^{2/3}$] for post-installed [cast-in-place] bars; [14] $\tau_{Rd,PI} = \tau_{Rk,PI} / (\gamma_M \cdot \gamma_{inst})$ [$\tau_{Rd,CI} = \tau_{Rk,CI} / \gamma_M$] for post-installed [cast-in-place] bars; Notes: Material safety factors $\gamma_c = \gamma_{Mc} = 1.5$ [1.3] and $\gamma_s = \gamma_{Ms} = 1.15$ [1.0] for fundamental [seismic] load case was assumed for monotonic [cyclic] testing; Installation safety factor $\gamma_{inst} = 1.4$ [1.0] was assumed for post-installed [cast-in-place] bars irrespective of bar diameter; [15] Installation safety factor

Table D.6 Characteristic and design material strengths of numerically tested specimens used for the validation of the enhanced bonded anchor design provisions (6/8)

| Monotonic loading: mon<br>Cyclic loading: cyc | Anchorage detailing | Starter bar layout | $\phi$[1]; $\ell_b$[2]<br>[mm]<br>$f_c$[3]<br>[MPa] | $f_{yk}$[4]<br>[MPa] | $f_{yd}$[5]<br>[MPa] | $f_{ck}$[6]<br>[MPa] | $f_{cd}$[7]<br>[MPa] | $f_{ctk}$[8]<br>[MPa] | $f_{ctd}$[9]<br>[MPa] | $f_{bd}$[10]<br>[MPa] | $f_{bk}$[11]<br>[MPa] | $f_b$[12]<br>[MPa] | $\tau_{Rk}$[13]<br>[MPa] | $\tau_{Rd}$[14]<br>[MPa] | $\gamma_{inst}$[15]<br>[-] |
|---|---|---|---|---|---|---|---|---|---|---|---|---|---|---|---|
| num3mon-PI50-d16-s | Post-installed | 4 bars | 16; 240 | 535 | 465 | 50.0 | 33.3 | 2.9 | 1.9 | 4.3 | 6.4 | 8.6 | 7.6 | 3.6 | 1.4 |
| num3cyc-PI50-d16-s | w/o hook | per face | 58.0 | 535 | 535 | 50.0 | 38.5 | 2.9 | 2.2 | 4.9 | 6.4 | 8.6 | 7.6 | 4.2 | 1.4 |
| num3mon-PI50-d12-s | Post-installed | 4 bars | 12; 240 | 535 | 465 | 50.0 | 33.3 | 2.9 | 1.9 | 4.3 | 6.4 | 8.6 | 7.6 | 3.6 | 1.4 |
| num3cyc-PI50-d12-s | w/o hook | per face | 58.0 | 535 | 535 | 50.0 | 38.5 | 2.9 | 2.2 | 4.9 | 6.4 | 8.6 | 7.6 | 4.2 | 1.4 |
| num3mon-PI50-d25-s | Post-installed | 4 bars | 25; 240 | 535 | 465 | 50.0 | 33.3 | 2.9 | 1.9 | 4.3 | 6.4 | 8.6 | 7.6 | 3.6 | 1.4 |
| num3cyc-PI50-d25-s | w/o hook | per face | 58.0 | 535 | 535 | 50.0 | 38.5 | 2.9 | 2.2 | 4.9 | 6.4 | 8.6 | 7.6 | 4.2 | 1.4 |
| num3mon-PI50-d16-s-d[3] | Post-installed | 4 bars | 16; 240 | 535 | 465 | 50.0 | 33.3 | 2.9 | 1.9 | 4.3 | 6.4 | 8.6 | 7.6 | 3.6 | 1.4 |
| num3cyc-PI50-d16-s-d[3] | w/o hook | per face | 58.0 | 535 | 535 | 50.0 | 38.5 | 2.9 | 2.2 | 4.9 | 6.4 | 8.6 | 7.6 | 4.2 | 1.4 |
| num3mon-PI50-d16-s-q[4] | Post-installed | 4 bars | 16; 240 | 535 | 465 | 50.0 | 33.3 | 2.9 | 1.9 | 4.3 | 6.4 | 8.6 | 7.6 | 3.6 | 1.4 |
| num3cyc-PI50-d16-s-q[4] | w/o hook | per face | 58.0 | 535 | 535 | 50.0 | 38.5 | 2.9 | 2.2 | 4.9 | 6.4 | 8.6 | 7.6 | 4.2 | 1.4 |
| num4mon-PI50-d25-s | Post-installed | 2 bars | 25; 240 | 535 | 465 | 50.0 | 33.3 | 2.9 | 1.9 | 4.3 | 6.4 | 8.6 | 7.6 | 3.6 | 1.4 |
| num4cyc-PI50-d25-s | w/o hook | per face | 58.0 | 535 | 535 | 50.0 | 38.5 | 2.9 | 2.2 | 4.9 | 6.4 | 8.6 | 7.6 | 4.2 | 1.4 |
| num4mon-PI50-d16-s | Post-installed | 2 bars | 16; 240 | 535 | 465 | 50.0 | 33.3 | 2.9 | 1.9 | 4.3 | 6.4 | 8.6 | 7.6 | 3.6 | 1.4 |
| num4cyc-PI50-d16-s | w/o hook | per face | 58.0 | 535 | 535 | 50.0 | 38.5 | 2.9 | 2.2 | 4.9 | 6.4 | 8.6 | 7.6 | 4.2 | 1.4 |
| num4mon-PI50-d32-s | Post-installed | 2 bars | 32; 240 | 535 | 465 | 50.0 | 33.3 | 2.9 | 1.9 | 4.3 | 6.4 | 8.6 | 7.6 | 3.6 | 1.4 |
| num4cyc-PI50-d32-s | w/o hook | per face | 58.0 | 535 | 535 | 50.0 | 38.5 | 2.9 | 2.2 | 4.9 | 6.4 | 8.6 | 7.6 | 4.2 | 1.4 |

[1] Starter bar diameter; [2] Anchorage length; [3] Compressive strength of foundation concrete (monotonically tested specimen, cyclically tested specimen)
[4] $f_{yk} = f_y$; [5] $f_{ck} = f_c$; [6] $f_{yd} = f_{ck} / \gamma_s$; [7] $f_{cd} = f_{ck} / \gamma_c$; [8] $f_{ctk} = 0.7 f_{ctm} = 0.7 \cdot 0.30 f_{ck}^{2/3}$; [9] $f_{ctd} = f_{ctk} / \gamma_c$; [10] $f_{bd} = 2.25 \cdot \min\{1.0; (132 - \phi\ [\text{mm}]) / 100\} \cdot f_{ctd}$ (starter bars have vertical orientation during casting); [11] $f_{bk} = f_{bd} \cdot \gamma_c$; [12] $f_b = f_{bk} / 0.75$; [13] $\tau_{Rk,PI} = \tau_{Rk,cr} \cdot \psi_c$ [$\tau_{Rk,CI} = f_{bk} = 0.473 f_{ck}^{2/3}$] for post-installed [cast-in-place] bars; [14] $\tau_{Rd,PI} = \tau_{Rk,PI} / (\gamma_M \cdot \gamma_{inst})$ [$\tau_{Rd,CI} = \tau_{Rk,CI} / \gamma_M$] for post-installed [cast-in-place] bars; Notes: Material safety factors $\gamma_c = \gamma_{Mc} = 1.5$ [1.3] and $\gamma_s = \gamma_{Ms} = 1.15$ [1.0] for fundamental [seismic] load case was assumed for monotonic [cyclic] testing; Installation safety factor $\gamma_{inst} = 1.4$ [1.0] was assumed for post-installed [cast-in-place] bars irrespective of bar diameter; [15] Installation safety factor

Table D.6 Characteristic and design material strengths of numerically tested specimens used for the validation of the enhanced bonded anchor design provisions (7/8)

| Monotonic loading: mon<br>Cyclic loading: cyc | Anchorage detailing | Starter bar layout | $\phi$ [1]; $\ell_b$ [2] [mm]<br>$f_c$ [3] [MPa] | $f_{yk}$ [4] [MPa] | $f_{yd}$ [5] [MPa] | $f_{ck}$ [6] [MPa] | $f_{cd}$ [7] [MPa] | $f_{ctk}$ [8] [MPa] | $f_{ctd}$ [9] [MPa] | $f_{bd}$ [10] [MPa] | $f_{bk}$ [11] [MPa] | $f_b$ [12] [MPa] | $\tau_{Rk}$ [13] [MPa] | $\tau_{Rd}$ [14] [MPa] | $\gamma_{inst}$ [15] [-] |
|---|---|---|---|---|---|---|---|---|---|---|---|---|---|---|---|
| num5mon-CI50-d32-s | Cast-in-place | 2 bars | 32; 420 | 535 | 465 | 50.0 | 33.3 | 2.9 | 1.9 | 4.3 | 6.4 | 8.6 | 6.4 | 4.3 | – |
| num5cyc'-CI50-d32-s | w/ hook | per face | 58.0 | 535 | 535 | 50.0 | 38.5 | 2.9 | 2.2 | 4.9 | 6.4 | 8.6 | 6.4 | 4.9 | – |
| num5mon-CI50-d25-h | Cast-in-place | 2 bars | 25; 420 | 535 | 465 | 50.0 | 33.3 | 2.9 | 1.9 | 4.3 | 6.4 | 8.6 | 6.4 | 4.3 | – |
| num5cyc-CI50-d25-h | w/ hook | per face | 58.0 | 535 | 535 | 50.0 | 38.5 | 2.9 | 2.2 | 4.9 | 6.4 | 8.6 | 6.4 | 4.9 | – |
| num5mon-CI50-d40-h | Cast-in-place | 2 bars | 40; 420 | 535 | 465 | 50.0 | 33.3 | 2.9 | 1.9 | 3.9 | 5.9 | 7.9 | 6.4 | 4.3 | – |
| num5cyc-CI50-d40-h | w/ hook | per face | 58.0 | 535 | 535 | 50.0 | 38.5 | 2.9 | 2.2 | 4.5 | 5.9 | 7.9 | 6.4 | 4.9 | – |
| num6mon-CI50-d32-s | Cast-in-place | 2 bars | 32; 420 | 535 | 465 | 50.0 | 33.3 | 2.9 | 1.9 | 4.3 | 6.4 | 8.6 | 6.4 | 4.3 | – |
| num6cyc-CI50-d32-s | w/o hook | per face | 58.0 | 535 | 535 | 50.0 | 38.5 | 2.9 | 2.2 | 4.9 | 6.4 | 8.6 | 6.4 | 4.9 | – |
| num6mon-CI50-d25-s | Cast-in-place | 2 bars | 25; 420 | 535 | 465 | 50.0 | 33.3 | 2.9 | 1.9 | 4.3 | 6.4 | 8.6 | 6.4 | 4.3 | – |
| num6cyc-CI50-d25-s | w/o hook | per face | 58.0 | 535 | 535 | 50.0 | 38.5 | 2.9 | 2.2 | 4.9 | 6.4 | 8.6 | 6.4 | 4.9 | – |
| num6mon-CI50-d40-s | Cast-in-place | 2 bars | 40; 420 | 535 | 465 | 50.0 | 33.3 | 2.9 | 1.9 | 3.9 | 5.9 | 7.9 | 6.4 | 4.3 | – |
| num6cyc-CI50-d40-s | w/o hook | per face | 58.0 | 535 | 535 | 50.0 | 38.5 | 2.9 | 2.2 | 4.5 | 5.9 | 7.9 | 6.4 | 4.9 | – |

[1] Starter bar diameter; [2] Anchorage length; [3] Compressive strength of foundation concrete (monotonically tested specimen, cyclically tested specimen) [4] $f_{yk} = f_y$; [5] $f_{ck} = f_c$; [6] $f_{yd} = f_{ck} / \gamma_s$; [7] $f_{cd} = f_{ck} / \gamma_c$; [8] $f_{ctk} = 0.7 f_{ctm} = 0.7 \cdot 0.30 f_{ck}^{2/3}$; [9] $f_{ctd} = f_{ctk} / \gamma_c$; [10] $f_{bd} = 2.25 \cdot \min\{1.0; (132 - \phi\ [\text{mm}]) / 100\} \cdot f_{ctd}$ (starter bars have vertical orientation during casting); [11] $f_{bk} = f_{bd} \cdot \gamma_c$; [12] $f_b = f_{bk} / 0.75$; [13] $\tau_{Rk,PI} = \tau_{Rk,cr} \cdot \psi_c$ [$\tau_{Rk,CI} = f_{bk} = 0.473 f_{ck}^{2/3}$] for post-installed [cast-in-place] bars; [14] $\tau_{Rd,PI} = \tau_{Rk,PI} / (\gamma_M \cdot \gamma_{inst})$ [$\tau_{Rd,CI} = \tau_{Rk,CI} / \gamma_M$] for post-installed [cast-in-place] bars; Notes: Material safety factors $\gamma_c = \gamma_{Mc} = 1.5$ [1.3] and $\gamma_s = \gamma_{Ms} = 1.15$ [1.0] for fundamental [seismic] load case was assumed for monotonic [cyclic] testing; Installation safety factor $\gamma_{inst} = 1.4$ [1.0] was assumed for post-installed [cast-in-place] bars irrespective of bar diameter; [15] Installation safety factor

Table D.6 Characteristic and design material strengths of numerically tested specimens used for the validation of the enhanced bonded anchor design provisions (8/8)

| Monotonic loading: mon<br>Cyclic loading: cyc | Anchorage detailing | Starter bar layout | $\phi$[1]; $\ell_b$[2]<br>[mm]<br>$f_c$[3]<br>[MPa] | $f_{yk}$[4]<br>[MPa] | $f_{yd}$[5]<br>[MPa] | $f_{ck}$[6]<br>[MPa] | $f_{cd}$[7]<br>[MPa] | $f_{ctk}$[8]<br>[MPa] | $f_{ctd}$[9]<br>[MPa] | $f_{bd}$[10]<br>[MPa] | $f_{bk}$[11]<br>[MPa] | $f_b$[12]<br>[MPa] | $\tau_{Rk}$[13]<br>[MPa] | $\tau_{Rd}$[14]<br>[MPa] | $\gamma_{inst}$[15]<br>[-] |
|---|---|---|---|---|---|---|---|---|---|---|---|---|---|---|---|
| num7mon'-PI50-d32-s | Post-installed | 2 bars | 32; 420 | 535 | 465 | 50.0 | 33.3 | 2.9 | 1.9 | 4.3 | 6.4 | 8.6 | 7.6 | 3.6 | 1.4 |
| num7cyc'-PI50-d32-s | w/o hook | per face | 58.0 | 535 | 535 | 50.0 | 38.5 | 2.9 | 2.2 | 4.9 | 6.4 | 8.6 | 7.6 | 4.2 | 1.4 |
| num7mon-PI50-d25-s | Post-installed | 2 bars | 25; 420 | 535 | 465 | 50.0 | 33.3 | 2.9 | 1.9 | 4.3 | 6.4 | 8.6 | 7.6 | 3.6 | 1.4 |
| num7cyc-PI50-d25-s | w/o hook | per face | 58.0 | 535 | 535 | 50.0 | 38.5 | 2.9 | 2.2 | 4.9 | 6.4 | 8.6 | 7.6 | 4.2 | 1.4 |
| num7mon-PI50-d40-s | Post-installed | 2 bars | 40; 420 | 535 | 465 | 50.0 | 33.3 | 2.9 | 1.9 | 3.9 | 5.9 | 7.9 | 7.6 | 3.6 | 1.4 |
| num7cyc-PI50-d40-s | w/o hook | per face | 58.0 | 535 | 535 | 50.0 | 38.5 | 2.9 | 2.2 | 4.5 | 5.9 | 7.9 | 7.6 | 4.2 | 1.4 |
| num7mon-PI50-d32-s-d[3] | Post-installed | 2 bars | 32; 420 | 535 | 465 | 50.0 | 33.3 | 2.9 | 1.9 | 4.3 | 6.4 | 8.6 | 7.6 | 3.6 | 1.4 |
| num7cyc-PI50-d32-s-d[3] | w/o hook | per face | 58.0 | 535 | 535 | 50.0 | 38.5 | 2.9 | 2.2 | 4.9 | 6.4 | 8.6 | 7.6 | 4.2 | 1.4 |
| num7mon-PI50-d32-s-q[4] | Post-installed | 2 bars | 32; 420 | 535 | 465 | 50.0 | 33.3 | 2.9 | 1.9 | 4.3 | 6.4 | 8.6 | 7.6 | 3.6 | 1.4 |
| num7cyc-PI50-d32-s-q[4] | w/o hook | per face | 58.0 | 535 | 535 | 50.0 | 38.5 | 2.9 | 2.2 | 4.9 | 6.4 | 8.6 | 7.6 | 4.2 | 1.4 |
| num8mon-PI50-d25-s | Post-installed | 2 bars | 25; 420 | 535 | 465 | 50.0 | 33.3 | 2.9 | 1.9 | 4.3 | 6.4 | 8.6 | 7.6 | 3.6 | 1.4 |
| num8cyc-PI50-d25-s | w/o hook | per face | 58.0 | 535 | 535 | 50.0 | 38.5 | 2.9 | 2.2 | 4.9 | 6.4 | 8.6 | 7.6 | 4.2 | 1.4 |

[1] Starter bar diameter; [2] Anchorage length; [3] Compressive strength of foundation concrete (monotonically tested specimen, cyclically tested specimen) [4] $f_{yk} = f_y$; [5] $f_{ck} = f_c$; [6] $f_{yd} = f_{ck} / \gamma_s$; [7] $f_{cd} = f_{ck} / \gamma_c$; [8] $f_{ctk} = 0.7 f_{ctm} = 0.7 \cdot 0.30 f_{ck}^{2/3}$; [9] $f_{ctd} = f_{ctk} / \gamma_c$; [10] $f_{bd} = 2.25 \cdot \min\{1.0; (132 - \phi\ [\text{mm}]) / 100\} \cdot f_{ctd}$ (starter bars have vertical orientation during casting); [11] $f_{bk} = f_{bd} \cdot \gamma_c$; [12] $f_b = f_{bk} / 0.75$; [13] $\tau_{Rk,PI} = \tau_{Rk,cr} \cdot \psi_c$ [$\tau_{Rk,CI} = f_{bk} = 0.473 f_{ck}^{2/3}$] for post-installed [cast-in-place] bars; [14] $\tau_{Rd,PI} = \tau_{Rk,PI} / (\gamma_M \cdot \gamma_{inst})$ [$\tau_{Rd,CI} = \tau_{Rk,CI} / \gamma_M$] for post-installed [cast-in-place] bars; Notes: Material safety factors $\gamma_c = \gamma_{Mc} = 1.5$ [1.3] and $\gamma_s = \gamma_{Ms} = 1.15$ [1.0] for fundamental [seismic] load case was assumed for monotonic [cyclic] testing; Installation safety factor $\gamma_{inst} = 1.4$ [1.0] was assumed for post-installed [cast-in-place] bars irrespective of bar diameter; [15] Installation safety factor

## D.5 Tested and Simulated versus Calculated Connections Capacities

Table D.7 compares the experimentally tested and Table D.8 the numerically simulated column-to-foundation connection capacities and failure modes to the calculated mean and characteristic capacities and failure modes on the basis of the enhanced bonded anchor design.

Table D.7 Mean and characteristic connection capacities and failure modes experimentally tested and calculated on the basis of the enhanced bonded anchor design provisions

| Monotonic loading: mon<br>Cyclic loading: cyc | Anchorage detailing | Starter bar layout | $\phi$[1]; $\ell_b$[2] [mm]<br>$f_c$[3] [MPa] | exp$M_R$[4] [kNm] | Failure mode tested | cal$M_R$[5] [kNm] | Failure mode calculated[5] | cal$M_{Rk}$[6] [kNm] | Failure mode calculated[6] | $N_{Rk,s}$ / $N_{Rk,p/c}$ [-] |
|---|---|---|---|---|---|---|---|---|---|---|
| exp1mon | Cast-in-place | 4 bars | 16; 240 | 106.5 | Y | 85.7 | C | 62.1 | C | – |
| exp1cyc | w/ hook | per face | 24.1, 22.4 | 98.3 | Y | 79.9 | C | 60.0 | C | 2.40 |
| exp2mon | Cast-in-place | 4 bars | 16; 240 | 76.2 | P/C | 65.0 | P | 25.1 | P | – |
| exp2cyc | w/o hook | per face | 21.7, 24.1 | 85.1 | P/C | 65.8 | P | 24.3 | P | 2.40 |
| exp3mon | Post-installed | 4 bars | 16; 240 | 97.5 | Y | 78.8 | C | 41.8 | P | – |
| exp3cyc | w/o hook | per face | 20.4, 23.2 | 89.4 | P/C | 81.3 | C | 40.5 | P | 2.71 |
| exp4mon | Post-installed | 2 bars | 25; 240 | 91.1 | P/C | 78.5 | C | 36.7 | P | – |
| exp4cyc | w/o hook | per face | 21.3, 20.6 | 69.5 | P/C | 72.7 | C | 34.6 | P | 3.34 |
| exp5mon | Cast-in-place | 2 bars | 32; 420 | 194.3 | Y | 180.7 | Y | 151.7 | C | – |
| exp5cyc | w/ hook | per face | 23.0, 22.5 | 192.0 | Y | 180.7 | Y | 145.5 | C | 1.94 |
| exp6mon | Cast-in-place | 2 bars | 32; 420 | 174.8 | Y | 174.2 | P | 58.1 | P | – |
| exp6cyc | w/o hook | per face | 21.9, 24.7 | 190.5 | Y | 176.6 | P | 55.8 | P | 1.94 |
| exp7mon | Post-installed | 2 bars | 32; 420 | 178.5 | Y | 180.7 | Y | 94.5 | P | – |
| exp7cyc | w/o hook | per face | 20.5, 22.2 | 178.5 | Y | 180.7 | Y | 90.7 | P | 2.08 |
| exp8mon | Post-installed | 2 bars | 25; 420 | 120.0 | Y | 112.7 | Y | 81.0 | P | – |
| exp8cyc | w/o hook | per face | 21.8, 20.7 | 120.0 | Y | 112.7 | Y | 79.0 | P | 1.25 |

[1] Starter bar diameter; [2] Anchorage length; [3] Compressive strength of foundation concrete (monotonically tested specimen, cyclically tested specimen);

[4] $expM_R = expM_{R,p/c} = expM_{max}$ for brittle failure and $expM_R = expM_{R,y}$ for ductile failure; [5] $calM_R = N_R \cdot z = \min\{N_{R,p}; N_{R,p}; N_{R,y}\} \cdot z$ according to Section 8.2 using tested mean material strengths $f_c$, $f_y$, $\tau_u$ (Table D.1); [6] $calM_{Rk} = N_{Rk} \cdot z = \min\{N_{Rk,p}; N_{Rk,p}; N_{Rk,y}\} \cdot z$ according to Section 9.2 using characteristic material strengths $f_{ck}$, $f_{yk}$, $\tau_{Rk}$ (Table D.5)

Table D.8 Mean and characteristic connection capacities and failure modes numerically tested and calculated on the basis of the enhanced bonded anchor design provisions (1/8)

| Monotonic loading: mon<br>Cyclic loading: cyc | Anchorage detailing | Starter bar layout | $\phi$[1]; $\ell_b$[2] [mm]<br>$f_c$[3] [MPa] | $numM_R$[4] [kNm] | Failure mode tested | $calM_R$[5] [kNm] | Failure mode calculated[5] | $calM_{Rk}$[6] [kNm] | Failure mode calculated[6] | $N_{Rk,s}$ / $N_{Rk,p/c}$ [-] |
|---|---|---|---|---|---|---|---|---|---|---|
| num1mon | Cast-in-place | 4 bars | 16; 240 | 102.0 | Y | 92.3 | C | 58.9 | C | – |
| num1cyc | w/ hook | per face | 28 | 99.0 | Y | 89.3 | C | 57.0 | C | 2.54 |
| num1mon-CI20-d12-h | Cast-in-place | 4 bars | 12; 240 | 63.0 | Y | 55.2 | Y | 55.2 | Y | – |
| num1cyc-CI20-d12-h | w/ hook | per face | 28 | 60.0 | Y | 55.2 | Y | 55.2 | Y | 1.72 |
| num1mon-CI20-d25-h | Cast-in-place | 4 bars | 25; 240 | 149.7 | P/C | 89.9 | C | 57.3 | C | – |
| num1cyc-CI20-d25-h | w/ hook | per face | 28 | 141.7 | P/C | 84.8 | C | 54.1 | C | 5.01 |
| num2mon | Cast-in-place | 4 bars | 16; 240 | 95.6 | P/C | 70.2 | C | 23.6 | P | – |
| num2cyc | w/o hook | per face | 28 | 84.1 | P/C | 67.9 | C | 22.9 | P | 2.54 |
| num2mon-CI20-d12-s | Cast-in-place | 4 bars | 12; 240 | 61.5 | Y | 55.2 | Y | 19.4 | Y | – |
| num2cyc-CI20-d12-s | w/o hook | per face | 28 | 58.5 | Y | 55.2 | Y | 19.2 | Y | 1.72 |
| num2mon-CI20-d25-s | Cast-in-place | 4 bars | 25; 240 | 102.8 | P/C | 73.5 | C | 31.5 | P | – |
| num2cyc-CI20-d25-s | w/o hook | per face | 28 | 87.7 | P/C | 69.3 | C | 29.7 | P | 5.01 |

[1] Starter bar diameter; [2] Anchorage length; [3] Compressive strength of foundation concrete; [4] $numM_R = numM_{R,p/c} = numM_{max}$ for brittle failure and $numM_R = expM_{R,y}$ for ductile failure; [5] $calM_R = N_R \cdot z = \min\{N_{R,p}; N_{R,p}; N_{R,y}\} \cdot z$ according to Section 8.2 using specified material strengths $f_c$, $f_y$, $\tau_u$ (Table D.2); [6] $calM_{Rk} = N_{Rk} \cdot z = \min\{N_{Rk,p}; N_{Rk,p}; N_{Rk,y}\} \cdot z$ according to Section 9.2 using characteristic material strengths $f_{ck}$, $f_{yk}$, $\tau_{Rk}$ (Table D.6)

Table D.8 Mean and characteristic connection capacities and failure modes numerically tested and calculated on the basis of the enhanced bonded anchor design provisions (2/8)

| Monotonic loading: mon<br>Cyclic loading: cyc | Anchorage detailing | Starter bar layout | $\phi$[1]; $\ell_b$[2] [mm]<br>$f_c$[3] [MPa] | num$M_R$[4] [kNm] | Failure mode tested | cal$M_R$[5] [kNm] | Failure mode calculated[5] | cal$M_{Rk}$[6] [kNm] | Failure mode calculated[6] | $N_{Rk,s}$ / ($N_{Rk,p/c} \cdot \gamma_{inst}$) [-] |
|---|---|---|---|---|---|---|---|---|---|---|
| num3mon | Post-installed | 4 bars | 16; 240 | 106.4 | P/C | 92.3 | C | 41.4 | C | – |
| num3cyc | w/o hook | per face | 28.0 | 97.2 | P/C | 89.3 | C | 40.0 | C | 2.84 |
| num3mon-PI20-d12-s | Post-installed | 4 bars | 12; 240 | 62.3 | Y | 55.2 | Y | 34.7 | Y | – |
| num3cyc-PI20-d12-s | w/o hook | per face | 28.0 | 59.3 | Y | 55.2 | Y | 34.3 | Y | 1.57 |
| num3mon-PI20-d25-s | Post-installed | 4 bars | 25; 240 | 106.4 | P/C | 89.9 | C | 52.0 | C | – |
| num3cyc-PI20-d25-s | w/o hook | per face | 28.0 | 93.9 | P/C | 84.8 | C | 49.0 | C | 7.02 |
| num3mon-PI20-d16-s-d3) | Post-installed | 4 bars | 16; 240 | 102.8 | P/C | 92.3 | C | 41.4 | C | – |
| num3cyc-PI20-d16-s-d3) | w/o hook | per face | 28.0 | 101.4 | P/C | 89.3 | C | 40.0 | C | 2.84 |
| num3mon-PI20-d16-s-q4) | Post-installed | 4 bars | 16; 240 | 102.6 | P/C | 92.3 | C | 41.4 | C | – |
| num3cyc-PI20-d16-s-q4) | w/o hook | per face | 28.0 | 104.1 | P/C | 89.3 | C | 40.0 | C | 2.84 |
| num4mon | Post-installed | 2 bars | 25; 240 | 87.9 | P/C | 89.9 | C | 36.3 | C | – |
| num4cyc | w/o hook | per face | 28.0 | 76.3 | P/C | 84.8 | C | 34.3 | C | 3.51 |
| num4mon-PI20-d16-s | Post-installed | 2 bars | 16; 240 | 55.5 | Y | 48.2 | Y | 27.1 | Y | – |
| num4cyc-PI20-d16-s | w/o hook | per face | 28.0 | 52.5 | Y | 48.2 | Y | 26.2 | Y | 1.55 |
| num4mon-PI20-d32-s | Post-installed | 2 bars | 32; 240 | 89.9 | P/C | 87.9 | C | 42.1 | C | – |
| num4cyc-PI20-d32-s | w/o hook | per face | 28.0 | 74.8 | P/C | 82.1 | C | 39.3 | C | 5.74 |

[1] Starter bar diameter; [2] Anchorage length; [3] Compressive strength of foundation concrete; [4] $numM_R = numM_{R,p/c} = numM_{max}$ for brittle failure and $numM_R = expM_{R,y}$ for ductile failure; [5] $calM_R = N_R \cdot z = \min\{N_{R,p}; N_{R,p}; N_{R,y}\} \cdot z$ according to Section 8.2 using specified material strengths $f_c$, $f_y$, $\tau_u$ (Table D.2); [6] $calM_{Rk} = N_{Rk} \cdot z = \min\{N_{Rk,p}; N_{Rk,p}; N_{Rk,y}\} \cdot z$ according to Section 9.2 using characteristic material strengths $f_{ck}$, $f_{yk}$, $\tau_{Rk}$ (Table D.6)

Table D.8 Mean and characteristic connection capacities and failure modes numerically tested and calculated on the basis of the enhanced bonded anchor design provisions (3/8)

| Monotonic loading: mon<br>Cyclic loading: cyc | Anchorage detailing | Starter bar layout | $\phi$[1]; $\ell_b$[2] [mm]<br>$f_c$[3] [MPa] | $numM_R$[4] [kNm] | Failure mode tested | $calM_R$[5] [kNm] | Failure mode calculated[5] | $calM_{Rk}$[6] [kNm] | Failure mode calculated[6] | $N_{Rk,s}$ / $N_{Rk,p/c}$ [-] |
|---|---|---|---|---|---|---|---|---|---|---|
| num5mon | Cast-in-place | 2 bars | 32; 420 | 202.5 | Y | 179.0 | Y | 144.0 | C | – |
| num5cyc' | w/ hook | per face | 28.0 | 198.0 | Y | 179.0 | Y | 138.1 | C | 2.18 |
| num5mon-CI20-d25-h | Cast-in-place | 2 bars | 25; 420 | 129.0 | Y | 112.9 | Y | 112.9 | Y | – |
| num5cyc-CI20-d25-h | w/ hook | per face | 28.0 | 126.0 | Y | 112.9 | Y | 112.9 | Y | 1.59 |
| num5mon-CI20-d40-h | Cast-in-place | 2 bars | 40; 420 | 226.5 | P/C | 217.9 | C | 139.0 | C | – |
| num5cyc-CI20-d40-h | w/ hook | per face | 28.0 | 235.6 | P/C | 206.4 | C | 131.7 | C | 2.89 |
| num6mon | Cast-in-place | 2 bars | 32; 420 | 179.3 | P/C | 165.7 | P | 51.4 | P | – |
| num6cyc' | w/o hook | per face | 28.0 | 177.1 | P/C | 158.9 | P | 49.3 | P | 2.18 |
| num6mon-CI20-d25-s | Cast-in-place | 2 bars | 25; 420 | 129.0 | Y | 112.9 | Y | 43.8 | P | – |
| num6cyc-CI20-d25-s | w/o hook | per face | 28.0 | 126.0 | Y | 112.9 | Y | 42.7 | P | 1.59 |
| num6mon-CI20-d40-s | Cast-in-place | 2 bars | 40; 420 | 238.8 | P/C | 181.3 | P | 59.1 | P | – |
| num6cyc-CI20-d40-s | w/o hook | per face | 28.0 | 239.4 | P/C | 171.7 | P | 56.0 | P | 2.89 |

[1] Starter bar diameter; [2] Anchorage length; [3] Compressive strength of foundation concrete; [4] $numM_R = numM_{R,p/c} = numM_{max}$ for brittle failure and $numM_R = expM_{R,y}$ for ductile failure; [5] $calM_R = N_R \cdot z = \min\{N_{R,p}; N_{R,p}; N_{R,y}\} \cdot z$ according to Section 8.2 using specified material strengths $f_c$, $f_y$, $\tau_u$ (Table D.2); [6] $calM_{Rk} = N_{Rk} \cdot z = \min\{N_{Rk,p}; N_{Rk,p}; N_{Rk,y}\} \cdot z$ according to Section 9.2 using characteristic material strengths $f_{ck}$, $f_{yk}$, $\tau_{Rk}$ (Table D.6)

Table D.8 Mean and characteristic connection capacities and failure modes numerically tested and calculated on the basis of the enhanced bonded anchor design provisions (4/8)

| Monotonic loading: mon<br>Cyclic loading: cyc | Anchorage detailing | Starter bar layout | $\phi$[1]; $\ell_b$[2] [mm]<br>$f_c$[3] [MPa] | num$M_R$[4] [kNm] | Failure mode tested | cal$M_R$[5] [kNm] | Failure mode calculated[5] | cal$M_{Rk}$[6] [kNm] | Failure mode calculated[6] | $N_{Rk,s}$ / ($N_{Rk,p/c} \cdot \gamma_{inst}$) [-] |
|---|---|---|---|---|---|---|---|---|---|---|
| num7mon-PI20-d32-s | Post-installed | 2 bars | 32; 420 | 196.5 | Y | 179.0 | Y | 93.6 | P | – |
| num7cyc-PI20-d32-s | w/o hook | per face | 28.0 | 193.5 | Y | 179.0 | Y | 89.7 | P | 2.18 |
| num7mon-PI20-d25-s | Post-installed | 2 bars | 25; 420 | 54.0 | Y | 48.2 | Y | 48.2 | Y | – |
| num7cyc-PI20-d25-s | w/o hook | per face | 28.0 | 51.0 | Y | 48.2 | Y | 48.2 | Y | 0.68 |
| num7mon-PI20-d40-s | Post-installed | 2 bars | 40; 420 | 162.9 | P/C | 217.9 | C | 105.9 | P | – |
| num7cyc-PI20-d40-s | w/o hook | per face | 28.0 | 163.5 | P/C | 206.4 | C | 100.3 | P | 3.43 |
| num7mon-PI20-d32-s-d'3) | Post-installed | 2 bars | 32; 420 | 201.8 | Y | 179.0 | Y | 93.6 | P | – |
| num7cyc-PI20-d32-s-d3) | w/o hook | per face | 28.0 | 198.8 | Y | 179.0 | Y | 89.7 | P | 2.18 |
| num7mon-PI20-d32-s-q4) | Post-installed | 2 bars | 32; 420 | 197.3 | Y | 179.0 | Y | 93.6 | P | – |
| num7cyc-PI20-d32-s-q4) | w/o hook | per face | 28.0 | 194.3 | Y | 179.0 | Y | 89.7 | P | 2.18 |
| num8mon | Post-installed | 2 bars | 25; 420 | 126.0 | Y | 112.9 | Y | 80.3 | P | – |
| num8cyc | w/o hook | per face | 28.0 | 123.0 | Y | 112.9 | Y | 78.3 | P | 1.31 |

[1] Starter bar diameter; [2] Anchorage length; [3] Compressive strength of foundation concrete; [4] num$M_R$ = num$M_{R,p/c}$ = num$M_{max}$ for brittle failure and num$M_R$ = exp$M_{R,y}$ for ductile failure; [5] cal$M_R$ = $N_R \cdot z$ = min{$N_{R,p}$; $N_{R,p}$; $N_{R,y}$} $\cdot z$ according to Section 8.2 using specified material strengths $f_c$, $f_y$, $\tau_u$ (Table D.2); [6] cal$M_{Rk}$ = $N_{Rk} \cdot z$ = min{$N_{Rk,p}$; $N_{Rk,p}$; $N_{Rk,y}$} $\cdot z$ according to Section 9.2 using characteristic material strengths $f_{ck}$, $f_{yk}$, $\tau_{Rk}$ (Table D.6)

Table D.8 Mean and characteristic connection capacities and failure modes numerically tested and calculated on the basis of the enhanced bonded anchor design provisions (5/8)

| Monotonic loading: mon<br>Cyclic loading: cyc | Anchorage detailing | Starter bar layout | $\phi$[1]; $\ell_b$[2] [mm]<br>$f_c$[3] [MPa] | $numM_R$[4] [kNm] | Failure mode tested | $calM_R$[5] [kNm] | Failure mode calculated[5] | $calM_{Rk}$[6] [kNm] | Failure mode calculated[6] | $N_{Rk,s}$ / $N_{Rk,p/c}$ [-] |
|---|---|---|---|---|---|---|---|---|---|---|
| num1mon-CI50-d16-h | Cast-in-place | 4 bars | 16; 240 | 108.0 | Y | 96.4 | Y | 93.1 | C | – |
| num1cyc-CI50-d16-h | w/ hook | per face | 58.0 | 105.0 | Y | 96.4 | Y | 90.1 | C | 1.49 |
| num1mon-CI50-d12-h | Cast-in-place | 4 bars | 12; 240 | 61.5 | Y | 55.2 | Y | 55.2 | Y | – |
| num1cyc-CI50-d12-h | w/ hook | per face | 58.0 | 61.5 | Y | 55.2 | Y | 55.2 | Y | 1.01 |
| num1mon-CI50-d25-h | Cast-in-place | 4 bars | 25; 240 | 201.3 | P/C | 129.4 | C | 90.7 | C | – |
| num1cyc-CI50-d25-h | w/ hook | per face | 58.0 | 196.8 | P/C | 122.0 | C | 85.5 | C | 3.17 |
| num2mon-CI50-d16-s | Cast-in-place | 4 bars | 16; 240 | 109.5 | Y | 96.4 | Y | 40.2 | P | – |
| num2cyc-CI50-d16-s | w/o hook | per face | 58.0 | 106.5 | Y | 93.4 | P | 38.9 | P | 1.49 |
| num2mon-CI50-d12-s | Cast-in-place | 4 bars | 12; 240 | 66.0 | Y | 55.2 | Y | 33.0 | P | – |
| num2cyc-CI50-d12-s | w/o hook | per face | 58.0 | 63.0 | Y | 55.2 | Y | 32.7 | P | 1.01 |
| num2mon-CI50-d25-s | Cast-in-place | 4 bars | 25; 240 | 147.3 | P/C | 101.9 | P | 53.8 | P | – |
| num2cyc-CI50-d25-s | w/o hook | per face | 58.0 | 152.6 | P/C | 96.1 | P | 50.7 | P | 3.17 |

[1] Starter bar diameter; [2] Anchorage length; [3] Compressive strength of foundation concrete; [4] $numM_R = numM_{R,p/c} = numM_{max}$ for brittle failure and $numM_R = expM_{R,y}$ for ductile failure; [5] $calM_R = N_R \cdot z = \min\{N_{R,p}; N_{R,p}; N_{R,y}\} \cdot z$ according to Section 8.2 using specified material strengths $f_c$, $f_y$, $\tau_u$ (Table D.2); [6] $calM_{Rk} = N_{Rk} \cdot z = \min\{N_{Rk,p}; N_{Rk,p}; N_{Rk,y}\} \cdot z$ according to Section 9.2 using characteristic material strengths $f_{ck}$, $f_{yk}$, $\tau_{Rk}$ (Table D.6)

Table D.8 Mean and characteristic connection capacities and failure modes numerically tested and calculated on the basis of the enhanced bonded anchor design provisions (6/8)

| Monotonic loading: mon<br>Cyclic loading: cyc | Anchorage detailing | Starter bar layout | $\phi$[1]; $\ell_b$[2] [mm]<br>$f_c$[3] [MPa] | num$M_R$[4] [kNm] | Failure mode tested | cal$M_R$[5] [kNm] | Failure mode calculated[5] | cal$M_{Rk}$[6] [kNm] | Failure mode calculated[6] | $N_{Rk,s}$ / ($N_{Rk,p/c} \cdot \gamma_{inst}$) [-] |
|---|---|---|---|---|---|---|---|---|---|---|
| num3mon-PI50-d16-s | Post-installed | 4 bars | 16; 240 | 106.5 | Y | 96.4 | Y | 46.4 | P | – |
| num3cyc-PI50-d16-s | w/o hook | per face | 58.0 | 103.5 | Y | 96.4 | Y | 44.8 | P | 1.81 |
| num3mon-PI50-d12-s | Post-installed | 4 bars | 12; 240 | 67.5 | Y | 55.2 | Y | 38.2 | P | – |
| num3cyc-PI50-d12-s | w/o hook | per face | 58.0 | 64.5 | Y | 55.2 | Y | 37.8 | P | 1.23 |
| num3mon-PI50-d25-s | Post-installed | 4 bars | 25; 240 | 152.9 | P/C | 129.4 | C | 61.4 | P | – |
| num3cyc-PI50-d25-s | w/o hook | per face | 58.0 | 156.7 | P/C | 122.0 | C | 58.0 | P | 4.44 |
| num3mon-PI50-d16-s-d3) | Post-installed | 4 bars | 16; 240 | 118.7 | P/C | 96.4 | Y | 46.4 | P | – |
| num3cyc-PI50-d16-s-d3) | w/o hook | per face | 58.0 | 118.5 | P/C | 96.4 | Y | 44.8 | P | 1.81 |
| num3mon-PI50-d16-s-q4) | Post-installed | 4 bars | 16; 240 | 119.0 | P/C | 96.4 | Y | 46.4 | P | – |
| num3cyc-PI50-d16-s-q4) | w/o hook | per face | 58.0 | 117.0 | P/C | 96.4 | Y | 44.8 | P | 1.81 |
| num4mon-PI50-d25-s | Post-installed | 2 bars | 25; 240 | 124.0 | P/C | 112.9 | Y | 40.2 | P | – |
| num4cyc-PI50-d25-s | w/o hook | per face | 58.0 | 123.0 | P/C | 112.9 | Y | 37.9 | P | 2.51 |
| num4mon-PI50-d16-s | Post-installed | 2 bars | 16; 240 | 59.3 | Y | 48.2 | Y | 29.4 | P | – |
| num4cyc-PI50-d16-s | w/o hook | per face | 58.0 | 56.3 | Y | 48.2 | Y | 28.4 | P | 1.42 |
| num4mon-PI50-d32-s | Post-installed | 2 bars | 32; 240 | 126.6 | P/C | 126.5 | C | 47.5 | P | – |
| num4cyc-PI50-d32-s | w/o hook | per face | 58.0 | 129.4 | P/C | 118.1 | C | 44.4 | P | 3.63 |

[1] Starter bar diameter; [2] Anchorage length; [3] Compressive strength of foundation concrete; [4] $numM_R = numM_{R,p/c} = numM_{max}$ for brittle failure and $numM_R = expM_{R,y}$ for ductile failure; [5] $calM_R = N_R \cdot z = \min\{N_{R,p}; N_{R,p}; N_{R,y}\} \cdot z$ according to Section 8.2 using specified material strengths $f_c$, $f_y$, $\tau_u$ (Table D.2); [6] $calM_{Rk} = N_{Rk} \cdot z = \min\{N_{Rk,p}; N_{Rk,p}; N_{Rk,y}\} \cdot z$ according to Section 9.2 using characteristic material strengths $f_{ck}$, $f_{yk}$, $\tau_{Rk}$ (Table D.6)

Table D.8 Mean and characteristic connection capacities and failure modes numerically tested and calculated on the basis of the enhanced bonded anchor design provisions (7/8)

| Monotonic loading: mon<br>Cyclic loading: cyc | Anchorage detailing | Starter bar layout | $\phi$[1]; $\ell_b$[2] [mm]<br>$f_c$[3] [MPa] | $numM_R$[4] [kNm] | Failure mode tested | $calM_R$[5] [kNm] | Failure mode calculated[5] | $calM_{Rk}$[6] [kNm] | Failure mode calculated[6] | $N_{Rk,s}$ / $N_{Rk,p/c}$ [-] |
|---|---|---|---|---|---|---|---|---|---|---|
| num5mon-CI50-d32-s | Cast-in-place | 2 bars | 32; 420 | 207.0 | Y | 179.0 | Y | 179.0 | Y | – |
| num5cyc'-CI50-d32-s | w/ hook | per face | 58.0 | 204.0 | Y | 179.0 | Y | 179.0 | Y | 1.26 |
| num5mon-CI50-d25-h | Cast-in-place | 2 bars | 25; 420 | 132.8 | Y | 112.9 | Y | 112.9 | Y | – |
| num5cyc-CI50-d25-h | w/ hook | per face | 58.0 | 129.8 | Y | 112.9 | Y | 112.9 | Y | 0.92 |
| num5mon-CI50-d40-h | Cast-in-place | 2 bars | 40; 420 | 316.0 | P/C | 268.9 | Y | 219.8 | C | – |
| num5cyc-CI50-d40-h | w/ hook | per face | 58.0 | 313.7 | P/C | 268.9 | Y | 208.2 | C | 1.65 |
| num6mon-CI50-d32-s | Cast-in-place | 2 bars | 32; 420 | 210.0 | Y | 179.0 | Y | 89.4 | P | – |
| num6cyc'-CI50-d32-s | w/o hook | per face | 58.0 | 207.0 | Y | 179.0 | Y | 85.8 | P | 1.26 |
| num6mon-CI50-d25-s | Cast-in-place | 2 bars | 25; 420 | 131.3 | Y | 112.9 | Y | 75.6 | P | – |
| num6cyc-CI50-d25-s | w/o hook | per face | 58.0 | 129.8 | Y | 112.9 | Y | 73.8 | P | 0.92 |
| num6mon-CI50-d40-s | Cast-in-place | 2 bars | 40; 420 | 238.8 | P/C | 251.5 | P | 103.4 | P | – |
| num6cyc-CI50-d40-s | w/o hook | per face | 58.0 | 239.4 | P/C | 238.3 | P | 97.9 | P | 1.65 |

[1] Starter bar diameter; [2] Anchorage length; [3] Compressive strength of foundation concrete; [4] $numM_R = numM_{R,p/c} = numM_{max}$ for brittle failure and $numM_R = expM_{R,y}$ for ductile failure; [5] $calM_R = N_R \cdot z = \min\{N_{R,p}; N_{R,p}; N_{R,y}\} \cdot z$ according to Section 8.2 using specified material strengths $f_c$, $f_y$, $\tau_u$ (Table D.2); [6] $calM_{Rk} = N_{Rk} \cdot z = \min\{N_{Rk,p}; N_{Rk,p}; N_{Rk,y}\} \cdot z$ according to Section 9.2 using characteristic material strengths $f_{ck}$, $f_{yk}$, $\tau_{Rk}$ (Table D.6)

Table D.8 Mean and characteristic connection capacities and failure modes numerically tested and calculated on the basis of the enhanced bonded anchor design provisions (8/8)

| Monotonic loading: mon<br>Cyclic loading: cyc | Anchorage detailing | Starter bar layout | $\phi$[1]; $\ell_b$[2] [mm]<br>$f_c$[3] [MPa] | $numM_R$[4] [kNm] | Failure mode tested | $calM_R$[5] [kNm] | Failure mode calculated[5] | $calM_{Rk}$[6] [kNm] | Failure mode calculated[6] | $N_{Rk,s}$ / ($N_{Rk,p/c} \cdot \gamma_{inst}$) [-] |
|---|---|---|---|---|---|---|---|---|---|---|
| num7mon'-PI50-d32-s | Post-installed | 2 bars | 32; 420 | 210.8 | Y | 179.0 | Y | 104.1 | P | – |
| num7cyc'-PI50-d32-s | w/o hook | per face | 58.0 | 207.8 | Y | 179.0 | Y | 99.9 | P | 1.51 |
| num7mon-PI50-d25-s | Post-installed | 2 bars | 25; 420 | 59.3 | Y | 48.2 | Y | 48.2 | Y | – |
| num7cyc-PI50-d25-s | w/o hook | per face | 58.0 | 56.3 | Y | 48.2 | Y | 48.2 | Y | 0.63 |
| num7mon-PI50-d40-s | Post-installed | 2 bars | 40; 420 | 236.2 | P/C | 268.9 | Y | 120.0 | P | – |
| num7cyc-PI50-d40-s | w/o hook | per face | 58.0 | 241.3 | P/C | 268.9 | Y | 113.7 | P | 2.17 |
| num7mon-PI50-d32-s-d'3) | Post-installed | 2 bars | 32; 420 | 204.8 | Y | 179.0 | Y | 104.1 | P | – |
| num7cyc-PI50-d32-s-d3) | w/o hook | per face | 58.0 | 201.8 | Y | 179.0 | Y | 99.9 | P | 1.51 |
| num7mon-PI50-d32-s-q4) | Post-installed | 2 bars | 32; 420 | 206.3 | Y | 179.0 | Y | 104.1 | P | – |
| num7cyc-PI50-d32-s-q4) | w/o hook | per face | 58.0 | 203.3 | Y | 179.0 | Y | 99.9 | P | 1.51 |
| num8mon-PI50-d25-s | Post-installed | 2 bars | 25; 420 | 131.3 | Y | 112.9 | Y | 88.2 | P | – |
| num8cyc-PI50-d25-s | w/o hook | per face | 58.0 | 129.8 | Y | 112.9 | Y | 86.0 | P | 1.10 |

[1] Starter bar diameter; [2] Anchorage length; [3] Compressive strength of foundation concrete; [4] $numM_R = numM_{R,p/c} = numM_{max}$ for brittle failure and $numM_R = expM_{R,y}$ for ductile failure; [5] $calM_R = N_R \cdot z = \min\{N_{R,p}; N_{R,p}; N_{R,y}\} \cdot z$ according to Section 8.2 using specified material strengths $f_c$, $f_y$, $\tau_u$ (Table D.2); [6] $calM_{Rk} = N_{Rk} \cdot z = \min\{N_{Rk,p}; N_{Rk,p}; N_{Rk,y}\} \cdot z$ according to Section 9.2 using characteristic material strengths $f_{ck}$, $f_{yk}$, $\tau_{Rk}$ (Table D.6)

## Curriculum Vitae

### Personal Data

Christoph Mahrenholtz
Born on the 25th of February, 1974
in Brunswick, Germany.

### Education

| | |
|---|---|
| 1980 – 1986 | Elementary School, Brunswick |
| 1986 – 1993 | Highschool 'Gymnasium Kleine Burg', Brunswick |
| 1993 – 1998 | University of Karlsruhe (KIT), Germany |
| 1998 | University of Edinburgh, United Kingdom |
| 1998 | *Diplom-Ingenieur (M.Sc.)* |
| 2006 – 2012 | University of Stuttgart, Germany |
| 2010 – 2011 | University of Canterbury, Christchurch, New Zealand |
| 2012 | *Doktor-Ingenieur (Ph.D.)* |

### Experience

| | |
|---|---|
| 1998 – 2001 | Hochtief AG, Essen, Germany<br>Site Engineer |
| 2001 – 2003 | Hochtief International Taichung, Taiwan and Essen, Germany<br>Project Engineer |
| 2003 – 2005 | Züblin AG, Stuttgart and Hamburg, Germany<br>Project Engineer |
| 2005 – 2006 | Züblin International Shanghai, China<br>Project Manager |
| 2007 – 2012 | University of Stuttgart, Germany<br>Test Engineer, Teaching Assistant, Research Engineer |
| 2010 – 2011 | University of Canterbury, Christchurch, New Zealand<br>Visiting Researcher |
| 2012 | National Taiwan University, Taipei, Taiwan<br>Post-doctoral Researcher |

*In the construction of a country, it is not the practical workers but the idealists and visionaries that are difficult to find.*

Dr. Y.-S. Sun, 1866 – 1925

Hiermit versichere ich, die vorliegende Dissertation ohne Hilfe Dritter nur mit den angegebenen Quellen und Hilfsmitteln angefertigt zu haben. Alle Stellen, die aus den Quellen entnommen wurden, sind als solche kenntlich gemacht worden. Diese Arbeit hat in gleicher oder ähnlicher Form noch keiner Prüfungsbehörde vorgelegen.